The Origin and Evolution of V-rich, Magnetite Dominated Fe-Ti Oxide Mineralization; Northwest River Anorthosite, South-Central Labrador, Canada

Anthony A. Valvasori

A thesis submitted to the Department of Earth Sciences in partial fulfillment of the requirements for the degree of Master of Science.

Memorial University of Newfoundland

Abstract

The Northwest River Anorthosite (NWRA) is a ca. 1625 Ma Paleoproterozoic massif anorthosite located in the Grenville Province of south-central Labrador. Abundant zones of coarse-grained massive to semi-massive Fe-Ti oxide mineralization and disseminated oxide mineralization, which occur in sharp irregular contact with the host anorthosite are present in the NWRA. The Fe-Ti oxide minerals in the NWRA are dominated by magnetite with less abundant ilmenite and pleonaste; all oxide minerals contain abundant and complex exsolution features.

Whole-rock geochemistry, petrography and in situ analyses show that regardless of field texture, oxide mineralization is similar in all of the samples analyzed. Whole-rock analyses of massive to semi-massive Fe-Ti oxide mineralization in the NWRA show values of ~10 wt. % TiO_2 and 2700 ppm V (0.48 wt. % V_2O_5). In-situ magnetite analyses contain <0.5 wt. % TiO_2 and 0.6-0.7 wt. % V_2O_5. Composite ilmenite contains ~1 wt. % Mg, 5-7 mol% hematite component and negligible Cr and Al content.

Based on oxide mineral chemistry, oxide-anorthosite field relationships, and whole-rock geochemistry, it can be inferred that the formation of the oxide mineralization occurred in a three step process: 1) late-stage magmatic crystallization of impure magnetite; 2) concentration by solid-state remobilization and/or crystal sorting; and 3) reequilibration during subsequent post-emplacement cooling and subsequent Grenvillian metamorphism. These subsolidus processes significantly modified the primary magmatic composition of the oxide minerals through exsolution and reequilibration.

Acknowledgments

This research could not have been undertaken without funding provided by the Ignite R&D Program of the Research and Development Corporation (RDC) of Newfoundland and Labrador, the Atlantic Canada Opportunities Agency (ACOA) and Innovation, Business and Rural Development (IBRD) to M.L.D. Fonkwe.

Tom Benoit and Craig Coady of Ferrum Resources are thanked for allowing access to the field area, permission for sampling, and many days in the field doing geology, which are the best kind of days.

M.L.D. Fonkwe and S.J. Piercey are thanked for helping to get the project off to a good start, and A. Kerr and J. M. Hanchar are thanked for helping get this project back on track to bring it to completion. The entire supervisory team is thanked for their knowledge, editing prowess, and willingness to help.

A big thanks to others who helped with logistics along the way, specifically Brian Joy (EPMA analyses), Marko Prasek and Dany Savard (LA-ICPMS analyses), and the entire staff of the Labrador Institute.

The grad school experience would have been much more unpleasant without the support and friendship of other grad students. You know who you are. Thanks.

Finally, I would like to acknowledge my two girls, Meghan and Qimmie. Thanks for your unwavering faith in me.

Table of Contents

Abstract……..ii
Acknowledgments……iii
Table of Contents……iv
List of Figures……vii
List of Appendices……ix
Chapter 1: Introduction……1
1.1 Overview……1
1.2 Previous Work……2
1.3 Study Area: Location and Physiography……3
1.4 Regional and Local Geology……5
1.4.1 Overview of the regional geology of the Eastern Grenville Province in Labrador……5
1.4.2 Local geology……7
1.5 Fe-Ti oxide mineralization in Proterozoic anorthosite massifs……9
1.5.1 Liquid Immiscibility……11
1.5.2 Fractional Crystallization……12
1.5.3 Magma Mixing……13
1.5.4 Hydrothermal remobilization……13
1.5.5 Solid state remobilization……14
1.6 Rationale and Objectives……15
Chapter 2: Methods……26
2.1 Sampling……26
2.2 Whole-rock geochemistry……27
2.3 EPMA……27
2.3.1 EPMA WDS analyses……27
2.3.2 EPMA WDS X-ray maps……28
2.3.3 Calculation of Fe^{2+} and Fe^{3+} from EPMA analyses……29
2.4 LA-ICPMS analyses……32
Chapter 3: Results……35
3.1 Massive to semi-massive oxide mineralization……35
3.1.1 General Features……36
3.1.2 Oxide-rich Pods……37

3.1.3 Oxide-rich Veins 38
3.1.4 Oxide-rich Bands 38
3.2 Disseminated oxide mineralization 40
3.3 Host rock mineralization 35
3.4 Petrography 42
3.4.1 Massive to semi-massive oxide mineralization 42
3.4.2 Disseminated oxide mineralization 49
3.4.3 Host rock Mineralization 52
3.5 Whole-rock geochemistry 53
3.5.1 Geochemistry overview 53
3.5.2 Unmineralized host rocks 54
3.5.3 Massive to semi-massive oxide mineralization 55
3.5.4 Disseminated oxide mineralization 56
3.5.5 Geochemical correlations 58
3.6 Electron microprobe analyses 59
3.6.1 Magnetite Compositions 59
3.6.2 Ilmenite 63
3.6.3 Pleonaste 63
3.7 Mineral compositions determined by LA-ICPMS 70
3.7.1 Magnetite 70
3.7.2 Ilmenite 73
3.7.3 Pleonaste 76
3.7.4 Wavelength Dispersal Spectroscopy (WDS) of Oxide Grains 79
Chapter 4: Discussion 84
4.1 Interpretation of results 84
4.1.1 Field observations 84
4.1.2 Petrography 85
4.1.3 Whole rock major and trace element geochemistry. 86
4.1.4 In situ oxide chemistry 88
4.1.5 EPMA discrimination diagrams 94
4.1.6 LA-ICPMS Discrimination diagrams 100
4.2 Genesis and evolution of oxide mineralization 100
4.2.1 Liquid Immiscibility 105

4.2.2 Magma mixing 107
4.2.3 Hydrothermal remobilization 108
4.2.4 Fractional Crystallization 109
4.2.5 Solid state remobilization 109
4.2.6 Effect of cooling and metamorphism on oxide chemistry 110
4.2.7 Oxygeothermometry 113
4.2.8 Oxide genesis, concentration and evolution in the NWRA 115
4.3 Economic Potential of Fe-Ti oxide mineralization in the NWRA 116
Chapter 5: Conclusions and Future Work 127
5.1 Conclusions 127
5.2 Future Work 129

List of Figures

Figure 1.1 Simplified geological map of Labrador 4
Figure 1.2 Map of local geology. 8
Figure 1.3 Regional aeromagnetic map of the Cape Caribou River allochthon. 10
Figure 3.1 Field photos; barren host rocks and disseminated oxide 37
Figure 3.2 Field photos; pods of massive to semi-massive oxide mineralization 39
Figure 3.3 Field photos; veins of oxide mineralization 40
Figure 3.4 Field photos; bands of oxide mineralization 42
Figure 3.5. Photomicrographs of massive to semi-massive oxide mineralization 443
Figure 3.6 Photomicrographs of massive to semi-massive oxide mineralization 45
Figure 3.7. Photomicrographs of exsolution features in Fe-Ti oxides 47
Figure 3.8. Photomicrographs of exsolution features in Fe-Ti oxides. 50
Figure 3.9. Photomicrographs of Fe-Ti oxides and host rock. 51
Figure 3.10 Whole-rock geochemistry element correlation matrix 59
Figure 3.11a, b. Magnetite EPMA box and whisker diagram 60
Figure 3.12a, b. Ilmenite EPMA box and whisker diagram 67
Figure 3.13a, b. Pleonaste EPMA box and whisker diagram 68
Figure 3.14a, b. Magnetite LA-ICPMS box and whisker diagram 71
Figure 3.15a, b. Ilmenite LA-ICPMS box and whisker diagram 75
Figure 3.16a, b. Pleonaste LA-ICPMS box and whisker diagram 77
Figure 3.17. X-ray maps of oxide minerals 79
Figure 4.1. Whole-rock binary variation diagrams of whole-rock analyses 86
Figure 4.2. EPMA magnetite binary element variation diagrams 90
Figure 4.3. LA-ICPMS magnetite binary variation diagrams 91
Figure 4.4. EPMA ilmenite binary variation diagrams 92
Figure 4.5. LA-ICPMS ilmenite binary element variation diagrams 92
Figure 4.7a, b. Dupuis and Beaudoin (2011) magnetite ore deposit discrimination diagrams 96
Figure 4.8. Knipping et al. (2015) hydrothermal vs magmatic magnetite discrimination diagram 98
Figure 4.9. Dare et al. (2014) hydrothermal vs magmatic magnetite discrimination diagram. 99
Figure 4.10a-c. Dare et al. (2014) multielement magnetite discrimination diagram 101-103

Figure 4.11. Data matrix showing plotting position of elements on the Dare et al. (2014) multi-element magnetite discrimination diagram..... 104
Figure 4.12. Oxygeothermometry results 114

List of Appendices

Appendix I. List of samples analyzed with EPMA and LA-ICPMS. 131

Appendix II. Average (mean) and standard deviation of whole-rock, EPMA and LA-ICPMS analyses 132

Appendix III. Whole-rock geochemistry results. 159

Appendix IV All EPMA analyses results. 168

Appendix V All LA-ICPMS analyses results. 233

Appendix VI. LA-ICPMS and EPMA spot and line analyses. 274

Appendix VII: LA-ICPMS secondary standards 394

List of Abbreviations

AMCG	Anorthosite mangerite charnockite granite
CCRA	Cape Caribou River allochthon
EPMA	Electron probe microanalyzer
fO_2	Oxygen fugacity
HLIS	Harp Lake intrusive suite
LA-ICPMS	Laser ablation inductively coupled plasma mass spectrometery
LOD	Level of detection
MMIS	Mealy Mountains intrusive suite
Myr	Million years
NPS	Nain plutonic suite
NWRA	North West River anorthosite
PGE	Platinum group elements
WDS	Wavelength dispersive spectroscopy

Chapter 1: Introduction

1.1 Overview

Titanium and Vanadium are important industrial elements that are commonly processed from the Fe-Ti oxide minerals magnetite (Fe_3O_4) and ilmenite ($FeTiO_3$) (Force, 1991; Fabjan et al., 2001; Dill, 2010). Economic concentrations of Fe-Ti oxide mineralization are a common feature in Proterozoic anorthosite intrusive complexes including three with currently active mines including Lac Tio, Québec (Charlier et al., 2009), Tellnes, SW Norway (Charlier et al., 2006), and Damiao, China (Chen et al., 2013). Other anorthosite massifs are known to host large, but currently uneconomic concentrations of Fe-Ti oxides including Suwalki (Poland) (Charlier et al., 2009b.), Lac St. Jean (Québec) (Morisset et al., 2010) and Marcy (New York State) (Ashwal, 1982).

Proterozoic anorthosite massifs were defined by Ashwal (2010) as temporally restricted (e.g., largely forming between ~1790 and ~1060 Ma) large composite igneous intrusive suites (i.e., massifs) dominantly composed of anorthositic rocks. Labrador contains several anorthosite massifs (Fig. 1.1) including the Nain Plutonic Suite, Mealy Mountains Intrusive Suite (MMIS), including the genetically related North-West River anorthosite (NWRA), as well as the Harp Lake Intrusive Suite, Mistastin Massif, and the Atikonak River Complex (Ashwal, 1993; Kerr et al., 2013).

During the exploration boom following the Voiseys Bay discovery, in 1994, in Labrador (Ryan et al., 1995), numerous occurrences of Fe-Ti-V oxide mineralization were discovered (or rediscovered) in various geological settings throughout Labrador (e.g., Hinchey et al., 1999; MacDonald, 1999; Kerr et al., 2001; Dyke et al., 2004; Kerr

et al., 2013). Only a few of these occurrences, however, underwent follow-up evaluation and detailed descriptions, as exploration efforts largely targeted magmatic Ni-Cu-Co sulphide deposits (Kerr et al., 2013, and references therein). The oxide zones were considered to be of limited interest, unless they were associated with sulphides and Ni, Cu, Co and PGE enrichment.

There is a general consensus that Fe-Ti oxide mineralization in Proterozoic anorthosite massifs suites is broadly magmatic in origin (e.g., Ashwal, 1982; Duchesne, 1999; Dymek and Owens, 2001; Charlier et al., 2015 and references therein). However, the nature of the processes responsible for oxide formation and/or concentration are subject to ongoing debate. Petrogenetic processes proposed for the formation of oxide-rich mineralization include liquid immiscibility, fractional crystallization, magma mixing, hydrothermal remobilization, and solid state remobilization. The various models and their assumptions and limitations are summarized by Charlier et al. (2015) and are described in more detail in section 1.5.

1.2 Previous Work

The study area for the current project, the North West River anorthosite (NWRA) which forms the uppermost unit of the CCRA, was first mapped at the 250,000 scale by Stevenson (1969) with the Geological Survey of Canada, and was subsequently remapped at 1:100,000 (Ryan et al., 1982) and 1:50,000 scale Wardle and Ash (1984; 1986) by the Department of Mines and Energy of the Government of Newfoundland and Labrador. Several other research studies were completed following the second phase of mapping, including structural and metamorphic studies (Gower

and Krogh, 2002; Krauss and Rivers, 2004) as well as U-Pb zircon geochronology which dated the host anorthosite as 1625-1650 Ma (Philippe et al., 1993; Bussy et al., 1995; and Corrigan et al., 1997).

Despite the presence of several known Fe-Ti oxide mineralized areas as well as a large aeromagnetic anomaly (Fig. 1.3), the NWRA has yet to be widely explored for economic mineralization. There were only sporadic prospecting and exploration activities following the Voisey's Bay discovery (Kerr et al., 2013, and references therein). However, semi-massive to massive Fe-Ti oxide mineralization in the NWRA was identified by prospectors T. Benoit and C. Coady in 2011 in anorthositic outcrops in the area west of Grand Lake (Figs. 1.2, 1.3) and this formed the starting point for the present investigation. This study marks the first descriptive work done on oxide mineralization hosted within the NWRA and includes field descriptions, transmitted and reflected light petrography, whole-rock geochemistry, and in-situ EPMA and LA-ICPMS analyses of magnetite, ilmenite, and pleonaste (a low-Mg spinel intermediate of the spinel-hercynite solid solution).

1.3 Study Area: Location and Physiography

The study area for this project is located between latitudes 53.50ºN and 53.37ºN and longitudes 60.67ºW and 60.52ºW, approximately 30 km northwest of Happy Valley-Goose Bay, Labrador (Figs. 1.1-1.3). It covers approximately 6 square

kilometers on the western edge of the CCRA, and is largely underlain by anorthositic

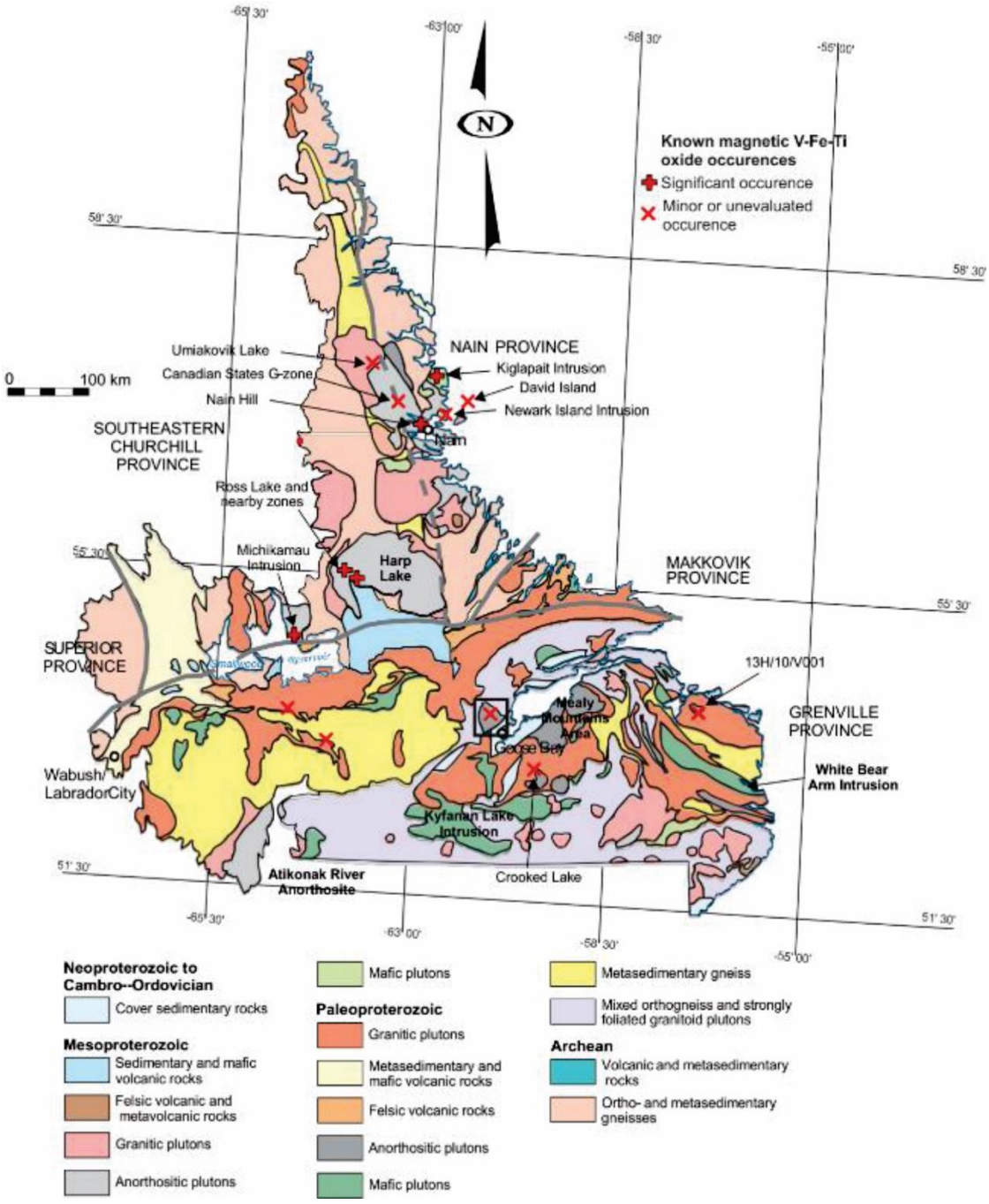

Figure 1.1 Simplified geological map of Labrador showing locations of known magmatic Fe-Ti-V oxide mineralization (shown by red x and + symbols). The Cape Caribou River allochthon is outlined by a black box (modified from Kerr et al., 2013).

rocks, grouped as the NWRA by Wardle and Ash, (1984). Field access is via the Grand Lake Road, a well-maintained gravel forestry road that branches from the paved Route 520, which extends from Happy Valley-Goose Bay to North West River. The field area is forested with jack pine, spruce, and fir, with several burnt over zones resulting from forest fires. Although bedrock outcrops are abundant in the area, recovering fresh samples is locally difficult because of surface weathering and the typically smooth, glacially-rounded outcrop surfaces. There is an 80 m elevation change in the field area, marked by a ridge to the west and low-lying muskeg to the east**.**

1.4 Regional and Local Geology

1.4.1 Overview of the regional geology of the Central and Eastern Grenville Province in Labrador

The rocks of the eastern Grenville province were assembled over ~700 Myr along the southeastern ancestral margin of the Laurentian craton, using present-day coordinates; most of these rock units have experienced polyphase, high-grade metamorphism and are gneisses (Li et al., 2008; Rivers, 2015). The oldest exposed rocks within the eastern Grenville province (>1710 Ma; termed pre-Labradorian (Gower, 1992; Gower et al., 1996; Gower and Krogh, 2002; Rivers, 2007) are migmatitic gneisses, the protoliths of which are interpreted to consist of sedimentary rocks that originally formed within a continental-margin basin. Four key subsequent tectono-metamorphic events are recognized within the rocks of the eastern Grenville Province: 1) the Labradorian orogeny (~1710-1600 Ma); 2) the Pinwarian orogeny

(1520-1460 Ma); 3) the Elsonian orogeny (1460-1230 Ma); and 4) the Grenvillian orogeny (1250-980 Ma) (Gower and Krogh, 2002; Rivers, 2007).

The oldest components of the Labradorian terrane consist of a volcanic arc dated at 1710 and 1680 Ma (Gower and Krogh, 2002). Arc magmatism ceased at ~1660 Ma likely due to arc accretion, which led to the continental crust becoming overthickened leading to penetrative ductile deformation coupled with low pressure metamorphism peaking at granulite facies (Gower, 1996; Rivers, 1997; Gower and Krogh, 2002). Subsequent to the arc-accretion events, a pulse of bimodal mafic-anorthositic-monzogranitic magmatism was emplaced within the eastern Grenville province (Rivers, 1997; Gower and Krogh, 2002). This magmatic pulse, dated at 1650-1625 Ma, includes the MMIS and the NWRA which at present lies within the CCRA (Ashwal, 1993; Gower and Krogh, 2002). The MMIS and NWRA and interpreted to have formed as components of a single body and were subsequently separated (Krauss and Rivers, 2004).

The Pinwarian orogeny (1520-1460 Ma) is thought to be associated with arc accretion and active margin shortening in an island arc or continental arc-margin setting (Gower and Krogh, 2002; Augland et al., 2015). The rock record from the Pinwarian orogeny includes dominantly felsic magmatism that intruding into Labradorian crust (Gower and Krogh, 2002; Gower et al., 2008). Deformation and metamorphism associated with the Pinwarian orogeny has been observed throughout the eastern Grenville Province (Augland et al., 2015).

Following the Pinwarian orogeny is the Elsonian orogeny (1460-1230 Ma). The Elsonian orogeny is thought to have occurred through the complex interactions between the subducting slab and the overriding Laurentian continental margin (Gower and Krogh, 2002). According to Gower and Krogh, rocks of the Elsonian orogeny include the Michael-Shabogamo gabbroic dike swarm as well as numerous anorthosite-mangerite-charnockite-granite (AMCG) suites including the NPS (Rivers, 1997; Gower and Krogh, 2002).

The Grenvillian orogeny (1090 and 980 Ma), occurred due to the terminal continental collision between Laurentia and Amazonia which led to extensive crustal thickening via imbrication of thrust slices, as well as intense deformation and metamorphism (e.g., Rivers, 1997; Li et al., 2008; Rivers et al., 2012; Rivers, 2015) and references therein). Post-Grenvillian rifting, possibly associated with the opening of the early Paleozoic Iapetus Ocean, created a series of grabens in the Lake Melville area, which now separate the CCRA from the MMIS (Fig. 1.1). The CCRA is believed to represent a portion of the MMIS that was separated during the formation of the Lake Melville rift as a similar assemblage of lithologies occurs in both the CCRA and the MMIS (Wardle et al., 1990; Philippe et al., 1993; Krauss and Rivers, 2004).

1.4.2 Local geology

The CCRA (Fig. 1.2) is a ~20-25 km wide lobate thrust sheet with an aerial extent of ~500km^2 that is dominantly composed of Paleoproterozoic AMCG rocks, and also includes minor layered gabbro monzonite, dioritic to granodioritic orthogneiss, amphibolite, mafic granulite, and minor metasedimentary gneiss (Wardle and Ash, 1984; 1986; Ryan et al., 1982). Penetrative deformation in the CCRA is limited to the

basal high-strain shear zone whereas the uppermost units including the NWRA have

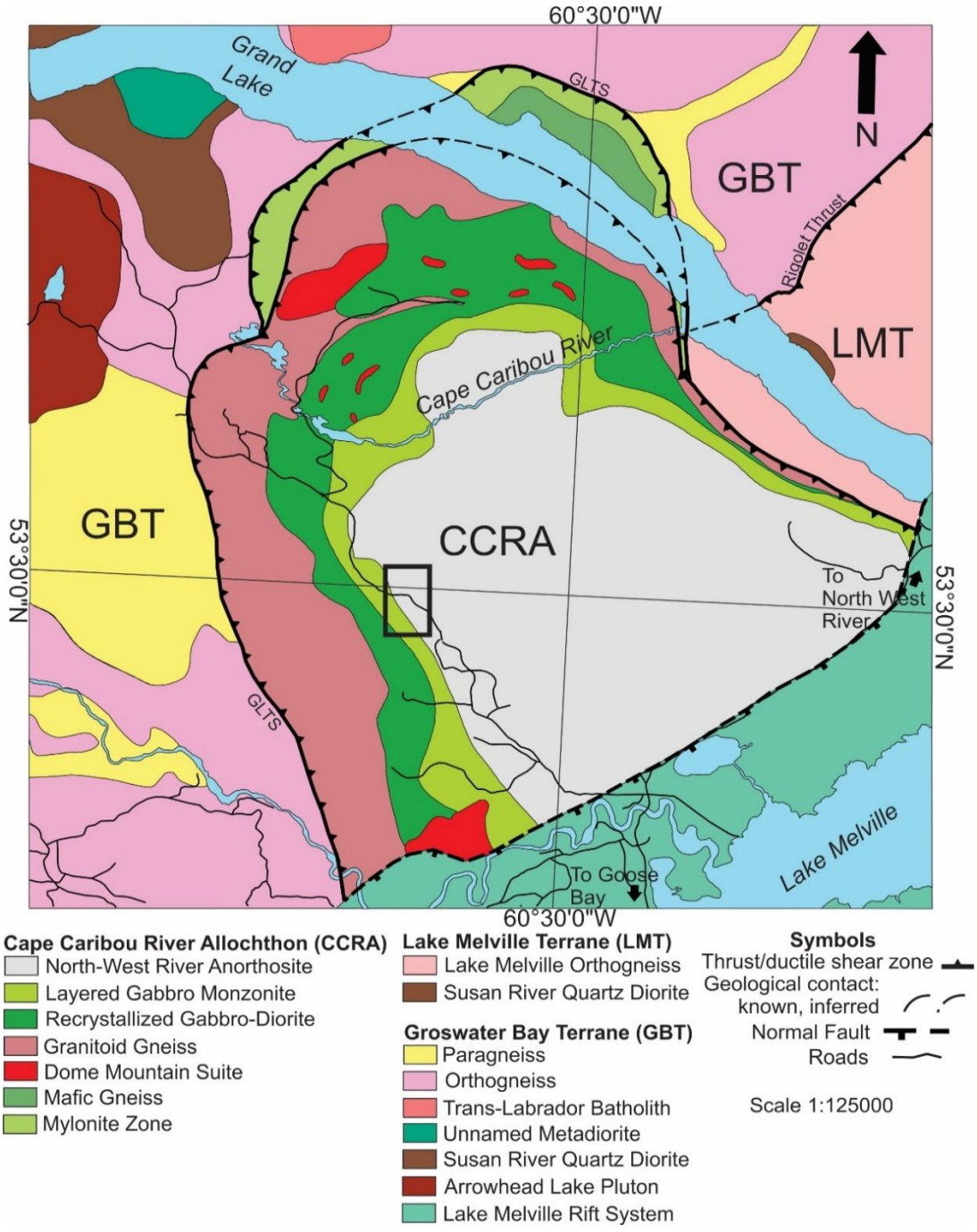

Figure 1.2 Geological map of the Cape Caribou River allochthon showing the North West River anorthosite in the center and surrounding rock units (modified from Krauss and Rivers, 2004). The field area for this study is outlined by the black box.

undergone only static recrystallization (Krauss and Rivers, 2002). The NWRA is an anorthositic body located at the structural top of the CCRA Allochthon (Fig. 1.2) (Bussy et al., 1995; Krauss and Rivers, 2004).

The NWRA is a heterogeneous unit composed primarily of anorthosite to gabbronoritic rocks composed of several coalesced anorthosite plutons, each with variable mafic components and textures (Krauss, 2002). In general, plagioclase crystals in all coalesced plutons ranges from a few mm to 20 cm in size and are unaltered to weakly sericitized. Despite the lack of penetrative deformation associated with thrusting, the NWRA shows evidence of static recrystallization including the presence of garnet in gabbronorites as well as recrystallization textures in plagioclase in the host anorthosite (Krauss, 2002). Fe-Ti oxide mineralization in the NWRA is dominated by magnetite (Valvasori et al., 2015).

1.5 Fe-Ti oxide mineralization in Proterozoic anorthosite massifs

Zones of voluminous Fe-Ti oxide mineralization commonly occur in Proterozoic massif anorthosite massifs (Ashwal, 1993; Charlier et al., 2014). The mineralization is generally composed of a combination of ilmenite ($FeTiO_3$), magnetite (Fe_3O_4), and/or spinel, typically pleonaste ($(Fe,Mg)Al_2O_4$) in composition. Although there is a consensus that the Fe-Ti oxide minerals have a magmatic origin, the specific processes by which the oxides formed and subsequently concentrated is not well constrained.

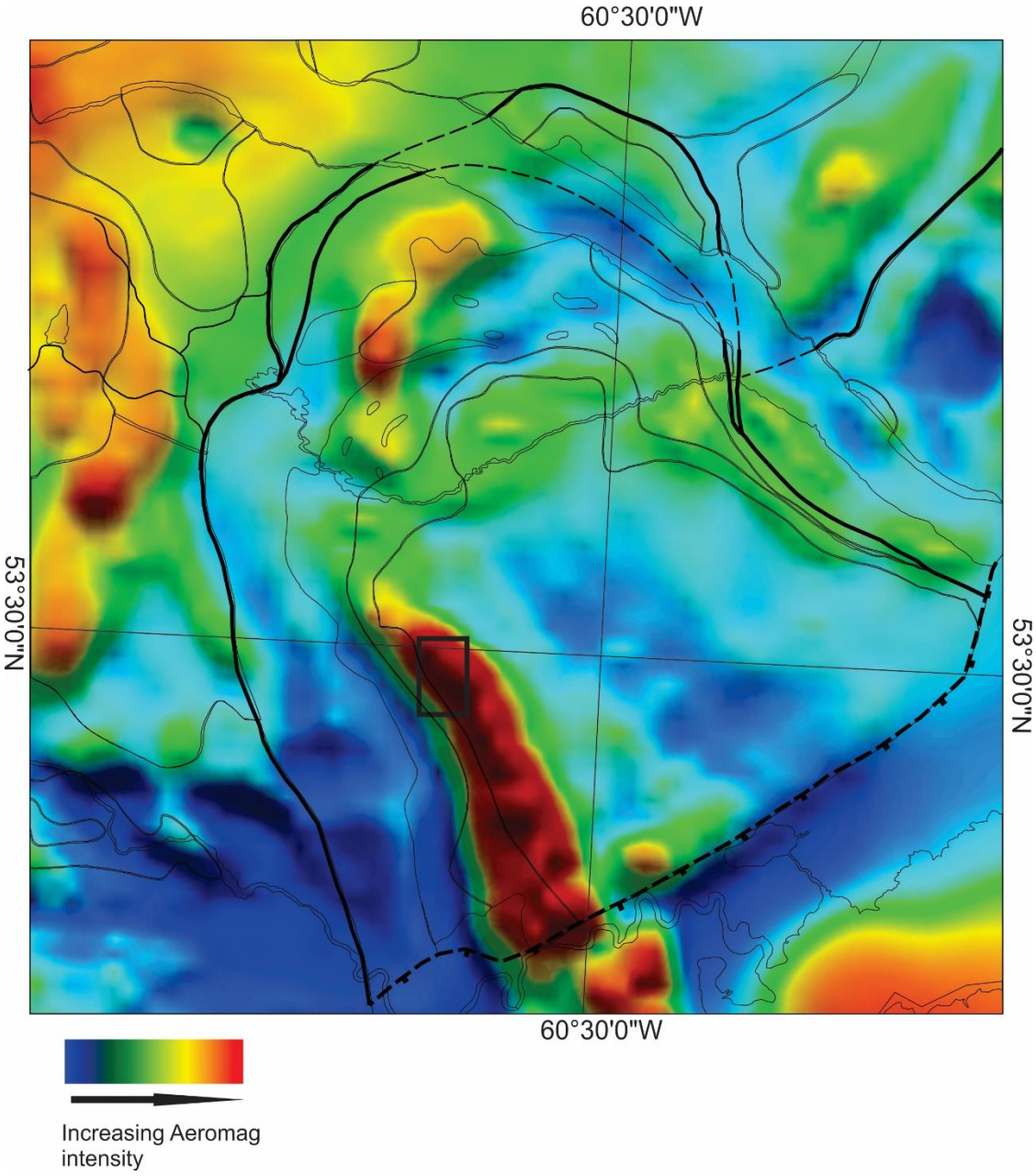

Figure 1.3 Regional aeromagnetic map (NL Geoscience Atlas) overlain by the unit boundaries of the rock units contained within Cape Caribou River allochthon from the NL Geoscience Atlas. Note the relationship between the large aeromagnetic high and the contact between the North West River anorthosite and basal layered monzonite. The field area for this study is outlined by a black solid box.

Current models for the formation of concentrations of Fe-Ti oxide minerals include: 1) liquid immiscibility; 2) fractional crystallization; 3) magma mixing; 4) hydrothermal remobilization; and 5) subsolidus remobilization (e.g., Charlier et al., 2015 and references therein). These are discussed in the next section and one of the main objectives of this present study is an attempt to test these models for ore formation by assessing the features (i.e., distribution, morphology, size, and chemistry) of oxide mineral accumulations in the study area.

1.5.1 Liquid Immiscibility

Liquid immiscibility is a process which has been proposed by some researchers to result in the formation of large zones of nearly pure Fe-Ti oxide mineralization in sharp contact with the host anorthosite. The textural features predicted by this process includes veins of massive oxide mineralization crosscutting the host anorthosite, as well as oxide minerals interstitial to plagioclase in the host anorthosite (Philpotts, 1967; He et al., 2016). In this model, the residual magma after the anorthosite crystallization is inferred to be a ferrodiorite which is a Fe, Ti, and P rich mafic silicate magma. Eutectic crystallization of ferrodioritic magma is proposed to lead to the formation of oxide-apatite gabbronoritic rocks (OAGN), whereas fractional crystallization of ferrodioritic magma is thought to lead to the generation of an immiscible Fe-Ti-P oxide magma under high fO_2 (Chen et al., 2013).

Critics of this model point to a lack of experimental evidence under naturally occurring conditions to support the theory of coexisting oxide and silicate magmas within a single magma chamber (Lindsley, 2003; Lindsley and Epler, 2017).

Furthermore, no direct evidence of coexisting immiscible silicate and Fe-Ti-P oxide melts have been reported in plutonic settings (Charlier and Grove, 2012).

1.5.2 Fractional Crystallization

Jotunites, which are also referred to as ferrodiorites, are a clan of Fe-Ti-P-enriched intermediate rocks commonly associated with Proterozoic massif anorthosite suites (Vander Auwera et al., 1998). All known jotunites share similar chemical and textural features, but their origin and relationship, if any, to anorthosites massifs has been debated (Dymek and Owens, 2001). Some researchers suggest that jotunites are genetically linked to anorthosite massifs as either a residual melt from anorthosite crystallization, or the parent magma to the anorthosite massif (e.g., Duchesne et al., 1974; Ashwal, 1982; Owens et al., 1993; Emslie et al., 1994). However, others suggest that jotunites are unrelated to anorthosites (e.g., Philpotts, 1981; Emslie, 1985; Duchesne, 1990). Unlike basaltic magmas, magmas with jotunitic compositions are believed to crystallize Fe-Ti oxide minerals as early liquidus phase minerals (Charlier et al., 2006; 2009; and 2010).

According to the fractional crystallization model for the formation of Fe-Ti oxide minerals, jotunitic magma is carried from depth along with the anorthosite crystal mush as both have similar densities (Vander Auwera and Longhi, 1994). Within the anorthosite crystal mush the jotunitic liquid pools in zones of low pressure, where it begins to fractionally crystallize. Cotectic crystallization values calculated by Charlier et al. (2007; 2008) suggest that Fe-Ti oxide minerals should make up ~20% of the crystallized jotunite, along with a combination of olivine, orthopyroxene, clinopyroxene, and apatite. As such, this model cannot adequately explain high-grade

zones of Fe-Ti oxide minerals, unless the latter are accumulated in some way. Proponents of fractional crystallization suggest cumulate sorting to “upgrade” the content of Fe-Ti oxides either by lateral remobilization of oxides, or flotation of less dense plagioclase (Charlier et al., 2008).

1.5.3 Magma Mixing

Magma mixing has been proposed to explain the formation of stratiform layers of pure oxide minerals including those in layered chromite deposits (e.g., Bushveld complex: Irvine, 1977; Cawthorn, 2003), and Fe-Ti oxide deposits (e.g., Tellnes: Robinson et al., 2003). The magma mixing model suggests that a fractionating magma is intruded by a more primitive magma, creating a hybrid magma which crystallizes a single oxide phase, which then sinks to the base of the magma chamber, and, thorough adcumulate growth creates a monomineralic layer of oxides (Irvine, 1975; Irvine et al., 1983; Charlier et al., 2010).

Evidence for magma mixing in the field includes parallel layers of massive, monomineralic oxides in sharp, in direct linear contact with the host rock at both the base and top of each layer or, rarely, a sharp contact at the base and a gradational contact at the top of the layer. Geochemical evidence of magma chamber replenishment includes sharp, sawtooth variations in Mg, Mn, V, and Cr contents of both whole rock geochemical analyses and in-situ magnetite, ilmenite and chromite chemical analyses (Charlier et al., 2010).

1.5.4 Hydrothermal remobilization

Hydrothermal remobilization is a process that was proposed by Li et al. (2014) in which primary plagioclase, which contains abundant Fe-Ti oxide as

microinclusions, is metasomatically altered by a late stage F-rich magmatic hydrothermal fluid. The alteration releases Fe and other metallic elements into the fluid, depositing zones of pure Fe-Ti oxide in pre-existing fractures in anorthosite (Li et al., 2014).

Evidence for hydrothermal remobilization as an ore-forming process include presence of altered anorthosite, often with individual plagioclase grains within anorthosite having unaltered cores as well as low homogenization temperatures in fluid inclusions within apatite (Li et al., 2014).

1.5.5 Solid state remobilization

Solid-state remobilization suggests that the presence of seams and veins of pure Fe-Ti oxides as well as the interstitial nature of Fe-Ti oxide minerals are the result of a subsolidus process rather than a magmatic process (Duchesne, 1996; 1999). During subsolidus conditions, evidence for oxide-oxide and oxide-silicate reequilibration is commonly observed; microtextural evidence of oxide grain boundary migration is also common (Krause and Pedall, 1980). Fe-Ti oxide minerals behave more ductily than adjacent plagioclase grains and as such, deformation has been shown to cause Fe-Ti oxide minerals to migrate towards pressure shadows, and zones of low stress (Paludan et al., 1994). On the scale of an anorthosite massif, particularly those deformed at high temperature, it is plausible that solid state remobilization is responsible for large bodies of pure Fe-Ti oxide in sharp contact with the host anorthosite, as well as interstitial to anorthosite (Duchesne, 1996; 1999).

Evidence of solid state remobilization includes the interstitial nature of Fe-Ti oxide minerals to plagioclase in anorthosite and Fe-Ti oxide minerals in the pressure

shadows of ferromagnesian silicate minerals, as well as larger concentrations of monomineralic Fe-Ti oxide minerals within the host anorthosite.

1.6 Rationale and Objectives

The CCRA was previously mapped at the 1:125000 scale in the early 1980s by the Department of Mines and Energy of the Government of Newfoundland and Labrador, and potential for Fe-Ti oxide mineralization was noted (Ryan et al., 1982; Wardle and Ash, 1984; 1986). Further research was completed regarding the tectonic and metamorphic history of the CCRA (Bussy et al., 1995; Butt, 2000; Krauss and Rivers, 2004; Gower and Krogh, 2002). No detailed work, however, has been completed on Fe-Ti oxide mineralization hosted within the CCRA.

The results from this study are used to: 1) test various models of Fe-Ti oxide genesis; 2) test various models of Fe-Ti oxide genesis in a Proterozoic anorthosite suite; and 3) propose a model for the genesis of Fe-Ti oxide mineralization specific to the NWRA will be proposed. The data from this study will also be used to investigate the utility and validity of magnetite trace element discrimination diagrams that have been previously used in an attempt to classify the geologic environment in which the magnetite crystallized. This marks the first application of this technique to a Proterozoic massif anorthosite suite. Finally, oxide mineralization from the NWRA is compared to other known Fe-Ti-V oxide deposits to determine the economic potential of the study area within the NWRA.

As such, the specific research objectives of this present study are as follows:

1) Characterize the Fe-Ti oxide mineralization hosted in the NWRA in terms of field occurrences, geographic distribution, mineralogy, major, minor and trace element oxide chemistry, microtextures, deduced physicochemical conditions of formation;

2) To compare Fe-Ti-V oxide mineralization from the NWRA to other known Fe-Ti deposits worldwide;

3) To determine if discrimination diagrams based on oxide mineral chemistry are of use in classifying and understanding magmatic Fe-Ti oxide mineralization in the NWRA;

4) Based on the aforementioned information, and existing formation models for oxide mineralization, to determine the formation processes of the Fe-Ti-V oxide mineralization in the NWRA.

REFERENCES

Ashwal LD (1982) Mineralogy of mafic and Fe-Ti oxide-rich differentiates of the Marcy anorthosite massif, Adirondacks, New York. American Mineralogist 67: 14-27

Ashwal LD (1993) Anorthosites. Spinger-Verlag, Berlin

Ashwal LD (2010) The temporality of anorthosites. Canadian Mineralogist 48: 711-728

Augland LE, Moukhsil A, Solgadi F, Indares A (2015) Pinwarian to Grenvillian magmatic evolution in the central Grenville Province: new constraints from ID-TIMS U-Pb ages and coupled Lu-Hf S-MC-ICP-MS data. Canadian Journal of Earth Sciences 52: 701-721.

Bussy F, Krogh T., Wardle RJ (1995) Late Labradorian metamorphism and anorthosite- granitoid intrusion, Cape Caribou River Allochthon, Grenville Province, Labrador: evidence from U-Pb geochronology. Canadian Journal of Earth Sciences 32: 1411-1425

Butt JM (2000) Mineral chemistry and mineral reactions in a meta-anorthosite complex, Cape Caribou River Allochthon, Grenville Province, Labrador. Unpublished B.Sc. Thesis, Memorial University of Newfoundland, St. John's NL, 111 pages

Cawthorn G (2003) Genesis of magmatic oxide deposits – a view from the Bushveld Complex. Norges geologiske undersøkelse Special Publication 9: 11-21

Charlier B, Namur O, Bolle O, Latypov R, Duchesne JC (2015) Fe-Ti-V-P ore deposits associated with Proterozoic massif-type anorthosites and related rocks. Earth-Science Reviews 141: 56-81

Charlier B, Namur O, Malpas S, de Marneffe C, Duschene JC, Vander Auwera J, Bolle O (2010) Origin of the giant Allard Lake ilmenite ore deposit (Canada) by fractional crystallization, multiple magma pulses and mixing. Lithos 117: 119-134

Charlier B, Namur O, Duchesne JC, Wisniewska J, Parecki A, Vander Auwera J (2009) Cumulate origin and polybaric crystallization of Fe-Ti oxide ores in the Suwalki anorthosite, NE Poland. Economic Geology 104: 205-221

Charlier B, Sakoma E, Sauvé M, Stanaway K, Vander Auwera J, Duchesne JC (2008) The Grader layered intrusion (Havre-Saint-Pierre Anorthosite, Quebec) and genesis of nelsonite and other Fe–Ti–P ores. Lithos 101: 359-378

Charlier B, Duchesne JC, Vander Auwera J (2006) Magma chamber processes in the Tellnes ilmenite deposit (Rogaland Anorthosite Province, SW Norway) and the formation of Fe-Ti ores in massif type anorthosites. Chemical Geology 234: 264-290

Charlier B, Skår Ø, Korneliussen A, Duchesne JC, Vander Auwera J (2007) Ilmenite composition in the Tellnes Fe–Ti deposit, SW Norway: fractional crystallization, postcumulus evolution and ilmenite–zircon relation. Contributions to Mineralogy and Petrology 154: 119-134

Chen WT, Zhou MF, Zhao TP (2013) Differentiation of nelsonitic magmas in the formation of the ~1.74Ga Damiao Fe-Ti-P ore deposit, North China. Contribution Mineralogy Petrology 165: 1342-1362

Corrigan D, Rivers T, Dunning GR (1997) Preliminary report on the evolution of the Allochthon Boundary Thrust in eastern Labrador, Mechin River to Goose Bay. East Coast Seismic Offshore-Onshore Transect Meeting 61: 45-56

Dill HG (2010) The "chessboard' classification scheme of mineral deposits: Mineralogy and geology from aluminum to zirconium. Earth-Science Reviews 100: 1-420

Duchesne JC, Roelandts I, Demaiffe D, Hertogen J, Gijbels R, De Winter J (1974) Rare-earth data on monzonoritic rocks related to anorthosites and their bearing on the nature of the parental magma of the anorthositic series. Earth and Planetary Science Letters 24: 325-335

Duchesne JC (1990) Origin and evolution of monzonorites related to anorthosites. Schweizerische Mineralogische und Petrographische Mitteilungen 70: 189-198

Duchesne JC (1996) Liquid ilmenite or liquidus ilmenite: a comment on the nature of ilmenite vein deposits. In: Demaiffe D. (ed) Petrology and geochemistry of magmatic suites of rocks in the continental and oceanic crusts. A volume dedicated to Professor Jean Michot. Tervuren, Brussels pp 73-82

Duchesne JC (1999) Fe-Ti deposits in Rogaland anorthosites (South Norway): geochemical characteristics and problems of interpretation. Mineralium Deposita 34: 182-198

Dyke B, Kerr A, Sylvester PJ (2004) Magmatic sulfide mineralization at the Fraser Lake prospect (NTS Map Area 13L/5), Michikamau Intrusion, Labrador. Current Research, Newfoundland and Labrador Geological Survey, Report 04: 7-22

Dymek RF, Owens BE (2001) Petrogenesis of apatite rich rocks (nelsonites and oxide-apatite gabbronorites) associated with massif anorthosites. Economic Geology 96: 797-815

Emslie RF (1985) Proterozoic anorthosite massifs. In: Tobi AC, Jacques LR (ed) The deep Proterozoic crust in the North Atlantic provinces. Springer, Dordrecht, pp. 39-60

Emslie RF, Hamilton MA, Thériault RJ (1994) Petrogenesis of a Mid-Proterozoic Anorthosite-Mangerite-Charnockite-Granite (AMCG) Complex: isotopic and chemical evidence from the Nain Plutonic Suite. Journal of Geology 102: 539-558

Fabjan C, Garche J, Harrer B, Kolbeck C, Philippi F, Tomazic G, Wagner F (2001) The vanadium redox-battery: an efficient storage unit for photovoltaic systems. Electrochimica Acta 47: 825-831

Force E (1991) Geology of titanium-mineral deposits. Geological Society of America, Special Paper 259, 112 p

Gower CF (1996) The evolution of the Grenville Province in Eastern Labrador, Canada. Geological Society of London Special Publications 112: 197-218

Gower CF, Schärer U, Heaman LM (1992) The Labradorian Orogeny in the Grenville Province, Eastern Labrador. Canadian Journal of Earth Sciences 29: 1944-1957

Gower CF, Krogh TE (2002) A U-Pb geochronological review of the Proterozoic history of the eastern Grenville Province. Canadian Journal of Earth Sciences 39: 795-829

He HL, Yu SY, Song XY, Du ZS, Dai ZH, Xie W (2016) Origin of nelsonite and Fe–Ti oxide ore of the Damiao anorthosite complex, NE China: Evidence from trace element geochemistry of apatite, plagioclase, magnetite and ilmenite. Ore Geology Reviews 79: 367-381

Hinchey JG (1999) Magmatic sulphide-oxide mineralization in the Nain area, northern Labrador: A petrological and geochemical study. Unpublished B.Sc. Thesis, Memorial University, St. John's, NL, 131 pages

Irvine TN (1975) Crystallization sequences in the Muskox intrusion and other layered intrusions—II. Origin of chromitite layers and similar deposits of other magmatic ores. Geochimica et Cosmochimica Acta 39: 991-1020

Irvine TN (1977) Origin of chromitite layers in the Muskox intrusion and other stratiform intrusions: A new interpretation. Geology 5: 273-277

Irvine TN, Keith DW, Todd SG (1983) The JM platinum-palladium reef of the Stillwater Complex, Montana; II, Origin by double-diffusive convective magma mixing and implications for the Bushveld Complex. Economic Geology 78: 1287-1334

Kerr A, Macdonald HE, Naldrett AJ (2001) Geochemistry of the Pants Lake Intrusion, Labrador: implications for future mineral exploration. Current Research, Newfoundland and Labrador Geological Survey 2001: 191-228

Kerr A, Walsh JA, Sparkes GW, Hinchey JG (2013) Vanadium potential in Newfoundland and Labrador: a review and assessment. Current Research, Newfoundland and Labrador Geological Survey 13: 137-165

Kilfoil G (2009) Geophysical data from recent airborne surveys, Newfoundland and Labrador. Newfoundland and Labrador Department of Natural Resources, Geological Survey, Report 09-1: 305-314

Krause H, Pedall G (1980) Fe–Ti mineralizations in the Åna–Sira anorthosite, Southern Norway. Metallogeny of the Baltic Shield. Finland Geological Survey Bulletin 307: 56-83

Krauss JB (2002) High-pressure (HP), granulite-facies thrusting in a thick-skinned thrust system in the eastern Grenville Province, central Labrador. Unpublished M.Sc. Thesis, Memorial University of Newfoundland, St. John's NL, 377 pages

Krauss JB, Rivers T (2004) High pressure granulites in the Grenvillian Grand Lake Thrust System, Labrador: pressure-temperature conditions and tectonic evolution *in* Proterozoic Tectonic Evolution of the Grenville Orogen in North America: Geological Society of America Memoir 197: 105-134

Li ZX, Bogdanova SV, Collins AS, Davidson A, De Waele B, Ernst RE, Fitzsimons ICW, Fuck RA, Gladkochub DP, Jacobs J, Karlstrom KE, Lu S, Natapov LM, Pease V, Pisarevsky SA, Thrane K, Vernikovsky V (2008) Assembly, configuration, and break-up history of Rodinia: A synthesis. Precambrian Research 160: 179-210

Li H, Li L, Zhang Z, Santosh M, Liu M, Cui Y, Yang X, Chen J, Yao T (2014) Alteration of the Damiao anorthosite complex in the northern North China Craton: Implications for high-grade iron mineralization. Ore Geology Reviews 57: 574-588

Lindsley DH (2003) Do Fe-Ti oxide magmas exist? Geology: yes; Experiments: no! (Extended abstract) Norges geologiske undersøkelse Special Publication 9: 34-36

Lindsley and Epler (2017) Do Fe-Ti-oxide magmas exist? Probably not! American Mineralogist 102(11): 2157-2169

MacDonald HE (1999) The geology, petrography and geochemistry of gabbroic rocks of the Pants Lake Intrusive Suite on the Donner/Teck South Voisey's Bay Property, north-central Labrador, Canada Unpublished M.Sc. Thesis, University of Toronto, Toronto, ON, 176 pages

Morisset CE, Scoates JS, Weis D (2010) Rutile-bearing ilmenite deposits associated with the Proterozoic Saint-Urbain and Lac Allard anorthosite massif, Grenville Province, Quebec. The Canadian Mineralogist 44: 821-849

Namur O, Charlier B, Holness MB (2012) Dual origin of Fe–Ti–P gabbros by immiscibility and fractional crystallization of evolved tholeiitic basalts in the Sept Iles layered intrusion. Lithos 154: 100-114

Owens BE, Rockow MW, Dymek RF (1993) Jotunites from the Grenville Province, Quebec: petrological characteristics and implications for massif anorthosite petrogenesis. Lithos 30: 57-80

Paludan JO, Hansen UB, Olesen NØ (1994) Structural evolution of the Precambrian Bjerkreim–Sokndal intrusion, south Norway. Norsk Geologisk Tidsskrift 74: 185-198

Philippe S, Wardle RJ, Scharer U (1993) Labradorian and Grenvillian crustal evolution of the Goose Bay Region, Labrador: new U-Pb geochronological constraints. Canadian Journal of Earth Sciences 30: 2315-2327

Philpotts AR (1967) Origin of certain iron-titanium oxide and apatite rocks. Economic Geology 62: 303-315

Philpotts AR (1981) A model for the generation of massif-type anorthosites. Canadian Mineralogist 19: 233-253

Rivers T (1997) Lithotectonic elements of the Grenville Province: review and tectonic implications. Precambrian research 86: 117-154

Rivers T, Culshaw NG, Hynes A, Indares A, Jamieson R, Martignole J (2012) The Grenville Orogen – A post-Lithoprobe perspective. In Percival JA, Cook FA, and Clowes Rm (ed) Tectonic Styles in Canada: the Lithoprobe perspective. Geological Association of Canada Special Paper, St. John's, pp 97-236

Robinson P, Kullerud K, Tegner C, Robins B, McEnroe SA (2003) Could the Tellnes ilmenite deposit have been produced by in-situ magma mixing? Ilmenite deposits and their geological environments, Norwegian Geological Survey Bulletin, Special Publication 9: 74-76

Ryan B, Neale T, McGuire J (1982) Descriptive notes to accompany geological maps of the Grand Lake area, Labrador 13F/10, 11, 14, 15: St.-John's, Newfoundland, Newfoundland and Labrador Department of Mines and Energy, Mineral Development Division Maps 82-64 to 82-67

Ryan B, Wardle RJ, Gower CF, Nunn GAG (1995) Nickel-copper-sulfide mineralization in Labrador: the Voisey's Bay discovery and its exploration implications. Current Research, Newfoundland and Labrador Geological Survey 95: 177-204

Stevenson IM (1967) Goose Bay map-area, Labrador. Geological Survey of Canada, Paper 67-33: 17-32

Valvasori A, Fonkwe MLD, Piercey SJ, Conliffe J (2015) Magmatic Fe-Ti-V oxide mineralization hosted in Paleoproterozoic anorthosite in the Cape Caribou River Allochthon, Grenville Province, southeast Labrador: preliminary results. Current Research, Newfoundland and Labrador Geological 15: 125-138

Vander Auwera J, Longhi J (1994) Experimental study of a jotunite (hypersthene monzodiorite): constraints on the parent magma composition and crystallization conditions (P, T, fO_2) of the Bjerkreim-Sokndal layered intrusion (Norway). Contributions to Mineralogy and Petrology 118: 60-78

Vander Auwera J, Longhi J, Duchesne JC (1998) A liquid line of descent of the jotunite (hypersthene monzodiorite) suite. Journal of Petrology 39: 439-468.

Wardle RJ, Ash C (1984) Geology of the Northwest River area, Current Research, Newfoundland and Labrador Geological 84: 53-67

Wardle RJ, Ash C (1986) Geology of the Goose Bay–Goose River area. Current Research, Newfoundland and Labrador Geological Survey 86: 113-123

Wardle RJ, Ryan B, Philippe S, Scharer U (1990) Proterozoic crustal development, Goose Bay Region, Grenville Province, Labrador, Canada *in* Gower, C.F., Rivers, T., and Ryan, B., eds., Mid-Proterozoic Laurentia-Baltica: Geological Association of Canada, Special Paper 38: 297-214

Chapter 2: Sampling and Analytical Methods

2.1 Sampling

One hundred and sixty four mineralized and unmineralized samples representative of anorthosite and gabbronorite observed in the field area as well as all associated Fe-Ti oxide mineralization were collected during the summers of 2014, 2015, and 2016. Samples were subdivided into three broad categories: massive to semi-massive oxide mineralization (50-100% oxide minerals); disseminated oxide mineralization (10-50 % oxide minerals); and barren anorthosite host rocks (<10 vol% oxide minerals). The samples were cleaned of any weathering rind by sawing and then cut into blocks for whole-rock major and trace element geochemical analyses and chips for polished thin sections.

Ninety-six samples were sent to Actlabs for whole rock major, minor and trace element geochemical analysis, and 113 samples were sent to Vancouver Petrographics to be made into polished thin sections. Both polished thin sections and the samples for geochemical analysis were taken from the same sample, with multiple thin sections made from selected coarse-grained massive to semi-massive oxide mineralized samples in order to obtain a more representative petrographic sample set. As a result the number of thins sections is greater than the number of samples analyzed for major and trace elements.

Polished thin sections were examined using both reflected and transmitted cross polarized light microscopy. Thin sections were organized based on Fe-Ti oxide mineralization styles observed within the NWRA, with petrographic description focusing on variations in mineralogy and exsolution textures within samples, between

samples from the same mineralization style, and between samples from different mineralization styles. Representative grains and microtextures of magnetite, ilmenite, and pleonaste were analyzed using both electron probe microanalyzer (EPMA) and laser ablation inductively coupled plasma mass spectrometry (LA-ICPMS) where the grains were sufficiently coarse (i.e., when minerals analyzed were larger than 25 micrometers in their shortest axis).

2.2 Whole-rock geochemistry

The samples sent to Actlabs were powdered and prepared for analysis using a lithium metaborate/tetraborate fusion followed by digestion in weak nitric acid. Samples were analyzed using a combination of inductively coupled plasma mass spectrometry (ICP-MS) and inductively coupled plasma optical emission spectroscopy (ICP-OES), with 59 elements quantified including major, minor and trace elements using the Code 4LITHO + 4B1(11+) Major Elements Fusion ICP(WRA)/Trace Elements Fusion ICP/MS(WRA4B2)/Total Digestion ICP(TOTAL) analytical package. Duplicate samples were inserted every 10 analyses to ensure quality of analyses.

2.3 EPMA

2.3.1 EPMA WDS analyses

Electron microprobe microanalysis (EPMA) using wavelength dispersive spectroscopy (WDS) was performed on nine representative thin sections selected based on field and petrographic observations (i.e. mineralization styles). The analyses were carried out in order to determine if there is any compositional differences between

similar textures of magnetite, ilmenite and pleonaste between different mineralization styles. The analyses were also intended to provide more chemical information on the various exsolution features in the oxide minerals. The analytical work was carried out at the Queens Facility for Isotope Research (QFIR) in the Department of Geological Sciences and Geological Engineering at Queens University, Kingston, Ontario. A JEOL JXA-8230 electron microprobe equipped with five WDS tunable spectrometers was used to determine the major and minor element compositions magnetite, ilmenite, and spinel in a variety of microtextural settings from the 9 polished thin sections. Specifically, the concentrations of Si, Ti, Al, Cr, V, Fe, Mn, Mg, Ni, Ca, Cu and K were quantified. Analyses with totals outside 100±1.5 wt. %, as well as analyses below the calculated detection limits were discarded. For details on the diffracting crystal used, X-ray lines used, counting times, standard used and range of detection limits for each element analyzed, see Table 2.2.

2.3.2 EPMA WDS X-ray maps

EPMA WDS X-ray maps were made for eight representative textural features on six of the thin sections. Specifically, the major elements Fe and Ti were measured in magnetite and ilmenite, and Mg, Fe and Al were measured in spinel, and the trace element V was also measured as exploratory analyses showed that its concentration varied significantly. An accelerating voltage of 15 kV, a sample current of 250 nA, and a dwell time of 200 ms per step were used for X-ray mapping. Pixel size ranged from 0.5-2µm depending on the grain size of features within the section.

2.3.3 Calculation of Fe^{2+} and Fe^{3+} from EPMA analyses

Fe^{2+} and Fe^{3+} values in oxide minerals in this study were approximated using a method involving charge balance (B. Joy, personal communication). In order to make this approximation, all measured oxides values are first converted to their elemental values which are then divided by their respective molar masses to determine the amount of each cation present assuming all Fe is Fe^{2+}. The cations of each element were then normalized to a fixed number equivalent to that in the ideal formula unit of the mineral in question; in spinel group minerals such as magnetite and pleonaste, cations are normalized to 3, whereas in ilmenite cations were normalized to 2. All normalized Fe is assumed to be divalent. The amount of Fe^{3+} present was calculated by subtracting the divalent Fe content from the charge value of the anions in the formula unit (8 in spinel minerals, 6 in ilmenite.) The Fe^{2+} content is then adjusted by subtracting the calculated value Fe^{3+} cations from it. Finally, Fe^{2+} and Fe^{3+} are converted into their respective oxides and divided by the normalization factor originally used to achieve the correct cation sum.

However, using charge balance to approximate Fe^{2+} and Fe^{3+} contents relies on the assumption that the mineral in question does not contain vacancies within its crystal structure and is charge balanced. As such, calculated values for Fe^{2+} and Fe^{3+} contents may be inaccurate when compared to analyses by Mössbauer spectroscopy that can precisely and accurately measure the Fe^{2+} and Fe^{3+} contents of minerals which contain both Fe oxidation states. Compared to Mössbauer spectroscopy charge balance calculations as described above can have errors of ~10-15% relative (M.D. Dyar and J.M. Hanchar, personal communication).

Table 2.1: Summaries of instrumentation and analytical protocols for EPMA and LA-ICPMS analyses of magnetite, ilmenite and pleonaste.

EPMA	
Model	JEOL JXA-8230 Superprobe
Voltage	15kV
Current	50nA
Spot size	Focused beam
Other relevant information	See Table 2.2
LA-ICPMS	
Laser ablation system	Laurin technic S155 RESOlution (193nm) ArF laser
ICP-MS	Agilent 7700x quadrupole ICPMS
Laser frequency	10 hz
Fluence	5mJ/cm^2
Stage speed	5-10µm/s
Beam size	33-75µm
Dwell time	10ms/peak
Analysis	Line
	100-300µm
	30s gas blank
	~60s signal
Internal standard	Al, Ti, Fe (From EPMA)
Reference material for calibration	GSD-1g
Secondary standards	GSE-1g, G probe 6
In-House monitor	BC-28
Data reduction	Iolite software package version 2.5

Table 2.2: Details of EPMA analytical settings and standards used for elements that were analyzed.

Element	Element X-ray Line	Diffracting Crystal	On-peak Counting Time	Off-Peak Counting Time (on each side of peak)	Standard	Range of detection limits (ppm)
Si	Kα	TAP	60	30	S-021 synthetic diopside	50-150
Ti	Kα	PET	30	15	S-208 rutile NMNH 120812	130-160
Al	Kα	TAP	60	30	S-354 synthetic spinel	90-110
Cr	Kα	LiFL	60	30	S-417 synthetic Cr_2O_3	100-120
V	Kα	LiFL	60	30	S-403 synthetic V_2O_3	100-120
Fe	Kα	LIF	10	5	S-125 hematite	300-420
Mn	Kα	LiFL	60	30	S-314 synthetic Mn_3O_4	90-120
Mg	Kα	TAP	60	30	S-194 Tiebaghi chromite NMNH 117075	90-160
Zn	Kα	LiFH	60	30	S-394 gahnite NMNH 145883	170-230
Ni	Kα	LiFH	60	30	S-493 synthetic liebenbergite	110-140
Ca	Kα	PET	60	30	S-021 synthetic diopside	40-70
Cu	Kα	LiFH	60	30	S-061 Cu metal	120-150
K	Kα	PET	60	30	S-096 adularia Penn State Or-1	40-60

To determine the accuracy of charge balance calculations, EPMA and Mössbauer spectroscopy data for two magnetite samples from the magnetite-apatite ores in Kiruna, Sweden, unrelated to this study were obtained (M.D. Dyar and J.M. Hanchar, personal communication). $Fe_{(t)}$ values from the EPMA analyses were recalculated via the charge balance method used in this study and the resulting Fe^{2+} and Fe^{3+} values were compared to the measured values obtained using Mössbauer spectroscopy. Using the charge balance calculations, both magnetite samples were calculated to contain, on average, 66.6 wt.% Fe_2O_3 and 29.6 wt.% FeO, whereas when analyzed using Mössbauer spectroscopy, the same samples were measured to contain 65 wt.% Fe_2O_3 and 35 wt.% FeO (the stoichiometric end-member proportions for magnetite). It should be noted, that while this difference is real, the EPMA analyses were done in situ and the Mössbauer analyses were done on bulk sample powder. Regardless of this discrepancy, the variation does not significantly affect the results or interpretation of the data.

2.4 LA-ICPMS analyses

LA-ICPMS analyses were done on the same thin sections and when possible on the same grains analyzed by EPMA. Like the EPMA analyses, the LA-ICPMS analyses were done to characterize the variation in minor and trace element composition within oxide minerals, between oxide minerals within each sample, and between oxides from different mineralization styles. Line analyses were done on all observed textural variations of magnetite, ilmenite, and pleonaste where coarse enough to do so in order to determine the mean value of the mineral analyzed including both inclusions and micro exsolution features. Large-scale observable exsolution features were avoided in order to ensure that only the targeted oxide mineral was analyzed. However, many smaller scale

intergrowths could not be analyzed due to spatial limitations of the laser beam diameter. LA-ICPMS analyses for ^{24}Mg, ^{25}Mg, ^{27}Al, ^{29}Si, ^{31}P, ^{34}S, ^{44}Ca, ^{45}Sc, ^{47}Ti, ^{51}V, ^{52}Cr, ^{55}Mn, ^{57}Fe, ^{59}Co,^{60}Ni, ^{63}Cu, ^{66}Zn, ^{71}Ga, ^{74}Ge, ^{89}Y, ^{90}Zr, ^{93}Nb, ^{95}Mo,^{118}Sn, ^{178}Hf, ^{181}Ta, ^{182}W and ^{208}Pb were done on magnetite, ilmenite, and pleonaste. However, depending on the target mineral, many of these elements proved to be below detection limits, and are therefore not discussed.

Analyses were done at LabMaTer, University of Quebec at Chicoutimi (UQaC) following the methods of Dare et al. (2014) and using an Agilent 7700x ICPMS interfaced to a Laurin technic S155 RESolution (193 nm) ArF excimer laser ablation system.). Variations in Ti, S, Ca, P, Al and Cu content in the oxide minerals were monitored to ensure the mineral analyzed was correctly identified and no mineral inclusions were included in the data integration. Instrument settings are presented in Table 2.1. Line analyses were done in this study in order to monitor elemental zonation as well as to homogenize microscopic exsolution microtextures. During line analyses, visible microtextures were avoided in order to minimize risk of contamination with unwanted material. The ICPMS was calibrated using reference material GSD-1g (USGS) using GeoReM preferred values (Jochum et al., 2005), and reduced using the Iolite version 2.5 software suite (Paton et al., 2011). Values of Al, Ti and $Fe_{(t)}$ from the EPMA analyses were used as internal standards for pleonaste (^{27}Al), ilmenite (^{47}Ti) and magnetite (^{57}Fe) respectively. Reference material GSE-1g (USGS) and G-probe 6 (BNV-1g, USGS) as well as in-house monitor BC-28 (a natural magnetite from the Bushveld Complex in South Africa) were used as secondary standards. LA-ICPMS results, which include average compositions and standard deviations from each mineralization style, are

presented in appendix II. However in analyses where n=≤3, standard deviations are not calculated.

REFERENCES

Dare SA, Barnes SJ, Beaudoin G, Meric J, Boutroy E, Potvin-Doucet C (2014) Trace elements in magnetite as petrogenetic indicators. Mineralium Deposita 49: 785-796

Jochum KP, Willbold M, Raczek I, Stoll B, Herwig K (2005) Chemical Characterization of the USGS reference glasses GSA-1G, GSC-1g, GSD-1g, GSE-1g, BCR-2G, BHVO-2G, and BIR-1G using EPMA, ID-TIMS, ID-ICP-MS and LA-ICPMS. Geostandards and Geoanalytical Research 29: 285-302

Paton C, Hellstrom J, Paul B, Woodhead J, Hergt J (2011) Iolite: freeware for the visualization and processing of mass spectrometric data. Journal of Analytical Atomic Spectrometry 26: 2508-2518

Chapter 3: Results

3.1 Host rock

The host rock to the oxide mineralization is the NWRA, a heterogeneous unit ranging in composition from anorthosite to gabbronorite (Fig. 3.1 a, b). Within the field area which is wooded and dominated by small, rounded outcrops, the host rocks are dominated by medium to coarse-grained plagioclase crystals that range in diameter from <1 cm to ~25 cm. Plagioclase crystals are white to light grey, and in rare cases mauve to lilac colour in hand sample. Texturally, the plagioclase is granoblastic to prismatic and weakly saussuritized (i.e., altered to epidote group minerals), with the most intense alteration occurring nearest to the oxide-rich zones. Labradorescence (i.e., blue or green iridescence) is locally found associated with plagioclase in the study area.

The primary ferromagnesian minerals observed in the NWRA include pyroxene (with clinopyroxene in greater abundance than orthopyroxene), amphiboles (hornblende and pargasite) and rare olivine. In hand specimens, orthopyroxene crystals are generally tan to buff in colour, whereas amphiboles are dark green to black. Ferromagnesian silicates occur as individual grains or as clusters of grains, and are irregular in form varying in size proportionally to the adjacent plagioclase grains (commonly between 5 mm and 20 cm). Ferromagnesian minerals occur in patches in host anorthosite accounting for between 0-70% of the total rock volume.

Fe-Ti oxide minerals are abundant in the NWRA and including massive to semi-massive mineralization and disseminated mineralization styles. Oxide mineralization is in sharp irregular contact with host anorthosite. Zones of massive to semi-massive oxide

mineralization are on the meter scale, discontinuous and dwarfed in size by surrounding anorthosite.

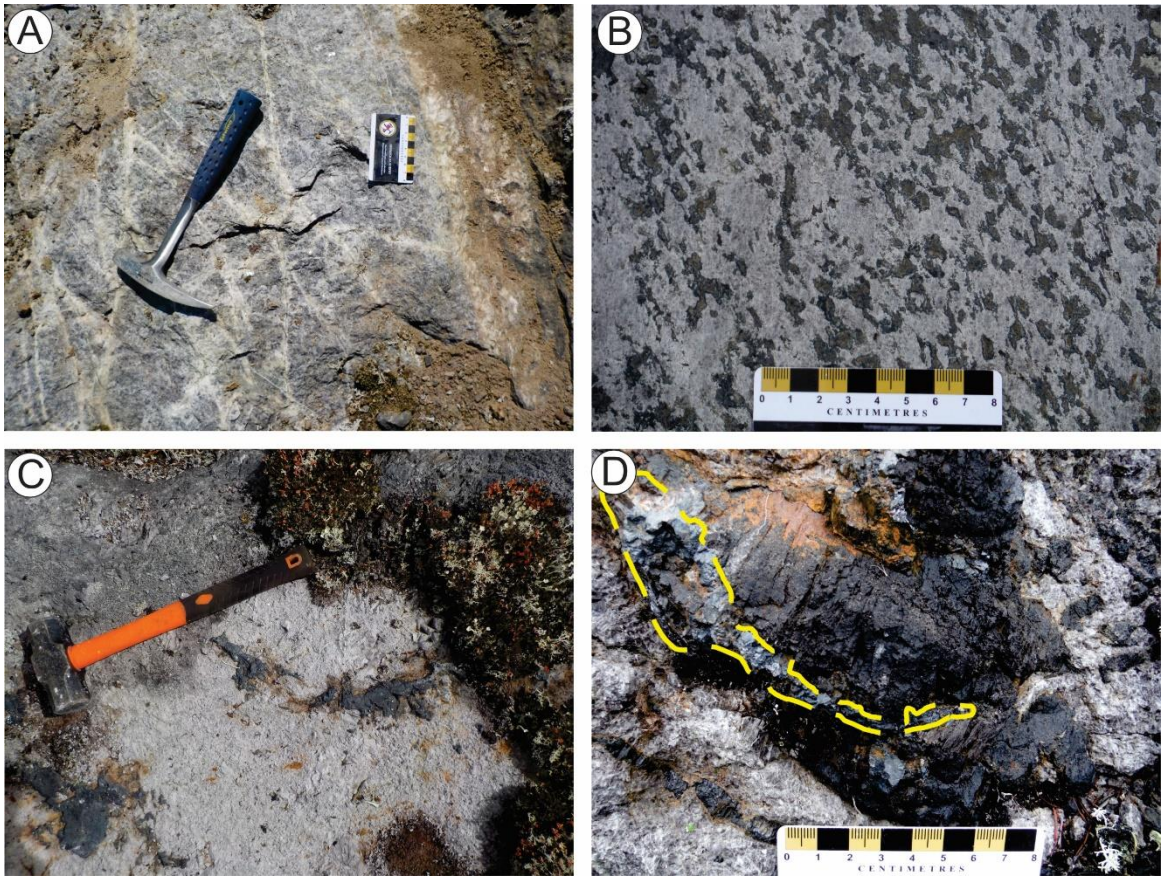

Figure 3.1. Representative field photographs of host rocks as well as disseminated oxide mineralization: A) Outcrop of anorthosite; B) Outcrop of anorthosite, exhibiting irregular-shaped blebs of pyroxene rimmed by amphibole and biotite; C) Anorthosite hosted disseminated oxide that is irregular in form; and D) Oxide mineralization (outlined in yellow) crosscutting and partially rimming an orthopyroxene megacryst.

3.2 Massive to semi-massive oxide mineralization

3.2.1 General Features

Massive to semi-massive oxide mineralization (50-100 vol. % oxide minerals on the outcrop scale) occurs in 1) oxide-rich pods; 2) oxide-rich veins; and 3) alternating bands of oxide mineralization and host anorthosite (Figs. 3.2, 3.3). Regardless of field context, oxide minerals in massive to semi-massive oxide mineralization are generally

coarse grained in hand sample (0.5cm-3cm) (Fig. 3.2b), and composed of magnetite (Fe_3O_4), ilmenite ($FeTiO_3$), and pleonaste ($[Fe,Mg]Al_2O_4$) in this order of abundance. Aside from the oxide minerals, plagioclase, orthopyroxene, pyrrhotite, pyrite, and chalcopyrite are also commonly observed in hand sample and thin section. Texturally, plagioclase and orthopyroxene occur as resorbed grains or in monomineralic clusters of grains with a dark rim of amphibole and biotite present at the contact between both orthopyroxene and plagioclase and surrounding oxide minerals. Contacts between massive to semi-massive oxide mineralization, and host rock, are sharp and irregular, and commonly show a mm- to cm- scale rim of hydrous minerals (e.g., biotite, pargasite, hornblende) at the oxide-silicate contact (Fig. 3.3c).

3.2.2 Oxide-rich Pods

The oxide-rich pods are the most commonly observed style of massive to semi-massive oxide mineralization within the field area (Fig. 3.2a). They vary in size with the largest observed pod measured at more than 8 m x 4.5 m at surface, with most 1-2 m in diameter. Although the pods are generally of equant dimensions, they can locally be lenticular to elongate in shape. Surfaces of these oxide-rich pods vary in colour from steel blue to grey. A portable drill was used on a massive oxide pod by prospectors T. Benoit and C. Coady to obtain an 8 m deep drill core of unknown orientation, which indicates that the minimum length of oxide mineralization in at least one location might be at least 8 m, as the lower contact with the surrounding anorthosite was not intersected during the drilling.

3.2.3 Oxide-rich Veins

Veins of oxide mineralization are rarely observed in the field area. However where present, they are typically 3-30 cm in width, and have straight irregular contacts with the host anorthosite (Fig. 3.3a-c). These veins vary in width along strike and can be discontinuous over tens of meters (Fig. 3.3 b). Oxide-rich veins locally contain small inclusions of host anorthosite (Fig. 3.3 c).

3.2.4 Oxide-rich Bands

Alternating oxide and anorthosite bands was observed in only two localities where a maximum of three parallel oxide bands were observed in sequence. When observed, bands of oxide mineralization occurs as two or more broadly parallel bands of continuous massive oxide that are >30 cm wide and alternate with variably-sized, but generally thicker bands of anorthosite (Fig. 3.4a). Contacts between the oxide bands and the host anorthosite are sharp and irregular (Fig. 3.4b, c).

Although individual oxide bands appear similar to vein occurrences, they differ in several key ways: 1) The contacts between oxide bands and anorthositic rocks are characterized by thinner bands of hydrous minerals than observed in vein-anorthosite contacts; 2) The oxide bands are more clearly defined and traceable along strike; 3) The larger oxide bands locally contain large anorthosite inclusions (Fig. 3.4d); and 4) the oxide abundance varies within bands, from massive to semi-massive.

3.2.5 Relationship between massive to semi-massive oxide mineralization styles

For the purpose of this study, massive to semi-massive oxide mineralization styles were defined solely using their surface expression. As such, it is unclear if there is continuity between various mineralization styles at depth.

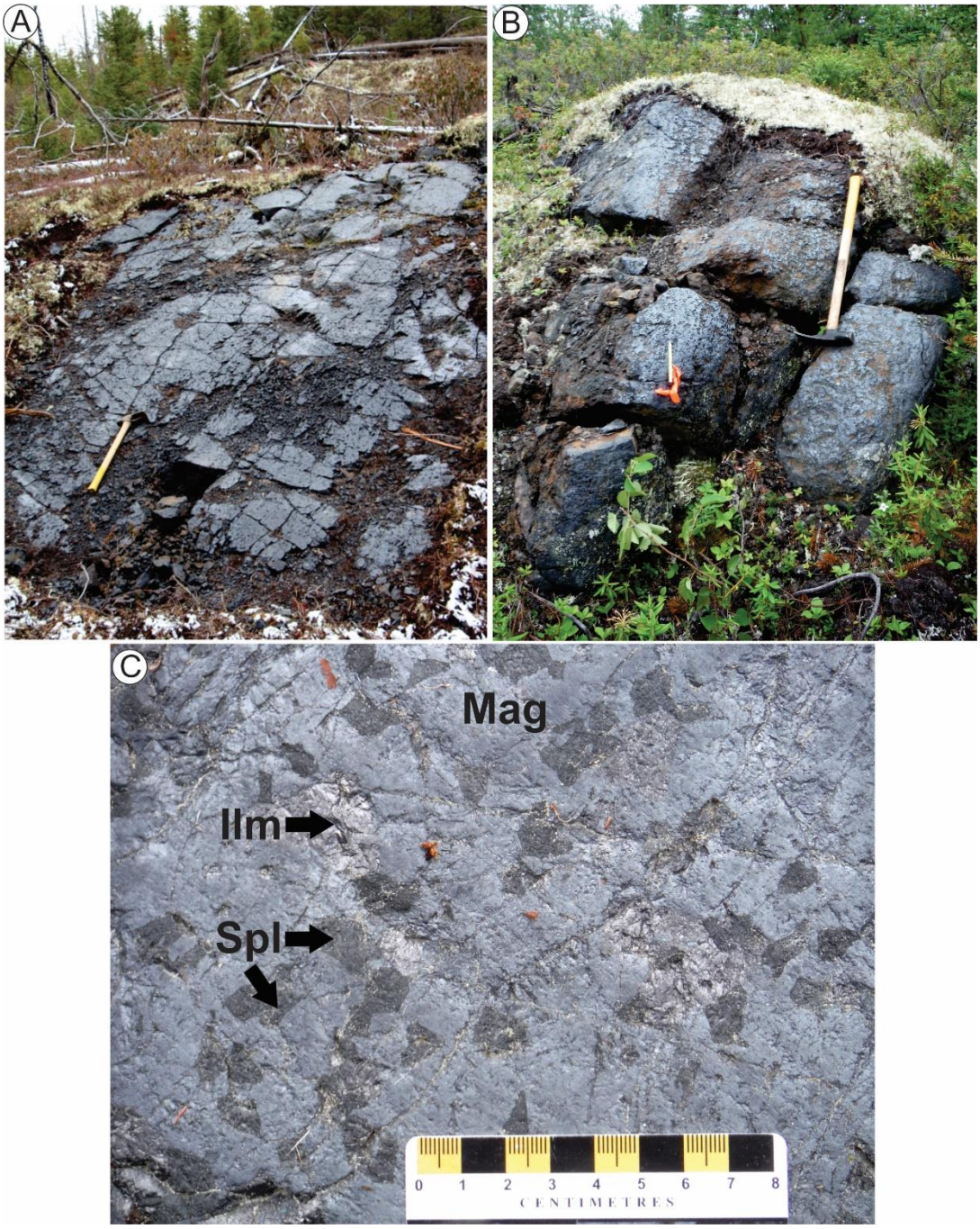

Figure 3.2 Representative field photographs showing pods of massive oxide mineralization: A) large pod of massive to semi-massive oxide mineralization (The hammer is 75 cm long); B) large pod of oxide mineralization; and C) close-up view of outcrop in A. Note coarse-grained nature of oxide minerals. Abbreviations: Mag- magnetite; Ilm- ilmenite; Spl- spinel (pleonaste).

Figure 3.3 Representative field photographs of oxide veins: A) Large vein of oxide mineralization with sharp, recessively weathered contacts with host gabbronorite; B) Discontinuous, discordant vein of oxide mineralization tapering in diameter from bottom to top of the outcrop; and C) Vein of oxide mineralization with sharp irregular contact with host anorthosite and a small inclusion of host anorthosite.

3.3 Disseminated oxide mineralization

Disseminated oxide mineralization (~10-50% of the mineralized rocks are composed of oxide minerals on the outcrop scale) is the most commonly observed mineralization style in the field area. There are two subtypes of disseminated oxide mineralization present: 1) disseminated oxide mineralization associated with pyroxene (Fig. 3.1d); and 2) disseminated oxide mineralization in the host anorthosite (Fig. 3.1c).

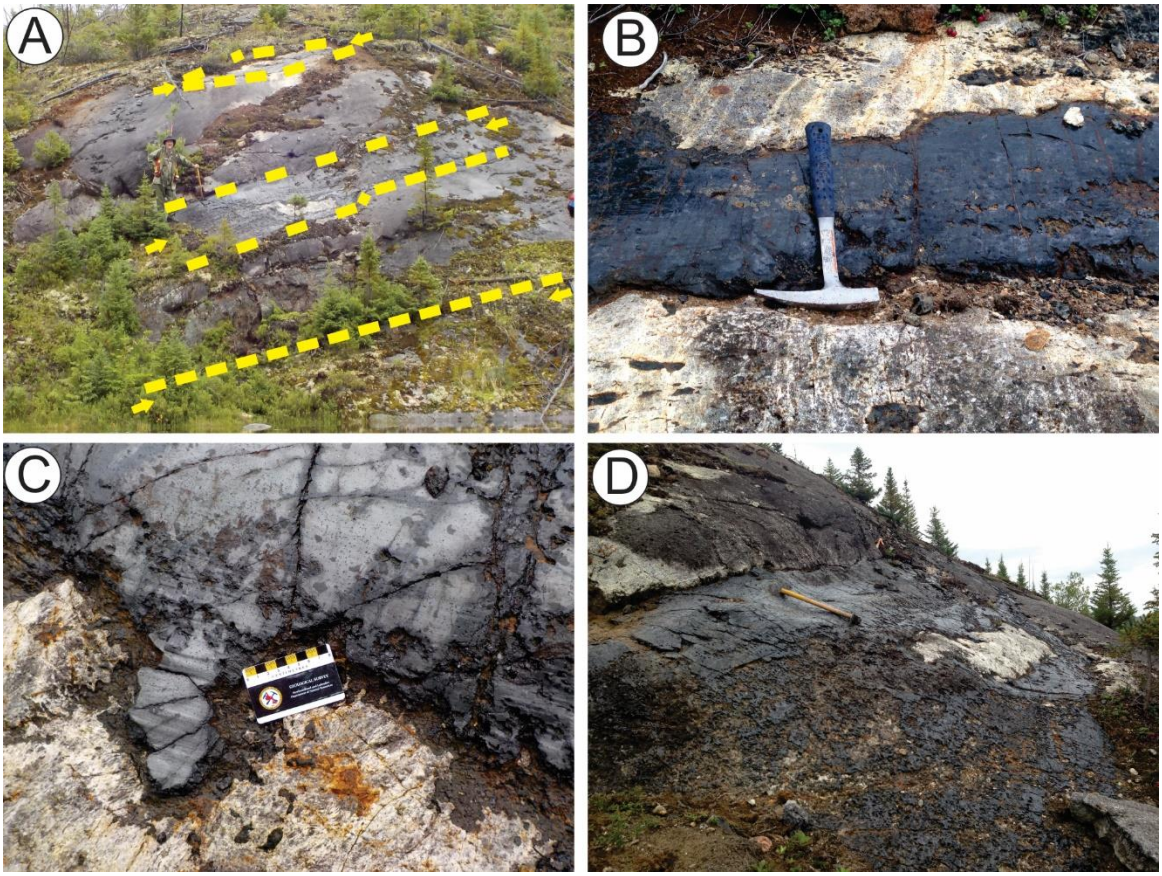

Figure 3.4. Representative field photographs of bands of oxide mineralization: A) large outcrop with three parallel bands of massive oxide mineralization as indicated by the arrows and yellow dashed lines, alternating with anorthosite layers; B) Detail of a band of oxide mineralization (dark grey) shown in A and having sharp, irregular contacts to the host anorthosite (light grey); C) close-up of irregular contact between band of oxide mineralization and host anorthosite, perhaps a density-driven structure; and D) Raft of host anorthosite in thick band of oxide mineralization.

Oxide grains associated with pyroxene are variable in size, and generally form rims around orthopyroxene or occur as cross-cutting features. In contrast, disseminated oxide mineralization hosted by anorthosite tends to be heterogeneously distributed with oxide grains interstitial to plagioclase grains. In both cases, there are polymineralic rims of biotite and amphibole developed around the oxides, ranging from ~3mm-2cm in width.

Disseminated oxide mineralization observed in this study is not composed of small grains of oxide minerals that are evenly distributed throughout the host rock, but instead consists of relatively coarse-grained, irregular-shaped aggregates of Fe-Ti oxide minerals that are widely dispersed throughout the host rock.

Oxide grains associated with pyroxene are variable in size, and generally form rims around orthopyroxene or occur as cross-cutting features. In contrast, disseminated oxide mineralization hosted by anorthosite tends to be heterogeneously distributed with oxide grains interstitial to plagioclase grains. In both cases, there are polymineralic rims of biotite and amphibole developed around the oxides, ranging from ~3mm-2cm in width.

Disseminated oxide mineralization observed in this study is not composed of small grains of oxide minerals that are evenly distributed throughout the host rock, but instead consists of relatively coarse-grained, irregular-shaped aggregates of Fe-Ti oxide minerals that are widely dispersed throughout the host rock.

3.4 Petrography

3.4.1 Massive to semi-massive oxide mineralization

3.4.1.1 Mineralogy

Representative thin sections from massive to semi-massive oxide mineralization including pods, veins, and bands were examined using transmitted and reflected light microscopy. Regardless of the mineralization style, the massive to semi-massive oxide mineralization is dominated by magnetite (Fe_3O_4) (~50-70%), ilmenite ($FeTiO_3$) (~20-35%), and pleonaste ($[Fe,Mg]Al_2O_4$) (~15-20%). Pleonaste is a spinel group mineral that

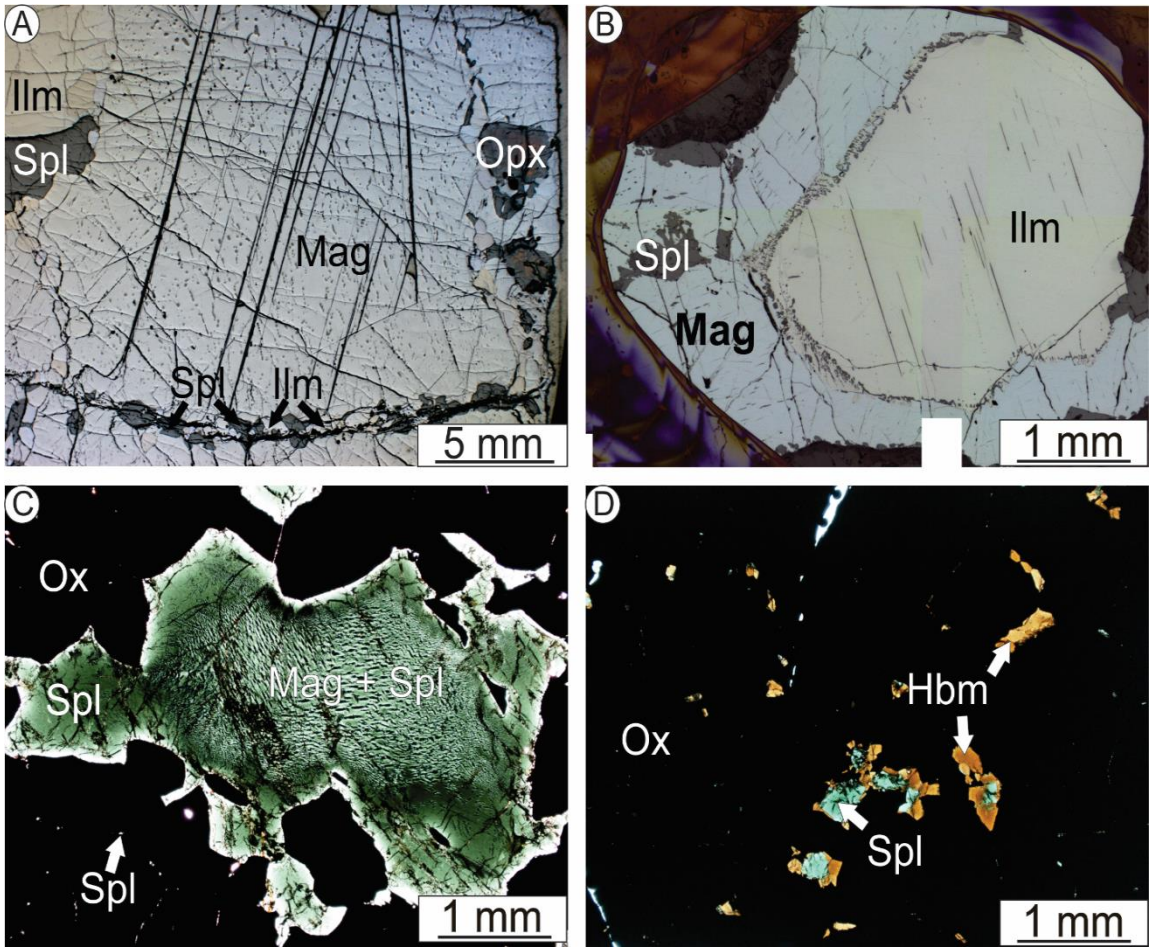

Figure 3.5. Representative photomicrographs of Fe-Ti oxide mineralization: A) Large grain of magnetite containing abundant exsolution microtextures including large lamellae of ilmenite and pleonaste as well as fine-grained granules of pleonaste which occur abundantly throughout magnetite grain. Note granoblastic zone of pleonaste and ilmenite rimming magnetite; B) Composite photomicrograph of coarse grained ilmenite containing lamellae of pleonaste shown by yellow arrow. Note the irregular contact with magnetite and the zone of ilmenite dotted by pleonaste microcrystals at the contact; C) Large grain of pleonaste in massive to semi-massive oxide mineralization. Magnetite lamellae are present in the core of the grain and diminish towards the Fe-Ti oxide minerals. ; D) Pleonaste partially to completely replaced by högbomite [ideally $[(Fe^{2+},Mg,Zn,Al)_3(Al,Ti,Fe^{3+})_8O_{15}(OH)]_2$] . Abbreviations: Mag- magnetite; Ilm-ilmenite; Spl-spinel (pleonaste); Opx- orthopyroxene; Ox- oxide minerals; Hbm-högbomite.

is intermediate in composition between the end-members spinel ($MgAl_2O_4$) and hercynite ($FeAl_2O_4$). It is commonly observed in magnetite-dominated Fe-Ti oxide mineralization hosted in anorthosite (Charlier et al., 2015). In transmitted light pleonaste it is forest green and isotropic.

Two textural varieties of magnetite are present in the NWRA; primary magnetite and recrystallized magnetite. Primary magnetite (Fig. 3.5a) is the magnetite interpreted to be the first forming magnetite still present in the samples. It is typically coarse-grained (~1 mm - 2 cm), subhedral in form, and contains abundant exsolution microtextures of pleonaste and ilmenite including granules, lamellae, and lenses. Recrystallized magnetite is finer-grained than primary magnetite (1-3mm) and is granoblastic in nature. The ilmenite ranges in size from ~6 mm - 2 cm and is typically subhedral to anhedral in form (Fig. 3.5b). Only the coarsest ilmenite grains contain lenses or lamellae of hematite, pleonaste and magnetite. Pleonaste is forest green in transmitted light and ranges in diameter from ~3mm-1cm (Fig. 3.5c). It is subhedral in form and commonly associated with ilmenite grains of similar size.

Locally, pleonaste is rimmed or replaced by högbomite $[(Fe^{2+},Mg,Zn,Al)_3(Al,Ti,Fe^{3+})_8O_{15}(OH)]_2$ (Fig. 3.5d), a rare, high-T metamorphic Fe-Mg-Al-Ti oxide mineral with similar major and minor element composition and visual appearance as the högbomite reported by Sengupta et al. (2009) and Rakotonandrasana et al. (2010). The coarsest granules of pleonaste contain magnetite lamellae. Contacts between oxide minerals are sharp and irregular, commonly with pleonaste occurring at the contact between magnetite and ilmenite, or within ilmenite adjacent to magnetite.

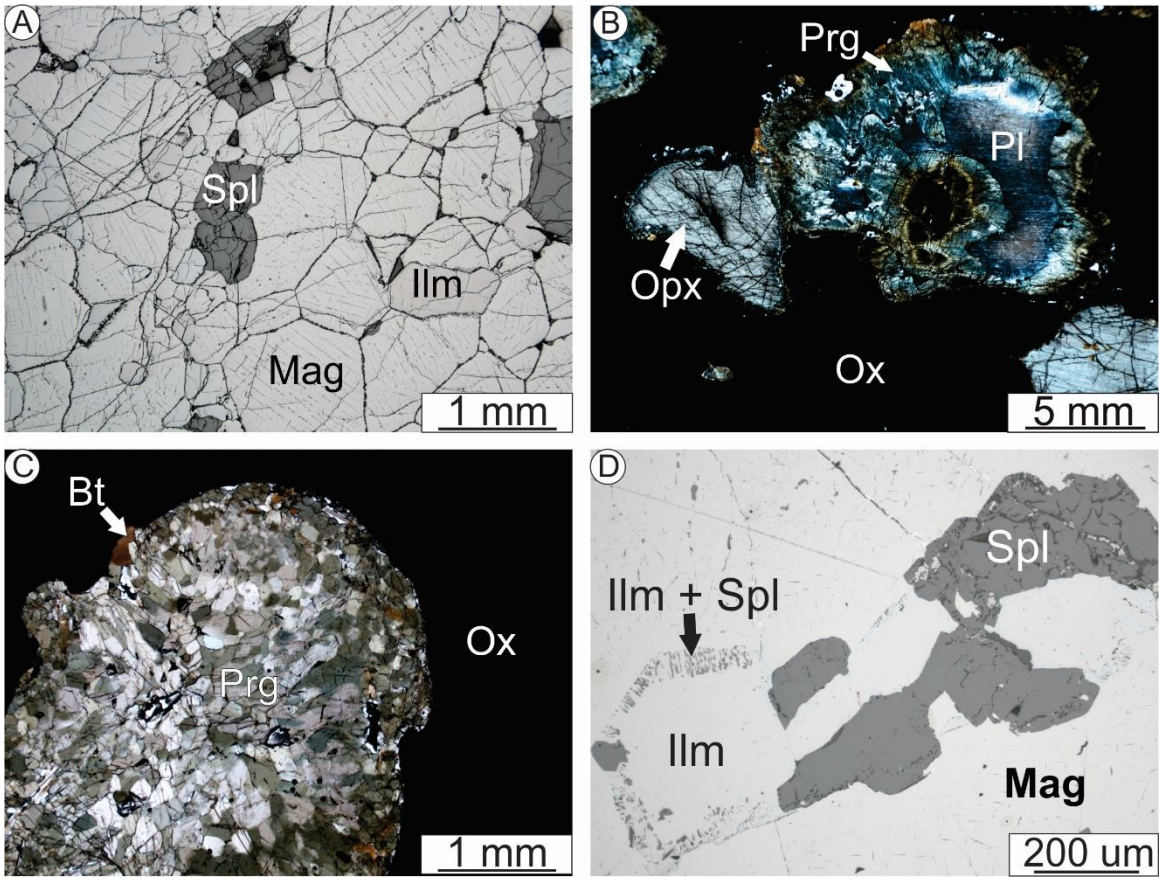

Figure 3.6. Representative photomicrographs of Fe-Ti oxide mineralization. A) Granoblastic zone of oxide mineralization; B) Representative silicate minerals in massive to semi-massive oxide mineralization including dusty resorbed plagioclase rimmed by pleonaste, and rounded orthopyroxene; C) Cluster of granoblastic pargasite and biotite within massive to semi-massive oxide mineralization; D) Association of composite ilmenite and pleonaste in magnetite. Abbreviations: Mag- magnetite; Ilm- ilmenite; Spl- spinel (pleonaste); Opx- orthopyroxene; Pl- plagioclase; Ox- oxide minerals; Prg- pargasite.

Granoblastic zones (Fig. 3.6a) of magnetite, ilmenite, and pleonaste (average grain size within these zones is ~0.5 – 2 mm) are common within the massive to semi-massive oxide mineralization. Where present, these zones are found either at grain boundaries between coarse-grained oxide minerals, or in patches randomly distributed within samples. It is common for whole areas of thin sections to consist of granoblastic massive

to semi-massive oxide; a texture normally associated with static recrystallization. Zones of granoblastic oxide are rarely observed in samples containing orthopyroxene or plagioclase.

Plagioclase (Fig. 3.6b) is the most common silicate mineral observed in massive to semi-massive oxide mineralization. It ranges from ~0.4-1 cm in diameter and occurs as subhedral grains that are equant to partially resorbed or as monomineralic clusters. The plagioclase within the massive to semi-massive oxide mineralization contains more microinclusions compared to plagioclase in the host anorthosite. Orthopyroxene (Fig. 3.6b) is light brown in hand sample and ranges from ~4 mm - 1 cm in diameter. It is subhedral to slightly round in form and ubiquitously rimmed by fine-grained symplectic intergrowths of magnetite and orthopyroxene.

Pargasite, ± hornblende, ± biotite ± garnet commonly occur in clusters (Fig. 3.6c) that range in diameter from ~2 mm- 1 cm. Mineral grains within these clusters range from ~0.3 – 0.5 mm and are granoblastic, with the exception of biotite which occurs as laths. Coronas are present at contacts between plagioclase and oxide minerals within the massive to semi-massive mineralization. These coronas are typically composed of three visually distinct amphiboles (Fe-Mg amphibole, pargasite, and hornblende) and biotite (Butt, 2000) and are perpendicular to the oxide grain boundaries.

3.4.1.2 Exsolution features

Exsolution textures are common in the magnetite, ilmenite, and pleonaste in the massive to semi-massive oxide mineralization. These textures observed in magnetite include lenses, granules, and lamellae of pleonaste, and lamellae and granules of ilmenite. Common magnetite-hosted ilmenite exsolution textures were defined by Haggerty (1991)

using examples from various magnetite -bearing gabbroic rocks from several localities. The exsolution textures observed, using the definitions discussed in Haggerty (1991) in the NWRA include “composite ilmenite”, which refers to granular ilmenite within or adjacent to magnetite, “trellis ilmenite” which refers to thin ilmenite lamellae which grow along the {111} planes of magnetite (Fig. 3.7c), and “sandwich ilmenite”, which are thick ilmenite lamellae growing parallel to only one set of {111} planes in magnetite (Fig. 3.7a). “Cloth-textured” ilmenite exsolution was defined by Haggerty (1991) as very fine lamellae of ilmenite parallel to the {100} plane of the host magnetite. Cloth-textured ilmenite is commonly observed in the orthopyroxene-bearing magnetite in massive to semi-massive oxide mineralization (Fig. 3.8b).

Texturally similar features are also observed where ilmenite is dotted with pleonaste microcrystals within magnetite. Furthermore, ilmenite dotted with pleonaste microcrystals also occurs at the contact between magnetite and ilmenite (Fig. 3.7d). Microcrystals of pleonaste typically form linear bands where observed in coarse ilmenite (Fig. 3.8a).

Pleonaste occurs as coarse- to fine-grained granules in magnetite as well as in lenses and lamellae (Fig. 3.7b). Coarse-grained granular pleonaste is associated with composite ilmenite of similar grain size (Fig. 3.6d); mid-sized granular pleonaste is found capping ilmenite sandwiches, and fine-grained granules of pleonaste are found randomly scattered throughout the magnetite. Pleonaste is also observed rimming unfilled fractures in magnetite (Fig. 3.7c).

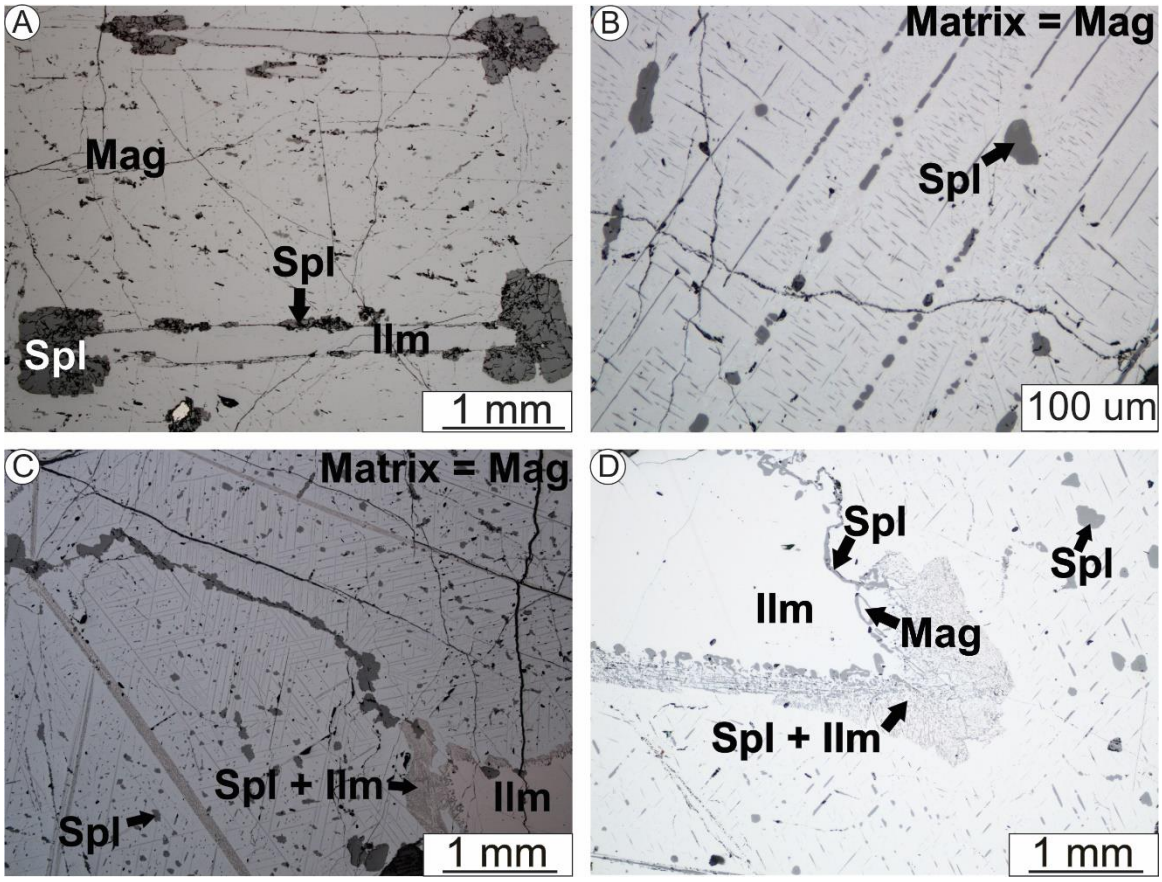

Figure 3.7. Representative photomicrographs of Fe-Ti oxide mineralization: A) Sandwich ilmenite in magnetite capped by granules of pleonaste; B) Variability of pleonaste exsolution in magnetite, note lenses, granules and lamellae; C) Trellis exsolution in magnetite, along with sandwich of ilmenite with microcrystals of pleonaste. Note pleonaste rimming fracture in magnetite; and D) Composite ilmenite in magnetite. Contact between Fe-Ti oxide minerals either ilmenite dotted with pleonaste microcrystals, or irregular with a rim of pleonaste. Abbreviations: Mag- magnetite; Ilm- ilmenite; Spl- spinel (pleonaste).

Coarse-grained ilmenite contains lamellae of magnetite with variable amounts of pleonaste (Fig. 3.8c), as well as hematite lenses (Fig. 3.8d). Hematite lenses can vary in size by orders of magnitude within the same ilmenite grain with the largest lenses being ~10um by ~40 um and the smallest being <1um by <1um, with irregular ilmenite that is <1um in diameter contained within the coarsest hematite lenses. Coarse pleonaste commonly contains lenses of magnetite (Fig. 3.5c).

The abundance of several exsolution features including pleonaste in magnetite, magnetite in pleonaste, and hematite in ilmenite, are most abundant at the core of their host minerals and least abundant directly adjacent to the contact with other oxide minerals (Fig. 3.5c, 3.7d, 3.8a-d).

3.4.1.3 Similarities and Contrasts

Textural and crystal size differences are observed between the massive to semi-massive oxide mineralization that contains orthopyroxene, and mineralization that lacks orthopyroxene. Oxide minerals within orthopyroxene-bearing massive oxide mineralization is coarser grained (commonly >1 cm in diameter), and contains more abundant lamellae and granules of pleonaste as well as cloth texture ilmenite. In contrast, the massive to semi-massive oxide mineralization without orthopyroxene is finer grained, commonly granoblastic, and contains equigranular magnetite, ilmenite, and pleonaste. Granoblastic magnetite contains fine-grained pleonaste and ilmenite lenses compared to the coarser magnetite, in which these intergrowth textures are markedly coarser grained.

3.4.2 Disseminated oxide mineralization

3.4.2.1 Mineralogy

Disseminated oxide mineralization is present within the host anorthosite, which contains no clinopyroxene or orthopyroxene, and in the orthopyroxene- and clinopyroxene-bearing anorthosite. Regardless of the host rock mineralogy, disseminated oxide mineralization is irregular in form, and typically occurs as clustered aggregates (Fig. 3.9a). Oxide minerals are typically proportional in size to the size of the aggregate

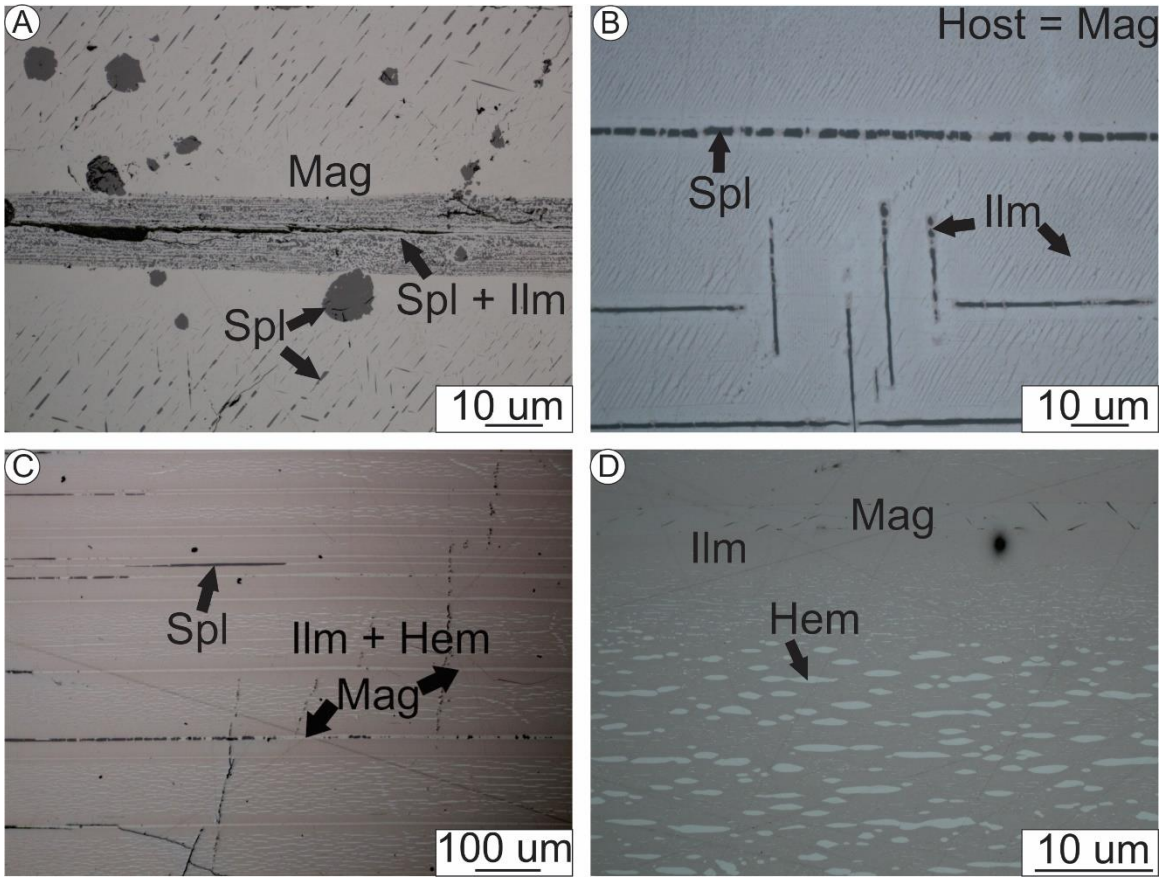

Figure 3.8. Representative photomicrographs of Fe-Ti oxide mineralization: A) Close-up photomicrograph of ilmenite dotted with spinel microcrystals. Pleonaste forms linear features in ilmenite. Note diminishing spinel content in magnetite adjacent to ilmenite dotted with pleonaste microcrystals; B) Cloth texture ilmenite in magnetite. Ilmenite is also present as rims of pleonaste lamellae. Note zones of low ilmenite adjacent to pleonaste; C) Composite ilmenite with lamellae of magnetite and pleonaste parallel to hematite lenses; and D) Close-up photomicrograph of exsolution microtextures in ilmenite including magnetite lamellae and hematite lenses. Note the fine hematite lenses between coarser lenses. Hematite content depletes approaching magnetite lamellae. Abbreviations: Mag- magnetite; Ilm- ilmenite; Spl- spinel (pleonaste); Hem- hematite.

they are contained within; oxide aggregates range in size from 1mm-5cm whereas individual oxide minerals range in diameter from ~0.5 mm- 2 cm. Where hosted by gabbronorite, the oxide minerals are typically spatially associated with pyroxene, and the oxide minerals commonly form as partial rims (Fig. 3.9d). Where hosted in anorthosite, the oxide minerals tend to be interstitial to plagioclase (Fig. 3.9a).

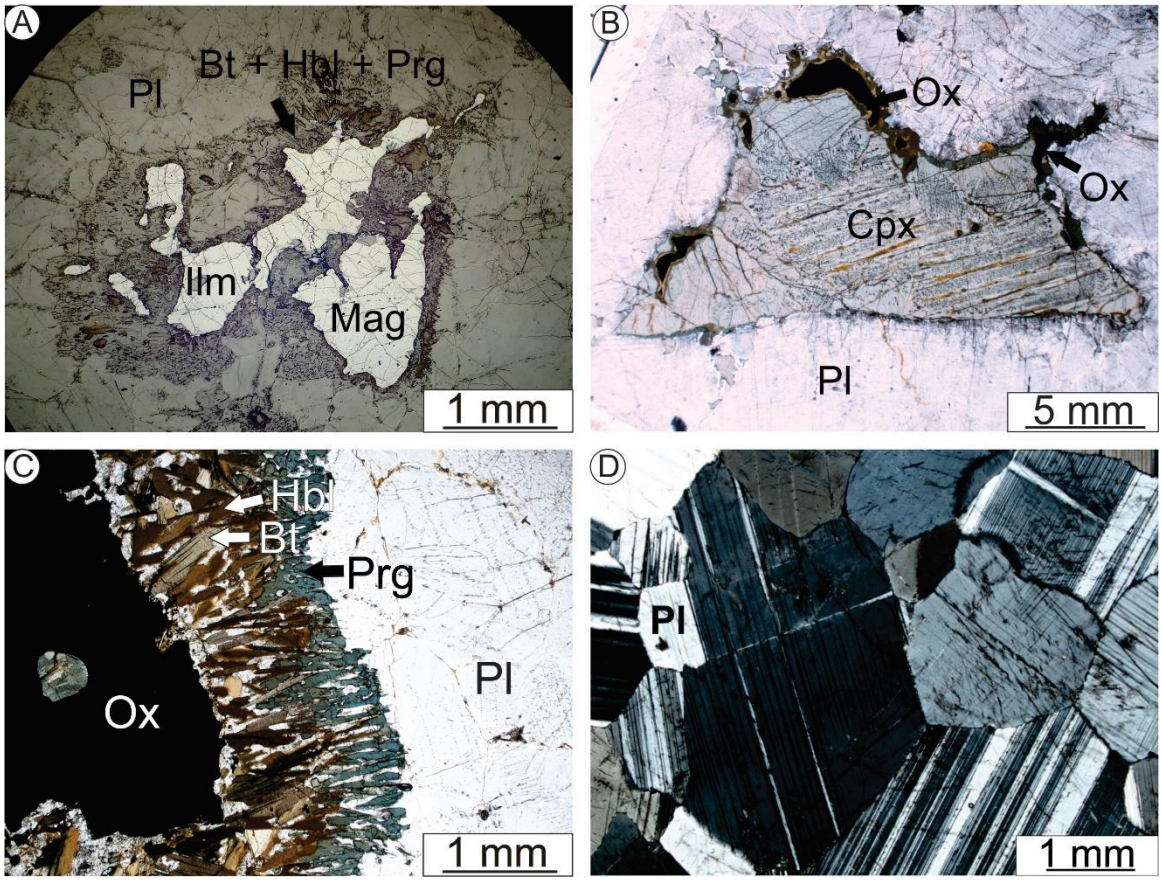

Figure 3.9. Representative photomicrographs of Fe-Ti oxide mineralization and host rocks: A) Typical disseminated oxide mineralization hosted in anorthosite. Note irregular nature and clustered habit; B) Coarse grained clinopyroxene partially rimmed by oxide mineralization.; C) Corona of hydrous minerals at contact between oxide mineralization and host anorthosite; and D) Typical host anorthosite with granoblastic plagioclase Abbreviations: Mag- magnetite; Ilm- ilmenite; Pl- plagioclase; Ox- oxide minerals; Bt- biotite; Prg- pargasite; Hbl- hornblende; Cpx- clinopyroxene.

Magnetite and ilmenite are the most abundant oxide minerals in the disseminated oxide mineralization. In contrast to massive to semi-massive oxide mineralization, coarse-grained pleonaste granules are not observed in disseminated oxide mineralization. Typically, clusters of Fe-Ti oxides range in size from ~5 to 8 mm in diameter. Single grains of ilmenite or magnetite within the clusters are between ~3 and 5 mm in diameter.

3.4.2.2 Coronas

Coronas of hydrous minerals are ubiquitous and rim all observed disseminated oxide mineralization throughout the NWRA (Fig. 3.9c). Where associated with the disseminated oxide mineralization, coronas are composed of pargasite, hornblende, and biotite ±garnet. Hydrous minerals in the coronas typically grew perpendicular to the contact between the oxide and plagioclase.

3.4.2.3 Exsolution features

Disseminated oxide mineralization shares many of the same types of exsolution features that are observed in massive to semi-massive oxide mineralization; although in the disseminated oxide mineralization the exsolution features tend to be finer grained than those that occur in the massive to semi-massive oxide mineralization. The larger the cluster of disseminated oxide mineralization is, the coarser the exsolution features tend to be. In contrast to massive to semi-massive oxide mineralization, the disseminated oxide mineralization typically occurs as lenses and lamellae of pleonaste in ilmenite and magnetite, and only rarely contains fine-grained granules of pleonaste.

As seen in massive to semi-massive oxide mineralization, ilmenite contains hematite lenses, lamellae of pleonaste and thin magnetite lamellae containing variable amounts of pleonaste. Unlike in massive to semi-massive oxide mineralization, thick magnetite lamellae are not present.

3.4.3 Host-rock to the Fe-Ti Oxide Mineralization

As previously mentioned, the NWRA is the host rock to the Fe-Ti oxide mineralization that is the focus of this study; it is a heterogeneous unit that ranges from true anorthosite to gabbronorite. Anorthosite and gabbronorite have similar silicate,

oxide, and sulfide mineral assemblages and exsolution textures, with the distinction resting on the amount of the pyroxene they contain. Silicate minerals in the host rocks include plagioclase, clinopyroxene, biotite and pargasite, with rare orthopyroxene, olivine and apatite.

The most common silicate mineral in the NWRA is plagioclase (Fig. 3.9b). In thin section, plagioclase is typically granoblastic in texture, ranging in size from several mm to a few cm in diameter. Rarely, large plagioclase grains are observed to be tabular. Plagioclase is commonly "dusty" in nature, a result of opaque micro-inclusions, likely Fe-Ti oxide minerals. Cores of plagioclase grains tend to be dustier than the rims.

Clinopyroxene is the most abundant ferromagnesian mineral in the anorthosite and gabbronorite. It is light green in colour in hand sample and is typically anhedral to interstitial in form, and commonly occurs in monomineralic clusters (Fig. 3.9d).

Biotite and pargasite are typically found either rimming oxide minerals or mafic silicates, or randomly distributed in the host rock adjacent to oxide minerals and mafic silicates.

3.5 Whole-rock geochemistry

3.5.1 Geochemistry overview

Eighty-six whole-rock analyses were done for major, minor, and trace elements on mineralized and unmineralized samples representative of all the rock types encountered in the study area. A complete list of the samples analyzed and the elements analyzed is presented in Appendix 3.3.

These analyses were grouped into the following categories: 1) barren host rocks (anorthosite, gabbronorite and olivine-bearing anorthosite); 2) disseminated Fe-Ti oxide

mineralization (anorthosite-hosted and gabbronorite-hosted); and 3) massive to semi-massive oxide mineralization (orthopyroxene-bearing and orthopyroxene-poor), based on field and petrographic observations. Averages and standard deviations from each sample group are provided in the appendices. In analyses where n = <3, however, standard deviations are not calculated. During the field work sample collecting, many samples were classified as disseminated oxide mineralization (10-25 % oxide); however, later geochemical analyses indicated that many of these samples should instead be classified as barren host rocks (0-10 % oxide minerals). In reality, there is a continuum between barren host rocks and disseminated oxide mineralization with the distinction between the two rock types resting in an artificial boundary meant to help simplify classifying the analyses.

3.5.2 Unmineralized host rocks

The unmineralized host rocks account for about half of the samples analyzed, and includes samples from barren anorthosite, barren gabbronorite and barren olivine-bearing anorthosite.

3.5.2.1 Major elements

The barren anorthosite (n=37), gabbronorite (n=7) and olivine-bearing anorthosite (n=3) samples share similar major-element compositions. The average SiO_2 content in the barren samples ranges from 48.65-57.15 wt. %, and Al_2O_3 content ranges from 16.8-28.01 wt. %. The alkali oxides CaO, Na_2O, and K_2O range from 6.93-11.0 wt. % CaO, 2.84-5.82 wt. % Na_2O, and 0.4-1.77 wt. % K_2O respectively. Transition metal oxides including MnO, MgO, $FeO_{(t)}$ and TiO_2 range from 0.01-0.17 wt. % MnO, 0.05-9.89 wt. % MgO, 0.57-11.12 wt. % $FeO_{(t)}$, and 0.07-1.07 wt. % TiO_2 respectively. The P_2O_5 content

has a compositional range of 0.21-0.54 wt. %. Loss on ignition (LOI) values range from 0-2.61 wt. %.

3.5.2.2 Minor and trace elements

Appreciable amounts of Ba (441-1330 ppm) and Sr (866-1536 ppm) are present in unmineralized host rocks, whereas all other minor and trace elements are present in low concentrations, typically < 100ppm, and for many elements nearing the minimum detection limits.

3.5.2.3 Variation between unmineralized sample types

Although all unmineralized host rock sample types have similar major- and trace-element compositions, there are some key differences. Samples containing ferromagnesian silicate minerals, including the barren gabbronorite and the olivine-bearing anorthosite have higher $FeO_{(t)}$, MgO, Co, Ni, and Zn content and lower abundances of SiO_2, Al_2O_3, alkali oxides, Sr and Ba compared to true anorthosite. These differences are consistent with the contrasts in mineralogy, as ferromagnesian minerals would have exactly these attributes, and Sr and Ba are largely measures of feldspar abundance.

3.5.3 Massive to semi-massive oxide mineralization

3.5.3.1 Major elements

Samples of orthopyroxene-rich (n=8) and orthopyroxene-poor (n=21) massive to semi-massive oxide mineralization share similar major element compositions. These oxide-rich rocks are predominantly composed of transition metal oxides including 48.35-73.59 wt. % $FeO_{(t)}$, 5.70-14.14 wt. % TiO_2, 1.52-7.28 wt. % MgO, and 0.16-0.37 wt. % MnO. SiO_2 contents have a wide compositional range of 0.48-18.70 wt. %, whereas

Al_2O_3 ranges from 7.24-14.83 wt. %. The alkali oxides, CaO, Na_2O, and K_2O range from 0.01-3.26 wt.% CaO, 0.02-1.66 wt.% Na_2O, and 0.02-2.34 wt. % K_2O respectively, depending on the abundance of oxide minerals present. Samples of massive to semi-massive oxide mineralization contain low P_2O_5 contents ranging from 0.01-0.03 wt. % which indicates the low abundance of phosphate minerals including apatite. LOI is below detection limits within massive to semi-massive mineralization, confirming the absence of any hydrous phases.

3.5.3.2 Minor and trace elements

The massive to semi-massive oxide mineralized samples are enriched in transition metals relative to the unmineralized host rocks. Vanadium and Cr range from 2,052-3,471 ppm and 690-4,410 ppm respectively, whereas Co, Ni, and Zn have ranges of ~100 to ~400 ppm. Sr and Ba have wide ranges from a few ppm to several hundred ppm.

3.5.3.3 Variation between massive to semi-massive oxide mineralization sample types

Regardless of the presence or absence of orthopyroxene, the massive to semi-massive oxide mineralization shows similar ranges of most major, minor, and trace elements. Exceptions include relative enrichment in Mg and Cr in the orthopyroxene-bearing samples, coupled with relative depletions in Al, Sr, and Ba.

3.5.4 Disseminated oxide mineralization

Only a small number of samples of disseminated oxide mineralization hosted in anorthosite (n=2) and gabbronorite (n=2) were collected and analyzed.

3.5.4.1 Major elements

Samples of disseminated oxide mineralization hosted in both anorthosite and gabbronorite show large variations in major element compositions. SiO_2 content ranges

from 33.19-47.47 wt. %, whereas Al_2O_3 content ranges from 14.49-23.03 wt. %. The alkali oxides, range from 4.69-9.02 wt. %; CaO, 2.5-4.43 wt. %, Na_2O, and 0.68-1.07 wt. % K_2O respectively. The transition metal oxides, $FeO_{(t)}$, TiO_2, MgO, and MnO range from 11.59-29.87 wt.%, FeO, 1.94-4.91 wt.% TiO_2, 0.99-6.34 wt.% MgO, and 0.05-0.19 wt.% MnO respectively. P_2O_5 content ranges from 0.03-0.06 wt. %, which indicates the low abundance of phosphate minerals, whereas LOI ranges from 1.06-2.18 wt. %.

3.5.4.2 Minor and trace elements

The minor and trace element compositions of the disseminated oxide mineralized samples are intermediate between values for the unmineralized host rock and the massive to semi-massive oxide mineralization. Vanadium, Cr, Sr, and Ba were the most abundant elements detected ranging from 429-1,163 ppm V, 10-1,370 ppm Cr, 13-643 ppm Sr, and 475-925 ppm Ba, respectively. Cobalt, Ni, and Zn, ranged from tens of ppm to a few hundred ppm. Copper, Zn, and S are especially enriched in one sample that contained observable sulfide minerals. In other samples, however, these elements are typically in the range of 100-300 ppm.

3.5.4.2 Variation between disseminated mineralization sample types

As in the unmineralized host rocks, analyses of the gabbronoritic rocks contain higher concentrations of MgO, Co, and Ni, and lower concentrations of Sr and Ba. This reflects a higher abundance of Fe-Mg silicate minerals.

3.5.5 Geochemical correlations

A correlation matrix (Fig. 3.10) was used to display positive and negative correlations between elements detected in appreciable amount in whole-rock analyses.

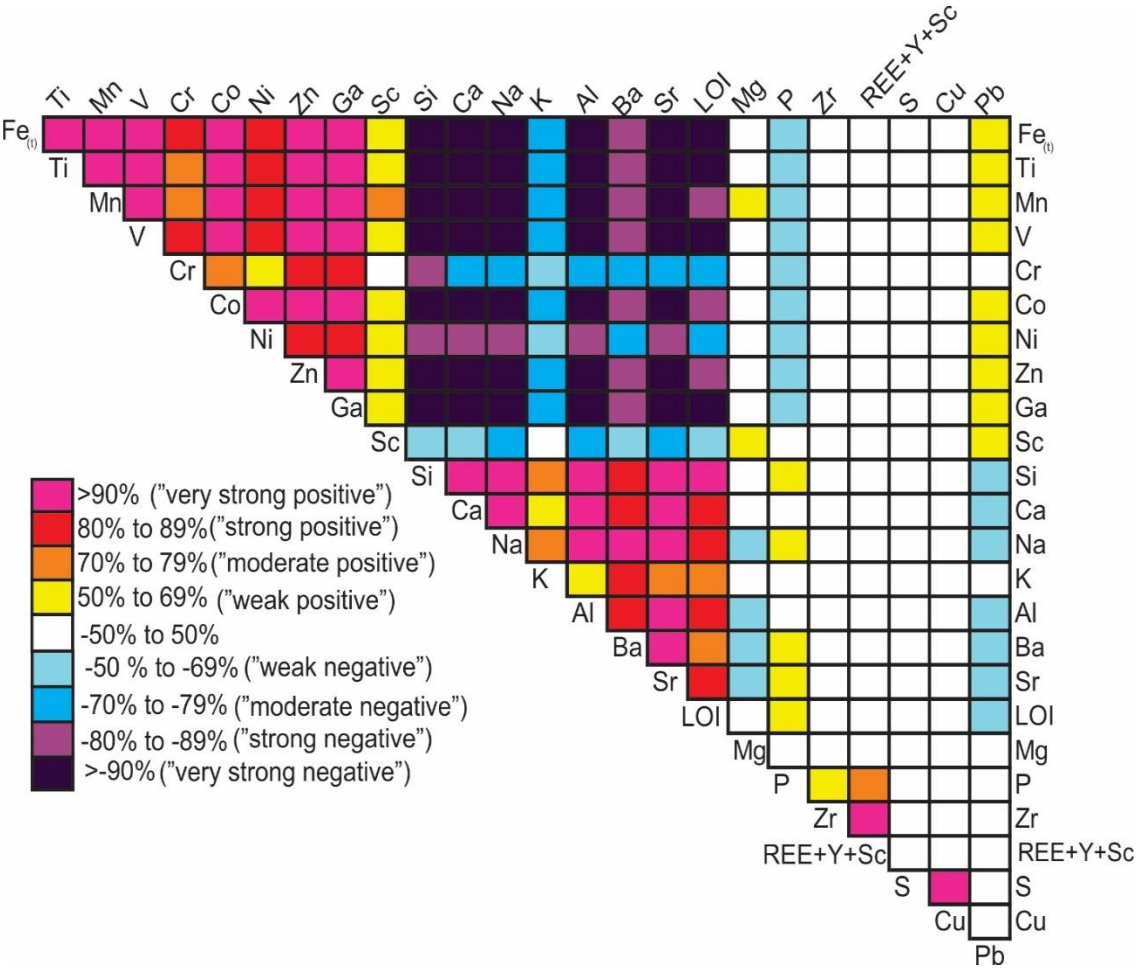

Fig. 3.10 Correlation matrix of elements from whole-rock analyses. Positive correlations are present between all elements associated with Fe-Ti oxide minerals (Fe, Ti, Mn, Cr, Co, Ni, Zn, Ga, and Sc), as well as between all elements associated with plagioclase (Si, Ca, Na, K, Al, Ba, Sr, and LOI). Elements associated with Fe-Ti oxide mineralization are negatively correlated with elements associated with plagioclase. Phosphorus, which is correlated to the presence of apatite is weakly positively correlated with plagioclase associated elements and weakly negatively associated with elements associated with Fe-Ti oxide minerals.

Two trends were observed; strong to very strong positive correlations are present between elements compatible in Fe-Ti oxide minerals including Fe, Ti, Mn, V, Cr, Co, Ni, Zn, Ga,

and Sc as well as between elements that are compatible within plagioclase including Si, Ca, Na, K, Al, Ba, and Sr. In contrast, elements associated with Fe-Ti oxide minerals are negatively to strongly negatively correlated to elements associated with plagioclase. Like elements associated with plagioclase, LOI values are strongly correlated to Si content. Phosphorus, which is typically associated with apatite, is weakly negatively correlated with elements associated with Fe-Ti oxide minerals.

3.6 Electron microprobe analyses

3.6.1 Magnetite Compositions

3.6.1.1 Overview

Primary (n=142) and recrystallized (n=12) magnetite grains were analyzed in all of the samples. Magnetite lenses and lamellae in ilmenite (n=49), and pleonaste (n=24) were also analyzed where intergrowths were coarse enough to permit the EPMA analyses to be done. Regardless of petrographic context, magnetite typically contains impurities accounting for, on average, <2 wt. % to a maximum value of 6 wt. % (Fig 3.11 a,b). Magnetite was analyzed for Si, Ti, Al, Cr, V, Fe, Mn, Mg, Zn, Ni, Ca, Cu, and K, although some of these present as trace elements proved to be below detection limits and were subsequently not analyzed in those samples. Fe^{2+} and Fe^{3+} were approximated from measured $Fe_{(t)}$ values using calculations based on charge as described previously. However, as noted this approximation may have up to a 10-15% error compared to the actual values of Fe^{2+} and Fe^{3+} in the sample (M.D. Dyar and J.M. Hanchar, personal communication). This does not materially affect the interpretation of the EPMA data.

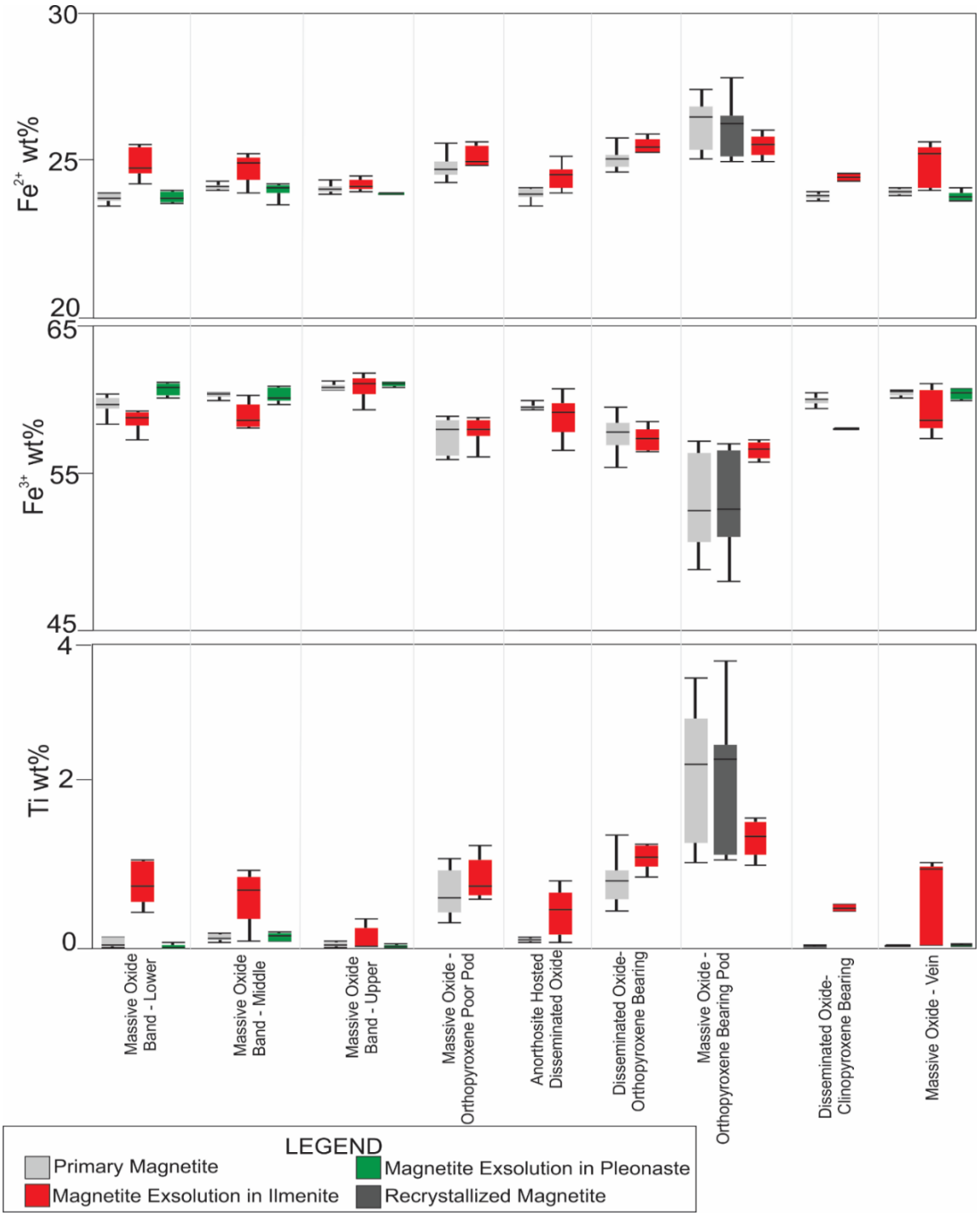

Figure 3.11a Box and whisker plots of $Fe^{2+,}$ Fe^{3+}, Ti, V, Al and Mg in magnetite from different textural settings, plotted as weight % metal. These plots show the range between the first and third quartiles or data (as the range of the box), the median of the data as the center line and the lines outside of the box showing 95% of the data.

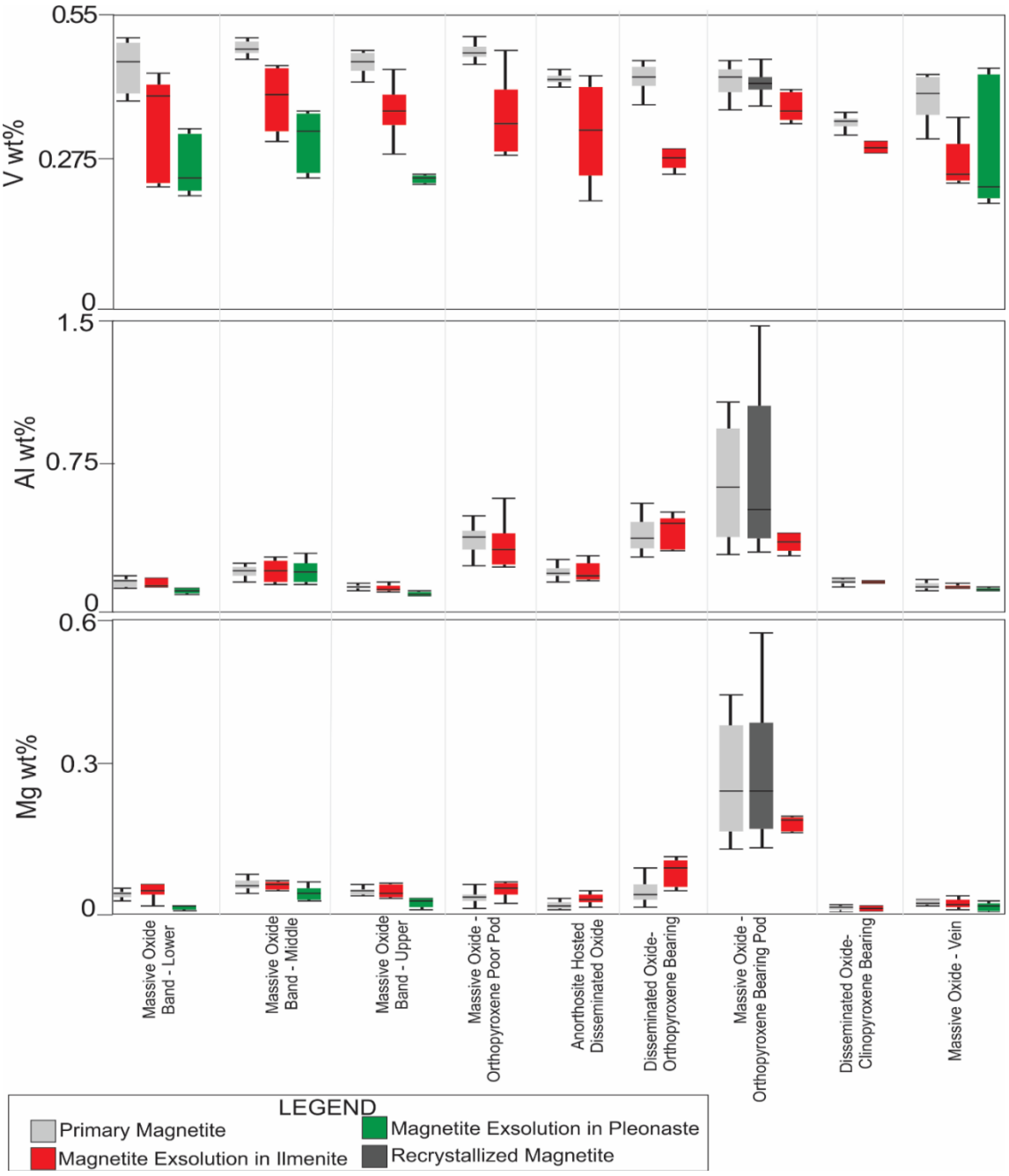

Figure 3.11b Box and whisker plots of Fe^{2+}, Fe^{3+}, Ti, V, Al and Mg in magnetite. These plots show the range between the first and third quartiles of data (as the range of the box), the median of the data as the center line and the lines outside of the box showing 95% of the data from the style of magnetite.

3.6.1.2 Primary magnetite

The texturally most primitive magmatic magnetite, hereafter referred to as "primary magnetite" contains ~48-62 wt. % Fe^{2+} and ~23-37 wt. % Fe^{3+}. The Ti contents ranges from 0.09-3.78 wt. %, whereas Al, Cr, and V, contents range from 0.1-1.5 wt. % Al, 0.16-0.53% Cr, and 0.31-0.51 wt. % V, respectively. Magnesium and Mn are commonly below the minimum detection limits and, where present, analyzed magnetite contains between 0.06-0.57 wt. % Mg, and 0.07-0.28 wt. % Mn (Fig. 3.11 a,b).

3.6.1.3 Magnetite lamellae in ilmenite

Magnetite lamellae hosted in ilmenite are predominantly composed of Fe^{2+}, and Fe^{3+}, with contents ranging from ~24-31 wt. % Fe^{2+} and ~56-62 wt. % Fe^{3+}, respectively. Their Ti content ranged from 0.03-1.8 wt. % whereas Al, Cr, and V contents range from 0.1-0.6 wt. % Al, 0.01-1.16 wt. % Cr, and 0.08-0.49 wt. % V, respectively. Magnesium contents range from below detection limits to 0.19 wt. %. In samples containing both primary magnetite and magnetite lamellae in ilmenite, the magnetite hosted in ilmenite is generally richer in Ti, and poorer in V and Cr, compared to the primary magnetite (Fig. 3.11 a,b).

3.6.1.4 Magnetite lenses in pleonaste

Magnetite lenses hosted in pleonaste are near end-member in composition with Fe^{2+}, and Fe^{3+} contents ranging from ~24-25 wt. % and ~60-61 wt. % respectively. Aluminum, Cr, and V contents are between 0.1-0.3wt. % Al, 0.1-0.3 wt. % Cr, and 0.2-0.4 wt. % V, respectively. In samples containing both primary magnetite and magnetite lenses in pleonaste, the magnetite hosted in pleonaste is generally poorer in V and Cr compared to the primary magnetite (Fig. 3.11 a,b).

3.6.2 Ilmenite

3.6.2.1 Overview

The EPMA analyses were done on granular and composite ilmenite with (n=90) and without exsolution (n=42) features, sandwich ilmenite (n=42) and ilmenite dotted with spinel microcrystals (n=49). Regardless of petrographic context, all ilmenite contains measurable amounts of V, Mn, and Mg (Fig. 3.12 a,b).

3.6.2.2 Composite ilmenite with exsolution lamellae

Composite ilmenite containing exsolution lamellae is predominantly composed of Ti and Fe^{2+} with 28.0-31.7 wt. % Ti, and ~30-34 wt. % Fe^{2+}, respectively. Fe^{3+}, V, Mn and Mg range from ~1-8 wt.% Fe^{3+}, 0.11-0.24 wt.%, V, 0.22-0.94 wt. % Mn, and 0.24-2.18 wt.% Mg (Fig. 3.12 a,b).

3.6.2.3 Composite ilmenite without exsolution

Composite ilmenite grains without exsolution lamellae have Ti and Fe^{2+} contents that range from 28.6-31.7 wt. % Ti, and ~30-35 wt. % Fe^{2+} respectively. Fe^{3+}, V, Mn, and Mg range from ~0-7 wt. % Fe^{3+}, 0.10-0.24 wt. % V, 0.32-1.6 wt. % Mg, and 0.18-2.17 wt. % Mn, respectively. The overall compositions differ little from those of grains that show exsolution lamellae (Fig. 3.12 a,b).

3.6.2.4 Sandwich ilmenite

Thick ilmenite lamellae growing parallel to only one set of {111} planes in magnetite, termed sandwich ilmenite, contain 29.2-31.8 wt. % Ti and ~31-36 wt. % Fe^{2+}. Fe^{3+}, V, Mn, and Mg, range from ~0-6 wt. % Fe^{3+}, 0.09-0.25 wt. % V, 0.39-2.29 wt. % Mn, and 0.15-1.39 wt. % Mg, respectively (Fig. 3.12 a,b).

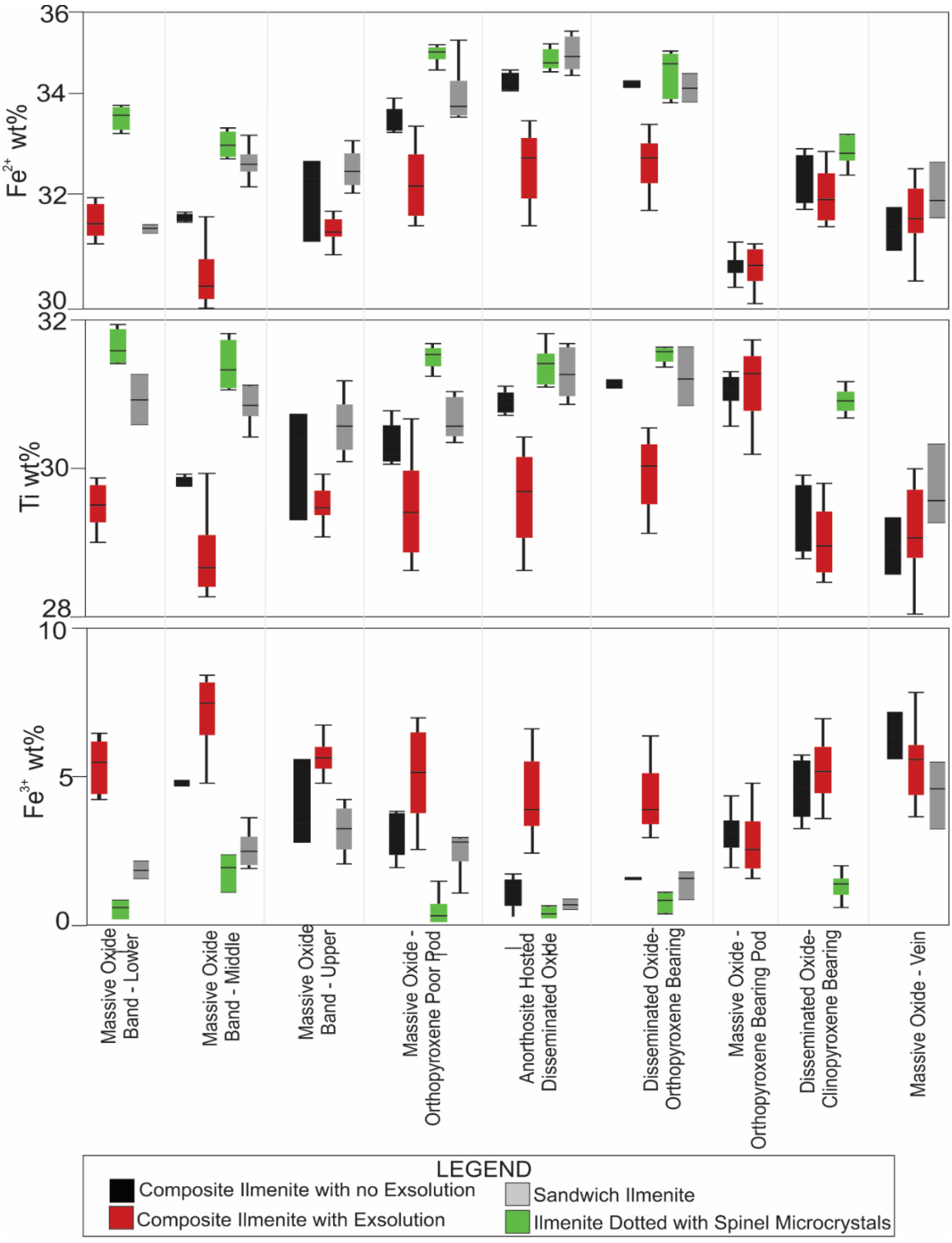

Figure 3.12a. Box and whisker type plot showing variation in $Fe^{2+,}$ Ti, Fe^{3+} , V, Mg, and Mn content in ilmenite from various textures and various mineralization styles.

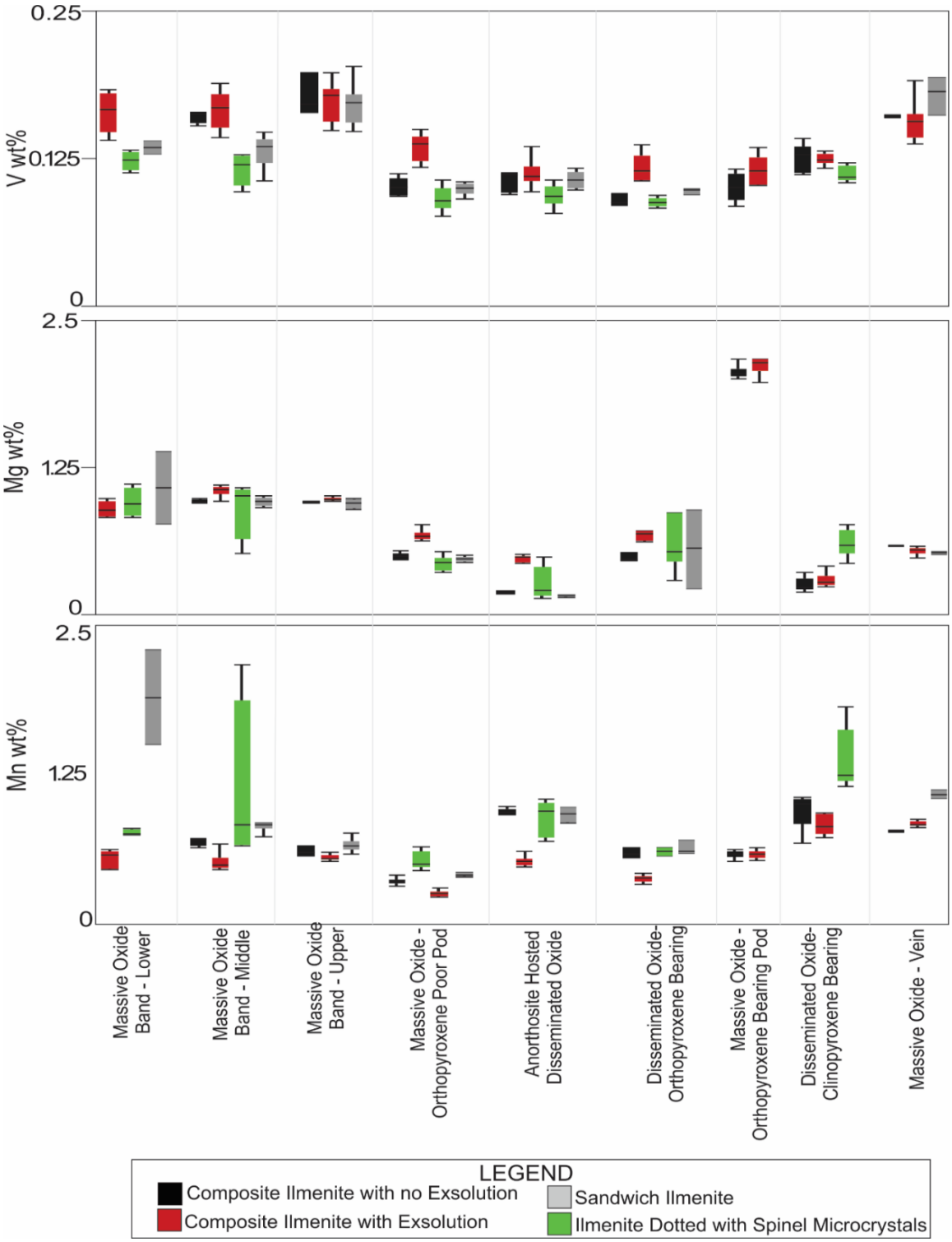

Figure 3.12b Box and whisker type plot showing variation in $Fe^{2+,}$ Ti, Fe^{3+} , V, Mg, and Mn content in ilmenite from various textures and various mineralization styles.

3.6.2.5 Ilmenite "dotted" with spinel microcrystals

The ilmenite fraction of ilmenite that is dotted with spinel microcrystals was also analyzed. In terms of Ti and Fe^{2+} content, this ilmenite contains 30.7-31.8 wt. % Ti, and ~33-35 wt. % Fe^{2+}, respectively. Fe^{3+}, V, Mn and Mg range from ~0-2 wt. % Fe^{3+}, 0.09-0.14 wt. % V, 0.44-1.82 wt. % Mn, and 0.14-1.0 wt. % Mg respectively (Fig. 3.12 a,b).

3.6.3 Pleonaste

3.6.3.1 Overview

Only a few pleonaste analyses were done compared to the number of analyses of magnetite and ilmenite, because coarse-grained analyzable pleonaste is relatively uncommon in the samples studied. As such, it is not clear if these pleonaste analyses presented are truly representative of the chemical composition of pleonaste in the NWRA.

Pleonaste within the NWRA occurs with a variety of exsolution textures within the oxide mineralization. Coarse-grained pleonaste containing magnetite exsolution (n=15), coarse-grained pleonaste without magnetite exsolution (n=12), pleonaste exsolution microtextures in ilmenite (n=11), and the pleonaste component of spinel dotted with pleonaste microcrystals (n=4) were analyzed by EPMA. Where analyzed, pleonaste typically contains detectable amounts of Ti, Al, Cr, Fe^{3+}, Fe^{2+}, Mn, Mg, and Zn (Fig 3.13a,b).

3.6.3.2 Pleonaste with magnetite exsolution

Pleonaste containing magnetite exsolution is predominantly composed of Mg, Fe^{2+} and Al, containing 4.6-7.1 wt. % Mg, ~17-21 wt. % Fe^{2+}, and 29.6-31.7 wt. % Al respectively. Other elements detected include Cr, Fe^{3+}, Mn, and Zn which range from 0.16-0.40 wt. % Cr, ~3-5 wt. % Fe^{3+}, 0.15-0.35 wt. % Mn, and 0.46-1.47 wt. % Zn, respectively (Fig 3.13 a,b).

3.6.3.3 Pleonaste without magnetite exsolution

Pleonaste without magnetite exsolution is predominantly composed of Mg, Fe^{2+}, and Al, containing 4.3-8.8 wt. % Mg, ~14-22 wt. % Fe^{2+}, and 29.7-32.8 wt. % Al, respectively. Other elements detected include Cr, Fe^{3+}, Mn, and Zn, which range from 0.22-0.35 wt. % Cr, ~2-5 wt. % Fe^{3+}, 0.14-0.19 wt. % Mn, and 0.18-0.73 wt. % Zn (Fig 3.13a,b), respectively.

3.6.3.4 Pleonaste lamellae in ilmenite

Pleonaste lamellae in ilmenite are composed of Mg, Fe^{2+}, and Al, containing 4.1-9.0 wt. % Mg, ~15-24 wt. % Fe^{2+}, and 30.1-33.3 wt. % Al, respectively. Other elements detected include Ti, Cr, Fe^{3+}, Mn, and Zn ranging from 0.30-0.68 wt. % Ti, 0.34-0.93 wt.% Cr, ~1-3 wt.% Fe^{3+}, 0.1-0.5 wt.% Mn, and 0.29-0.65 wt.% Zn, respectively (Fig 3.13a,b).

3.6.3.5 Pleonaste from ilmenite dotted with pleonaste microcrystals

Pleonaste from ilmenite dotted with pleonaste microcrystals was only analyzed in one sample where it is predominantly composed of Mg, Fe^{2+}, and Al, with ranges from 4.3-4.5 wt. % Mg, ~22-23 wt. % Fe^{2+}, and 29.6-29.9 wt. % Al, respectively. Other elements detected include Ti, Cr, Fe^{3+}, Mn and Zn which range from 0.44-0.78 wt.% Ti, 0.81-1.02 wt.% Cr, ~1-2 wt.% Fe^{3+}, 0.02-0.12 wt.% Mn, and 0.46-0.61 wt.% Zn, respectively (Fig 3.13a,b).

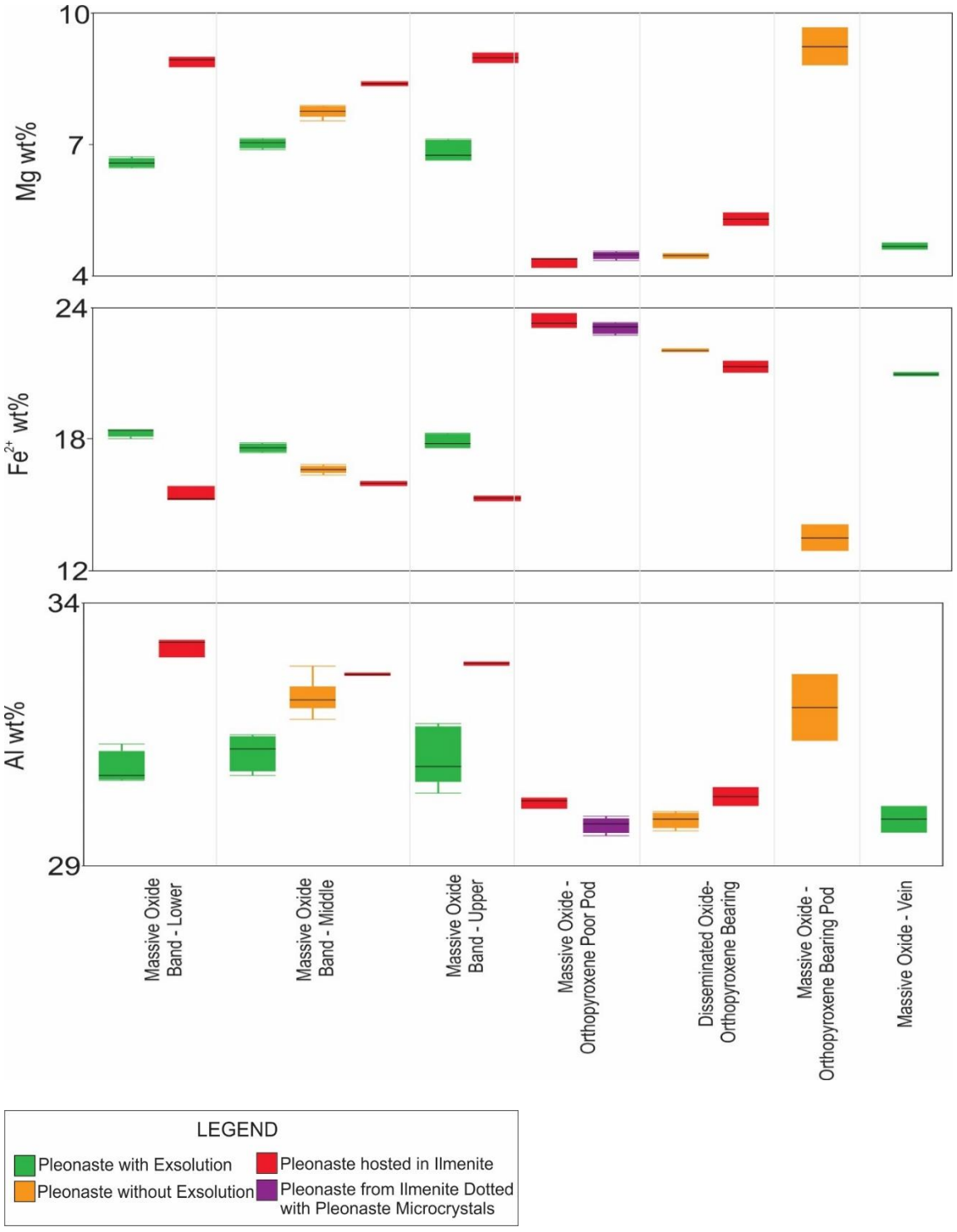

Figure 3.13a. Box and whisker plot showing variation in Mg, Fe^{2+}, Al, Fe^{3+}, Ti and Mn content between various textures of pleonaste from various mineralization styles.

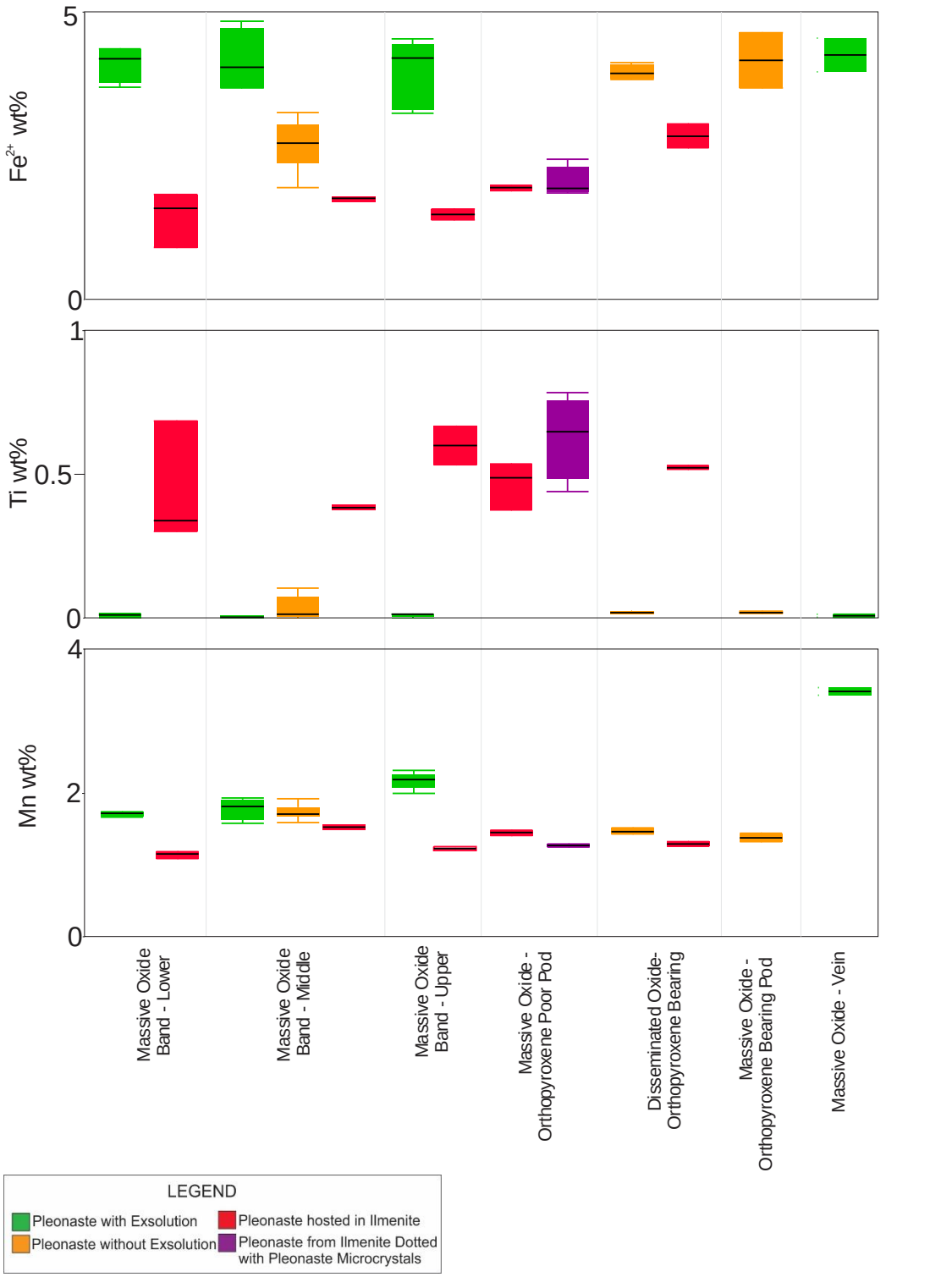

Figure 3.13b. Box and whisker plot showing variation in Mg, Fe^{2+}, Al, Fe^{3+}, Ti and Mn content between various textures of pleonaste from various mineralization styles.

3.7 Mineral compositions determined by LA-ICPMS

3.7.1 Magnetite

3.7.1.1 Overview

Primary magmatic (n=103) and granoblastic (n=13) magnetite grains from all mineralization styles were analyzed in situ using LA-ICPMS to determine their trace element compositions (Fig 3.14 a,b). In magnetite, Si, Al, Ga, Mn, Mg, Ti, Zn, Co, V, Ni, and Cr were detected in appreciable amounts, whereas Ca, Y, P, Pb, Zr, Hf, Ge, W, Sc, Ta, Nb, Mo, Sn, As, and Sb were limited to < ~10 ppm at maximum when detected.

3.7.1.2 Results

The most abundant trace elements detected in primary magmatic magnetite were Al, Ti, V, Cr, Mg, and Si which ranged from 1,852 ppm-3.3 wt. % Al, 313 ppm - 4.3 wt. % Ti, 3,124-6,469 ppm V, 1,464-4,539 ppm Cr, 333-6,000 ppm Mg, and 50-3,000 ppm Si, respectively. Other elements detected include Ga, Mn, Zn, Co, and Ni which range from 31-85 ppm Ga, 67-1896 ppm Mn, 3-500ppm Zn, 47-206 ppm Co, and 93-507 ppm Ni, respectively (Fig. 3.14 a,b). Analyses show that the recrystallized granoblastic magnetite, like the primary magnetite, contain abundant Al, Ti, V, Cr, Mg, and Si, ranging from 1.4-2.8 wt. % Al, 2.4-3.2 wt. % Ti, 4223-4519 ppm V, 2085-2417 ppm Cr, 5129-6257 ppm Mg, and 56-726 ppm Si, respectively. As in the primary magnetite, in the recrystallized granoblastic magnetite the less abundant elements include Ga, Mn, Zn, Co, and Ni with ranges of 55-67 ppm Ga, 1,848-2,270 ppm Mn, 52-455 ppm Zn, 16-20 ppm Co, and 306-342 ppm Ni, respectively (Fig. 3.14 a,b).

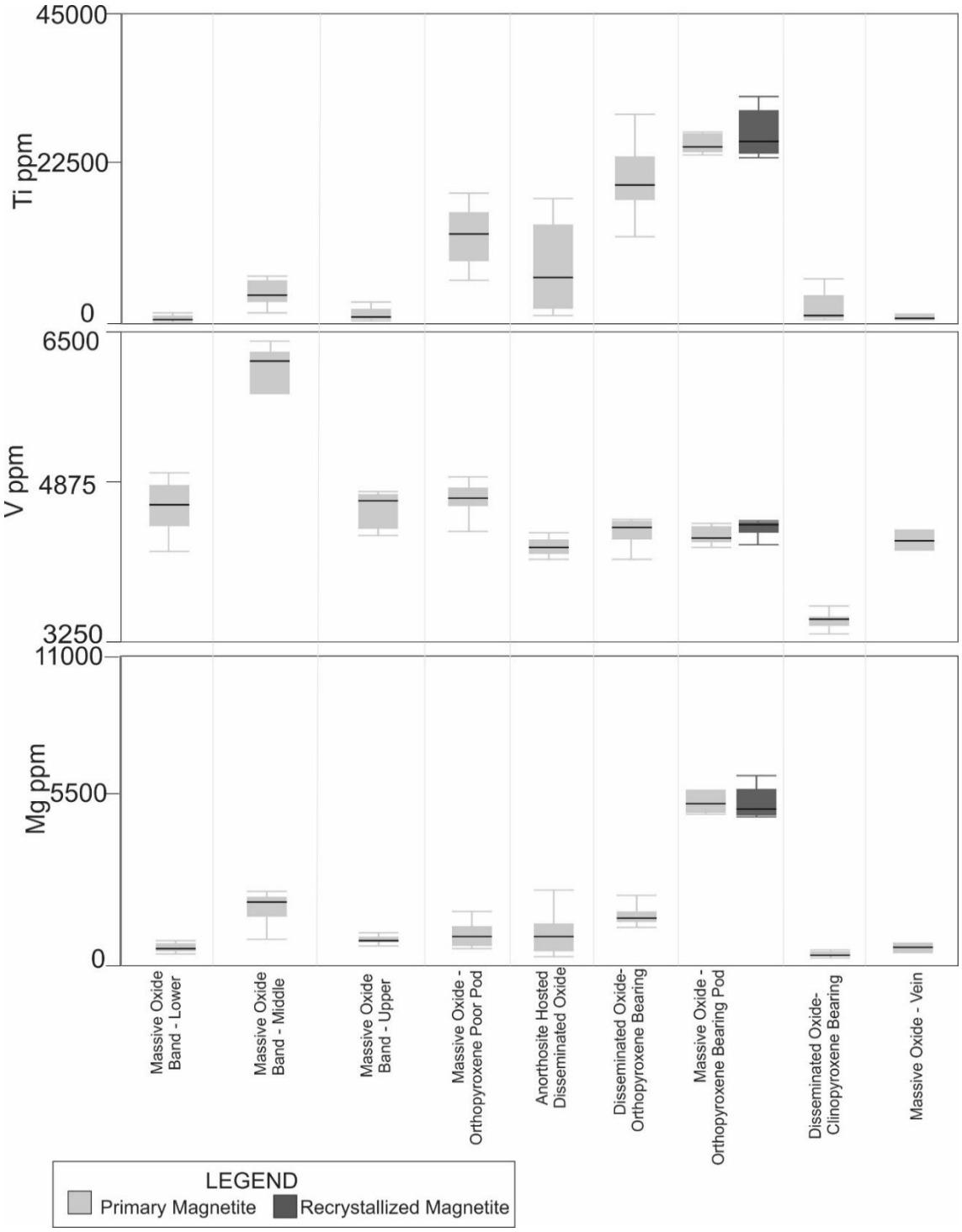

Figure 3.14a. Box and whisker type plots of LA-ICPMS data showing variation in Ti, V, Mg, Mn, Cr, and Ni content in magnetite from various mineralization styles.

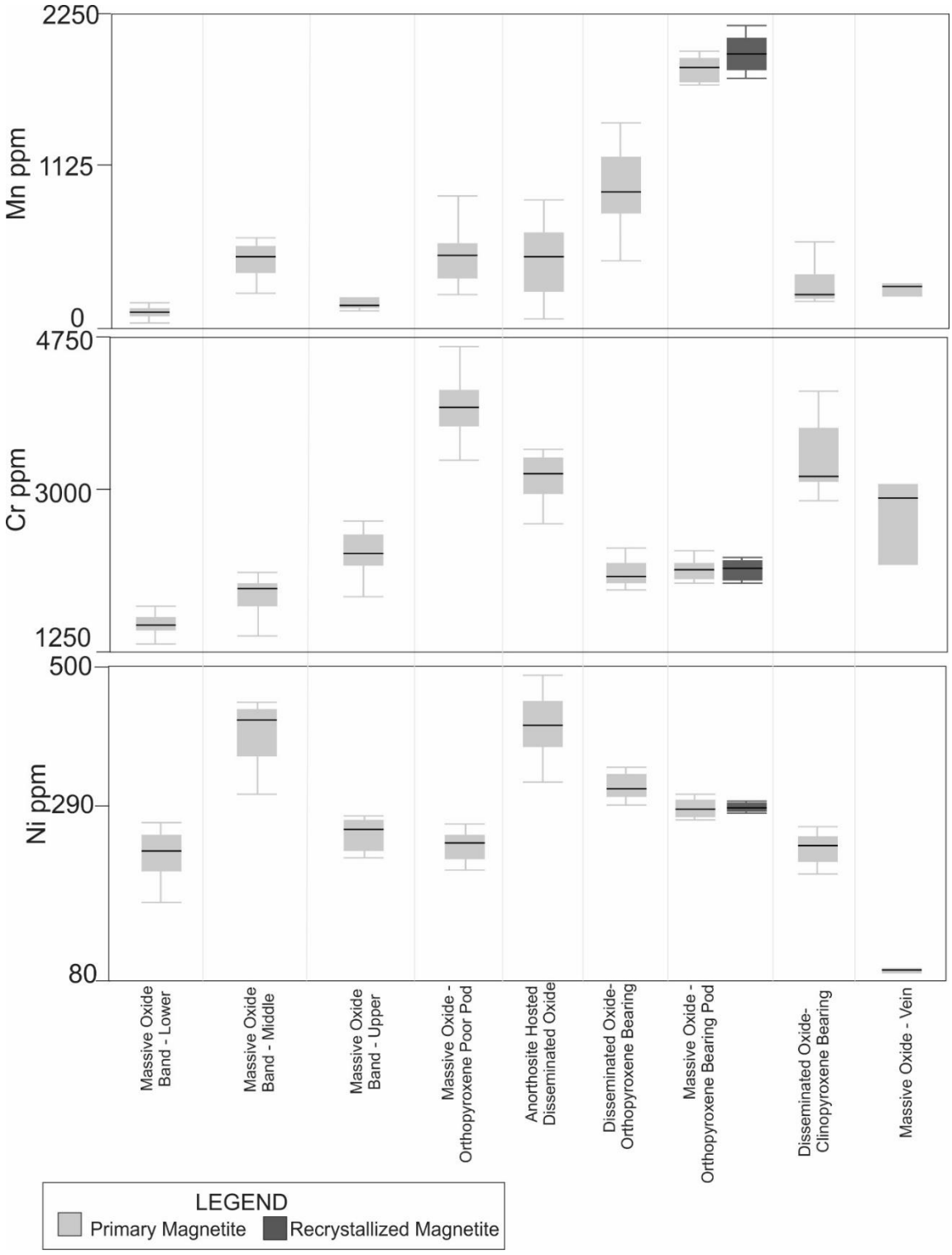

Figure 3.14 b. Box and whisker type plots of LA-ICPMS data showing variation in Ti, V, Mg, Mn, Cr, and Ni content in magnetite from various mineralization styles.

3.7.2 Ilmenite

3.7.2.1 Overview

Composite ilmenite with exsolution of magnetite, hematite and pleonaste, without exsolution, and sandwich ilmenite were also analyzed by LA-ICPMS (Fig. 3.15 a,b). Of all the elements analyzed, Mg, Al, Si, Sc, V, Cr, Mn, Co, Ni, Zr and Zn were present in appreciable concentrations whereas P, Ca, Cu, Ga, Ge, As, Y, Mo, Sn, Sb, Hf, Ta, W and Pb were limited to <~10 ppm at maximum when detected.

3.7.2.2 Results

Ilmenite containing exsolution lamellae of magnetite, hematite and pleonaste contain abundant Mg, Al, Si, V, and Mn ranging from 3,076 ppm to 2.2 wt. % Mg, 134-4,470 ppm Al, 45-3,760 ppm Si, 395-2,800 ppm V, and 2.5 ppm to 1.3 wt. % Mn, respectively. Less abundant elements include Sc, Cr, Co, Ni, Zn, Zr, and Nb which range from 20-69 ppm Sc, 30-434 ppm Cr, 64-123 ppm Co, 14-84 ppm Ni, 5-172 ppm Zn, 6-223 ppm Zr, and 2-40 ppm Nb, respectively (Fig. 3.15 a,b).

Composite ilmenite grains without exsolution contain abundant Mg, Al, Si, V, and Mn with ranges including 2,089 ppm to 2.4 wt. % Mg, 134 ppm to 1.6 wt. % Al, 44-3,760 ppm Si, 311-2,800 ppm V, and 2,446 ppm to 1.3 wt. % Mn, respectively. Less abundant elements include Sc, Cr, Co, Ni, Zn, Zr, and Nb, which range from 18-76 ppm Sc, 30-432 ppm Cr, 47-146 ppm Co, 14-84 ppm Ni, 3-226 ppm Zn, 13-223 ppm Zr, and 2-40 ppm Nb (Fig. 3.24).

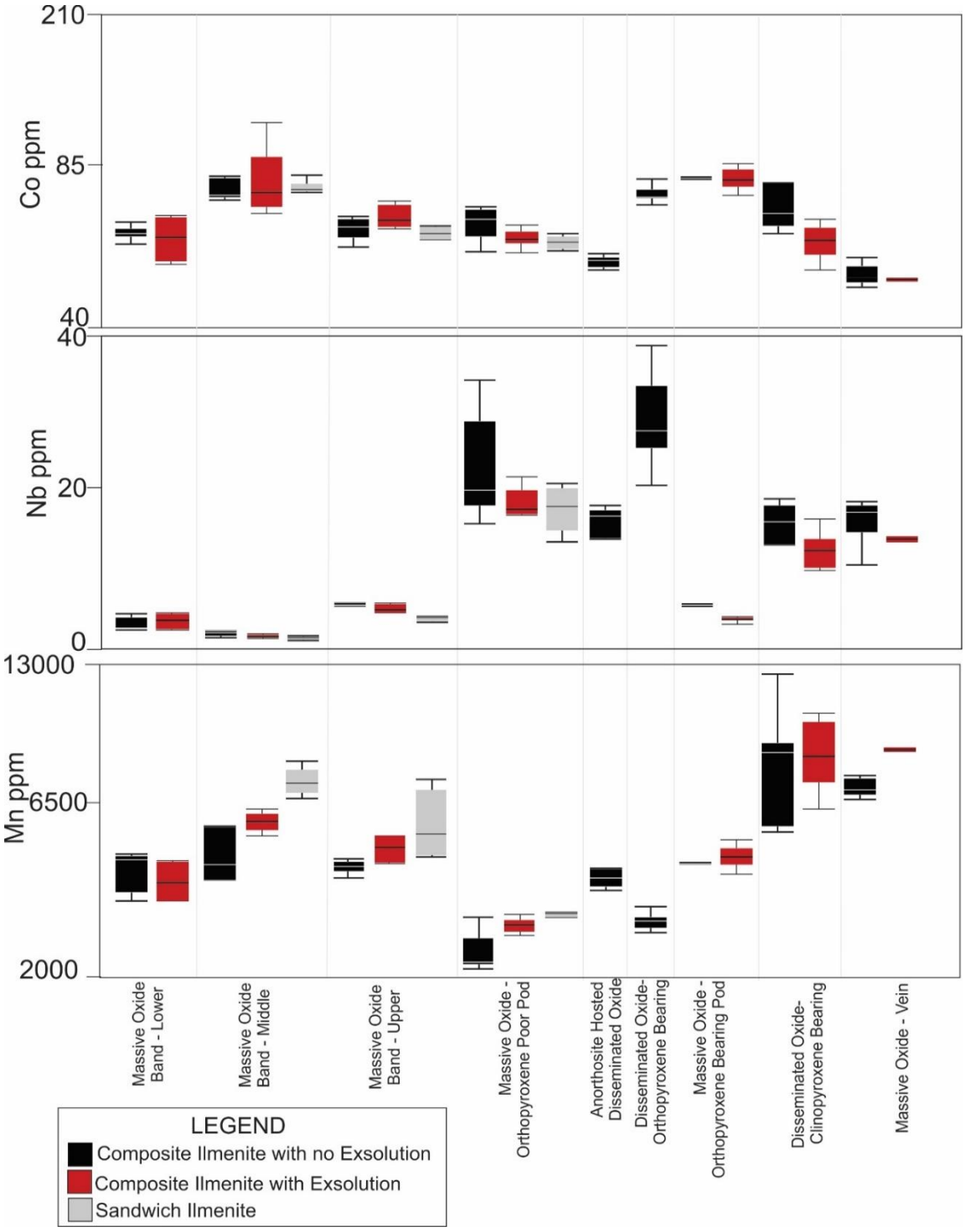

Figure 3.15a. Box and whisker type plots of LA-ICPMS data showing variation in Co, Nb, Mn, V, Sc, and Zr content in ilmenite from various textures and various mineralization styles.

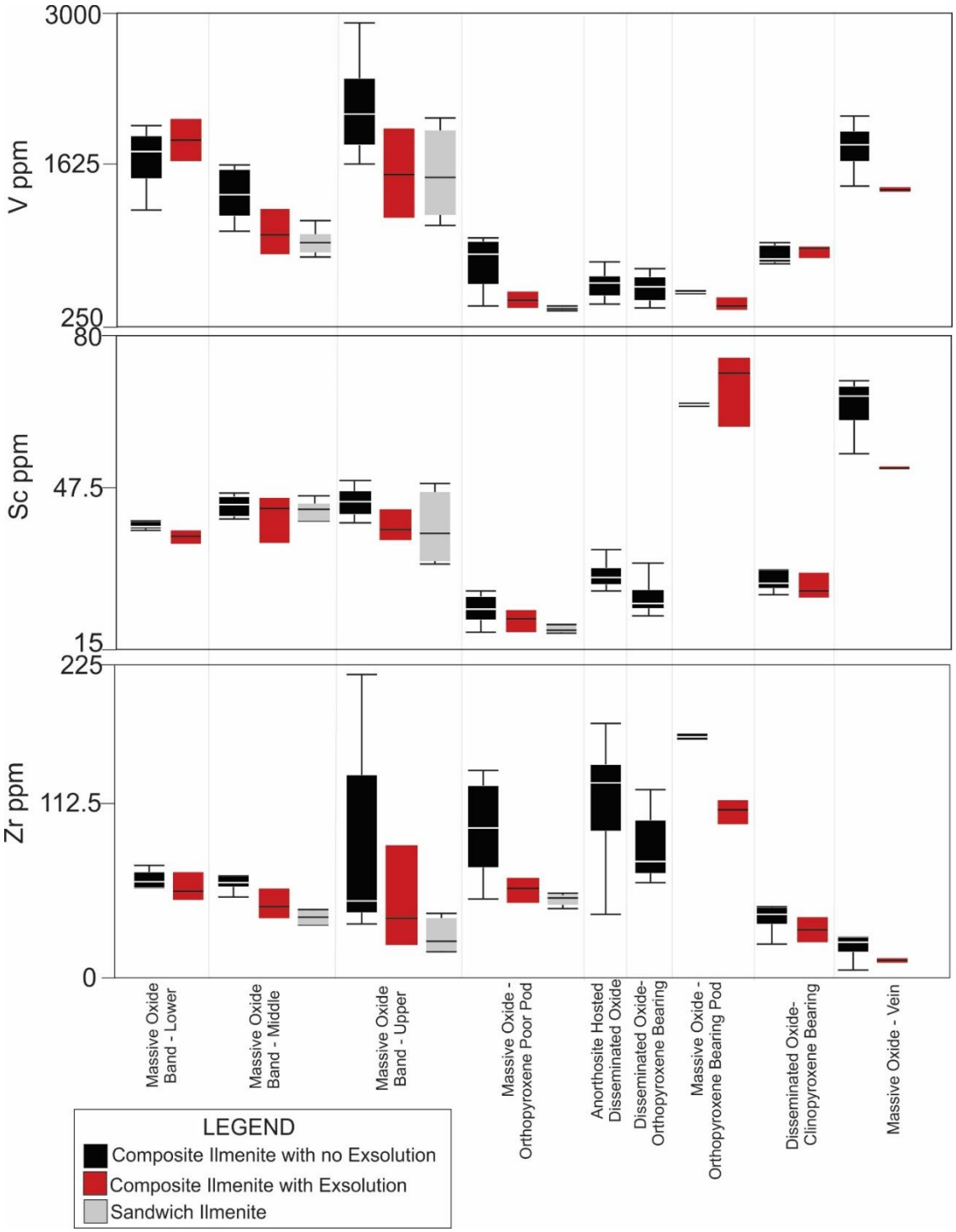

Figure 3.15b. Box and whisker type plots of LA-ICPMS data showing variation in Co, Nb, Mn, V, Sc, and Zr content in ilmenite from various textures and various mineralization styles.

Sandwich ilmenite contains abundant Mg, Al, Si, V, and Mn, which range from 4,755 ppm to 1.1 wt. % Mg, 109-1,060 ppm Al, 374-2,000 ppm Si, 109-1,060 ppm V, and 4,213-9,550 ppm Mn, respectively. Less abundant elements include Sc, Cr, Co, Ni, Zn and Zr which range from 20-49 ppm Sc, 99-256 ppm Cr, 83-124 ppm Co, 43-81 ppm Ni, 4-100 ppm Zn, and 19-109 ppm Zr, respectively (Fig. 3.15 a,b).

3.7.3 Pleonaste

3.7.3.1 Overview

As noted above, relatively few LA-ICPMS analyses of pleonaste were completed compared to the magnetite and ilmenite analyses due to a lack of coarse-grained pleonaste. Pleonaste containing magnetite exsolution, and medium grained pleonaste without magnetite exsolution were analyzed. Fe, Mg, Si, Pb, Ca, V, Cr, Mn, Co, Ni, Zn, and Ga were detected in appreciable amounts (>~1 ppm).

3.7.3.2 Results

Pleonaste granules without exsolution predominantly contain Si, Pb, Ca, and V. Specifically, contents range from 500 ppm-1.2 wt. % Si, 2-189 ppm Pb, 8-352 ppm Ca and 387-2560 ppm V respectively. Chromium, Mn, Co, Ni, Zn, and Ga contents range from 2068-4733 ppm Cr, 1368-2674 ppm Mn, 472-1410 ppm Co, 557-1121 ppm Ni, 3164-9380 ppm Zn, and 166-372 ppm Ga respectively (Fig 3.16 a,b).

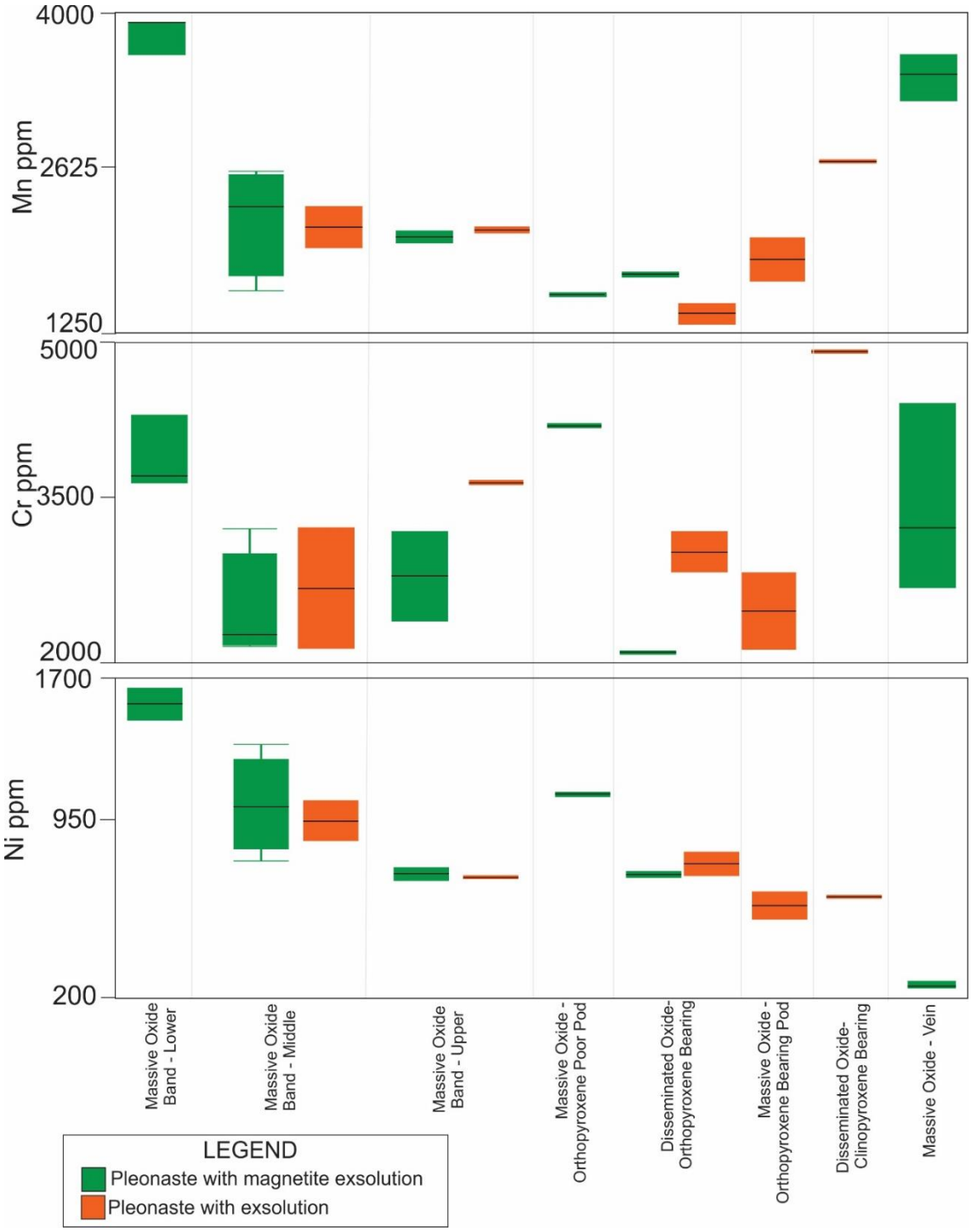

Figure 3.16a. Box and whisker type plots of LA-ICPMS data showing variation in Fe, Mg, Cr, Mn, Co, and Zn content in pleonaste from various textures and various mineralization styles.

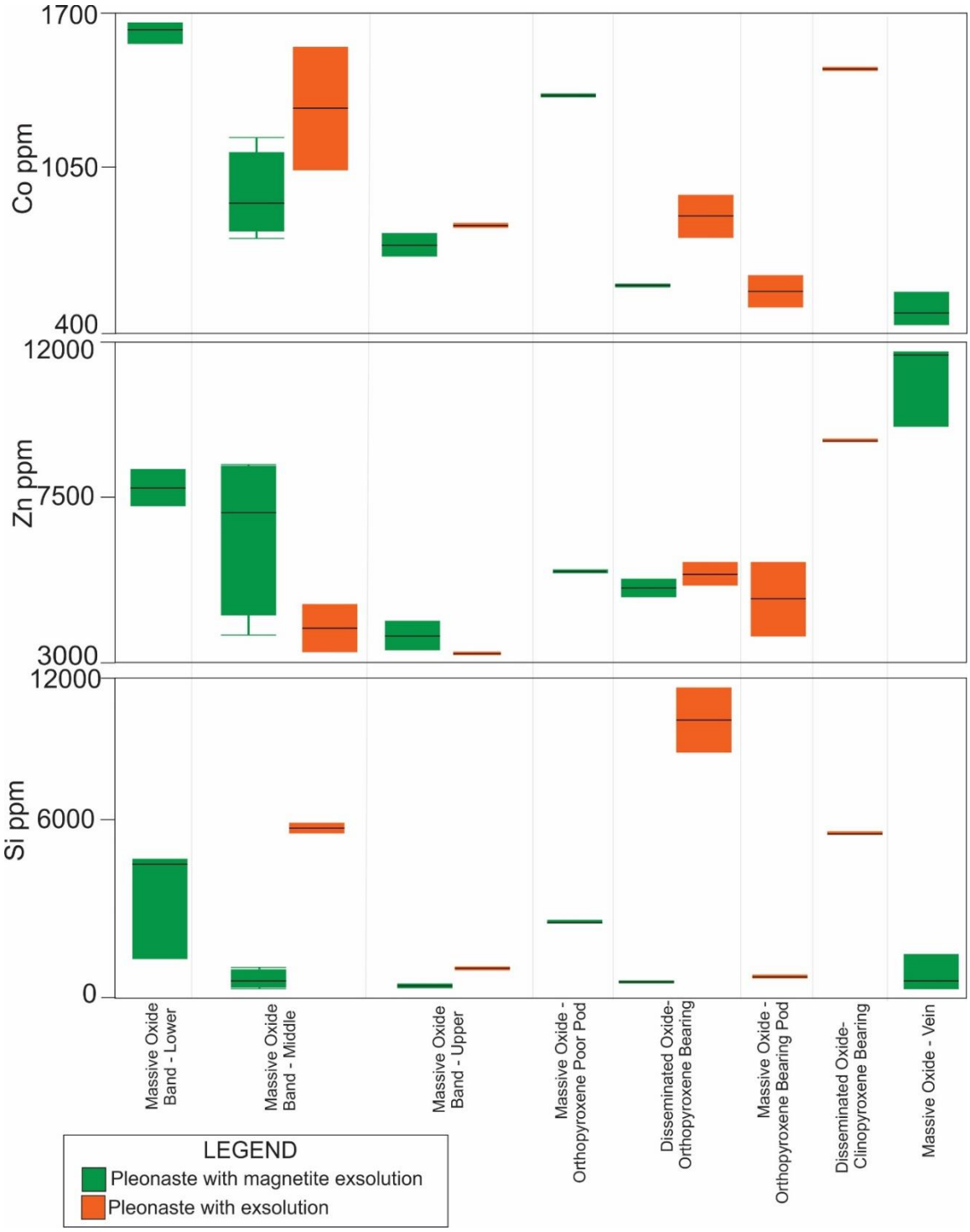

Figure 3.16b Box and whisker type plots of LA-ICPMS data showing variation in Fe, Mg, Cr, Mn, Co, and Zn content in pleonaste from various textures and various mineralization styles.

3.7.4 Wavelength Dispersal Spectroscopy (WDS) X-ray maps of Oxide Grains

Wavelength dispersal spectroscopy (WDS) X-ray maps using the EPMA were made on representative grains of magnetite and ilmenite as well as at contacts between magnetite and ilmenite in order to elucidate the presence of spatial chemical variation and to better understand exsolution features and related textures. Cryptic spatial zonation, as well as growth zoning, has been observed in hydrothermal magnetite by Dare et al. (2014); Knipping et al. (2015); and Broughm et al. (2017).

In this study Fe, Ti, V, Al, and Mg contents were mapped in eight regions from six thin sections. Maps containing representative results are shown in Fig. 3.17. These maps are semi-quantitative and shown with a colour gradient scale; warm colours representing relative higher abundance of the element in question, whereas cooler colours represent lower abundances of that element (Fig 3.17). In general, similar chemical features are observed for each element in all of the maps made using this technique. Magnetite is relatively homogeneous with a few exceptions. Adjacent to ilmenite, magnetite has a narrow rim that is slightly enriched in Ti, coupled with a slight depletion of V. An increase in Ti, Mg, and Al coupled with a depletion of Fe is present in structures that mimic the typical shape of spinel lenses and ilmenite lamellae observed in magnetite under reflected light. These lenses and lamellae are typically most abundant in the cores of magnetite grains and least abundant in areas near contacts with adjacent silicates or ilmenite.

Ilmenite grains that are adjacent to magnetite typically display a narrow rim enriched in Ti, coupled with a depletion in Fe. Locally, this zone contains irregular zones enriched in Mg and Al, which correspond to zones of aluminous spinel identified during

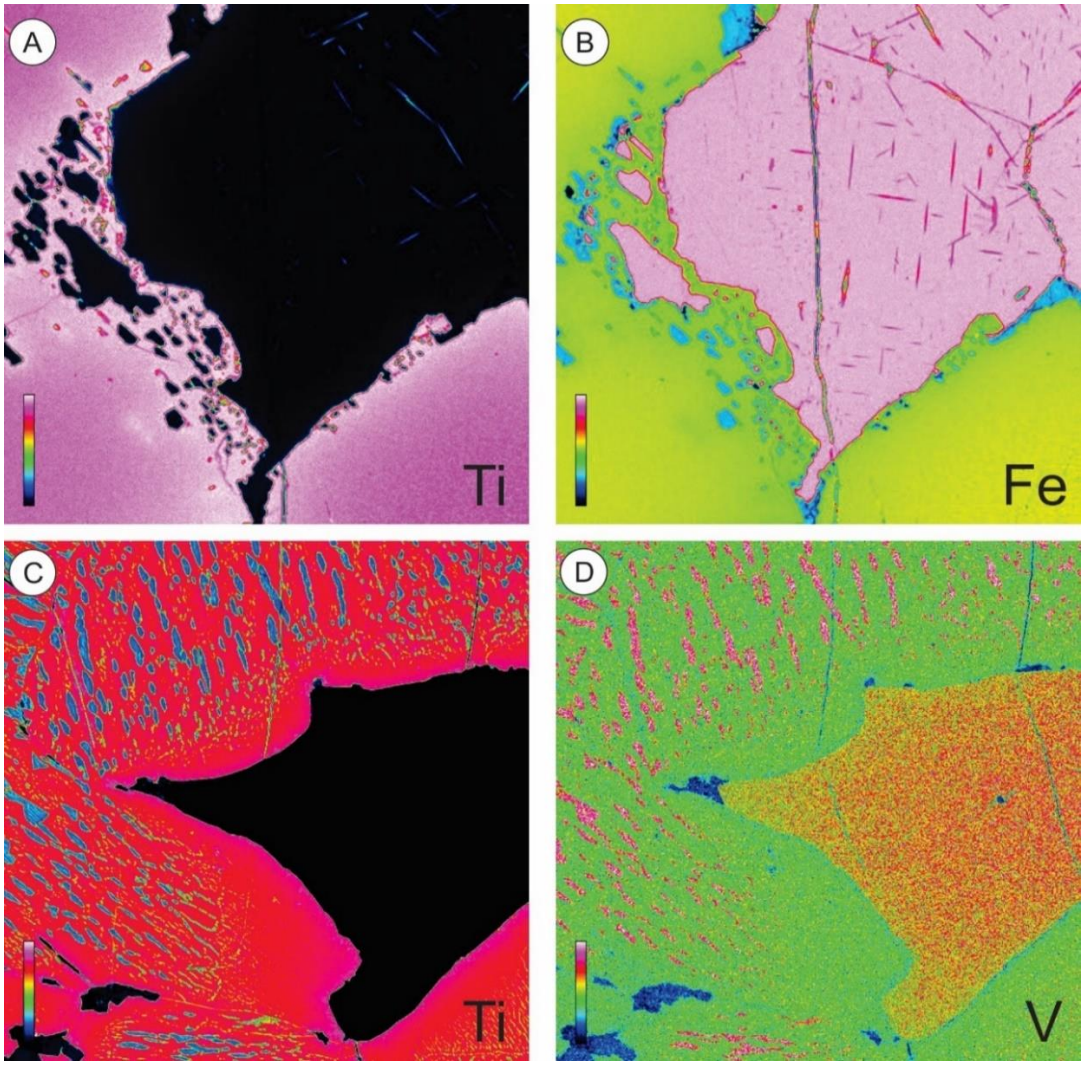

Figure 3.17. Representative EPMA WDS X-ray maps of magnetite, ilmenite, and pleonaste from selected mineralized samples. Maps have a relative "temperature" scale with the warmest colours representing the highest abundance of the element in question: A) Ti content variations at the contact between magnetite and ilmenite; note high Ti rim in ilmenite (pink in colour) at contact with magnetite and lamellae in magnetite slightly enriched in Ti; B) map showing variation in Fe content from the area analyzed in figure A. Note zone of low Fe at contact between magnetite (pink) and ilmenite (yellow). Dark pink lenses in magnetite correspond with pleonaste exsolution features as observed with transmitted light microscopy; C) WDS map of Ti content variation at contact between ilmenite and magnetite. As in A, a high Ti rim is present in ilmenite (red) immediately adjacent to contact between magnetite (black) and ilmenite. Note low Ti lenses in ilmenite correspond with hematite as observed with reflected light microscopy; and D) V content variation from the area analyzed in C. Note slight enrichment in V content in core of magnetite grain vs rim and enriched V content in hematite lenses in ilmenite.

petrography. Two exsolution textures within ilmenite are illustrated well by WDS X-ray mapping.

The first shares a textural form with hematite lenses identified petrographically, and is chemically defined by an enrichment in Fe and V coupled, with a depletion of Ti. Within the largest of these hematite lenses, lamellae enriched in Ti are present. In general, hematite lenses are most abundant at the core of ilmenite grains and gradationally diminish in abundance approaching the contacts between ilmenite and magnetite. The second intergrowth texture is composed of lamellar features that are enriched in Al and Mg and depleted in Fe compared to the host ilmenite. These lamellae correspond with pleonaste observed in thin section. Surrounding these lamellae are zones slightly enriched in Ti and slightly depleted in Fe.

REFERENCES

Broughm SG, Hanchar JM, Tornos F, Westhaus A, Attersley S (2017) Mineral chemistry of magnetite from magnetite-apatite mineralization and their host rocks: examples from Kiruna, Sweden, and El Laco, Chile. Mineralium Deposita 51: 1223-1244

Butt JM (2000) Mineral chemistry and mineral reactions in a meta-anorthosite complex, Cape Caribou River Allochthon, Grenville Province, Labrador. Unpublished B.Sc. thesis, Memorial University of Newfoundland, St. John's NL, 111 pages

Charlier B, Namur O, Bolle O, Latypov R, Duchesne JC (2015) Fe-Ti-V-P ore deposits associated with Proterozoic massif-type anorthosites and related rocks. Earth-Science Reviews 141: 56-81

Dare SA, Barnes SJ, Beaudoin G, Meric J, Boutroy E, Potvin-Doucet C (2014) Trace elements in magnetite as petrogenetic indicators. Mineralium Deposita 49: 785-796

Duchesne JC (1970) Microtextures of Fe-Ti oxide minerals in the South Rogaland anorthositic complex (Norway). Annales de la Societe Geologique de Belgique 93: 197-251

Dupuis C, Beaudoin G (2011) Discriminant diagrams for iron oxide trace element fingerprinting of mineral deposit types. Mineralium Deposita 36: 319-355

Knipping JL, Bilenker LD, Simon AC, Reich M, Barra F, Deditus AP, Walle M, Heinrich CA, Holtz F, Munizaga R (2015) Trace elements in magnetite from massive iron oxide-apatite deposits indicate a combined formation by igneous and magmatic-hydrothermal processes. Geochimica Cosmochimica Acta 171: 15-38

Nadoll P, Angerer T, Mauk JL, French D, Walshe J (2014) The chemistry of hydrothermal magnetite: a review. Ore Geology Reviews 61: 1-32

Rakotonandrasana NOT, Arima M, Miyawaki R, Rambeloson RA (2010) Widespread occurrences of högbomite-2N2S in UHT metapelites from the Betroka Belt, Southern Madagascar; implications on melt or fluid activity during regional metamorphism. Journal of Petrology 51: 869-895.

Ramdohr P (1953) Ulvospinel and its significance in titaniferous iron ores. Economic Geology 48: 677-688

Rudnick R, Gao S (2003) Composition of the continental crust. Treatise on Geochemistry 3: 1-64

Sengupta P, Bhui EK, Braun I, Dutta U, Mukhopadhyay D (2009) Chemical substitutions, paragenetic relations and physical conditions of formation of högbomite in the Sittampundi layered anorthosite complex, Southern India. American Mineralogist. 94: 1520-1534

Velasco F, Tornos F, Hanchar JM (2016) Immiscible iron- and silica-rich melts and magnetite geochemistry at the El Laco volcano (northern Chile): Evidence for a magmatic origin for the magnetite deposits. Ore Geology Reviews 79: 346-366

Chapter 4: Discussion

4.1 Interpretation of results

4.1.1 Field observations

Massive to semi-massive and disseminated Fe and Ti oxide mineralization hosted in granoblastic anorthosite commonly occurs throughout the field area of this study. The mineralization is coarse to very coarse grained (1-5 cm) and dominated by magnetite (~60-70%) along with abundant ilmenite (10-20%) and pleonaste (10-20%). Disseminated oxide mineralization occurs interstitial to plagioclase in the host anorthosite, or associated with or partially rimming clinopyroxene when present. Massive to semi-massive oxide mineralization is observed in discordant veins, pods and bands. Apatite is not observed to be directly associated with the Fe-Ti oxide mineralization but is a common mineral in the samples studied.

Oxide mineralization in the NWRA is separated into various mineralization styles observed at the outcrop scale during field work to facilitate comparisons between various textural occurrences of Fe-Ti oxide mineralization. An in depth study of the mineralization styles showed that all of the oxide mineralization observed has remarkably similar oxide and silicate mineralogy, mineral textures, and textural relationships with host anorthosite and mineral inclusions. Contact relationships between all massive to semi-massive mineralization styles and the host anorthosite are sharp and irregular, oftentimes with disseminated oxide mineralization adjacent to the massive oxide zone within the host anorthosite. Inclusions of rafts of host anorthosite are commonly observed in massive oxide mineralization.

4.1.2 Petrography

Thin sections representative of each mineralization style observed during fieldwork were examined using transmitted and reflected light microscopy. All observed Fe-Ti oxide mineralization is dominated by magnetite with less abundant ilmenite and pleonaste. Orthopyroxene is present in some samples of bands of oxide mineralization, pods of oxide mineralization, as well as associated with some of the disseminated oxide mineralization. Magnetite, ilmenite, and pleonaste from all mineralization styles observed contain complex microtextures including examples of miscibility gap exsolution, oxidation exsolution, reduction exsolution, and contain evidence of reequilibration between oxide minerals. The presence of these textures shows that the primary magmatic compositions of oxide minerals cannot be accurately determined using in situ, or any other kinds of analyses.

Similar exsolution features are observed in all thin sections examined including massive to semi-massive oxide mineralization and disseminated oxide mineralization. Exsolution features are finer grained in the disseminated oxide mineralization compared to those in massive to semi-massive oxide mineralization; coarse grained granules of pleonaste and ilmenite are not observed associated with disseminated oxide mineralization. Granoblastic zones consisting of equigranular magnetite, ilmenite, and pleonaste are commonly observed within all oxide mineralization. Granoblastic magnetite contains fine grained pleonaste and “cloth textured” (i.e., submicroscopic to microscopic ilmenite lamellae growing parallel to the {111} plane in the host magnetite (Duchesne, 1970)).

4.1.3 Whole rock major and trace element geochemistry.

Whole rock geochemistry data from barren host-rock and mineralized samples show strong to very-strong positive correlations between elements associated within Fe-Ti oxide minerals (e.g., $FeO_{(t)}$, TiO_2, V_2O_5, Cr_2O_3, Co, Ni, Zn, and Ga) as well as between elements associated with plagioclase feldspar (SiO_2, CaO, Al_2O_3, Na_2O, K_2O, Sr, and Ba). In contrast, SiO_2 and $FeO_{(t)}$ values are strongly negatively correlated. Phosphorus is weakly positively correlated with elements associated with plagioclase and weakly negatively correlated with elements associated with Fe-Ti oxide minerals suggesting apatite is not associated with Fe-Ti oxide mineralization in the NWRA. Magnesium contents are not correlated with either SiO_2 or $FeO_{(t)}$ and rather are likely controlled by the presence of ferromagnesian silicates like orthopyroxene, clinopyroxene, or rarely olivine, as observed during the petrographic investigation.

Binary variation diagrams were generated using SiO_2 and $FeO_{(t)}$ as variation indices (Fig. 4.1). Each figure contains grey ellipses labelled with a mineral abbreviation which represents the compositional range of that mineral. When the compositional range of that mineral plots outside of the bounds of the graph, the direction of its compositional range is denoted by an arrow. Aside from showing some of the aforementioned correlations, these diagrams show that two distinct clusters of data are present; one cluster is rich in elements that are associated with Fe-Ti oxide minerals and poor in elements that are associated with plagioclase, and the other is rich in elements that are associated with plagioclase and poor in elements that are associated with Fe-Ti oxide minerals. With the exception of a few intermediate samples, the gap in these clusters spans between ~20-45 wt.% SiO_2 content as well as ~20-45 wt.% $FeO_{(t)}$.

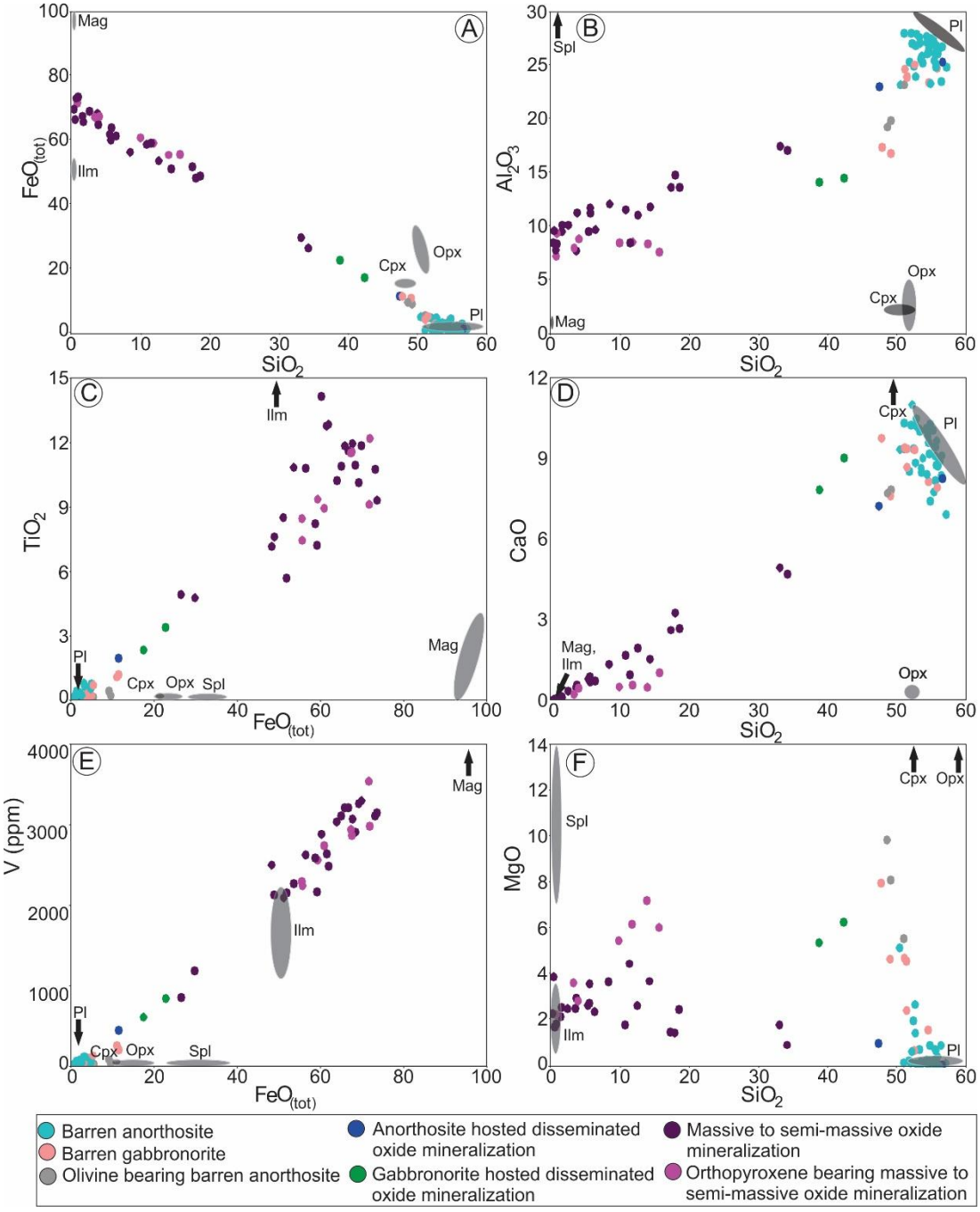

Figure 4.1. Binary variation diagrams of whole-rock geochemical analyses from the North West-River anorthosite (NWRA). Axis units are in wt. % except for V which is in ppm. Composition ranges of minerals observed are represented by ellipses or indicated by an arrow when beyond the bounds of the graph. Silicate mineral ellipses are based on the typical compositional ranges of those minerals in labradorite-type Proterozoic massif anorthosite suites Charlier et al. (2009). Pl = plagioclase, Opx = orthopyroxene, Cpx = clinopyroxene, Mag = magnetite, Ilm = ilmenite, and Spl = spinel (pleonaste) spinel.

The nature of this gap is unclear, however it may be associated with the lack of observed semi-massive oxide mineralization, or a sampling bias due to the coarse grained nature of the rocks within the study area.

4.1.4 In situ oxide chemistry

4.1.4.1 Magnetite chemistry

Magnetite hosted in the NWRA contains abundant and complex exsolution microtextures suggesting that primary magmatic composition of magnetite has not been preserved. This is corroborated by the Ti-poor nature of the magnetite analyzed compared to other known anorthosite hosted Fe-Ti oxide mineralization such as those in the layered Fedorivka complex in which magnetite can contain up to 28 wt.% TiO_2 (Duchesne et al., 2006). Further evidence of modification of the primary magmatic magnetite composition lies in the strong positive correlation between Fe^{2+} and Ti, Al, Mg and Mn, and strongly negatively correlated with Fe^{3+} in all analyses (Fig. 4.2). This relationship geochemically confirms the presence of pleonaste and ilmenite exsolution from primary magnetite observed in thin section. In contrast, the Cr_2O_3 and V_2O_5 contents are similar in all coarse-grained magnetite and is not correlated to any other elements, suggesting that Cr_2O_3 and V_2O_5 are largely unaffected by exsolution and reequilibration during cooling and metamorphism.

Magnetite from orthopyroxene-bearing oxide mineralization is relatively enriched in Fe^{2+}, Ti, Al, Mg, and Mn, and relatively depleted in Fe^{3+} compared to orthopyroxene-poor samples. Such enrichments suggest that magnetite from orthopyroxene bearing samples has undergone less exsolution and reequilibration compared to orthopyroxene-poor samples.

Similar trends are present in the magnetite in situ trace element data (Fig. 4.3). Bands of oxide mineralization are depleted in Al and Ga relative to the other mineralization styles, whereas orthopyroxene-bearing bands of oxide mineralization are enriched in Mg, Mn, Ti, Co, V, Ni, and Ga.

Magnetite in orthopyroxene-poor pods are relatively enriched in Mn, Ti, Cr, and Ga, whereas magnetite in orthopyroxene-bearing pods are highly enriched in Mg, as well as somewhat enriched in Mn, Al, Ti, Co, and Ni. The clinopyroxene-bearing disseminated oxide mineralization is relatively enriched in Cr and depleted in V and Ni. The anorthosite-hosted disseminated oxide mineralization magnetite is enriched in Mn, Ti, Ni and Cr, whereas the orthopyroxene-associated disseminated oxide mineralization is highly enriched in Mg as well as slightly enriched in Mn, Al, Ti, Co, and Ni. These variations are likely a function of different local bulk compositions and perhaps due to high-T breakdown of orthopyroxene which could release Mg, Al and Ni to be taken up by proximal magnetite.

4.1.4.2 Ilmenite chemistry

Like in magnetite, ilmenite in the NWRA contains abundant and complex exsolution microtextures, including pleonaste, hematite, and magnetite, suggesting subsolidus chemical modification of ilmenite has occurred, and that ilmenite analyzed is not representative of the primary magmatic ilmenite composition. In situ analyses were done on all four of the observed textural varieties of ilmenite. A strong positive correlation between Ti and Fe^{2+} coupled with a strong negative correlation between Fe^{2+} and Fe^{3+} is present in all ilmenite analyses (Fig 4.4).

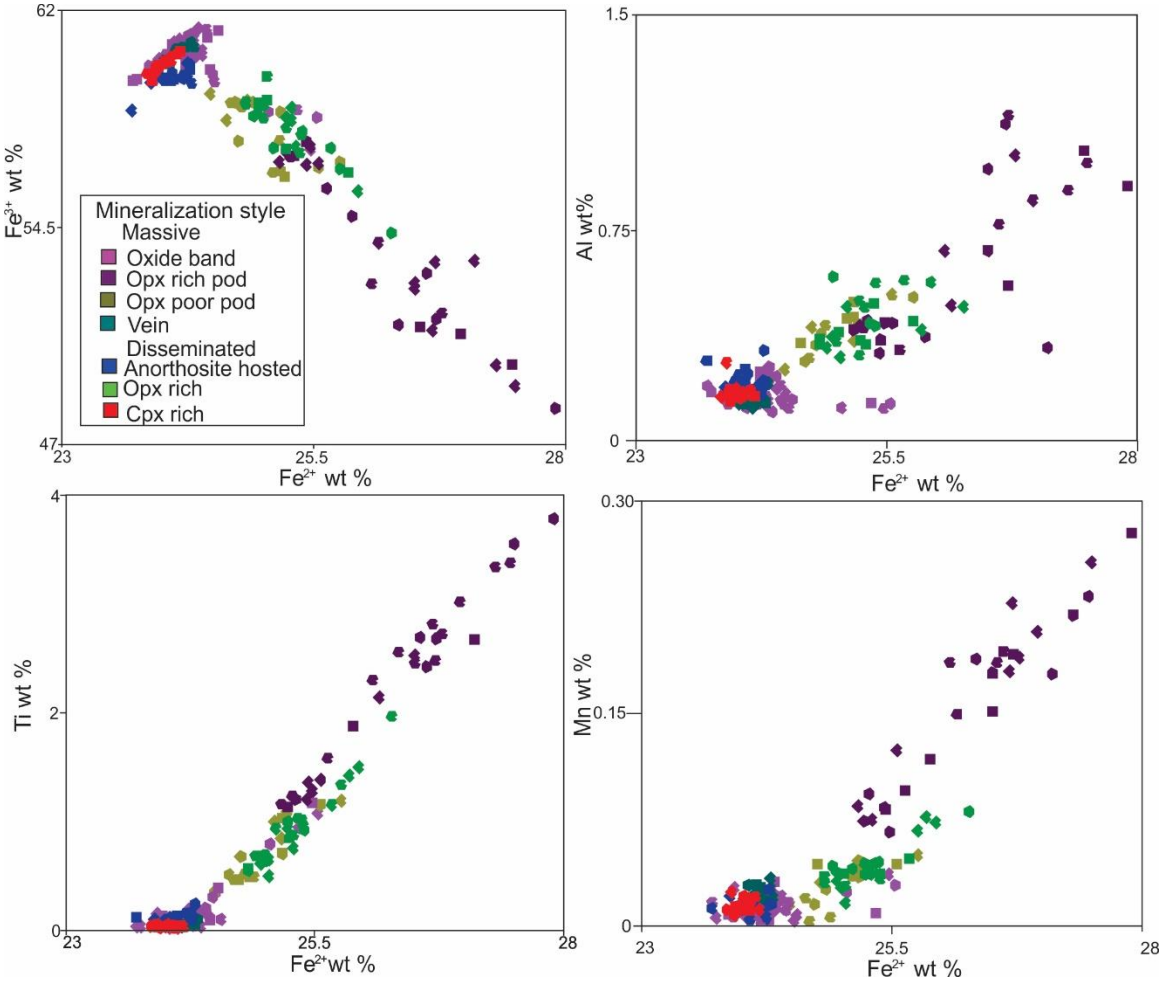

Figure 4.2. Binary element variation diagrams of EPMA magnetite analyses showing a negative correlation between Fe^{2+} and Fe^{3+} coupled with positive correlations between Fe^{2+} and Mn, Al (hercynite substitution), and Ti (ilmenite substitution). The positive correlation between Mn and Fe^{2+} suggests the presence of the pyrophanite ($MgTiO_3$) substitution which is commonly associated with ilmenite.

Amongst the various ilmenite textural types, a pattern of variation of the ilmenite textures was observed. Ferrous iron is most abundant in the ilmenite containing spinel microcrystals, slightly less abundant in the sandwich ilmenite, and least abundant

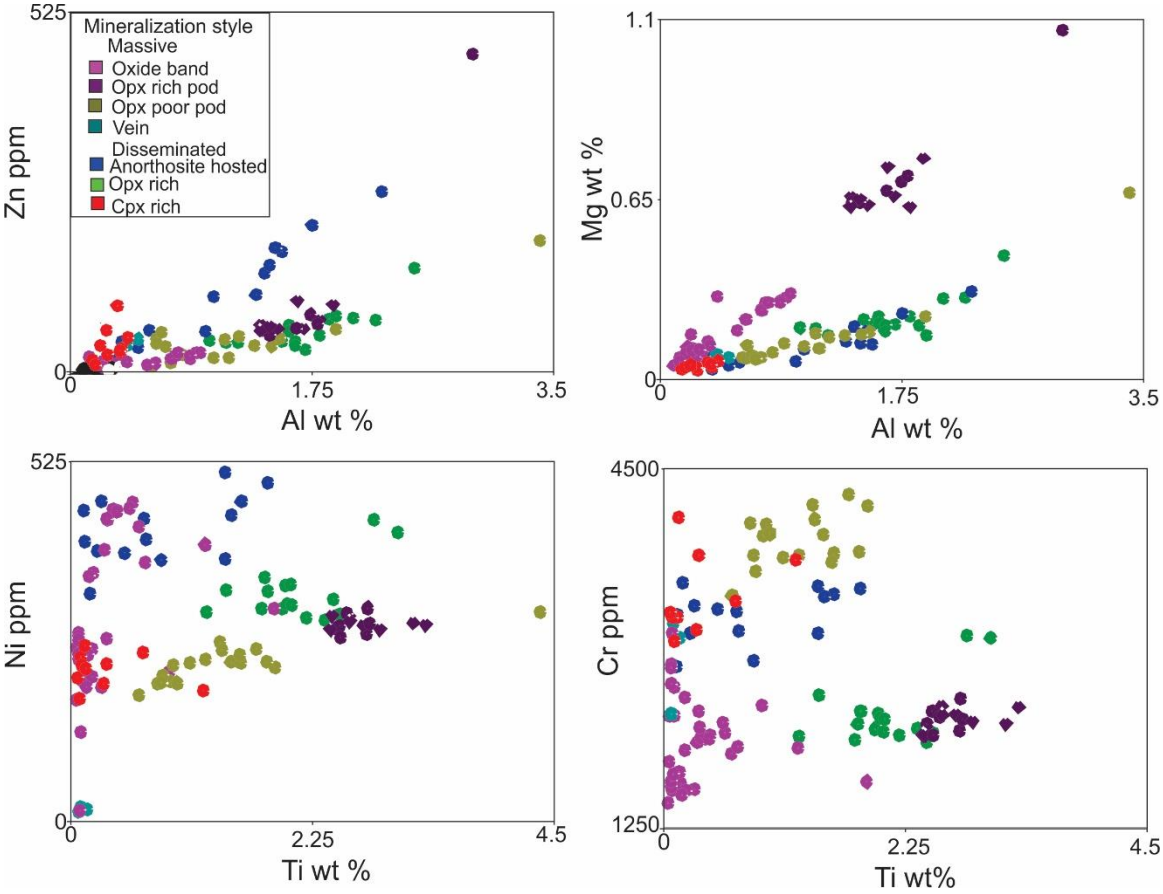

Figure 4.3. Binary variation diagram from LA-ICPMS magnetite analyses showing positive correlations between Al, and Mg (spinel substitution) as well as Zn, and Al (gahnite substitution). Two trends are observed on the Ti vs Ni graph; one with a low Ti:Ni ratio and one with a high Ti:Ni ratio. Two trends are also observed on the Ti vs Cr graph, one with a low Ti:Cr ratio and one with a high ratio.

in composite ilmenite grains with exsolution lamellae. The same pattern is shown by Ti, which is most abundant in samples containing abundant Fe^{2+}, and least abundant in samples that are richer in Fe^{3+}. This pattern suggests a paragenesis of ilmenite; first coarse grained ilmenite with exsolution features are formed, then coarse ilmenite without exsolution features are formed, then sandwich ilmenite, and then finally the ilmenite containing spinel microcrystals are exsolved.

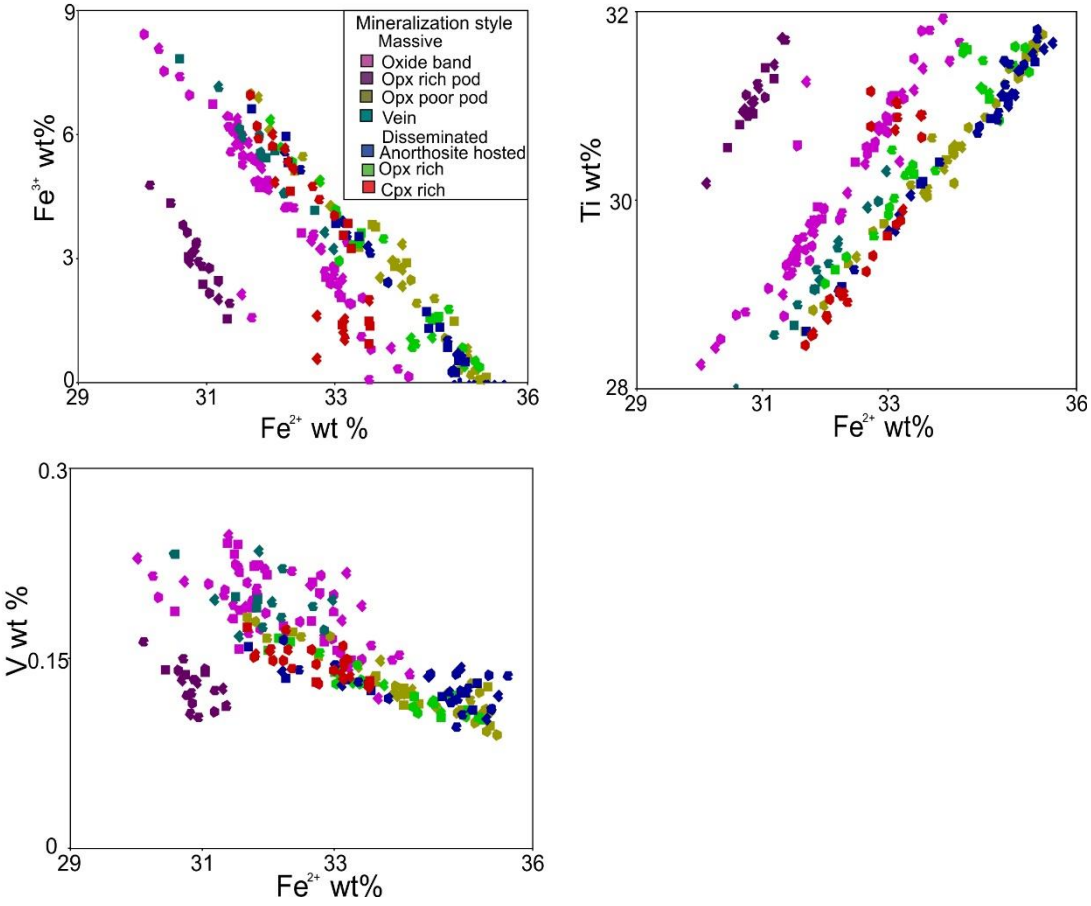

Figure 4.4. Binary variation diagram from EPMA ilmenite analyses showing negative correlations between Fe^{2+} and both V and Fe^{3+} and a positive correlation between Fe^{2+} and Ti.

The major- and minor-element chemical variation in ilmenite between the different mineralization styles is minimal; V and Mg are slightly enriched in bands of oxide mineralization. The largest variation is observed in the orthopyroxene-bearing massive oxide pods in which Ti and Mg are enriched, and coupled with a depletion in Fe^{2+} relative to other samples.

Variations in the trace element composition of ilmenite occur in the different mineralization styles (Fig. 4.5). Orthopyroxene-poor bands of oxide mineralization are

enriched in Mg, Ni, and Sc, and slightly depleted in Nb compared to other mineralization styles. Whereas orthopyroxene-bearing bands are also enriched in Ni and Mn. Orthopyroxene-poor pods are depleted in Sc and Mn, and orthopyroxene-bearing pods are relatively enriched in Mg and Sc, and depleted in Nb, Cr, and Mn.

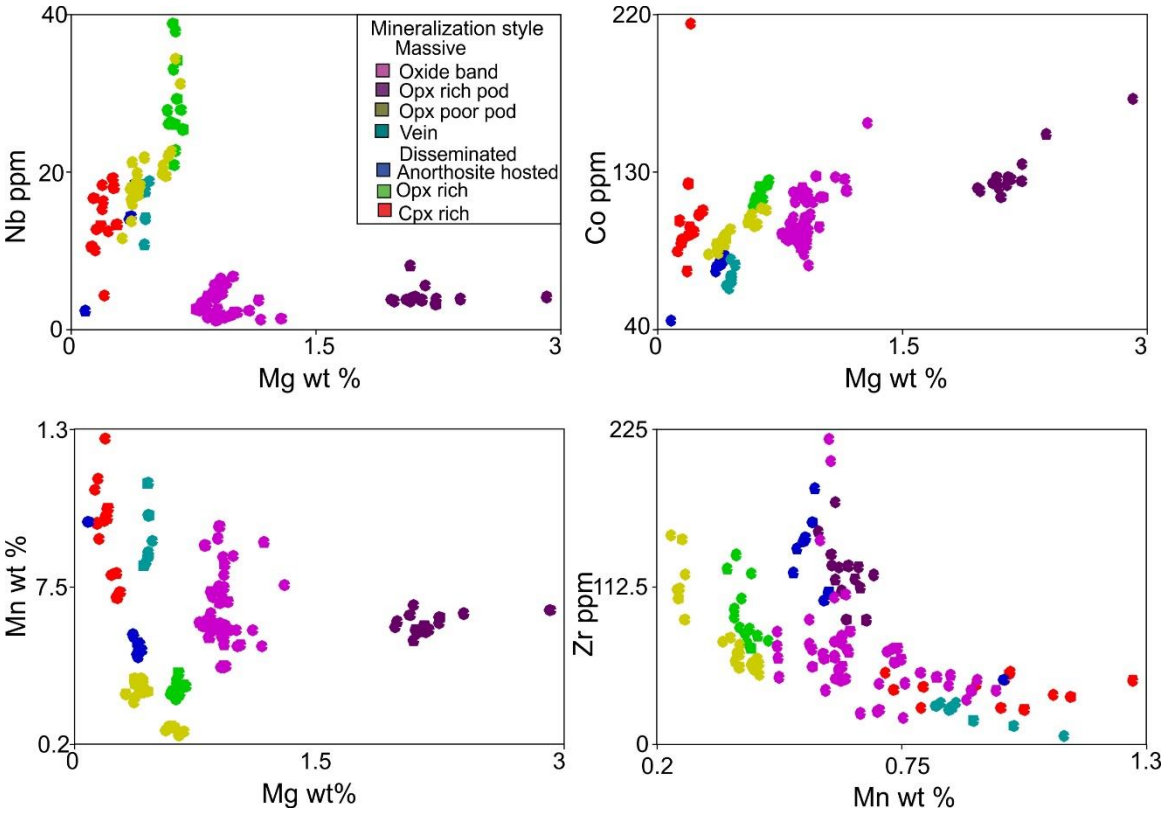

Figure 4.5. Binary element variation diagrams from ilmenite LA-ICPMS analyses. Two trends observed in the Mg vs Nb graph, one with high Nb and low Mg and the other with low Nb and high Mg. A positive correlation is present between Mg and Co. A negative correlation is present between Mn and Zr. Vertical linear trends in several mineralization styles in the Mg vs Mn binary variation diagram.

Veins of oxide mineralization are relatively enriched in Sc, moderately enriched in Zn, Cr, V, and Mn, and depleted in Co, Zr, and Ni relative to other samples. Anorthosite-hosted disseminated oxide mineralization and orthopyroxene-bearing disseminated oxide mineralization are enriched in Ni compared to other types, and anorthosite-hosted

disseminated oxide mineralization is depleted in Co. The clinopyroxene-bearing disseminated oxide mineralization is enriched in Zn, Cr, and Mn, and depleted in Mg and Zr relative to other ilmenite samples.

4.1.4.3 Pleonaste chemistry

Relatively few pleonaste analyses were done during the course of this study due to the lack of analyzable pleonaste in the samples studied rendering it difficult to infer trends in the pleonaste compositions from the different sample types and pleonaste mineralization styles. Pleonaste lamellae hosted in ilmenite, however, are higher in Ti and lower in Fe^{3+} compared to coarse-grained pleonaste hosted in magnetite suggesting the chemical composition of pleonaste is associated with the host oxide mineralogy.

4.1.5 EPMA discrimination diagrams

The trace- and minor-element composition of magnetite is thought to systematically vary with changes in factors such as temperature of crystallization, as well as both the chemical composition, and redox state of parental fluid or magma during magnetite crystallization (Buddington and Lindsley, 1964; Lindsley, 1976; Dupuis and Beaudoin, 2011; Dare et al., 2014; Knipping et al., 2015).

Based on this principle, several magnetite discrimination diagrams have been proposed with fields based on empirical observations generated from a database of in-situ analyses that have been previously interpreted as hydrothermal and magmatic magnetite associated with various types of ore deposits. Two groups of discrimination diagrams exist: those which differentiate hydrothermal and magmatic magnetite; and those which differentiate magnetite from various ore deposit types. Both types of discrimination diagrams have commonly been used and/or modified in a number of recent studies (e.g.,

Huang et al., 2014; Hu et al., 2015). However, other recent studies have questioned the accuracy, validity, and usefulness of these diagrams (e.g. Hu et al., 2015; Broughm et al., 2017; Wen et al., 2017). In this section, the effectiveness of empirical magnetite discrimination diagrams will be evaluated using analyses from a magnetite dominated magmatic Fe-Ti-V deposit hosted in a Proterozoic massif anorthosite suite.

Dupuis and Beaudoin (2011) proposed two empirical diagrams which discriminate magnetite from various ore deposits. The first, which uses Ca + Al + Mn in wt. % as the Y-axis variable, and Ti + V in wt. % as the X-axis variable (Fig. 4.7a), does not provide meaningful results for the analyses from the present study. Approximately half of the data plot in the Fe-Ti, V field, whereas other samples plot between the "porphyry" and "Kiruna-type" fields. The data show a strong positive correlation between Ti + V content and Ca + Al + Mn content, with orthopyroxene -bearing samples containing the most abundant amounts of both Ca + Al + Mn and Ti + V.

Likewise, the second Dupuis and Beaudoin (2011) discrimination diagram, which uses Ni/(Cr+Mn) that is calculated from ppm values of each element as the Y-axis variable and Ti + V in wt.% as the X-axis variable (Fig. 4.7b) also does not effectively discriminate magnetite data from this study. The data are spread across the "Fe-Ti, V oxide", "porphyry" and "skarn" fields. All magnetite analyses in the present study show similar Ni/(Cr+Mn) ratios with widely variable Ti contents; the highest Ti content is present in the orthopyroxene -bearing samples. In both of the Dupuis and Beaudoin (2011) discrimination diagrams, the samples with the highest Ti contents plot correctly within the "Fe-Ti, V oxide field".

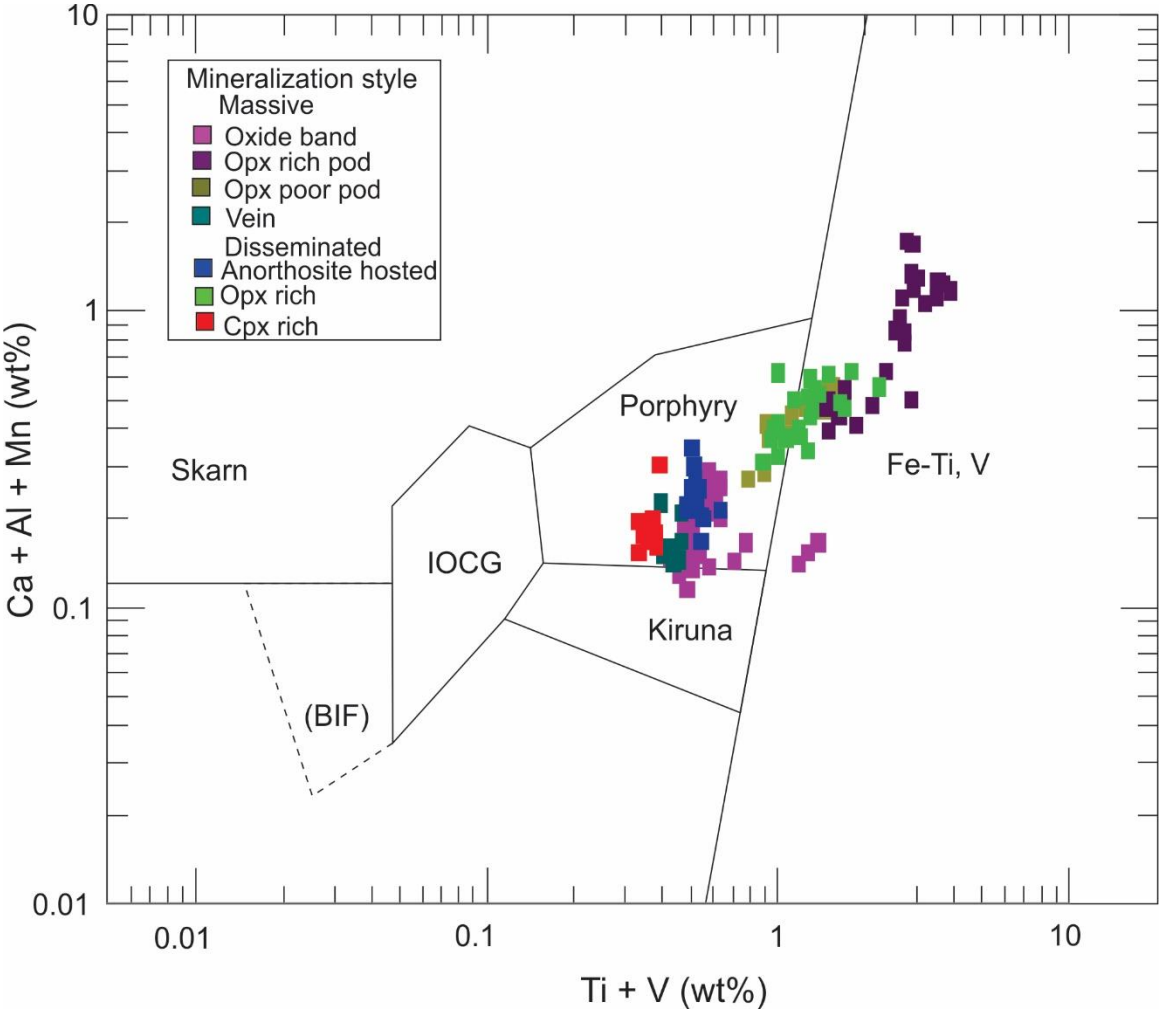

Figure 4.7a. Magnetite ore deposit discrimination diagrams of Dupuis and Beaudoin (2011). A) Diagram using Ca + Al + Mn (wt. %) as the Y axis and Ti + V (wt. %) as the X axis, B) Diagram using Ni/(Cr + Mn) as the Y axis and Ti + V (wt. %) as the X axis. Magnetite analyses from this study were plotted on the diagram. See text for details.

Knipping et al. (2015) proposed an empirical discrimination diagram for discriminating magmatic and hydrothermal magnetite using the in situ Ti and V (ppm) content in magnetite as the respective X and Y axes (Fig. 4.8).

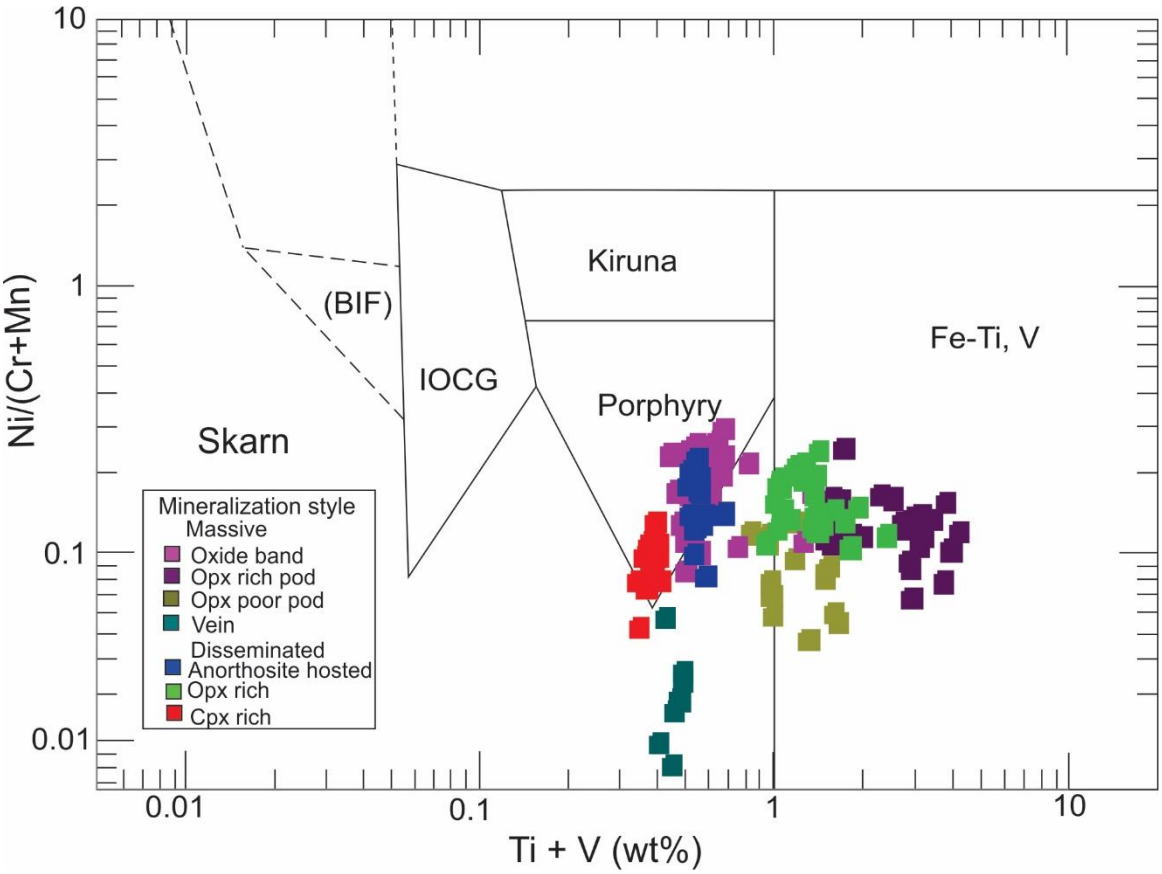

Figure 4.7b. Magnetite ore deposit discrimination diagrams of Dupuis and Beaudoin (2011). A) Diagram using Ca + Al + Mn (wt. %) as the Y axis and Ti + V (wt. %) as the X axis, B) Diagram using Ni/(Cr + Mn) as the Y axis and Ti + V (wt. %) as the X axis. Magnetite analyses from this study were plotted on the diagram. See text for details.

This diagram is not effective for most of the data from the present study; the majority of coarse-grained magnetite data plot above the defined discrimination fields. Data points for primary magnetite have similar V contents, with the exception of analyses from clinopyroxene associated disseminated oxide mineralization which have slightly lower V contents. The Ti content is much more variable; samples with the highest Ti content plot correctly within the magmatic magnetite field.

Dare et al. (2014) presented an empirical diagram to discriminate magmatic and hydrothermal magnetite. The diagram uses Ni/Cr and Ti content as the X and Y axes,

respectively (Fig. 4.9). Data from this study plot within the magmatic magnetite field, thus this diagram appears to be effective for the analyses in the present study.

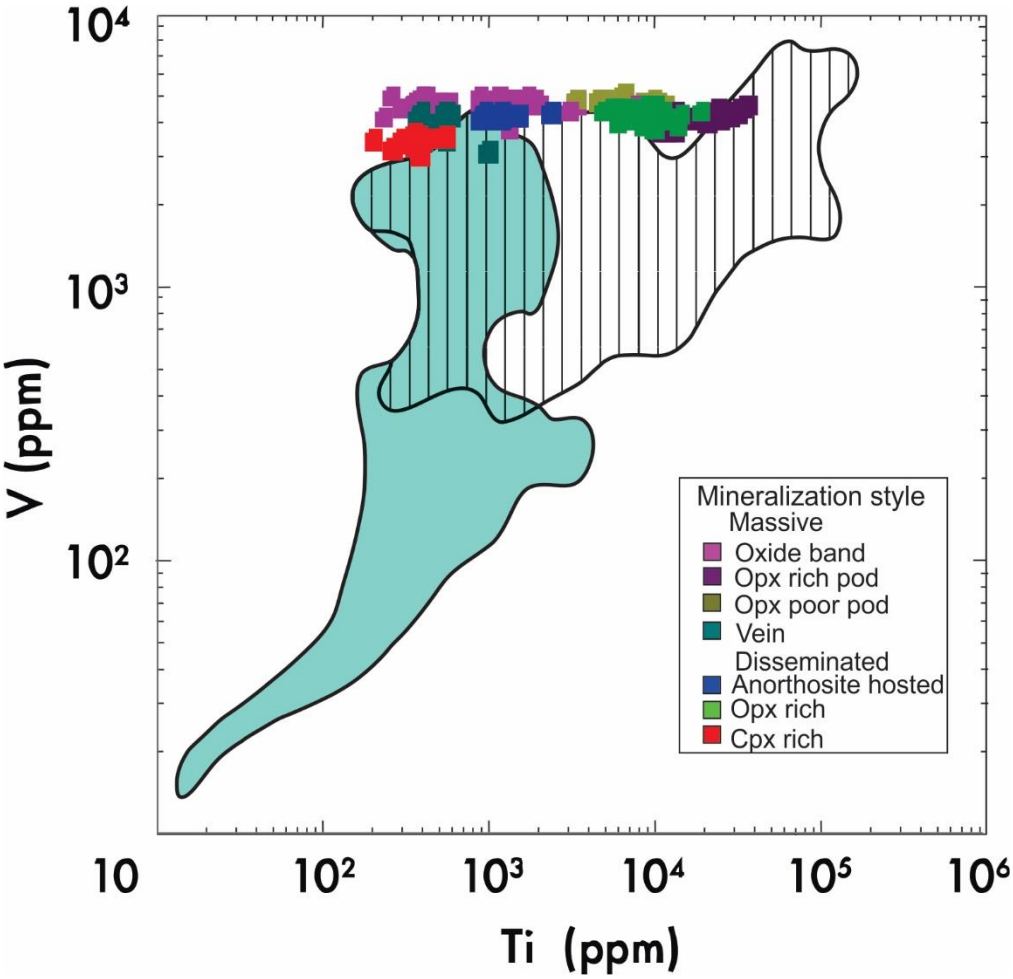

Figure 4.8. Hydrothermal vs magmatic discrimination diagram proposed by Knipping et al. (2015) using Ti as the X axis and V for the Y axis. The diagram contains three fields; a magmatic magnetite field (vertical lines), a hydrothermal magnetite field (teal field) and a magmatic-hydrothermal magnetite field (vertical lines on a teal field) Most primary magnetite data from this study plots above all fields of the discrimination diagram due to its high V content.

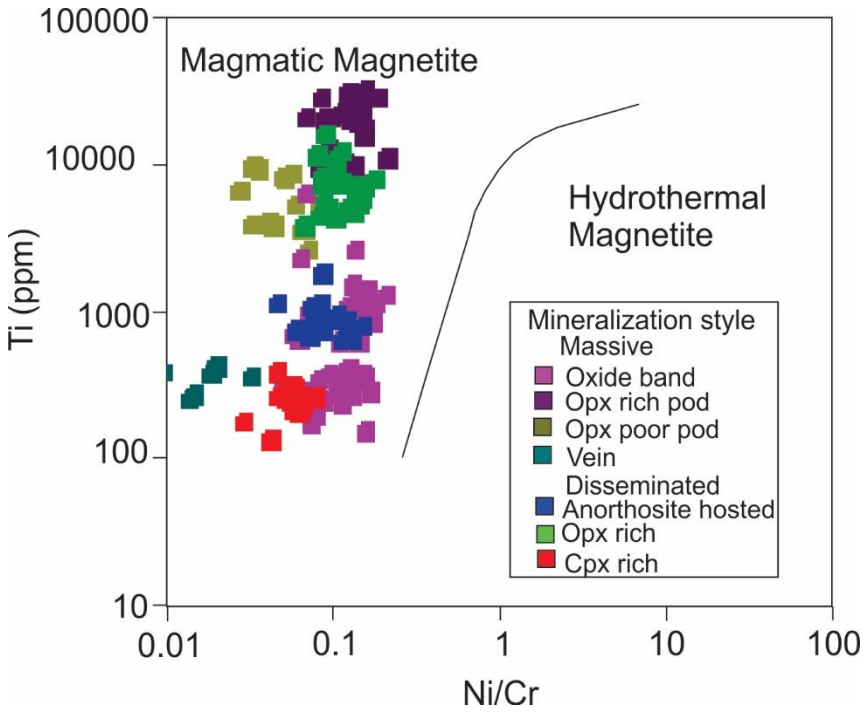

Figure 4.9. Hydrothermal vs magmatic discrimination diagram proposed by Dare et al. (2014) using Ni/Cr as the X axis and Ti (ppm) as the Y axis. All magnetite analyses, regardless of mineralization style plot in the magmatic field.

With the exception of the Dare et al. (2014) diagram, the aforementioned discrimination diagrams, which make use of the major- and minor-element composition of magnetite, were ineffective when considering data from this study. There are two possible reasons for this. First, the Ti and/or Al contents are used as axis variables in each of the discrimination diagrams. However, the Ti and Al contents in magnetite are known to be modified by exsolution of ilmenite and pleonaste, respectively. Furthermore, reequilibration processes are known to occur during cooling and metamorphism. Because in situ analyses from this study systematically avoided exsolution microtextures, the magnetite analyzed is not representative of its primary magmatic compositions, which is what the fields on the discrimination diagrams are based on. Secondly, the data used to

generate the Fe-Ti, V field on the Dupuis and Beaudoin (2011) diagrams does not include data from magnetite-dominated Proterozoic massif anorthosite hosted Fe-Ti-V deposits. For this reason, magnetite from the present study most likely do not plot within the Fe-Ti, V oxide field. As such, the Fe-Ti, V oxide field needs to be modified or removed, or magnetite mineral separate analyses could be used instead of in situ analyses. Analyzing magnetite mineral separates could re-homogenized magnetite and contained exsolution features in order to gain insight into the primary magmatic composition of magnetite.

4.1.6 LA-ICPMS Discrimination diagrams

Dare et al. (2014) proposed a multi-element empirical discrimination diagram for magnetite. LA-ICPMS analyses of Mg, Al, Si, P, Ca, Sc, Ti, V, Cr, Mn, Co, Ni, Cu, Zn, Ga, Ge, Y, Zr, Nb, Mo, Sn, Hf, Ta, W, and Pb are used in the diagram (Fig. 4.10 a-c). The data are normalized to bulk continental crust values (Rudnick and Gao, 2003). The normalized values are plotted on a line diagram in order of increasing compatibility in magnetite.

Because the trace element composition of magnetite is thought to reflect the composition of the melt or fluid from which it crystallized, discrimination fields for magnetite from magmatic Fe-Ti-V deposits (primitive magnetite), Fe-Ti-P deposits (evolved magnetite), high-T hydrothermal deposits, felsic plutons, and andesite were proposed as different fields on the diagram. For the purpose of this study, only the high-T hydrothermal magnetite and magmatic Fe-Ti-V oxide fields were considered because those fields most closely match proposed models for genesis of Fe-Ti oxide mineralization in Proterozoic massif anorthosite suites (Charlier et al., 2014). The high-T

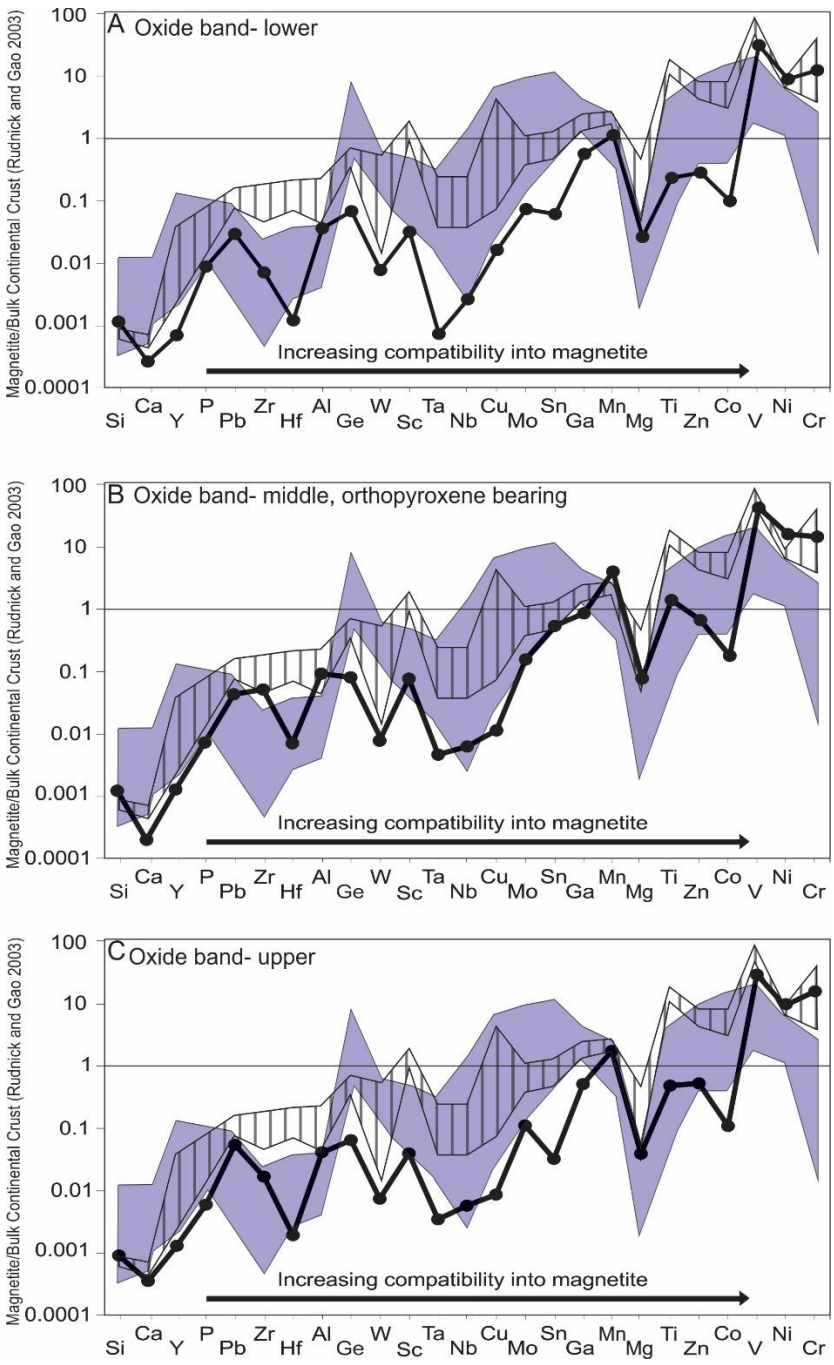

Figure 4.10a. Discrimination diagram for trace-element LA-ICPMS analyses proposed by Dare et al. (2014). The trace element composition of magnetite is normalized to bulk continental crust of Rudnick and Gao (2003) and organized in order of compatibility in magnetite. Discriminant fields for Fe-Ti-V magmatic magnetite (vertical stripes) and high-T hydrothermal magnetite (periwinkle) are plotted. Data from this study were averaged and plotted on separate figures by mineralization style as labelled on each diagram.

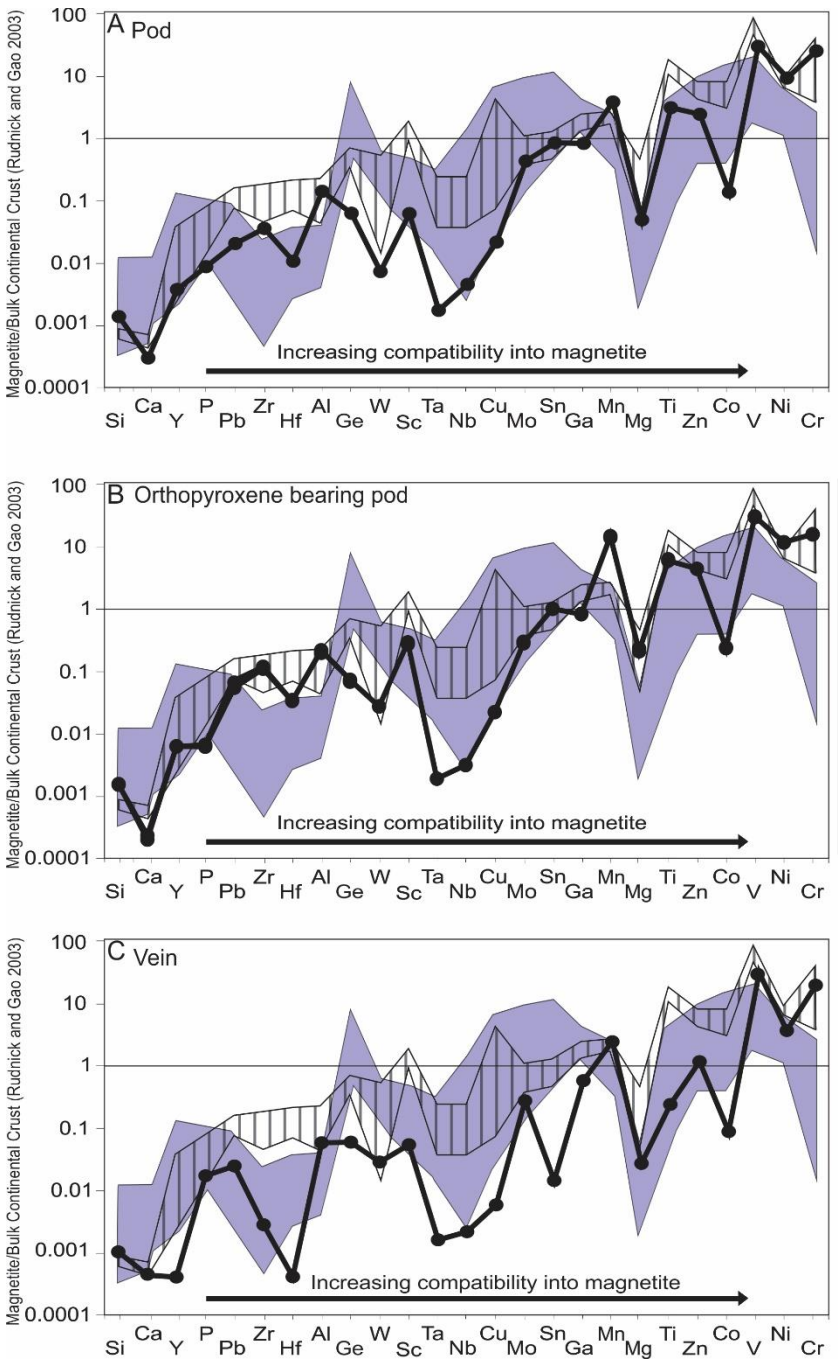

Figure 4.10 b. Discrimination diagram for trace-element LA-ICPMS analyses proposed by Dare et al. (2014). The trace element composition of magnetite is normalized to bulk continental crust of Rudnick and Gao (2003) and organized in order of compatibility in magnetite. Discriminant fields for Fe-Ti-V magmatic magnetite (vertical stripes) and high-T hydrothermal magnetite (periwinkle) are plotted. Data from this study were averaged and plotted on separate figures by mineralization style as labelled on each diagram.

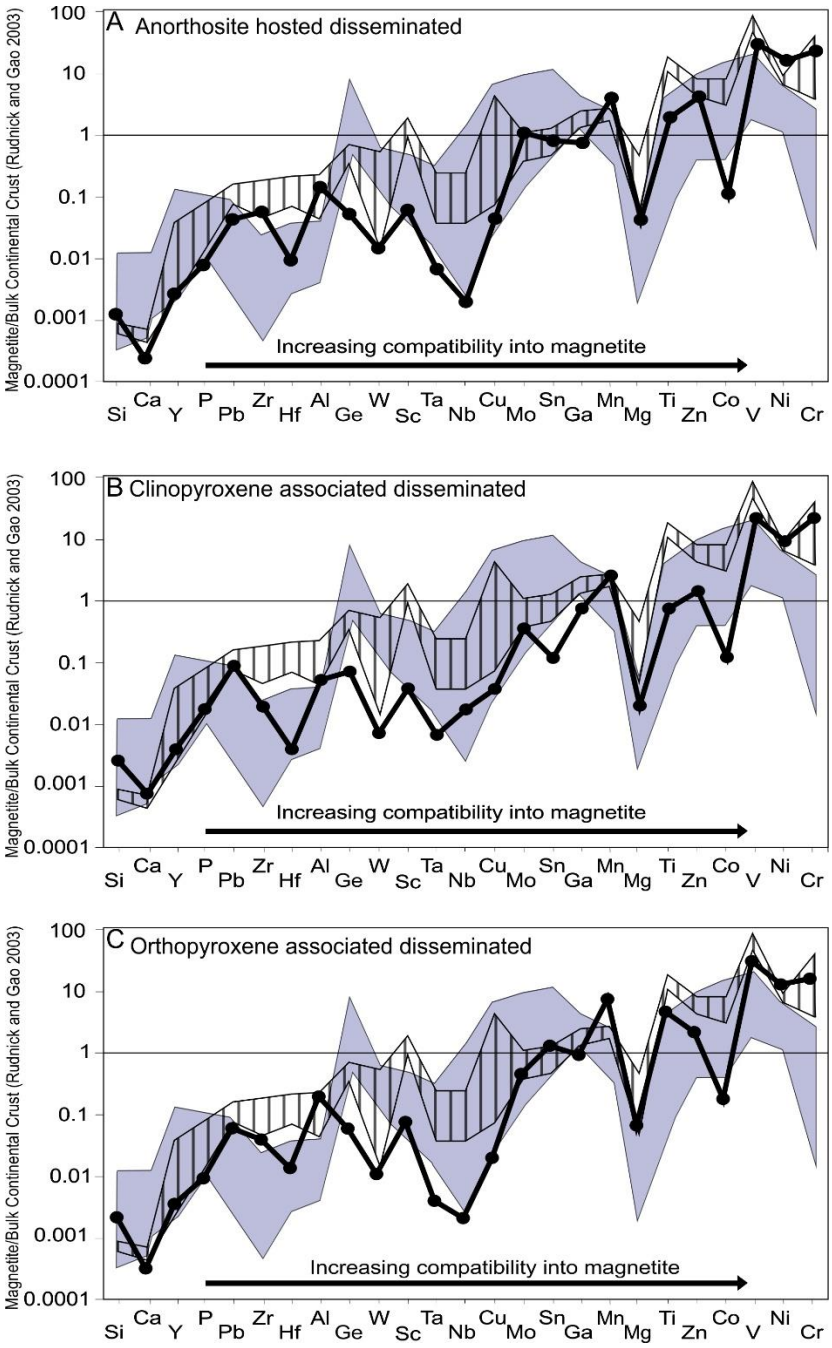

Figure 4.10 c. Discrimination diagram for trace-element LA-ICPMS analyses proposed by Dare et al. (2014). The trace element composition of magnetite is normalized to bulk continental crust of Rudnick and Gao (2003) and organized in order of compatibility in magnetite. Discriminant fields for Fe-Ti-V magmatic magnetite (vertical stripes) and high-T hydrothermal magnetite (periwinkle) are plotted. Data from this study were averaged and plotted on separate figures by mineralization style as labelled on each diagram.

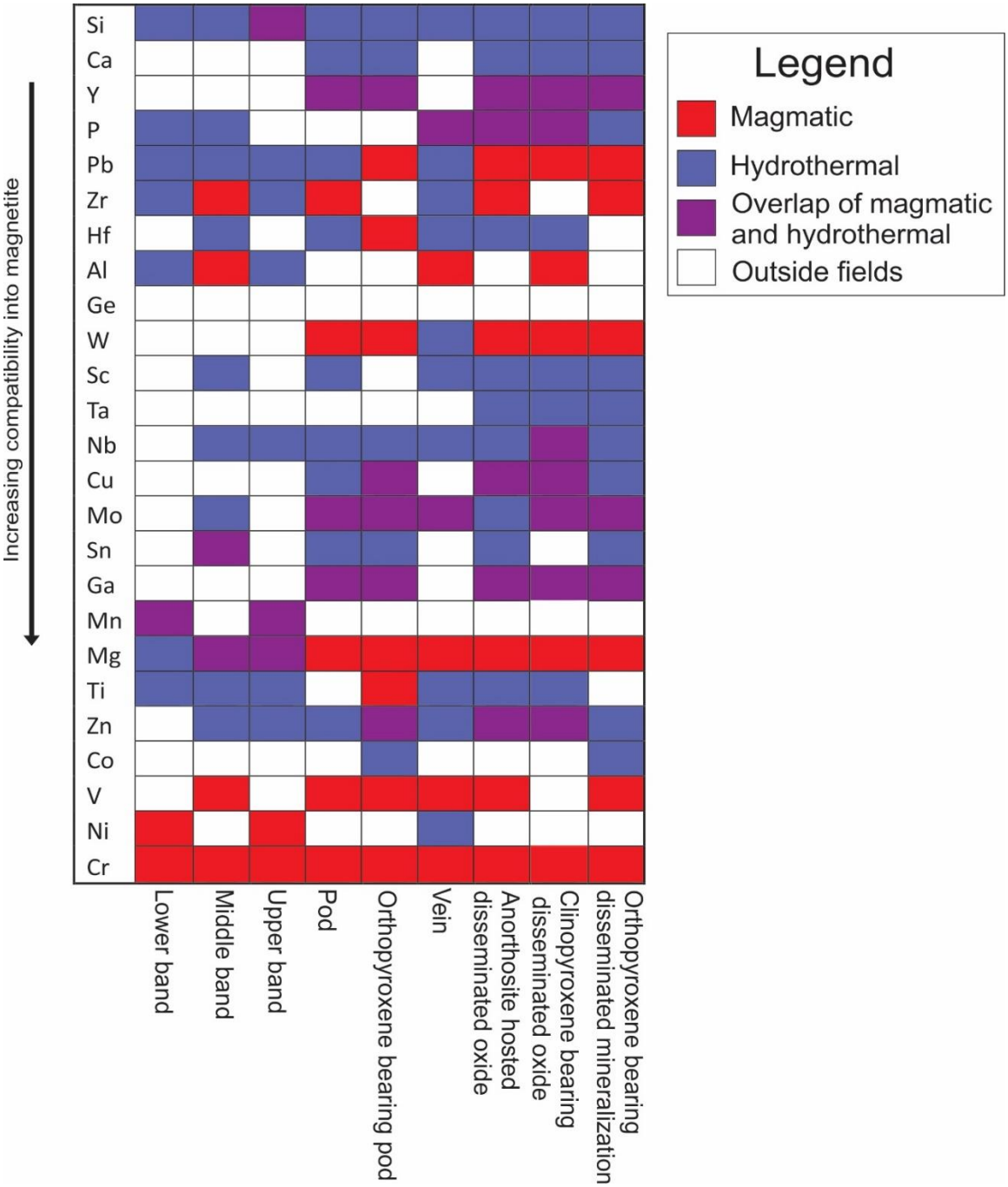

Figure 4.11. Companion figure to Fig. 3.5.7a-c showing the plotting area of magnetite analyses from various mineralization styles. Red squares represent points plotting within the magmatic magnetite field, blue squares represent points plotting within the hydrothermal field, purple squares represent points plotting in the overlap between magmatic and hydrothermal fields and white squares represent points plotting outside of any field.

hydrothermal and magmatic Fe-Ti-V magnetite fields overlap in the majority of the elements measured in the present study.

Complete overlap occurs with Si, Y, P, Ta, Nb, Cu, Mo, Sn, Ga, Mn, Zn, and Co, and partial overlap occurs in Ca, Ge, and W, so these elements are not useful for discrimination purposes using this empirical discrimination diagram. Only Pb, Zr, Hf, Al, Ti, V, Ni, and Cr do not have any overlap, so these elements are the most useful for discriminating between magmatic and high-T hydrothermal magnetite, however, the geological rationale for why these elements plot where they do needs to be more adequately explained.

Regardless of the mineralization style, data from this study did not consistently plot uniquely in either field; the analyses plotted variably within the high-T magmatic field, hydrothermal field, at the overlap of both fields, or outside of the fields (Fig. 4.10 a-c). The lack of clear affinity with either of the fields defined by Dare et al. (2014) is also illustrated by the block diagram in Fig. 4.11 and suggests a limited utility of this diagram.

The reason that these empirical discrimination diagrams are ineffective is unclear, however, it may have to do with the chemical modification of oxide minerals during sub-solidus exsolution and reequilibration of magnetite during hydrothermal alteration or metamorphism, or that the geologic rationale behind the fields defined on the diagrams is not valid.

4.2 Genesis and evolution of oxide mineralization

It is well known that Fe-Ti oxide mineralization hosted in Proterozoic massif anorthosite suites is broadly magmatic in nature (Charlier et al., 2014, and references therein). However, the specific processes for oxide formation and concentration varies

between deposits. In this section, oxide formation models proposed by other workers are summarized, and Fe-Ti oxide mineralization from this study is compared to each model.

4.2.1 Liquid Immiscibility

Proponents of liquid immiscibility as a formation process for Fe-Ti oxide mineralization in massif anorthosite suites suggest that residual magma from anorthosite crystallization is mafic in nature and enriched in Fe, Ti, and P. Fractional crystallization of this residual magma is thought to lead to the formation of an immiscible Fe-Ti-P melt and conjugate K_2O-rich silicate rocks, thought to include perthitic norite or mangerite (Chen et al., 2013). The immiscible Fe-Ti-P melt crystallizes into zones of massive apatite-bearing Fe-Ti oxide mineralization that is devoid of silicate minerals, sometimes referred to as nelsonites (Chen et al., 2013).

Liquid immiscibility is thought to generate large zones of nelsonite in discordant veins or pods that have sharp irregular contacts with host anorthosite; disseminated nelsonite is interstitial to plagioclase in the host anorthosite (Philpotts, 1967; Chen et al., 2013; He et al., 2016). Disseminated nelsonite is also known to crosscut plagioclase or pyroxene crystals, form rims on ferromagnesian silicates, and can contain rafts of host anorthosite (Chen et al., 2013).

However, it is unclear if immiscible Fe-Ti oxide melts can exist in nature in these systems. Evidence of coexisting immiscible Fe-Ti oxide and silicate melts has not been observed in the NWRA and has also not been reported in plutonic settings globally. Experiments that generated immiscible Fe-Ti oxide and silicate melts were done at 1420˚C, which is a geologically unreasonable high temperature (Philpotts, 1967; Lindsley, 2003; Charlier and Grove, 2012; Lindsley and Epler, 2017).

Within the NWRA, discordant zones of massive to semi-massive oxide mineralization, vein-like massive oxide mineralization are commonly observed, and disseminated Fe-Ti oxide minerals occur both interstitial to host plagioclase and partially rimming pyroxene, as predicted by the liquid immiscibility model. However, apatite is not observed to be associated with oxide mineralization in the NWRA, and nelsonites are not observed in the field area as is typical of Fe-Ti oxide mineralization generated via liquid immiscibility (e.g., Kolker, 1982; Chen et al., 2013; She et al., 2014; Peng et al., 2015; She et al., 2016); in fact, in whole rock geochemical analyses, there is a negative correlation between FeO content (which is associated with Fe-Ti oxide mineralization) and P content (which is associated with apatite). As such, it is unlikely that liquid immiscibility is responsible for the genesis of Fe-Ti oxide mineralization in the NWRA.

4.2.2 Magma mixing

Magma mixing is a process thought to be responsible for formation of stratiform chromite deposits and has been extrapolated for use in stratiform Fe-Ti oxide deposits. In this process, a fractionating mafic magma is intruded by a more primitive mafic magma, or contaminated by a pre-existing siliceous rock. The interaction between the two magmas generates a hybrid magma which crystallizes a single mineral which sinks to the base of the magma chamber creating a mono-mineralic layer of the crystallized mineral (Irvine, 1975; Irvine et al., 1983; Charlier et al., 2010).

Evidence of magma mixing includes rhythmically alternating monomineralic layers of oxide and silicate minerals in sharp, straight contact with the underlying layer and in sharp to gradational contact with the overlying layer (Irvine, 1975; Irvine et al., 1983). Geochemical evidence of magma mixing includes large variations in compatible

elements such as Mg, Mn, V, and Cr in Fe-Ti oxide minerals between layers (Charlier et al., 2010).

Rhythmically alternating mono-mineralic layers of oxides and silicates are not observed in the NWRA. In fact, aside from host anorthosite, mono-mineralic zones of any texture or composition are not observed in the NWRA. Although all massive oxide mineralization is in sharp contact with host anorthosite the contacts are irregular. Furthermore, the in situ analyses of magnetite and ilmenite show little to no variation in Cr and V between samples. As such, it is unlikely that magma mixing is responsible for oxide genesis.

4.2.3 Hydrothermal remobilization

Hydrothermal remobilization is a process in which plagioclase containing microinclusions of Fe-Ti oxide minerals is pervasively altered to fine-grained albite, clinozoisite, and sericite (Li et al., 2014). During alteration, the Fe-Ti oxide microinclusions are dissolved into solution until they reprecipitate along pre-existing fractures, or in lenticular bodies generating zones of nelsonite in sharp, irregular contact with the adjacent anorthosite (Li et al., 2014). Contacts with host anorthosite are lined by zones of massive chlorite or chloritized anorthosite (Li et al., 2014).

Irregular unconformable zones of massive Fe-Ti oxide mineralization are observed in the NWRA, however these zones are not associated with pre-existing fractures, do not contain apatite, and are not associated with chlorite. Furthermore, plagioclase in the host anorthosite has been minimally altered. As such, hydrothermal remobilization is likely not responsible for the genesis of Fe-Ti oxide mineralization.

4.2.4 Fractional Crystallization

Fe-Ti-P enriched mafic magma termed jotunites or ferrodiorites associated with anorthosite genesis are thought to be carried from depth with diapirically rising anorthosite crystal mush (Vander Auwera and Longhi, 1994). Due to rheological differences, the Fe-Ti-P enriched mafic magma pools in zones of low pressure where it begins to fractionally crystallize. Calculated cotectic crystallization values suggest the resulting rock would be an oxide-bearing gabbronorite containing ~20 wt. % Fe-Ti oxide minerals along with a combination of clinopyroxene, orthopyroxene, olivine, and apatite (Charlier et al., 2007; 2008). Oxide-bearing gabbronorite is not observed in the NWRA and as such, fractional crystallization is likely not the sole process responsible for genesis of oxide mineralization in the NWRA.

4.2.5 Solid state remobilization

Solid-state remobilization is a process that concentrates existing oxide minerals into zones of massive to semi-massive mineralization rather than generating new oxide minerals. Due to ductility differences between oxide minerals and plagioclase, Fe-Ti oxide minerals can recrystallize and migrate to zones of low pressure via diffusion creep in subsolidus conditions, such as those present during diapiric uplift of the host anorthosite (Krause and Pedall, 1980; Duchesne 1996; 1999). On the scale of an anorthosite suite, this deformation could concentrate large irregular zones of massive to semi-massive oxide mineralization in sharp, irregular contact with the host anorthosite, disseminated oxide mineralization that is interstitial to plagioclase in the host anorthosite, as well as disseminated oxide mineralization rimming ferromagnesian silicate minerals (Duchesne, 1996; 1999).

Evidence of solid state remobilization includes zones of massive oxide mineralization in sharp, irregular contact with host anorthosite, veins of oxide discordantly crosscutting host anorthosite, oxide minerals interstitial to plagioclase, and oxides partially rimming and crosscutting clinopyroxene. Furthermore, solid-state remobilization does not predict the presence of apatite associated with oxide mineralization, as is the case in the NWRA. Finally, inclusions and rafts of plagioclase, anorthosite, and orthopyroxene can also be explained via solid state remobilization.

Solid-state remobilization predicts the presence of mono-mineralic ilmenite bodies; however, it is unclear if the process can be used to explain the presence of magnetite, ilmenite and pleonaste which are observed in the NWRA. The presence of orthopyroxene-bearing massive to semi-massive oxide mineralization spatially associated with orthopyroxene-poor massive to semi-massive oxide mineralization cannot be easily explained using this model. Finally, solid-state remobilization can explain concentrations of Fe-Ti oxide minerals, however it cannot explain the genesis of the oxide minerals observed.

4.2.6 Effect of cooling and metamorphism on oxide chemistry

Fe-Ti oxide minerals are known to experience extensive amounts of subsolidus reequilibration during periods of slow cooling as well as during metamorphism (Buddington and Lindsley, 1964; Duchesne, 1970; Lindsley, 1991). The net effect of reequilibration is purification of the oxide minerals towards their end-member compositions by means of exsolution, oxide-oxide reequilibration and oxide-silicate reequilibration (Buddington and Lindsley, 1964).

The presence of abundant and complex exsolution features observed in oxide minerals in the NWRA suggest that the in situ oxide analyses are not representative of primary magmatic compositions, rather, they are representative of the point at which exsolution and inter-oxide reequilibration ceased. Microtextures composed of pleonaste and ilmenite in magnetite, as well as granular ilmenite and pleonaste adjacent to magnetite suggests that primary magmatic magnetite contained higher abundances of Ti, Al and Mg compared to the magnetite analyzed. Likewise, the presence of hematite lenses, spinel lamellae and magnetite lamellae in ilmenite suggest that primary ilmenite had a higher hematite component as well as higher Mg and Al contents compared to the analyzed ilmenite. Magnetite lenses in pleonaste suggest that primary pleonaste contained more Fe than analyzed pleonaste. Inter-oxide reequilibration is also responsible for oxide purification. For example, adjacent Ti-magnetite and ilmenite interact following the reaction $FeTi_2O_4$ (in magnetite) + Fe_2O_3 (in ilmenite) -> Fe_3O_4 (in magnetite) + $FeTiO_3$ (in ilmenite) (Buddington and Lindsley, 1964; Duchesne, 1972).

Oxide minerals in the NWRA underwent two periods of reequilibration; 1) during autometamorphism caused by the residual heat of the host anorthosite and 2) during overprinting Grenvillian metamorphism. It is difficult to differentiate which exsolution features are associated with autometamorphism and which are associated with overprinting Grenvillian metamorphism as the grade of Grenvillian metamorphism has not been well constrained within the NWRA. According to Rivers, 2008, the NWRA is located within the Grenvillian orogenic lid, which is thought to have reached a maximum temperature of ~650 ˚C (Cherniak, 2000). As coarse-grained granular exsolution features as well as pleonaste exsolution in magnetite occur at >750 ˚C (Buddington and Lindsley,

1964; Mucke, 2003), those features can be ascribed as autometamorphic features. In contrast, ulvospinel can exsolve from magnetite can occur until ~600 ˚C (Buddington and Lindsley, 1964). Ulvospinel exsolution can be subsequently oxidized to ilmenite at a wide range of temperatures (Buddington and Lindsley, 1964). This suggests that finer grained ilmenite exsolutions in magnetite formed at lower temperatures including during Grenvillian metamorphism. The combined effects of autometamorphism and Grenvillian metamorphism significantly modified primary Fe-Ti oxide compositions to their current near end-member compositions, representing a nearly complete reequilibration process.

Recent studies of Fe-Ti oxide mineralization (e.g., Charlier et al., 2009; Charlier et al., 2010) suggest analyzing oxide mineral separates results in a more accurate representation of true magmatic oxide compositions. Re-integration of exsolution features into the host magnetite using relative abundances of exsolution features coupled with in situ analyses of each type of exsolution feature observed has been used in the past (e.g., Bowles, 1977; Pang et al., 2008). However, these approaches are flawed because they cannot accurately constrain inter-oxide reequilibration, oxide-silicate reequilibration, reequilibration between oxide minerals and trapped liquid or the presence and amount of external granule exsolution, wherein ilmenite and pleonaste granules form at the grain boundaries of magnetite during subsolidus conditions (Buddington and Lindsley, 1964; Duchesne, 1972; Charlier et al., 2009).

The relative proportions of primary oxides and those formed through external granule exsolution in the NWRA is unclear. However, the following observations suggest that ilmenite and pleonaste made up only minor components of the primary magmatic oxide mineral assemblage and the ilmenite and pleonaste granules are instead the product

of external granule exsolution based: 1) in massive oxide mineralization the magnetite is coarser grained than granular ilmenite and pleonaste; 2) in massive oxide mineralization the coarsest ilmenite and pleonaste are spatially associated with each other and are present in clusters; 3) zones enriched in ilmenite or pleonaste relative to magnetite are not observed in either massive to semi-massive mineralization or disseminated oxide mineralization; 4) no coarse granular pleonaste or ilmenite is observed associated with disseminated oxide mineralization; and 5) no disseminated mineralization that is dominated by ilmenite or pleonaste is observed. Similar conclusions are drawn to explain the presence of magnetite-dominated ilmenite-bearing Fe-Ti oxide mineralization hosted in the late Permian, Panzhihua layered gabbro intrusion of southwest China (Pang et al., 2008). Because external granule exsolution occurs at such high temperatures (between <880-600˚C; Buddington and Lindsley, 1964), the exsolution product itself will be impure and upon cooling will contain exsolution features as are observed in coarse granular ilmenite and pleonaste in the NWRA.

4.2.7 Oxygeothermometry

Buddington et al. (1955) showed that in the presence of independent coexisting grains of ilmenite and magnetite, the TiO_2 content of magnetite is a function of the temperature of magnetite crystallization, making it a potential candidate for use as a geothermometer. Further work by Buddington and Lindsley (1964) showed that at a constant temperature, higher fO_2 leads to a decrease in the TiO_2 content of magnetite and an increase in the Fe_2O_3 content of ilmenite, thereby providing a potential magnetite-ilmenite oxygeothermometer. More recent improvements of the oxygeothermometer including additional new experimental data, thermodynamic calculations, and improved

algorithms for data calculation allow for estimates of the equilibrium conditions of magnetite and ilmenite to ±30˚C and the fO_2 to within one order of magnitude (Powell and Powell, 1977; Andersen et al., 1993; Lattard et al., 2005; Ghiorso and Evans, 2008).

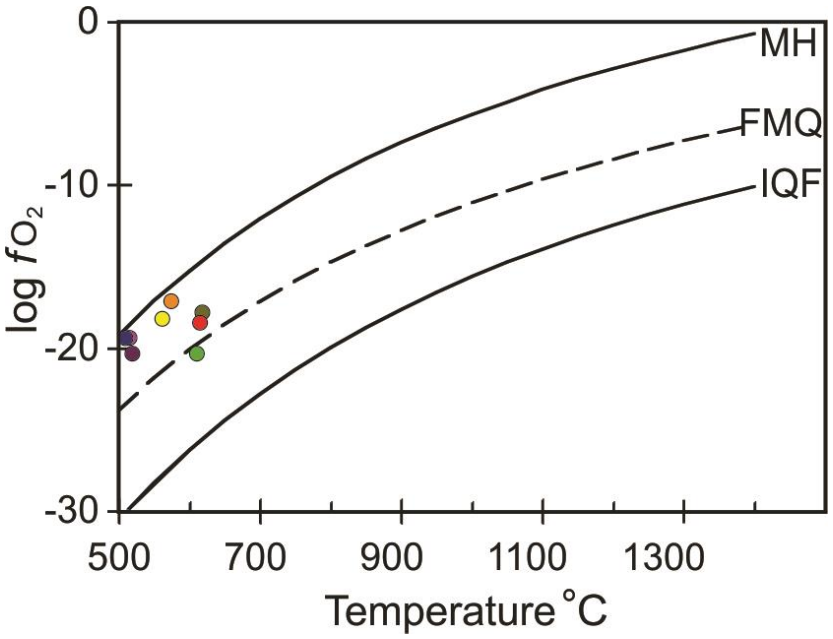

Figure 4.12. Diagram of log fO_2 vs T (in ˚C) values calculated using the magnetite-ilmenite oxygeothermometer calculated using in-situ values from ILMAT (Lepage, 2003). The calculated values show the temperature and fO_2 conditions at which oxide reequilibration ceased in the NWRA. Buffer assemblage abbreviations: MH- magnetite-hematite, FMQ- fayalite magnetite quartz, IQF- iron-quartz-fayalite.

Magnetite-ilmenite oxygeothermometry was applied to analyses of the earliest texturally identifiable magnetite and composite ilmenite containing exsolution microtextures from in situ analyses of samples collected in the NWRA. These textural varieties were selected as they were inferred to have formed at the earliest point of crystallization or subsolidus processes. The method of Stormer (1983) was used to determine the ulvospinel component in magnetite and the ilmenite component in ilmenite and the oxygeothermometer calibration of Andersen and Lindsley (1985) was used to

calculate the T and fO_2 values for each mineralization style. Calculated equilibration temperatures from all mineralization styles ranged from 487-619˚C, and log fO_2 values ranged from -17.1 to -20.3 (Fig. 4.12). The calculated temperature ranges corresponds with the end of subsolidus reequilibration and exsolution associated with autometamorphism and Grenvillian metamorphism rather than primary magmatic compositions of magnetite and ilmenite (Vincent et al., 1957; Buddington and Lindsley, 1964; Tan et al., 2017).

4.2.8 Oxide genesis, concentration and evolution in the NWRA

Summarising the previous conclusions, Fe-Ti oxide mineralization in the NWRA shows evidence of a three-step formation process: 1) late-stage magmatic crystallization of impure magnetite; 2) concentration by solid-state remobilization and/or crystal sorting; and 3) reequilibration during subsequent post-emplacement cooling and subsequent Grenvillian metamorphism. Evidence of the process responsible for the genesis of the oxide mineralization has largely been destroyed during recrystallization of oxides and host anorthosite, oxide remobilization, and subsolidus exsolution and reequilibration of the oxide minerals.

The original formation process of the Fe-Ti oxide mineralization must be able to explain the presence of large quantities of impure magnetite, as well as both orthopyroxene -bearing and orthopyroxene poor oxide mineralization. Either magma mixing or fractional crystallization of a Fe-Ti-P -bearing mafic silicate magma may have been responsible for the genesis of the oxide mineralization, however without further evidence the specific formation process is not clear at present.

During diapiric rise of the anorthosite suite, two processes are thought to be able to concentrate oxide minerals: 1) differential stress on the host anorthosite causes the more ductile Fe-Ti oxide minerals to concentrate in zones of low pressure in the less ductile anorthosite via diffusion creep (Duchesne, 1996; 1999); or 2) density based crystal sorting concentrates Fe-Ti oxide mineralization (Pang et al., 2008). Either process could create zones of pure mono-mineralic Ti, Al, Mg -bearing magnetite in sharp, irregular contact with the host anorthosite. It is evident that deformation ceased at high temperatures as exsolution lamellae of pleonaste and ilmenite in magnetite have not undergone subsequent deformation.

Finally, as the massive mono-mineralic magnetite cooled, it began to exsolve, and reequilibrate to form the textures observed at present. At highest temperatures, coarse granules of pleonaste and ilmenite were formed at grain boundaries of magnetite followed by all other textures of pleonaste, magnetite and ilmenite exsolution. The long period of slow cooling resulted in the coarse to very coarse-grained nature of the oxide mineralization as well as the near end-member concentrations of magnetite and ilmenite.

4.3 Economic Potential of Fe-Ti oxide mineralization in the NWRA

Proterozoic massif anorthosite suites are known to contain large concentrations of Fe, Ti, V and P which are typically hosted in or associated with Fe-Ti oxide mineralization (Charlier et al., 2014). Fe-Ti oxide mineralization in the NWRA contains magnetite and ilmenite which are the typical sources of Fe, Ti and V. The economic potential of Fe-Ti-V oxide mineralization is linked to the grade and abundance of oxide minerals as well as oxide mineralogy, the in situ compositions of oxide minerals including economic and deleterious elements. Presently, Ti can only be economically

extracted from ilmenite and rutile; Ti hosted in magnetite and titanite is of little value and has low demand because it cannot be economically extracted (Force, 1991; Charlier et al., 2014). In contrast, Fe and V can be economically extracted from magnetite. The trace element composition of oxide minerals also affects economic potential. Cr, V, Mn, Mg and hematite component in ilmenite are deleterious to extraction of high quality TiO_2 and thus, impure ilmenite is less attractive for processing than more pure ilmenite (Force, 1991).

There are currently two operating mines in massif anorthosite suites that predominantly mine Ti. The Lac Tio deposit (Québec), is the largest known hard-rock ilmenite deposit where an ilmenite-rich norite that grades at 32-38 wt.% TiO_2 over 138Mt is mined (Charlier et al., 2010). Ilmenite from the Lac Tio deposit typically contains 2.5-3 wt. % MgO which is considered a moderate value compared to other known deposits (Charlier et al., 2010). The ore of the Tellnes deposit (Norway) is also an ilmenite-rich norite which grades at ~18 wt. % TiO_2 with over 57 Mt of ore. The MgO content in ilmenite in the Tellnes deposit ranges from 1.4-4.4 wt. % with hematite content of ilmenite ranging from 10-14 mol% (Charlier et al., 2006; 2007). Unlike the two aforementioned deposits, the Damiao (China) deposit contains magnetite, ilmenite, and apatite and is mined for Ti, Fe, V and P. The Damiao deposit averages grades of 36 wt. % Fe_2O_3, 7.0 wt. % TiO_2, 0.3 wt. % V_2O_5 and 2 wt. % P and its oxide mineralization is predominantly massive in nature with minor occurrences of disseminated oxides (Charlier et al., 2014). Ilmenite from the Damiao deposit has low concentrations of Cr and Mg and a low mol fraction hematite (<7 wt. %) (Chen et al., 2013).

Vanadium is not typically mined as the primary commodity in any deposit at present, instead, it is extracted as a byproduct of mining for other metals. The largest global sources of V are contained within vanadiferous magnetite hosted in large layered mafic intrusions. The Rhovan deposit, which is a part of the Bushveld Complex in South Africa contains the largest reserves of V currently being mined. Ore from the Rhovan deposits is hosted in a titaniferous magnetite gabbro and grades on average at 0.5 wt. % V_2O_5 in bulk samples over 26Mt in proven reserves and ~200Mt in other types of resource estimates (Glencore website http://www.glencore.com/investors/reports-and-results/reserves-and-resources).

The Panzhihua deposit (China) is hosted in mafic-ultramafic intrusions in the Emishian Large Igneous Province in southwest China and contains reserves of 1.2 Bt grading at 33.2% Fe_2O_3, 11.6% TiO_2 and 0.3% V_2O_5 (Zhou et al., 2013). Undeveloped Canadian V deposits include the Lac Doré and De La Blache deposits which are anorthosite-hosted magnetite-dominated Fe-Ti oxide deposits in the Grenville province of Québec (Charlier et al., 2014). Of the North American deposits, the Lac Doré deposit is the largest with reserves of about 100 Mt at a grade of 0.49% V_2O_5 (0.28% V) (Taner et al., 2000). The Maracas deposit of Brazil is an orebody of vanadium-rich titanomagnetite which has ore reserves that grade at 1.17 wt.% V_2O_5 over 18.4 Mt and ~50Mt grading between 0.85 and 1.24 wt.% V_2O_5 (Largo resources website http://www.largoresources.com/investors/financial-reports/default.aspx).

Mineralization in the NWRA is predominantly hosted in irregular zones of massive to semi-massive oxide that is dominated by V-rich magnetite and minor ilmenite. On average, whole-rock geochemistry results of massive to semi-massive oxide

mineralization in this study show that it contains ~10 wt.% TiO_2, 62 wt.% $FeO_{(t)}$ and 2700 ppm V (0.48 wt.% V_2O_5). In-situ magnetite analyses typically contain <0.5 wt. % TiO_2 to a maximum value of ~4 wt. % whereas V_2O_5 contents typically range from 0.6-0.7 wt. %. In-situ analyses of coarse ilmenite typically have values of ~1 wt. % Mg, 5-7 mol% hematite component and negligible Cr and Al content which is amenable to economic potential.

Zones of massive to semi-massive oxide mineralization within the NWRA have similar to slightly lower Fe, Ti, and V grades compared to the deposits described above. However, at surface, zones of massive oxide mineralization are sporadically distributed and dwarfed in volume by barren anorthosite. The amount of barren anorthosite between zones of massive oxide mineralization significantly dilutes the grades of the ore. Furthermore, individual pods of massive to semi-massive oxide mineralization are too small to be efficiently targeted for extraction while avoiding the unmineralized anorthosite. If mineralization at depth is similar to the mineralization observed at surface, the economic potential of the NWRA is limited. However, it is impossible to accurately determine the grade and abundance of oxide mineralization without having a proper 3-D context provided by either detailed geophysical analysis or drill core. Unfortunately, this work has not yet been completed in the NWRA.

REFERENCES

Andersen DJ, Lindsley DH, Davidson PM (1993) QUILF: A pascal program to assess equilibria among Fe-Mg-Mn-Ti oxides, pyroxenes, olivine, and quartz. Computers & Geosciences 19: 1333-1350

Andersen DJ, Lindsley DH (1985) New (and final!) models for the Ti-magnetite/ilmenite geothermometer and oxygen barometer. Abstract AGU 1985 Spring Meeting EOS Transactions. American Geophysical Union 66, 416

Ashwal LD (1993) Anorthosites. Spinger-Verlag, Berlin

Bowles JF (1977) A method of tracing the temperature and oxygen-fugacity histories of complex magnetite-ilmenite grains. Mineralogical Magazine 41: 103-109

Broughm SG, Hanchar JM, Tornos F, Westhaus A, Attersley S (2017) Mineral chemistry of magnetite from magnetite-apatite mineralization and their host rocks: examples from Kiruna, Sweden and El Laco, Chile. Mineralium Deposita 52: 1223-1244

Buddington AF, Lindsley DH (1964) Iron-titanium oxide minerals and synthetic equivalents. Journal of Petrology 5: 310-357

Buddington AF, Fahey J, Vlisidis A (1955) Thermometric and petrogenetic significance of titaniferous magnetite. American Journal of Science 497-532

Charlier B, Grove TL (2012) Experiments on liquid immiscibility along tholeiitic liquid lines of descent. Contributions to Mineralogy and Petrology 164: 27-44

Charlier B, Namur O, Bolle O, Latypov R, Duchesne JC (2014) Fe-Ti-V-P ore deposits associated with Proterozoic massif-type anorthosites and related rocks. Earth-Science Reviews 141: 56-81

Charlier B, Namur O, Malpas S, de Marneffe C, Duschene JC, Vander Auwera J, Bolle O (2010) Origin of the giant Allard Lake ilmenite ore deposit (Canada) by fractional crystallization, multiple magma pulses and mixing. Lithos 117: 119-134

Charlier B, Namur O, Duchesne JC, Wisniewska J, Parecki A, Vander Auwera J (2009) Cumulate origin and polybaric crystallization of Fe-Ti oxide ores in the Suwalki anorthosite, NE Poland. Economic Geology 104: 205-221

Charlier B, Sakoma E, Sauvé M, Stanaway K, Vander Auwera J, Duchesne JC (2008) The Grader layered intrusion (Havre-Saint-Pierre Anorthosite, Quebec) and genesis of nelsonite and other Fe–Ti–P ores. Lithos 101: 359-378

Charlier B, Duchesne JC, Vander Auwera J (2006) Magma chamber processes in the Tellnes ilmenite deposit (Rogaland Anorthosite Province, SW Norway) and the formation of Fe-Ti ores in massif type anorthosites. Chemical Geology 234: 264-290

Charlier B, Skår Ø, Korneliussen A, Duchesne JC, Vander Auwera J (2007) Ilmenite composition in the Tellnes Fe–Ti deposit, SW Norway: fractional crystallization, postcumulus evolution and ilmenite–zircon relation. Contributions to Mineralogy and Petrology 154: 119-134

Chen WT, Zhou MF, Zhao TP (2013) Differentiation of nelsonitic magmas in the formation of the ~1.74Ga Damiao Fe-Ti-P ore deposit, North China. Contributions to Mineralogy and Petrology 165: 1342-1362

Dare SA, Barnes SJ, Beaudoin G, Meric J, Boutroy E, Potvin-Doucet C (2014) Trace elements in magnetite as petrogenetic indicators. Mineralium Deposita 49: 785-796

Duchesne JC (1970) Microtextures of Fe-Ti oxide minerals in the South Rogaland anorthositic complex (Norway). Annales de la Societe Geologique de Belgique 93: 197-251

Duchesne JC (1972) Iron-titanium oxide minerals in the Bjerkrem-Sogndal Massif, southwestern Norway. Journal of Petrology 13: 57-81

Duchesne JC (1996) Liquid ilmenite or liquidus ilmenite: a comment on the nature of ilmenite vein deposits. In: Demaiffe D. (ed) Petrology and geochemistry of magmatic suites of rocks in the continental and oceanic crust. A volume dedicated to Professor Jean Michot, Universite Libre de Bruxelles, Royal Museum for Central Africa, pp 73-82

Duchesne JC (1999) Fe-Ti deposits in Rogaland anorthosites (South Norway): geochemical characteristics and problems of interpretation. Mineralium Deposita 34: 182-198

Dupuis C, Beaudoin G (2011) Discriminant diagrams for iron oxide trace element fingerprinting of mineral deposit types. Mineralium Deposita 36: 319-355.

Force E (1991) Geology of titanium-mineral deposits. Geological Society of America, Special Paper 259

Ghiorso MS, Evans BW (2008) Thermodynamics of rhombohedral oxide solid solutions and a revision of the Fe-Ti two oxide geothermometer and oxygen-barometer. American Journal of Science 308: 957-1039

Glencore Resources (2016) 2016 reserves and resources report, August 2, 2017. [For updated information see Glencore Resources website - http://www.glencore.com/investors/reports-and-results/reserves-and-resources)

He HL, Yu SY, Song XY, Du ZS, Dai ZH, Xie W (2016) Origin of nelsonite and Fe–Ti oxide ore of the Damiao anorthosite complex, NE China: Evidence from trace element geochemistry of apatite, plagioclase, magnetite and ilmenite. Ore Geology Reviews 79: 367-381

Hu H, Li JW, Lentz D, Ren Z, Zhao XF, Deng XD, Hall D (2014) Dissolution-reprecipitation process of magnetite from the Chengchao iron deposit: insights into ore genesis and implication for in-situ chemical analysis of magnetite. Ore Geology Reviews 57: 393-405

Huang XW, Gao JF, Qi L, Meng YM, Wang YC, Dai ZH (2015) In-situ LA-ICPMS trace element analysis of magnetite: the Fenghuangshan Cu-Fe-Au deposit, Tongling, Eastern China. Ore Geology Reviews 72: 746-759

Irvine TN (1975) Crystallization sequences in the Muskox intrusion and other layered intrusions—II. Origin of chromitite layers and similar deposits of other magmatic ores. Geochimica et Cosmochimica Acta 39: 991-1020

Irvine TN, Keith DW, Todd SG (1983) The JM platinum-palladium reef of the Stillwater Complex, Montana; II, Origin by double-diffusive convective magma mixing and implications for the Bushveld Complex. Economic Geology 78: 1287-1334

Kerr A, Walsh JA, Sparkes GW, Hinchey JG (2013) Vanadium potential in Newfoundland and Labrador: a review and assessment. Current Research, Newfoundland and Labrador Geological Survey 13: 137-165

Knipping JL, Bilenker LD, Simon AC, Reich M, Barra F, Deditus AP, Walle M, Heinrich CA, Holtz F, Munizaga R (2015) Trace elements in magnetite from massive iron oxide-apatite deposits indicate a combined formation by igneous and magmatic-hydrothermal processes. Geochimica Cosmochimica Acta 171: 15-38

Krause H, Pedall G (1980) Fe–Ti mineralization in the Åna–Sira anorthosite, Southern Norway. Metallogeny of the Baltic Shield. Finland Geological Survey Bulletin 307: 56-83

Largo Resources (2016) Annual consolidated financial statements for the years ending December 31, 2016 and 2015, August 2, 2017. [For updated information see Largo Resources website - http://www.largoresources.com/investors/financial-reports/default.aspx]

Li H, Li L, Zhang Z, Santosh M, Liu M, Cui Y, Yang X, Chen J, Yao T (2014) Alteration of the Damiao anorthosite complex in the northern North China Craton: Implications for high-grade iron mineralization. Ore Geology Reviews 57: 574-588

Lindsley and Epler (2017) Do Fe-Ti-oxide magmas exist? Probably not! American Mineralogist 102: 2157-2169

Lindsley DH (1976) The crystal chemistry and structure of oxide minerals as exemplified by the Fe-Ti oxides. In Oxide Minerals. Mineralogical Society of America, Short Course Notes 3: L1-L60

Lindsley DH (1991) Experimental studies of oxide minerals. Reviews in Mineralogy and Geochemistry 25: 69-109

Lindsley DH (2003) Do Fe-Ti oxide magmas exist? Geology: yes; Experiments: no! (Extended abstract) Norges geologiske undersøkelse Special Publication 9: 34-36

Pang KN, Zhou MF, Lindsley D, Zhao D, Malpas J (2008) Origin of Fe-Ti oxide ores in mafic intrusions: evidence from the Panzhihua intrusion, SW China. Journal of Petrology 49: 295-313

Philpotts AR (1967) Origin of certain iron-titanium oxide and apatite rocks. Economic Geology 62: 303-315

Powell R, Powell M (1977) Geothermometry and oxygen barometry using coexisting iron-titanium oxides: a reappraisal. Mineralogical Magazine 41: 257-263.

Rudnick RL, Gao S (2003) Composition of the continental crust. Treatise on Geochemistry 3: 1-64

Stormer JC (1983) The effects of recalculation on estimates of temperature and oxygen fugacity from analyses of multicomponent iron-titanium oxides. American Mineralogist 68: 586-594

Tan W, Lie P, He H, Wang CY, Liang X (2017) Mineralogy and origin of exsolution in Ti-rich magnetite from different magmatic Fe-Ti oxide-bearing intrusions. The Canadian Mineralogist 54: 539-55

Taner MF, Gault RA, Ercit TA (2000) Vanadium mineralization and its industry in Canada. Geological Association of Canada, Mineral Deposits Division. The Gangue, Issue 65.

Vander Auwera J, Longhi J (1994) Experimental study of a jotunite (hypersthene monzodiorite): constraints on the parent magma composition and crystallization conditions (P, T, fO_2) of the Bjerkreim-Sokndal layered intrusion (Norway). Contributions to Mineralogy and Petrology 118: 60-78

Vincent EA, Wright JB, Chevallier R, Mathieu S (1957) Heating experiments on some natural titaniferous magnetites. Mineralogical Magazine 31: 625-655

Wen G, Li JW, Hofstra AH, Koenig AE, Lowers HA, Adams D (2017) Hydrothermal reequilibration of igneous magnetite in altered granitic plutons and its implications for magnetite classification schemes: Insights from the Handan-Xingtai iron district, North China Craton. Geochimica et Cosmochimica Acta 213: 255-270

Zhou T, Fan Y, Yuan F, Zhang L, Qian B, Ma L, Yang X (2013) Geology and Geochronology of magnetite-apatite deposits in the Ning-Wu volcanic basin, eastern China. Journal of Asian Earth Sciences 66: 90-107

Chapter 5: Conclusions and Future Work

5.1 Conclusions

1) Fe-Ti oxide mineralization in the NWRA is coarse-grained and magnetite-dominated, containing minor ilmenite and pleonaste. Fe-Ti oxide mineralization is present in zones of massive to semi-massive oxide mineralization and as disseminated oxide mineralization. Fe-Ti oxide mineralization is in sharp, irregular, contact with the host anorthosite. No textural or in situ chemical variation is observed between mineralization styles.

2) Subsolidus processes including exsolution and reequilibration that occurred during slow cooling of the host anorthosite body coupled with Grenvillian metamorphism have significantly modified the magnetite, ilmenite, and pleonaste chemical compositions, and as a result primary magmatic oxide compositions are not preserved. Therefore the in situ analyses are not representative of the equilibrium conditions of magnetite, ilmenite and pleonaste, rather than their crystallization conditions. It is clear that subsolidus processes occurred both during the post-emplacement period and in response to Grenvillian metamorphism. However, the extent of the subsolidus processes during each event is unclear.

3) EPMA magnetite discrimination diagrams including those by Dupuis and Beaudoin (2011) and Knipping et al. (2015) were not effective. The reason for this ineffectiveness is unclear; however, the use of Ti and/or Al as axis variables for each discrimination diagram may play a role as the Ti and Al content in magnetite is known to be significantly modified during subsolidus exsolution of ilmenite and pleonaste respectively as well as during reequilibration.

4) The multi-element magnetite LA-ICPMS discrimination diagram of Dare et al. (2014) is ineffective for discrimination of magnetite in the case of this study with analyses spread between the magmatic and high-T hydrothermal fields as well as outside of either field.

5) The formation and evolution of Fe-Ti oxide mineralization in the NWRA occurred through three distinct processes: 1) late-stage magmatic crystallization of impure magnetite; 2) concentration by solid-state remobilization and/or crystal sorting; and 3) reequilibration during subsequent post-emplacement cooling and subsequent Grenvillian metamorphism. Textural and chemical evidence of the primary oxide forming process has largely not been preserved during subsequent slow cooling and metamorphism. However, magma mixing or fractional crystallization of Fe-Ti-P enriched mafic silicate magma could also be responsible. Impure magnetite is concentrated in zones of low pressure during the diapiric rise of the host anorthosite through either solid-state remobilization (Duchesne, 1996; 1999) or crystal sorting. During slow cooling and metamorphism the zones of mono-mineralic magnetite underwent exsolution and reequilibration giving rise to the present magnetite, ilmenite and pleonaste mineral assemblage, as well as oxide textures and chemical composition including the coarse-grained granoblastic nature of the Fe-Ti oxide mineralization.

6) Whole-rock massive to semi-massive oxide mineralization and in situ magnetite and ilmenite analyses from the NWRA have similar chemical compositions as ores in presently operating mines and advanced Fe-Ti-V prospects. Whole-rock analyses of massive to semi-massive Fe-Ti oxide mineralization in the NWRA contains ~10 wt. % TiO_2 and 2700 ppm V (0.48 wt. % V_2O_5). In-situ magnetite typically contain <0.5 wt. %

TiO_2 and 0.6-0.7 wt. % V_2O_5. Composite ilmenite contains ~1 wt. % Mg, 5-7 mol% hematite component and negligible Cr and Al content. However, in the NWRA the observed zones of massive to semi-massive oxide mineralization are relatively small and discontinuous compared to the amounts of adjacent anorthosite. It is unclear, due to lack of drill core and geophysical surveys, if the mineralization at depth is similar to that observed at surface, but if so, the economic potential of the field area within the NWRA is limited.

5.2 Future Work

1) A detailed geological map of the area of this study including the spatial relationships between oxide mineralization and host anorthosite, and specifically the orientation of veins and bands of massive to semi-massive oxide mineralization would be invaluable to better understand the formation processes of the Fe-Ti oxide mineralization in the NWRA

2) A detailed geophysical study would help test formation model in 3-D environment and determine continuity of mineralization at depth

3) Oxygen isotope studies to help determine the origin of the Fe-Ti oxide mineralization in the NWRA

4) Ar-Ar geochronology on biotite observed in coronas surrounding oxide mineralization could help to constrain timing of oxide formation/emplacement and cooling history of the NWRA.

5) U-Pb geochronology of zircon and apatite in the oxide mineralization and host anorthosite, and Lu-Hf in zircon and Sm-Nd in the apatite to add additional constraints to

the timing of emplacement, alteration, mineralization, and metamorphism, and the source of the mineralizing fluids.

6) Mineral separate analyses of magnetite, ilmenite and pleonaste to better understand the pre-exsolution chemistry of oxide minerals and to help determine if chemical variations between mineral separate analysis and in situ oxide analysis affect the interpretations and model presented in this study. It is noted, however, that due to external granule exsolution as well as oxide-silicate reequilibration, it is impossible to recreate the primary magnetite chemical composition.

Appendix I. **Sample list with GPS location, and mineralization style of samples analyzed with EPMA and LA-ICPMS.**

Sample	UTM easting	UTM northing	Mineralization style	Notes
CC008	658736	5929043	Massive to semi-massive oxide mineralization	Bands of oxide mineralization - lower
CC010	658736	5929043	Massive to semi-massive oxide mineralization	Bands of oxide mineralization - middle
CC013	658736	5929043	Massive to semi-massive oxide mineralization	Bands of oxide mineralization - upper
CC025	657619	5929902	Massive to semi-massive oxide mineralization	Pod of oxide mineralization
CC031	657605	5929747	Disseminated oxide mineralization	Anorthosite hosted
CC054	667754	5919493	Disseminated oxide mineralization	Orthopyroxene-bearing
CC072	657744	5929747	Massive to semi-massive oxide mineralization	Orthopyroxene-bearing
CC074	658516	5930210	Disseminated oxide mineralization	Clinopyroxene-bearing
CC076B	658237	5929903	Massive to semi-massive oxide mineralization	Vein of oxide mineralization

Appendix II a. Average (mean) and 2σ standard deviation of major, minor and trace element compositions of whole-rock analyses from various rock types observed in the field area.

	Barren Ol - bearing anorthosite avg	n=3 stdev	Barren anorthosite avg	n=37 stdev	Barren gabbronorite avg	n=7 stdev	Disseminated oxide avg	n=2 stdev	disseminated hosted in gabbronorite avg	n=2 stdev
wt.%										
SiO2	49.65	1.29	54.38	1.66	52.86	1.93	40.33	10.10	38.35	5.73
Al2O3	20.79	2.11	26.17	1.31	24.31	0.64	20.26	3.92	15.79	1.83
FeO(t)	8.18	2.29	2.00	1.33	4.18	1.12	20.74	12.92	22.03	6.38
MnO	0.12	0.03	0.02	0.02	0.05	0.03	0.10	0.06	0.16	0.04
MgO	7.89	2.15	0.60	0.96	2.41	1.94	1.46	0.57	3.67	3.78
CaO	8.30	0.92	9.22	0.91	8.81	0.66	6.09	1.63	6.86	3.06
Na2O	3.22	0.41	5.01	0.47	4.49	0.67	3.64	1.12	2.92	0.59
K2O	0.61	0.03	1.14	0.29	1.04	0.33	1.03	0.06	0.83	0.21
TiO2	0.25	0.13	0.27	0.19	0.29	0.22	3.34	1.98	3.63	1.82
P2O5	0.05	0.01	0.06	0.06	0.05	0.03	0.05	0.01	0.04	0.01
LOI	0.17	0.20	0.97	0.58	0.86	0.31	1.17	0.11	1.62	0.79
ppm										
V	43	30	37	27	53	49	796	519	712	169
Cr	10	0	31	37	23	20	455	7	690	962
Co	53	14	7	7	23	7	51	29	96	44
Ni	130	36	25	23	91	64	109	8	184	141
Zn	56	16	16	15	27	11	128	95	135	44
S	440	61	882	1080	2666.7	3201.4	1610	1075	9110	8613
Cu	16	8	44	58	143	181	229	110	698	639
Ga	14	1	18	1	17	2	30	8	27	6
Sr	985	114	1379	114	1272	142	1074	323	798	218
Ba	573	61	929	239	925	330	851	105	576	142
ΣREE + Y + Sc	14	3	15	3	20	9	19	0.3	20	11

Appendix IIa. (Continued)

	Massive to semi-massive oxide mineralization	n=21	Opx -bearing massive to semi-massive oxide mineralization	n=8
	avg	stdev	avg	stdev
wt.%				
SiO2	7.30	6.12	7.68	5.99
Al2O3	10.61	1.97	8.32	0.68
FeO(t)	61.71	7.71	63.76	6.72
MnO	0.27	0.05	0.30	0.01
MgO	2.70	0.82	4.48	2.07
CaO	0.99	0.97	0.41	0.32
Na2O	0.44	0.50	0.11	0.10
K2O	0.36	0.60	0.05	0.04
TiO2	10.25	2.18	9.81	1.72
P2O5	0.01	0.01	0.01	0.01
LOI	0.00	0.00	0.00	0.00
ppm				
V	2704	415	2717	411
Cr	1625	875	2029	1311
Co	154	31	154	15
Ni	234	69	212	41
Zn	338	71	328	38
S	511	641	80	56
Cu	102	62	59	21
Ga	65	7	63	7
Sr	150	157	35	35
Ba	135	129	24	28
ΣREE + Y + Sc	14	4	15	4

Appendix II b. Average (mean) and 2σ standard deviation of in-situ EPMA analyses of observed oxide minerals from various textural occurrences. Total*: total accounting for recalculated FeO; FeO*: measured FeO content.

Magnetite- most primary	Massive oxide band-lower n=9		Massive oxide band-middle n=13		Massive oxide band-upper n=19		Massive oxide pod n=15		Massive oxide vein n=12		Orthopyroxene-bearing oxide pod n=12	
	avg	stdev	avg	stdev	avg	stdev	avg	stdev	avg	stdev	avg	stdev
SiO_2	0.02	0.01	0.01	0.01	0.02	0.01	0.03	0.01	0.01	0.00	0.03	0.01
TiO_2	0.11	0.08	0.27	0.11	0.30	0.51	1.22	0.49	0.09	0.03	3.59	1.34
Al_2O_3	0.32	0.03	0.40	0.05	0.25	0.03	0.73	0.15	0.26	0.05	1.41	0.82
Cr_2O_3	0.27	0.02	0.27	0.04	0.42	0.06	0.60	0.04	0.48	0.05	0.33	0.02
V_2O_3	0.69	0.05	0.72	0.02	0.67	0.03	0.71	0.02	0.60	0.06	0.62	0.04
FeO*	90.80	0.53	91.79	0.32	91.99	0.74	89.98	0.81	91.72	0.34	87.38	1.98
Fe_2O_3 recalculated	66.71	0.42	67.23	0.33	67.35	1.21	64.26	1.20	67.36	0.26	59.64	3.21
FeO recalculated	30.77	0.17	31.30	0.11	31.39	0.43	32.16	0.45	31.10	0.12	33.72	1.04
MnO	0.01	0.01	0.02	0.01	0.02	0.01	0.04	0.02	0.03	0.01	0.19	0.08
MgO	0.06	0.01	0.09	0.02	0.07	0.01	0.05	0.02	0.03	0.01	0.48	0.24
ZnO	0.02	0.01	0.01	0.00	0.02	0.01	0.02	0.01	0.01	0.00	0.02	0.01
NiO	0.03	0.01	0.04	0.01	0.03	0.01	0.03	0.01	0.01	0.00	0.03	0.01
total*	99.00		100.38		100.53		99.85		99.99		100.07	
Total measured	92.32	0.53	93.64	0.26	93.79	0.39	93.41	0.52	93.24	0.32	94.10	0.53

Appendix II b. (Continued)

Magnetite host	Disseminated oxide hosted in anorthosite n=17		Orthopyroxene -bearing disseminated oxide n=24		Clinopyroxene -bearing disseminated oxide n=18	
	avg	stdev	avg	stdev	avg	stdev
SiO_2	0.03	0.01	0.03	0.01	0.02	0.01
TiO_2	0.21	0.06	1.55	0.59	0.06	0.01
Al_2O_3	0.41	0.07	0.78	0.17	0.32	0.05
Cr_2O_3	0.52	0.09	0.34	0.03	0.57	0.08
V_2O_3	0.63	0.01	0.64	0.03	0.51	0.02
FeO*	90.69	0.52	90.32	0.79	91.06	0.36
Fe_2O_3 recalculated	66.32	0.39	64.21	1.32	66.86	0.28
FeO recalculated	31.01	0.20	32.54	0.48	30.89	0.11
MnO	0.02	0.01	0.06	0.02	0.02	0.01
MgO	0.02	0.01	0.07	0.04	0.02	0.01
ZnO	0.01	0.01	0.02	0.01	0.01	0.00
NiO	0.04	0.01	0.03	0.01	0.03	0.00
total*	99.22		100.27		99.31	
Total measured	92.58	0.56	93.84	0.36	92.61	0.34

Appendix II b. (Continued)

Magnetite in ilmenite	Massive oxide band-lower avg n=5	stdev	Massive oxide band-middle avg n=2	stdev	Massive oxide band-upper avg n=10	stdev	Massive oxide pod avg n=8	stdev	Massive oxide vein avg n=9	stdev	Orthopyroxene-bearing oxide pod avg n=5	stdev
SiO_2	0.01	0.00	0.02	0.01	0.01	0.00	0.01	0.00	0.01	0.00	0.01	0.00
TiO_2	1.18	0.32	0.51	0.46	0.10	0.10	1.53	0.43	1.58	0.57	2.43	0.41
Al_2O_3	0.28	0.04	0.50	0.08	0.25	0.03	0.67	0.23	0.26	0.02	0.70	0.10
Cr_2O_3	0.23	0.12	0.21	0.01	0.32	0.05	0.40	0.05	0.25	0.07	0.20	0.02
V_2O_3	0.47	0.15	0.48	0.03	0.56	0.09	0.52	0.10	0.38	0.06	0.56	0.04
FeO*	91.17	0.54	91.49	0.09	92.58	0.49	90.72	0.55	91.47	0.68	89.93	0.38
Fe_2O_3 recalculated	65.70	0.37	66.74	0.69	68.09	0.44	64.63	0.92	65.37	1.00	63.22	0.61
FeO recalculated	32.05	0.49	31.43	0.53	31.29	0.22	32.56	0.41	32.65	0.61	33.05	0.49
MnO	0.01	0.01	0.02	0.00	0.01	0.00	0.01	0.01	0.03	0.01	0.04	0.01
MgO	0.07	0.03	0.10	0.01	0.07	0.02	0.09	0.04	0.03	0.01	0.30	0.03
ZnO	0.02	0.01	0.01	0.00	0.02	0.01	0.01	0.00	0.01	0.00	0.01	0.00
NiO	0.02	0.01	0.03	0.01	0.03	0.01	0.03	0.01	0.01	0.01	0.04	0.01
total*	100.04		100.05		100.75		100.47		100.58		100.57	
Total measured	93.45	0.70	93.37	0.41	93.95	0.44	93.99	0.30	94.04	0.68	94.23	0.54

Appendix II b. (Continued)

	Disseminated oxide hosted in anorthosite		Orthopyroxene -bearing disseminated oxide	
Magnetite in ilmenite	avg n=5	stdev	avg n=5	stdev
SiO_2	0.01	0.00	0.01	0.01
TiO_2	1.04	0.31	2.03	0.28
Al_2O_3	0.48	0.20	0.81	0.17
Cr_2O_3	0.38	0.01	0.23	0.01
V_2O_3	0.36	0.05	0.42	0.03
FeO*	91.12	0.45	90.58	0.82
Fe_2O_3 recalculated	65.74	0.57	63.98	0.86
FeO recalculated	31.96	0.40	33.01	0.32
MnO	0.01	0.00	0.02	0.01
MgO	0.07	0.04	0.14	0.05
ZnO	0.02	0.01	0.02	0.01
NiO	0.05	0.01	0.04	0.01
total*	100.12		100.70	
Total measured	93.52	0.46	94.28	0.58

Appendix II b. (Continued)

Magnetite in pleonaste	Massive oxide band-lower n=6 avg	stdev	Massive oxide band-middle n=10 avg	stdev	Massive oxide band-upper n=4 avg	stdev	Massive oxide vein n=4 avg	stdev
SiO_2	0.01	0.00	0.01	0.00	0.02	0.01	0.01	0.00
TiO_2	0.06	0.04	0.29	0.08	0.07	0.03	0.07	0.04
Al_2O_3	0.21	0.03	0.40	0.11	0.18	0.02	0.21	0.03
Cr_2O_3	0.16	0.01	0.17	0.01	0.26	0.02	0.38	0.03
V_2O_3	0.39	0.08	0.46	0.07	0.36	0.01	0.31	0.02
FeO*	91.77	0.66	91.67	0.65	92.24	0.16	91.41	0.39
Fe_2O_3 recalculated	67.68	0.50	67.24	0.49	68.03	0.17	67.38	0.35
FeO recalculated	30.87	0.23	31.17	0.26	31.03	0.03	30.77	0.09
MnO	0.02	0.01	0.03	0.01	0.03	0.01	0.05	0.01
MgO	0.02	0.01	0.07	0.02	0.03	0.02	0.02	0.01
ZnO	0.03	0.03	0.04	0.02	0.04	0.02	0.12	0.03
NiO	0.03	0.01	0.03	0.01	0.04	0.01	0.01	0.00
Total*	99.48		99.90		100.09		99.33	
Total measured	92.71	0.69	93.18	0.75	93.28	0.10	92.59	0.39

Appendix II b. (Continued)

Composite ilmenite with exsolution	Massive oxide band-lower n=8 average	stdev	Massive oxide band-middle n=6 average	stdev	Massive oxide band-upper n=15 average	stdev	Massive oxide pod n=9 average	stdev	Massive oxide vein n=9 average	stdev
SiO_2	0.01	0.00	0.01	-	0.01	0.00	0.01	0.00	0.01	0.00
TiO_2	49.20	0.48	48.04	0.99	49.18	0.50	49.18	1.11	48.62	1.02
Al_2O_3	0.02	0.01	0.04	0.00	0.02	0.01	0.05	0.01	0.03	0.03
Cr_2O_3	0.01	0.01	0.01	0.01	0.02	0.01	0.02	0.01	0.02	0.01
V_2O_3	0.36	0.03	0.36	0.04	0.38	0.03	0.29	0.02	0.34	0.03
FeO*	47.79	0.69	48.67	0.83	48.01	0.52	48.41	1.08	48.06	0.76
Fe_2O_3 recalculated	7.69	1.22	10.29	1.85	8.06	0.80	7.24	2.18	7.83	1.78
FeO recalculated	40.87	0.43	39.41	0.85	40.66	0.31	41.90	0.89	41.02	0.86
MnO	0.71	0.10	0.67	0.10	0.72	0.03	0.33	0.03	1.09	0.03
MgO	1.49	0.11	1.75	0.08	1.64	0.03	1.12	0.07	0.91	0.05
ZnO	0.01	0.00	0.01	0.00	0.01	0.00	0.01	0.00	0.01	0.00
NiO	0.01	-	0.01	-	0.01	0.00	0.01	0.00	0.01	0.00
Total measured	99.54	0.39	99.51	0.27	99.92	0.29	99.37	0.33	99.03	0.39

Appendix II b. (Continued)

Composite ilmenite with exsolution	Orthopyroxene -bearing oxide pod n=6		Disseminated oxide hosted in anorthosite n=13		Orthopyroxene -bearing disseminated oxide n=12		Clinopyroxene -bearing disseminated oxide n=12	
	average	stdev	average	stdev	average	stdev	average	stdev
SiO_2	0.01	-	0.01	0.00	0.01	0.00	0.01	0.00
TiO_2	51.96	0.90	49.96	0.78	49.37	0.96	48.45	0.77
Al_2O_3	0.03	0.02	0.04	0.01	0.02	0.01	0.01	0.01
Cr_2O_3	0.01	0.00	0.01	0.01	0.02	0.01	0.04	0.02
V_2O_3	0.25	0.03	0.25	0.02	0.25	0.02	0.27	0.02
FeO*	43.22	0.91	47.82	0.78	47.90	0.84	48.31	0.74
Fe_2O_3 recalculated	3.93	1.63	6.00	1.50	6.24	1.87	7.46	1.49
FeO recalculated	39.69	0.56	42.42	0.67	42.29	0.86	41.60	0.69
MnO	0.76	0.05	0.49	0.04	0.69	0.05	1.08	0.11
MgO	3.51	0.13	1.12	0.16	0.79	0.04	0.49	0.09
ZnO	0.02	0.01	0.02	0.01	0.01	0.00	0.01	0.00
NiO	0.01	0.00	0.01	0.01	0.01	0.00	0.01	-
Total measured	99.72	0.14	99.69	0.25	99.02	0.30	98.64	0.49

Appendix II b. (Continued)

Composite ilmenite without exsolution	Massive oxide band-middle n=4		Massive oxide band-upper n=3		Massive oxide pod n=7		Massive oxide vein n=2		Orthopyroxene-bearing oxide pod n=13		Disseminated oxide hosted in anorthosite n=3	
	average	stdev	average	stdev	average	stdev	average	stdev	average	stdev	average	stdev
SiO_2	0.01	-	0.01	-	0.01	0.00	0.01	-	0.01	0.00	0.01	-
TiO_2	49.74	0.12	50.29	1.23	50.61	0.49	48.31	0.90	51.81	0.46	51.94	0.09
Al_2O_3	0.04	0.01	0.02	0.01	0.03	0.01	0.02	0.00	0.03	0.01	0.02	0.01
Cr_2O_3	0.01	0.01	0.02	0.01	0.02	0.01	0.02	0.01	0.01	0.01	0.01	-
V_2O_3	0.35	0.01	0.39	0.04	0.22	0.02	0.35	0.00	0.22	0.02	0.19	0.01
FeO*	47.11	0.08	46.66	0.80	47.59	0.68	48.90	0.62	43.70	0.56	46.49	0.13
Fe_2O_3 recalculated	6.83	0.14	5.62	2.10	4.44	1.10	9.12	1.56	4.42	0.93	2.23	0.06
FeO recalculated	40.97	0.11	41.60	1.09	43.60	0.36	40.69	0.79	39.72	0.30	44.48	0.08
MnO	0.90	0.05	0.79	0.05	0.47	0.04	1.01	0.02	0.76	0.04	0.77	0.06
MgO	1.60	0.03	1.59	0.01	0.80	0.10	0.97	0.01	3.42	0.08	0.81	0.06
ZnO	0.01	-	0.01	0.00	0.02	0.01	0.02	0.01	0.01	0.00	0.02	0.02
NiO	0.01	-	0.01	-	0.01	0.01	0.01	-	0.01	0.00	0.01	0.01
Total measured	99.71	0.12	99.71	0.41	99.74	0.19	99.53	0.30	99.94	0.29	100.24	0.08

Appendix II b. (Continued)

Composite ilmenite without exsolution	Orthopyroxene -bearing disseminated oxide n=5 average	stdev	Clinopyroxene -bearing disseminated oxide n=5 average	stdev
SiO_2	0.01	-	0.01	-
TiO_2	51.53	0.25	48.82	0.80
Al_2O_3	0.02	0.01	0.02	0.01
Cr_2O_3	0.02	0.01	0.05	0.02
V_2O_3	0.23	0.02	0.27	0.03
FeO*	46.00	0.50	47.81	0.66
Fe_2O_3 recalculated	1.62	0.77	6.57	1.42
FeO recalculated	44.54	0.23	41.89	0.67
MnO	1.22	0.03	1.23	0.20
MgO	0.31	0.02	0.42	0.11
ZnO	0.02	0.01	0.02	0.01
NiO	0.01	0.00	0.01	0.01
Total measured	99.31	0.27	98.61	0.37

Appendix II b. (Continued)

Sandwich ilmenite	Massive oxide band-lower n=2 average	Massive oxide band-middle n=10 average	stdev	Massive oxide band-upper n=9 average	stdev	Massive oxide pod n=9 average	stdev	Massive oxide vein n=3 average	Disseminated oxide hosted in anorthosite n=3 average	Orthopyroxene-bearing disseminated oxide n=6 average	stdev
SiO_2	0.02	0.01	0.00	0.01	0.00	0.01	0.00	0.01	0.01	0.01	0.00
TiO_2	51.60	51.60	0.64	50.85	0.95	51.26	0.75	49.58	52.10	52.19	0.59
Al_2O_3	0.46	0.02	0.01	0.03	0.00	0.02	0.01	0.01	0.01	0.01	0.00
Cr_2O_3	0.05	0.01	0.01	0.02	0.01	0.01	0.01	0.10	0.02	0.01	0.01
V_2O_3	0.29	0.29	0.03	0.37	0.04	0.21	0.02	0.39	0.21	0.23	0.02
FeO*	43.07	45.47	0.92	46.54	0.83	46.93	0.82	47.32	46.16	45.00	0.83
Fe_2O_3 recalculated	2.65	3.40	1.42	4.91	1.70	3.16	1.46	6.34	2.00	0.51	0.55
FeO recalculated	40.69	42.41	0.38	42.13	0.76	44.14	0.66	41.62	44.36	45.25	0.46
MnO	2.46	1.11	0.19	0.86	0.07	0.54	0.03	1.40	0.82	1.19	0.08
MgO	1.79	1.60	0.06	1.53	0.14	0.78	0.03	0.87	0.93	0.26	0.01
ZnO	0.06	0.02	0.01	0.01	0.01	0.02	0.01	0.01	0.02	0.02	0.01
NiO	0.01	0.01	0.00	0.01	0.00	0.01	0.00	0.01	0.01	0.01	0.00
Total measured	99.74	100.08	0.29	100.17	0.25	99.76	0.27	99.62	100.24	98.89	0.33

Appendix II b. (Continued)

Ilmenite dotted with pleonaste microcrystals	Massive oxide band-lower n=4		Massive oxide band-middle n=4		Massive oxide pod n=12		Disseminated oxide hosted in anorthosite n=7		Orthopyroxene-bearing disseminated oxide n=12		Clinopyroxene-bearing disseminated oxide n=10	
	average	stdev	average	stdev	average	stdev	average	stdev	average	stdev	average	stdev
SiO_2	0.01	0.00	0.01	0.00	0.01	0.00	0.01	0.00	0.01	0.00	0.01	0.00
TiO_2	52.77	0.39	52.35	0.58	52.54	0.24	52.61	0.17	52.35	0.41	51.56	0.24
Al_2O_3	0.03	0.03	0.01	0.01	0.06	0.12	0.02	0.01	0.04	0.06	0.03	0.05
Cr_2O_3	0.02	0.01	0.01	0.00	0.03	0.01	0.02	0.01	0.03	0.02	0.04	0.01
V_2O_3	0.27	0.02	0.25	0.03	0.20	0.02	0.19	0.01	0.20	0.02	0.24	0.01
FeO*	44.28	0.25	44.45	1.32	45.53	0.56	45.69	0.30	44.87	0.78	44.42	0.76
Fe_2O_3 recalculated	0.76	0.49	1.94	1.48	0.48	0.63	1.07	0.45	0.29	0.36	1.88	0.57
FeO recalculated	43.60	0.32	42.88	0.34	45.25	0.21	44.73	0.57	45.10	0.26	42.73	0.41
MnO	0.99	0.03	1.45	0.92	0.69	0.09	0.79	0.04	1.17	0.18	1.80	0.32
MgO	1.58	0.21	1.50	0.43	0.72	0.09	0.99	0.36	0.44	0.21	1.01	0.19
ZnO	0.04	0.01	0.05	0.01	0.02	0.01	0.02	0.01	0.02	0.01	0.03	0.02
NiO	0.01	0.01	0.01	0.00	0.01	0.00	0.01	0.00	0.01	0.00	0.01	0.00
Total measured	99.94	0.75	100.07	0.32	99.76	0.39	100.33	0.27	99.10	0.37	99.11	0.36

Appendix II b. (Continued)

Pleonaste with magnetite exsolution	Massive oxide band-lower n=4 average	stdev	Massive oxide band-middle n=4 average	stdev	Massive oxide band-upper n=5 average	stdev	Massive oxide vein n=2 average	stdev
SiO_2	0.01	-	0.01	-	0.01	-	0.01	-
TiO_2	0.02	0.01	0.01	-	0.01	-	0.01	-
Al_2O_3	58.28	0.61	58.88	0.67	58.72	1.05	56.47	0.66
Cr_2O_3	0.28	0.04	0.26	0.01	0.46	0.09	0.55	0.06
V_2O_3	0.09	0.01	0.08	0.02	0.08	0.01	0.09	0.02
FeO*	28.85	0.31	27.99	0.98	28.09	1.12	32.46	0.68
Fe_2O_3 recalculated	5.88	0.46	5.93	0.80	5.62	0.86	6.09	0.59
FeO recalculated	23.56	0.25	22.65	0.27	23.03	0.43	26.98	0.14
MnO	0.22	0.00	0.23	0.02	0.28	0.02	0.44	0.01
MgO	10.93	0.18	11.65	0.20	11.36	0.39	7.76	0.18
ZnO	0.64	0.03	0.67	0.03	0.60	0.02	1.77	0.09
NiO	0.11	0.00	0.10	0.01	0.10	0.01	0.05	0.01
Total	100.01	0.38	100.48	0.24	100.28	0.38	100.20	0.21

Appendix II b. (Continued)

Pleonaste with no exsolution	Massive oxide band- middle n=6		Orthopyroxene -bearing oxide pod n=2		Disseminated oxide hosted in anorthosite n=4	
Comment	average	stdev	average	stdev	average	stdev
SiO_2	0.02	0.03	0.01	-	0.01	-
TiO_2	0.06	0.07	0.03	0.01	0.03	0.00
Al_2O_3	60.86	0.63	60.50	1.68	56.45	0.30
Cr_2O_3	0.36	0.04	0.39	0.01	0.47	0.03
V_2O_3	0.07	0.01	0.06	0.00	0.07	0.00
FeO*	24.82	0.64	22.70	1.95	33.47	0.16
Fe_2O_3 recalculated	3.84	0.64	5.95	0.97	5.66	0.18
FeO recalculated	21.36	0.23	17.35	1.08	28.38	0.04
MnO	0.22	0.01	0.18	0.01	0.19	0.01
MgO	12.85	0.23	15.33	1.00	7.39	0.10
ZnO	0.43	0.10	0.77	0.04	0.89	0.02
NiO	0.10	0.01	0.06	0.01	0.11	0.02
Total	100.17	0.16	100.61	0.62	99.65	0.34

Appendix II b. (Continued)

Pleonaste in ilmenite Comment	Massive oxide band-lower n=3 average	Massive oxide band-middle n=1	Massive oxide band-upper n=2 average	Massive oxide pod n=3 average	Disseminated oxide hosted in anorthosite n=2 average
SiO_2	0.02	0.01	0.01	0.09	0.01
TiO_2	0.74	0.64	1.00	0.78	0.87
Al_2O_3	62.68	61.66	62.07	57.07	57.28
Cr_2O_3	0.57	0.50	0.73	1.07	0.51
V_2O_3	0.06	0.06	0.08	0.08	0.07
FeO*	21.72	22.83	21.56	32.59	31.09
Fe_2O_3 recalculated	2.06	2.52	2.11	2.78	4.07
FeO recalculated	19.87	20.56	19.66	30.09	27.42
MnO	0.15	0.20	0.16	0.19	0.17
MgO	14.76	13.92	14.90	7.17	8.79
ZnO	0.38	0.42	0.49	0.51	0.80
NiO	0.08	0.07	0.07	0.11	0.12
Total	101.36	100.57	101.26	99.93	100.10

Appendix II b. (Continued)

Pleonaste from ilmenite dotted with spinel microcrystals	Massive oxide pod n=4	
Comment	average	stdev
SiO_2	0.10	0.07
TiO_2	1.05	0.24
Al_2O_3	56.26	0.29
Cr_2O_3	1.38	0.14
V_2O_3	0.07	0.01
FeO*	32.33	0.23
Fe_2O_3 recalculated	2.91	0.39
FeO recalculated	29.71	0.33
MnO	0.16	0.00
MgO	7.41	0.15
ZnO	0.67	0.08
NiO	0.11	0.01
Total	99.84	0.42

Appendix II c. Average (mean) and 2σ standard deviation of LA-ICPMS magnetite analyses from various observed textural occurrences.

	Massive oxide band- lower		Massive oxide band- middle		Massive oxide band- upper		Massive oxide pod	
	n=12		n=14		n=10		n=18	
ppm	avg	stdev	avg	stdev	avg	stdev	avg	stdev
^{29}Si	269	152	305	240	197	152	338	293
^{44}Ca	10	5	8	5	12	18	11	8
^{89}Y	0.001	0.000	0.003	0.003	0.003	0.004	0.008	0.007
^{31}P	3	1	3	1	2	0.3	3	2
^{208}Pb	0.3	0.1	0.4	0.4	1	0.2	0.2	0.1
^{90}Zr	0.1	0.1	1	1	0.3	0.3	1	0.4
^{178}Hf	0.00	0.00	0.02	0.03	0.01	0.01	0.04	0.02
^{27}Al	2758	614	7291	1982	3097	468	11663	6393
^{74}Ge	1	0.11	1	0.14	1	0.1	1	0.11
^{182}W	0.01	0.01	0.01	0.00	0.01	0.01	0.01	0.00
^{45}Sc	1	0	2	0	1	0	1	0
^{181}Ta	0.000	0.000	0.003	0.005	0.002	0.002	0.001	0.001
^{93}Nb	0.02	0.01	0.05	0.08	0.04	0.05	0.03	0.03
^{63}Cu	1	1	1	0.4	0.4	0.2	1	1
^{95}Mo	0.05	0.04	0.12	0.03	0.08	0.02	0.35	0.06
^{118}Sn	0.1	0.1	1	0.2	0.0	0.1	1	0.1
^{69}Ga	39	3	60	9	36	2	62	10
^{55}Mn	151	41	531	137	243	111	559	189
^{24}Mg	668	162	2052	540	983	191	1332	1138
^{47}Ti	928	676	5687	4520	1994	2568	13904	8122
^{66}Zn	7	5	17	8	14	20	70	114
^{59}Co	72	8	131	17	78	3	104	30
^{51}V	4682	264	5960	716	4660	190	4734	181
^{60}Ni	248	57	428	39	288	21	274	23
^{52}Cr	1764	406	1954	211	2407	234	3903	284
^{75}As	0.3	0.2	1	0.2	1	0.1	0.3	0.2
^{121}Sb	0.01	0.01	0.04	0.07	0.03	0.02	0.01	0.01

Appendix II c. (Continued)

	Massive oxide vein		Orthopyroxene - bearing oxide pod		Disseminated oxide hosted in anorthosite		Orthopyroxene -bearing disseminated oxide		Clinopyroxene - bearing disseminated oxide	
	n=3		n=7		n=14		n=16		n=10	
ppm	avg	stdev	avg	stdev	avg	stdev	avg	stdev	avg	stdev
^{29}Si	235	121	381	250	309	198	593	688	526	474
^{44}Ca	16	17	8	2	9	4	14	13	23	30
^{89}Y	0.001	0.01	0.014	0.01	0.006	0.01	0.009	0.01	0.007	0.01
^{31}P	6	7	3	1	3	1	4	2	6	8
^{208}Pb	0.2	0.1	1	0.1	0.4	0.1	1	0.2	1	0.2
^{90}Zr	0.0	0.1	2	0.4	1	0.4	1	0.2	0.3	0.3
^{178}Hf	0.00	0.00	0.11	0.01	0.03	0.02	0.05	0.01	0.01	0.01
^{27}Al	4387	1421	17501	5057	11286	5669	16744	3649	3700	843
^{74}Ge	1	0.15	1	0.06	1	0.1	1	0.1	1	0.14
^{182}W	0.03	0.00	0.01	0.01	0.01	0.03	0.01	0.01	0.01	0.01
^{45}Sc	1	1	6	1	1	0	2	0	1	0
^{181}Ta	0.001	0.01	0.001	0.01	0.004	0.01	0.003	0.05	0.004	0.01
^{93}Nb	0.01	0.00	0.02	0.02	0.01	0.01	0.02	0.01	0.11	0.17
^{63}Cu	0.3	0.2	1	1	2	2	1	1	2	4
^{95}Mo	0.21	0.10	0.22	0.05	0.85	0.11	0.37	0.06	0.26	0.04
^{118}Sn	0.0	0.0	2	0.1	1	0.3	2	0.3	0.2	0.1
^{69}Ga	40	5	59	4	52	9	69	7	52	4
^{55}Mn	325	46	1943	93	533	268	1057	288	355	172
^{24}Mg	675	146	6360	1871	1115	666	1901	594	455	94
^{47}Ti	940	420	25637	1399	7960	6070	20522	4537	3015	3645
^{66}Zn	31	21	121	148	113	75	61	28	38	25
^{59}Co	62	4	179	13	82	25	140	18	83	8
^{51}V	4307	110	4358	102	4194	204	4480	297	3438	79
^{60}Ni	98	3	322	13	438	41	362	35	267	21
^{52}Cr	2783	443	2228	111	3178	242	2274	297	3348	357
^{75}As	1	0.3	1	0.1	1	0.2	1	0.3	2	0.4
^{121}Sb	0.02	0.02	0.03	0.01	0.04	0.02	0.04	0.04	0.05	0.06

Appendix II c. (Continued)

Composite ilmenite with exsolution ppm	Massive oxide band-lower n=8 average	stdev	Massive oxide band-middle n=7 average	stdev	Massive oxide band- upper n=11 average	stdev	Massive oxide pod n=11 average	stdev
^{24}Mg	9196	552	10468	1133	9831	309	6477	898
^{27}Al	987	1484	272	72	405	172	362	109
^{29}Si	278	125	363	333	400	278	235	99
^{31}P	3	1	2	1	5	3	2	0
^{44}Ca	6	1	7	5	17	11	8	6
^{45}Sc	41	1	44	2	45	3	24	2
^{47}Ti	293338	2265	287281	6652	295364	5842	290618	3794
^{51}V	1661	233	1351	206	2082	363	811	181
^{52}Cr	135	38	136	29	243	35	147	40
^{55}Mn	5832	671	6321	895	5926	205	2875	557
^{59}Co	93	3	115	5	95	6	99	7
^{60}Ni	46	6	69	9	47	4	50	2
^{63}Cu	4	5	1	0.2	3	1	3	1
^{66}Zn	15	14	8	4	17	17	8	2
^{69}Ga	3	3	1	0.3	2	0.5	1	0.2
^{74}Ge	0.2	0.03	0.1	0.03	0.2	0.1	0.1	0.01
^{75}As	0.5	0.1	1	0.2	1	0.3	0.2	0.1
^{89}Y	0.1	0.01	0.1	0.01	0.1	0.01	0.1	0.01
^{90}Zr	70	10	72	10	95	68	107	28
^{93}Nb	4	1	3	1	6	1	23	6
^{95}Mo	0.4	0.1	0	0.1	1	0.1	1	0.1
^{118}Sn	3	1	3	0.2	2	1	3	1
^{121}Sb	0.1	0.01	0.04	0.01	0.1	0.04	0.1	0.03
^{178}Hf	2	0.3	2	0.2	2	1	4	1
^{181}Ta	0	0.1	0.1	0.1	0.4	0.1	1	1
^{182}W	0.009	0.005	0.02	0.01	0.1	0.01	0.1	0.04
^{208}Pb	1	0.15	1	0.2	2	1	0.5	0.1

Appendix II c. (Continued)

Composite ilmenite with exsolution	Massive oxide vein n=8		Orthopyroxene - bearing oxide pod n=1	Disseminated oxide hosted in anorthosite n=8	
ppm	average	stdev		average	stdev
^{24}Mg	5526	139	21680	4922	165
^{27}Al	812	1117	203	243	48
^{29}Si	565	583	264	227	156
^{31}P	5	5	2	2	0
^{44}Ca	19	26	6	7	3
^{45}Sc	64	5	64	31	2
^{47}Ti	287860	5796	310900	289660	6360
^{51}V	1749	189	530	610	100
^{52}Cr	273	29	30	171	63
^{55}Mn	8868	904	6038	5477	272
^{59}Co	70	5	122	78	3
^{60}Ni	17	2	52	81	2
^{63}Cu	2	2	1	2	0.2
^{66}Zn	22	23	15	7	2
^{69}Ga	3	2	0.5	1	0.2
^{74}Ge	0.2	0.04	0.1	0.1	0.02
^{75}As	1	0.1	1	1	0.1
^{89}Y	0.1	0.01	0.2	0.2	0.02
^{90}Zr	23	8	177	141	27
^{93}Nb	17	3	6	18	2
^{95}Mo	1	0.03	0.4	1	0.2
^{118}Sn	2	1	2	2	0.3
^{121}Sb	0.2	0.1	0.1	0.2	0.05
^{178}Hf	2	1	5	4	1
^{181}Ta	1	0.2	0.3	1	0.2
^{182}W	0.1	0.04	0.004	1	1
^{208}Pb	1	0.3	2	1	0.2

Appendix II c. (Continued)

Composite ilmenite with exsolution	Orthopyroxene -bearing disseminated oxide n=11		Clinopyroxene -bearing disseminated oxide n=5	
ppm	average	stdev	average	stdev
^{24}Mg	7311	206	3514	375
^{27}Al	288	87	263	90
^{29}Si	397	213	536	651
^{31}P	3	2	6	5
^{44}Ca	12	9	10	7
^{45}Sc	27	3	31	2
^{47}Ti	301712	7482	291480	2080
^{51}V	559	119	862	69
^{52}Cr	82	14	379	73
^{55}Mn	4087	250	8416	1337
^{59}Co	114	4	100	5
^{60}Ni	67	4	48	4
^{63}Cu	3	1	2	0.4
^{66}Zn	14	5	28	11
^{69}Ga	1	0.4	2	0.1
^{74}Ge	0.1	0.04	0.2	0.02
^{75}As	1	0.2	2	1
^{89}Y	0.1	0.02	0.1	0.03
^{90}Zr	96	25	47	6
^{93}Nb	30	6	17	2
^{95}Mo	0.4	0.1	1	0.2
^{118}Sn	2	0.4	2	0.3
^{121}Sb	0.04	0.01	0.1	0.04
^{178}Hf	3	1	2	0.2
^{181}Ta	1	0.4	1	0.1
^{182}W	0.1	0.02	0.04	0.01
^{208}Pb	1	0.5	2	1

Appendix II c. (Continued)

Composite ilmenite without exsolution	Massive oxide band-lower n=2 average	stdev	Massive oxide band-middle n=4 average	stdev	Massive oxide band- upper n=1 none	Massive oxide pod n=9 average	stdev	Massive oxide vein n=1 none
^{24}Mg	9872	182	9881	208	10250	5230	714	5558
^{27}Al	366	80	240	55	479	252	137	237
^{29}Si	1436	1647	425	175	279	208	169	385
^{31}P	7	8	2	1	3	2	0	2
^{44}Ca	198	271	7	7	9	6	3	4
^{45}Sc	40	0	43	4	45	22	3	52
^{47}Ti	295800	566	292750	1708	293500	300244	2589	284300
^{51}V	1893	195	1076	199	1861	497	135	1393
^{52}Cr	150	28	148	20	270	173	54	267
^{55}Mn	4777	14	7439	371	6027	3830	457	9928
^{59}Co	79	4	110	5	110	90	5	68
^{60}Ni	29	2	62	9	76	48	3	18
^{63}Cu	2	2	1	0	3	3	3	1
^{66}Zn	7	2	14	10	12	8	6	11
^{69}Ga	2	0	1	0	4	0.5	0.2	1
^{74}Ge	0	0	0	0	0	0.1	0.02	0.2
^{75}As	1	1	1	0	1	0.2	0.1	0.5
^{89}Y	0	0	0	0	0	0.1	0.01	0.1
^{90}Zr	72	14	57	11	63	70	22	13
^{93}Nb	5	0	3	0	7	19	3	15
^{95}Mo	0	0	0	0	1	0.4	0.04	1
^{118}Sn	3	0	3	0	2	2	0.3	0.1
^{121}Sb	0	0	0	0	0	0.04	0.03	0.2
^{178}Hf	3	0	2	0	2	3	1	0.5
^{181}Ta	0	0	0	0	0	1	0.2	0.5
^{182}W	0	0	0	0	0	0.1	0.04	0.2
^{208}Pb	1	1	1	0	2	0.5	0.1	1

Appendix II c. (Continued)

Composite ilmenite without exsolution	Orthopyroxene -bearing oxide pod n=12 average	stdev	Disseminated oxide hosted in anorthosite n=1	Clinopyroxene -bearing disseminated oxide n=5 average	stdev
^{24}Mg	21253	1099	2089	2878	348
^{27}Al	937	1936	310	367	268
^{29}Si	325	165	488	816	237
^{31}P	2	1	2	4	3
^{44}Ca	9	8	12	16	10
^{45}Sc	67	8	29	28	2
^{47}Ti	305608	5813	294900	290894	3745
^{51}V	432	76	433	862	90
^{52}Cr	93	45	216	328	54
^{55}Mn	6244	333	9711	9515	1178
^{59}Co	122	9	47	89	10
^{60}Ni	58	9	53	39	6
^{63}Cu	2	1	3	4	4
^{66}Zn	29	62	10	32	17
^{69}Ga	1	2	1	1	1
^{74}Ge	0.1	0.03	0.03	0.2	0.03
^{75}As	1	0.1	1	2	0.2
^{89}Y	0.2	0.02	0.1	0.2	0.1
^{90}Zr	124	16	47	35	9
^{93}Nb	5	1	3	14	2
^{95}Mo	0.4	0.04	1	1	0.1
^{118}Sn	2	0.3	2	2	0.4
^{121}Sb	0.1	0.03	0.1	0.1	0.01
^{178}Hf	4	0.4	2	2	0.3
^{181}Ta	0.1	0.1	0.1	1	0.3
^{182}W	0.01	0.004	0.2	0.04	0.02
^{208}Pb	1	0.2	1	1	0.3

Appendix II c. (Continued)

Sandwich ilmenite ppm	Massive oxide band-middle n=5 average	stdev	Massive oxide band-upper n=6 average	stdev	Massive oxide pod n=5 average	stdev
^{24}Mg	9877	346	9414	403	4931	213
^{27}Al	222	171	297	175	142	19
^{29}Si	342	349	395	337	336	205
^{31}P	3	2	6	5	2	0.4
^{44}Ca	6	4	15	9	6	2
^{45}Sc	43	2	39	5	21	1
^{47}Ti	309780	2616	297483	9953	304340	1313
^{51}V	965	111	1401	345	391	16
^{52}Cr	125	26	192	55	130	22
^{55}Mn	8800	531	7202	934	4300	76
^{59}Co	117	4	94	5	87	4
^{60}Ni	73	9	48	6	47	2
^{63}Cu	2	0	3	1	2	1
^{66}Zn	32	38	31	22	5	1
^{69}Ga	1	1	1	1	0.3	0.04
^{74}Ge	0.1	0.03	0.2	0.05	0.05	0.03
^{75}As	1	0.2	1	0	0.2	0.1
^{89}Y	0.1	0.004	0.12	0.01	0.1	0.02
^{90}Zr	45	5	28	10	57	4
^{93}Nb	2	0.2	5	1	19	3
^{95}Mo	1	0.1	0.5	0.1	0.5	0.1
^{118}Sn	3	0.2	1	0.4	2	0.1
^{121}Sb	0.1	0.01	0.1	0.03	0.04	0.01
^{178}Hf	2	0.1	1	0.3	2	0.2
^{181}Ta	0.1	0.04	0.3	0.1	1	0.2
^{182}W	0.02	0.01	0.1	0.02	0.05	0.02
^{208}Pb	1	0.1	2	0.5	0.5	0.2

Appendix II c. (Continued)

Composite pleonaste with magnetite exsolution	Massive oxide band-lower	Massive oxide band-middle		Massive oxide band-upper	Massive oxide pod	Massive oxide vein	Disseminated oxide hosted in anorthosite
	n=3	n=4		n=2	n=1	n=3	n=2
ppm	average	average	stdev	average		average	average
^{24}Mg	141030	81785	11926	62280	47560	46157	40855
^{29}Si	3697	441	391	180	2590	602	345
^{31}P	38	12	9	10	3	8	21
^{44}Ca	36	10	1	11	24	12	37
^{45}Sc	0.5	0.1	0.1	0.1	1	0.1	0.1
^{47}Ti	0.01	0.04	0.04	0.02	0.3	363	0.04
^{51}V	1233	752	176	561	484	544	590
^{52}Cr	3781	2411	499	2723	4067	3349	2045
^{55}Mn	3712	2213	439	2070	1607	3361	1767
^{59}Co	1465	875	153	697	1237	463	552
^{60}Ni	1583	1102	230	772	1155	240	769
^{66}Zn	8007	6740	2380	3685	5580	11237	5068
^{69}Ga	455	254	34	219	363	211	183
^{74}Ge	0.3	0.3	0.1	0.4	0.03	0.2	1
^{89}Y	0.004	0.004	0.001	0.004	0.003	0.003	0.003
^{90}Zr	0.04	0.02	0.01	0.02	3	0.1	0.5
^{93}Nb	0.008	0.01	0.003	0.01	1	0.01	0.02
^{95}Mo	0.2	0.1	0.01	0.2	0.3	0.1	0.1
^{118}Sn	0.1	0.1	0.1	0.1	0.3	0.2	0.1
^{178}Hf	0.004	0.03	0.03	0.03	0.1	0.01	0.1
^{181}Ta	0.003	0.01	0.02	0.01	0.02	0.001	0.03
^{182}W	0.03	0.03	0.01	0.03	0.02	0.02	0.02
^{208}Pb	0.4	0.3	0.2	0.3	0.003	0.3	0.5
^{75}As	1	1	0.3	1	0.5	1	1
^{121}Sb	0.04	0.01	0.01	0.02	0.03	0.04	0.02

Appendix II c. (Continued)

Composite pleonaste with no exsolution	Massive oxide band-lower	Massive oxide band-middle	Massive oxide band-upper	Orthopyroxene-bearing oxide pod	Orthopyroxene-bearing disseminated oxide	Clinopyroxene-bearing disseminated oxide
	n=1	n=2		n=2	n=2	n=1
ppm		average		average	average	
^{24}Mg	73730	74735	65850	83650	42155	36040
^{29}Si	2300	6220	860	540	10370	6000
^{31}P	3	6	3	5	165	63
^{44}Ca	300	36	10	18	286	149
^{45}Sc	2	1	0.4	0.4	1	0.02
^{47}Ti	22800	3900	4450	0.002	0.1	0.001
^{51}V	1780	1497	546	603	549	388
^{52}Cr	3110	2617	3560	2409	2939	4733
^{55}Mn	2390	2147	2125	1885	1450	2674
^{59}Co	1054	1190	765	529	801	1333
^{60}Ni	963	1025	755	622	821	661
^{66}Zn	5710	3903	3164	4750	5490	9380
^{69}Ga	301	352	206	195	179	251
^{74}Ge	0.5	0.5	0.3	0.3	0.3	0.2
^{89}Y	0.02	0.02	0.002	0.003	0.2	0.003
^{90}Zr	2	1	1	0.2	0.2	0
^{93}Nb	0.4	0.01	0.004	0.01	0.01	0.01
^{95}Mo	0.1	0.1	0.1	0.1	0.3	0.1
^{118}Sn	0.6	0.5	0.1	0.1	0.3	0.01
^{178}Hf	0.1	0.02	0.004	0.03	0.01	0.002
^{181}Ta	0.03	0.3	0.01	0.01	0.001	0.00
^{182}W	0.02	0.1	0.024	0.0	0.2	0.01
^{208}Pb	0.3	1	1	0.5	1	0.4
^{75}As	1	1	1	1	1	1
^{121}Sb	0.2	0.1	0.004	0.1	0.04	0.04

Appendix III. Whole-rock geochemistry results.

Sample ID				CC001	CC002	CC003	CC004	CC007	CC008	CC009	CC010A
Easting				658748	658748	658748	658748	658778	658736	658736	658736
Westing				5929229	5929229	5929229	5929229	5928890	5929043	5929043	5929043
Description				BAR	BAR	MAS	MAS	TRO	MAS	BAR	OMAS
		Idl									
SiO_2	%	0.01	FUS-ICP	55.22	54.53	18.08	5.8	49.18	2.7	53.53	11.91
Al_2O_3	%	0.01	FUS-ICP	27.53	26.23	14.83	11.75	19.89	10.15	25.63	8.54
$Fe_2O_{3(T)}$	%	0.01	FUS-ICP	1.14	0.91	53.73	66.99	10.3	76.9	3.93	65.95
MnO	%	0.001	FUS-ICP	0.012	0.009	0.156	0.239	0.128	0.218	0.022	0.31
MgO	%	0.01	FUS-ICP	0.2	0.17	1.52	2.79	8.17	2.56	0.25	6.24
CaO	%	0.01	FUS-ICP	10.05	9.82	3.26	0.88	7.84	0.35	8.65	0.56
Na_2O	%	0.01	FUS-ICP	5.06	5.01	1.66	0.26	3.18	0.17	5.09	0.13
K_2O	%	0.01	FUS-ICP	0.98	1.07	0.29	0.19	0.6	0.05	1.22	0.05
TiO_2	%	0.001	FUS-ICP	0.166	0.09	7.144	14.14	0.403	10.14	0.52	9.347
P_2O_5	%	0.01	FUS-ICP	0.05	0.05	0.03	< 0.01	0.05	0.02	0.04	< 0.01
LOI	%		FUS-ICP	0.46	0.65	-1.61	-2.49	0	-2.58	1.07	-2.2
Total	%	0.01	FUS-ICP	100.9	98.55	99.08	100.6	99.75	100.7	99.95	100.9
Sc	ppm	1	FUS-ICP	< 1	< 1	6	12	5	9	< 1	17
Be	ppm	1	FUS-ICP	< 1	< 1	< 1	< 1	< 1	< 1	< 1	< 1
V	ppm	5	FUS-ICP	20	7	2454	2829	77	3200	96	2511
Cr	ppm	20	FUS-MS	< 20	< 20	820	910	< 20	1330	120	1090
Co	ppm	1	FUS-MS	4	3	126	169	57	208	14	146
Ni	ppm	1	TD-ICP	21	28	226	239	115	318	78	226
Zn	ppm	1	TD-ICP	14	6	229	353	65	360	23	351
Cd	ppm	0.5	TD-ICP	< 0.5	< 0.5	0.5	0.7	< 0.5	0.8	< 0.5	1.1
S	%	0.001	TD-ICP	0.05	0.097	0.062	0.013	0.041	0.22	0.182	0.018
Cu	ppm	1	TD-ICP	16	61	93	44	21	231	231	61
Ag	ppm	0.3	TD-ICP	< 0.3	0.3	< 0.3	0.7	< 0.3	0.8	0.6	0.5
Pb	ppm	5	TD-ICP	< 5	< 5	14	15	< 5	16	< 5	15
Ga	ppm	1	FUS-MS	18	17	56	67	15	74	19	56
Ge	ppm	1	FUS-MS	< 1	1	1	2	1	2	1	2
As	ppm	5	FUS-MS	< 5	< 5	< 5	< 5	< 5	< 5	< 5	< 5
Rb	ppm	2	FUS-MS	8	4	< 2	3	< 2	< 2	10	2
Sr	ppm	2	FUS-ICP	1390	1413	451	112	995	52	1449	34
Y	ppm	2	FUS-ICP	2	< 2	< 2	< 2	< 2	< 2	< 2	< 2
Zr	ppm	4	FUS-ICP	9	5	6	12	5	7	5	9
Nb	ppm	1	FUS-MS	< 1	< 1	< 1	< 1	< 1	< 1	< 1	< 1
Mo	ppm	2	FUS-MS	< 2	< 2	< 2	3	< 2	< 2	< 2	< 2
In	ppm	0.2	FUS-MS	< 0.2	< 0.2	< 0.2	< 0.2	< 0.2	< 0.2	< 0.2	< 0.2
Sn	ppm	1	FUS-MS	< 1	< 1	1	2	< 1	1	< 1	1
Sb	ppm	0.5	FUS-MS	< 0.5	< 0.5	< 0.5	< 0.5	< 0.5	< 0.5	< 0.5	< 0.5
Cs	ppm	0.5	FUS-MS	< 0.5	< 0.5	< 0.5	< 0.5	< 0.5	< 0.5	< 0.5	< 0.5
Ba	ppm	3	FUS-ICP	919	937	264	98	609	38	1043	21
La	ppm	0.1	FUS-MS	3.7	2.8	1	0.3	2.4	0.2	3.7	< 0.1
Ce	ppm	0.1	FUS-MS	6.7	4.6	1.7	0.6	4.2	0.3	5.9	0.2
Pr	ppm	0.05	FUS-MS	0.79	0.53	0.2	0.07	0.53	< 0.05	0.71	< 0.05
Nd	ppm	0.1	FUS-MS	3.3	2	0.9	0.3	2.2	0.1	2.8	0.2
Sm	ppm	0.1	FUS-MS	0.5	0.3	0.1	< 0.1	0.4	< 0.1	0.4	< 0.1
Eu	ppm	0.05	FUS-MS	0.87	0.74	0.22	0.09	0.62	< 0.05	0.82	0.05
Gd	ppm	0.1	FUS-MS	0.4	0.2	< 0.1	< 0.1	0.3	< 0.1	0.2	0.1
Tb	ppm	0.1	FUS-MS	< 0.1	< 0.1	< 0.1	< 0.1	< 0.1	< 0.1	< 0.1	< 0.1
Dy	ppm	0.1	FUS-MS	0.3	< 0.1	< 0.1	< 0.1	0.3	< 0.1	0.1	0.1
Ho	ppm	0.1	FUS-MS	< 0.1	< 0.1	< 0.1	< 0.1	< 0.1	< 0.1	< 0.1	< 0.1
Er	ppm	0.1	FUS-MS	< 0.1	< 0.1	< 0.1	< 0.1	0.1	< 0.1	< 0.1	0.1
Tm	ppm	0.05	FUS-MS	< 0.05	< 0.05	< 0.05	< 0.05	< 0.05	< 0.05	< 0.05	< 0.05
Yb	ppm	0.1	FUS-MS	< 0.1	< 0.1	< 0.1	< 0.1	0.1	< 0.1	< 0.1	0.1
Lu	ppm	0.04	FUS-MS	< 0.04	< 0.04	< 0.04	< 0.04	< 0.04	< 0.04	< 0.04	< 0.04
Hf	ppm	0.2	FUS-MS	< 0.2	< 0.2	0.2	0.5	< 0.2	0.3	< 0.2	0.4
Ta	ppm	0.1	FUS-MS	< 0.1	< 0.1	< 0.1	0.1	< 0.1	< 0.1	< 0.1	< 0.1
W	ppm	1	FUS-MS	2	1	2	8	1	4	< 1	3
Tl	ppm	0.1	FUS-MS	0.2	< 0.1	< 0.1	0.1	< 0.1	< 0.1	< 0.1	< 0.1
Bi	ppm	0.4	FUS-MS	< 0.4	< 0.4	< 0.4	< 0.4	< 0.4	< 0.4	< 0.4	< 0.4
Th	ppm	0.1	FUS-MS	< 0.1	< 0.1	< 0.1	< 0.1	< 0.1	< 0.1	< 0.1	< 0.1
U	ppm	0.1	FUS-MS	0.1	< 0.1	0.2	0.3	< 0.1	0.1	< 0.1	< 0.1

Abbreviations:	Rock types		
MAS	Massive to semi-massive oxide mineralization	BAR	Barren anorthosite
OMAS	Orthopyroxene -bearing massive-semi-massive oxide mineralization	DIS	Disseminated oxide mineralization
GAB	Gabbronorite	TRO	Troctolite

Appendix III. (Continued)

Sample ID				CC001	CC002	CC003	CC004	CC007	CC008	CC009	CC010A
Easting				658748	658748	658748	658748	658778	658736	658736	658736
Westing				5929229	5929229	5929229	5929229	5928890	5929043	5929043	5929043
Description				BAR	BAR	MAS	MAS	TRO	MAS	BAR	OMAS
		Idl									
SiO_2	%	0.01	FUS-ICP	55.22	54.53	18.08	5.8	49.18	2.7	53.53	11.91
Al_2O_3	%	0.01	FUS-ICP	27.53	26.23	14.83	11.75	19.89	10.15	25.63	8.54
$Fe_2O_{3(T)}$	%	0.01	FUS-ICP	1.14	0.91	53.73	66.99	10.3	76.9	3.93	65.95
MnO	%	0.001	FUS-ICP	0.012	0.009	0.156	0.239	0.128	0.218	0.022	0.31
MgO	%	0.01	FUS-ICP	0.2	0.17	1.52	2.79	8.17	2.56	0.25	6.24
CaO	%	0.01	FUS-ICP	10.05	9.82	3.26	0.88	7.84	0.35	8.65	0.56
Na_2O	%	0.01	FUS-ICP	5.06	5.01	1.66	0.26	3.18	0.17	5.09	0.13
K_2O	%	0.01	FUS-ICP	0.98	1.07	0.29	0.19	0.6	0.05	1.22	0.05
TiO_2	%	0.001	FUS-ICP	0.166	0.09	7.144	14.14	0.403	10.14	0.52	9.347
P_2O_5	%	0.01	FUS-ICP	0.05	0.05	0.03	< 0.01	0.05	0.02	0.04	< 0.01
LOI	%		FUS-ICP	0.46	0.65	-1.61	-2.49	0	-2.58	1.07	-2.2
Total	%	0.01	FUS-ICP	100.9	98.55	99.08	100.6	99.75	100.7	99.95	100.9
Sc	ppm	1	FUS-ICP	< 1	< 1	6	12	5	9	< 1	17
Be	ppm	1	FUS-ICP	< 1	< 1	< 1	< 1	< 1	< 1	< 1	< 1
V	ppm	5	FUS-ICP	20	7	2454	2829	77	3200	96	2511
Cr	ppm	20	FUS-MS	< 20	< 20	820	910	< 20	1330	120	1090
Co	ppm	1	FUS-MS	4	3	126	169	57	208	14	146
Ni	ppm	1	TD-ICP	21	28	226	239	115	318	78	226
Zn	ppm	1	TD-ICP	14	6	229	353	65	360	23	351
Cd	ppm	0.5	TD-ICP	< 0.5	< 0.5	0.5	0.7	< 0.5	0.8	< 0.5	1.1
S	%	0.001	TD-ICP	0.05	0.097	0.062	0.013	0.041	0.22	0.182	0.018
Cu	ppm	1	TD-ICP	16	61	93	44	21	231	231	61
Ag	ppm	0.3	TD-ICP	< 0.3	0.3	< 0.3	0.7	< 0.3	0.8	0.6	0.5
Pb	ppm	5	TD-ICP	< 5	< 5	14	15	< 5	16	< 5	15
Ga	ppm	1	FUS-MS	18	17	56	67	15	74	19	56
Ge	ppm	1	FUS-MS	< 1	1	1	2	1	2	1	2
As	ppm	5	FUS-MS	< 5	< 5	< 5	< 5	< 5	< 5	< 5	< 5
Rb	ppm	2	FUS-MS	8	4	< 2	3	< 2	< 2	10	2
Sr	ppm	2	FUS-ICP	1390	1413	451	112	995	52	1449	34
Y	ppm	2	FUS-ICP	2	< 2	< 2	< 2	< 2	< 2	< 2	< 2
Zr	ppm	4	FUS-ICP	9	5	6	12	5	7	5	9
Nb	ppm	1	FUS-MS	< 1	< 1	< 1	< 1	< 1	< 1	< 1	< 1
Mo	ppm	2	FUS-MS	< 2	< 2	< 2	3	< 2	< 2	< 2	< 2
In	ppm	0.2	FUS-MS	< 0.2	< 0.2	< 0.2	< 0.2	< 0.2	< 0.2	< 0.2	< 0.2
Sn	ppm	1	FUS-MS	< 1	< 1	1	2	< 1	1	< 1	1
Sb	ppm	0.5	FUS-MS	< 0.5	< 0.5	< 0.5	< 0.5	< 0.5	< 0.5	< 0.5	< 0.5
Cs	ppm	0.5	FUS-MS	< 0.5	< 0.5	< 0.5	< 0.5	< 0.5	< 0.5	< 0.5	< 0.5
Ba	ppm	3	FUS-ICP	919	937	264	98	609	38	1043	21
La	ppm	0.1	FUS-MS	3.7	2.8	1	0.3	2.4	0.2	3.7	< 0.1
Ce	ppm	0.1	FUS-MS	6.7	4.6	1.7	0.6	4.2	0.3	5.9	0.2
Pr	ppm	0.05	FUS-MS	0.79	0.53	0.2	0.07	0.53	< 0.05	0.71	< 0.05
Nd	ppm	0.1	FUS-MS	3.3	2	0.9	0.3	2.2	0.1	2.8	0.2
Sm	ppm	0.1	FUS-MS	0.5	0.3	0.1	< 0.1	0.4	< 0.1	0.4	< 0.1
Eu	ppm	0.05	FUS-MS	0.87	0.74	0.22	0.09	0.62	< 0.05	0.82	0.05
Gd	ppm	0.1	FUS-MS	0.4	0.2	< 0.1	< 0.1	0.3	< 0.1	0.2	0.1
Tb	ppm	0.1	FUS-MS	< 0.1	< 0.1	< 0.1	< 0.1	< 0.1	< 0.1	< 0.1	< 0.1
Dy	ppm	0.1	FUS-MS	0.3	< 0.1	< 0.1	< 0.1	0.3	< 0.1	0.1	0.1
Ho	ppm	0.1	FUS-MS	< 0.1	< 0.1	< 0.1	< 0.1	< 0.1	< 0.1	< 0.1	< 0.1
Er	ppm	0.1	FUS-MS	< 0.1	< 0.1	< 0.1	< 0.1	0.1	< 0.1	< 0.1	0.1
Tm	ppm	0.05	FUS-MS	< 0.05	< 0.05	< 0.05	< 0.05	< 0.05	< 0.05	< 0.05	< 0.05
Yb	ppm	0.1	FUS-MS	< 0.1	< 0.1	< 0.1	< 0.1	0.1	< 0.1	< 0.1	0.1
Lu	ppm	0.04	FUS-MS	< 0.04	< 0.04	< 0.04	< 0.04	< 0.04	< 0.04	< 0.04	< 0.04
Hf	ppm	0.2	FUS-MS	< 0.2	< 0.2	0.2	0.5	< 0.2	0.3	< 0.2	0.4
Ta	ppm	0.1	FUS-MS	< 0.1	< 0.1	< 0.1	0.1	< 0.1	< 0.1	< 0.1	< 0.1
W	ppm	1	FUS-MS	2	1	2	8	1	4	< 1	3
Tl	ppm	0.1	FUS-MS	0.2	< 0.1	< 0.1	0.1	< 0.1	< 0.1	< 0.1	< 0.1
Bi	ppm	0.4	FUS-MS	< 0.4	< 0.4	< 0.4	< 0.4	< 0.4	< 0.4	< 0.4	< 0.4
Th	ppm	0.1	FUS-MS	< 0.1	< 0.1	< 0.1	< 0.1	< 0.1	< 0.1	< 0.1	< 0.1
U	ppm	0.1	FUS-MS	0.1	< 0.1	0.2	0.3	< 0.1	0.1	< 0.1	< 0.1

Abbreviations:	Rock types		
MAS	Massive to semi-massive oxide mineralization	BAR	Barren anorthosite
OMAS	Orthopyroxene -bearing massive-semi-massive oxide mineralization	DIS	Disseminated oxide mineralization
GAB	Gabbronorite	TRO	Troctolite

Appendix III. (Continued)

Sample ID				CC021	CC022	CC023	CC024	CC025	CC026A	CC026B	CC027A
Easting				658257	658257	658257	658177	657619	657488	657488	657488
Westing				5929027	5929027	5929027	5929766	5929902	5929960	5929960	5929960
Description				MAS	OMAS	MAS	BAR	MAS	BAR	OMAS	GAB
		Idl									
SiO_2	%	0.01	FUS-ICP	12.67	15.8	34.29	57.15	10.97	55.39	0.99	55.83
Al_2O_3	%	0.01	FUS-ICP	11.05	7.62	17.08	24.89	11.6	25.47	9.39	24.77
$Fe_2O_{3(T)}$	%	0.01	FUS-ICP	59.65	61.89	29.5	1.63	65.34	2.27	79.7	2.83
MnO	%	0.001	FUS-ICP	0.287	0.308	0.135	0.013	0.225	0.016	0.296	0.017
MgO	%	0.01	FUS-ICP	2.69	6.09	0.99	0.19	1.86	0.26	2.3	0.19
CaO	%	0.01	FUS-ICP	1.95	1.01	4.69	6.93	1.68	7.76	0.04	7.93
Na_2O	%	0.01	FUS-ICP	1.08	0.31	3.33	5.82	0.68	5.54	0.04	5.46
K_2O	%	0.01	FUS-ICP	0.25	0.12	0.98	1.77	0.28	1.44	0.02	1.46
TiO_2	%	0.001	FUS-ICP	10.83	7.43	4.913	0.406	8.204	0.272	9.103	0.152
P_2O_5	%	0.01	FUS-ICP	0.02	0.02	0.03	0.03	< 0.01	0.08	< 0.01	0.05
LOI	%		FUS-ICP	-2.15	-2.29	2.18	0.82	-2.38	2.21	-3.34	1.17
Total	%	0.01	FUS-ICP	98.32	98.31	98.13	99.66	98.47	100.7	98.56	99.86
Sc	ppm	1	FUS-ICP	14	16	6	< 1	9	1	8	1
Be	ppm	1	FUS-ICP	< 1	< 1	< 1	< 1	< 1	< 1	< 1	< 1
V	ppm	5	FUS-ICP	2221	2198	831	57	2533	58	3471	20
Cr	ppm	20	FUS-MS	940	980	1370	40	2620	60	1380	20
Co	ppm	1	FUS-MS	125	129	127	6	133	6	182	22
Ni	ppm	1	TD-ICP	143	136	284	31	178	25	263	105
Zn	ppm	1	TD-ICP	317	283	166	13	461	13	303	11
Cd	ppm	0.5	TD-ICP	0.7	0.9	< 0.5	< 0.5	0.9	< 0.5	< 0.5	< 0.5
S	%	0.001	TD-ICP	0.026	0.005	1.52	0.158	0.015	0.055	0.007	0.747
Cu	ppm	1	TD-ICP	90	43	1150	127	34	107	45	268
Ag	ppm	0.3	TD-ICP	0.7	0.4	0.4	< 0.3	0.7	< 0.3	0.5	< 0.3
Pb	ppm	5	TD-ICP	14	13	5	6	15	< 5	17	< 5
Ga	ppm	1	FUS-MS	52	56	31	20	70	19	74	18
Ge	ppm	1	FUS-MS	1	2	1	1	2	1	2	1
As	ppm	5	FUS-MS	< 5	< 5	< 5	< 5	< 5	< 5	< 5	< 5
Rb	ppm	2	FUS-MS	< 2	3	7	6	3	8	< 2	6
Sr	ppm	2	FUS-ICP	333	101	952	1280	285	1525	10	1460
Y	ppm	2	FUS-ICP	< 2	< 2	< 2	< 2	< 2	2	< 2	< 2
Zr	ppm	4	FUS-ICP	24	15	17	8	33	7	7	7
Nb	ppm	1	FUS-MS	2	< 1	2	< 1	< 1	< 1	< 1	< 1
Mo	ppm	2	FUS-MS	< 2	< 2	< 2	< 2	< 2	< 2	< 2	< 2
In	ppm	0.2	FUS-MS	< 0.2	< 0.2	< 0.2	< 0.2	< 0.2	< 0.2	< 0.2	< 0.2
Sn	ppm	1	FUS-MS	2	2	< 1	< 1	2	< 1	2	< 1
Sb	ppm	0.5	FUS-MS	< 0.5	< 0.5	< 0.5	< 0.5	< 0.5	< 0.5	< 0.5	< 0.5
Cs	ppm	0.5	FUS-MS	< 0.5	< 0.5	< 0.5	< 0.5	< 0.5	< 0.5	< 0.5	< 0.5
Ba	ppm	3	FUS-ICP	232	71	676	1072	208	1293	< 3	1288
La	ppm	0.1	FUS-MS	1.2	0.6	3.4	6.6	1.6	5.8	< 0.1	5.3
Ce	ppm	0.1	FUS-MS	2	1.2	5.4	9.6	2.9	9.9	0.1	8.6
Pr	ppm	0.05	FUS-MS	0.18	0.16	0.56	0.97	0.36	1.19	< 0.05	0.94
Nd	ppm	0.1	FUS-MS	0.7	0.8	2.3	3.6	1.3	4.7	< 0.1	3.6
Sm	ppm	0.1	FUS-MS	0.1	0.2	0.2	0.4	0.2	0.6	< 0.1	0.5
Eu	ppm	0.05	FUS-MS	0.23	0.11	0.67	1.21	0.2	1.07	< 0.05	1.17
Gd	ppm	0.1	FUS-MS	< 0.1	0.2	0.2	0.2	0.2	0.5	< 0.1	0.3
Tb	ppm	0.1	FUS-MS	< 0.1	< 0.1	< 0.1	< 0.1	< 0.1	< 0.1	< 0.1	< 0.1
Dy	ppm	0.1	FUS-MS	< 0.1	0.2	0.1	< 0.1	0.1	0.3	< 0.1	0.2
Ho	ppm	0.1	FUS-MS	< 0.1	< 0.1	< 0.1	< 0.1	< 0.1	< 0.1	< 0.1	< 0.1
Er	ppm	0.1	FUS-MS	< 0.1	0.2	< 0.1	< 0.1	< 0.1	0.1	< 0.1	0.1
Tm	ppm	0.05	FUS-MS	< 0.05	< 0.05	< 0.05	< 0.05	< 0.05	< 0.05	< 0.05	< 0.05
Yb	ppm	0.1	FUS-MS	< 0.1	0.2	< 0.1	< 0.1	< 0.1	0.1	< 0.1	< 0.1
Lu	ppm	0.04	FUS-MS	< 0.04	< 0.04	< 0.04	< 0.04	< 0.04	< 0.04	< 0.04	< 0.04
Hf	ppm	0.2	FUS-MS	0.7	0.6	0.4	< 0.2	0.9	< 0.2	0.3	< 0.2
Ta	ppm	0.1	FUS-MS	0.1	< 0.1	< 0.1	< 0.1	< 0.1	< 0.1	< 0.1	< 0.1
W	ppm	1	FUS-MS	1	2	< 1	< 1	2	1	2	2
Tl	ppm	0.1	FUS-MS	< 0.1	< 0.1	< 0.1	< 0.1	< 0.1	< 0.1	< 0.1	< 0.1
Bi	ppm	0.4	FUS-MS	< 0.4	< 0.4	< 0.4	< 0.4	< 0.4	< 0.4	< 0.4	< 0.4
Th	ppm	0.1	FUS-MS	< 0.1	< 0.1	< 0.1	< 0.1	< 0.1	< 0.1	< 0.1	< 0.1
U	ppm	0.1	FUS-MS	< 0.1	< 0.1	< 0.1	< 0.1	< 0.1	< 0.1	< 0.1	< 0.1

Abbreviations:	Rock types		
MAS	Massive to semi-massive oxide mineralization	BAR	Barren anorthosite
OMAS	Orthopyroxene -bearing massive-semi-massive oxide mineralization	DIS	Disseminated oxide mineralization
GAB	Gabbronorite	TRO	Troctolite

Appendix III. (Continued)

Sample ID				CC027B	CC028A	CC029A	CC030	CC031	CC032	CC034	CC035
Easting				657488	656993	657661	657734	657605	657605	659545	659379
Westing				5929960	5930964	5929749	5929752	5929747	5929747	5927682	5927636
Description				BAR	MAS	MAS	OMAS	DIS	BAR	BAR	BAR
		Idl									
SiO_2	%	0.01	FUS-ICP	56.43	67.91	3.96	4.16	47.47	55.39	54.63	55.66
Al_2O_3	%	0.01	FUS-ICP	23.52	16.1	11.31	8.84	23.03	27.06	26.61	24.89
$Fe_2O_{3(T)}$	%	0.01	FUS-ICP	3.32	3.38	72.31	75.04	12.89	1.25	0.74	2.56
MnO	%	0.001	FUS-ICP	0.045	0.022	0.294	0.313	0.054	0.013	0.008	0.029
MgO	%	0.01	FUS-ICP	0.97	0.7	3.03	2.91	1.06	0.2	0.11	0.73
CaO	%	0.01	FUS-ICP	8.38	3.43	0.56	0.45	7.24	9.44	9.61	8.75
Na_2O	%	0.01	FUS-ICP	5.25	5.13	0.26	0.18	4.43	5.16	5.06	5.16
K_2O	%	0.01	FUS-ICP	1.45	0.99	0.07	0.08	0.99	1.18	1.1	1.37
TiO_2	%	0.001	FUS-ICP	0.219	0.296	10.89	11.56	1.941	0.149	0.101	0.324
P_2O_5	%	0.01	FUS-ICP	0.06	0.24	0.01	< 0.01	0.04	0.04	0.05	0.08
LOI	%		FUS-ICP	1.17	0.89	-2.56	-2.79	1.09	1	0.42	0.53
Total	%	0.01	FUS-ICP	100.8	99.09	100.1	100.7	100.2	100.9	98.44	100.1
Sc	ppm	1	FUS-ICP	7	< 1	11	14	4	1	< 1	3
Be	ppm	1	FUS-ICP	< 1	3	< 1	< 1	< 1	< 1	< 1	< 1
V	ppm	5	FUS-ICP	28	38	3049	2815	429	20	10	52
Cr	ppm	20	FUS-MS	30	20	1200	1690	450	< 20	< 20	60
Co	ppm	1	FUS-MS	20	23	168	157	30	4	< 1	7
Ni	ppm	1	TD-ICP	95	46	262	199	103	24	10	31
Zn	ppm	1	TD-ICP	16	27	369	332	61	8	6	17
Cd	ppm	0.5	TD-ICP	< 0.5	< 0.5	0.6	1	< 0.5	< 0.5	< 0.5	< 0.5
S	%	0.001	TD-ICP	0.579	0.547	0.009	0.004	0.085	0.091	0.052	0.089
Cu	ppm	1	TD-ICP	191	266	107	68	151	45	7	60
Ag	ppm	0.3	TD-ICP	0.4	0.5	0.7	0.5	< 0.3	< 0.3	< 0.3	0.4
Pb	ppm	5	TD-ICP	< 5	26	77	20	6	< 5	< 5	< 5
Ga	ppm	1	FUS-MS	18	21	72	65	24	18	17	18
Ge	ppm	1	FUS-MS	1	1	2	2	1	1	1	1
As	ppm	5	FUS-MS	< 5	< 5	< 5	< 5	< 5	< 5	< 5	< 5
Rb	ppm	2	FUS-MS	7	30	< 2	< 2	7	8	2	4
Sr	ppm	2	FUS-ICP	1365	1601	86	74	1302	1382	1369	1451
Y	ppm	2	FUS-ICP	4	4	< 2	< 2	< 2	< 2	< 2	3
Zr	ppm	4	FUS-ICP	11	154	12	14	9	6	5	11
Nb	ppm	1	FUS-MS	< 1	2	< 1	< 1	< 1	< 1	< 1	< 1
Mo	ppm	2	FUS-MS	< 2	< 2	< 2	< 2	< 2	< 2	< 2	< 2
In	ppm	0.2	FUS-MS	< 0.2	< 0.2	< 0.2	< 0.2	< 0.2	< 0.2	< 0.2	< 0.2
Sn	ppm	1	FUS-MS	< 1	< 1	2	2	< 1	< 1	< 1	< 1
Sb	ppm	0.5	FUS-MS	< 0.5	< 0.5	< 0.5	< 0.5	< 0.5	< 0.5	< 0.5	< 0.5
Cs	ppm	0.5	FUS-MS	< 0.5	0.7	< 0.5	< 0.5	< 0.5	< 0.5	< 0.5	< 0.5
Ba	ppm	3	FUS-ICP	1213	467	57	60	925	1021	978	1196
La	ppm	0.1	FUS-MS	5.7	97.9	0.2	0.2	3.7	3.9	3.7	5.1
Ce	ppm	0.1	FUS-MS	9.7	174	0.4	0.3	6.1	6.1	6.3	8.8
Pr	ppm	0.05	FUS-MS	1.21	18	0.05	< 0.05	0.68	0.71	0.74	1.07
Nd	ppm	0.1	FUS-MS	5.4	57.7	0.2	0.2	2.7	2.7	2.6	4.1
Sm	ppm	0.1	FUS-MS	0.9	6.2	< 0.1	< 0.1	0.4	0.4	0.4	0.7
Eu	ppm	0.05	FUS-MS	1.33	1.24	0.06	< 0.05	0.78	0.95	0.84	1.08
Gd	ppm	0.1	FUS-MS	0.7	2.3	< 0.1	< 0.1	0.2	0.3	0.2	0.5
Tb	ppm	0.1	FUS-MS	0.1	0.2	< 0.1	< 0.1	< 0.1	< 0.1	< 0.1	< 0.1
Dy	ppm	0.1	FUS-MS	0.7	0.9	< 0.1	< 0.1	0.1	0.1	0.2	0.4
Ho	ppm	0.1	FUS-MS	0.1	0.1	< 0.1	< 0.1	< 0.1	< 0.1	< 0.1	< 0.1
Er	ppm	0.1	FUS-MS	0.3	0.3	< 0.1	< 0.1	< 0.1	< 0.1	< 0.1	0.2
Tm	ppm	0.05	FUS-MS	< 0.05	< 0.05	< 0.05	< 0.05	< 0.05	< 0.05	< 0.05	< 0.05
Yb	ppm	0.1	FUS-MS	0.2	0.2	< 0.1	< 0.1	< 0.1	< 0.1	< 0.1	0.2
Lu	ppm	0.04	FUS-MS	< 0.04	< 0.04	< 0.04	< 0.04	< 0.04	< 0.04	< 0.04	< 0.04
Hf	ppm	0.2	FUS-MS	< 0.2	3.2	0.4	0.5	0.2	< 0.2	< 0.2	< 0.2
Ta	ppm	0.1	FUS-MS	< 0.1	< 0.1	< 0.1	< 0.1	< 0.1	< 0.1	< 0.1	< 0.1
W	ppm	1	FUS-MS	< 1	< 1	2	2	< 1	< 1	< 1	2
Tl	ppm	0.1	FUS-MS	< 0.1	< 0.1	< 0.1	< 0.1	< 0.1	< 0.1	< 0.1	< 0.1
Bi	ppm	0.4	FUS-MS	< 0.4	< 0.4	< 0.4	< 0.4	< 0.4	< 0.4	< 0.4	< 0.4
Th	ppm	0.1	FUS-MS	< 0.1	25.4	< 0.1	< 0.1	< 0.1	< 0.1	< 0.1	< 0.1
U	ppm	0.1	FUS-MS	< 0.1	0.8	< 0.1	< 0.1	< 0.1	< 0.1	< 0.1	< 0.1

Abbreviations:	Rock types		
MAS	Massive to semi-massive oxide mineralization	BAR	Barren anorthosite
OMAS	Orthopyroxene -bearing massive-semi-massive oxide mineralization	DIS	Disseminated oxide mineralization
GAB	Gabbronorite	TRO	Troctolite

Appendix III. (Continued)

Sample ID				CC036	CC037	CC038	CC039	CC041	CC042A	CC043	CC045	CC046
Easting				659118	659390	659554	658920	658884	659021	658632	658107	657985
Westing				5927608	5927870	5927859	5927761	5928070	5928177	5928536	5928784	5928761
Description				BAR	BAR	BAR	TRO	GAB	BAR	GAB	TRO	BAR
		Idl										
SiO_2	%	0.01	FUS-ICP	56.53	50.5	54.37	51.11	47.85	54.74	51.15	48.65	52.88
Al_2O_3	%	0.01	FUS-ICP	26.77	23.19	27.15	23.2	17.37	26.93	24.7	19.27	27.97
$Fe_2O_{3(T)}$	%	0.01	FUS-ICP	1.01	5.76	0.89	6.16	12.86	0.88	4.98	10.8	1.08
MnO	%	0.001	FUS-ICP	0.009	0.08	0.012	0.083	0.173	0.012	0.067	0.141	0.01
MgO	%	0.01	FUS-ICP	0.09	5.2	0.32	5.62	8.04	0.29	4.77	9.89	0.18
CaO	%	0.01	FUS-ICP	9.12	9.35	10.15	9.36	9.77	9.18	9.4	7.71	10.5
Na_2O	%	0.01	FUS-ICP	5.36	3.52	4.82	3.65	2.72	5.14	3.8	2.84	4.82
K_2O	%	0.01	FUS-ICP	1.25	0.55	0.96	0.65	0.53	1.31	0.75	0.59	0.4
TiO_2	%	0.001	FUS-ICP	0.124	0.171	0.104	0.151	1.173	0.07	0.094	0.2	0.136
P_2O_5	%	0.01	FUS-ICP	0.05	0.05	0.03	0.05	0.11	0.03	0.02	0.04	0.05
LOI	%		FUS-ICP	0.64	1.96	0.51	0.39	0.23	1.48	1.23	0.13	0.75
Total	%	0.01	FUS-ICP	101	100.3	99.31	100.4	100.8	100.1	101	100.3	98.79
Sc	ppm	1	FUS-ICP	< 1	2	< 1	2	27	< 1	2	2	1
Be	ppm	1	FUS-ICP	< 1	< 1	< 1	< 1	< 1	< 1	< 1	< 1	< 1
V	ppm	5	FUS-ICP	18	24	10	21	195	9	12	32	16
Cr	ppm	20	FUS-MS	20	< 20	< 20	< 20	140	< 20	< 20	< 20	< 20
Co	ppm	1	FUS-MS	1	34	2	38	58	2	30	65	3
Ni	ppm	1	TD-ICP	7	97	8	104	161	11	84	171	13
Zn	ppm	1	TD-ICP	8	38	6	38	72	4	32	65	7
Cd	ppm	0.5	TD-ICP	< 0.5	< 0.5	< 0.5	< 0.5	< 0.5	< 0.5	< 0.5	< 0.5	< 0.5
S	%	0.001	TD-ICP	0.047	0.041	0.041	0.051	0.076	0.043	0.04	0.04	0.06
Cu	ppm	1	TD-ICP	8	7	< 1	20	97	9	4	6	20
Ag	ppm	0.3	TD-ICP	< 0.3	< 0.3	< 0.3	< 0.3	< 0.3	< 0.3	< 0.3	< 0.3	0.4
Pb	ppm	5	TD-ICP	< 5	< 5	< 5	< 5	< 5	< 5	< 5	< 5	< 5
Ga	ppm	1	FUS-MS	18	16	17	15	20	18	15	13	18
Ge	ppm	1	FUS-MS	1	1	1	1	2	1	1	2	1
As	ppm	5	FUS-MS	< 5	< 5	< 5	< 5	< 5	< 5	< 5	< 5	< 5
Rb	ppm	2	FUS-MS	3	8	4	2	13	29	8	< 2	3
Sr	ppm	2	FUS-ICP	1525	1020	1313	1093	264	1400	1113	866	1373
Y	ppm	2	FUS-ICP	< 2	< 2	< 2	< 2	19	< 2	< 2	< 2	2
Zr	ppm	4	FUS-ICP	6	5	5	6	80	5	< 4	< 4	7
Nb	ppm	1	FUS-MS	< 1	< 1	< 1	< 1	6	< 1	< 1	< 1	< 1
Mo	ppm	2	FUS-MS	< 2	< 2	< 2	< 2	< 2	< 2	< 2	< 2	< 2
In	ppm	0.2	FUS-MS	< 0.2	< 0.2	< 0.2	< 0.2	< 0.2	< 0.2	< 0.2	< 0.2	< 0.2
Sn	ppm	1	FUS-MS	< 1	< 1	< 1	< 1	2	1	< 1	< 1	< 1
Sb	ppm	0.5	FUS-MS	< 0.5	< 0.5	< 0.5	< 0.5	< 0.5	< 0.5	< 0.5	< 0.5	< 0.5
Cs	ppm	0.5	FUS-MS	< 0.5	0.6	< 0.5	< 0.5	< 0.5	0.7	< 0.5	< 0.5	< 0.5
Ba	ppm	3	FUS-ICP	1100	441	816	608	137	870	521	503	724
La	ppm	0.1	FUS-MS	3.9	2.6	3	2.7	8.2	3.2	2	2.1	3.9
Ce	ppm	0.1	FUS-MS	6.5	4.7	5	5	18.5	5.1	3.4	3.8	7.1
Pr	ppm	0.05	FUS-MS	0.71	0.56	0.6	0.61	2.59	0.56	0.42	0.45	0.89
Nd	ppm	0.1	FUS-MS	2.9	2.5	2.2	2.5	11.6	2	1.6	1.6	3.7
Sm	ppm	0.1	FUS-MS	0.4	0.4	0.4	0.4	3.2	0.3	0.3	0.3	0.6
Eu	ppm	0.05	FUS-MS	0.92	0.59	0.79	0.66	1.12	0.72	0.51	0.57	0.83
Gd	ppm	0.1	FUS-MS	0.2	0.2	0.2	0.3	3.2	0.2	0.2	0.2	0.4
Tb	ppm	0.1	FUS-MS	< 0.1	< 0.1	< 0.1	< 0.1	0.6	< 0.1	< 0.1	< 0.1	< 0.1
Dy	ppm	0.1	FUS-MS	0.1	0.2	< 0.1	0.2	3.5	0.1	< 0.1	< 0.1	0.3
Ho	ppm	0.1	FUS-MS	< 0.1	< 0.1	< 0.1	< 0.1	0.7	< 0.1	< 0.1	< 0.1	< 0.1
Er	ppm	0.1	FUS-MS	< 0.1	< 0.1	< 0.1	0.1	2	< 0.1	< 0.1	< 0.1	0.1
Tm	ppm	0.05	FUS-MS	< 0.05	< 0.05	< 0.05	< 0.05	0.29	< 0.05	< 0.05	< 0.05	< 0.05
Yb	ppm	0.1	FUS-MS	< 0.1	< 0.1	< 0.1	< 0.1	1.8	< 0.1	< 0.1	< 0.1	0.1
Lu	ppm	0.04	FUS-MS	< 0.04	< 0.04	< 0.04	< 0.04	0.31	< 0.04	< 0.04	< 0.04	< 0.04
Hf	ppm	0.2	FUS-MS	< 0.2	< 0.2	< 0.2	< 0.2	1.8	< 0.2	< 0.2	< 0.2	< 0.2
Ta	ppm	0.1	FUS-MS	< 0.1	< 0.1	< 0.1	< 0.1	0.4	< 0.1	< 0.1	< 0.1	< 0.1
W	ppm	1	FUS-MS	< 1	1	< 1	1	1	1	< 1	< 1	2
Tl	ppm	0.1	FUS-MS	< 0.1	< 0.1	< 0.1	< 0.1	0.4	0.4	0.3	0.1	0.1
Bi	ppm	0.4	FUS-MS	< 0.4	< 0.4	< 0.4	< 0.4	< 0.4	< 0.4	< 0.4	< 0.4	< 0.4
Th	ppm	0.1	FUS-MS	< 0.1	0.1	< 0.1	< 0.1	1	0.1	< 0.1	< 0.1	< 0.1
U	ppm	0.1	FUS-MS	< 0.1	0.2	< 0.1	< 0.1	0.4	< 0.1	< 0.1	< 0.1	< 0.1

Abbreviations:	Rock types		
MAS	Massive to semi-massive oxide mineralization	BAR	Barren anorthosite
OMAS	Orthopyroxene -bearing massive-semi-massive oxide mineralization	DIS	Disseminated oxide mineralization
GAB	Gabbronorite	TRO	Troctolite

Appendix III. (Continued)

Sample ID				CC047	CC048	CC050A	CC050BA	CC050C	CC051A	CC051B	CC052A
Easting				658396	658384	658392	658392	658392	667719	667719	667982
Westing				5928496	5928579	5928617	5928617	5928617	5919434	5919434	5919407
Description				GAB	BAR	MAS	BAR	MAS	BAR	BAR	BAR
		Idl									
SiO_2	%	0.01	FUS-ICP	51.49	54.4	1.04	52.7	18.7	51.07	52.13	53.36
Al_2O_3	%	0.01	FUS-ICP	24.03	26.08	8.42	23.96	13.67	28.01	28	27.1
$Fe_2O_{3(T)}$	%	0.01	FUS-ICP	5.63	3.8	81.78	5.44	54.42	1.16	1.27	1.72
MnO	%	0.001	FUS-ICP	0.075	0.024	0.304	0.066	0.259	0.013	0.013	0.025
MgO	%	0.01	FUS-ICP	4.62	0.27	1.9	2.74	2.53	0.23	0.21	0.78
CaO	%	0.01	FUS-ICP	9.38	8.41	0.07	8.85	2.68	10.32	10.24	10.01
Na_2O	%	0.01	FUS-ICP	3.84	5.35	0.05	4.42	1.46	4.39	4.32	4.36
K_2O	%	0.01	FUS-ICP	0.7	1.22	0.04	1.07	0.4	1.33	1.37	1.07
TiO_2	%	0.001	FUS-ICP	0.202	0.671	9.302	0.525	7.616	0.146	0.175	0.161
P_2O_5	%	0.01	FUS-ICP	0.05	0.05	< 0.01	0.07	0.02	0.03	0.04	0.03
LOI	%		FUS-ICP	0.64	0.49	-3.08	0.46	-1.31	2.57	2.61	0.94
Total	%	0.01	FUS-ICP	100.7	100.8	99.83	100.3	100.4	99.26	100.4	99.56
Sc	ppm	1	FUS-ICP	2	1	9	6	11	1	< 1	2
Be	ppm	1	FUS-ICP	< 1	< 1	< 1	< 1	< 1	< 1	< 1	< 1
V	ppm	5	FUS-ICP	25	111	3091	74	2088	22	26	28
Cr	ppm	20	FUS-MS	< 20	180	3480	60	2590	< 20	< 20	30
Co	ppm	1	FUS-MS	30	9	160	20	112	2	2	4
Ni	ppm	1	TD-ICP	84	21	212	39	143	9	10	13
Zn	ppm	1	TD-ICP	37	26	336	39	303	10	7	12
Cd	ppm	0.5	TD-ICP	< 0.5	< 0.5	1.2	< 0.5	< 0.5	< 0.5	< 0.5	< 0.5
S	%	0.001	TD-ICP	0.045	0.065	0.001	0.079	0.017	0.052	0.049	0.047
Cu	ppm	1	TD-ICP	10	27	29	30	147	3	11	12
Ag	ppm	0.3	TD-ICP	< 0.3	< 0.3	0.8	< 0.3	0.4	< 0.3	< 0.3	< 0.3
Pb	ppm	5	TD-ICP	< 5	< 5	17	< 5	9	< 5	< 5	< 5
Ga	ppm	1	FUS-MS	15	20	71	19	59	17	17	17
Ge	ppm	1	FUS-MS	1	1	2	1	2	1	< 1	1
As	ppm	5	FUS-MS	< 5	< 5	< 5	< 5	< 5	< 5	< 5	< 5
Rb	ppm	2	FUS-MS	3	3	< 2	3	< 2	17	17	9
Sr	ppm	2	FUS-ICP	1101	1491	16	1281	502	1286	1285	1305
Y	ppm	2	FUS-ICP	< 2	< 2	< 2	3	< 2	< 2	< 2	< 2
Zr	ppm	4	FUS-ICP	6	7	9	13	14	6	6	5
Nb	ppm	1	FUS-MS	< 1	< 1	< 1	< 1	1	< 1	< 1	< 1
Mo	ppm	2	FUS-MS	< 2	< 2	< 2	< 2	< 2	< 2	< 2	< 2
In	ppm	0.2	FUS-MS	< 0.2	< 0.2	< 0.2	< 0.2	< 0.2	< 0.2	< 0.2	< 0.2
Sn	ppm	1	FUS-MS	< 1	1	2	< 1	2	< 1	< 1	< 1
Sb	ppm	0.5	FUS-MS	< 0.5	< 0.5	< 0.5	< 0.5	< 0.5	< 0.5	< 0.5	< 0.5
Cs	ppm	0.5	FUS-MS	< 0.5	< 0.5	< 0.5	< 0.5	< 0.5	0.9	1	< 0.5
Ba	ppm	3	FUS-ICP	629	1162	9	1053	389	577	569	574
La	ppm	0.1	FUS-MS	3.3	4.2	0.1	5	1.5	2.3	2.3	2.5
Ce	ppm	0.1	FUS-MS	6	6.8	0.2	8.9	2.4	4.2	4.1	4.3
Pr	ppm	0.05	FUS-MS	0.75	0.79	< 0.05	1.1	0.29	0.5	0.52	0.51
Nd	ppm	0.1	FUS-MS	3.3	2.5	< 0.1	4.5	0.9	2.4	2.2	2.3
Sm	ppm	0.1	FUS-MS	0.5	0.5	< 0.1	0.9	0.2	0.4	0.4	0.3
Eu	ppm	0.05	FUS-MS	0.71	0.93	< 0.05	1.03	0.33	0.59	0.58	0.64
Gd	ppm	0.1	FUS-MS	0.4	0.3	< 0.1	0.7	0.1	0.2	0.3	0.2
Tb	ppm	0.1	FUS-MS	< 0.1	< 0.1	< 0.1	0.1	< 0.1	< 0.1	< 0.1	< 0.1
Dy	ppm	0.1	FUS-MS	0.3	0.2	< 0.1	0.6	< 0.1	0.2	0.2	0.2
Ho	ppm	0.1	FUS-MS	< 0.1	< 0.1	< 0.1	0.1	< 0.1	< 0.1	< 0.1	< 0.1
Er	ppm	0.1	FUS-MS	0.1	< 0.1	< 0.1	0.3	< 0.1	< 0.1	< 0.1	< 0.1
Tm	ppm	0.05	FUS-MS	< 0.05	< 0.05	< 0.05	< 0.05	< 0.05	< 0.05	< 0.05	< 0.05
Yb	ppm	0.1	FUS-MS	< 0.1	< 0.1	< 0.1	0.3	< 0.1	< 0.1	< 0.1	< 0.1
Lu	ppm	0.04	FUS-MS	< 0.04	< 0.04	< 0.04	0.04	< 0.04	< 0.04	< 0.04	< 0.04
Hf	ppm	0.2	FUS-MS	< 0.2	< 0.2	0.4	0.3	0.5	< 0.2	< 0.2	< 0.2
Ta	ppm	0.1	FUS-MS	< 0.1	< 0.1	< 0.1	< 0.1	< 0.1	< 0.1	< 0.1	< 0.1
W	ppm	1	FUS-MS	< 1	< 1	1	< 1	1	< 1	< 1	< 1
Tl	ppm	0.1	FUS-MS	< 0.1	< 0.1	< 0.1	< 0.1	< 0.1	0.1	0.1	< 0.1
Bi	ppm	0.4	FUS-MS	< 0.4	< 0.4	< 0.4	< 0.4	< 0.4	< 0.4	< 0.4	< 0.4
Th	ppm	0.1	FUS-MS	< 0.1	< 0.1	< 0.1	< 0.1	< 0.1	0.4	0.3	< 0.1
U	ppm	0.1	FUS-MS	< 0.1	< 0.1	< 0.1	< 0.1	< 0.1	< 0.1	< 0.1	< 0.1

Abbreviations:	Rock types		
MAS	Massive to semi-massive oxide mineralization	BAR	Barren anorthosite
OMAS	Orthopyroxene -bearing massive-semi-massive oxide mineralization	DIS	Disseminated oxide mineralization
GAB	Gabbronorite	TRO	Troctolite

Appendix III. (Continued)

Sample ID				CC052B	CC052D	CC053	CC054A	CC059A	CC059B	CC060	CC061
Easting				667982	667982	667754	667754	658741	658741	659434	657858
Westing				5919407	5919407	5919493	5919493	5929050	5929050	5928198	5929930
Description				BAR	BAR	MAS	GAB	MAS	GAB	MAS	BAR
		Idl									
SiO_2	%	0.01	FUS-ICP	54.84	51.86	17.49	51.51	8.59	52.56	0.48	55.93
Al_2O_3	%	0.01	FUS-ICP	23.35	25.31	13.65	23.86	12.08	25.1	8.52	26.1
$Fe_2O_{3(T)}$	%	0.01	FUS-ICP	5.14	5.59	57.69	6.04	62.82	3.47	77.61	2.07
MnO	%	0.001	FUS-ICP	0.113	0.082	0.193	0.071	0.277	0.022	0.287	0.018
MgO	%	0.01	FUS-ICP	0.97	0.29	1.56	2.49	3.73	0.74	2.34	0.48
CaO	%	0.01	FUS-ICP	7.42	8.53	2.61	8.68	1.34	9.33	< 0.01	8.73
Na_2O	%	0.01	FUS-ICP	5.48	4.85	1.28	4.1	0.46	4.9	0.02	5.33
K_2O	%	0.01	FUS-ICP	1.51	1.22	0.45	1.01	0.19	0.9	0.04	1.22
TiO_2	%	0.001	FUS-ICP	0.625	0.752	5.695	0.681	10.8	0.213	11.86	0.273
P_2O_5	%	0.01	FUS-ICP	0.2	0.34	0.01	0.04	0.02	0.03	< 0.01	0.04
LOI	%		FUS-ICP	1.32	1.15	-1.27	0.46	-2.02	0.95	-2.83	0.69
Total	%	0.01	FUS-ICP	101	99.98	99.36	98.93	98.29	98.21	98.31	100.9
Sc	ppm	1	FUS-ICP	8	4	7	6	15	2	13	1
Be	ppm	1	FUS-ICP	< 1	1	< 1	< 1	< 1	< 1	< 1	< 1
V	ppm	5	FUS-ICP	39	41	2109	127	2573	34	3231	48
Cr	ppm	20	FUS-MS	< 20	< 20	1280	60	1210	< 20	1700	20
Co	ppm	1	FUS-MS	7	8	118	20	191	24	177	6
Ni	ppm	1	TD-ICP	17	16	188	54	300	205	283	24
Zn	ppm	1	TD-ICP	69	63	306	39	339	17	311	15
Cd	ppm	0.5	TD-ICP	< 0.5	< 0.5	0.8	< 0.5	0.6	< 0.5	0.7	< 0.5
S	%	0.001	TD-ICP	0.079	0.104	0.04	0.094	0.184	0.603	0.004	0.065
Cu	ppm	1	TD-ICP	47	89	64	91	229	454	71	42
Ag	ppm	0.3	TD-ICP	< 0.3	< 0.3	< 0.3	0.3	0.4	0.4	0.4	0.4
Pb	ppm	5	TD-ICP	5	6	12	< 5	15	6	19	< 5
Ga	ppm	1	FUS-MS	22	20	62	20	62	17	71	18
Ge	ppm	1	FUS-MS	2	1	2	1	2	1	2	1
As	ppm	5	FUS-MS	< 5	< 5	< 5	< 5	< 5	< 5	< 5	< 5
Rb	ppm	2	FUS-MS	12	14	5	4	2	5	< 2	5
Sr	ppm	2	FUS-ICP	1101	1275	419	1269	193	1333	4	1536
Y	ppm	2	FUS-ICP	7	8	< 2	2	< 2	< 2	< 2	< 2
Zr	ppm	4	FUS-ICP	34	11	23	7	11	5	10	5
Nb	ppm	1	FUS-MS	< 1	4	< 1	< 1	< 1	< 1	< 1	< 1
Mo	ppm	2	FUS-MS	< 2	< 2	< 2	< 2	< 2	< 2	< 2	< 2
In	ppm	0.2	FUS-MS	< 0.2	< 0.2	< 0.2	< 0.2	< 0.2	< 0.2	< 0.2	< 0.2
Sn	ppm	1	FUS-MS	< 1	< 1	2	< 1	2	< 1	1	< 1
Sb	ppm	0.5	FUS-MS	< 0.5	< 0.5	< 0.5	< 0.5	< 0.5	< 0.5	< 0.5	< 0.5
Cs	ppm	0.5	FUS-MS	< 0.5	< 0.5	< 0.5	< 0.5	< 0.5	< 0.5	< 0.5	< 0.5
Ba	ppm	3	FUS-ICP	857	752	299	841	149	950	< 3	1104
La	ppm	0.1	FUS-MS	11.6	10.1	1.2	3.7	0.6	3.1	< 0.1	3.5
Ce	ppm	0.1	FUS-MS	21.2	21.4	2.2	5.9	1.1	5.1	< 0.1	5.6
Pr	ppm	0.05	FUS-MS	2.77	2.91	0.27	0.65	0.14	0.59	< 0.05	0.65
Nd	ppm	0.1	FUS-MS	11.6	12.9	1.1	2.8	0.5	2.3	< 0.1	2.3
Sm	ppm	0.1	FUS-MS	2.2	2.4	0.2	0.4	< 0.1	0.4	< 0.1	0.4
Eu	ppm	0.05	FUS-MS	2.03	1.45	0.25	0.86	0.13	0.74	< 0.05	0.79
Gd	ppm	0.1	FUS-MS	1.8	2	0.1	0.3	< 0.1	0.2	< 0.1	0.2
Tb	ppm	0.1	FUS-MS	0.3	0.2	< 0.1	< 0.1	< 0.1	< 0.1	< 0.1	< 0.1
Dy	ppm	0.1	FUS-MS	1.6	1.4	< 0.1	0.2	< 0.1	0.1	< 0.1	0.1
Ho	ppm	0.1	FUS-MS	0.3	0.2	< 0.1	< 0.1	< 0.1	< 0.1	< 0.1	< 0.1
Er	ppm	0.1	FUS-MS	0.8	0.7	< 0.1	0.1	< 0.1	< 0.1	< 0.1	< 0.1
Tm	ppm	0.05	FUS-MS	0.12	0.1	< 0.05	< 0.05	< 0.05	< 0.05	< 0.05	< 0.05
Yb	ppm	0.1	FUS-MS	0.8	0.6	< 0.1	0.1	< 0.1	< 0.1	< 0.1	< 0.1
Lu	ppm	0.04	FUS-MS	0.11	0.09	< 0.04	< 0.04	< 0.04	< 0.04	< 0.04	< 0.04
Hf	ppm	0.2	FUS-MS	0.7	0.3	0.6	< 0.2	0.4	< 0.2	0.4	< 0.2
Ta	ppm	0.1	FUS-MS	< 0.1	< 0.1	< 0.1	< 0.1	< 0.1	< 0.1	< 0.1	< 0.1
W	ppm	1	FUS-MS	< 1	< 1	2	2	2	< 1	1	< 1
Tl	ppm	0.1	FUS-MS	< 0.1	0.1	< 0.1	< 0.1	< 0.1	0.1	< 0.1	< 0.1
Bi	ppm	0.4	FUS-MS	< 0.4	< 0.4	< 0.4	< 0.4	< 0.4	< 0.4	< 0.4	< 0.4
Th	ppm	0.1	FUS-MS	< 0.1	< 0.1	< 0.1	< 0.1	< 0.1	< 0.1	< 0.1	< 0.1
U	ppm	0.1	FUS-MS	< 0.1	< 0.1	< 0.1	< 0.1	0.2	0.2	0.3	< 0.1

Abbreviations:	Rock types		
MAS	Massive to semi-massive oxide mineralization	BAR	Barren anorthosite
OMAS	Orthopyroxene -bearing massive-semi-massive oxide mineralization	DIS	Disseminated oxide mineralization
GAB	Gabbronorite	TRO	Troctolite

Appendix III. (Continued)

Sample ID				CC063A	CC063B	CC064	CC065A	CC065B	CC066	CC067A	CC067B	CC068
Easting				657451	657451	657507	657731	657731	657825	657914	657914	658275
Westing				5929961	5929961	5929978	5930062	5930062	5930109	5930069	5930069	5929492
Description				MAS	BAR	DIS	BAR	BAR	BAR	OMAS	BAR	BAR
		ldl										
SiO_2	%	0.01	FUS-ICP	14.46	53.62	56.61	56.21	56.13	55.77	14.12	53.78	52.26
Al_2O_3	%	0.01	FUS-ICP	11.81	25.88	25.35	26.65	26.63	26.53	8.39	25.27	27.07
$Fe_2O_{3(T)}$	%	0.01	FUS-ICP	56.87	3.64	1.77	0.72	0.63	1.3	61.77	2.5	2.06
MnO	%	0.001	FUS-ICP	0.271	0.022	0.012	0.007	0.006	0.012	0.298	0.015	0.022
MgO	%	0.01	FUS-ICP	3.76	0.22	0.13	0.05	0.06	0.3	7.28	0.18	0.7
CaO	%	0.01	FUS-ICP	1.53	8.48	8.26	8.9	8.92	9.66	0.47	9.01	11
Na_2O	%	0.01	FUS-ICP	0.24	5.25	5.55	5.5	5.54	5.14	0.04	5.13	4.32
K_2O	%	0.01	FUS-ICP	2.34	1.12	1.46	1.19	1.18	1.02	0.03	1.19	0.97
TiO_2	%	0.001	FUS-ICP	8.494	0.781	0.11	0.102	0.099	0.136	8.443	0.346	0.254
P_2O_5	%	0.01	FUS-ICP	0.01	0.04	0.06	0.05	0.05	0.04	0.01	0.04	0.1
LOI	%		FUS-ICP	-0.09	0.55	0.76	0.66	0.71	0.8	-2.06	0.95	1.9
Total	%	0.01	FUS-ICP	99.7	99.63	100.1	100	99.95	100.7	98.79	98.4	100.7
Sc	ppm	1	FUS-ICP	13	1	< 1	< 1	< 1	< 1	17	< 1	3
Be	ppm	1	FUS-ICP	< 1	< 1	< 1	< 1	< 1	< 1	< 1	< 1	< 1
V	ppm	5	FUS-ICP	2052	107	9	6	6	21	2246	69	34
Cr	ppm	20	FUS-MS	760	100	< 20	< 20	< 20	< 20	3770	70	20
Co	ppm	1	FUS-MS	135	9	14	< 1	< 1	3	154	5	6
Ni	ppm	1	TD-ICP	260	27	60	7	6	23	243	23	27
Zn	ppm	1	TD-ICP	283	21	6	7	4	8	273	15	15
Cd	ppm	0.5	TD-ICP	< 0.5	< 0.5	< 0.5	< 0.5	< 0.5	< 0.5	0.7	< 0.5	< 0.5
S	%	0.001	TD-ICP	0.111	0.048	0.441	0.04	0.039	0.071	0.007	0.069	0.05
Cu	ppm	1	TD-ICP	111	22	203	5	6	40	72	41	14
Ag	ppm	0.3	TD-ICP	< 0.3	< 0.3	0.4	0.4	0.4	0.4	0.5	0.4	< 0.3
Pb	ppm	5	TD-ICP	14	< 5	< 5	< 5	< 5	< 5	11	< 5	< 5
Ga	ppm	1	FUS-MS	50	20	18	18	18	17	53	18	17
Ge	ppm	1	FUS-MS	2	1	1	1	1	1	2	1	1
As	ppm	5	FUS-MS	< 5	< 5	< 5	< 5	< 5	< 5	< 5	< 5	< 5
Rb	ppm	2	FUS-MS	57	4	4	5	5	3	< 2	5	17
Sr	ppm	2	FUS-ICP	211	1496	1460	1520	1519	1450	8	1467	1296
Y	ppm	2	FUS-ICP	< 2	< 2	< 2	< 2	< 2	< 2	< 2	< 2	3
Zr	ppm	4	FUS-ICP	11	8	6	5	5	5	9	5	11
Nb	ppm	1	FUS-MS	< 1	< 1	< 1	2	< 1	< 1	< 1	< 1	< 1
Mo	ppm	2	FUS-MS	< 2	< 2	< 2	< 2	< 2	< 2	< 2	< 2	< 2
In	ppm	0.2	FUS-MS	< 0.2	< 0.2	< 0.2	< 0.2	< 0.2	< 0.2	< 0.2	< 0.2	< 0.2
Sn	ppm	1	FUS-MS	1	< 1	< 1	< 1	< 1	< 1	1	1	< 1
Sb	ppm	0.5	FUS-MS	< 0.5	< 0.5	< 0.5	< 0.5	< 0.5	< 0.5	< 0.5	< 0.5	< 0.5
Cs	ppm	0.5	FUS-MS	2.5	< 0.5	< 0.5	< 0.5	< 0.5	< 0.5	< 0.5	< 0.5	< 0.5
Ba	ppm	3	FUS-ICP	422	1078	1330	1156	1100	956	< 3	1042	463
La	ppm	0.1	FUS-MS	1	3.8	4.6	4.1	3.6	2.7	< 0.1	3.3	3.2
Ce	ppm	0.1	FUS-MS	1.7	6.3	7.6	6.8	5.9	4.2	0.2	5.2	6.3
Pr	ppm	0.05	FUS-MS	0.22	0.71	0.84	0.78	0.65	0.48	< 0.05	0.56	0.88
Nd	ppm	0.1	FUS-MS	0.7	2.6	3.3	3.1	2.5	2	0.2	2.3	3.8
Sm	ppm	0.1	FUS-MS	0.1	0.4	0.5	0.3	0.4	0.3	< 0.1	0.3	0.8
Eu	ppm	0.05	FUS-MS	0.28	0.9	1.11	0.92	0.86	0.72	< 0.05	0.78	0.69
Gd	ppm	0.1	FUS-MS	0.1	0.3	0.3	0.2	0.2	0.2	< 0.1	0.2	0.7
Tb	ppm	0.1	FUS-MS	< 0.1	< 0.1	< 0.1	< 0.1	< 0.1	< 0.1	< 0.1	< 0.1	< 0.1
Dy	ppm	0.1	FUS-MS	< 0.1	0.2	0.2	0.1	0.1	< 0.1	< 0.1	< 0.1	0.5
Ho	ppm	0.1	FUS-MS	< 0.1	< 0.1	< 0.1	< 0.1	< 0.1	< 0.1	< 0.1	< 0.1	0.1
Er	ppm	0.1	FUS-MS	< 0.1	< 0.1	< 0.1	< 0.1	< 0.1	< 0.1	< 0.1	< 0.1	0.3
Tm	ppm	0.05	FUS-MS	< 0.05	< 0.05	< 0.05	< 0.05	< 0.05	< 0.05	< 0.05	< 0.05	< 0.05
Yb	ppm	0.1	FUS-MS	< 0.1	< 0.1	< 0.1	< 0.1	< 0.1	< 0.1	0.1	< 0.1	0.2
Lu	ppm	0.04	FUS-MS	< 0.04	< 0.04	< 0.04	< 0.04	< 0.04	< 0.04	< 0.04	< 0.04	< 0.04
Hf	ppm	0.2	FUS-MS	0.5	< 0.2	< 0.2	< 0.2	< 0.2	< 0.2	0.4	< 0.2	< 0.2
Ta	ppm	0.1	FUS-MS	0.1	< 0.1	< 0.1	< 0.1	< 0.1	< 0.1	< 0.1	< 0.1	< 0.1
W	ppm	1	FUS-MS	1	1	< 1	< 1	< 1	< 1	1	< 1	< 1
Tl	ppm	0.1	FUS-MS	< 0.1	0.1	< 0.1	< 0.1	< 0.1	< 0.1	< 0.1	< 0.1	< 0.1
Bi	ppm	0.4	FUS-MS	< 0.4	< 0.4	< 0.4	< 0.4	< 0.4	< 0.4	< 0.4	< 0.4	< 0.4
Th	ppm	0.1	FUS-MS	< 0.1	< 0.1	< 0.1	0.5	< 0.1	< 0.1	< 0.1	< 0.1	< 0.1
U	ppm	0.1	FUS-MS	0.2	< 0.1	< 0.1	< 0.1	< 0.1	< 0.1	< 0.1	< 0.1	< 0.1

Abbreviations: Rock types

MAS Massive to semi-massive oxide mineralization

OMAS Orthopyroxene -bearing massive-semi-massive oxide mineralization

BAR Barren anorthosite

DIS Disseminated oxide mineralization

Appendix III. (Continued)

Sample ID				CC069	CC071	CC072	CC073	CC074	CC075	CC076A	CC076B
Easting				658424	658527	657744	658070	658516	658220	658237	658237
Westing				5929537	5929467	5929747	5930061	5930210	5930258	5929903	5929903
Description				MAS	MAS	OMAS	BAR	BAR	BAR	BAR	MAS
		Idl									
SiO_2	%	0.01	FUS-ICP	0.64	1.78	3.49	55.64	52.76	53.3	54.31	6.57
Al_2O_3	%	0.01	FUS-ICP	9.6	10.16	8.02	26.89	26.9	27.66	27.71	9.69
$Fe_2O_{3(T)}$	%	0.01	FUS-ICP	74.07	73.19	74.89	1.3	2.99	1.13	1.56	68.4
MnO	%	0.001	FUS-ICP	0.315	0.302	0.325	0.009	0.034	0.01	0.014	0.365
MgO	%	0.01	FUS-ICP	3.94	2.62	3.7	0.1	1.51	0.11	0.23	2.42
CaO	%	0.01	FUS-ICP	0.01	0.09	0.21	9.43	10.23	10.1	10.07	0.72
Na_2O	%	0.01	FUS-ICP	0.03	0.07	0.04	5.26	4.34	4.96	5.18	0.23
K_2O	%	0.01	FUS-ICP	0.05	0.04	0.02	1.1	0.65	0.93	0.61	0.76
TiO_2	%	0.001	FUS-ICP	11.63	11.84	11.51	0.189	0.227	0.164	0.257	12.78
P_2O_5	%	0.01	FUS-ICP	0.01	0.01	< 0.01	0.03	0.04	0.03	0.05	0.02
LOI	%		FUS-ICP	-2.2	-2.17	-2.81	0.45	0.73	1.06	0.67	-1.9
Total	%	0.01	FUS-ICP	98.1	97.93	99.4	100.4	100.4	99.46	100.7	100
Sc	ppm	1	FUS-ICP	17	13	16	< 1	2	< 1	< 1	20
Be	ppm	1	FUS-ICP	< 1	< 1	< 1	< 1	< 1	< 1	< 1	< 1
V	ppm	5	FUS-ICP	3154	3147	2883	31	39	23	34	2584
Cr	ppm	20	FUS-MS	1330	1190	1740	< 20	40	< 20	< 20	1880
Co	ppm	1	FUS-MS	209	160	162	2	11	1	3	87
Ni	ppm	1	TD-ICP	333	333	220	10	27	9	11	82
Zn	ppm	1	TD-ICP	306	296	354	14	19	12	11	533
Cd	ppm	0.5	TD-ICP	< 0.5	0.8	0.8	< 0.5	< 0.5	< 0.5	< 0.5	1
S	%	0.001	TD-ICP	0.01	0.067	0.006	0.044	0.053	0.045	0.047	0.031
Cu	ppm	1	TD-ICP	24	107	97	11	18	5	8	53
Ag	ppm	0.3	TD-ICP	1	0.4	0.4	< 0.3	< 0.3	< 0.3	< 0.3	0.5
Pb	ppm	5	TD-ICP	13	18	17	< 5	< 5	< 5	< 5	12
Ga	ppm	1	FUS-MS	71	72	65	18	16	16	18	64
Ge	ppm	1	FUS-MS	2	2	2	1	1	1	1	2
As	ppm	5	FUS-MS	< 5	< 5	< 5	< 5	< 5	< 5	< 5	< 5
Rb	ppm	2	FUS-MS	< 2	< 2	< 2	< 2	< 2	8	5	18
Sr	ppm	2	FUS-ICP	6	20	10	1462	1270	1332	1399	105
Y	ppm	2	FUS-ICP	< 2	< 2	< 2	< 2	< 2	< 2	2	< 2
Zr	ppm	4	FUS-ICP	8	8	13	5	5	5	10	41
Nb	ppm	1	FUS-MS	< 1	< 1	< 1	< 1	< 1	< 1	< 1	1
Mo	ppm	2	FUS-MS	< 2	< 2	< 2	< 2	< 2	< 2	< 2	< 2
In	ppm	0.2	FUS-MS	< 0.2	< 0.2	< 0.2	< 0.2	< 0.2	< 0.2	< 0.2	< 0.2
Sn	ppm	1	FUS-MS	2	1	2	< 1	< 1	< 1	< 1	1
Sb	ppm	0.5	FUS-MS	< 0.5	< 0.5	< 0.5	< 0.5	< 0.5	< 0.5	< 0.5	< 0.5
Cs	ppm	0.5	FUS-MS	< 0.5	< 0.5	< 0.5	< 0.5	< 0.5	< 0.5	< 0.5	0.9
Ba	ppm	3	FUS-ICP	3	11	< 3	1073	649	638	685	163
La	ppm	0.1	FUS-MS	0.3	< 0.1	< 0.1	3.1	2.2	2.5	3.5	0.8
Ce	ppm	0.1	FUS-MS	0.7	< 0.1	0.2	5	3.8	4.2	6.6	1.8
Pr	ppm	0.05	FUS-MS	0.09	< 0.05	< 0.05	0.58	0.46	0.51	0.81	0.19
Nd	ppm	0.1	FUS-MS	0.5	< 0.1	0.2	2.1	2	2	3.2	0.8
Sm	ppm	0.1	FUS-MS	< 0.1	< 0.1	< 0.1	0.3	0.4	0.4	0.5	0.1
Eu	ppm	0.05	FUS-MS	< 0.05	< 0.05	< 0.05	0.84	0.65	0.58	0.68	0.18
Gd	ppm	0.1	FUS-MS	0.1	< 0.1	< 0.1	0.2	0.2	0.2	0.4	0.1
Tb	ppm	0.1	FUS-MS	< 0.1	< 0.1	< 0.1	< 0.1	< 0.1	< 0.1	< 0.1	< 0.1
Dy	ppm	0.1	FUS-MS	< 0.1	< 0.1	< 0.1	< 0.1	0.2	< 0.1	0.3	< 0.1
Ho	ppm	0.1	FUS-MS	< 0.1	< 0.1	< 0.1	< 0.1	< 0.1	< 0.1	< 0.1	< 0.1
Er	ppm	0.1	FUS-MS	< 0.1	< 0.1	< 0.1	< 0.1	< 0.1	< 0.1	< 0.1	< 0.1
Tm	ppm	0.05	FUS-MS	< 0.05	< 0.05	< 0.05	< 0.05	< 0.05	< 0.05	< 0.05	< 0.05
Yb	ppm	0.1	FUS-MS	< 0.1	< 0.1	< 0.1	< 0.1	< 0.1	< 0.1	0.1	< 0.1
Lu	ppm	0.04	FUS-MS	< 0.04	< 0.04	< 0.04	< 0.04	< 0.04	< 0.04	< 0.04	< 0.04
Hf	ppm	0.2	FUS-MS	0.4	0.3	0.6	< 0.2	< 0.2	< 0.2	< 0.2	1.1
Ta	ppm	0.1	FUS-MS	< 0.1	< 0.1	< 0.1	< 0.1	< 0.1	< 0.1	< 0.1	0.1
W	ppm	1	FUS-MS	2	1	2	< 1	1	< 1	< 1	1
Tl	ppm	0.1	FUS-MS	< 0.1	< 0.1	< 0.1	< 0.1	< 0.1	< 0.1	< 0.1	< 0.1
Bi	ppm	0.4	FUS-MS	< 0.4	< 0.4	< 0.4	< 0.4	< 0.4	< 0.4	< 0.4	< 0.4
Th	ppm	0.1	FUS-MS	< 0.1	< 0.1	< 0.1	< 0.1	< 0.1	< 0.1	< 0.1	< 0.1
U	ppm	0.1	FUS-MS	< 0.1	0.1	< 0.1	< 0.1	< 0.1	< 0.1	< 0.1	< 0.1

Abbreviations:	Rock types		
MAS	Massive to semi-massive oxide mineralization	BAR	Barren anorthosite
OMAS	Orthopyroxene -bearing massive-semi-massive oxide mineralization	DIS	Disseminated oxide mineralization
GAB	Gabbronorite	TRO	Troctolite

Appendix IV a. **EPMA magnetite analyses results. Spot locations are shown on BSE images in Appendix VI. Total recalculated refers to the total value with recalculated FeO content.**

Sample	CC008	CC008	CC008	CC008	CC008	CC008	CC008	CC008	CC008
Mineralization type	MAS	MAS	MAS	MAS	MAS	MAS	MAS	MAS	MAS
Descriptor	BAN	BAN	BAN	BAN	BAN	BAN	BAN	BAN	BAN
Circle Number	A	A	A	B	B	B	B	C	C
Mineral analyzed	MAG	MAG	MAG	MAG	MAG	MAG	MAG	MAG	MAG
Mineral host	MAG	MAG	MAG	PLE	PLE	PLE	PLE	ILM	ILM
Point	7	8	9	10	11	12	13	16	17
SiO_2	0.03	0.01	0.01	0.00	0.00	0.01	0.02	-	-
TiO_2	0.09	0.09	0.22	0.14	0.05	0.04	0.01	1.03	1.07
Al_2O_3	0.34	0.31	0.32	0.22	0.18	0.25	0.24	0.26	0.25
Cr_2O_3	0.25	0.25	0.25	0.17	0.14	0.16	0.15	0.37	0.35
V_2O_3	0.68	0.68	0.57	0.38	0.35	0.48	0.50	0.65	0.62
FeO*	91.56	90.79	90.71	90.95	91.51	92.51	92.36	91.43	90.88
Fe_2O_3 recalculated	67.27	66.77	66.54	66.97	67.56	68.20	68.08	65.92	65.57
FeO recalculated	31.03	30.71	30.83	30.69	30.72	31.14	31.10	32.11	31.88
MnO	0.01	0.01	0.02	0.02	0.02	0.02	0.02	0.01	0.02
MgO	0.07	0.07	0.05	0.02	0.02	0.01	0.00	0.02	0.07
ZnO	-	0.00	0.04	0.02	0.06	0.02	0.02	0.01	0.01
NiO	0.02	0.03	0.02	0.03	0.03	0.05	0.02	0.01	0.03
CaO	0.00	0.00	-	0.00	-	-	0.01	-	-
Cu_2O	-	0.01	-	-	-	0.00	-	0.00	-
K_2O	0.00	-	-	-	0.00	0.00	0.00	-	0.00
Total measured	93.05	92.25	92.21	91.95	92.36	93.54	93.34	93.80	93.30
Total recalculated	99.80	98.94	98.88	98.66	99.13	100.37	100.16	100.40	99.87

MAS	Massive to semi-massive mineralization	OBAN	Orthopyroxene -bearing bands of oxide mineralization
DIS	Disseminated mineralization	POD	Pod of oxide mineralization
BAN	Bands of oxide mineralization	OPOD	Orthopyroxene -bearing pod of oxide mineralization
ANO	Anorthosite hosted disseminated	VEIN	Vein of oxide mineralization
ORT	Orthopyroxene associated	MAG	Magnetite
CLI	Clinopyroxene associated	ILM	Ilmenite
		PLE	Pleonaste

Appendix IV a. (Continued)

Sample	CC008	CC008	CC008	CC008	CC008	CC008	CC008	CC008	CC008
Mineralization type	MAS	MAS	MAS	MAS	MAS	MAS	MAS	MAS	MAS
Descriptor	BAN	BAN	BAN	BAN	BAN	BAN	BAN	BAN	BAN
Circle Number	C	C	C	D	D	D	D	F	F
Mineral analyzed	MAG	MAG	MAG	MAG	MAG	MAG	MAG	MAG	MAG
Mineral host	MAG	MAG	MAG	PLE	PLE	MAG	MAG	MAG	MAG
Point	23	24	25	29	30	36	37	42	43
SiO_2	0.01	0.02	0.02	0.01	0.02	0.02	0.01	0.02	0.01
TiO_2	0.07	0.06	0.09	0.07	0.04	0.07	0.04	1.58	1.80
Al_2O_3	0.32	0.36	0.33	0.19	0.21	0.29	0.32	0.25	0.24
Cr_2O_3	0.25	0.25	0.28	0.14	0.18	0.28	0.27	0.37	0.37
V_2O_3	0.73	0.69	0.71	0.31	0.33	0.74	0.75	0.60	0.58
FeO*	90.19	90.08	90.93	91.14	92.16	91.18	91.42	91.18	91.17
Fe_2O_3 recalculated	66.28	66.21	66.84	67.28	68.02	67.06	67.23	65.10	64.81
FeO recalculated	30.55	30.50	30.78	30.60	30.95	30.84	30.93	32.60	32.85
MnO	0.01	0.02	0.03	0.02	0.04	0.02	0.01	0.01	0.04
MgO	0.04	0.05	0.08	0.02	0.02	0.06	0.05	0.06	0.06
ZnO	-	0.01	0.00	0.07	0.04	0.01	0.02	0.03	0.01
NiO	0.03	0.03	0.03	0.04	0.03	0.04	0.02	0.03	0.03
CaO	0.01	0.00	-	-	0.00	-	-	0.02	0.01
Cu_2O	-	-	0.01	-	-	0.01	-	0.00	-
K_2O	-	-	-	-	-	0.00	-	0.00	0.00
Total measured	91.66	91.57	92.52	92.01	93.07	92.73	92.91	94.16	94.32
Total recalculated	98.30	98.21	99.22	98.75	99.88	99.44	99.65	100.68	100.82

MAS	Massive to semi-massive mineralization	OBAN	Orthopyroxene -bearing bands of oxide mineralization		
DIS	Disseminated mineralization			POD	Pod of oxide mineralization
BAN	Bands of oxide mineralization			OPOD	Orthopyroxene -bearing pod of oxide mineralization
ANO	Anorthosite hosted disseminated			VEIN	Vein of oxide mineralization

Appendix IV a. (Continued)

Sample	CC008	CC008	CC008	CC008	CC008	CC008	CC010	CC010
Mineralization type	MAS	MAS	MAS	MAS	MAS	MAS	MAS	MAS
Descriptor	BAN	BAN	BAN	BAN	BAN	BAN	OBAN	OBAN
Circle Number	F	F	F	I	I	I	A	A
Mineral analyzed	MAG	MAG	MAG	MAG	MAG	MAG	MAG	MAG
Mineral host	MAG	ILM	ILM	ILM	ILM	ILM	PLE	PLE
Point	44	47	48	49	50	51	1	2
SiO_2	0.02	0.01	0.01	0.01	0.00	-	0.01	0.02
TiO_2	0.26	1.93	1.94	0.79	1.39	1.60	0.17	0.35
Al_2O_3	0.24	0.25	1.01	0.27	0.35	0.28	0.44	0.48
Cr_2O_3	0.30	0.33	0.33	0.16	0.14	0.14	0.16	0.16
V_2O_3	0.68	0.62	0.59	0.39	0.35	0.34	0.49	0.49
FeO*	90.36	91.57	90.54	90.88	90.67	91.99	92.14	91.41
Fe_2O_3 recalculated	66.22	64.97	63.98	66.08	65.12	65.81	67.75	66.90
FeO recalculated	30.77	33.11	32.97	31.43	32.08	32.78	31.18	31.21
MnO	0.01	0.05	0.04	-	0.02	0.01	0.04	0.03
MgO	0.07	0.06	0.21	0.08	0.09	0.07	0.08	0.06
ZnO	-	0.03	0.04	0.03	-	-	0.04	0.03
NiO	0.04	0.03	0.04	0.03	0.00	0.02	0.04	0.04
CaO	0.00	0.01	0.01	0.01	-	-	-	-
Cu_2O	0.01	0.02	-	0.01	-	-	-	0.01
K_2O	-	-	0.00	0.00	0.01	0.00	-	-
Total measured	91.99	94.91	94.76	92.65	93.03	94.46	93.62	93.09
Total recalculated	98.63	101.42	101.18	99.27	99.55	101.05	100.40	99.79

MAS	Massive to semi-massive mineralization	OBAN	Orthopyroxene -bearing bands of oxide mineralization		
DIS	Disseminated mineralization	POD	Pod of oxide mineralization		
BAN	Bands of oxide mineralization	OPOD	Orthopyroxene -bearing pod of oxide mineralization		
ANO	Anorthosite hosted disseminated	VEIN	Vein of oxide mineralization		
ORT	Orthopyroxene associated	MAG	Magnetite		
CLI	Clinopyroxene associated	ILM	Ilmenite	PLE	Pleonaste

Appendix IV a. (Continued)

Sample	CC010	CC010	CC010	CC010	CC010	CC010	CC010	CC010
Mineralization type	MAS	MAS	MAS	MAS	MAS	MAS	MAS	MAS
Descriptor	OBAN	OBAN	OBAN	OBAN	OBAN	OBAN	OBAN	OBAN
Circle Number	A	A	A	A	C	C	C	C
Mineral analyzed	MAG	MAG	MAG	MAG	MAG	MAG	MAG	MAG
Mineral host	PLE	PLE	PLE	PLE	PLE	PLE	PLE	PLE
Point	3	4	5	6	10	11	12	13
SiO_2	0.01	0.01	0.01	0.02	0.02	0.01	0.01	0.01
TiO_2	0.31	0.16	0.35	0.37	0.19	0.29	0.30	0.38
Al_2O_3	0.28	0.30	0.60	0.53	0.41	0.40	0.30	0.30
Cr_2O_3	0.15	0.16	0.18	0.17	0.15	0.17	0.16	0.19
V_2O_3	0.38	0.38	0.55	0.54	0.50	0.54	0.41	0.36
FeO*	91.24	90.40	91.72	91.60	92.38	92.26	92.41	91.14
Fe_2O_3 recalculated	66.98	66.52	67.08	67.04	67.89	67.62	67.82	66.78
FeO recalculated	30.97	30.54	31.36	31.28	31.29	31.41	31.38	31.05
MnO	0.02	0.03	0.03	0.04	0.03	0.02	0.02	0.02
MgO	0.04	0.04	0.09	0.10	0.08	0.07	0.05	0.04
ZnO	0.06	0.02	0.01	0.05	0.06	0.02	0.04	0.04
NiO	0.04	0.05	0.04	0.04	0.01	0.03	0.03	0.03
CaO	0.01	0.00	0.01	0.00	-	0.00	0.00	-
Cu_2O	-	-	-	-	0.02	-	-	-
K_2O	-	0.01	-	0.00	-	0.01	0.00	-
Total measured	92.55	91.56	93.58	93.46	93.85	93.81	93.74	92.52
Total recalculated	99.26	98.22	100.30	100.18	100.66	100.59	100.53	99.21

MAS	Massive to semi-massive mineralization	OBAN	Orthopyroxene -bearing bands of oxide mineralization		
DIS	Disseminated mineralization	POD	Pod of oxide mineralization		
BAN	Bands of oxide mineralization	OPOD	Orthopyroxene -bearing pod of oxide mineralization		
ANO	Anorthosite hosted disseminated	VEIN	Vein of oxide mineralization		
ORT	Orthopyroxene associated	MAG	Magnetite		
CLI	Clinopyroxene associated	ILM	Ilmenite	PLE	Pleonaste

Appendix IV a. (Continued)

Sample	CC010	CC010	CC010	CC010	CC010	CC010	CC010	CC010
Mineralization type	MAS	MAS	MAS	MAS	MAS	MAS	MAS	MAS
Descriptor	OBAN	OBAN	OBAN	OBAN	OBAN	OBAN	OBAN	OBAN
Circle Number	D	D	D	D	D	E	E	E
Mineral analyzed	MAG	MAG	MAG	MAG	MAG	MAG	MAG	MAG
Mineral host	MAG	MAG	MAG	ILM	ILM	MAG	MAG	MAG
Point	18	19	20	24	25	38	39	40
SiO_2	0.02	0.03	0.02	0.00	0.01	0.02	0.02	0.01
TiO_2	0.19	0.24	0.25	1.71	1.52	0.21	0.28	0.58
Al_2O_3	0.37	0.42	0.42	0.31	0.27	0.49	0.43	0.31
Cr_2O_3	0.24	0.25	0.25	0.31	0.33	0.28	0.26	0.39
V_2O_3	0.75	0.69	0.73	0.60	0.59	0.72	0.73	0.70
FeO*	92.53	91.57	91.60	90.98	91.10	91.94	92.01	91.33
Fe_2O_3 recalculated	67.88	67.12	67.07	64.78	65.13	67.40	67.37	66.47
FeO recalculated	31.45	31.18	31.25	32.69	32.49	31.30	31.39	31.52
MnO	0.01	0.03	0.03	0.01	0.03	0.04	0.03	0.00
MgO	0.09	0.12	0.06	0.08	0.07	0.11	0.09	0.08
ZnO	0.01	-	0.01	0.00	-	0.01	-	-
NiO	0.04	0.03	0.03	0.04	0.04	0.03	0.03	0.05
CaO	-	-	-	-	-	-	0.01	-
Cu_2O	-	0.00	-	-	-	-	0.00	0.00
K_2O	-	-	-	0.01	-	-	0.01	0.00
Total measured	94.24	93.37	93.40	94.05	93.97	93.85	93.89	93.45
Total recalculated	101.04	100.09	100.12	100.54	100.50	100.60	100.64	100.11

MAS	Massive to semi-massive mineralization	OBAN	Orthopyroxene -bearing bands of oxide mineralization		
DIS	Disseminated mineralization	POD	Pod of oxide mineralization		
BAN	Bands of oxide mineralization	OPOD	Orthopyroxene -bearing pod of oxide mineralization		
ANO	Anorthosite hosted disseminated	VEIN	Vein of oxide mineralization		
ORT	Orthopyroxene associated	MAG	Magnetite		
CLI	Clinopyroxene associated	ILM	Ilmenite	PLE	Pleonaste

Appendix IV a. (Continued)

Sample	CC010	CC010	CC010	CC010	CC010	CC010	CC010	CC010
Mineralization type	MAS	MAS	MAS	MAS	MAS	MAS	MAS	MAS
Descriptor	OBAN	OBAN	OBAN	OBAN	OBAN	OBAN	OBAN	OBAN
Circle Number	F	F	F	F	F	H	H	H
Mineral analyzed	MAG	MAG	MAG	MAG	MAG	MAG	MAG	MAG
Mineral host	MAG	MAG	MAG	ILM	ILM	MAG	MAG	MAG
Point	44	45	46	47	48	57	58	59
SiO_2	0.02	0.02	0.02	0.02	0.02	0.01	0.01	0.01
TiO_2	0.15	0.34	0.21	1.33	1.26	0.26	0.29	0.22
Al_2O_3	0.37	0.34	0.35	0.51	0.41	0.40	0.44	0.46
Cr_2O_3	0.27	0.31	0.26	0.36	0.36	0.26	0.26	0.24
V_2O_3	0.74	0.69	0.72	0.66	0.67	0.72	0.74	0.71
FeO*	91.79	91.88	91.81	90.66	91.47	91.93	91.73	91.89
Fe_2O_3 recalculated	67.37	67.22	67.34	64.96	65.67	67.39	67.15	67.37
FeO recalculated	31.17	31.39	31.22	32.21	32.38	31.30	31.31	31.27
MnO	0.01	0.02	0.03	0.04	0.03	0.02	0.03	0.04
MgO	0.08	0.09	0.07	0.11	0.09	0.10	0.09	0.10
ZnO	0.02	-	0.02	0.01	0.01	0.02	-	-
NiO	0.03	0.04	0.03	0.05	0.05	0.04	0.05	0.04
CaO	-	-	0.00	-	0.00	-	-	-
Cu_2O	-	0.01	-	-	0.02	-	0.01	-
K_2O	0.00	-	0.00	-	0.00	-	0.00	0.00
Total measured	93.49	93.75	93.50	93.75	94.39	93.76	93.64	93.71
Total recalculated	100.24	100.48	100.25	100.26	100.97	100.52	100.36	100.47

MAS	Massive to semi-massive mineralization	OBAN	Orthopyroxene -bearing bands of oxide mineralization
DIS	Disseminated mineralization	POD	Pod of oxide mineralization
BAN	Bands of oxide mineralization	OPOD	Orthopyroxene -bearing pod of oxide mineralization
ANO	Anorthosite hosted disseminated	VEIN	Vein of oxide mineralization
ORT	Orthopyroxene associated	MAG	Magnetite
CLI	Clinopyroxene associated	ILM	Ilmenite
		PLE	Pleonaste

Appendix IV a. (Continued)

Sample	CC010	CC010	CC010	CC010	CC010	CC013A	CC013A	CC013A
Mineralization type	MAS	MAS	MAS	MAS	MAS	MAS	MAS	MAS
Descriptor	OBAN	OBAN	OBAN	OBAN	OBAN	BAN	BAN	BAN
Circle Number	L	L	P	P	P	A	A	A
Mineral analyzed	MAG	MAG	MAG	MAG	MAG	MAG	MAG	MAG
Mineral host	ILM	ILM	Opx	Opx	MAG	MAG	MAG	MAG
Point	60	61	80	81	82	7	8	9
SiO_2	0.02	0.02	0.02	0.01	0.02	0.01	0.01	0.02
TiO_2	0.83	0.19	0.21	0.22	0.32	0.15	0.07	0.07
Al_2O_3	0.55	0.44	0.39	0.53	0.46	0.27	0.27	0.29
Cr_2O_3	0.20	0.21	0.27	0.25	0.26	0.42	0.37	0.40
V_2O_3	0.46	0.50	0.71	0.70	0.72	0.66	0.70	0.68
FeO*	91.42	91.55	91.43	91.07	91.30	92.82	92.36	92.38
Fe_2O_3 recalculated	66.26	67.23	67.04	66.83	66.82	68.21	67.93	67.93
FeO recalculated	31.80	31.06	31.10	30.93	31.18	31.45	31.23	31.26
MnO	0.02	0.02	0.07	0.09	0.03	0.01	0.02	0.01
MgO	0.10	0.09	0.05	0.12	0.13	0.10	0.07	0.08
ZnO	0.01	-	0.01	0.03	-	0.02	-	0.04
NiO	0.03	0.04	0.03	0.03	0.04	0.02	0.04	0.02
CaO	0.00	0.00	0.02	0.02	0.01	0.01	0.00	0.00
Cu_2O	0.00	0.00	0.02	0.00	-	0.00	-	0.00
K_2O	0.01	-	0.00	0.00	0.00	0.00	-	0.00
Total measured	93.66	93.08	93.21	93.06	93.28	94.50	93.91	94.00
Total recalculated	100.29	99.81	99.93	99.75	99.98	101.34	100.71	100.81

MAS	Massive to semi-massive mineralization	OBAN	Orthopyroxene -bearing bands of oxide mineralization		
DIS	Disseminated mineralization	POD	Pod of oxide mineralization		
BAN	Bands of oxide mineralization	OPOD	Orthopyroxene -bearing pod of oxide mineralization		
ANO	Anorthosite hosted disseminated	VEIN	Vein of oxide mineralization		
ORT	Orthopyroxene associated	MAG	Magnetite		
CLI	Clinopyroxene associated	ILM	Ilmenite	PLE	Pleonaste

Appendix IV a. (Continued)

Sample	CC013A	CC013A	CC013A	CC013A	CC013A	CC013A	CC013A	CC013A	CC013A
Mineralization type	MAS	MAS	MAS	MAS	MAS	MAS	MAS	MAS	MAS
Descriptor	BAN	BAN	BAN	BAN	BAN	BAN	BAN	BAN	BAN
Circle Number	B	B	B	C	C	C	D	D	D
Mineral analyzed	MAG	MAG	MAG	MAG	MAG	MAG	MAG	MAG	MAG
Mineral host	MAG	MAG	MAG	MAG	MAG	MAG	ILM	ILM	ILM
Point	18	19	20	24	25	26	27	28	29
SiO_2	0.00	0.01	0.01	0.01	0.02	0.01	0.01	0.00	0.01
TiO_2	0.15	0.08	0.05	0.08	0.16	0.08	0.08	0.07	0.39
Al_2O_3	0.24	0.25	0.22	0.26	0.27	0.23	0.31	0.26	0.28
Cr_2O_3	0.36	0.37	0.37	0.42	0.46	0.41	0.31	0.34	0.29
V_2O_3	0.63	0.69	0.67	0.71	0.69	0.71	0.53	0.53	0.53
FeO*	91.93	92.34	91.84	92.11	92.92	92.49	92.13	92.48	92.84
Fe_2O_3 recalculated	67.57	67.92	67.61	67.74	68.15	68.04	67.62	67.83	68.13
FeO recalculated	31.13	31.23	31.01	31.16	31.59	31.27	31.78	31.10	31.18
MnO	0.01	0.01	0.01	0.01	0.01	0.03	0.00	0.00	0.01
MgO	0.08	0.07	0.07	0.08	0.06	0.06	0.10	0.10	0.10
ZnO	0.00	0.02	0.01	0.02	0.02	0.03	-	0.01	-
NiO	0.04	0.04	0.03	0.03	0.02	0.04	0.03	0.02	0.02
CaO	0.00	0.00	0.01	0.00	-	0.01	0.00	0.00	-
Cu_2O	-	0.00	-	-	-	-	0.01	0.00	0.00
K_2O	-	0.01	0.01	-	0.00	-	0.00	0.00	-
Total measured	93.44	93.90	93.30	93.73	94.63	94.11	93.51	93.82	94.47
Total recalculated	100.21	100.70	100.07	100.52	101.46	100.92	100.78	100.27	100.94

MAS	Massive to semi-massive mineralization	OBAN	Orthopyroxene -bearing bands of oxide mineralization
DIS	Disseminated mineralization	POD	Pod of oxide mineralization
BAN	Bands of oxide mineralization	OPOD	Orthopyroxene -bearing pod of oxide mineralization
ANO	Anorthosite hosted disseminated	VEIN	Vein of oxide mineralization
ORT	Orthopyroxene associated	MAG	Magnetite
CLI	Clinopyroxene associated	ILM	Ilmenite
		PLE	Pleonaste

Appendix IV a. (Continued)

Sample	CC013A	CC013A	CC013A	CC013A	CC013A	CC013A	CC013A	CC013A	CC013A
Mineralization type	MAS	MAS	MAS	MAS	MAS	MAS	MAS	MAS	MAS
Descriptor	BAN	BAN	BAN	BAN	BAN	BAN	BAN	BAN	BAN
Circle Number	D	E	E	I	I	I	I	I	L
Mineral analyzed	ILM	MAG	MAG	MAG	MAG	MAG	MAG	MAG	MAG
Mineral host	ILM	ILM	ILM	PLE	PLE	ILM	ILM	ILM	PLE
Point	33	37	38	39	40	46	47	48	52
SiO_2	0.01	0.00	0.01	0.03	0.01	0.02	0.02	0.01	0.03
TiO_2	0.55	0.05	0.05	0.11	0.07	0.08	0.06	0.07	0.03
Al_2O_3	0.25	0.20	0.26	0.21	0.18	0.22	0.24	0.22	0.17
Cr_2O_3	0.24	0.25	0.26	0.25	0.22	0.33	0.34	0.34	0.27
V_2O_3	0.41	0.43	0.45	0.36	0.34	0.57	0.57	0.56	0.37
FeO*	92.63	92.76	93.03	92.02	92.40	92.88	92.37	93.43	92.29
Fe_2O_3 recalculated	10.50	68.41	68.60	67.79	68.18	68.35	67.97	68.80	68.13
FeO recalculated	39.54	31.20	31.30	31.02	31.05	31.38	31.21	31.52	30.99
MnO	0.01	0.00	0.00	0.03	0.04	0.01	-	-	0.03
MgO	0.05	0.05	0.08	0.05	0.04	0.06	0.05	0.07	0.04
ZnO	0.01	0.03	0.02	0.04	0.02	-	0.02	0.03	0.05
NiO	0.03	0.02	0.03	0.03	0.05	0.03	0.02	0.03	0.05
CaO	0.01	0.00	-	-	0.01	0.00	0.00	-	0.00
Cu_2O	-	-	0.01	0.00	-	0.01	0.00	-	-
K_2O	0.00	0.00	0.00	0.00	-	0.00	-	-	0.00
Total measured	94.19	93.79	94.20	93.15	93.38	94.21	93.70	94.75	93.33
Total recalculated	51.59	100.65	101.08	99.94	100.21	101.05	100.51	101.65	100.15

MAS	Massive to semi-massive mineralization	OBAN	Orthopyroxene -bearing bands of oxide mineralization
DIS	Disseminated mineralization	POD	Pod of oxide mineralization
BAN	Bands of oxide mineralization	OPOD	Orthopyroxene -bearing pod of oxide mineralization
ANO	Anorthosite hosted disseminated	VEIN	Vein of oxide mineralization

ORT Orthopyroxene associated MAG Magnetite

Appendix IV a. (Continued)

Sample	CC013A	CC013A	CC013A	CC013A	CC013A	CC013A	CC013A	CC013A
Mineralization type	MAS	MAS	MAS	MAS	MAS	MAS	MAS	MAS
Descriptor	BAN	BAN	BAN	BAN	BAN	BAN	BAN	BAN
Circle Number	L	L	L	L	M	M	M	P
Mineral analyzed	MAG	MAG	MAG	MAG	MAG	MAG	MAG	MAG
Mineral host	PLE	MAG	MAG	MAG	MAG	MAG	MAG	MAG
Point	53	56	57	58	62	63	64	65
SiO_2	0.01	0.02	0.02	0.01	0.02	0.02	0.03	0.02
TiO_2	0.07	0.04	0.09	0.07	0.06	0.09	0.07	0.65
Al_2O_3	0.17	0.24	0.26	0.27	0.19	0.26	0.33	0.21
Cr_2O_3	0.28	0.38	0.37	0.37	0.39	0.39	0.36	0.52
V_2O_3	0.36	0.63	0.63	0.62	0.71	0.70	0.68	0.66
FeO*	92.25	91.95	92.37	92.10	92.73	92.35	91.87	91.10
Fe_2O_3 recalculated	68.02	67.70	67.97	67.79	68.23	67.86	67.56	66.18
FeO recalculated	31.04	31.03	31.21	31.10	31.34	31.29	31.08	31.55
MnO	0.02	0.02	0.01	0.02	0.02	0.01	0.01	0.00
MgO	0.01	0.06	0.08	0.09	0.07	0.05	0.09	0.05
ZnO	0.05	0.02	0.03	0.01	0.01	0.03	0.03	0.02
NiO	0.04	0.05	0.05	0.04	0.03	0.03	0.02	0.03
CaO	0.01	-	-	-	0.00	-	0.01	0.00
Cu_2O	-	0.01	0.00	-	0.01	-	-	-
K_2O	0.00	-	0.01	-	-	0.00	-	0.00
Total measured	93.27	93.41	93.91	93.60	94.24	93.94	93.49	93.28
Total recalculated	100.09	100.19	100.71	100.39	101.07	100.74	100.26	99.91

MAS	Massive to semi-massive mineralization	OBAN	Orthopyroxene -bearing bands of oxide mineralization		
DIS	Disseminated mineralization	POD	Pod of oxide mineralization		
BAN	Bands of oxide mineralization	OPOD	Orthopyroxene -bearing pod of oxide mineralization		
ANO	Anorthosite hosted disseminated	VEIN	Vein of oxide mineralization		
ORT	Orthopyroxene associated	MAG	Magnetite		
CLI	Clinopyroxene associated	ILM	Ilmenite	PLE	Pleonaste

Appendix IV a. (Continued)

Sample	CC013A	CC013A	CC013A	CC013A	CC013A	CC025A	CC025A	CC025A
Mineralization type	MAS	MAS	MAS	MAS	MAS	MAS	MAS	MAS
Descriptor	BAN	BAN	BAN	BAN	BAN	POD	POD	POD
Circle Number	P	P	P	R	R	A	A	A
Mineral analyzed	MAG	MAG	MAG	ILM	ILM	MAG	MAG	MAG
Mineral host	MAG	MAG	MAG	MAG	MAG	ILM	ILM	ILM
Point	66	67	68	69	70	4	5	6
SiO_2	0.04	0.03	0.03	0.02	0.02	0.01	0.01	-
TiO_2	1.96	0.52	1.33	0.10	0.06	1.99	1.79	2.26
Al_2O_3	0.21	0.24	0.22	0.24	0.26	0.48	0.45	1.15
Cr_2O_3	0.54	0.48	0.52	0.39	0.37	0.46	0.47	0.43
V_2O_3	0.65	0.66	0.68	0.71	0.71	0.42	0.44	0.43
FeO*	89.97	91.45	90.73	92.00	91.90	91.12	90.56	89.54
Fe_2O_3 recalculated	63.57	66.64	65.02	67.61	67.59	64.37	64.26	62.69
FeO recalculated	32.77	31.49	32.23	31.16	31.08	33.20	32.73	33.13
MnO	0.05	0.02	0.03	0.01	0.00	0.01	0.00	0.01
MgO	0.05	0.07	0.07	0.06	0.08	0.03	0.07	0.18
ZnO	-	0.02	0.02	0.02	0.02	0.01	0.01	0.01
NiO	0.02	0.03	0.03	0.04	0.03	0.04	0.03	0.02
CaO	0.00	-	-	0.00	0.00	0.01	0.01	-
Cu_2O	-	-	-	-	0.00	-	-	-
K_2O	0.00	0.00	-	0.00	0.00	0.00	-	-
Total measured	93.49	93.51	93.65	93.60	93.45	94.58	93.83	94.02
Total recalculated	99.86	100.19	100.16	100.38	100.22	101.03	100.27	100.31

MAS	Massive to semi-massive mineralization	OBAN	Orthopyroxene -bearing bands of oxide mineralization		
DIS	Disseminated mineralization	POD	Pod of oxide mineralization		
BAN	Bands of oxide mineralization	OPOD	Orthopyroxene -bearing pod of oxide mineralization		
ANO	Anorthosite hosted disseminated	VEIN	Vein of oxide mineralization		
ORT	Orthopyroxene associated	MAG	Magnetite		
CLI	Clinopyroxene associated	ILM	Ilmenite	PLE	Pleonaste

Appendix IV a. (Continued)

Sample	CC025A	CC025A	CC025A	CC025A	CC025A	CC025A	CC025A	CC025A
Mineralization type	MAS	MAS	MAS	MAS	MAS	MAS	MAS	MAS
Descriptor	POD	POD	POD	POD	POD	POD	POD	POD
Circle Number	A	A	A	B	B	C	C	C
Mineral analyzed	MAG	MAG	MAG	MAG	MAG	MAG	MAG	MAG
Mineral host	MAG	MAG	MAG	ILM	ILM	MAG	MAG	MAG
Point	7	8	9	13	14	20	21	22
SiO_2	0.03	0.04	0.03	-	0.01	0.02	0.02	0.04
TiO_2	0.78	0.78	0.86	1.09	1.18	0.58	0.85	1.13
Al_2O_3	0.53	0.55	0.63	0.82	0.49	0.47	0.65	0.75
Cr_2O_3	0.66	0.63	0.62	0.34	0.34	0.63	0.61	0.63
V_2O_3	0.72	0.72	0.70	0.71	0.63	0.72	0.72	0.75
FeO*	90.58	90.65	90.56	90.94	91.09	90.63	89.91	89.34
Fe_2O_3 recalculated	65.37	65.39	65.20	65.30	65.40	65.71	64.69	63.89
FeO recalculated	31.76	31.82	31.90	32.18	32.24	31.50	31.70	31.85
MnO	0.00	0.02	0.04	0.02	0.00	0.02	0.03	0.06
MgO	0.07	0.05	0.04	0.10	0.06	0.03	0.02	0.05
ZnO	-	-	-	-	-	0.03	-	0.03
NiO	0.04	0.04	0.02	0.03	0.04	0.04	0.02	0.03
CaO	-	-	-	-	0.00	0.01	0.00	0.00
Cu_2O	-	0.02	0.01	0.02	0.01	-	-	0.00
K_2O	0.00	-	0.01	0.00	0.00	-	0.00	-
Total measured	93.41	93.50	93.52	94.09	93.86	93.17	92.83	92.82
Total recalculated	99.96	100.05	100.05	100.63	100.41	99.76	99.31	99.22

MAS	Massive to semi-massive mineralization	OBAN	Orthopyroxene -bearing bands of oxide mineralization		
DIS	Disseminated mineralization	POD	Pod of oxide mineralization		
BAN	Bands of oxide mineralization	OPOD	Orthopyroxene -bearing pod of oxide mineralization		
ANO	Anorthosite hosted disseminated	VEIN	Vein of oxide mineralization		
ORT	Orthopyroxene associated	MAG	Magnetite		
CLI	Clinopyroxene associated	ILM	Ilmenite	PLE	Pleonaste

Appendix IV a. (Continued)

Sample	CC025A	CC025A	CC025A	CC025A	CC025A	CC025A	CC025A	CC025A
Mineralization type	MAS	MAS	MAS	MAS	MAS	MAS	MAS	MAS
Descriptor	POD	POD	POD	POD	POD	POD	POD	POD
Circle Number	D	D	D	E	E	E	I	I
Mineral analyzed	MAG	MAG	MAG	MAG	MAG	MAG	MAG	MAG
Mineral host	MAG	MAG	MAG	MAG	MAG	MAG	MAG	MAG
Point	35	36	37	48	49	50	62	63
SiO_2	0.02	0.05	0.03	0.03	0.03	0.03	0.04	0.05
TiO_2	1.41	1.99	1.93	1.72	1.67	1.81	0.82	0.82
Al_2O_3	0.82	0.95	0.97	0.92	0.81	0.78	0.77	0.71
Cr_2O_3	0.59	0.58	0.60	0.60	0.57	0.60	0.64	0.51
V_2O_3	0.70	0.69	0.67	0.68	0.72	0.70	0.71	0.71
FeO*	89.89	89.92	89.44	88.85	88.69	88.70	90.86	90.85
Fe_2O_3 recalculated	63.91	63.09	62.86	62.75	62.68	62.52	65.39	65.45
FeO recalculated	32.38	33.15	32.87	32.38	32.29	32.44	32.03	31.96
MnO	0.05	0.06	0.06	0.06	0.05	0.06	0.01	0.03
MgO	0.06	0.06	0.08	0.09	0.05	0.06	0.06	0.04
ZnO	-	0.01	0.02	0.01	-	-	0.00	0.03
NiO	0.01	0.02	0.02	0.03	0.03	0.03	0.02	0.02
CaO	-	0.00	-	0.01	0.01	0.01	0.01	0.01
Cu_2O	0.02	-	0.00	0.01	0.02	0.01	0.01	-
K_2O	0.00	0.00	0.00	0.00	-	-	-	0.01
Total measured	93.59	94.34	93.81	93.01	92.64	92.77	93.94	93.79
Total recalculated	99.99	100.66	100.11	99.29	98.92	99.04	100.49	100.34

MAS	Massive to semi-massive mineralization	OBAN	Orthopyroxene -bearing bands of oxide mineralization
DIS	Disseminated mineralization	POD	Pod of oxide mineralization
BAN	Bands of oxide mineralization	OPOD	Orthopyroxene -bearing pod of oxide mineralization
ANO	Anorthosite hosted disseminated	VEIN	Vein of oxide mineralization
ORT	Orthopyroxene associated	MAG	Magnetite
CLI	Clinopyroxene associated	ILM	Ilmenite
		PLE	Pleonaste

Appendix IV a. (Continued)

Sample	CC025A	CC025A	CC025A	CC025A	CC031A	CC031A	CC031A	CC031A	CC031A
Mineralization type	MAS	MAS	MAS	MAS	DIS	DIS	DIS	DIS	DIS
Descriptor	POD	POD	POD	POD	ANO	ANO	ANO	ANO	ANO
Circle Number	I	K	K	K	A	A	A	B	B
Mineral analyzed	MAG	MAG	MAG	MAG	MAG	MAG	MAG	MAG	MAG
Mineral host	MAG	ILM	ILM	ILM	MAG	MAG	MAG	MAG	MAG
Point	64	68	69	70	1	2	3	12	13
SiO_2	0.03	0.01	0.01	0.01	0.02	0.02	0.04	0.03	0.02
TiO_2	1.18	1.29	1.49	1.17	0.22	0.15	0.20	0.20	0.19
Al_2O_3	0.66	0.62	0.71	0.63	0.44	0.39	0.60	0.40	0.39
Cr_2O_3	0.52	0.37	0.40	0.40	0.52	0.51	0.49	0.44	0.41
V_2O_3	0.70	0.52	0.53	0.51	0.64	0.62	0.61	0.64	0.65
FeO*	90.88	90.59	90.60	91.30	90.65	90.56	91.19	90.67	90.61
Fe_2O_3 recalculated	65.01	64.88	64.60	65.57	66.26	66.35	66.64	66.33	66.33
FeO recalculated	32.38	32.21	32.47	32.30	31.03	30.86	31.23	30.99	30.93
MnO	0.04	0.01	0.02	0.02	0.02	0.02	0.03	0.01	0.02
MgO	0.01	0.08	0.09	0.08	0.01	0.02	0.04	0.02	-
ZnO	-	0.02	0.01	-	-	0.01	0.01	-	0.01
NiO	0.04	0.03	0.05	0.02	0.05	0.05	0.03	0.04	0.06
CaO	-	-	-	0.00	0.00	0.00	0.00	-	-
Cu_2O	0.01	0.01	-	-	-	0.02	0.00	0.00	0.00
K_2O	-	0.00	-	0.00	-	-	-	0.00	-
Total measured	94.07	93.54	93.90	94.13	92.57	92.37	93.27	92.46	92.36
Total recalculated	100.58	100.04	100.37	100.70	99.21	99.02	99.94	99.10	99.00

MAS	Massive to semi-massive mineralization	OBAN	Orthopyroxene -bearing bands of oxide mineralization
DIS	Disseminated mineralization	POD	Pod of oxide mineralization
BAN	Bands of oxide mineralization	OPOD	Orthopyroxene -bearing pod of oxide mineralization
ANO	Anorthosite hosted disseminated	VEIN	Vein of oxide mineralization
ORT	Orthopyroxene associated	MAG	Magnetite
CLI	Clinopyroxene associated	ILM	Ilmenite
		PLE	Pleonaste

Appendix IV a. (Continued)

Sample	CC031A	CC031A	CC031A	CC031A	CC031A	CC031A	CC031A	CC031A	CC031A
Mineralization type	DIS	DIS	DIS	DIS	DIS	DIS	DIS	DIS	DIS
Descriptor	ANO	ANO	ANO	ANO	ANO	ANO	ANO	ANO	ANO
Circle Number	B	C	C	C	C	C	D	D	D
Mineral analyzed	MAG	MAG	MAG	MAG	MAG	MAG	MAG	MAG	MAG
Mineral host	MAG	ILM	ILM	MAG	MAG	MAG	MAG	MAG	MAG
Point	14	18	19	22	23	24	30	31	32
SiO_2	0.04	0.02	0.00	0.04	0.04	0.03	0.03	-	0.04
TiO_2	0.26	1.48	1.08	0.25	0.20	0.20	0.20	0.17	0.15
Al_2O_3	0.36	0.38	0.53	0.31	0.48	0.40	0.53	0.35	0.36
Cr_2O_3	0.68	1.68	1.71	0.77	0.56	0.51	0.47	0.46	0.41
V_2O_3	0.63	0.64	0.61	0.63	0.65	0.65	0.63	0.61	0.63
FeO*	90.81	89.24	89.03	90.98	90.57	91.36	89.05	90.25	90.54
Fe_2O_3 recalculated	66.31	63.22	63.58	66.44	66.21	66.83	65.07	66.14	66.31
FeO recalculated	31.14	32.35	31.82	31.20	30.99	31.23	30.50	30.74	30.87
MnO	0.01	0.03	0.04	0.01	0.02	0.02	0.02	0.03	0.01
MgO	0.03	0.04	0.05	0.03	0.05	0.01	0.03	0.01	-
ZnO	0.04	0.02	0.04	0.01	0.01	0.00	0.00	0.00	0.01
NiO	0.03	0.04	0.04	0.05	0.04	0.06	0.04	0.04	0.05
CaO	-	-	0.00	-	0.00	-	0.01	0.00	0.01
Cu_2O	-	0.02	0.00	0.02	0.01	-	-	0.00	-
K_2O	0.00	-	0.01	-	-	0.00	0.00	0.01	-
Total measured	92.89	93.60	93.14	93.11	92.61	93.24	91.00	91.93	92.21
Total recalculated	99.54	99.93	99.51	99.76	99.25	99.94	97.52	98.56	98.86

MAS	Massive to semi-massive mineralization	OBAN	Orthopyroxene -bearing bands of oxide mineralization
DIS	Disseminated mineralization	POD	Pod of oxide mineralization
BAN	Bands of oxide mineralization	OPOD	Orthopyroxene -bearing pod of oxide mineralization
ANO	Anorthosite hosted disseminated	VEIN	Vein of oxide mineralization
ORT	Orthopyroxene associated	MAG	Magnetite
CLI	Clinopyroxene associated	ILM	Ilmenite
		PLE	Pleonaste

Appendix IV a. (Continued)

Sample	CC031A	CC031A	CC031A	CC031A	CC031A	CC031A	CC031A	CC031A
Mineralization type	DIS	DIS	DIS	DIS	DIS	DIS	DIS	DIS
Descriptor	ANO	ANO	ANO	ANO	ANO	ANO	ANO	ANO
Circle Number	E	E	E	F	F	F	G	G
Mineral analyzed	MAG	MAG	MAG	MAG	MAG	MAG	MAG	MAG
Mineral host	MAG	MAG	MAG	ILM	ILM	ILM	ILM	ILM
Point	42	43	44	48	49	50	53	54
SiO_2	0.02	0.02	0.02	0.02	0.03	0.01	0.02	0.01
TiO_2	0.40	0.16	0.17	0.35	0.30	0.18	1.24	1.18
Al_2O_3	0.37	0.39	0.44	0.32	0.33	0.40	0.30	0.32
Cr_2O_3	0.51	0.52	0.50	0.47	0.49	0.54	0.85	1.07
V_2O_3	0.65	0.66	0.63	0.47	0.52	0.55	0.58	0.60
FeO*	90.75	91.40	90.50	90.74	91.25	91.62	90.32	90.03
Fe_2O_3 recalculated	66.12	66.90	66.22	66.36	66.72	67.14	64.65	64.44
FeO recalculated	31.26	31.21	30.91	31.03	31.22	31.21	32.15	32.05
MnO	0.02	-	0.02	0.01	0.02	0.01	0.02	0.02
MgO	-	-	0.02	0.04	0.03	0.04	0.02	0.02
ZnO	0.03	0.02	0.02	0.01	-	0.00	0.00	0.01
NiO	0.04	0.03	0.03	0.06	0.05	0.06	0.06	0.05
CaO	-	0.01	-	0.00	-	0.01	-	0.00
Cu_2O	-	-	0.00	0.01	0.01	-	0.01	-
K_2O	0.00	0.00	0.00	-	-	-	0.01	0.01
Total measured	92.79	93.21	92.36	92.50	93.03	93.44	93.43	93.31
Total recalculated	99.41	99.92	98.99	99.15	99.72	100.17	99.91	99.77

MAS	Massive to semi-massive mineralization	OBAN	Orthopyroxene -bearing bands of oxide mineralization		
DIS	Disseminated mineralization	POD	Pod of oxide mineralization		
BAN	Bands of oxide mineralization	OPOD	Orthopyroxene -bearing pod of oxide mineralization		
ANO	Anorthosite hosted disseminated	VEIN	Vein of oxide mineralization		
ORT	Orthopyroxene associated	MAG	Magnetite		
CLI	Clinopyroxene associated	ILM	Ilmenite	PLE	Pleonaste

Appendix IV a. (Continued)

Sample	CC031A	CC031A	CC031A	CC031A	CC031A	CC031A	CC031A	CC031A
Mineralization type	DIS	DIS	DIS	DIS	DIS	DIS	DIS	DIS
Descriptor	ANO	ANO	ANO	ANO	ANO	ANO	ANO	ANO
Circle Number	G	G	H	H	H	I	I	I
Mineral analyzed	MAG	MAG	MAG	MAG	MAG	MAG	MAG	MAG
Mineral host	MAG	MAG	ILM	ILM	ILM	ILM	ILM	ILM
Point	56	57	58	59	60	64	65	66
SiO_2	0.02	0.02	-	0.01	0.01	0.00	0.00	0.01
TiO_2	0.26	0.18	1.26	1.48	0.15	0.74	0.90	0.84
Al_2O_3	0.36	0.40	0.79	0.38	0.35	0.35	0.57	0.32
Cr_2O_3	0.56	0.53	0.37	0.36	0.52	0.38	0.37	0.39
V_2O_3	0.63	0.62	0.31	0.30	0.64	0.42	0.39	0.36
FeO*	90.92	90.84	90.47	91.43	92.37	90.83	91.32	91.54
Fe_2O_3 recalculated	66.42	66.50	64.91	65.42	67.73	65.96	66.05	66.36
FeO recalculated	31.15	31.00	32.06	32.57	31.43	31.47	31.89	31.82
MnO	0.01	0.02	-	0.01	0.00	-	0.01	0.01
MgO	-	0.02	0.13	0.02	0.04	0.06	0.07	0.05
ZnO	0.02	0.01	-	0.04	-	0.02	0.01	-
NiO	0.04	0.06	0.06	0.06	0.06	0.04	0.06	0.05
CaO	0.00	0.00	-	-	0.00	-	0.01	0.00
Cu_2O	-	-	-	0.01	-	-	-	-
K_2O	0.00	-	0.00	0.01	0.01	-	0.00	-
Total measured	92.83	92.71	93.39	94.11	94.16	92.85	93.71	93.56
Total recalculated	99.48	99.37	99.89	100.66	100.94	99.46	100.33	100.21

MAS	Massive to semi-massive mineralization	OBAN	Orthopyroxene -bearing bands of oxide mineralization		
DIS	Disseminated mineralization	POD	Pod of oxide mineralization		
BAN	Bands of oxide mineralization	OPOD	Orthopyroxene -bearing pod of oxide mineralization		
ANO	Anorthosite hosted disseminated	VEIN	Vein of oxide mineralization		
ORT	Orthopyroxene associated	MAG	Magnetite		
CLI	Clinopyroxene associated	ILM	Ilmenite	PLE	Pleonaste

Appendix IV a. (Continued)

Sample	CC054B	CC054B	CC054B	CC054B	CC054B	CC054B	CC054B	CC054B
Mineralization type	DIS	DIS	DIS	DIS	DIS	DIS	DIS	DIS
Descriptor	ORT	ORT	ORT	ORT	ORT	ORT	ORT	ORT
Circle Number	B	B	B	B	B	C	C	C
Mineral analyzed	MAG	MAG	MAG	MAG	MAG	MAG	MAG	MAG
Mineral host	garnet	garnet	MAG	MAG	MAG	garnet	garnet	MAG
Point	1	2	3	4	5	6	7	11
SiO_2	0.08	0.04	0.04	0.03	0.03	0.06	0.02	0.03
TiO_2	2.83	1.33	1.03	1.46	1.07	0.68	0.45	1.42
Al_2O_3	0.60	0.75	0.69	0.64	0.72	0.48	0.48	0.67
Cr_2O_3	0.19	0.26	0.32	0.35	0.33	0.13	0.14	0.33
V_2O_3	0.50	0.55	0.60	0.59	0.62	0.56	0.57	0.61
FeO*	87.99	89.91	90.92	90.74	90.93	90.90	91.22	90.79
Fe_2O_3 recalculated	61.02	64.33	65.36	64.68	65.28	66.08	66.70	64.81
FeO recalculated	33.09	32.03	32.11	32.54	32.19	31.44	31.21	32.47
MnO	0.16	0.12	0.04	0.05	0.05	0.06	0.07	0.06
MgO	0.02	-	0.05	0.04	0.04	0.01	0.01	0.07
ZnO	0.04	0.00	0.01	-	0.00	0.02	0.02	0.02
NiO	0.04	0.05	0.04	0.05	0.04	0.05	0.03	0.04
CaO	0.11	0.12	0.01	0.00	0.00	0.14	0.14	0.00
Cu_2O	0.00	-	0.01	-	-	-	-	-
K_2O	0.01	0.02	0.00	0.01	0.01	0.02	0.01	0.01
Total measured	92.56	93.14	93.76	93.96	93.84	93.11	93.17	94.03
Total recalculated	98.68	99.59	100.31	100.44	100.38	99.73	99.86	100.53

MAS	Massive to semi-massive mineralization	OBAN	Orthopyroxene -bearing bands of oxide mineralization		
DIS	Disseminated mineralization	POD	Pod of oxide mineralization		
BAN	Bands of oxide mineralization	OPOD	Orthopyroxene -bearing pod of oxide mineralization		
ANO	Anorthosite hosted disseminated	VEIN	Vein of oxide mineralization		
ORT	Orthopyroxene associated	MAG	Magnetite		
CLI	Clinopyroxene associated	ILM	Ilmenite	PLE	Pleonaste

Appendix IV a. (Continued)

Sample	CC054B	CC054B	CC054B	CC054B	CC054B	CC054B	CC054B	CC054B
Mineralization type	DIS	DIS	DIS	DIS	DIS	DIS	DIS	DIS
Descriptor	ORT	ORT	ORT	ORT	ORT	ORT	ORT	ORT
Circle Number	C	C	D	D	E	E	E	F
Mineral analyzed	MAG	MAG	MAG	MAG	MAG	MAG	MAG	MAG
Mineral host	MAG	MAG	ILM	ILM	MAG	MAG	MAG	MAG
Point	12	13	14	15	29	30	31	34
SiO_2	0.04	0.04	0.00	-	0.03	0.05	0.02	0.02
TiO_2	1.61	1.09	2.02	2.29	0.92	1.70	0.95	1.03
Al_2O_3	0.76	0.55	0.90	0.62	0.64	0.91	0.68	1.09
Cr_2O_3	0.34	0.35	0.24	0.22	0.34	0.35	0.36	0.33
V_2O_3	0.62	0.62	0.41	0.44	0.68	0.69	0.67	0.67
FeO*	90.37	91.12	90.63	91.25	90.80	89.73	90.72	90.60
Fe_2O_3 recalculated	64.14	65.46	64.06	64.14	65.41	63.45	65.32	65.00
FeO recalculated	32.66	32.22	32.99	33.54	31.95	32.64	31.95	32.12
MnO	0.05	0.04	0.02	0.01	0.04	0.06	0.05	0.05
MgO	0.06	0.05	0.19	0.07	0.03	0.07	0.05	0.09
ZnO	0.00	0.01	0.03	0.01	0.03	0.01	-	0.03
NiO	0.03	0.03	0.04	0.04	0.03	0.03	0.03	0.04
CaO	0.00	-	-	-	0.00	-	0.01	0.01
Cu_2O	-	0.00	-	0.01	-	-	0.03	0.00
K_2O	0.00	0.00	0.01	0.00	-	0.01	0.00	-
Total measured	93.88	93.91	94.48	94.97	93.54	93.60	93.55	93.95
Total recalculated	100.31	100.47	100.89	101.40	100.09	99.95	100.10	100.46

MAS	Massive to semi-massive mineralization	OBAN	Orthopyroxene -bearing bands of oxide mineralization		
DIS	Disseminated mineralization	POD	Pod of oxide mineralization		
BAN	Bands of oxide mineralization	OPOD	Orthopyroxene -bearing pod of oxide mineralization		
ANO	Anorthosite hosted disseminated	VEIN	Vein of oxide mineralization		
ORT	Orthopyroxene associated	MAG	Magnetite		
CLI	Clinopyroxene associated	ILM	Ilmenite	PLE	Pleonaste

Appendix IV a. (Continued)

Sample	CC054B	CC054B	CC054B	CC054B	CC054B	CC054B	CC054B	CC054B
Mineralization type	DIS	DIS	DIS	DIS	DIS	DIS	DIS	DIS
Descriptor	ORT	ORT	ORT	ORT	ORT	ORT	ORT	ORT
Circle Number	F	F	G	G	G	H	H	H
Mineral analyzed	MAG	MAG	MAG	MAG	MAG	MAG	MAG	MAG
Mineral host	MAG	MAG	MAG	MAG	MAG	opx	opx	MAG
Point	35	36	42	43	44	47	48	52
SiO_2	0.04	0.04	0.02	0.02	0.01	0.03	0.05	0.04
TiO_2	1.14	1.16	3.28	1.67	1.56	1.57	1.40	1.26
Al_2O_3	0.62	0.66	0.89	0.93	0.57	1.02	0.76	0.89
Cr_2O_3	0.33	0.33	0.34	0.35	0.33	0.25	0.23	0.35
V_2O_3	0.67	0.64	0.66	0.64	0.62	0.62	0.61	0.67
FeO*	90.40	90.46	88.12	89.69	90.41	89.10	89.67	91.17
Fe_2O_3 recalculated	64.85	64.78	60.37	63.61	64.40	63.18	64.06	65.17
FeO recalculated	32.04	32.17	33.80	32.46	32.46	32.25	32.03	32.53
MnO	0.05	0.03	0.10	0.06	0.05	0.07	0.09	0.05
MgO	0.05	0.02	0.14	0.12	0.07	0.04	0.10	0.10
ZnO	0.03	0.02	0.03	-	-	-	-	-
NiO	0.04	0.03	0.03	0.06	0.03	0.02	0.04	0.05
CaO	-	0.01	0.01	0.01	0.00	0.04	0.05	-
Cu_2O	-	0.01	-	0.01	0.01	0.02	0.00	0.00
K_2O	0.00	0.00	0.00	0.01	0.00	0.00	0.00	0.00
Total measured	93.38	93.41	93.62	93.55	93.66	92.79	93.00	94.58
Total recalculated	99.88	99.90	99.67	99.92	100.12	99.12	99.42	101.11

MAS	Massive to semi-massive mineralization	OBAN	Orthopyroxene -bearing bands of oxide mineralization		
DIS	Disseminated mineralization	POD	Pod of oxide mineralization		
BAN	Bands of oxide mineralization	OPOD	Orthopyroxene -bearing pod of oxide mineralization		
ANO	Anorthosite hosted disseminated	VEIN	Vein of oxide mineralization		
ORT	Orthopyroxene associated	MAG	Magnetite		
CLI	Clinopyroxene associated	ILM	Ilmenite	PLE	Pleonaste

Appendix IV a. (Continued)

Sample	CC054B	CC054B	CC054B	CC054B	CC054B	CC054B	CC054B	CC054B
Mineralization type	DIS	DIS	DIS	DIS	DIS	DIS	DIS	DIS
Descriptor	ORT	ORT	ORT	ORT	ORT	ORT	ORT	ORT
Circle Number	H	H	J	J	J	L	L	L
Mineral analyzed	MAG	MAG	MAG	MAG	MAG	MAG	MAG	MAG
Mineral host	MAG	MAG	MAG	MAG	MAG	MAG	MAG	MAG
Point	53	54	60	61	62	68	69	70
SiO_2	0.02	0.02	0.04	0.02	0.03	0.02	0.04	0.03
TiO_2	1.54	1.93	2.24	2.38	1.72	1.57	2.50	0.83
Al_2O_3	1.05	1.07	0.79	0.74	0.78	0.89	1.05	0.55
Cr_2O_3	0.36	0.37	0.30	0.31	0.31	0.47	0.36	0.35
V_2O_3	0.68	0.66	0.61	0.59	0.56	0.64	0.64	0.66
FeO*	90.49	90.28	89.67	89.67	89.88	89.56	89.14	91.94
Fe_2O_3 recalculated	64.26	63.63	62.82	62.70	63.67	63.64	61.97	66.37
FeO recalculated	32.67	33.03	33.15	33.26	32.59	32.30	33.38	32.22
MnO	0.04	0.06	0.09	0.10	0.06	0.05	0.09	0.02
MgO	0.12	0.15	0.05	0.06	0.04	0.13	0.09	0.03
ZnO	-	0.00	0.02	0.00	0.03	0.02	0.02	-
NiO	0.04	0.03	0.03	0.02	0.02	0.05	0.04	0.02
CaO	0.01	-	-	-	0.01	0.01	-	-
Cu_2O	-	-	0.00	-	-	0.00	-	0.02
K_2O	0.00	-	0.01	0.01	0.00	-	0.01	0.00
Total measured	94.36	94.57	93.85	93.91	93.44	93.41	93.97	94.47
Total recalculated	100.80	100.95	100.14	100.19	99.82	99.79	100.18	101.12

MAS	Massive to semi-massive mineralization	OBAN	Orthopyroxene -bearing bands of oxide mineralization		
DIS	Disseminated mineralization	POD	Pod of oxide mineralization		
BAN	Bands of oxide mineralization	OPOD	Orthopyroxene -bearing pod of oxide mineralization		
ANO	Anorthosite hosted disseminated	VEIN	Vein of oxide mineralization		
ORT	Orthopyroxene associated	MAG	Magnetite		
CLI	Clinopyroxene associated	ILM	Ilmenite	PLE	Pleonaste

Appendix IV a. (Continued)

Sample	CC054B	CC054B	CC054B	CC072	CC072	CC072	CC072	CC072	CC072
Mineralization type	DIS	DIS	DIS	MAS	MAS	MAS	MAS	MAS	MAS
Descriptor	ORT	ORT	ORT	OPOD	OPOD	OPOD	OPOD	OPOD	OPOD
Circle Number	O	O	O	A	A	A	A	A	A
Mineral analyzed	MAG	MAG	MAG	MAG	MAG	MAG	MAG	MAG	MAG
Mineral host	ILM	ILM	ILM	MAG	MAG	MAG	MAG	MAG	MAG
Point	74	75	76	1	2	3	4	5	6
SiO_2	0.00	0.02	-	0.03	0.03	0.02	0.02	0.05	0.02
TiO_2	1.58	2.01	2.24	4.47	4.46	6.31	4.70	5.64	5.93
Al_2O_3	0.64	1.01	0.89	2.17	0.62	1.70	2.11	1.93	1.85
Cr_2O_3	0.24	0.20	0.23	0.33	0.33	0.32	0.31	0.32	0.33
V_2O_3	0.42	0.44	0.37	0.66	0.64	0.69	0.66	0.68	0.68
FeO*	91.49	89.55	89.99	85.71	88.22	84.15	85.27	85.10	84.41
Fe_2O_3 recalculated	65.29	63.13	63.28	57.05	59.29	53.63	56.61	55.30	54.49
FeO recalculated	32.75	32.75	33.05	34.37	34.87	35.90	34.33	35.34	35.38
MnO	0.02	0.03	0.02	0.25	0.23	0.36	0.23	0.30	0.33
MgO	0.10	0.15	0.16	0.63	0.29	0.49	0.74	0.72	0.71
ZnO	-	-	0.02	0.01	0.02	0.03	0.02	0.01	-
NiO	0.05	0.04	0.03	0.03	0.04	0.05	0.03	0.05	0.04
CaO	0.00	-	0.00	-	0.00	-	0.01	-	-
Cu_2O	-	0.01	-	-	-	-	0.01	0.01	-
K_2O	0.00	-	-	-	0.01	-	0.00	0.01	-
Total measured	94.54	93.47	93.97	94.29	94.88	94.10	94.11	94.82	94.30
Total recalculated	101.08	99.79	100.31	100.00	100.82	99.47	99.79	100.36	99.76

MAS	Massive to semi-massive mineralization	OBAN	Orthopyroxene -bearing bands of oxide mineralization
DIS	Disseminated mineralization	POD	Pod of oxide mineralization
BAN	Bands of oxide mineralization	OPOD	Orthopyroxene -bearing pod of oxide mineralization
ANO	Anorthosite hosted disseminated	VEIN	Vein of oxide mineralization
ORT	Orthopyroxene associated	MAG	Magnetite
CLI	Clinopyroxene associated	ILM	Ilmenite

PLE	Pleonaste

Appendix IV a. (Continued)

Sample	CC072	CC072	CC072	CC072	CC072	CC072	CC072	CC072	CC072
Mineralization type	MAS	MAS	MAS	MAS	MAS	MAS	MAS	MAS	MAS
Descriptor	OPOD	OPOD	OPOD	OPOD	OPOD	OPOD	OPOD	OPOD	OPOD
Circle Number	B	B	B	B	B	B	C	C	C
Mineral analyzed	MAG	MAG	MAG	MAG	MAG	MAG	MAG	MAG	MAG
Mineral host	opx	opx	opx	MAG	MAG	MAG	MAG	MAG	MAG
Point	15	16	17	18	19	20	26	27	28
SiO_2	0.02	0.03	0.04	0.02	0.03	0.02	0.02	0.02	0.03
TiO_2	4.40	4.77	2.34	4.14	4.04	2.31	3.84	5.58	4.55
Al_2O_3	1.38	2.15	0.84	1.03	1.44	0.78	1.26	1.67	1.90
Cr_2O_3	0.28	0.33	0.30	0.33	0.36	0.33	0.32	0.32	0.32
V_2O_3	0.61	0.62	0.51	0.68	0.62	0.65	0.64	0.65	0.65
FeO*	86.44	84.88	89.13	87.66	87.18	89.60	86.11	84.87	86.01
Fe_2O_3 recalculated	57.92	56.09	62.55	59.23	58.82	63.03	58.40	55.27	57.29
FeO recalculated	34.33	34.41	32.85	34.37	34.25	32.88	33.56	35.14	34.46
MnO	0.27	0.45	0.15	0.29	0.25	0.16	0.24	0.28	0.25
MgO	0.44	0.52	0.22	0.36	0.41	0.28	0.41	0.63	0.60
ZnO	-	0.02	0.02	-	0.00	-	0.01	0.02	0.01
NiO	0.03	0.04	0.02	0.03	0.04	0.03	0.04	0.02	0.04
CaO	0.01	0.01	0.00	0.00	-	0.01	0.01	-	-
Cu_2O	0.03	0.01	0.00	-	-	-	-	0.01	0.01
K_2O	0.01	-	-	0.00	-	-	0.00	-	-
Total measured	93.92	93.81	93.57	94.54	94.38	94.17	92.90	94.07	94.37
Total recalculated	99.72	99.43	99.84	100.48	100.27	100.48	98.75	99.61	100.11

MAS	Massive to semi-massive mineralization	OBAN	Orthopyroxene -bearing bands of oxide mineralization
DIS	Disseminated mineralization	POD	Pod of oxide mineralization
BAN	Bands of oxide mineralization	OPOD	Orthopyroxene -bearing pod of oxide mineralization
ANO	Anorthosite hosted disseminated	VEIN	Vein of oxide mineralization
ORT	Orthopyroxene associated	MAG	Magnetite
CLI	Clinopyroxene associated	ILM	Ilmenite
		PLE	Pleonaste

Appendix IV a. (Continued)

Sample	CC072	CC072	CC072	CC072	CC072	CC072	CC072	CC072
Mineralization type	MAS	MAS	MAS	MAS	MAS	MAS	MAS	MAS
Descriptor	OPOD	OPOD	OPOD	OPOD	OPOD	OPOD	OPOD	OPOD
Circle Number	C	C	C	D	D	D	D	D
Mineral analyzed	MAG	MAG	MAG	MAG	MAG	MAG	MAG	MAG
Mineral host	MAG	MAG	MAG	MAG	MAG	MAG	opx	opx
Point	29	30	31	35	36	37	38	39
SiO_2	0.04	0.02	0.02	0.03	0.05	0.03	0.03	0.06
TiO_2	1.89	5.04	3.57	2.14	2.01	2.06	3.13	3.40
Al_2O_3	0.76	1.60	0.90	0.78	0.80	0.75	1.30	0.97
Cr_2O_3	0.31	0.32	0.33	0.37	0.33	0.33	0.32	0.30
V_2O_3	0.55	0.63	0.60	0.61	0.56	0.55	0.58	0.62
FeO*	89.60	85.50	87.63	90.09	89.55	89.45	87.70	87.39
Fe_2O_3 recalculated	63.51	56.48	60.00	63.69	63.34	63.28	60.50	59.90
FeO recalculated	32.45	34.68	33.64	32.78	32.56	32.51	33.26	33.49
MnO	0.10	0.27	0.19	0.09	0.10	0.12	0.16	0.22
MgO	0.24	0.62	0.37	0.37	0.28	0.28	0.44	0.31
ZnO	-	0.00	0.00	0.04	0.02	-	-	0.00
NiO	0.02	0.04	0.05	0.04	0.02	0.04	0.04	0.04
CaO	-	0.00	0.00	0.00	0.01	-	0.00	0.01
Cu_2O	0.01	-	-	-	0.00	0.01	-	0.01
K_2O	-	-	0.00	0.00	0.00	0.00	-	0.00
Total measured	93.53	94.05	93.67	94.56	93.72	93.62	93.69	93.33
Total recalculated	99.89	99.71	99.68	100.94	100.07	99.96	99.76	99.33

MAS	Massive to semi-massive mineralization	OBAN	Orthopyroxene -bearing bands of oxide mineralization		
DIS	Disseminated mineralization	POD	Pod of oxide mineralization		
BAN	Bands of oxide mineralization	OPOD	Orthopyroxene -bearing pod of oxide mineralization		
ANO	Anorthosite hosted disseminated	VEIN	Vein of oxide mineralization		
ORT	Orthopyroxene associated	MAG	Magnetite		
CLI	Clinopyroxene associated	ILM	Ilmenite	PLE	Pleonaste

Appendix IV a. (Continued)

Sample	CC072	CC072	CC072	CC072	CC072	CC072	CC072	CC072	CC072
Mineralization type	MAS	MAS	MAS	MAS	MAS	MAS	MAS	MAS	MAS
Descriptor	OPOD	OPOD	OPOD	OPOD	OPOD	OPOD	OPOD	OPOD	OPOD
Circle Number	D	E	E	E	G	G	G	G	H
Mineral analyzed	MAG	MAG	MAG	MAG	MAG	MAG	MAG	MAG	MAG
Mineral host	opx	MAG	MAG	MAG	ILM	ILM	opx	opx	ILM
Point	40	43	44	45	52	53	54	55	59
SiO_2	0.03	0.04	0.03	0.04	0.00	-	0.03	0.03	-
TiO_2	3.73	2.64	4.22	1.94	2.70	2.88	3.54	3.51	1.83
Al_2O_3	1.60	0.60	1.27	0.74	0.80	0.78	1.53	1.01	0.71
Cr_2O_3	0.31	0.32	0.31	0.31	0.24	0.22	0.28	0.28	0.21
V_2O_3	0.62	0.62	0.63	0.61	0.53	0.51	0.57	0.56	0.60
FeO*	86.21	88.83	86.49	89.15	89.30	90.28	87.02	87.34	89.91
Fe_2O_3 recalculated	58.55	62.07	58.22	63.09	62.38	62.88	59.43	59.77	63.98
FeO recalculated	33.52	32.98	34.10	32.38	33.17	33.70	33.54	33.56	32.34
MnO	0.20	0.12	0.23	0.11	0.05	0.05	0.19	0.20	0.02
MgO	0.53	0.29	0.46	0.22	0.32	0.32	0.50	0.32	0.31
ZnO	0.01	-	0.02	0.00	0.02	-	0.01	0.02	0.01
NiO	0.03	0.03	0.02	0.04	0.04	0.04	0.02	0.02	0.03
CaO	-	-	0.01	-	0.00	0.00	0.01	0.01	-
Cu_2O	-	0.01	0.02	-	-	0.00	-	-	0.01
K_2O	-	-	-	-	-	-	0.00	0.01	0.00
Total measured	93.28	93.50	93.69	93.15	94.01	95.09	93.73	93.31	93.64
Total recalculated	99.15	99.72	99.52	99.47	100.26	101.39	99.68	99.30	100.05

MAS	Massive to semi-massive mineralization	OBAN	Orthopyroxene -bearing bands of oxide mineralization
DIS	Disseminated mineralization	POD	Pod of oxide mineralization
BAN	Bands of oxide mineralization	OPOD	Orthopyroxene -bearing pod of oxide mineralization
ANO	Anorthosite hosted disseminated	VEIN	Vein of oxide mineralization
ORT	Orthopyroxene associated	MAG	Magnetite
CLI	Clinopyroxene associated	ILM	Ilmenite
		PLE	Pleonaste

Appendix IV a. (Continued)

Sample	CC072	CC072	CC072	CC072	CC072	CC072	CC072	CC072
Mineralization type	MAS	MAS	MAS	MAS	MAS	MAS	MAS	MAS
Descriptor	OPOD	OPOD	OPOD	OPOD	OPOD	OPOD	OPOD	OPOD
Circle Number	H	H	I	I	I	I	I	I
Mineral analyzed	MAG	MAG	MAG	MAG	MAG	MAG	MAG	MAG
Mineral host	ILM	ILM	MAG	MAG	MAG	MAG	MAG	MAG
Point	60	61	62	63	64	65	66	67
SiO_2	0.00	0.02	0.03	0.04	0.03	0.02	0.03	0.02
TiO_2	2.46	2.28	4.50	4.27	4.10	3.13	2.27	2.01
Al_2O_3	0.66	0.56	2.86	2.88	1.81	0.69	0.67	0.58
Cr_2O_3	0.18	0.18	0.33	0.33	0.33	0.31	0.31	0.31
V_2O_3	0.59	0.54	0.64	0.61	0.63	0.61	0.55	0.60
FeO*	90.05	90.12	85.22	85.02	86.69	88.19	89.40	90.19
Fe_2O_3 recalculated	63.28	63.55	56.74	56.82	58.44	61.00	62.99	63.88
FeO recalculated	33.11	32.93	34.17	33.89	34.10	33.30	32.72	32.71
MnO	0.05	0.03	0.24	0.24	0.20	0.15	0.11	0.11
MgO	0.28	0.27	0.95	0.91	0.65	0.31	0.26	0.21
ZnO	0.01	-	0.02	0.01	-	0.01	0.00	0.00
NiO	0.06	0.03	0.04	0.04	0.03	0.04	0.06	0.03
CaO	0.00	-	0.00	0.00	0.00	-	0.01	0.01
Cu_2O	0.01	0.02	0.02	0.01	-	0.00	-	0.00
K_2O	0.00	0.00	-	0.00	0.00	-	-	0.01
Total measured	94.36	94.06	94.84	94.37	94.46	93.47	93.67	94.07
Total recalculated	100.70	100.43	100.53	100.06	100.32	99.58	99.98	100.47

MAS	Massive to semi-massive mineralization	OBAN	Orthopyroxene -bearing bands of oxide mineralization		
DIS	Disseminated mineralization	POD	Pod of oxide mineralization		
BAN	Bands of oxide mineralization	OPOD	Orthopyroxene -bearing pod of oxide mineralization		
ANO	Anorthosite hosted disseminated	VEIN	Vein of oxide mineralization		
ORT	Orthopyroxene associated	MAG	Magnetite		
CLI	Clinopyroxene associated	ILM	Ilmenite	PLE	Pleonaste

Appendix IV a. (Continued)

Sample	CC074	CC074	CC074	CC074	CC074	CC074	CC074	CC074
Mineralization type	DIS	DIS	DIS	DIS	DIS	DIS	DIS	DIS
Descriptor	CLI	CLI	CLI	CLI	CLI	CLI	CLI	CLI
Circle Number	A	A	A	A	A	B	B	B
Mineral analyzed	MAG	MAG	MAG	MAG	MAG	MAG	MAG	MAG
Mineral host	ILM	ILM	MAG	MAG	MAG	MAG	MAG	MAG
Point	6	7	8	9	10	22	23	24
SiO_2	0.01	0.00	0.01	0.02	0.02	0.00	0.01	0.01
TiO_2	0.97	0.84	0.09	0.06	0.06	0.08	0.06	0.07
Al_2O_3	0.29	0.32	0.52	0.29	0.28	0.31	0.32	0.30
Cr_2O_3	1.24	1.20	0.68	0.54	0.53	0.52	0.51	0.49
V_2O_3	0.46	0.43	0.53	0.51	0.54	0.53	0.52	0.52
FeO*	90.23	89.78	90.33	90.51	91.13	91.15	91.31	91.17
Fe_2O_3 recalculated	64.85	64.75	66.22	66.48	66.91	66.95	67.06	66.96
FeO recalculated	31.87	31.52	30.75	30.69	30.92	30.91	30.97	30.92
MnO	0.04	0.04	0.03	0.02	0.01	0.00	0.02	0.02
MgO	0.00	0.02	0.07	0.01	0.00	0.02	-	0.01
ZnO	0.00	-	-	-	0.00	0.01	0.01	0.01
NiO	0.04	0.05	0.03	0.03	0.03	0.03	0.03	0.03
CaO	0.01	-	0.00	0.00	-	0.01	0.00	-
Cu_2O	-	0.00	0.01	-	0.01	0.01	0.02	-
K_2O	-	0.00	0.00	0.00	-	0.01	0.01	0.00
Total measured	93.29	92.69	92.31	91.99	92.62	92.67	92.83	92.63
Total recalculated	99.79	99.17	98.94	98.65	99.33	99.38	99.55	99.33

MAS	Massive to semi-massive mineralization	OBAN	Orthopyroxene -bearing bands of oxide mineralization
DIS	Disseminated mineralization	POD	Pod of oxide mineralization
BAN	Bands of oxide mineralization	OPOD	Orthopyroxene -bearing pod of oxide mineralization
ANO	Anorthosite hosted disseminated	VEIN	Vein of oxide mineralization
ORT	Orthopyroxene associated	MAG	Magnetite
CLI	Clinopyroxene associated	ILM	Ilmenite

PLE Pleonaste

Appendix IV a. (Continued)

Sample	CC074	CC074	CC074	CC074	CC074	CC074
Mineralization type	DIS	DIS	DIS	DIS	DIS	DIS
Descriptor	CLI	CLI	CLI	CLI	CLI	CLI
Circle Number	C	C	C	D	D	D
Mineral analyzed	MAG	MAG	MAG	MAG	MAG	MAG
Mineral host	MAG	MAG	MAG	MAG	MAG	MAG
Point	30	31	32	38	39	40
SiO_2	0.02	0.01	0.02	0.01	0.03	0.05
TiO_2	0.06	0.06	0.06	0.07	0.05	0.05
Al_2O_3	0.30	0.34	0.34	0.31	0.29	0.31
Cr_2O_3	0.64	0.51	0.49	0.71	0.54	0.54
V_2O_3	0.48	0.50	0.53	0.45	0.52	0.51
FeO*	91.36	90.77	91.05	91.16	90.89	90.63
Fe_2O_3 recalculated	67.11	66.65	66.87	66.96	66.74	66.51
FeO recalculated	30.98	30.80	30.88	30.91	30.84	30.78
MnO	0.01	0.01	0.02	0.03	0.02	0.01
MgO	0.02	0.00	0.02	0.02	0.00	0.02
ZnO	0.03	-	-	0.00	0.00	-
NiO	0.03	0.02	0.03	0.03	0.03	0.03
CaO	0.01	0.01	0.01	0.01	-	0.01
Cu_2O	0.01	0.01	-	0.00	-	-
K_2O	-	-	-	0.00	-	-
Total measured	92.98	92.25	92.57	92.81	92.37	92.15
Total recalculated	99.70	98.93	99.27	99.52	99.06	98.82

MAS	Massive to semi-massive mineralization	OBAN	Orthopyroxene -bearing bands of oxide mineralization		
DIS	Disseminated mineralization	POD	Pod of oxide mineralization		
BAN	Bands of oxide mineralization	OPOD	Orthopyroxene -bearing pod of oxide mineralization		
ANO	Anorthosite hosted disseminated	VEIN	Vein of oxide mineralization		
ORT	Orthopyroxene associated	MAG	Magnetite		
CLI	Clinopyroxene associated	ILM	Ilmenite	PLE	Pleonaste

Appendix IV a. (Continued)

Sample	CC074	CC074	CC074	CC074	CC074	CC074	CC076B	CC076B
Mineralization type	DIS	DIS	DIS	DIS	DIS	DIS	MAS	MAS
Descriptor	CLI	CLI	CLI	CLI	CLI	CLI	VEIN	VEIN
Circle Number	E	E	E	F	F	F	B	B
Mineral analyzed	MAG	MAG	MAG	MAG	MAG	MAG	MAG	MAG
Mineral host	MAG	MAG	MAG	MAG	MAG	MAG	MAG	MAG
Point	46	47	48	54	55	56	1	2
SiO_2	0.02	0.02	0.01	0.01	0.03	0.01	0.01	0.02
TiO_2	0.05	0.07	0.08	0.04	0.03	0.05	0.17	0.09
Al_2O_3	0.32	0.33	0.31	0.26	0.30	0.29	0.38	0.26
Cr_2O_3	0.51	0.50	0.52	0.72	0.68	0.67	0.42	0.49
V_2O_3	0.51	0.52	0.52	0.48	0.52	0.51	0.47	0.52
FeO*	90.95	91.57	91.23	90.81	91.26	91.71	92.03	91.89
Fe_2O_3 recalculated	66.81	67.25	67.00	66.69	66.98	67.35	67.50	67.49
FeO recalculated	30.83	31.06	30.94	30.80	31.00	31.11	31.29	31.16
MnO	0.02	0.03	0.02	0.02	0.02	0.01	0.03	0.02
MgO	0.02	0.01	0.02	0.02	0.01	0.01	0.04	0.03
ZnO	-	0.01	0.00	-	0.00	0.01	-	-
NiO	0.03	0.02	0.03	0.02	0.03	0.04	-	0.00
CaO	0.00	-	-	0.00	0.00	0.01	0.00	-
Cu_2O	-	0.00	-	-	-	0.00	-	-
K_2O	0.00	0.00	0.00	0.01	0.00	-	-	-
Total measured	92.43	93.08	92.74	92.39	92.89	93.32	93.55	93.33
Total recalculated	99.12	99.82	99.45	99.08	99.60	100.07	100.31	100.09

MAS	Massive to semi-massive mineralization	OBAN	Orthopyroxene -bearing bands of oxide mineralization		
DIS	Disseminated mineralization	POD	Pod of oxide mineralization		
BAN	Bands of oxide mineralization	OPOD	Orthopyroxene -bearing pod of oxide mineralization		
ANO	Anorthosite hosted disseminated	VEIN	Vein of oxide mineralization		
ORT	Orthopyroxene associated	MAG	Magnetite		
CLI	Clinopyroxene associated	ILM	Ilmenite	PLE	Pleonaste

Appendix IV a. (Continued)

Sample	CC076B	CC076B	CC076B	CC076B	CC076B	CC076B	CC076B	CC076B	CC076B
Mineralization type	MAS	MAS	MAS	MAS	MAS	MAS	MAS	MAS	MAS
Descriptor	VEIN	VEIN	VEIN	VEIN	VEIN	VEIN	VEIN	VEIN	VEIN
Circle Number	B	B	B	C	C	C	C	C	C
Mineral analyzed	MAG	MAG	MAG	MAG	MAG	MAG	MAG	MAG	MAG
Mineral host	MAG	PLE	PLE	MAG	MAG	MAG	MAG	MAG	MAG
Point	3	11	12	16	17	18	19	20	21
SiO_2	0.01	0.01	0.01	0.02	0.02	0.01	0.01	0.01	0.02
TiO_2	0.09	0.08	0.02	0.10	0.09	0.07	0.10	0.07	0.09
Al_2O_3	0.24	0.23	0.18	0.26	0.33	0.25	0.24	0.23	0.25
Cr_2O_3	0.53	0.36	0.38	0.46	0.48	0.46	0.60	0.48	0.47
V_2O_3	0.55	0.34	0.29	0.64	0.65	0.65	0.62	0.65	0.66
FeO*	91.68	91.69	91.74	92.06	91.23	91.22	91.13	91.75	92.15
Fe_2O_3 recalculated	67.39	67.58	67.73	67.58	66.98	67.03	66.86	67.45	67.68
FeO recalculated	31.04	30.89	30.80	31.25	30.96	30.91	30.97	31.06	31.25
MnO	0.03	0.04	0.04	0.03	0.04	0.02	0.02	0.04	0.04
MgO	0.05	0.01	0.01	0.03	0.04	0.03	0.02	0.04	0.03
ZnO	0.02	0.14	0.14	-	0.02	0.02	-	0.01	0.01
NiO	0.02	0.02	-	0.01	0.01	0.01	-	-	-
CaO	0.00	0.00	0.00	-	0.01	-	0.00	0.01	0.01
Cu_2O	-	-	-	0.01	0.00	0.00	-	0.00	0.01
K_2O	0.00	-	0.00	-	-	0.00	-	0.00	0.00
Total measured	93.21	92.91	92.81	93.63	92.91	92.74	92.75	93.28	93.75
Total recalculated	99.96	99.68	99.60	100.40	99.62	99.45	99.45	100.04	100.53

MAS	Massive to semi-massive mineralization	OBAN	Orthopyroxene -bearing bands of oxide mineralization		
DIS	Disseminated mineralization	POD	Pod of oxide mineralization		
BAN	Bands of oxide mineralization	OPOD	Orthopyroxene -bearing pod of oxide mineralization		
ANO	Anorthosite hosted disseminated	VEIN	Vein of oxide mineralization		
ORT	Orthopyroxene associated	MAG	Magnetite		
CLI	Clinopyroxene associated	ILM	Ilmenite	PLE	Pleonaste

Appendix IV a. (Continued)

Sample	CC076B	CC076B	CC076B	CC076B	CC076B	CC076B	CC076B	CC076B	CC076B
Mineralization type	MAS	MAS	MAS	MAS	MAS	MAS	MAS	MAS	MAS
Descriptor	VEIN	VEIN	VEIN	VEIN	VEIN	VEIN	VEIN	VEIN	VEIN
Circle Number	D	D	D	D	D	D	E	E	E
Mineral analyzed	MAG	MAG	MAG	MAG	MAG	MAG	MAG	MAG	MAG
Mineral host	ILM	ILM	ILM	ILM	ILM	ILM	Grt	Grt	Grt
Point	22	23	24	25	26	27	31	32	33
SiO_2	0.01	0.01	0.01	0.01	0.02	0.02	0.01	0.03	0.02
TiO_2	1.49	1.75	1.81	0.08	0.08	0.09	0.08	0.05	0.10
Al_2O_3	0.31	0.24	0.23	0.24	0.29	0.27	0.28	0.32	0.30
Cr_2O_3	0.22	0.21	0.21	0.39	0.41	0.42	0.64	0.66	0.65
V_2O_3	0.37	0.37	0.36	0.46	0.53	0.53	0.86	0.72	0.70
FeO*	91.87	91.42	92.15	92.46	92.03	92.04	91.66	91.02	91.04
Fe_2O_3 recalculated	65.78	65.16	65.59	68.04	67.61	67.64	67.16	66.82	66.85
FeO recalculated	32.68	32.79	33.13	31.24	31.19	31.17	31.22	30.90	30.89
MnO	0.02	0.03	0.04	0.00	0.02	0.02	0.01	0.15	0.17
MgO	0.04	0.04	0.03	0.05	0.02	0.03	0.03	0.01	0.01
ZnO	0.02	0.02	-	-	0.02	0.02	0.02	0.00	-
NiO	0.01	0.01	0.01	-	0.00	0.02	-	0.00	0.02
CaO	0.01	-	-	0.01	-	0.00	-	0.04	0.06
Cu_2O	0.01	0.01	0.02	0.00	0.01	0.00	0.01	-	-
K_2O	-	0.00	-	0.00	0.01	0.01	-	0.02	0.01
Total measured	94.38	94.11	94.87	93.70	93.43	93.45	93.60	93.02	93.07
Total recalculated	100.97	100.64	101.44	100.52	100.20	100.23	100.33	99.72	99.77

MAS	Massive to semi-massive mineralization	OBAN	Orthopyroxene -bearing bands of oxide mineralization		
DIS	Disseminated mineralization	POD	Pod of oxide mineralization		
BAN	Bands of oxide mineralization	OPOD	Orthopyroxene -bearing pod of oxide mineralization		
ANO	Anorthosite hosted disseminated	VEIN	Vein of oxide mineralization		
ORT	Orthopyroxene associated	MAG	Magnetite		
CLI	Clinopyroxene associated	ILM	Ilmenite	PLE	Pleonaste

Appendix IV a. (Continued)

Sample	CC076B	CC076B	CC076B	CC076B	CC076B	CC076B	CC076B	CC076B	CC076B	CC076B
Mineralization type	MAS	MAS	MAS	MAS	MAS	MAS	MAS	MAS	MAS	MAS
Descriptor	VEIN	VEIN	VEIN	VEIN	VEIN	VEIN	VEIN	VEIN	VEIN	VEIN
Circle Number	F	F	F	G	G	G	G	G	G	G
Mineral analyzed	MAG	MAG	MAG	MAG	MAG	MAG	MAG	MAG	MAG	MAG
Mineral host	ILM	ILM	ILM	ILM	ILM	PLE	PLE	MAG	MAG	MAG
Point	34	35	36	40	41	42	43	44	45	46
SiO_2	0.00	0.00	0.01	0.01	0.01	0.02	0.02	0.02	0.01	0.02
TiO_2	1.89	1.75	1.88	1.82	1.72	0.10	0.07	0.08	0.09	0.06
Al_2O_3	0.25	0.27	0.26	0.24	0.25	0.22	0.22	0.25	0.24	0.22
Cr_2O_3	0.23	0.23	0.22	0.25	0.26	0.35	0.42	0.44	0.44	0.44
V_2O_3	0.38	0.39	0.35	0.35	0.35	0.31	0.32	0.60	0.59	0.63
FeO*	92.09	91.52	91.34	90.15	90.68	90.90	91.29	91.86	91.81	91.78
Fe_2O_3 recalculated	65.43	65.24	64.84	64.07	64.61	66.92	67.32	67.48	67.45	67.45
FeO recalculated	33.21	32.82	32.99	32.50	32.55	30.69	30.72	31.14	31.12	31.08
MnO	0.01	0.02	0.02	0.03	0.05	0.05	0.06	0.03	0.04	0.03
MgO	0.04	0.05	0.01	0.01	0.02	0.00	0.03	0.03	0.02	0.02
ZnO	0.01	0.01	-	-	0.02	0.08	0.14	-	-	0.00
NiO	0.00	0.03	-	0.01	-	0.01	0.01	-	0.00	0.01
CaO	-	0.00	0.00	0.00	-	-	-	-	0.00	0.01
Cu_2O	-	-	0.00	0.01	-	-	-	0.00	-	0.00
K_2O	0.01	-	0.00	-	0.00	0.00	0.01	-	-	0.01
Total measured	94.92	94.27	94.09	92.89	93.37	92.04	92.58	93.31	93.25	93.22
Total recalculated	101.48	100.81	100.58	99.31	99.84	98.75	99.32	100.07	100.01	99.98

MAS	Massive to semi-massive mineralization	OBAN	Orthopyroxene -bearing bands of oxide mineralization
DIS	Disseminated mineralization	POD	Pod of oxide mineralization
BAN	Bands of oxide mineralization	OPOD	Orthopyroxene -bearing pod of oxide mineralization
ANO	Anorthosite hosted disseminated	VEIN	Vein of oxide mineralization
ORT	Orthopyroxene associated	MAG	Magnetite
CLI	Clinopyroxene associated	ILM	Ilmenite
		PLE	Pleonaste

Appendix IV a. (Continued)

Sample #	CC008	CC008	CC008	CC008	CC008	CC008	CC008	CC008	CC008	CC008	CC008	CC008
Circle Number	A	A	A	C	C	C	C	C	D	D	D	E
Mineralization type	MAS	MAS	MAS	MAS	MAS	MAS	MAS	MAS	MAS	MAS	MAS	MAS
Descriptor	BAN	BAN	BAN	BAN	BAN	BAN	BAN	BAN	BAN	BAN	BAN	BAN
mineral host	ILM	ILM	ILM	ILM	ILM	ILM	MAG	MAG	ILM	ILM	ILM	MAG
Mineral analyzed	ILM	ILM	ILM	ILM	ILM	ILM	ILM	ILM	ILM	ILM	ILM	ILM
exsolution feature type	host	host	host	host	host	host	in rim	in rim	host	host	host	lens
Point	4	5	6	20	21	22	26	27	33	34	35	38
SiO_2	0.00	0.01	0.00	0.01	0.00	0.01	0.00	0.00	0.01	0.00	0.00	0.03
TiO_2	50.07	48.78	49.25	50.27	49.16	50.56	52.86	52.53	49.72	48.39	49.83	51.03
Al_2O_3	0.02	0.02	0.02	0.04	0.01	0.03	0.02	0.02	0.03	0.03	0.03	0.89
Cr_2O_3	0.00	0.01	0.02	0.00	0.00	0.01	0.02	0.03	0.00	0.01	0.01	0.06
V_2O_3	0.31	0.28	0.33	0.30	0.32	0.27	0.20	0.22	0.26	0.29	0.25	0.23
FeO*	46.55	48.51	47.17	46.47	48.05	46.14	44.11	44.14	46.89	48.60	46.99	43.34
Fe_2O_3 recalculated	5.40	8.91	6.98	5.04	8.05	4.37	0.21	0.47	6.04	9.22	6.09	3.06
FeO recalculated	41.69	40.50	40.89	41.93	40.81	42.20	43.92	43.72	41.45	40.31	41.51	40.59
MnO	0.79	0.74	0.80	0.76	0.79	0.76	0.98	1.04	0.79	0.77	0.81	2.96
MgO	1.41	1.48	1.46	1.41	1.46	1.39	1.46	1.37	1.39	1.37	1.39	1.29
ZnO	0.03	0.00	0.00	0.00	0.00	0.01	0.04	0.03	0.00	0.00	0.01	0.05
NiO	0.00	0.00	0.00	0.00	0.00	0.02	0.00	0.00	0.00	0.00	0.01	0.00
CaO	0.01	0.00	0.01	0.00	0.00	0.00	0.00	0.00	0.00	0.00	0.00	0.00
Cu_2O	0.00	0.00	0.00	0.00	0.01	0.01	0.00	0.01	0.00	0.00	0.00	0.00
K_2O	0.00	0.00	0.00	0.00	0.01	0.00	0.00	0.00	0.01	0.00	0.00	0.00
Total measured	99.19	99.84	99.04	99.27	99.82	99.21	99.69	99.41	99.09	99.48	99.33	99.88

MAS	Massive to semi-massive mineralization	OBAN	Orthopyroxene -bearing bands of oxide mineralization
DIS	Disseminated mineralization	POD	Pod of oxide mineralization
BAN	Bands of oxide mineralization	OPOD	Orthopyroxene -bearing pod of oxide mineralization
ANO	Anorthosite hosted disseminated	VEIN	Vein of oxide mineralization
ORT	Orthopyroxene associated	MAG	Magnetite
CLI	Clinopyroxene associated	ILM	Ilmenite PLE Pleonaste

Appendix IV a. (Continued)

Sample #	CC008	CC008	CC008	CC008	CC008	CC008	CC008	CC010	CC010	CC010	CC010	CC010
Circle Number	E	F	F	F	I	I	I	A	C	C	D	D
Mineralization type	MAS	MAS	MAS	MAS	MAS	MAS	MAS	MAS	MAS	MAS	MAS	MAS
Descriptor	BAN	BAN	BAN	BAN	BAN	BAN	BAN	BAN	OBAN	OBAN	OBAN	OBAN
mineral host	MAG	MAG	ILM	ILM	ILM	ILM	ILM	PLE	PLE	PLE	ILM	ILM
Mineral analyzed	ILM	ILM	ILM	ILM	ILM	ILM	ILM	ILM	ILM	ILM	ILM	ILM
exsolution feature type	lens	ig	host	host	host	host	host	lath	lath	lath	Host	Host
Point	39	41	45	46	52	53	54	7	16	17	21	22
SiO_2	0.01	0.00	0.01	0.00	0.01	0.01	0.00	0.00	0.00	0.00	0.00	0.00
TiO_2	52.16	53.28	49.69	51.41	48.96	49.18	49.48	51.75	51.62	51.49	47.45	47.15
Al_2O_3	0.02	0.01	0.02	0.02	0.03	0.03	0.02	0.03	0.03	0.03	0.04	0.05
Cr_2O_3	0.04	0.00	0.00	0.01	0.01	0.01	0.02	0.02	0.02	0.02	0.02	0.01
V_2O_3	0.25	0.22	0.31	0.25	0.33	0.31	0.30	0.20	0.21	0.19	0.32	0.34
FeO*	42.80	44.65	47.35	45.61	48.29	47.78	48.05	44.51	46.03	45.67	49.32	49.47
Fe_2O_3 recalculated	2.24	1.19	6.65	3.04	8.56	7.80	7.89	2.32	3.53	3.17	11.55	12.05
FeO recalculated	40.79	43.58	41.36	42.88	40.58	40.76	40.95	42.42	42.86	42.82	38.93	38.62
MnO	1.95	0.97	0.78	0.83	0.60	0.60	0.60	1.28	1.05	1.16	0.66	0.67
MgO	2.30	1.84	1.42	1.41	1.59	1.60	1.64	1.55	1.39	1.28	1.73	1.74
ZnO	0.06	0.06	0.02	0.00	0.02	0.01	0.02	0.06	0.02	0.03	0.00	0.00
NiO	0.01	0.02	0.00	0.01	0.00	0.00	0.01	0.01	0.02	0.00	0.01	0.00
CaO	0.00	0.01	0.00	0.01	0.00	0.00	0.00	0.00	0.00	0.00	0.00	0.00
Cu_2O	0.00	0.00	0.00	0.00	0.00	0.00	0.00	0.01	0.01	0.01	0.01	0.00
K_2O	0.00	0.01	0.00	0.00	0.00	0.00	0.00	0.00	0.00	0.00	0.00	0.00
Total measured	99.60	101.06	99.60	99.55	99.83	99.54	100.15	99.42	100.40	99.89	99.55	99.44

MAS	Massive to semi-massive mineralization	OBAN	Orthopyroxene -bearing bands of oxide mineralization
DIS	Disseminated mineralization	POD	Pod of oxide mineralization
BAN	Bands of oxide mineralization	OPOD	Orthopyroxene -bearing pod of oxide mineralization
ANO	Anorthosite hosted disseminated	VEIN	Vein of oxide mineralization
ORT	Orthopyroxene associated	MAG	Magnetite
CLI	Clinopyroxene associated	ILM	Ilmenite PLE Pleonaste

Appendix IV a. (Continued)

Sample #	CC010	CC010	CC010	CC010	CC010	CC010	CC010	CC010
Circle Number	D	D	E	E	E	E	E	E
Mineralization type	MAS	MAS	MAS	MAS	MAS	MAS	MAS	MAS
Descriptor	OBAN	OBAN	OBAN	OBAN	OBAN	OBAN	OBAN	OBAN
mineral host	ILM	ILM	MAG	MAG	MAG	MAG	MAG	MAG
Mineral analyzed	ILM	ILM	ILM	ILM	ILM	ILM	ILM	ILM
exsolution feature type	Host	rim	Sandwich	Sandwich	Sandwich	rim around sandwich	Composite	Composite
Point	23	26	28	29	30	31	32	33
SiO_2	0.01	0.00	0.00	0.00	0.00	0.01	0.01	0.01
TiO_2	49.09	51.82	51.00	51.91	50.74	53.07	49.41	51.61
Al_2O_3	0.03	0.03	0.03	0.02	0.03	0.02	0.03	0.03
Cr_2O_3	0.01	0.01	0.01	0.01	0.01	0.02	0.02	0.02
V_2O_3	0.33	0.23	0.26	0.23	0.26	0.17	0.29	0.24
FeO*	48.18	45.56	46.53	45.23	46.43	42.61	47.61	45.86
Fe_2O_3 recalculated	8.77	3.39	5.03	2.95	5.17	-0.78	7.66	3.80
FeO recalculated	40.29	42.51	42.01	42.57	41.78	43.31	40.72	42.44
MnO	0.70	0.85	0.96	1.07	0.95	2.81	0.90	1.00
MgO	1.77	1.79	1.60	1.68	1.60	0.87	1.56	1.66
ZnO	0.01	0.05	0.02	0.03	0.04	0.04	0.03	0.01
NiO	0.00	0.00	0.01	0.01	0.02	0.00	0.00	0.01
CaO	0.00	0.01	0.00	0.00	0.00	0.00	0.00	0.00
Cu_2O	0.00	0.02	0.00	0.00	0.01	0.00	0.00	0.00
K_2O	0.00	0.00	0.01	0.00	0.00	0.00	0.00	0.00
Total measured	100.12	100.35	100.45	100.19	100.09	99.62	99.88	100.45

MAS	Massive to semi-massive mineralization	OBAN	Orthopyroxene -bearing bands of oxide mineralization		
DIS	Disseminated mineralization	POD	Pod of oxide mineralization		
BAN	Bands of oxide mineralization	OPOD	Orthopyroxene -bearing pod of oxide mineralization		
ANO	Anorthosite hosted disseminated	VEIN	Vein of oxide mineralization		
ORT	Orthopyroxene associated	MAG	Magnetite		
CLI	Clinopyroxene associated	ILM	Ilmenite	PLE	Pleonaste PLE

Appendix IV a. (Continued)

Sample #	CC010	CC010	CC010	CC010	CC010	CC010	CC010	CC010
Circle Number	E	F	F	F	I	I	I	H
Mineralization type	MAS	MAS	MAS	MAS	MAS	MAS	MAS	MAS
Descriptor	OBAN	OBAN	OBAN	OBAN	OBAN	OBAN	OBAN	OBAN
mineral host	MAG	ILM	ILM	ILM	MAG	MAG	MAG	MAG
Mineral analyzed	ILM	ILM	ILM	ILM	ILM	ILM	ILM	ILM
exsolution feature type	Composite	Host	Host	Host	Composite	Composite	Composite	Composite
Point	34	41	42	43	51	52	53	54
SiO_2	0.00	0.00	0.00	0.01	0.00	0.00	0.00	0.01
TiO_2	49.53	49.70	49.71	48.08	51.42	49.91	53.36	51.63
Al_2O_3	0.05	0.03	0.04	0.04	0.03	0.03	0.00	0.02
Cr_2O_3	0.02	0.01	0.02	0.03	0.02	0.02	0.01	0.01
V_2O_3	0.30	0.29	0.29	0.31	0.21	0.27	0.21	0.22
FeO*	47.61	47.19	47.00	48.48	45.75	47.13	42.74	45.42
Fe_2O_3 recalculated	7.60	6.93	6.74	9.94	3.88	6.68	-2.23	3.35
FeO recalculated	40.77	40.95	40.94	39.53	42.26	41.11	44.75	42.40
MnO	0.91	0.93	0.93	0.87	0.88	0.83	2.48	1.00
MgO	1.59	1.57	1.58	1.60	1.72	1.64	0.39	1.68
ZnO	0.03	0.00	0.00	0.00	0.03	0.00	0.04	0.04
NiO	0.00	0.00	0.01	0.00	0.01	0.01	0.00	0.00
CaO	0.00	0.00	0.00	0.00	0.00	0.01	0.00	0.00
Cu_2O	0.00	0.00	0.00	0.00	0.02	0.00	0.00	0.00
K_2O	0.00	0.01	0.00	0.00	0.00	0.00	0.00	0.00
Total measured	100.04	99.74	99.58	99.41	100.09	99.86	99.24	100.03

MAS	Massive to semi-massive mineralization	OBAN	Orthopyroxene -bearing bands of oxide mineralization
DIS	Disseminated mineralization	POD	Pod of oxide mineralization
BAN	Bands of oxide mineralization	OPOD	Orthopyroxene -bearing pod of oxide mineralization
ANO	Anorthosite hosted disseminated	VEIN	Vein of oxide mineralization
ORT	Orthopyroxene associated	MAG	Magnetite
CLI	Clinopyroxene associated	ILM	Ilmenite
		PLE	Pleonaste

Appendix IV a. (Continued)

Sample #	CC010	CC010	CC010	CC010	CC010	CC010	CC010	CC010	CC010
Circle Number	H	H	L	L	L	L	M	M	M
Mineralization type	MAS	MAS	MAS	MAS	MAS	MAS	MAS	MAS	MAS
Descriptor	OBAN	OBAN	OBAN	OBAN	OBAN	OBAN	OBAN	OBAN	OBAN
mineral host	MAG	MAG	ILM	ILM	Opx	Opx	MAG	MAG	MAG
Mineral analyzed	ILM	ILM	ILM	ILM	ILM	ILM	ILM	ILM	ILM
exsolution feature type	Composite	Composite	Host	Host	Granule	Granule	Sandwich	Sandwich	Sandwich
Point	55	56	62	63	65	66	69	70	71
SiO_2	0.00	0.00	0.01	0.00	0.05	0.03	0.00	0.00	0.00
TiO_2	49.64	51.63	48.03	47.60	49.65	51.02	51.86	51.30	51.32
Al_2O_3	0.05	0.03	0.04	0.03	0.02	0.03	0.02	0.02	0.02
Cr_2O_3	0.02	0.01	0.01	0.01	0.04	0.03	0.01	0.00	0.01
V_2O_3	0.29	0.22	0.28	0.29	0.34	0.36	0.22	0.25	0.24
FeO*	47.12	45.57	48.87	48.72	44.75	44.14	45.23	45.56	45.44
Fe_2O_3 recalculated	6.96	3.48	10.59	10.78	4.01	2.07	2.73	3.66	3.43
FeO recalculated	40.86	42.44	39.34	39.02	41.14	42.28	42.77	42.27	42.35
MnO	0.91	0.99	0.63	0.59	0.57	0.80	1.09	1.08	1.09
MgO	1.60	1.67	1.80	1.79	1.62	1.46	1.52	1.54	1.52
ZnO	0.02	0.01	0.00	0.00	0.03	0.05	0.03	0.03	0.00
NiO	0.00	0.01	0.01	0.01	0.01	0.00	0.01	0.00	0.00
CaO	0.00	0.00	0.01	0.00	0.06	0.14	0.01	0.01	0.00
Cu_2O	0.00	0.01	0.01	0.01	0.00	0.00	0.00	0.00	0.00
K_2O	0.00	0.00	0.00	0.00	0.00	0.00	0.00	0.00	0.00
Total measured	99.64	100.16	99.69	99.07	97.13	98.06	100.01	99.79	99.64

MAS	Massive to semi-massive mineralization	OBAN	Orthopyroxene -bearing bands of oxide mineralization
DIS	Disseminated mineralization	POD	Pod of oxide mineralization
BAN	Bands of oxide mineralization	OPOD	Orthopyroxene -bearing pod of oxide mineralization
ANO	Anorthosite hosted disseminated	VEIN	Vein of oxide mineralization
ORT	Orthopyroxene associated	MAG	Magnetite
CLI	Clinopyroxene associated	ILM	Ilmenite
		PLE	Pleonaste

Appendix IV a. (Continued)

Sample #	CC010	CC010	CC010	CC010	CC010	CC010	CC010	CC013A	CC013A	CC013A
Circle Number	M	M	M	M	M	O	O	A	A	A
Mineralization type	MAS	MAS	MAS	MAS	MAS	MAS	MAS	MAS	MAS	MAS
Descriptor	OBAN	OBAN	OBAN	OBAN	OBAN	OBAN	OBAN	BAN	BAN	BAN
mineral host	MAG	ILM	ILM	MAG	MAG	MAG	MAG	MAG	MAG	MAG
Mineral analyzed	ILM	PLE	PLE	PLE	PLE	ILM	ILM	ILM	ILM	ILM
exsolution feature type	Sandwich	Cap	Cap	granule	granule	Sandwich	Sandwich	Sandwich	Sandwich	Sandwich
Point	72	73	74	75	76	77	79	1	2	3
SiO_2	0.01	0.00	0.02	0.00	0.09	0.00	0.00	0.01	0.00	0.00
TiO_2	53.06	0.00	0.01	0.17	0.03	51.37	51.89	51.53	50.75	51.09
Al_2O_3	0.02	60.61	60.05	60.89	61.97	0.03	0.02	0.03	0.03	0.03
Cr_2O_3	0.01	0.34	0.33	0.43	0.34	0.02	0.03	0.02	0.02	0.03
V_2O_3	0.19	0.08	0.08	0.06	0.06	0.24	0.21	0.26	0.32	0.32
FeO*	43.23	25.16	25.83	24.45	24.09	45.72	45.27	45.83	47.07	46.35
Fe_2O_3 recalculated	0.10	4.24	4.65	3.59	2.79	3.85	3.04	3.58	4.86	4.62
FeO recalculated	43.14	21.34	21.64	21.22	21.58	42.26	42.53	42.61	42.70	42.19
MnO	1.63	0.20	0.22	0.23	0.25	1.06	1.10	0.80	0.81	0.85
MgO	1.64	12.76	12.49	12.98	13.06	1.61	1.68	1.63	1.19	1.61
ZnO	0.03	0.47	0.50	0.43	0.23	0.00	0.03	0.02	0.00	0.03
NiO	0.00	0.11	0.09	0.09	0.09	0.01	0.01	0.00	0.00	0.00
CaO	0.00	0.01	0.00	0.01	0.00	0.00	0.00	0.01	0.00	0.00
Cu_2O	0.00	0.00	0.00	0.01	0.01	0.00	0.01	0.00	0.02	0.00
K_2O	0.00	0.01	0.00	0.00	0.00	0.00	0.00	0.00	0.01	0.00
Total measured	99.82	99.75	99.61	99.75	100.22	100.06	100.25	100.14	100.21	100.32

MAS	Massive to semi-massive mineralization	OBAN	Orthopyroxene -bearing bands of oxide mineralization
DIS	Disseminated mineralization	POD	Pod of oxide mineralization
BAN	Bands of oxide mineralization	OPOD	Orthopyroxene -bearing pod of oxide mineralization
ANO	Anorthosite hosted disseminated	VEIN	Vein of oxide mineralization
ORT	Orthopyroxene associated	MAG	Magnetite
CLI	Clinopyroxene associated	ILM	Ilmenite
		PLE	Pleonaste

Appendix IV a. (Continued)

Sample #	CC013A	CC013A	CC013A	CC013A	CC013A	CC013A	CC013A	CC013A	CC013A
Circle Number	A	A	A	B	B	B	C	C	D
Mineralization type	MAS	MAS	MAS	MAS	MAS	MAS	MAS	MAS	MAS
Descriptor	BAN	BAN	BAN	BAN	BAN	BAN	BAN	BAN	BAN
mineral host	MAG	MAG	MAG	ILM	ILM	ILM	MAG	MAG	ILM
Mineral analyzed	ILM	ILM	ILM	ILM	ILM	ILM	ILM	ILM	MAG
exsolution feature type	Composite	Composite	Composite	Host	Host	Host	Sandwich	Sandwich	thick lam
Point	4	5	6	15	16	17	22	23	30
SiO_2	0.01	0.00	0.01	0.00	0.00	0.00	0.01	0.01	0.00
TiO_2	49.68	49.73	49.91	49.11	49.20	49.10	50.99	50.87	49.46
Al_2O_3	0.03	0.02	0.02	0.03	0.01	0.03	0.02	0.03	0.03
Cr_2O_3	0.02	0.02	0.02	0.01	0.00	0.03	0.03	0.03	0.02
V_2O_3	0.33	0.32	0.32	0.35	0.32	0.33	0.30	0.31	0.29
FeO*	47.67	47.38	47.30	47.97	47.66	48.18	46.32	46.65	47.76
Fe_2O_3 recalculated	7.43	6.99	6.84	8.22	7.85	8.51	4.62	5.14	67.96
FeO recalculated	40.99	41.09	41.14	40.57	40.60	40.52	42.16	42.03	31.69
MnO	0.77	0.72	0.75	0.75	0.73	0.71	0.88	0.88	0.69
MgO	1.64	1.62	1.68	1.59	1.63	1.63	1.57	1.59	1.65
ZnO	0.01	0.02	0.00	0.00	0.01	0.02	0.01	0.01	0.00
NiO	0.00	0.01	0.00	0.00	0.00	0.00	0.01	0.00	0.00
CaO	0.00	0.00	0.00	0.00	0.00	0.00	0.00	0.00	0.00
Cu_2O	0.00	0.00	0.00	0.00	0.00	0.00	0.00	0.02	0.01
K_2O	0.00	0.01	0.01	0.00	0.00	0.00	0.00	0.00	0.01
Total measured	100.15	99.85	100.02	99.83	99.56	100.04	100.13	100.40	99.91

MAS	Massive to semi-massive mineralization	OBAN	Orthopyroxene -bearing bands of oxide mineralization
DIS	Disseminated mineralization	POD	Pod of oxide mineralization
BAN	Bands of oxide mineralization	OPOD	Orthopyroxene -bearing pod of oxide mineralization
ANO	Anorthosite hosted disseminated	VEIN	Vein of oxide mineralization
ORT	Orthopyroxene associated	MAG	Magnetite
CLI	Clinopyroxene associated	ILM	Ilmenite PLE Pleonaste

Appendix IV a. (Continued)

Sample #	CC013A	CC013A	CC013A	CC013A	CC013A	CC013A	CC013A	CC013A	CC013A
Circle Number	D	E	E	E	I	I	I	L	L
Mineralization type	MAS	MAS	MAS	MAS	MAS	MAS	MAS	MAS	MAS
Descriptor	BAN	BAN	BAN	BAN	BAN	BAN	BAN	BAN	BAN
mineral host	ILM	ILM	ILM	ILM	ILM	ILM	ILM	ILM	ILM
Mineral analyzed	ILM	ILM	ILM	ILM	ILM	ILM	ILM	ILM	ILM
exsolution feature type	Host	Host	Host	Host	Host	Host	Host	Composite	Composite
Point	32	34	35	36	43	44	45	49	51
SiO_2	0.00	0.00	0.00	0.00	0.01	0.01	0.00	0.02	0.01
TiO_2	48.00	49.36	48.99	49.41	48.50	49.02	49.49	50.70	51.26
Al_2O_3	0.02	0.02	0.02	0.03	0.03	0.03	0.03	0.02	0.01
Cr_2O_3	0.01	0.02	0.02	0.01	0.01	0.02	0.01	0.01	0.01
V_2O_3	0.30	0.28	0.27	0.28	0.31	0.34	0.33	0.31	0.29
FeO*	48.98	47.40	47.91	48.19	48.67	48.71	47.78	46.40	46.02
Fe_2O_3 recalculated	8.86	7.55	8.26	8.30	9.63	9.12	7.64	4.90	3.98
FeO recalculated	40.32	40.61	40.47	40.72	40.00	40.50	40.91	41.99	42.44
MnO	0.69	0.71	0.70	0.78	0.71	0.68	0.70	0.78	0.85
MgO	1.63	1.71	1.60	1.63	1.63	1.63	1.61	1.59	1.58
ZnO	0.03	0.00	0.01	0.01	0.01	0.00	0.00	0.00	0.00
NiO	0.01	0.02	0.01	0.01	0.01	0.00	0.00	0.00	0.00
CaO	0.00	0.00	0.00	0.01	0.00	0.00	0.01	0.00	0.00
Cu_2O	0.01	0.00	0.00	0.00	0.02	0.01	0.01	0.00	0.00
K_2O	0.00	0.01	0.01	0.01	0.00	0.00	0.00	0.01	0.01
Total measured	99.69	99.53	99.54	100.36	99.89	100.46	99.99	99.84	100.04

MAS	Massive to semi-massive mineralization	OBAN	Orthopyroxene -bearing bands of oxide mineralization
DIS	Disseminated mineralization	POD	Pod of oxide mineralization
BAN	Bands of oxide mineralization	OPOD	Orthopyroxene -bearing pod of oxide mineralization
ANO	Anorthosite hosted disseminated	VEIN	Vein of oxide mineralization
ORT	Orthopyroxene associated	MAG	Magnetite
CLI	Clinopyroxene associated	ILM	Ilmenite
		PLE	Pleonaste

Appendix IV a. (Continued)

Sample #	CC013A	CC013A	CC013A	CC025A	CC025A	CC025A	CC025A	CC025A	CC025A	CC025A
Circle Number	M	M	M	A	A	A	B	B	B	C
Mineralization type	MAS	MAS	MAS	MAS	MAS	MAS	MAS	MAS	MAS	MAS
Descriptor	BAN	BAN	BAN	POD	POD	POD	POD	POD	POD	POD
mineral host	MAG	MAG	MAG	ILM	ILM	ILM	ILM	ILM	ILM	MAG
Mineral analyzed	ILM	ILM	ILM	ILM	ILM	ILM	ILM	ILM	ILM	ILM
exsolution feature type	lath	lath	lath	host	host	host	host	host	host	sandwich
Point	59	60	61	1	2	3	10	11	12	15
SiO_2	0.01	0.02	0.02	0.00	0.00	0.00	0.00	0.00	0.00	0.00
TiO_2	50.19	48.72	51.46	50.33	49.64	48.20	51.16	48.93	48.11	51.01
Al_2O_3	0.03	0.03	0.03	0.03	0.05	0.06	0.03	0.06	0.05	0.02
Cr_2O_3	0.03	0.03	0.04	0.03	0.03	0.01	0.00	0.01	0.01	0.02
V_2O_3	0.32	0.36	0.28	0.21	0.25	0.24	0.22	0.25	0.26	0.18
FeO*	47.07	48.23	45.75	47.15	47.86	49.01	46.62	48.24	49.79	47.61
Fe_2O_3 recalculated	6.05	8.70	3.69	4.69	6.10	8.74	3.62	7.33	9.86	4.14
FeO recalculated	41.63	40.40	42.43	42.93	42.37	41.14	43.36	41.64	40.92	43.88
MnO	0.82	0.76	0.91	0.39	0.34	0.33	0.38	0.30	0.29	0.53
MgO	1.51	1.48	1.64	1.09	1.08	1.05	1.26	1.16	1.14	0.82
ZnO	0.00	0.02	0.01	0.00	0.00	0.01	0.01	0.00	0.00	0.00
NiO	0.01	0.01	0.00	0.00	0.01	0.00	0.01	0.00	0.01	0.00
CaO	0.00	0.00	0.01	0.00	0.00	0.00	0.00	0.00	0.01	0.01
Cu_2O	0.02	0.00	0.00	0.00	0.01	0.00	0.01	0.00	0.01	0.00
K_2O	0.01	0.00	0.01	0.00	0.00	0.00	0.00	0.00	0.00	0.00
Total measured	100.01	99.67	100.15	99.23	99.27	98.91	99.70	98.95	99.69	100.20

MAS	Massive to semi-massive mineralization	OBAN	Orthopyroxene -bearing bands of oxide mineralization
DIS	Disseminated mineralization	POD	Pod of oxide mineralization
BAN	Bands of oxide mineralization	OPOD	Orthopyroxene -bearing pod of oxide mineralization
ANO	Anorthosite hosted disseminated	VEIN	Vein of oxide mineralization
ORT	Orthopyroxene associated	MAG	Magnetite
CLI	Clinopyroxene associated	ILM	Ilmenite
		PLE	Pleonaste

Appendix IV a. (Continued)

Sample #	CC025A	CC025A	CC025A	CC025A	CC025A	CC025A	CC025A	CC025A	CC025A
Circle Number	C	C	C	D	D	D	D	D	D
Mineralization type	MAS	MAS	MAS	MAS	MAS	MAS	MAS	MAS	MAS
Descriptor	POD	POD	POD	POD	POD	POD	POD	POD	POD
mineral host	MAG	MAG	MAG	MAG	MAG	MAG	MAG	MAG	MAG
Mineral analyzed	ILM	ILM	ILM	ILM	ILM	ILM	ILM	ILM	ILM
exsolution feature type	sandwich	thin ig	thin ig	composite	composite	composite	thick ig	thick ig	thick ig
Point	16	18	19	23	24	25	26	27	28
SiO_2	0.00	0.01	0.01	0.00	0.00	0.01	0.01	0.02	0.02
TiO_2	50.62	52.60	52.85	51.02	50.95	50.26	52.23	52.33	44.97
Al_2O_3	0.03	0.01	0.01	0.01	0.03	0.04	0.07	0.09	5.82
Cr_2O_3	0.03	0.03	0.03	0.01	0.02	0.04	0.03	0.05	0.20
V_2O_3	0.18	0.16	0.14	0.18	0.18	0.19	0.19	0.15	0.16
FeO*	47.40	45.42	44.97	46.82	47.34	48.11	45.87	45.42	43.73
Fe_2O_3 recalculated	4.21	0.09	-0.57	3.35	3.96	5.38	0.84	0.26	6.65
FeO recalculated	43.61	45.34	45.49	43.81	43.77	43.27	45.12	45.18	37.74
MnO	0.53	0.63	0.65	0.48	0.49	0.46	0.77	0.79	0.68
MgO	0.77	0.75	0.77	0.90	0.87	0.83	0.60	0.60	1.11
ZnO	0.00	0.00	0.02	0.00	0.00	0.00	0.00	0.02	0.06
NiO	0.01	0.01	0.00	0.00	0.01	0.00	0.01	0.01	0.01
CaO	0.00	0.01	0.00	0.00	0.00	0.00	0.00	0.00	0.01
Cu_2O	0.00	0.03	0.00	0.01	0.00	0.00	0.01	0.00	0.00
K_2O	0.00	0.00	0.00	0.00	0.00	0.00	0.00	0.01	0.00
Total measured	99.57	99.65	99.46	99.42	99.89	99.94	99.80	99.48	96.76

MAS	Massive to semi-massive mineralization	OBAN	Orthopyroxene -bearing bands of oxide mineralization
DIS	Disseminated mineralization	POD	Pod of oxide mineralization
BAN	Bands of oxide mineralization	OPOD	Orthopyroxene -bearing pod of oxide mineralization
ANO	Anorthosite hosted disseminated	VEIN	Vein of oxide mineralization
ORT	Orthopyroxene associated	MAG	Magnetite
CLI	Clinopyroxene associated	ILM	Ilmenite
		PLE	Pleonaste

Appendix IV a. (Continued)

Sample #	CC025A	CC025A	CC025A	CC025A	CC025A	CC025A	CC025A	CC025A	CC025A
Circle Number	D	D	E	E	E	E	E	E	E
Mineralization type	MAS	MAS	MAS	MAS	MAS	MAS	MAS	MAS	MAS
Descriptor	POD	POD	POD	POD	POD	POD	POD	POD	POD
mineral host	ILM	ILM	MAG	MAG	MAG	MAG	MAG	MAG	MAG
Mineral analyzed	ILM	ILM	ILM	ILM	ILM	ILM	ILM	ILM	ILM
exsolution feature type	intergrowth inside	intergrowth	sandwich	sandwich	sandwich	comp ig	comp ig	thick ig	thick ig
Point	31	32	38	39	40	41	42	45	46
SiO_2	0.00	0.00	0.01	0.00	0.00	0.01	0.02	0.00	0.00
TiO_2	52.12	52.77	53.00	50.78	50.78	52.82	52.40	52.68	52.67
Al_2O_3	0.01	0.01	0.01	0.02	0.03	0.01	0.43	0.01	0.01
Cr_2O_3	0.00	0.03	0.00	0.02	0.01	0.03	0.03	0.03	0.05
V_2O_3	0.16	0.16	0.13	0.18	0.19	0.14	0.16	0.16	0.19
FeO*	46.75	45.64	45.12	47.40	47.25	45.52	45.33	44.89	44.72
Fe_2O_3 recalculated	2.12	0.17	-0.55	4.14	4.01	0.12	0.44	-0.56	-0.79
FeO recalculated	44.84	45.48	45.62	43.67	43.64	45.41	44.94	45.40	45.43
MnO	0.58	0.63	0.62	0.53	0.51	0.65	0.62	0.84	0.80
MgO	0.81	0.74	0.80	0.80	0.84	0.81	0.88	0.63	0.63
ZnO	0.00	0.03	0.00	0.03	0.00	0.00	0.00	0.02	0.00
NiO	0.00	0.00	0.00	0.01	0.02	0.00	0.01	0.00	0.00
CaO	0.00	0.00	0.00	0.00	0.00	0.00	0.00	0.00	0.00
Cu_2O	0.00	0.00	0.00	0.00	0.01	0.02	0.00	0.00	0.00
K_2O	0.01	0.00	0.00	0.00	0.00	0.00	0.00	0.00	0.00
Total measured	100.44	100.01	99.69	99.76	99.64	100.00	99.89	99.26	99.08

MAS	Massive to semi-massive mineralization	OBAN	Orthopyroxene -bearing bands of oxide mineralization
DIS	Disseminated mineralization	POD	Pod of oxide mineralization
BAN	Bands of oxide mineralization	OPOD	Orthopyroxene -bearing pod of oxide mineralization
ANO	Anorthosite hosted disseminated	VEIN	Vein of oxide mineralization
ORT	Orthopyroxene associated	MAG	Magnetite
CLI	Clinopyroxene associated	ILM	Ilmenite
		PLE	Pleonaste

Appendix IV a. (Continued)

Sample #	CC025A	CC025A	CC025A	CC025A	CC025A	CC025A	CC025A	CC025A
Circle Number	G	G	G	G	G	G	G	I
Mineralization type	MAS	MAS	MAS	MAS	MAS	MAS	MAS	MAS
Descriptor	POD	POD	POD	POD	POD	POD	POD	POD
mineral host	MAG	MAG	MAG	MAG	MAG	MAG	MAG	MAG
Mineral analyzed	ILM	ILM	ILM	ILM	ILM	ILM	ILM	ILM
exsolution feature type	composite	composite	composite	sandwich	sandwich	ig contact	ig contact	composite
Point	51	52	53	54	56	57	58	59
SiO_2	0.00	0.00	0.00	0.00	0.00	0.00	0.00	0.01
TiO_2	51.35	50.20	49.86	51.77	50.87	52.38	52.60	52.04
Al_2O_3	0.03	0.05	0.04	0.01	0.03	0.01	0.01	0.02
Cr_2O_3	0.02	0.02	0.03	0.02	0.02	0.01	0.02	0.02
V_2O_3	0.17	0.19	0.21	0.18	0.19	0.17	0.18	0.19
FeO*	46.56	48.12	47.94	46.03	47.32	46.15	45.66	46.17
Fe_2O_3 recalculated	2.74	5.47	5.59	1.52	3.91	1.16	0.43	1.45
FeO recalculated	44.10	43.20	42.91	44.66	43.80	45.11	45.27	44.87
MnO	0.53	0.46	0.46	0.55	0.52	0.64	0.69	0.55
MgO	0.84	0.81	0.82	0.74	0.79	0.74	0.73	0.78
ZnO	0.04	0.03	0.00	0.01	0.03	0.02	0.03	0.00
NiO	0.02	0.00	0.00	0.00	0.00	0.01	0.02	0.00
CaO	0.00	0.00	0.00	0.01	0.00	0.00	0.00	0.00
Cu_2O	0.01	0.01	0.00	0.01	0.00	0.00	0.00	0.00
K_2O	0.01	0.00	0.01	0.00	0.00	0.00	0.00	0.00
Total measured	99.57	99.90	99.37	99.34	99.76	100.14	99.93	99.78

MAS	Massive to semi-massive mineralization	OBAN	Orthopyroxene -bearing bands of oxide mineralization
DIS	Disseminated mineralization	POD	Pod of oxide mineralization
BAN	Bands of oxide mineralization	OPOD	Orthopyroxene -bearing pod of oxide mineralization
ANO	Anorthosite hosted disseminated	VEIN	Vein of oxide mineralization
ORT	Orthopyroxene associated	MAG	Magnetite
CLI	Clinopyroxene associated	ILM	Ilmenite
		PLE	Pleonaste

Appendix IV a. (Continued)

Sample #	CC025A	CC025A	CC025A	CC025A	CC025A	CC031A	CC031A	CC031A
Circle Number	I	I	K	K	K	A	A	B
Mineralization type	MAS	MAS	MAS	MAS	MAS	DIS	DIS	DIS
Descriptor	POD	POD	POD	POD	POD	ANO	ANO	ANO
mineral host	MAG	MAG	ILM	ILM	ILM	MAG	MAG	MAG
Mineral analyzed	ILM	ILM	ILM	ILM	ILM	ILM	ILM	ILM
exsolution feature type	composite	composite	host	host	host	Thick Lamellae	Thick Lamellae	composite
Point	60	61	65	66	67	4	6	7
SiO_2	0.01	0.01	0.00	0.00	0.01	0.00	0.01	0.00
TiO_2	50.13	50.36	49.50	47.74	49.05	52.35	51.93	51.25
Al_2O_3	0.03	0.03	0.03	0.07	0.06	0.00	0.02	0.01
Cr_2O_3	0.05	0.02	0.01	0.02	0.03	0.02	0.03	0.03
V_2O_3	0.20	0.17	0.22	0.27	0.25	0.16	0.17	0.20
FeO*	48.09	48.11	48.43	49.75	48.85	45.01	45.11	46.49
Fe_2O_3 recalculated	5.38	4.79	6.99	9.99	7.82	-0.14	0.36	2.45
FeO recalculated	43.25	43.80	42.14	40.76	41.81	45.14	44.79	44.29
MnO	0.44	0.41	0.34	0.32	0.33	1.31	1.32	1.19
MgO	0.78	0.60	1.14	1.05	1.10	0.33	0.33	0.34
ZnO	0.00	0.01	0.00	0.00	0.00	0.03	0.00	0.00
NiO	0.01	0.00	0.00	0.00	0.01	0.01	0.00	0.00
CaO	0.00	0.00	0.00	0.00	0.00	0.00	0.00	0.00
Cu_2O	0.00	0.00	0.00	0.01	0.00	0.01	0.01	0.01
K_2O	0.00	0.00	0.01	0.01	0.00	0.01	0.00	0.00
Total measured	99.74	99.72	99.68	99.22	99.69	99.23	98.93	99.52

MAS	Massive to semi-massive mineralization	OBAN	Orthopyroxene -bearing bands of oxide mineralization
DIS	Disseminated mineralization	POD	Pod of oxide mineralization
BAN	Bands of oxide mineralization	OPOD	Orthopyroxene -bearing pod of oxide mineralization
ANO	Anorthosite hosted disseminated	VEIN	Vein of oxide mineralization
ORT	Orthopyroxene associated	MAG	Magnetite
CLI	Clinopyroxene associated	ILM	Ilmenite
		PLE	Pleonaste

Appendix IV a. (Continued)

Sample #	CC031A	CC031A	CC031A	CC031A	CC031A	CC031A	CC031A
Circle Number	B	B	B	B	C	C	C
Mineralization type	DIS	DIS	DIS	DIS	DIS	DIS	DIS
Descriptor	ANO	ANO	ANO	ANO	ANO	ANO	ANO
mineral host	MAG	MAG	MAG	MAG	MAG	MAG	ILM
Mineral analyzed	ILM	ILM	ILM	ILM	ILM	ILM	ILM
exsolution feature type	composite	composite	intergrowth contact	intergrowth contact	host	host	ILM PLE contact
Point	8	9	10	11	15	16	20
SiO_2	0.00	0.01	0.01	0.00	0.00	0.00	0.00
TiO_2	51.37	52.59	52.97	52.90	50.74	49.80	52.47
Al_2O_3	0.03	0.01	0.06	0.03	0.01	0.04	0.01
Cr_2O_3	0.02	0.03	0.03	0.03	0.04	0.03	0.02
V_2O_3	0.20	0.20	0.18	0.19	0.17	0.20	0.16
FeO*	46.02	46.04	44.80	44.65	46.63	47.29	45.02
Fe_2O_3 recalculated	1.88	0.72	-0.98	-36.03	3.47	5.10	0.08
FeO recalculated	44.33	45.39	45.68	77.07	43.51	42.70	44.95
MnO	1.22	1.29	1.33	1.37	0.79	0.75	0.89
MgO	0.34	0.34	0.35	0.34	0.73	0.74	0.74
ZnO	0.03	0.00	0.00	0.01	0.03	0.01	0.01
NiO	0.01	0.00	0.00	0.00	0.00	0.01	0.00
CaO	0.00	0.01	0.00	0.00	0.00	0.00	0.00
Cu_2O	0.00	0.00	0.00	0.00	0.01	0.00	0.00
K_2O	0.00	0.00	0.00	0.00	0.00	0.00	0.00
Total measured	99.25	100.51	99.72	99.52	99.16	98.86	99.33

MAS	Massive to semi-massive mineralization	OBAN	Orthopyroxene -bearing bands of oxide mineralization		
DIS	Disseminated mineralization	POD	Pod of oxide mineralization		
BAN	Bands of oxide mineralization	OPOD	Orthopyroxene -bearing pod of oxide mineralization		
ANO	Anorthosite hosted disseminated	VEIN	Vein of oxide mineralization		
ORT	Orthopyroxene associated	MAG	Magnetite		
CLI	Clinopyroxene associated	ILM	Ilmenite	PLE	Pleonaste

Appendix IV a. (Continued)

Sample #	CC031A	CC031A	CC031A	CC031A	CC031A	CC031A	CC031A	CC031A
Circle Number	C	D	D	D	D	D	D	D
Mineralization type	DIS	DIS	DIS	DIS	DIS	DIS	DIS	DIS
Descriptor	ANO	ANO	ANO	ANO	ANO	ANO	ANO	ANO
mineral host	ILM	MAG	MAG	MAG	MAG	MAG	MAG	MAG
Mineral analyzed	ILM	ILM	ILM	ILM	ILM	ILM	ILM	ILM
exsolution feature type	ILM PLE contact	composite	composite	composite	ig contact	ig contact	sandwich	sandwich
Point	21	25	26	27	28	29	33	34
SiO_2	0.00	0.00	0.02	0.00	0.00	0.00	0.00	0.01
TiO_2	52.53	51.89	51.61	51.51	52.65	52.46	52.74	52.52
Al_2O_3	0.13	0.01	0.01	0.03	0.01	0.02	0.00	0.01
Cr_2O_3	0.03	0.03	0.01	0.03	0.02	0.07	0.01	0.01
V_2O_3	0.14	0.20	0.17	0.18	0.15	0.19	0.18	0.20
FeO*	44.77	45.18	46.03	46.27	44.74	44.02	44.50	43.92
Fe_2O_3 recalculated	-0.08	0.40	1.46	1.91	-0.77	-1.35	-1.28	-1.71
FeO recalculated	44.84	44.82	44.72	44.55	45.43	45.24	45.65	45.46
MnO	0.94	1.27	1.18	1.22	1.31	1.35	1.26	1.27
MgO	0.81	0.31	0.29	0.29	0.34	0.31	0.28	0.28
ZnO	0.02	0.00	0.00	0.01	0.00	0.03	0.01	0.00
NiO	0.01	0.00	0.00	0.01	0.00	0.00	0.00	0.01
CaO	0.00	0.00	0.00	0.00	0.00	0.00	0.01	0.00
Cu_2O	0.00	0.00	0.00	0.00	0.00	0.01	0.00	0.01
K_2O	0.00	0.00	0.00	0.00	0.01	0.00	0.01	0.00
Total measured	99.37	98.89	99.33	99.56	99.22	98.47	98.98	98.24

MAS	Massive to semi-massive mineralization	OBAN	Orthopyroxene -bearing bands of oxide mineralization
DIS	Disseminated mineralization	POD	Pod of oxide mineralization
BAN	Bands of oxide mineralization	OPOD	Orthopyroxene -bearing pod of oxide mineralization
ANO	Anorthosite hosted disseminated	VEIN	Vein of oxide mineralization
ORT	Orthopyroxene associated	MAG	Magnetite
CLI	Clinopyroxene associated	ILM	Ilmenite

PLE Pleonaste

Appendix IV a. (Continued)

Sample #	CC031A	CC031A	CC031A	CC031A	CC031A	CC031A	CC031A	CC031A
Circle Number	E	E	E	E	E	E	F	F
Mineralization type	DIS	DIS	DIS	DIS	DIS	DIS	DIS	DIS
Descriptor	ANO	ANO	ANO	ANO	ANO	ANO	ANO	ANO
mineral host	MAG	MAG	MAG	MAG	MAG	MAG	ILM	ILM
Mineral analyzed	ILM	ILM	ILM	ILM	ILM	ILM	ILM	ILM
exsolution feature type	sandwich	sandwich	sandwich	Thick Lamellae	Thick Lamellae	Thick Lamellae	Host	Host
Point	36	37	38	39	40	41	45	46
SiO_2	0.00	0.00	0.00	0.00	0.00	0.00	0.00	0.01
TiO_2	51.78	51.49	51.73	51.95	51.93	51.87	50.39	48.83
Al_2O_3	0.01	0.02	0.01	0.01	0.02	0.01	0.02	0.00
Cr_2O_3	0.01	0.03	0.03	0.04	0.03	0.03	0.02	0.02
V_2O_3	0.18	0.18	0.21	0.18	0.19	0.18	0.18	0.21
FeO*	45.80	45.80	45.61	45.78	45.71	45.76	47.20	48.40
Fe_2O_3 recalculated	0.98	1.22	0.76	0.86	0.72	0.94	4.48	7.37
FeO recalculated	44.92	44.70	44.92	45.00	45.06	44.91	43.17	41.77
MnO	1.16	1.10	1.10	1.22	1.22	1.22	0.71	0.68
MgO	0.27	0.27	0.26	0.26	0.23	0.26	0.81	0.81
ZnO	0.01	0.02	0.03	0.02	0.00	0.03	0.00	0.03
NiO	0.00	0.00	0.00	0.00	0.00	0.02	0.00	0.00
CaO	0.00	0.00	0.00	0.00	0.00	0.00	0.00	0.00
Cu_2O	0.01	0.00	0.00	0.01	0.00	0.00	0.03	0.00
K_2O	0.00	0.00	0.00	0.01	0.00	0.00	0.00	0.00
Total measured	99.22	98.91	98.98	99.48	99.32	99.38	99.35	98.99

MAS	Massive to semi-massive mineralization	OBAN	Orthopyroxene -bearing bands of oxide mineralization
DIS	Disseminated mineralization	POD	Pod of oxide mineralization
BAN	Bands of oxide mineralization	OPOD	Orthopyroxene -bearing pod of oxide mineralization
ANO	Anorthosite hosted disseminated	VEIN	Vein of oxide mineralization
ORT	Orthopyroxene associated	MAG	Magnetite
CLI	Clinopyroxene associated	ILM	Ilmenite
		PLE	Pleonaste

Appendix IV a. (Continued)

Sample #	CC031A	CC031A	CC031A	CC031A	CC031A	CC031A	CC031A	CC031A	CC031A	CC054B
Circle Number	F	G	G	H	H	H	I	I	I	C
Mineralization type	DIS	DIS	DIS	DIS	DIS	DIS	DIS	DIS	DIS	DIS
Descriptor	ANO	ANO	ANO	ANO	ANO	ANO	ANO	ANO	ANO	ORT
mineral host	ILM	MAG	MAG	ILM	ILM	ILM	ILM	ILM	ILM	ILM
Mineral analyzed	ILM	ILM	ILM	ILM	ILM	ILM	ILM	ILM	ILM	ILM
exsolution feature type	Host	composite Ilm Spl ig	weird ILM box	Host	Host	Host	Host	Host	Host	host
Point	47	52	55	61	62	63	67	68	69	9
SiO_2	0.00	0.00	0.01	0.00	0.00	0.00	0.01	0.00	0.00	0.00
TiO_2	48.41	52.92	53.21	48.53	47.74	48.46	49.53	50.15	50.35	50.52
Al_2O_3	0.03	0.01	0.01	0.04	0.03	0.02	0.05	0.03	0.03	0.04
Cr_2O_3	0.01	0.05	0.07	0.02	0.03	0.02	0.02	0.01	0.02	0.02
V_2O_3	0.24	0.16	0.16	0.20	0.23	0.21	0.19	0.19	0.19	0.20
FeO*	49.13	44.19	43.64	48.36	49.30	48.63	47.63	47.48	47.35	47.63
Fe_2O_3 recalculated	8.52	-1.48	-2.11	7.62	9.47	7.98	5.58	5.06	4.70	5.17
FeO recalculated	41.46	45.52	45.54	41.50	40.78	41.45	42.61	42.93	43.12	42.98
MnO	0.63	0.92	1.00	0.64	0.62	0.66	0.64	0.70	0.69	0.54
MgO	0.80	0.63	0.72	0.83	0.85	0.82	0.72	0.82	0.81	1.06
ZnO	0.02	0.01	0.02	0.01	0.00	0.01	0.00	0.00	0.01	0.03
NiO	0.01	0.00	0.00	0.00	0.01	0.01	0.00	0.00	0.00	0.00
CaO	0.00	0.01	0.00	0.00	0.01	0.00	0.00	0.00	0.01	0.00
Cu_2O	0.01	0.00	0.00	0.00	0.01	0.00	0.00	0.00	0.00	0.00
K_2O	0.00	0.01	0.00	0.00	0.01	0.00	0.00	0.00	0.00	0.01
Total measured	99.29	98.91	98.85	98.63	98.85	98.82	98.79	99.40	99.46	100.04

MAS	Massive to semi-massive mineralization	OBAN	Orthopyroxene -bearing bands of oxide mineralization
DIS	Disseminated mineralization	POD	Pod of oxide mineralization
BAN	Bands of oxide mineralization	OPOD	Orthopyroxene -bearing pod of oxide mineralization
ANO	Anorthosite hosted disseminated	VEIN	Vein of oxide mineralization
ORT	Orthopyroxene associated	MAG	Magnetite
CLI	Clinopyroxene associated	ILM	Ilmenite
		PLE	Pleonaste

Appendix IV a. (Continued)

Sample #	CC054B	CC054B	CC054B	CC054B	CC054B	CC054B	CC054B
Circle Number	C	D	D	D	E	E	E
Mineralization type	DIS	DIS	DIS	DIS	DIS	DIS	DIS
Descriptor	ORT	ORT	ORT	ORT	ORT	ORT	ORT
mineral host	ILM	ILM	ILM	ILM	MAG	MAG	MAG
Mineral analyzed	ILM	ILM	ILM	ILM	ILM	ILM	ILM
exsolution feature type	host	host	host	host	composite	composite	composite
Point	10	16	17	18	21	22	23
SiO_2	0.01	0.00	0.00	0.01	0.01	0.00	0.01
TiO_2	50.09	50.68	49.05	50.59	52.03	51.95	51.85
Al_2O_3	0.03	0.03	0.04	0.04	0.01	0.02	0.03
Cr_2O_3	0.03	0.01	0.01	0.01	0.01	0.00	0.01
V_2O_3	0.21	0.19	0.24	0.21	0.17	0.16	0.15
FeO*	47.59	47.39	48.46	47.24	46.34	46.55	46.58
Fe_2O_3 recalculated	5.56	4.93	7.63	4.82	2.17	2.24	2.28
FeO recalculated	42.59	42.95	41.60	42.91	44.39	44.54	44.53
MnO	0.53	0.51	0.47	0.50	0.83	0.76	0.72
MgO	1.09	1.19	1.14	1.17	0.87	0.78	0.77
ZnO	0.00	0.00	0.00	0.00	0.00	0.04	0.01
NiO	0.00	0.00	0.00	0.00	0.02	0.00	0.01
CaO	0.00	0.00	0.01	0.01	0.00	0.00	0.00
Cu_2O	0.00	0.00	0.02	0.03	0.00	0.01	0.00
K_2O	0.00	0.00	0.00	0.00	0.00	0.00	0.01
Total measured	99.57	99.99	99.44	99.82	100.30	100.27	100.15

MAS	Massive to semi-massive mineralization	OBAN	Orthopyroxene -bearing bands of oxide mineralization
DIS	Disseminated mineralization	POD	Pod of oxide mineralization
BAN	Bands of oxide mineralization	OPOD	Orthopyroxene -bearing pod of oxide mineralization
ANO	Anorthosite hosted disseminated	VEIN	Vein of oxide mineralization
ORT	Orthopyroxene associated	MAG	Magnetite
CLI	Clinopyroxene associated	ILM	Ilmenite
		PLE	Pleonaste

Appendix IV a. (Continued)

Sample #	CC054B	CC054B	CC054B	CC054B	CC054B	CC054B	CC054B
Circle Number	E	E	E	E	G	G	G
Mineralization type	DIS	DIS	DIS	DIS	DIS	DIS	DIS
Descriptor	ORT	ORT	ORT	ORT	ORT	ORT	ORT
mineral host	MAG	MAG	MAG	MAG	MAG	MAG	MAG
Mineral analyzed	ILM	ILM	ILM	ILM	ILM	ILM	ILM
exsolution feature type	Ilm Spl composite	Ilm Spl composite	Ilm Spl contact	Ilm Spl contact	composite	composite	composite
Point	24	26	27	28	39	40	41
SiO_2	0.00	0.02	0.01	0.00	0.00	0.01	0.01
TiO_2	52.54	52.45	52.76	52.78	50.95	50.50	49.80
Al_2O_3	0.01	0.03	0.00	0.01	0.04	0.02	0.04
Cr_2O_3	0.01	0.03	0.02	0.02	0.00	0.01	0.01
V_2O_3	0.17	0.15	0.15	0.16	0.20	0.19	0.20
FeO*	45.82	46.09	45.92	45.56	46.32	47.09	47.85
Fe_2O_3 recalculated	1.57	1.20	0.73	0.57	4.21	4.76	5.99
FeO recalculated	44.40	45.01	45.26	45.05	42.53	42.81	42.46
MnO	0.77	0.83	0.74	0.79	0.52	0.50	0.47
MgO	1.15	0.75	0.80	0.89	1.54	1.16	1.03
ZnO	0.03	0.01	0.02	0.04	0.00	0.03	0.02
NiO	0.01	0.00	0.00	0.00	0.03	0.01	0.00
CaO	0.00	0.00	0.00	0.00	0.00	0.01	0.01
Cu_2O	0.01	0.00	0.01	0.00	0.01	0.00	0.00
K_2O	0.00	0.00	0.00	0.00	0.00	0.00	0.00
Total measured	100.51	100.37	100.45	100.26	99.62	99.54	99.45

MAS	Massive to semi-massive mineralization	OBAN	Orthopyroxene -bearing bands of oxide mineralization		
DIS	Disseminated mineralization	POD	Pod of oxide mineralization		
BAN	Bands of oxide mineralization	OPOD	Orthopyroxene -bearing pod of oxide mineralization		
ANO	Anorthosite hosted disseminated	VEIN	Vein of oxide mineralization		
ORT	Orthopyroxene associated	MAG	Magnetite		
CLI	Clinopyroxene associated	ILM	Ilmenite	PLE	Pleonaste

Appendix IV a. (Continued)

Sample #	CC054B	CC054B	CC054B	CC054B	CC054B	CC054B	CC054B	CC054B
Circle Number	H	H	J	J	J	L	L	L
Mineralization type	DIS	DIS	DIS	DIS	DIS	DIS	DIS	DIS
Descriptor	ORT	ORT	ORT	ORT	ORT	ORT	ORT	ORT
mineral host	MAG	MAG	MAG	MAG	MAG	MAG	MAG	MAG
Mineral analyzed	ILM	ILM	ILM	ILM	ILM	ILM	ILM	ILM
exsolution feature type	sandwich	sandwich	sandwich	sandwich	sandwich	composite	composite	composite
Point	49	50	57	58	59	63	64	65
SiO_2	0.02	0.00	0.01	0.00	0.00	0.00	0.00	0.00
TiO_2	51.47	52.05	52.33	53.43	53.59	52.29	50.59	49.93
Al_2O_3	0.02	0.02	0.01	0.02	0.00	0.02	0.03	0.03
Cr_2O_3	0.01	0.03	0.00	0.02	0.01	0.01	0.00	0.01
V_2O_3	0.18	0.17	0.18	0.17	0.18	0.15	0.19	0.19
FeO*	47.02	46.37	45.50	42.75	42.73	46.22	47.89	47.67
Fe_2O_3 recalculated	2.54	2.24	1.10	1.09	0.76	2.50	4.96	5.76
FeO recalculated	44.74	44.35	44.51	41.77	42.05	43.97	43.42	42.48
MnO	0.91	0.77	1.20	1.15	1.05	0.67	0.55	0.50
MgO	0.37	0.94	0.75	2.86	2.84	1.32	0.83	1.07
ZnO	0.01	0.00	0.00	0.00	0.00	0.02	0.03	0.00
NiO	0.00	0.00	0.00	0.02	0.02	0.01	0.02	0.02
CaO	0.00	0.01	0.00	0.01	0.01	0.00	0.00	0.00
Cu_2O	0.01	0.00	0.02	0.01	0.01	0.01	0.00	0.00
K_2O	0.00	0.00	0.00	0.00	0.00	0.00	0.00	0.00
Total measured	100.00	100.35	100.01	100.42	100.43	100.73	100.13	99.42

MAS	Massive to semi-massive mineralization	OBAN	Orthopyroxene -bearing bands of oxide mineralization
DIS	Disseminated mineralization	POD	Pod of oxide mineralization
BAN	Bands of oxide mineralization	OPOD	Orthopyroxene -bearing pod of oxide mineralization
ANO	Anorthosite hosted disseminated	VEIN	Vein of oxide mineralization
ORT	Orthopyroxene associated	MAG	Magnetite
CLI	Clinopyroxene associated	ILM	Ilmenite
PLE	Pleonaste		

Appendix IV a. (Continued)

Sample #	CC054B	CC054B	CC054B	CC054B	CC072A	CC072A	CC072A	CC072A
Circle Number	L	L	O	O	A	A	A	B
Mineralization type	DIS	DIS	DIS	DIS	MAS	MAS	MAS	MAS
Descriptor	ORT	ORT	ORT	ORT	OPOD	OPOD	OPOD	OPOD
mineral host	ILM	ILM	ILM	ILM	MAG	MAG	MAG	MAG
Mineral analyzed	ILM	ILM	ILM	ILM	ILM	ILM	ILM	ILM
exsolution feature type	in Ilm Spl rim	in Ilm Spl rim	host	host	composite	composite	composite	composite
Point	66	67	71	72	7	8	9	12
SiO_2	0.00	0.01	0.02	0.00	0.00	0.01	0.00	0.00
TiO_2	52.73	52.33	49.43	48.83	53.06	51.82	51.64	52.90
Al_2O_3	0.01	0.04	0.06	0.06	0.02	0.03	0.03	0.03
Cr_2O_3	0.00	0.04	0.00	0.00	0.01	0.01	0.00	0.00
V_2O_3	0.16	0.15	0.23	0.24	0.17	0.20	0.16	0.17
FeO*	45.28	45.82	48.44	48.69	42.29	43.49	43.82	42.82
Fe_2O_3 recalculated	1.34	0.53	6.97	8.13	1.99	4.19	4.63	2.75
FeO recalculated	44.07	45.34	42.17	41.37	40.50	39.72	39.65	40.35
MnO	0.74	0.83	0.45	0.44	0.86	0.81	0.79	0.79
MgO	1.43	0.49	1.03	1.18	3.56	3.40	3.36	3.60
ZnO	0.04	0.02	0.00	0.01	0.00	0.00	0.00	0.00
NiO	0.00	0.00	0.00	0.00	0.00	0.01	0.00	0.01
CaO	0.00	0.01	0.01	0.00	0.00	0.00	0.00	0.00
Cu_2O	0.00	0.02	0.00	0.00	0.00	0.00	0.01	0.02
K_2O	0.00	0.01	0.00	0.00	0.01	0.00	0.00	0.00
Total measured	100.40	99.75	99.67	99.45	99.98	99.77	99.81	100.34

MAS	Massive to semi-massive mineralization	OBAN	Orthopyroxene -bearing bands of oxide mineralization
DIS	Disseminated mineralization	POD	Pod of oxide mineralization
BAN	Bands of oxide mineralization	OPOD	Orthopyroxene -bearing pod of oxide mineralization
ANO	Anorthosite hosted disseminated	VEIN	Vein of oxide mineralization
ORT	Orthopyroxene associated	MAG	Magnetite
CLI	Clinopyroxene associated	ILM	Ilmenite
		PLE	Pleonaste

Appendix IV a. (Continued)

Sample #	CC072A	CC072A	CC072A	CC072A	CC072A	CC072A	CC072A	CC072A	CC072A
Circle Number	B	B	C	C	C	D	D	E	E
Mineralization type	MAS	MAS	MAS	MAS	MAS	MAS	MAS	MAS	MAS
Descriptor	OPOD	OPOD	OPOD	OPOD	OPOD	OPOD	OPOD	OPOD	OPOD
mineral host	MAG	MAG	MAG	MAG	MAG	ILM	ILM	ILM	ILM
Mineral analyzed	ILM	ILM	ILM	ILM	ILM	ILM	ILM	ILM	ILM
exsolution feature type	composite	composite	composite	composite	composite	host	host	host	host
Point	13	14	23	24	25	32	34	46	47
SiO_2	0.00	0.01	0.00	0.01	0.00	0.00	0.00	0.00	0.00
TiO_2	51.80	52.13	53.31	53.12	53.36	52.05	51.55	52.21	51.88
Al_2O_3	0.02	0.02	0.02	0.01	0.01	0.04	0.03	0.02	0.05
Cr_2O_3	0.00	0.02	0.01	0.00	0.00	0.03	0.00	0.01	0.01
V_2O_3	0.18	0.19	0.17	0.17	0.16	0.15	0.18	0.16	0.20
FeO*	44.01	43.41	42.55	41.90	42.10	42.86	43.59	43.28	43.49
Fe_2O_3 recalculated	4.82	4.02	2.02	1.42	1.42	3.39	4.46	3.52	3.95
FeO recalculated	39.67	39.79	40.73	40.63	40.82	39.81	39.58	40.12	39.93
MnO	0.73	0.76	0.86	0.88	0.86	0.80	0.73	0.81	0.79
MgO	3.45	3.54	3.55	3.51	3.52	3.48	3.39	3.38	3.32
ZnO	0.03	0.02	0.01	0.02	0.02	0.00	0.00	0.00	0.00
NiO	0.00	0.01	0.00	0.00	0.00	0.00	0.00	0.00	0.01
CaO	0.00	0.00	0.01	0.00	0.00	0.00	0.00	0.00	0.00
Cu_2O	0.00	0.00	0.00	0.00	0.00	0.00	0.00	0.00	0.00
K_2O	0.00	0.00	0.01	0.00	0.00	0.00	0.00	0.00	0.01
Total measured	100.23	100.12	100.49	99.63	100.04	99.41	99.49	99.87	99.76

MAS	Massive to semi-massive mineralization	OBAN	Orthopyroxene -bearing bands of oxide mineralization
DIS	Disseminated mineralization	POD	Pod of oxide mineralization
BAN	Bands of oxide mineralization	OPOD	Orthopyroxene -bearing pod of oxide mineralization
ANO	Anorthosite hosted disseminated	VEIN	Vein of oxide mineralization
ORT	Orthopyroxene associated	MAG	Magnetite
CLI	Clinopyroxene associated	ILM	Ilmenite
		PLE	Pleonaste

Appendix IV a. (Continued)

Sample #	CC072A	CC072A	CC072A	CC072A	CC072A	CC072A	CC072A	CC072A	CC072A	CC074
Circle Number	E	G	G	G	H	H	H	I	I	A
Mineralization type	MAS	MAS	MAS	MAS	MAS	MAS	MAS	MAS	MAS	DIS
Descriptor	OPOD	OPOD	OPOD	OPOD	OPOD	OPOD	OPOD	OPOD	OPOD	CLI
mineral host	ILM	ILM	ILM	ILM	ILM	ILM	ILM	ILM	ILM	MAG
Mineral analyzed	ILM	ILM	ILM	ILM	ILM	ILM	ILM	ILM	ILM	ILM
exsolution feature type	host	host	host	host	host	host	host	composite	composite	composite
Point	48	49	50	51	56	57	58	68	69	1
SiO_2	0.00	0.00	0.00	0.00	0.00	0.00	0.00	0.00	0.00	0.01
TiO_2	51.59	50.36	52.93	52.46	52.41	51.67	51.93	50.99	51.40	49.63
Al_2O_3	0.03	0.05	0.02	0.01	0.03	0.05	0.02	0.03	0.02	0.03
Cr_2O_3	0.01	0.00	0.00	0.02	0.00	0.00	0.00	0.01	0.01	0.05
V_2O_3	0.17	0.24	0.19	0.18	0.21	0.22	0.20	0.21	0.21	0.23
FeO*	44.04	44.88	42.28	42.73	42.72	43.43	43.30	44.76	44.30	47.21
Fe_2O_3 recalculated	4.84	6.82	2.21	2.89	3.10	4.35	4.17	6.22	5.44	5.10
FeO recalculated	39.68	38.74	40.29	40.13	39.93	39.51	39.54	39.16	39.41	42.62
MnO	0.76	0.69	0.83	0.77	0.77	0.73	0.75	0.68	0.71	1.21
MgO	3.33	3.27	3.61	3.52	3.60	3.49	3.59	3.36	3.41	0.44
ZnO	0.00	0.03	0.03	0.00	0.00	0.00	0.00	0.02	0.00	0.01
NiO	0.01	0.00	0.02	0.00	0.00	0.00	0.00	0.01	0.02	0.00
CaO	0.01	0.00	0.00	0.00	0.00	0.00	0.00	0.00	0.00	0.01
Cu_2O	0.01	0.00	0.00	0.00	0.00	0.00	0.03	0.00	0.01	0.00
K_2O	0.00	0.01	0.00	0.00	0.00	0.01	0.00	0.00	0.00	0.01
Total measured	99.95	99.53	99.90	99.70	99.75	99.60	99.83	100.06	100.09	98.84

MAS	Massive to semi-massive mineralization	OBAN	Orthopyroxene -bearing bands of oxide mineralization
DIS	Disseminated mineralization	POD	Pod of oxide mineralization
BAN	Bands of oxide mineralization	OPOD	Orthopyroxene -bearing pod of oxide mineralization
ANO	Anorthosite hosted disseminated	VEIN	Vein of oxide mineralization
ORT	Orthopyroxene associated	MAG	Magnetite
CLI	Clinopyroxene associated	ILM	Ilmenite
		PLE	Pleonaste

Appendix IV a. (Continued)

Sample #	CC074	CC074	CC074	CC074	CC074	CC074	CC074
Circle Number	A	A	A	A	B	B	B
Mineralization type	DIS	DIS	DIS	DIS	DIS	DIS	DIS
Descriptor	CLI	CLI	CLI	CLI	CLI	CLI	CLI
mineral host	MAG	MAG	MAG	MAG	MAG	MAG	MAG
Mineral analyzed	ILM	ILM	ILM	ILM	ILM	ILM	ILM
exsolution feature type	composite	composite	around rim	around rim	composite	composite	composite
Point	2	3	4	5	11	12	13
SiO_2	0.00	0.00	0.00	0.00	0.00	0.00	0.00
TiO_2	48.43	47.66	51.80	51.57	49.89	48.01	48.36
Al_2O_3	0.02	0.01	0.00	0.17	0.02	0.02	0.03
Cr_2O_3	0.06	0.06	0.03	0.05	0.04	0.07	0.06
V_2O_3	0.22	0.22	0.20	0.19	0.20	0.23	0.25
FeO*	48.74	48.88	44.18	44.91	46.94	48.56	48.39
Fe_2O_3 recalculated	8.10	8.89	1.73	1.95	4.63	8.18	7.64
FeO recalculated	41.45	40.89	42.63	43.15	42.77	41.20	41.52
MnO	1.20	1.15	2.10	1.55	1.33	1.30	1.28
MgO	0.50	0.46	1.01	0.92	0.42	0.37	0.38
ZnO	0.01	0.00	0.03	0.02	0.02	0.00	0.00
NiO	0.00	0.00	0.01	0.00	0.00	0.00	0.00
CaO	0.00	0.00	0.01	0.00	0.00	0.00	0.00
Cu_2O	0.00	0.00	0.01	0.00	0.00	0.00	0.01
K_2O	0.00	0.00	0.00	0.00	0.00	0.00	0.00
Total measured	99.18	98.45	99.37	99.38	98.85	98.57	98.77

MAS	Massive to semi-massive mineralization	OBAN	Orthopyroxene -bearing bands of oxide mineralization
DIS	Disseminated mineralization	POD	Pod of oxide mineralization
BAN	Bands of oxide mineralization	OPOD	Orthopyroxene -bearing pod of oxide mineralization
ANO	Anorthosite hosted disseminated	VEIN	Vein of oxide mineralization
ORT	Orthopyroxene associated	MAG	Magnetite
CLI	Clinopyroxene associated	ILM	Ilmenite
		PLE	Pleonaste

Appendix IV a. (Continued)

Sample #	CC074	CC074	CC074	CC074	CC074	CC074	CC074	CC074
Circle Number	B	B	B	B	B	B	B	C
Mineralization type	DIS	DIS	DIS	DIS	DIS	DIS	DIS	DIS
Descriptor	CLI	CLI	CLI	CLI	CLI	CLI	CLI	CLI
mineral host	MAG	MAG	MAG	MAG	MAG	ILM	ILM	ILM
Mineral analyzed	ILM	ILM	ILM	ILM	ILM	ILM	ILM	ILM
exsolution feature type	Ilm Spl ig composite	Ilm Spl ig composite	lamellae	lamellae	lamellae	in Spl Ilm ig	in Spl Ilm ig	Host
Point	15	16	17	18	19	20	21	25
SiO_2	0.00	0.01	0.00	0.00	0.01	0.01	0.00	0.00
TiO_2	51.56	51.53	51.99	51.37	51.30	51.76	51.57	49.70
Al_2O_3	0.02	0.02	0.01	0.01	0.08	0.01	0.01	0.02
Cr_2O_3	0.03	0.04	0.04	0.06	0.06	0.03	0.03	0.04
V_2O_3	0.19	0.21	0.21	0.19	0.20	0.22	0.19	0.22
FeO*	44.34	43.99	42.84	44.18	44.40	44.62	45.04	47.66
Fe_2O_3 recalculated	1.34	1.49	0.83	2.31	2.00	2.19	2.12	5.50
FeO recalculated	43.13	42.65	42.10	42.10	42.60	42.65	43.13	42.71
MnO	1.49	1.57	2.35	2.08	2.12	1.62	1.61	0.99
MgO	0.94	1.17	1.27	1.11	0.78	1.27	0.90	0.54
ZnO	0.07	0.04	0.02	0.00	0.01	0.02	0.02	0.02
NiO	0.00	0.00	0.01	0.02	0.00	0.01	0.00	0.01
CaO	0.00	0.00	0.00	0.00	0.01	0.00	0.00	0.00
Cu_2O	0.00	0.00	0.00	0.00	0.00	0.00	0.00	0.00
K_2O	0.00	0.00	0.01	0.00	0.00	0.00	0.01	0.00
Total measured	98.65	98.58	98.76	99.03	98.96	99.57	99.38	99.19

MAS	Massive to semi-massive mineralization	OBAN	Orthopyroxene -bearing bands of oxide mineralization
DIS	Disseminated mineralization	POD	Pod of oxide mineralization
BAN	Bands of oxide mineralization	OPOD	Orthopyroxene -bearing pod of oxide mineralization
ANO	Anorthosite hosted disseminated	VEIN	Vein of oxide mineralization
ORT	Orthopyroxene associated	MAG	Magnetite
CLI	Clinopyroxene associated	ILM	Ilmenite
		PLE	Pleonaste

Appendix IV a. (Continued)

Sample #	CC074	CC074	CC074	CC074	CC074	CC074	CC074	CC074	CC074
Circle Number	C	C	C	D	D	D	D	D	E
Mineralization type	DIS	DIS	DIS	DIS	DIS	DIS	DIS	DIS	DIS
Descriptor	CLI	CLI	CLI	CLI	CLI	CLI	CLI	CLI	CLI
mineral host	ILM	ILM	ILM	ILM	ILM	ILM	ILM	ILM	MAG
Mineral analyzed	ILM	ILM	ILM	ILM	ILM	ILM	ILM	ILM	ILM
exsolution feature type	Host	rim	rim	Host	Host	Host	Ilm Spl ig composite	Ilm Spl ig composite	thick lamellae
Point	26	28	29	33	34	35	36	37	41
SiO_2	0.01	0.00	0.01	0.01	0.00	0.00	0.00	0.00	0.00
TiO_2	48.80	51.48	51.44	48.25	47.70	48.30	51.33	51.47	52.03
Al_2O_3	0.02	0.02	0.02	0.01	0.02	0.01	0.07	0.01	0.04
Cr_2O_3	0.04	0.06	0.06	0.03	0.03	0.01	0.04	0.02	0.04
V_2O_3	0.23	0.20	0.20	0.21	0.23	0.22	0.17	0.20	0.19
FeO*	48.12	45.65	45.91	48.28	48.52	47.50	45.69	45.04	43.02
Fe_2O_3 recalculated	6.80	1.81	2.15	7.39	8.45	6.94	1.42	1.20	-0.60
FeO recalculated	42.01	44.02	43.98	41.63	40.92	41.25	44.42	43.96	43.56
MnO	1.05	1.17	1.20	0.98	0.94	0.94	1.51	2.21	3.15
MgO	0.46	0.58	0.58	0.42	0.58	0.68	0.09	0.02	0.01
ZnO	0.00	0.06	0.04	0.01	0.01	0.00	0.05	0.05	0.03
NiO	0.00	0.01	0.00	0.00	0.00	0.01	0.00	0.01	0.00
CaO	0.01	0.00	0.00	0.02	0.00	0.01	0.01	0.01	0.00
Cu_2O	0.00	0.02	0.00	0.02	0.01	0.01	0.00	0.00	0.00
K_2O	0.00	0.00	0.01	0.00	0.00	0.00	0.00	0.00	0.00
Total measured	98.73	99.26	99.47	98.24	98.03	97.70	98.96	99.04	98.52

MAS	Massive to semi-massive mineralization	OBAN	Orthopyroxene -bearing bands of oxide mineralization
DIS	Disseminated mineralization	POD	Pod of oxide mineralization
BAN	Bands of oxide mineralization	OPOD	Orthopyroxene -bearing pod of oxide mineralization
ANO	Anorthosite hosted disseminated	VEIN	Vein of oxide mineralization
ORT	Orthopyroxene associated	MAG	Magnetite
CLI	Clinopyroxene associated	ILM	Ilmenite

PLE Pleonaste

Appendix IV a. (Continued)

Sample #	CC074	CC074	CC074	CC074	CC074	CC074	CC074	CC074	CC076	CC076
Circle Number	E	E	E	F	F	F	F	F	B	B
Mineralization type	DIS	DIS	DIS	DIS	DIS	DIS	DIS	DIS	MAS	MAS
Descriptor	CLI	CLI	CLI	CLI	CLI	CLI	CLI	CLI	VEIN	VEIN
mineral host	MAG	MAG	MAG	MAG	MAG	ILM	ILM	ILM	ILM	ILM
Mineral analyzed	ILM	ILM	ILM	ILM	ILM	ILM	ILM	ILM	ILM	ILM
exsolution feature type	thick lamellae	composite	composite	lamellae	lamellae	Host	Host	Host	host	host
Point	42	44	45	49	50	51	52	53	4	5
SiO_2	0.00	0.00	0.00	0.00	0.06	0.00	0.00	0.00	0.00	0.00
TiO_2	51.96	49.43	48.41	51.10	50.72	50.12	47.96	47.49	47.67	48.94
Al_2O_3	0.00	0.01	0.03	0.05	0.28	0.03	0.01	0.03	0.02	0.03
Cr_2O_3	0.04	0.03	0.05	0.09	0.10	0.05	0.04	0.06	0.02	0.03
V_2O_3	0.19	0.21	0.23	0.21	0.20	0.23	0.23	0.26	0.29	0.29
FeO*	43.32	47.64	47.52	41.26	39.70	46.90	48.95	49.71	49.33	48.46
Fe_2O_3 recalculated	-0.19	5.78	6.63	2.10	1.94	4.20	8.60	9.95	10.23	8.02
FeO recalculated	43.49	42.44	41.55	39.37	37.95	43.12	41.21	40.75	40.13	41.25
MnO	3.13	0.88	1.37	6.47	7.45	1.22	1.19	1.20	0.99	1.02
MgO	0.02	0.60	0.32	0.00	0.06	0.38	0.40	0.41	0.96	0.98
ZnO	0.02	0.04	0.02	0.02	0.03	0.03	0.01	0.00	0.03	0.00
NiO	0.00	0.03	0.00	0.01	0.01	0.02	0.00	0.01	0.00	0.00
CaO	0.01	0.00	0.01	0.01	0.05	0.00	0.00	0.00	0.00	0.00
Cu_2O	0.00	0.00	0.02	0.00	0.02	0.00	0.00	0.00	0.00	0.00
K_2O	0.00	0.01	0.00	0.00	0.00	0.00	0.00	0.00	0.00	0.00
Total measured	98.72	98.87	97.98	99.23	98.66	98.98	98.79	99.18	99.31	99.74

MAS	Massive to semi-massive mineralization	OBAN	Orthopyroxene -bearing bands of oxide mineralization
DIS	Disseminated mineralization	POD	Pod of oxide mineralization
BAN	Bands of oxide mineralization	OPOD	Orthopyroxene -bearing pod of oxide mineralization
ANO	Anorthosite hosted disseminated	VEIN	Vein of oxide mineralization
ORT	Orthopyroxene associated	MAG	Magnetite
CLI	Clinopyroxene associated	ILM	Ilmenite
		PLE	Pleonaste

Appendix IV a. (Continued)

Sample #	CC076	CC076	CC076	CC076	CC076	CC076	CC076	CC076	CC076	CC076	CC076	CC076
Circle Number	B	C	C	C	D	D	F	F	F	G	G	G
Mineralization type	MAS	MAS	MAS	MAS	MAS	MAS	MAS	MAS	MAS	MAS	MAS	MAS
Descriptor	VEIN	VEIN	VEIN	VEIN	VEIN	VEIN	VEIN	VEIN	VEIN	VEIN	VEIN	VEIN
mineral host	ILM	MAG	MAG	MAG	ILM	ILM	ILM	ILM	ILM	ILM	ILM	ILM
Mineral analyzed	ILM	ILM	ILM	ILM	ILM	ILM	ILM	ILM	ILM	ILM	ILM	ILM
exsolution feature type	host	lath	lath	lath	host	host	host	host	host	host	host	host
Point	6	13	14	15	29	30	37	38	39	47	48	49
SiO_2	0.01	0.00	0.01	0.00	0.00	0.01	0.00	0.01	0.01	0.01	0.00	0.01
TiO_2	48.64	50.58	49.33	48.83	48.49	50.04	46.76	48.65	49.22	48.47	47.84	48.21
Al_2O_3	0.02	0.01	0.01	0.02	0.01	0.02	0.02	0.02	0.01	0.02	0.11	0.02
Cr_2O_3	0.02	0.10	0.09	0.11	0.03	0.00	0.02	0.02	0.02	0.02	0.02	0.01
V_2O_3	0.26	0.29	0.33	0.35	0.29	0.25	0.34	0.26	0.27	0.28	0.29	0.25
FeO*	48.87	46.59	47.35	48.02	48.12	46.93	49.42	48.06	47.32	48.63	48.44	48.26
Fe_2O_3 recalculated	-26.66	4.63	6.57	7.82	7.96	5.20	11.21	7.78	6.55	8.55	8.79	8.50
FeO recalculated	72.86	42.43	41.44	40.99	40.96	42.25	39.34	41.06	41.43	40.94	40.53	40.61
MnO	0.98	1.45	1.36	1.40	1.09	1.07	1.05	1.07	1.14	1.08	1.06	1.12
MgO	1.01	0.89	0.87	0.85	0.86	0.94	0.93	0.91	0.95	0.87	0.80	0.91
ZnO	0.02	0.01	0.00	0.00	0.00	0.00	0.00	0.00	0.00	0.01	0.01	0.00
NiO	0.00	0.00	0.00	0.00	0.00	0.00	0.00	0.00	0.00	0.01	0.00	0.01
CaO	0.00	0.00	0.00	0.00	0.01	0.01	0.00	0.00	0.01	0.00	0.00	0.00
Cu_2O	0.00	0.01	0.00	0.01	0.00	0.00	0.00	0.00	0.02	0.00	0.00	0.00
K_2O	0.00	0.00	0.00	0.00	0.00	0.00	0.01	0.00	0.00	0.00	0.00	0.00
Total measured	99.84	99.93	99.35	99.59	98.91	99.28	98.55	98.99	98.97	99.40	98.58	98.80

MAS	Massive to semi-massive mineralization	OBAN	Orthopyroxene -bearing bands of oxide mineralization
DIS	Disseminated mineralization	POD	Pod of oxide mineralization
BAN	Bands of oxide mineralization	OPOD	Orthopyroxene -bearing pod of oxide mineralization
ANO	Anorthosite hosted disseminated	VEIN	Vein of oxide mineralization
ORT	Orthopyroxene associated	MAG	Magnetite
CLI	Clinopyroxene associated	ILM	Ilmenite PLE Pleonaste

Appendix IV a. (Continued)

Sample #	CC076	CC076
Circle Number	M	M
Mineralization type	MAS	MAS
Descriptor	VEIN	VEIN
mineral host	Grt	Grt
Mineral analyzed	ILM	ILM
exsolution feature type	myrmekite	myrmekite
Point	50	51
SiO_2	0.02	0.02
TiO_2	51.43	50.92
Al_2O_3	0.02	0.02
Cr_2O_3	0.04	0.04
V_2O_3	0.25	0.23
FeO*	45.22	45.28
Fe_2O_3 recalculated	2.16	1.96
FeO recalculated	43.27	43.51
MnO	1.31	1.46
MgO	0.89	0.43
ZnO	0.02	0.03
NiO	0.00	0.00
CaO	0.06	0.03
Cu_2O	0.00	0.01
K_2O	0.00	0.03
Total measured	99.26	98.49

MAS	Massive to semi-massive mineralization	OBAN	Orthopyroxene -bearing bands of oxide mineralization
DIS	Disseminated mineralization	POD	Pod of oxide mineralization
BAN	Bands of oxide mineralization	OPOD	Orthopyroxene -bearing pod of oxide mineralization
ANO	Anorthosite hosted disseminated	VEIN	Vein of oxide mineralization
ORT	Orthopyroxene associated	MAG	Magnetite
CLI	Clinopyroxene associated	ILM	Ilmenite PLE Pleonaste

Appendix IV a. (Continued)

Sample #	CC008	CC008	CC008	CC008	CC008	CC008	CC008	CC010	CC010	CC010	CC010
Circle Number	B	B	C	C	C	D	D	A	A	C	C
Mineralization type	MAS	MAS	MAS	MAS	MAS	MAS	MAS	MAS	MAS	MAS	MAS
Descriptor	BAN	BAN	BAN	BAN	BAN	BAN	OBAN	OBAN	OBAN	OBAN	OBAN
mineral host	PLE	PLE	ILM	ILM	ILM	PLE	PLE	PLE	PLE	PLE	PLE
Mineral analyzed	PLE	PLE	PLE	PLE	PLE	PLE	PLE	PLE	PLE	PLE	PLE
exsolution feature type	host	host	box rims	box rims	lamellae	host	host	Host	Host	Host	Host
Point	14	15	18	19	28	31	32	8	9	14	15
SiO_2	0.00	0.00	0.03	0.00	0.01	0.01	0.00	0.01	0.00	0.01	0.00
TiO_2	0.00	0.01	0.56	0.50	1.14	0.02	0.03	0.01	0.00	0.01	0.02
Al_2O_3	59.18	57.99	62.91	62.83	62.31	58.11	57.85	59.50	58.67	59.32	58.04
Cr_2O_3	0.25	0.34	0.65	0.56	0.50	0.25	0.28	0.26	0.26	0.25	0.25
V_2O_3	0.09	0.08	0.06	0.06	0.06	0.09	0.09	0.06	0.10	0.07	0.10
FeO*	28.47	28.81	21.62	22.01	21.54	28.89	29.22	27.23	28.39	27.15	29.18
Fe_2O_3 recalculated	5.28	6.25	2.27	2.62	1.30	5.75	6.24	5.26	6.24	5.31	6.92
FeO recalculated	23.72	23.19	19.57	19.65	20.37	23.72	23.60	22.50	22.78	22.37	22.96
MnO	0.22	0.22	0.15	0.15	0.14	0.23	0.22	0.24	0.25	0.20	0.23
MgO	10.99	11.14	14.93	14.82	14.54	10.73	10.84	11.79	11.58	11.83	11.41
ZnO	0.68	0.62	0.39	0.37	0.37	0.65	0.61	0.67	0.64	0.70	0.67
NiO	0.11	0.10	0.09	0.09	0.06	0.11	0.11	0.12	0.10	0.10	0.10
Total (Mass %)	99.99	99.31	101.39	101.40	100.67	99.08	99.25	99.89	99.99	99.63	100.00
Total recalculated	100.52	99.94	101.62	101.66	100.80	99.66	99.88	100.42	100.61	100.16	100.69

MAS	Massive to semi-massive mineralization	OBAN	Orthopyroxene -bearing bands of oxide mineralization
DIS	Disseminated mineralization	POD	Pod of oxide mineralization
BAN	Bands of oxide mineralization	OPOD	Orthopyroxene -bearing pod of oxide mineralization
ANO	Anorthosite hosted disseminated	VEIN	Vein of oxide mineralization
ORT	Orthopyroxene associated	MAG	Magnetite
CLI	Clinopyroxene associated	ILM	Ilmenite
		PLE	Pleonaste

Appendix IV a. (Continued)

Sample #	CC010	CC010	CC010	CC010	CC010	CC010	CC010	CC013	CC013	CC013
Circle Number	E	E	F	M	M	M	M	A	A	A
Mineralization type	MAS	MAS	MAS	MAS	MAS	MAS	MAS	MAS	MAS	MAS
Descriptor	OBAN	OBAN	OBAN	OBAN	OBAN	OBAN	OBAN	BAN	BAN	BAN
mineral host	MAG	MAG	ILM	ILM	ILM	MAG	MAG	MAG	ILM	ILM
Mineral analyzed	PLE	PLE	PLE	PLE	PLE	PLE	PLE	PLE	PLE	PLE
exsolution feature type	cap	cap	rim	Cap	Cap	granule	granule	granule	lamellae	lamellae
Point	36	37	49	73	74	75	76	10	11	12
SiO_2	0.01	0.01	0.01	0.00	0.02	0.00	0.09	0.00	0.00	0.00
TiO_2	0.11	0.01	0.64	0.00	0.01	0.17	0.03	0.02	0.89	1.11
Al_2O_3	60.99	60.65	61.66	60.61	60.05	60.89	61.97	57.40	62.00	62.13
Cr_2O_3	0.38	0.34	0.50	0.34	0.33	0.43	0.34	0.59	0.72	0.75
V_2O_3	0.06	0.06	0.06	0.08	0.08	0.06	0.06	0.07	0.06	0.09
FeO*	24.35	25.03	22.83	25.16	25.83	24.45	24.09	28.74	21.82	21.29
Fe_2O_3 recalculated	3.70	4.08	2.52	4.24	4.65	3.59	2.79	6.50	2.24	1.97
FeO recalculated	21.02	21.36	20.56	21.34	21.64	21.22	21.58	22.89	19.80	19.51
MnO	0.22	0.22	0.20	0.20	0.22	0.23	0.25	0.26	0.16	0.16
MgO	13.09	12.73	13.92	12.76	12.49	12.98	13.06	11.19	14.71	15.08
ZnO	0.46	0.48	0.42	0.47	0.50	0.43	0.23	0.58	0.48	0.50
NiO	0.09	0.10	0.07	0.11	0.09	0.09	0.09	0.10	0.07	0.07
Total (Mass %)	99.76	99.63	100.31	99.74	99.61	99.74	100.21	98.95	100.90	101.17
Total recalculated	100.13	100.04	100.56	100.16	100.08	100.10	100.49	99.60	101.13	101.37

MAS	Massive to semi-massive mineralization	OBAN	Orthopyroxene -bearing bands of oxide mineralization
DIS	Disseminated mineralization	POD	Pod of oxide mineralization
BAN	Bands of oxide mineralization	OPOD	Orthopyroxene -bearing pod of oxide mineralization
ANO	Anorthosite hosted disseminated	VEIN	Vein of oxide mineralization
ORT	Orthopyroxene associated	MAG	Magnetite
CLI	Clinopyroxene associated	ILM	Ilmenite
		PLE	Pleonaste

Appendix IV a. (Continued)

Sample #	CC013	CC013	CC013	CC013	CC025	CC025	CC025	CC025	CC025	CC025
Circle Number	I	I	L	L	D	D	D	D	E	E
Mineralization type	MAS	MAS	MAS	MAS	MAS	MAS	MAS	MAS	MAS	MAS
Descriptor	BAN	BAN	BAN	BAN	POD	POD	POD	POD	POD	POD
mineral host	PLE	PLE	PLE	PLE	ILM	ILM	hercynite	PLE	PLE	PLE
Mineral analyzed	PLE	PLE	PLE	PLE	PLE	PLE	hercynite	PLE	PLE	PLE
exsolution feature type	host	host	Host	Host	thick ig	thick ig	intergrowth	intergrowth	comp ig	comp ig
Point	41	42	54	55	29	30	33	34	43	44
SiO_2	0.00	0.00	0.00	0.00	0.05	0.11	0.01	0.18	0.10	0.11
TiO_2	0.01	0.02	0.00	0.02	0.89	0.82	1.03	1.14	0.74	1.31
Al_2O_3	58.37	58.24	59.91	59.68	56.86	57.12	56.58	56.28	56.30	55.88
Cr_2O_3	0.40	0.35	0.49	0.49	1.36	0.99	1.45	1.49	1.18	1.40
V_2O_3	0.08	0.10	0.07	0.08	0.08	0.08	0.06	0.07	0.07	0.08
FeO*	28.93	29.03	26.81	26.92	33.07	32.52	32.39	32.52	32.43	31.99
Fe_2O_3 recalculated	6.01	6.21	4.64	4.77	2.79	2.84	2.75	2.76	3.49	2.65
FeO recalculated	23.52	23.45	22.63	22.63	30.56	29.96	29.91	30.03	29.29	29.61
MnO	0.30	0.29	0.28	0.28	0.19	0.19	0.16	0.16	0.16	0.17
MgO	11.01	11.03	11.80	11.76	6.94	7.29	7.21	7.40	7.45	7.56
ZnO	0.61	0.63	0.58	0.60	0.58	0.54	0.76	0.71	0.63	0.58
NiO	0.09	0.11	0.11	0.10	0.10	0.13	0.09	0.11	0.11	0.12
Total (Mass %)	99.81	99.80	100.04	99.93	100.12	99.78	99.74	100.07	99.18	99.19
Total recalculated	100.41	100.42	100.50	100.41	100.40	100.06	100.02	100.34	99.53	99.46

MAS	Massive to semi-massive mineralization	OBAN	Orthopyroxene -bearing bands of oxide mineralization
DIS	Disseminated mineralization	POD	Pod of oxide mineralization
BAN	Bands of oxide mineralization	OPOD	Orthopyroxene -bearing pod of oxide mineralization
ANO	Anorthosite hosted disseminated	VEIN	Vein of oxide mineralization
ORT	Orthopyroxene associated	MAG	Magnetite
CLI	Clinopyroxene associated	ILM	Ilmenite
		PLE	Pleonaste

Appendix IV a. (Continued)

Sample #	CC025	CC054	CC054	CC054	CC054	CC054	CC054	CC072	CC072	CC076	CC076
Circle Number	E	D	D	E	E	F	F	A	A	B	B
Mineralization type	MAS	DIS	DIS	DIS	DIS	DIS	DIS	MAS	MAS	MAS	MAS
Descriptor	POD	ORT	ORT	ORT	ORT	ORT	ORT	OPOD	OPOD	VEIN	VEIN
mineral host	ILM	ILM	ILM	MAG	MAG	MAG	MAG	MAG	MAG	PLE	PLE
Mineral analyzed	PLE	PLE	PLE	PLE	PLE	PLE	PLE	PLE	PLE	PLE	PLE
exsolution feature type	thick ig	lamellae	lamellae	granules	granule	granule	granule	granule	granule	host	host
Point	47	19	20	32	33	37	38	10	11	9	10
SiO_2	0.10	0.01	0.02	0.00	0.01	0.01	0.00	0.00	0.01	0.00	0.00
TiO_2	0.63	0.89	0.86	0.04	0.03	0.03	0.03	0.02	0.04	0.02	0.00
Al_2O_3	57.23	57.60	56.95	56.76	56.57	56.06	56.39	61.68	59.31	56.93	56.00
Cr_2O_3	0.86	0.51	0.51	0.51	0.46	0.46	0.46	0.38	0.39	0.60	0.51
V_2O_3	0.09	0.06	0.07	0.07	0.07	0.07	0.07	0.05	0.06	0.07	0.10
FeO*	32.19	30.49	31.68	33.42	33.46	33.69	33.30	21.32	24.08	31.98	32.94
Fe_2O_3 recalculated	2.71	3.77	4.37	5.55	5.71	5.89	5.48	5.27	6.63	5.67	6.51
FeO recalculated	29.76	27.10	27.75	28.42	28.33	28.39	28.37	16.58	18.11	26.88	27.08
MnO	0.18	0.16	0.17	0.19	0.18	0.20	0.19	0.17	0.19	0.43	0.45
MgO	7.28	9.02	8.55	7.48	7.48	7.29	7.31	16.03	14.62	7.88	7.63
ZnO	0.40	0.81	0.79	0.87	0.88	0.92	0.90	0.80	0.75	1.83	1.70
NiO	0.09	0.13	0.11	0.12	0.13	0.09	0.12	0.06	0.06	0.04	0.05
Total (Mass %)	99.06	99.69	99.70	99.46	99.28	98.81	98.76	100.51	99.51	99.78	99.38
Total recalculated	99.33	100.07	100.14	100.02	99.85	99.40	99.31	101.04	100.17	100.35	100.03

MAS	Massive to semi-massive mineralization	OBAN	Orthopyroxene -bearing bands of oxide mineralization
DIS	Disseminated mineralization	POD	Pod of oxide mineralization
BAN	Bands of oxide mineralization	OPOD	Orthopyroxene -bearing pod of oxide mineralization
ANO	Anorthosite hosted disseminated	VEIN	Vein of oxide mineralization
ORT	Orthopyroxene associated	MAG	Magnetite
CLI	Clinopyroxene associated	ILM	Ilmenite
		PLE	Pleonaste

Appendix V **LA-ICPMS line analyses of magnetite, ilmenite and pleonaste. Corresponding photomicrographs are in Appendix VI. Fe, Ti or Al (wt. %) is measured using EPMA analyses of the same samples.**

Sample	CC008	CC008	CC008	CC008	CC008	CC008	CC008
Circle number	A	A	C	C	D	D	F
Analysis	08-A-M1	08-A-M2	08-C-M1	08-C-M2	08-D-M1	08-D-M2	08-F-M1
Mineralization type	MAS	MAS	MAS	MAS	MAS	MAS	MAS
Descriptor	BAN	BAN	BAN	BAN	BAN	BAN	BAN
Mineral host	MAG	MAG	MAG	MAG	MAG	MAG	MAG
Mineral analyzed	MAG	MAG	MAG	MAG	MAG	MAG	MAG
Fe wt.% (EPMA)*	64	64	64	64	64	64	64
^{24}Mg	721	703	724	545	911	574	468
^{27}Al	3390	2264	3320	2175	3820	2745	1852
^{29}Si	249	417	430	<MDL	<MDL	355	<MDL
^{31}P	<MDL	5	<MDL	<MDL	<MDL	<MDL	<MDL
^{44}Ca	<MDL	<MDL	<MDL	<MDL	<MDL	<MDL	<MDL
^{45}Sc	1	1	1	1	1	1	1
^{47}Ti	700	2770	618	611	1530	631	313
^{51}V	5033	4457	4899	4895	4933	4899	4665
^{52}Cr	1580	1588	1654	1618	1642	1617	1464
^{55}Mn	159	187	143	158	205	139	113
^{59}Co	93	66	73	70	78	65	72
^{60}Ni	263	246	280	287	286	286	262
^{63}Cu	0.4	0.4	0.3	0.4	2	0.2	1
^{66}Zn	8	3	4	6	5	5	3
^{69}Ga	42	38	42	40	45	42	35
^{74}Ge	1	1	1	1	1	1	1
^{75}As	0.5	0.3	<MDL	<MDL	0.4	0.4	<MDL
^{89}Y	0.001	0.001	<MDL	<MDL	<MDL	0.002	<MDL
^{90}Zr	0.1	0.4	0.1	0.02	0.3	0.1	0.01
^{93}Nb	0.01	0.03	0.03	<MDL	0.02	0.03	0.001
^{95}Mo	0.1	0.1	<MDL	<MDL	0.03	0.1	<MDL
^{118}Sn	0.1	0.1	0.1	0.03	0.2	0.1	<MDL
^{121}Sb	0.02	<MDL	0.02	0.03	<MDL	0.01	0.01
^{178}Hf	0.001	0.01	<MDL	<MDL	0.004	<MDL	<MDL
^{181}Ta	<MDL	<MDL	0.000	<MDL	<MDL	0.000	<MDL
^{182}W	0.002	0.01	0.003	<MDL	0.02	<MDL	<MDL
^{208}Pb	0.4	0.3	0.2	0.3	0.2	0.3	0.5

MAS	Massive to semi-massive mineralization	OBAN	Orthopyroxene -bearing band
DIS	Disseminated mineralization	POD	Pod
BAN	Bands of oxide mineralization	OPOD	Orthopyroxene -bearing pod
ANO	Anorthosite hosted disseminated	VEIN	Vein
ORT	Orthopyroxene associated	MAG	Magnetite
CLI	Clinopyroxene associated	ILM	Ilmenite

* Internal calibrant was taken from EPMA analyses performed on the same grain as LA-ICPMS analyses; when LA-ICPMS analyses were performed on magnetite without EPMA analyses, the internal calibrant used was the average of all texturally similar magnetite in the sample. <MDL: below minimum detection level

Appendix V (Continued)

Sample	CC008	CC008	CC008	CC008	CC008	CC010
Circle number	F	H	H	J	J	D
Analysis	08-F-M2	08-H-M1	08-H-M2	08-J-M1	08-J-M2	10-D-M1
Mineralization type	MAS	MAS	MAS	MAS	MAS	MAS
Descriptor	BAN	BAN	BAN	BAN	BAN	OBAN
Mineral host	MAG	MAG	MAG	MAG	MAG	MAG
Mineral analyzed	MAG	MAG	MAG	MAG	MAG	MAG
Fe wt.% (EPMA)*	64	64	64	64	64	64
^{24}Mg	462	827	603	16780	933	1073
^{27}Al	2250	2700	2227	294	3120	4310
^{29}Si	<MDL	248	310	1040	550	<MDL
^{31}P	<MDL	<MDL	<MDL	<MDL	<MDL	<MDL
^{44}Ca	<MDL	<MDL	<MDL	41	<MDL	<MDL
^{45}Sc	0.5	1	0.3	56	1	1
^{47}Ti	610	1350	449	511300	839	1974
^{51}V	4728	4648	4457	2535	4393	4944
^{52}Cr	1668	1748	1847	193	1729	1579
^{55}Mn	137	156	76	8820	113	316
^{59}Co	70	76	68	115	68	96
^{60}Ni	303	247	231	34	192	384
^{63}Cu	0.3	0.3	2	2	2	0.5
^{66}Zn	4	5	21	8	7	7
^{69}Ga	39	38	36	1	40	44
^{74}Ge	1	1	1	0.3	1	1
^{75}As	<MDL	<MDL	<MDL	1	1	1
^{89}Y	<MDL	0.002	<MDL	0.2	0.002	<MDL
^{90}Zr	0.03	0.1	0.05	78	0.2	0.2
^{93}Nb	0.005	0.02	0.01	9	0.04	0.01
^{95}Mo	<MDL	<MDL	0.04	1	<MDL	0.1
^{118}Sn	<MDL	0.1	0.1	4	0.2	1
^{121}Sb	<MDL	<MDL	0.02	0.1	<MDL	<MDL
^{178}Hf	<MDL	<MDL	0.000	3	0.004	<MDL
^{181}Ta	0.001	<MDL	<MDL	1	0.001	<MDL
^{182}W	<MDL	0.002	0.003	0.05	<MQL	0.001
^{208}Pb	0.5	0.2	0.2	2	0.3	0.2

MAS	Massive to semi-massive mineralization	OBAN	Orthopyroxene -bearing band
DIS	Disseminated mineralization	POD	Pod
BAN	Bands of oxide mineralization	OPOD	Orthopyroxene -bearing pod
ANO	Anorthosite hosted disseminated	VEIN	Vein
ORT	Orthopyroxene associated	MAG	Magnetite
CLI	Clinopyroxene associated	ILM	Ilmenite

Appendix V (Continued)

Sample	CC010	CC010	CC010	CC010	CC010	CC010	CC010
Circle number	D	E	F	F	H	H	I
Analysis	10-D-M2	10-E-M2	10-F-M1	10-F-M2	10-H-M1	10-H-M2	10-I-M1
Mineralization type	MAS	MAS	MAS	MAS	MAS	MAS	MAS
Descriptor	OBAN	OBAN	OBAN	OBAN	OBAN	OBAN	OBAN
Mineral host	MAG	MAG	MAG	MAG	MAG	MAG	MAG
Mineral analyzed	MAG	MAG	MAG	MAG	MAG	MAG	MAG
Fe wt.% (EPMA)*	64	64	64	64	64	64	64
^{24}Mg	943	1855	2430	2350	2520	1860	2625
^{27}Al	3570	6730	9140	8110	9550	6780	9820
^{29}Si	<MDL	<MDL	414	293	692	793	573
^{31}P	<MDL	<MDL	<MDL	<MDL	<MDL	<MDL	<MDL
^{44}Ca	<MDL	<MDL	<MDL	22	<MDL	<MDL	<MDL
^{45}Sc	1	2	2	2	2	1	2
^{47}Ti	1604	4150	3800	5540	6160	2990	6740
^{51}V	4919	6346	6228	6318	6239	6201	6222
^{52}Cr	1536	2080	2053	2106	1914	2016	1982
^{55}Mn	304	562	555	576	704	483	638
^{59}Co	93	133	146	144	141	129	136
^{60}Ni	381	460	462	470	440	412	397
^{63}Cu	0.2	1	1	1	0.3	0.1	0.5
^{66}Zn	3	12	18	23	27	12	28
^{69}Ga	42	63	66	63	64	57	63
^{74}Ge	1	1	1	1	1	1	1
^{75}As	1	1	1	1	1	1	2
^{89}Y	0.002	0.005	0.001	0.001	<MDL	<MDL	0.003
^{90}Zr	0.1	0.4	1	1	1	0.4	1
^{93}Nb	0.003	0.02	0.02	0.03	0.03	0.01	0.03
^{95}Mo	0.1	<MDL	0.2	0.2	0.1	0.1	0.1
^{118}Sn	1	1	1	1	1	1	1
^{121}Sb	0.02	0.3	0.02	<MDL	0.03	0.02	0.04
^{178}Hf	0.001	0.01	0.01	0.03	0.01	0.004	0.02
^{181}Ta	0.000	<MDL	<MDL	<MDL	<MDL	<MDL	0.000
^{182}W	0.01	0.005	0.003	0.01	0.01	0.004	0.01
^{208}Pb	0.1	0.4	0.4	0.4	0.4	0.4	0.4

MAS	Massive to semi-massive mineralization	OBAN	Orthopyroxene -bearing band
DIS	Disseminated mineralization	POD	Pod
BAN	Bands of oxide mineralization	OPOD	Orthopyroxene -bearing pod
ANO	Anorthosite hosted disseminated	VEIN	Vein
ORT	Orthopyroxene associated	MAG	Magnetite
CLI	Clinopyroxene associated	ILM	Ilmenite

Appendix V (Continued)

Sample	CC010	CC010	CC010	CC010	CC010	CC010	CC013
Circle number	I	L	M	M	O	O	A
Analysis	10-I-M3	10-L-M3	10-M-M1	10-M-M2	10-O-M1	10-O-M2	13-A-M1
Mineralization type	MAS	MAS	MAS	MAS	MAS	MAS	MAS
Descriptor	OBAN	OBAN	OBAN	OBAN	OBAN	OBAN	BAN
Mineral host	MAG	MAG	MAG	MAG	MAG	MAG	MAG
Mineral analyzed	MAG	MAG	MAG	MAG	MAG	MAG	MAG
Fe wt.% (EPMA)*	64	64	64	64	64	64	65
^{24}Mg	1513	2550	2359	2153	2130	2360	963
^{27}Al	6190	4830	9110	7790	7850	8300	3460
^{29}Si	<MDL	210	344	354	<MDL	193	<MDL
^{31}P	<MDL	<MDL	<MDL	<MDL	<MDL	<MDL	<MDL
^{44}Ca	<MDL	<MDL	<MDL	12	<MDL	<MDL	<MDL
^{45}Sc	<MDL	2	2	2	2	2	1
^{47}Ti	<MDL	18500	3300	4120	3230	5330	665
^{51}V	6270	4187	6420	6308	6370	6469	4839
^{52}Cr	1964	1659	2063	2049	2156	2202	2729
^{55}Mn	<MDL	666	569	660	505	602	180
^{59}Co	122	128	145	141	138	143	78
^{60}Ni	419	342	450	459	450	463	288
^{63}Cu	<MDL	1	1	0.4	1	1	0.2
^{66}Zn	10	14	23	19	19	28	12
^{69}Ga	62	46	66	67	65	65	36
^{74}Ge	1	1	1	1	1	1	1
^{75}As	1	1	1	1	1	1	1
^{89}Y	<MDL	0.005	0.001	<MDL	0.000	<MDL	0.001
^{90}Zr	<MDL	3	1	0.4	0.3	1	0.2
^{93}Nb	<MDL	0.3	0.004	0.01	0.01	0.01	0.01
^{95}Mo	0.1	0.1	0.1	0.2	0.1	0.1	0.04
^{118}Sn	1	0.5	1	1	1	1	0.03
^{121}Sb	<MDL	0.02	0.02	0.02	0.02	0.04	0.01
^{178}Hf	<MDL	0.1	0.02	0.01	0.01	0.01	0.003
^{181}Ta	<MDL	0.01	<MDL	<MDL	0.001	0.000	0.000
^{182}W	<MDL	<MDL	0.01	0.01	0.01	0.01	0.001
^{208}Pb	<MDL	0.1	0.4	0.4	1	0.4	0.4

MAS	Massive to semi-massive mineralization	OBAN	Orthopyroxene -bearing band
DIS	Disseminated mineralization	POD	Pod
BAN	Bands of oxide mineralization	OPOD	Orthopyroxene -bearing pod
ANO	Anorthosite hosted disseminated	VEIN	Vein
ORT	Orthopyroxene associated	MAG	Magnetite
CLI	Clinopyroxene associated	ILM	Ilmenite

Appendix V (Continued)

Sample	CC013	CC013	CC013	CC013	CC013	CC013	CC013
Circle number	A	B	C	C	D	E	F
Analysis	13-A-M2	13-B-M2	13-C-M1	13-C-M2	13-D-M2	13-E-M1	13-F-M1
Mineralization type	MAS	MAS	MAS	MAS	MAS	MAS	MAS
Descriptor	BAN	BAN	BAN	BAN	BAN	BAN	BAN
Mineral host	MAG	MAG	MAG	MAG	ILM	ILM	MAG
Mineral analyzed	MAG	MAG	MAG	MAG	MAG	MAG	MAG
Fe wt.% (EPMA)*	65	64	65	65	64	65	65
^{24}Mg	878	905	1203	745	822	808	572
^{27}Al	2800	2950	4190	2443	2860	2792	1954
^{29}Si	<MDL	300	<MDL	<MDL	<MDL	228	<MDL
^{31}P	<MDL	<MDL	<MDL	<MDL	<MDL	<MDL	<MDL
^{44}Ca	<MDL	<MDL	<MDL	<MDL	<MDL	<MDL	<MDL
^{45}Sc	1	1	1	1	0.4	1	0.4
^{47}Ti	917	1840	627	602	421	660	160
^{51}V	4402	4691	4800	4789	3542	3124	2527
^{52}Cr	2527	2433	2553	2696	1990	1762	1273
^{55}Mn	161	215	191	195	110	98	67
^{59}Co	73	79	84	77	72	76	69
^{60}Ni	254	292	313	308	243	282	255
^{63}Cu	0.4	0.5	1	0.5	1	0.3	1
^{66}Zn	9	6	13	5	6	5	9
^{69}Ga	33	34	39	37	31	32	35
^{74}Ge	1	1	1	1	1	0.5	1
^{75}As	1	1	1	1	1	1	<MDL
^{89}Y	<MDL	0.002	<MDL	<MDL	<MDL	0.001	<MDL
^{90}Zr	0.1	0.4	0.2	0.02	0.2	0.2	0.2
^{93}Nb	0.01	0.04	0.01	0.01	0.01	0.02	<MDL
^{95}Mo	0.1	0.1	0.1	0.1	0.1	0.1	<MDL
^{118}Sn	0.03	<MDL	0.03	<MDL	0.03	0.05	<MDL
^{121}Sb	0.03	<MDL	0.04	0.1	0.02	0.01	0.1
^{178}Hf	0.001	0.01	<MDL	<MDL	0.003	0.005	0.003
^{181}Ta	0.001	0.001	<MDL	0.000	0.000	<MDL	<MDL
^{182}W	0.002	0.01	0.004	0.003	0.002	0.003	0.01
^{208}Pb	0.4	0.4	1	1	0.3	0.3	1

MAS	Massive to semi-massive mineralization	OBAN	Orthopyroxene -bearing band
DIS	Disseminated mineralization	POD	Pod
BAN	Bands of oxide mineralization	OPOD	Orthopyroxene -bearing pod
ANO	Anorthosite hosted disseminated	VEIN	Vein
ORT	Orthopyroxene associated	MAG	Magnetite
CLI	Clinopyroxene associated	ILM	Ilmenite

Appendix V (Continued)

Sample	CC013	CC013	CC013	CC013	CC013	CC025	CC025
Circle number	L	L	P	P	R	A	A
Analysis	13-L-M1	13-L-M2	13-P-M1	13-P-M2	13-R-M2	25-A-M1	25-A-M2
Mineralization type	MAS	MAS	MAS	MAS	MAS	MAS	MAS
Descriptor	BAN	BAN	BAN	BAN	BAN	POD	POD
Mineral host	MAG	MAG	MAG	MAG	MAG	MAG	MAG
Mineral analyzed	MAG	MAG	MAG	MAG	MAG	MAG	MAG
Fe wt.% (EPMA)*	65	65	65	65	65	63	63
^{24}Mg	1395	994	850	1030	863	1442	712
^{27}Al	3007	3139	3087	2780	3110	11510	6560
^{29}Si	367	511	162	198	165	<MDL	410
^{31}P	<MDL	<MDL	<MDL	<MDL	<MDL	<MDL	<MDL
^{44}Ca	64	<MDL	<MDL	<MDL	<MDL	<MDL	<MDL
^{45}Sc	1	1	1	1	1	1	1
^{47}Ti	8900	1860	900	3160	468	13520	18600
^{51}V	4353	4428	4826	4739	4736	5000	4868
^{52}Cr	2355	1946	2265	2307	2257	4186	4178
^{55}Mn	496	215	216	394	167	527	692
^{59}Co	81	77	74	78	77	110	85
^{60}Ni	264	259	297	305	294	301	270
^{63}Cu	1	1	0.2	0.5	0.3	2	1
^{66}Zn	70	7	4	8	6	46	8
^{69}Ga	35	36	38	39	37	67	58
^{74}Ge	1	1	1	1	1	1	1
^{75}As	1	1	1	0.5	1	0.5	<MDL
^{89}Y	0.01	0.001	0.001	0.001	0.001	0.01	0.02
^{90}Zr	1	0.5	0.1	0.3	0.2	1	0.5
^{93}Nb	0.2	0.1	0.01	0.1	0.01	0.1	0.01
^{95}Mo	0.1	0.1	0.1	0.1	0.1	0.4	0.3
^{118}Sn	0.2	0.1	0.1	<MDL	<MDL	2	2
^{121}Sb	0.1	0.03	0.02	<MDL	0.1	<MDL	<MDL
^{178}Hf	0.02	0.01	0.001	0.01	<MDL	0.02	0.03
^{181}Ta	0.01	0.005	0.000	0.002	<MDL	0.002	<MDL
^{182}W	0.02	0.02	0.002	0.01	0.004	0.01	0.005
^{208}Pb	1	1	0.4	1	0.4	0.2	0.2

MAS	Massive to semi-massive mineralization	OBAN	Orthopyroxene -bearing band
DIS	Disseminated mineralization	POD	Pod
BAN	Bands of oxide mineralization	OPOD	Orthopyroxene -bearing pod
ANO	Anorthosite hosted disseminated	VEIN	Vein
ORT	Orthopyroxene associated	MAG	Magnetite
CLI	Clinopyroxene associated	ILM	Ilmenite

Appendix V (Continued)

Sample	CC025	CC025	CC025	CC025	CC025	CC025	CC025
Circle number	A	A	C	C	D	D	D
Analysis	25-A-M3	25-A-M4	25-C-M1	25-C-M2	25-D-M1	25-D-M3	25-D-M2
Mineralization type	MAS	MAS	MAS	MAS	MAS	MAS	MAS
Descriptor	POD	POD	POD	POD	POD	POD	POD
Mineral host	MAG	MAG	MAG	MAG	MAG	MAG	MAG
Mineral analyzed	MAG	MAG	MAG	MAG	MAG	MAG	MAG
Fe wt.% (EPMA)*	63	63	63	63	62	62	62
^{24}Mg	1082	5660	1326	674	760	720	1371
^{27}Al	6850	32990	12460	6800	7170	7420	13520
^{29}Si	<MDL	<MDL	790	<MDL	279	462	601
^{31}P	<MDL	<MDL	<MDL	<MDL	<MDL	<MDL	<MDL
^{44}Ca	<MDL	<MDL	<MDL	<MDL	<MDL	<MDL	16
^{45}Sc	1	2	1	1	1	1	1
^{47}Ti	16870	42800	13740	7820	9020	8360	10820
^{51}V	4930	4403	4800	4893	4677	4649	4684
^{52}Cr	4280	4539	4055	4022	3900	3577	3702
^{55}Mn	621	1006	638	330	344	405	543
^{59}Co	102	206	109	71	78	81	109
^{60}Ni	292	338	290	251	253	260	275
^{63}Cu	2	6	1	2	1	1	1
^{66}Zn	48	188	51	40	57	500	37
^{69}Ga	71	83	72	47	49	54	65
^{74}Ge	1	1	1	1	1	1	1
^{75}As	<MDL	1	<MDL	<MDL	<MDL	<MDL	<MDL
^{89}Y	0.01	0.03	0.02	0.002	0.01	0.003	0.004
^{90}Zr	0.5	2	0.5	1	1	0.5	1
^{93}Nb	0.1	0.04	0.04	0.02	0.1	0.02	0.02
^{95}Mo	0.4	0.4	0.3	0.3	0.3	0.4	0.3
^{118}Sn	2	2	2	1	1	1	2
^{121}Sb	<MDL	<MDL	<MDL	<MDL	0.02	<MDL	<MDL
^{178}Hf	0.02	0.1	0.01	0.02	0.03	0.02	0.04
^{181}Ta	0.001	0.004	0.001	<MDL	0.002	<MDL	<MDL
^{182}W	<MDL	<MDL	0.01	<MQL	0.01	0.005	0.004
^{208}Pb	0.2	0.3	0.2	0.2	0.3	0.3	0.1

MAS	Massive to semi-massive mineralization	OBAN	Orthopyroxene -bearing band
DIS	Disseminated mineralization	POD	Pod
BAN	Bands of oxide mineralization	OPOD	Orthopyroxene -bearing pod
ANO	Anorthosite hosted disseminated	VEIN	Vein
ORT	Orthopyroxene associated	MAG	Magnetite
CLI	Clinopyroxene associated	ILM	Ilmenite

Appendix V (Continued)

Sample	CC025	CC025	CC025	CC025	CC025	CC025	CC025
Circle number	E	E	F	F	G	H	I
Analysis	25-E-M1	25-E-M2	25-F-M2	25-F-M3	25-G-M3	25-H-M1	25-I-M1
Mineralization type	MAS	MAS	MAS	MAS	MAS	MAS	MAS
Descriptor	POD	POD	POD	POD	POD	POD	POD
Mineral host	MAG	MAG	MAG	MAG	MAG	MAG	MAG
Mineral analyzed	MAG	MAG	MAG	MAG	MAG	MAG	MAG
Fe wt.% (EPMA)*	64	64	63	63	63	63	63
^{24}Mg	1047	874	1140	981	708	1480	1948
^{27}Al	10750	8590	9380	11780	7780	15220	19050
^{29}Si	240	<MDL	1200	<MDL	<MDL	430	347
^{31}P	<MDL	<MDL	<MDL	<MDL	<MDL	<MDL	<MDL
^{44}Ca	<MDL	<MDL	<MDL	<MDL	<MDL	<MDL	<MDL
^{45}Sc	1	1	1	2	1	1	1
^{47}Ti	14550	9310	6180	15490	8189	12260	15320
^{51}V	4687	4780	4300	4525	4726	4756	4841
^{52}Cr	3918	4012	3356	3741	3722	3722	3659
^{55}Mn	631	451	281	706	424	598	648
^{59}Co	103	92	102	104	82	114	131
^{60}Ni	277	273	237	275	252	280	285
^{63}Cu	0.2	2	<MDL	0.4	0.3	0.2	0.4
^{66}Zn	20	25	25	20	13	48	61
^{69}Ga	66	60	53	66	51	65	75
^{74}Ge	1	1	1	1	1	1	1
^{75}As	<MDL	0.4	<MDL	<MDL	<MDL	<MDL	1
^{89}Y	0.004	0.01	<MDL	0.002	0.003	0.01	0.01
^{90}Zr	0.4	1	1	0.4	1	1	1
^{93}Nb	0.02	0.02	0.01	0.003	0.01	0.02	0.03
^{95}Mo	0.3	0.4	0.4	0.3	0.3	0.4	0.4
^{118}Sn	2	2	1	1	1	1	1
^{121}Sb	0.03	<MDL	<MDL	<MDL	<MDL	<MDL	<MDL
^{178}Hf	0.03	0.04	0.05	0.05	0.02	0.04	0.04
^{181}Ta	<MDL	<MDL	<MDL	0.001	<MDL	0.000	<MDL
^{182}W	<MDL	0.01	0.01	0.001	0.004	0.01	0.01
^{208}Pb	0.1	0.4	0.2	0.2	0.2	0.2	0.2

MAS	Massive to semi-massive mineralization	OBAN	Orthopyroxene -bearing band
DIS	Disseminated mineralization	POD	Pod
BAN	Bands of oxide mineralization	OPOD	Orthopyroxene -bearing pod
ANO	Anorthosite hosted disseminated	VEIN	Vein
ORT	Orthopyroxene associated	MAG	Magnetite
CLI	Clinopyroxene associated	ILM	Ilmenite

Appendix V (Continued)

Sample	CC025	CC025	CC031	CC031	CC031	CC031	CC031
Circle number	L	L	A	A	B	B	C
Analysis	25-L-M1	25-L-M2	31-A-M1	31-A-M2	31-B-M1	31-B-M2	31-C-M1
Mineralization type	MAS	MAS	DIS	DIS	DIS	DIS	DIS
Descriptor	POD	POD	ANO	ANO	ANO	ANO	ANO
Mineral host	MAG	MAG	MAG	MAG	MAG	MAG	MAG
Mineral analyzed	MAG	MAG	MAG	MAG	MAG	MAG	MAG
Fe wt.% (EPMA)*	63	63	64	64	63	63	64
^{24}Mg	657	1391	1200	963	562	346	2030
^{27}Al	7430	14670	13610	10720	6320	4470	17440
^{29}Si	<MDL	191	230	356	153	<MDL	201
^{31}P	<MDL	<MDL	<MDL	<MDL	<MDL	<MDL	<MDL
^{44}Ca	<MDL	<MDL	<MDL	<MDL	<MDL	<MDL	<MDL
^{45}Sc	1	2	1	1	1	1	2
^{47}Ti	9640	17780	2710	6590	8190	2320	17920
^{51}V	4883	4802	4221	4307	4288	4383	4150
^{52}Cr	3919	3761	3261	3214	2765	3015	3420
^{55}Mn	374	841	461	582	627	320	977
^{59}Co	74	113	89	79	57	47	118
^{60}Ni	251	277	472	451	400	411	494
^{63}Cu	1	1	1	2	3	2	5
^{66}Zn	36	37	110	108	60	43	210
^{69}Ga	49	68	56	52	48	42	65
^{74}Ge	1	1	1	1	1	1	1
^{75}As	0.4	0.5	1	1	1	1	1
^{89}Y	0.004	0.01	0.001	0.01	0.003	<MDL	0.01
^{90}Zr	1	1	1	1	1	0.3	1
^{93}Nb	0.01	0.01	0.01	0.01	0.05	0.02	0.01
^{95}Mo	0.4	0.3	1	1	1	1	1
^{118}Sn	1	2	2	1	1	1	2
^{121}Sb	0.02	0.04	0.02	0.02	0.03	<MDL	0.04
^{178}Hf	0.02	0.03	0.02	0.03	0.03	0.003	0.04
^{181}Ta	0.000	0.000	0.000	<MDL	<MDL	<MDL	0.001
^{182}W	0.01	0.01	0.01	0.005	0.003	0.01	0.01
^{208}Pb	0.2	0.2	0.4	1	1	1	1

MAS	Massive to semi-massive mineralization	OBAN	Orthopyroxene -bearing band
DIS	Disseminated mineralization	POD	Pod
BAN	Bands of oxide mineralization	OPOD	Orthopyroxene -bearing pod
ANO	Anorthosite hosted disseminated	VEIN	Vein
ORT	Orthopyroxene associated	MAG	Magnetite
CLI	Clinopyroxene associated	ILM	Ilmenite

Appendix V (Continued)

Sample	CC031	CC031	CC031	CC031	CC031	CC031	CC031
Circle number	C	C	D	D	E	E	F
Analysis	31-C-M2	31-C-M3	31-D-M1	31-D-M2	31-E-M1	31-E-M2	31-F-M1
Mineralization type	DIS	DIS	DIS	DIS	DIS	DIS	DIS
Descriptor	ANO	ANO	ANO	ANO	ANO	ANO	ANO
Mineral host	MAG	MAG	MAG	MAG	MAG	MAG	MAG
Mineral analyzed	MAG	MAG	MAG	MAG	MAG	MAG	MAG
Fe wt.% (EPMA)*	64	64	63	63	64	64	64
^{24}Mg	1630	473	1103	1146	1479	605	897
^{27}Al	14200	5570	15390	14570	14930	10190	3920
^{29}Si	<MDL	191	390	580	540	560	<MDL
^{31}P	<MDL	<MDL	<MDL	<MDL	5	<MDL	<MDL
^{44}Ca	<MDL	<MDL	<MDL	<MDL	<MDL	<MDL	<MDL
^{45}Sc	2	1	2	1	2	1	0.2
^{47}Ti	15500	1173	14050	6780	14600	1650	1101
^{51}V	4163	4302	4216	4311	4099	4340	3544
^{52}Cr	3371	3186	3013	3033	3347	3479	2707
^{55}Mn	704	181	791	546	870	254	102
^{59}Co	105	58	79	85	95	60	89
^{60}Ni	471	423	402	425	455	359	460
^{63}Cu	1	0.2	2	3	7	5	0.3
^{66}Zn	141	35	172	153	177	58	18
^{69}Ga	57	45	58	53	62	48	34
^{74}Ge	1	1	1	1	1	1	1
^{75}As	1	1	1	1	1	1	1
^{89}Y	0.01	<MDL	0.003	0.002	0.01	0.002	0.01
^{90}Zr	1	0.4	1	1	2	1	2
^{93}Nb	0.01	0.01	0.02	0.005	0.02	0.01	0.01
^{95}Mo	1	1	1	1	1	1	1
^{118}Sn	1	1	1	2	2	1	0.3
^{121}Sb	0.03	0.02	0.04	0.1	0.02	0.04	<MDL
^{178}Hf	0.05	0.01	0.1	0.04	0.1	0.02	0.01
^{181}Ta	0.004	0.001	0.02	<MDL	<MDL	<MDL	<MDL
^{182}W	0.02	0.000	0.1	0.003	0.02	0.003	<MDL
^{208}Pb	1	0.3	0.4	0.5	0.4	0.2	0.4

MAS	Massive to semi-massive mineralization	OBAN	Orthopyroxene -bearing band
DIS	Disseminated mineralization	POD	Pod
BAN	Bands of oxide mineralization	OPOD	Orthopyroxene -bearing pod
ANO	Anorthosite hosted disseminated	VEIN	Vein
ORT	Orthopyroxene associated	MAG	Magnetite
CLI	Clinopyroxene associated	ILM	Ilmenite

Appendix V (Continued)

Sample	CC031	CC031	CC054	CC054	CC054	CC054	CC054
Circle number	F	F	B	B	C	C	E
Analysis	31-F-M2	31-F-M3	54-B-M1	54-B-M2	54-C-M1	54-C-M2	54-E-M1
Mineralization type	DIS	DIS	DIS	DIS	DIS	DIS	DIS
Descriptor	ANO	ANO	ORT	ORT	ORT	ORT	ORT
Mineral host	MAG	MAG	MAG	MAG	MAG	MAG	MAG
Mineral analyzed	MAG	MAG	MAG	MAG	MAG	MAG	MAG
Fe wt.% (EPMA)*	64	64	63	63	63	63	63
^{24}Mg	2690	487	1714	2504	1600	3770	2476
^{27}Al	22200	4470	16960	21760	10460	24400	20250
^{29}Si	630	<MDL	770	375	780	<MDL	<MDL
^{31}P	<MDL	<MDL	<MDL	<MDL	9	<MDL	<MDL
^{44}Ca	<MDL	<MDL	<MDL	<MDL	<MDL	<MDL	<MDL
^{45}Sc	2	1	2	2	1	1	1
^{47}Ti	14000	4860	29800	27610	12320	17650	19510
^{51}V	4167	4230	5187	5165	4194	4096	4348
^{52}Cr	3439	3235	2970	2993	2074	2184	2283
^{55}Mn	719	326	1553	1391	529	671	1054
^{59}Co	133	56	160	176	121	175	158
^{60}Ni	507	409	434	449	338	380	370
^{63}Cu	1	2	1	2	2	2	1
^{66}Zn	258	35	32	74	45	149	77
^{69}Ga	66	44	80	85	59	72	69
^{74}Ge	1	1	1	1	1	1	1
^{75}As	1	1	1	1	1	1	1
^{89}Y	0.01	0.003	0.01	0.01	0.01	0.01	0.01
^{90}Zr	1	0.5	1	1	1	1	1
^{93}Nb	0.01	0.01	0.02	0.01	0.02	0.01	0.01
^{95}Mo	1	1	0.4	0.4	0.3	0.3	0.4
^{118}Sn	1	1	3	3	2	2	2
^{121}Sb	0.04	0.1	0.1	0.04	0.04	0.03	0.2
^{178}Hf	0.1	0.01	0.1	0.1	0.03	0.1	0.05
^{181}Ta	<MDL	<MDL	0.000	0.02	0.002	0.000	0.002
^{182}W	0.003	<MDL	0.1	0.04	0.01	0.002	0.01
^{208}Pb	0.4	0.3	1	1	1	1	1

MAS	Massive to semi-massive mineralization	OBAN	Orthopyroxene -bearing band
DIS	Disseminated mineralization	POD	Pod
BAN	Bands of oxide mineralization	OPOD	Orthopyroxene -bearing pod
ANO	Anorthosite hosted disseminated	VEIN	Vein
ORT	Orthopyroxene associated	MAG	Magnetite
CLI	Clinopyroxene associated	ILM	Ilmenite

Appendix V (Continued)

Sample	CC054	CC054	CC054	CC054	CC054	CC054	CC054
Circle number	E	F	F	G	G	I	I
Analysis	54-E-M2	54-F-M1	54-F-M2	54-G-M1	54-G-M2	54-I-M1	54-I-M2
Mineralization type	DIS	DIS	DIS	DIS	DIS	DIS	DIS
Descriptor	ORT	ORT	ORT	ORT	ORT	ORT	ORT
Mineral host	MAG	MAG	MAG	MAG	MAG	MAG	MAG
Mineral analyzed	MAG	MAG	MAG	MAG	MAG	MAG	MAG
Fe wt.% (EPMA)*	63	63	63	63	63	63	63
^{24}Mg	1695	1685	1930	1846	1381	1581	1727
^{27}Al	15380	18600	15850	14790	19100	11560	15890
^{29}Si	340	<MDL	710	440	700	360	274
^{31}P	<MDL	<MDL	<MDL	<MDL	<MDL	8	<MDL
^{44}Ca	<MDL	<MDL	<MDL	23	<MDL	<MDL	<MDL
^{45}Sc	2	2	2	1	2	1	2
^{47}Ti	19210	21450	24500	17940	19680	14090	20020
^{51}V	4434	4303	4328	4538	4452	4470	4396
^{52}Cr	2140	2086	2105	2305	2241	2453	2115
^{55}Mn	945	1232	1379	928	860	668	1201
^{59}Co	130	130	138	136	129	128	142
^{60}Ni	342	331	334	363	347	364	371
^{63}Cu	0.3	1	3	1	1	1	2
^{66}Zn	43	76	67	53	81	41	58
^{69}Ga	63	66	66	65	65	78	71
^{74}Ge	1	1	1	1	1	1	1
^{75}As	1	1	1	<MDL	1	1	1
^{89}Y	0.001	0.01	0.01	0.01	0.02	0.001	0.01
^{90}Zr	1	1	1	1	1	1	1
^{93}Nb	0.01	0.01	0.01	0.02	0.03	0.01	0.02
^{95}Mo	0.3	0.4	0.4	0.4	0.4	0.3	0.4
^{118}Sn	2	2	3	2	2	2	2
^{121}Sb	<MDL	0.03	<MDL	0.01	0.1	0.04	0.02
^{178}Hf	0.05	0.1	0.1	0.04	0.1	0.04	0.04
^{181}Ta	<MDL	0.000	0.002	0.002	<MDL	<MDL	<MDL
^{182}W	<MDL	0.004	<MDL	0.01	0.003	0.004	0.01
^{208}Pb	1	1	1	0.5	1	1	1

MAS	Massive to semi-massive mineralization	OBAN	Orthopyroxene -bearing band
DIS	Disseminated mineralization	POD	Pod
BAN	Bands of oxide mineralization	OPOD	Orthopyroxene -bearing pod
ANO	Anorthosite hosted disseminated	VEIN	Vein
ORT	Orthopyroxene associated	MAG	Magnetite
CLI	Clinopyroxene associated	ILM	Ilmenite

Appendix V (Continued)

Sample	CC054	CC054	CC054	CC054	CC072	CC072	CC072
Circle number	L	L	M	M	A	A	B
Analysis	54-L-M1	54-L-M2	54-M-M1	54-M-M2	72-A-M1	72-A-M2	72-B-M2
Mineralization type	DIS	DIS	DIS	DIS	MAS	MAS	MAS
Descriptor	ORT	ORT	ORT	ORT	OPOD	OPOD	OPOD
Mineral host	MAG	MAG	MAG	MAG	MAG	MAG	MAG
Mineral analyzed	MAG	MAG	MAG	MAG	MAG	MAG	MAG
Fe wt.% (EPMA)*	63	63	63	63	60	60	59
^{24}Mg	1947	1680	1372	1505	5571	5240	10540
^{27}Al	17960	16290	12370	16280	16860	17980	28400
^{29}Si	730	529	3000	<MDL	726	178	<MDL
^{31}P	<MDL	<MDL	<MDL	<MDL	<MDL	<MDL	<MDL
^{44}Ca	<MDL	60	<MDL	<MDL	22	<MDL	<MDL
^{45}Sc	2	2	2	2	6	6	5
^{47}Ti	20110	23140	17390	23930	23620	23790	27050
^{51}V	4497	4462	4528	4278	4368	4252	4223
^{52}Cr	2232	2144	2045	2020	2088	2085	2417
^{55}Mn	1031	1136	1001	1325	1875	2070	2030
^{59}Co	139	125	123	137	170	180	206
^{60}Ni	346	327	342	353	316	334	342
^{63}Cu	0.4	0.3	0.4	1	12	1	4
^{66}Zn	52	43	42	38	62	75	455
^{69}Ga	66	63	65	66	56	61	67
^{74}Ge	1	1	1	1	1	1	1
^{75}As	1	1	0.5	1	1	1	1
^{89}Y	0.01	0.01	0.01	0.01	0.01	0.02	0.02
^{90}Zr	0.5	1	1	1	2	2	2
^{93}Nb	0.02	0.01	<MDL	0.04	0.02	0.01	0.1
^{95}Mo	0.3	0.4	1	0.4	0.2	0.2	0.2
^{118}Sn	2	2	2	2	2	2	2
^{121}Sb	0.1	<MDL	0.02	0.03	0.03	0.04	0.05
^{178}Hf	0.04	0.1	0.04	0.05	0.1	0.1	0.1
^{181}Ta	0.001	<MDL	<MDL	0.001	0.001	0.000	0.001
^{182}W	0.01	0.01	<MDL	0.01	0.01	0.004	0.01
^{208}Pb	0.4	0.4	1	1	0.5	1	1

MAS	Massive to semi-massive mineralization	OBAN	Orthopyroxene -bearing band
DIS	Disseminated mineralization	POD	Pod
BAN	Bands of oxide mineralization	OPOD	Orthopyroxene -bearing pod
ANO	Anorthosite hosted disseminated	VEIN	Vein
ORT	Orthopyroxene associated	MAG	Magnetite
CLI	Clinopyroxene associated	ILM	Ilmenite

Appendix V (Continued)

Sample	CC072	CC072	CC072	CC072	CC072	CC072	CC072
Circle number	C	C	D	D	E	E	G
Analysis	72-C-M2	72-C-M1	72-D-M1	72-D-M2	72-E-M1	72-E-M2	72-G-M1
Mineralization type	MAS	MAS	MAS	MAS	MAS	MAS	MAS
Descriptor	OPOD	OPOD	OPOD	OPOD	OPOD	OPOD	OPOD
Mineral host	MAG	MAG	MAG	MAG	MAG	MAG	MAG
Mineral analyzed	MAG	MAG	MAG	MAG	MAG	MAG	MAG
Fe wt.% (EPMA)*	62	62	60	60	61	61	62
^{24}Mg	6160	5720	6700	5540	6450	5299	5370
^{27}Al	17830	16380	18880	13930	16430	15090	14540
^{29}Si	526	<MDL	<MDL	502	454	710	410
^{31}P	<MDL	<MDL	<MDL	<MDL	<MDL	<MDL	<MDL
^{44}Ca	<MDL	<MDL	<MDL	<MDL	<MDL	<MDL	<MDL
^{45}Sc	7	6	6	6	7	7	6
^{47}Ti	26980	24560	26620	25300	32340	31170	27240
^{51}V	4289	4328	4519	4508	4498	4477	4482
^{52}Cr	2123	2086	2272	2351	2341	2190	2232
^{55}Mn	2083	1848	2013	2059	2270	2206	1957
^{59}Co	179	166	175	176	178	169	173
^{60}Ni	311	306	322	332	322	324	324
^{63}Cu	1	2	0.4	1	0.4	0.3	1
^{66}Zn	68	62	96	68	102	62	52
^{69}Ga	58	56	60	64	57	57	58
^{74}Ge	1	1	1	1	1	1	1
^{75}As	1	1	1	1	1	1	1
^{89}Y	0.01	0.01	0.01	0.01	0.02	0.02	0.01
^{90}Zr	3	2	2	2	3	3	2
^{93}Nb	0.02	0.01	0.01	0.01	0.1	0.02	0.02
^{95}Mo	0.3	0.2	0.3	0.3	0.2	0.2	0.1
^{118}Sn	2	2	2	2	2	2	2
^{121}Sb	0.04	0.02	0.1	0.04	0.05	0.02	0.04
^{178}Hf	0.1	0.1	0.1	0.1	0.2	0.2	0.1
^{181}Ta	0.000	0.000	<MDL	0.000	0.001	0.000	0.000
^{182}W	0.004	0.003	0.01	0.01	0.01	0.2	0.03
^{208}Pb	1	0.5	1	1	0.4	0.4	1

MAS	Massive to semi-massive mineralization	OBAN	Orthopyroxene -bearing band
DIS	Disseminated mineralization	POD	Pod
BAN	Bands of oxide mineralization	OPOD	Orthopyroxene -bearing pod
ANO	Anorthosite hosted disseminated	VEIN	Vein
ORT	Orthopyroxene associated	MAG	Magnetite
CLI	Clinopyroxene associated	ILM	Ilmenite

Appendix V (Continued)

Sample	CC072	CC072	CC072	CC072	CC072	CC074	CC074
Circle number	G	H	H	I	I	A	A
Analysis	72-G-M2	72-H-M1	72-H-M2	72-I-M1	72-I-M2	74-A-M1	74-A-M2
Mineralization type	MAS	MAS	MAS	MAS	MAS	DIS	DIS
Descriptor	OPOD	OPOD	OPOD	OPOD	OPOD	CLI	CLI
Mineral host	MAG	MAG	MAG	MAG	MAG	MAG	MAG
Mineral analyzed	MAG	MAG	MAG	MAG	MAG	MAG	MAG
Fe wt.% (EPMA)*	62	60	60	62	62	63	63
^{24}Mg	5380	5250	5490	6000	5350	411	333
^{27}Al	14000	13890	14520	17360	14000	4450	3460
^{29}Si	404	<MDL	180	780	404	<MDL	<MDL
^{31}P	<MDL	<MDL	<MDL	<MDL	<MDL	<MDL	<MDL
^{44}Ca	<MDL	<MDL	<MDL	<MDL	<MDL	<MDL	<MDL
^{45}Sc	5	6	5	6	5	1	1
^{47}Ti	25130	28140	25390	24010	24490	854	3180
^{51}V	4442	4456	4451	4283	4459	3584	3429
^{52}Cr	2253	2209	2268	2185	2300	3178	3722
^{55}Mn	1956	2105	1911	1830	1896	300	356
^{59}Co	181	173	179	172	177	86	76
^{60}Ni	335	317	326	317	321	283	275
^{63}Cu	1	0.3	1	0.4	1	0.5	<MDL
^{66}Zn	65	59	65	82	59	33	25
^{69}Ga	60	55	57	58	57	56	49
^{74}Ge	1	1	1	1	1	1	<MDL
^{75}As	1	1	1	1	1	2	<MDL
^{89}Y	0.01	0.01	0.01	0.02	0.01	<MDL	0.01
^{90}Zr	2	2	2	2	2	0.1	0.5
^{93}Nb	0.01	0.02	0.02	0.01	0.02	0.03	0.2
^{95}Mo	0.3	0.2	0.2	0.2	0.2	0.3	<MDL
^{118}Sn	2	2	2	2	2	0.3	<MDL
^{121}Sb	0.04	0.02	0.02	0.02	0.03	0.1	0.2
^{178}Hf	0.1	0.1	0.1	0.1	0.1	<MDL	0.01
^{181}Ta	0.002	0.000	0.01	<MDL	0.000	<MDL	0.004
^{182}W	0.002	0.01	0.01	0.002	0.003	0.001	<MQL
^{208}Pb	1	0.3	1	1	1	1	1

MAS	Massive to semi-massive mineralization	OBAN	Orthopyroxene -bearing band
DIS	Disseminated mineralization	POD	Pod
BAN	Bands of oxide mineralization	OPOD	Orthopyroxene -bearing pod
ANO	Anorthosite hosted disseminated	VEIN	Vein
ORT	Orthopyroxene associated	MAG	Magnetite
CLI	Clinopyroxene associated	ILM	Ilmenite

Appendix V (Continued)

Sample	CC074	CC074	CC074	CC074	CC074	CC074	CC074
Circle number	B	B	C	C	D	D	E
Analysis	74-B-M1	74-B-M2	74-C-M1	74-C-M2	74-D-M2	74-D-M2	74-E-M1
Mineralization type	DIS	DIS	DIS	DIS	DIS	DIS	DIS
Descriptor	CLI	CLI	CLI	CLI	CLI	CLI	CLI
Mineral host	MAG	MAG	MAG	MAG	MAG	MAG	MAG
Mineral analyzed	MAG	MAG	MAG	MAG	MAG	MAG	MAG
Fe wt.% (EPMA)*	64	64	64	64	64	64	64
^{24}Mg	610	571	367	504	<MDL	405	406
^{27}Al	4860	4150	2410	4360	4300	2618	3400
^{29}Si	<MDL	<MDL	584	680	708	395	310
^{31}P	<MDL	<MDL	<MDL	<MDL	6	<MDL	<MDL
^{44}Ca	<MDL	<MDL	<MDL	17	15	<MDL	<MDL
^{45}Sc	1	1	0.4	1	1	1	1
^{47}Ti	1170	6500	2930	887	12000	727	557
^{51}V	3486	3455	3380	3480	3294	3462	3447
^{52}Cr	3159	3310	3047	2945	3683	3159	3206
^{55}Mn	270	674	293	257	673	233	235
^{59}Co	82	91	74	84	98	73	78
^{60}Ni	297	288	250	273	242	232	258
^{63}Cu	0.2	1	1	0.3	1	14	0.3
^{66}Zn	49	95	17	27	30	9	60
^{69}Ga	53	55	46	55	54	47	49
^{74}Ge	1	1	1	1	1	1	1
^{75}As	2	2	2	2	2	1	1
^{89}Y	0.01	0.02	0.01	0.003	0.01	0.01	<MDL
^{90}Zr	0.3	1	0.2	0.1	1	0.03	0.1
^{93}Nb	0.02	0.2	0.1	0.01	1	0.02	0.01
^{95}Mo	0.3	0.3	0.2	0.3	0.3	0.3	0.2
^{118}Sn	0.2	0.4	0.1	0.1	0.4	0.1	0.1
^{121}Sb	0.1	0.1	0.02	0.03	0.1	0.01	<MDL
^{178}Hf	0.002	0.01	0.01	0.002	0.04	0.001	<MDL
^{181}Ta	0.001	0.003	0.002	0.000	0.02	0.000	<MDL
^{182}W	0.002	0.004	0.001	0.01	0.01	0.005	0.003
^{208}Pb	1	1	1	1	1	1	1

MAS	Massive to semi-massive mineralization	OBAN	Orthopyroxene -bearing band
DIS	Disseminated mineralization	POD	Pod
BAN	Bands of oxide mineralization	OPOD	Orthopyroxene -bearing pod
ANO	Anorthosite hosted disseminated	VEIN	Vein
ORT	Orthopyroxene associated	MAG	Magnetite
CLI	Clinopyroxene associated	ILM	Ilmenite

Appendix V (Continued)

Sample	CC074	CC074	CC076	CC076	CC076	CC076
Circle number	E	F	C	C	D	K
Analysis	74-E-M2	74-F-M1	76-C-M1	76-C-M2	76-D-M1	76-K-M1
Mineralization type	DIS	DIS	MAS	MAS	MAS	MAS
Descriptor	CLI	CLI	VEIN	VEIN	VEIN	VEIN
Mineral host	MAG	MAG	MAG	MAG	MAG	MAG
Mineral analyzed	MAG	MAG	MAG	MAG	MAG	MAG
Fe wt.% (EPMA)*	64	64	64	64	64	64
^{24}Mg	2940	489	517	702	624	806
^{27}Al	17700	2990	2810	5570	3610	4780
^{29}Si	240	1630	<MDL	<MDL	209	149
^{31}P	<MDL	7	<MDL	<MDL	<MDL	<MDL
^{44}Ca	16	72	<MDL	<MDL	<MDL	<MDL
^{45}Sc	1	0.4	1	1	1	1
^{47}Ti	1370	1340	601	808	524	1410
^{51}V	3453	3362	4200	4420	3476	4300
^{52}Cr	3792	4070	2277	3103	2591	2969
^{55}Mn	517	259	345	273	205	358
^{59}Co	181	90	58	64	59	64
^{60}Ni	337	269	96	101	93	98
^{63}Cu	0.4	1	1	0.2	0.1	0.1
^{66}Zn	1320	38	7	47	18	38
^{69}Ga	68	54	34	42	36	43
^{74}Ge	1	1	1	1	1	1
^{75}As	1	1	<MDL	<MDL	0.4	0.4
^{89}Y	0.001	0.002	<MDL	0.001	<MDL	0.001
^{90}Zr	0.1	0.1	0.01	0.02	0.1	0.1
^{93}Nb	0.02	0.03	<MDL	0.01	0.01	0.01
^{95}Mo	0.2	0.2	0.3	<MDL	0.2	0.2
^{118}Sn	0.3	0.1	<MDL	<MDL	0.05	<MDL
^{121}Sb	0.02	0.02	<MDL	<MDL	0.01	<MDL
^{178}Hf	0.001	<MDL	<MDL	<MDL	0.002	0.001
^{181}Ta	0.001	0.001	<MDL	<MDL	0.01	0.000
^{182}W	0.01	<MDL	<MDL	<MDL	0.001	<MDL
^{208}Pb	1	1	0.4	0.2	0.2	0.2

MAS	Massive to semi-massive mineralization	OBAN	Orthopyroxene -bearing band
DIS	Disseminated mineralization	POD	Pod
BAN	Bands of oxide mineralization	OPOD	Orthopyroxene -bearing pod
ANO	Anorthosite hosted disseminated	VEIN	Vein
ORT	Orthopyroxene associated	MAG	Magnetite
CLI	Clinopyroxene associated	ILM	Ilmenite

Appendix V (Continued)

Sample	CC008	CC008	CC008	CC008	CC008	CC008	CC008	CC008
Circle number	A	A	A	C	D	D	F	F
Analysis number	08-A-I1	08-A-I3	08-A-I4	08-C-I1	08-D-I1	08-D-I2	08-F-I1	08-F-I2
Mineralization style	MAS	MAS	MAS	MAS	MAS	MAS	MAS	MAS
Descriptor	BAN	BAN	BAN	BAN	BAN	BAN	BAN	BAN
Ilmenite texture	COMP	COMP	COMP	COMP	COMP	COMP	COMP	COMP
Exsolution?	y	y	y	y	y	y	n	n
Ti wt. % (EPMA)	29.1	29.0	29.1	29.4	29.5	29.6	29.6	29.7
^{24}Mg	8670	9710	8920	9050	8970	8488	8940	9140
^{27}Al	508	4470	204	266	1600	235	261	452
^{29}Si	296	259	307	231	123	252	540	410
^{31}P	4	<MDL	4	<MDL	<MDL	<MDL	<MDL	<MDL
^{44}Ca	<MDL	<MDL	<MDL	<MDL	<MDL	<MDL	36	32
^{45}Sc	41	40	41	41	40	40	37	38
^{51}V	1866	1603	1786	1929	1445	1719	1590	1867
^{52}Cr	116	140	99	179	150	184	193	208
^{55}Mn	6177	6178	6356	5769	6323	6283	6120	6010
^{57}Fe	413300	433700	436800	432200	416000	424000	404900	432800
^{59}Co	91	99	93	92	96	93	99	102
^{60}Ni	43	42	41	49	55	52	53	56
^{63}Cu	2	2	3	17	1	2	2	2
^{65}Cu	4	5	6	4	4	4	5	5
^{69}Ga	2	9	2	2	3	1	1	2
^{74}Ge	0.2	0.1	0.2	0.2	0.2	0.2	0.2	0.2
^{75}As	0.4	0.4	0.5	1	0.4	1	1	1
^{89}Y	0.1	0.1	0.1	0.1	0.1	0.1	0.1	0.1
^{90}Zr	73	79	82	66	67	69	55	64
^{93}Nb	3	3	3	4	4	3	3	4
^{95}Mo	0.4	0.5	1	0.4	0.4	0.4	0.4	0.4
^{118}Sn	3	3	3	4	3	4	4	4
^{121}Sb	0.1	0.1	0.1	0.1	0.1	0.1	0.1	0.05
^{178}Hf	2	2	2	3	2	3	2	2
^{181}Ta	0.1	0.1	0.1	0.1	0.1	0.1	0.2	0.2
^{182}W	0.01	0.00	0.02	0.01	0.00	0.01	0.01	0.01
^{208}Pb	1	1	1	1	1	1	1	1

MAS	Massive to semi-massive mineralization	OBAN	Orthopyroxene -bearing band
DIS	Disseminated mineralization	POD	Pod
BAN	Bands of oxide mineralization	OPOD	Orthopyroxene -bearing pod
ANO	Anorthosite hosted disseminated	VEIN	Vein
ORT	Orthopyroxene associated	COMP	composite ilmenite
CLI	Clinopyroxene associated	SAN	sandwich ilmenite

* Internal calibrant was taken from EPMA analyses performed on the same grain as LA-ICPMS analyses; when LA-ICPMS analyses were performed on magnetite without EPMA analyses, the internal calibrant used was the average of all texturally similar ilmenite in the sample

Appendix V (Continued)

Sample	CC008	CC008	CC008	CC008	CC010	CC010	CC010	CC010
Circle number	H	H	J	J	D	D	D	E
Analysis number	08-H-I1	08-H-I2	08-J-I1	08-J-I2	10-D-I1	10-D-I1	10-D-I2	10-E-S1
Mineralization style	MAS	MAS	MAS	MAS	MAS	MAS	MAS	MAS
Descriptor	BAN	BAN	BAN	BAN	OBAN	OBAN	OBAN	OBAN
Ilmenite texture	COMP	COMP	COMP	COMP	COMP	COMP	COMP	SAN
Exsolution?	y	y	n	n	y	y	y	n
Ti wt. % (EPMA)	29.5	29.5	29.6	29.5	29.8	28.2	28.3	30.69
^{24}Mg	9893	9870	10000	9743	11540	10840	10663	9940
^{27}Al	483	134	423	310	326	294	272	173
^{29}Si	552	201	2600	271	<MDL	290	986	668
^{31}P	5	4	13	<MDL	<MDL	<MDL	<MDL	<MDL
^{44}Ca	<MDL	<MDL	390	<MDL	<MDL	<MDL	17	<MDL
^{45}Sc	40	40	40	39	45	44	45	44
^{51}V	1717	1222	2031	1755	1565	1348	1601	975
^{52}Cr	141	74	170	130	148	132	108	113
^{55}Mn	4769	4804	4787	4767	6020	5522	5468	8249
^{57}Fe	463600	380500	479800	464000	442000	403000	413400	390000
^{59}Co	91	87	76	82	123	113	113	114
^{60}Ni	50	38	27	30	64	64	68	81
^{63}Cu	1	1	4	1	2	1	1	2
^{65}Cu	4	3	6	3	5	5	5	6
^{69}Ga	3	1	2	2	1	1	1	1
^{74}Ge	0.2	0.1	0.2	0.2	0.2	0.1	0.1	0.1
^{75}As	0.5	0.3	1	0.5	1	1	1	1
^{89}Y	0.1	0.1	0.1	0.1	0.1	0.1	0.1	0.1
^{90}Zr	71	48	63	82	75	69	91	49
^{93}Nb	5	5	5	5	3	3	3	2
^{95}Mo	0.4	0.3	0.4	0.4	0.4	0.3	0.4	0.5
^{118}Sn	3	2	4	3	4	3	3	3
^{121}Sb	0.04	0.03	0.1	0.04	0.04	0.02	0.02	0.04
^{178}Hf	3	2	3	3	2	2	2	2
^{181}Ta	0.4	0.4	0.5	0.4	0.1	0.1	0.1	0.1
^{182}W	0.01	0.01	0.03	0.02	0.02	0.01	0.01	0.02
^{208}Pb	1	1	2	1	1	1	1	1

MAS	Massive to semi-massive mineralization	OBAN	Orthopyroxene -bearing band
DIS	Disseminated mineralization	POD	Pod
BAN	Bands of oxide mineralization	OPOD	Orthopyroxene -bearing pod
ANO	Anorthosite hosted disseminated	VEIN	Vein
ORT	Orthopyroxene associated	COMP	composite ilmenite
CLI	Clinopyroxene associated	SAN	sandwich ilmenite

Appendix V (Continued)

Sample	CC010	CC010	CC010	CC010	CC010	CC010	CC010	CC010
Circle number	E	E	E	E	F	F	I	I
Analysis number	10-E-S2	10-E-C2	10-E-C1	10-E-S1	10-F-I1	10-F-I2	10-I-I1	10-I-I2
Mineralization style	MAS	MAS	MAS	MAS	MAS	MAS	MAS	MAS
Descriptor	OBAN	OBAN	OBAN	OBAN	OBAN	OBAN	OBAN	OBAN
Ilmenite texture	SAN	COMP	COMP	SAN	COMP	COMP	COMP	COMP
Exsolution?	n	y	y	n	n	n	n	n
Ti wt. % (EPMA)	30.7	28.3	28.1	31.2	29.5	29.3	31.2	29.2
^{24}Mg	9830	9244	9150	10430	9908	9890	13380	10115
^{27}Al	141	210	160	525	204	322	11630	209
^{29}Si	769	310	<MDL	<MDL	533	355	958	599
^{31}P	8	<MDL	<MDL	<MDL	<MDL	<MDL	8	4
^{44}Ca	14	<MDL	<MDL	<MDL	<MDL	<MDL	23	17
^{45}Sc	42	46	42	44	44	45	37	37
^{51}V	913	1174	1041	1129	1009	1148	857	840
^{52}Cr	117	165	119	169	132	141	337	144
^{55}Mn	8510	7161	7328	8549	7897	7469	7555	6990
^{57}Fe	379900	375000	370700	426000	382000	404000	398000	372000
^{59}Co	115	110	115	124	110	114	152	103
^{60}Ni	81	82	82	77	62	68	68	49
^{63}Cu	2	1	2	2	1	1	2	2
^{65}Cu	6	5	5	5	4	4	25	5
^{69}Ga	0.5	1	1	3	1	1	13	1
^{74}Ge	0.1	0.1	0.1	0.2	0.1	0.1	0.1	0.2
^{75}As	1	1	1	1	1	1	1	1
^{89}Y	0.1	0.1	0.1	0.1	0.1	0.1	0.1	0.1
^{90}Zr	42	67	59	50	52	62	44	44
^{93}Nb	2	3	2	3	2	3	2	2
^{95}Mo	1	0.4	1	0.5	0.4	0.4	0.4	0.4
^{118}Sn	3	4	4	3	3	3	3	2
^{121}Sb	0.1	0.05	0.04	0.1	0.03	0.04	0.1	0.05
^{178}Hf	1	2	2	2	2	2	2	1
^{181}Ta	0.1	0.1	0.1	0.1	0.1	0.1	0.04	0.04
^{182}W	0.03	0.01	0.01	0.03	0.01	0.03	0.01	0.03
^{208}Pb	1	1	1	1	1	1	1	1

MAS	Massive to semi-massive mineralization	OBAN	Orthopyroxene -bearing band
DIS	Disseminated mineralization	POD	Pod
BAN	Bands of oxide mineralization	OPOD	Orthopyroxene -bearing pod
ANO	Anorthosite hosted disseminated	VEIN	Vein
ORT	Orthopyroxene associated	COMP	composite ilmenite
CLI	Clinopyroxene associated	SAN	sandwich ilmenite

Appendix V (Continued)

Sample	CC010	CC010	CC010	CC010	CC010	CC010	CC013
Circle number	L	M	M	M	M	A	A
Analysis number	10-L-I2	10-M-S1	10-M-S2	10-M-I1	10-M-I2	10-O-S1	13-A-S1
Mineralization style	MAS	MAS	MAS	MAS	MAS	MAS	MAS
Descriptor	OBAN	OBAN	OBAN	OBAN	OBAN	OBAN	BAN
Ilmenite texture	COMP	SAN	SAN	COMP	COMP	SAN	SAN
Exsolution?	y	n	n	y	n	n	n
Ti wt. % (EPMA)	29.3	31.2	31.1	29.1	29.1	31	30.6
^{24}Mg	12090	9632	9552	9750	9609	12190	9940
^{27}Al	377	109	161	266	224	3920	630
^{29}Si	620	160	<MDL	207	213	2750	<MDL
^{31}P	4	<MDL	<MDL	<MDL	<MDL	<MDL	<MDL
^{44}Ca	9	<MDL	<MDL	<MDL	<MDL	10	<MDL
^{45}Sc	42	42	46	47	47	44	37
^{51}V	1464	826	984	1267	1307	875	1177
^{52}Cr	101	99	125	178	178	139	163
^{55}Mn	5472	9550	9140	7277	7398	9010	6998
^{57}Fe	460000	391000	399000	400000	406000	402000	378800
^{59}Co	122	118	116	112	114	116	101
^{60}Ni	61	62	64	65	68	68	47
^{63}Cu	2	1	3	1	1	132	3
^{65}Cu	5	5	5	4	4	141	6
^{69}Ga	2	0.4	1	1	1	3	1
^{74}Ge	0.2	0.1	0.2	0.1	0.1	0.1	<MDL
^{75}As	1	1	1	1	1	1	<MDL
^{89}Y	0.1	0.1	0.1	0.1	0.1	0.1	0.1
^{90}Zr	73	39	47	70	70	39	24
^{93}Nb	5	2	2	3	3	2	6
^{95}Mo	0.4	1	1	0.4	1	1	0.4
^{118}Sn	3	3	3	3	3	3	0.3
^{121}Sb	0.04	0.1	0.1	0.04	0.03	0.1	0.1
^{178}Hf	3	1	2	2	2	2	1
^{181}Ta	0.2	0.04	0.1	0.1	0.05	0.1	0.4
^{182}W	0.02	0.03	0.02	0.04	0.01	0.05	0.1
^{208}Pb	1	1	1	1	1	2	3

MAS	Massive to semi-massive mineralization	OBAN	Orthopyroxene -bearing band
DIS	Disseminated mineralization	POD	Pod
BAN	Bands of oxide mineralization	OPOD	Orthopyroxene -bearing pod
ANO	Anorthosite hosted disseminated	VEIN	Vein
ORT	Orthopyroxene associated	COMP	composite ilmenite
CLI	Clinopyroxene associated	SAN	sandwich ilmenite

Appendix V (Continued)

Sample	CC013	CC013	CC013	CC013	CC013	CC013
Circle number	A	A	A	B	B	C
Analysis number	13-A-S2	13-A-I1	13-A-I2	13-B-I2	13-B-I3	13-C-S1
Mineralization style	MAS	MAS	MAS	MAS	MAS	MAS
Descriptor	BAN	BAN	BAN	BAN	BAN	BAN
Ilmenite texture	SAN	COMP	COMP	COMP	SAN	SAN
Exsolution?	n	y	y	y	n	n
Ti wt. % (EPMA)	30.62	29.5	29.7	29.3	29.2	28.4
^{24}Mg	9647	9575	9978	9816	9670	9145
^{27}Al	239	573	240	366	1060	317
^{29}Si	350	473	178	559	334	1057
^{31}P	<MDL	<MDL	<MDL	4	<MDL	10
^{44}Ca	<MDL	28	<MDL	11	<MDL	32
^{45}Sc	39	44	41	45	41	33
^{51}V	1146	2208	2033	2329	1926	1443
^{52}Cr	146	236	247	256	198	241
^{55}Mn	6952	6157	6190	5786	6259	6582
^{57}Fe	369800	439200	438900	479300	420900	391300
^{59}Co	95	85	95	96	98	96
^{60}Ni	43	45	46	56	48	60
^{63}Cu	3	2	2	2	2	3
^{65}Cu	6	5	5	5	5	6
^{69}Ga	1	2	1	2	1	3
^{74}Ge	<MDL	0.2	0.2	0.2	0.1	0.2
^{75}As	<MDL	1	1	1	1	1
^{89}Y	0.1	0.1	0.1	0.1	0.2	0.1
^{90}Zr	24	46	57	62	109	22
^{93}Nb	5	7	6	6	6	5
^{95}Mo	0.4	1	1	1	1	0.4
^{118}Sn	0.3	3	2	2	1	1
^{121}Sb	0.1	0.1	0.1	0.1	0.1	0.1
^{178}Hf	1	2	2	2	2	1
^{181}Ta	0.4	0.4	0.4	0.5	0.4	0.3
^{182}W	0.1	0.05	0.1	0.1	0.1	0.1
^{208}Pb	2	2	1	1	1	2

MAS	Massive to semi-massive mineralization	OBAN	Orthopyroxene -bearing band
DIS	Disseminated mineralization	POD	Pod
BAN	Bands of oxide mineralization	OPOD	Orthopyroxene -bearing pod
ANO	Anorthosite hosted disseminated	VEIN	Vein
ORT	Orthopyroxene associated	COMP	composite ilmenite
CLI	Clinopyroxene associated	SAN	sandwich ilmenite

Appendix V (Continued)

Sample	CC013	CC013	CC013	CC013	CC013	CC013	CC013
Circle number	E	F	F	D	D	E	L
Analysis number	13-E-I1	13-F-I1	13-F-12	13-D-I1	13-D-I2	13-E-I2	13-L-I1
Mineralization style	MAS	MAS	MAS	MAS	MAS	MAS	MAS
Descriptor	BAN	BAN	BAN	BAN	BAN	BAN	BAN
Ilmenite texture	COMP	COMP	COMP	COMP	COMP	COMP	COMP
Exsolution?	y	y	y	y	y	n	y
Ti wt. % (EPMA)	29.7	29.6	29.6	31.0	29.0	29.4	29.0
^{24}Mg	9900	9780	9830	10609	9891	10250	9437
^{27}Al	298	234	296	523	460	479	422
^{29}Si	970	690	<MDL	458	446	279	<MDL
^{31}P	<MDL	<MDL	<MDL	5	<MDL	3	<MDL
^{44}Ca	<MDL	<MDL	<MDL	11	12	9	<MDL
^{45}Sc	45	48	46	49	45	45	43
^{51}V	1872	1770	1612	2800	2480	1861	2197
^{52}Cr	279	234	222	312	267	270	200
^{55}Mn	5700	5896	5933	6019	5532	6027	6045
^{57}Fe	527000	507400	503000	579300	518000	497300	435700
^{59}Co	101	100	102	97	90	110	88
^{60}Ni	49	45	45	48	48	76	43
^{63}Cu	3	4	4	4	3	3	2
^{65}Cu	7	6	6	6	5	6	5
^{69}Ga	2	2	2	3	3	4	2
^{74}Ge	0.5	<MDL	0.4	0.2	0.2	0.1	0.2
^{75}As	<MDL	<MDL	1	1	1	1	1
^{89}Y	0.1	0.1	0.1	0.1	0.1	0.1	0.1
^{90}Zr	149	223	207	107	56	63	48
^{93}Nb	7	6	7	8	7	7	6
^{95}Mo	0.4	1	1	1	1	1	1
^{118}Sn	2	2	2	4	3	2	2
^{121}Sb	0.2	0.2	0.1	0.1	0.1	0.1	0.1
^{178}Hf	3	4	3	3	2	2	2
^{181}Ta	0.4	0.4	0.4	0.5	0.5	0.4	0.3
^{182}W	0.1	0.1	0.04	0.04	0.1	0.05	0.1
^{208}Pb	3	2	2	3	2	2	2

MAS	Massive to semi-massive mineralization	OBAN	Orthopyroxene -bearing band
DIS	Disseminated mineralization	POD	Pod
BAN	Bands of oxide mineralization	OPOD	Orthopyroxene -bearing pod
ANO	Anorthosite hosted disseminated	VEIN	Vein
ORT	Orthopyroxene associated	COMP	composite ilmenite
CLI	Clinopyroxene associated	SAN	sandwich ilmenite

Appendix V (Continued)

Sample	CC013	CC013	CC013	CC025	CC025	CC025
Circle number	L	P	R	A	A	B
Analysis number	13-L-I2	13-P-S1	13-R-S1	25-A-I1	25-A-I2	25-B-I1
Mineralization style	MAS	MAS	MAS	MAS	MAS	MAS
Descriptor	BAN	BAN	BAN	POD	POD	POD
Ilmenite texture	COMP	SAN	SAN	COMP	COMP	COMP
Exsolution?	y	n	n	y	n	y
Ti wt. % (EPMA)	28.8	29.4	30.58	29.3	29.6	29.7
^{24}Mg	9525	8810	9605	7065	6882	7580
^{27}Al	790	178	144	511	274	291
^{29}Si	<MDL	377	<BDL	367	<MDL	<MDL
^{31}P	<MDL	4	14	<MDL	<MDL	<MDL
^{44}Ca	<MDL	11	<MDL	<MDL	<MDL	<MDL
^{45}Sc	41	49	36	28	25	22
^{51}V	1920	1553	1089	985	822	709
^{52}Cr	186	256	122	183	192	69
^{55}Mn	6112	8904	7515	2690	2756	2581
^{57}Fe	408800	385000	368300	406100	390100	377500
^{59}Co	90	90	95	98	97	106
^{60}Ni	44	46	48	52	52	52
^{63}Cu	2	2	3	5	4	4
^{65}Cu	5	5	5	10	10	7
^{69}Ga	2	1	1	1	1	1
^{74}Ge	0.2	0.2	<MDL	0.1	0.1	0.1
^{75}As	1	0.5	<MDL	0.3	<MDL	0.3
^{89}Y	0.1	0.1	0.1	0.1	0.1	0.1
^{90}Zr	53	32	19	150	124	113
^{93}Nb	5	4	5	23	23	32
^{95}Mo	1	1	1	0.5	0.5	1
^{118}Sn	1	1	0.3	3	2	3
^{121}Sb	0.1	0.1	0.04	0.1	0.1	0.1
^{178}Hf	1	1	1	5	4	4
^{181}Ta	0.3	0.2	0.3	1	1	2
^{182}W	0.1	0.04	0.1	0.1	0.1	0.1
^{208}Pb	2	2	3	1	0.5	0.5

MAS	Massive to semi-massive mineralization	OBAN	Orthopyroxene -bearing band
DIS	Disseminated mineralization	POD	Pod
BAN	Bands of oxide mineralization	OPOD	Orthopyroxene -bearing pod
ANO	Anorthosite hosted disseminated	VEIN	Vein
ORT	Orthopyroxene associated	COMP	composite ilmenite
CLI	Clinopyroxene associated	SAN	sandwich ilmenite

Appendix V (Continued)

Sample	CC025	CC025	CC025	CC025	CC025	CC025	CC025
Circle number	B	C	C	D	D	E	E
Analysis number	25-B-I2	25-C-S1	25-C-S2	25-D-I1	25-D-I2	25-E-I1	25-E-I2
Mineralization style	MAS	MAS	MAS	MAS	MAS	MAS	MAS
Descriptor	POD	POD	POD	POD	POD	POD	POD
Ilmenite texture	COMP	SAN	SAN	COMP	COMP	COMP	COMP
Exsolution?	y	n	n	n	n	n	n
Ti wt. % (EPMA)	29.4	30.5	30.5	30.3	30.3	30.3	30.1
^{24}Mg	7300	4765	4815	5137	5500	5170	5236
^{27}Al	349	124	124	174	147	158	151
^{29}Si	362	485	435	470	339	<MDL	<MDL
^{31}P	<MDL	<MDL	<MDL	<MDL	<MDL	<MDL	<MDL
^{44}Ca	<MDL	<MDL	10	<MDL	9	<MDL	<MDL
^{45}Sc	27	21	20	20	18	20	20
^{51}V	946	392	374	454	393	390	394
^{52}Cr	113	130	129	123	104	144	146
^{55}Mn	2446	4326	4227	3940	3935	4259	4313
^{57}Fe	404600	386300	379600	387300	386800	381700	387000
^{59}Co	107	85	88	92	95	87	90
^{60}Ni	53	48	49	51	53	46	48
^{63}Cu	4	3	3	11	2	1	1
^{65}Cu	8	7	6	5	5	4	4
^{69}Ga	1	0.3	0.3	0.3	0.3	0.4	0.3
^{74}Ge	0.1	<MDL	0.1	0.1	0.1	0.1	0.1
^{75}As	<MDL	<MDL	<MDL	0.2	0.3	1	<MDL
^{89}Y	0.1	0.1	0.1	0.1	0.1	0.1	0.1
^{90}Zr	152	62	59	65	56	54	53
^{93}Nb	35	17	22	18	23	19	19
^{95}Mo	0.5	0.5	1	0.4	0.4	0.4	0.4
^{118}Sn	3	2	1	2	1	2	1
^{121}Sb	0.2	0.04	0.05	0.1	0.03	0.02	0.02
^{178}Hf	6	3	2	3	2	2	2
^{181}Ta	2	1	1	1	1	1	1
^{182}W	0.1	0.1	0.1	0.05	0.1	0.1	0.1
^{208}Pb	0.4	1	1	0.5	0.3	0.4	0.3

MAS	Massive to semi-massive mineralization	OBAN	Orthopyroxene -bearing band
DIS	Disseminated mineralization	POD	Pod
BAN	Bands of oxide mineralization	OPOD	Orthopyroxene -bearing pod
ANO	Anorthosite hosted disseminated	VEIN	Vein
ORT	Orthopyroxene associated	COMP	composite ilmenite
CLI	Clinopyroxene associated	SAN	sandwich ilmenite

Appendix V (Continued)

Sample	CC025	CC025	CC025	CC025	CC025	CC025	CC025
Circle number	G	G	G	G	I	I	K
Analysis number	25-G-S1	25-G-S2	25-G-I1	25-G-I2	25-I-I1	25-I-I2	25-K-I1
Mineralization style	MAS	MAS	MAS	MAS	MAS	MAS	MAS
Descriptor	POD	POD	POD	POD	POD	POD	POD
Ilmenite texture	SAN	SAN	COMP	COMP	COMP	COMP	COMP
Exsolution?	n	n	n	n	n	n	y
Ti wt. % (EPMA)	30.2	30.4	30.2	30.0	29.7	29.86	29
^{24}Mg	4755	5212	5123	5051	4722	4247	6526
^{27}Al	142	152	217	241	327	580	310
^{29}Si	<MDL	181	<MDL	251	422	171	289
^{31}P	<MDL	<MDL	<MDL	<MDL	<MDL	<MDL	<MDL
^{44}Ca	<MDL	<MDL	<MDL	<MDL	14	<MDL	20
^{45}Sc	20	20	22	24	24	24	25
^{51}V	382	390	479	538	539	461	888
^{52}Cr	110	117	160	183	267	241	155
^{55}Mn	4371	4213	3894	3942	3580	3850	2606
^{57}Fe	379700	389500	390600	392800	390000	384000	397100
^{59}Co	83	92	89	89	88	82	99
^{60}Ni	43	47	46	46	48	46	48
^{63}Cu	2	2	2	2	2	3	2
^{65}Cu	4	4	4	5	4	5	4
^{69}Ga	0.3	0.4	0.5	1	1	1	1
^{74}Ge	<MDL	<MDL	0.1	0.1	0.1	<MDL	0.1
^{75}As	0.2	0.2	0.3	<MDL	0.3	0.3	0.2
^{89}Y	0.1	0.1	0.1	0.1	0.1	0.1	0.1
^{90}Zr	50	56	66	72	75	60	106
^{93}Nb	15	19	18	20	19	12	21
^{95}Mo	0.4	0.5	0.5	0.4	0.5	0.4	1
^{118}Sn	2	2	2	2	2	2	3
^{121}Sb	0.02	0.04	0.04	0.1	0.1	0.03	0.1
^{178}Hf	2	2	3	3	3	3	4
^{181}Ta	0.4	0.5	0.5	1	0.5	0.2	1
^{182}W	0.02	0.02	0.03	0.03	0.02	0.01	0.05
^{208}Pb	0.4	0.3	1	1	1	1	0.4

MAS	Massive to semi-massive mineralization	OBAN	Orthopyroxene -bearing band
DIS	Disseminated mineralization	POD	Pod
BAN	Bands of oxide mineralization	OPOD	Orthopyroxene -bearing pod
ANO	Anorthosite hosted disseminated	VEIN	Vein
ORT	Orthopyroxene associated	COMP	composite ilmenite
CLI	Clinopyroxene associated	SAN	sandwich ilmenite

Appendix V (Continued)

Sample	CC025	CC025	CC025	CC025	CC031	CC031	CC031	CC031
Circle number	K	L	L	L	B	C	C	F
Analysis number	25-K-I3	25-L-I1	25-L-I2	25-L-I3	31-B-I1	31-C-I1	31-C-I2	31-F-I1
Mineralization style	MAS	MAS	MAS	MAS	DIS	DIS	DIS	DIS
Descriptor	POD	POD	POD	POD	ANO	ANO	ANO	ANO
Ilmenite texture	COMP	COMP	COMP	COMP	COMP	COMP	COMP	COMP
Exsolution?	y	y	y	y	n	y	y	y
Ti wt. % (EPMA)	29.2	29.1	29.2	29.0	29.49	29.7	29.6	28.59
^{24}Mg	6590	4783	4809	5141	2089	4645	4729	4998
^{27}Al	441	220	557	175	310	203	154	307
^{29}Si	118	235	262	233	488	<MDL	314	394
^{31}P	<MDL	<MDL	<MDL	<MDL	<MDL	<MDL	<MDL	<MDL
^{44}Ca	<MDL	<MDL	<MDL	<MDL	12	<MDL	<MDL	12
^{45}Sc	25	24	20	20	29	30	29	31
^{51}V	954	563	418	505	433	519	489	642
^{52}Cr	169	218	138	95	216	286	255	141
^{55}Mn	2634	3743	4198	3627	9711	5883	5787	5378
^{57}Fe	399100	383600	368900	371200	360200	386200	384200	389000
^{59}Co	101	88	83	92	47	73	76	80
^{60}Ni	51	50	46	50	53	81	82	80
^{63}Cu	1	3	3	2	3	2	1	2
^{65}Cu	4	5	6	5	5	4	4	4
^{69}Ga	1	0.5	1	0.4	1	1	1	1
^{74}Ge	0.1	0.1	0.1	0.1	<MDL	0.1	0.1	0.1
^{75}As	<MDL	<MDL	<MDL	0.3	1	1	1	1
^{89}Y	0.1	0.1	0.1	0.1	0.1	0.1	0.2	0.1
^{90}Zr	114	78	58	68	47	111	105	151
^{93}Nb	22	19	17	20	3	15	15	18
^{95}Mo	1	0.5	0.5	1	1	1	1	1
^{118}Sn	3	2	1	2	2	2	2	2
^{121}Sb	0.1	0.1	0.04	0.05	0.1	0.2	0.2	0.2
^{178}Hf	4	3	2	3	2	4	3	5
^{181}Ta	1	0.5	0.5	1	0.1	1	1	1
^{182}W	0.1	0.04	0.04	0.03	0.2	3	3	1
^{208}Pb	0.4	1	1	1	1	1	1	1

MAS	Massive to semi-massive mineralization	OBAN	Orthopyroxene -bearing band
DIS	Disseminated mineralization	POD	Pod
BAN	Bands of oxide mineralization	OPOD	Orthopyroxene -bearing pod
ANO	Anorthosite hosted disseminated	VEIN	Vein
ORT	Orthopyroxene associated	COMP	composite ilmenite
CLI	Clinopyroxene associated	SAN	sandwich ilmenite

Appendix V (Continued)

Sample	CC031	CC031	CC031	CC031	CC054	CC054	CC054
Circle number	H	H	I	I	C	C	D
Analysis number	31-H-I1	31-H-I2	31-I-I1	31-I-I2	54-C-I1	54-C-I2	54-D-I1
Mineralization style	DIS	DIS	DIS	DIS	DIS	DIS	DIS
Descriptor	ANO	ANO	ANO	ANO	ORT	ORT	ORT
Ilmenite texture	COMP	COMP	COMP	COMP	COMP	COMP	COMP
Exsolution?	y	y	y	y	y	y	y
Ti wt. % (EPMA)	28.1	28.3	29.4	29.5	30.2	30.2	30.8
^{24}Mg	4919	4963	5035	4927	7715	7611	7372
^{27}Al	242	243	243	276	274	234	325
^{29}Si	223	161	123	<MDL	<MDL	<MDL	650
^{31}P	<MDL	<MDL	<MDL	<MDL	<MDL	<MDL	7
^{44}Ca	<MDL	<MDL	<MDL	<MDL	<MDL	<MDL	<MDL
^{45}Sc	30	28	33	36	25	25	33
^{51}V	604	518	682	786	521	533	706
^{52}Cr	151	129	112	140	91	92	89
^{55}Mn	5194	5115	5531	5590	4102	4156	3864
^{57}Fe	381200	365200	396700	406900	411000	403000	412500
^{59}Co	78	77	78	79	122	119	111
^{60}Ni	80	78	81	79	70	67	65
^{63}Cu	2	1	2	2	5	4	3
^{65}Cu	4	4	4	4	14	9	8
^{69}Ga	1	1	1	1	1	1	1
^{74}Ge	0.1	0.1	0.1	0.1	0.1	<MDL	0.1
^{75}As	1	1	1	1	1	1	1
^{89}Y	0.2	0.2	0.2	0.2	0.1	0.1	0.2
^{90}Zr	143	125	162	187	74	84	138
^{93}Nb	19	19	18	18	26	29	35
^{95}Mo	1	1	1	1	0.4	0.4	0.4
^{118}Sn	2	2	2	2	3	2	3
^{121}Sb	0.3	0.2	0.3	0.3	0.1	0.1	0.03
^{178}Hf	4	4	5	5	3	3	5
^{181}Ta	1	1	1	1	1	1	2
^{182}W	1	1	0.1	0.2	0.1	0.1	0.1
^{208}Pb	1	1	0.5	0.4	2	2	1

MAS	Massive to semi-massive mineralization	OBAN	Orthopyroxene -bearing band
DIS	Disseminated mineralization	POD	Pod
BAN	Bands of oxide mineralization	OPOD	Orthopyroxene -bearing pod
ANO	Anorthosite hosted disseminated	VEIN	Vein
ORT	Orthopyroxene associated	COMP	composite ilmenite
CLI	Clinopyroxene associated	SAN	sandwich ilmenite

Appendix V (Continued)

Sample	CC054	CC054	CC054	CC054	CC054	CC054	CC054
Circle number	D	D	E	G	G	L	L
Analysis number	54-D-I2	54-D-I3	54-E-I2	54-G-I1	54-G-I2	54-L-I1	54-L-I2
Mineralization style	DIS	DIS	DIS	DIS	DIS	DIS	DIS
Descriptor	ORT	ORT	ORT	ORT	ORT	ORT	ORT
Ilmenite texture	COMP	COMP	COMP	COMP	COMP	COMP	COMP
Exsolution?	y	y	y	y	y	y	y
Ti wt. % (EPMA)	30.6	30.8	30.9	30.0	29.8	29.6	29.6
^{24}Mg	7284	7180	6993	7257	7372	6829	6915
^{27}Al	154	416	306	291	243	256	257
^{29}Si	540	621	293	628	388	586	483
^{31}P	<MDL	6	<MDL	6	<MDL	<MDL	<MDL
^{44}Ca	<MDL	33	<MDL	27	<MDL	15	17
^{45}Sc	23	27	29	25	26	27	26
^{51}V	395	681	624	439	481	573	575
^{52}Cr	70	81	110	65	66	100	101
^{55}Mn	4567	4203	3982	4187	4064	3834	3949
^{57}Fe	393400	415400	402500	379900	388600	392300	398000
^{59}Co	114	118	112	111	112	108	111
^{60}Ni	63	74	69	64	65	61	63
^{63}Cu	3	4	3	3	3	1	1
^{65}Cu	7	9	6	7	6	4	4
^{69}Ga	0.4	1	1	1	1	1	1
^{74}Ge	0.1	0.1	0.1	0.1	0.1	0.1	0.1
^{75}As	1	1	1	1	1	1	1
^{89}Y	0.2	0.2	0.2	0.2	0.2	0.1	0.2
^{90}Zr	75	124	106	70	81	92	85
^{93}Nb	24	34	27	27	30	29	27
^{95}Mo	0.4	1	0.5	0.4	0.4	0.5	0.4
^{118}Sn	2	3	2	2	2	2	2
^{121}Sb	0.04	0.04	0.03	0.04	0.03	0.01	<MDL
^{178}Hf	3	5	4	3	3	3	3
^{181}Ta	1	2	1	1	1	1	1
^{182}W	0.1	0.1	0.05	0.1	0.1	0.1	0.1
^{208}Pb	1	2	1	1	1	0.2	0.2

MAS	Massive to semi-massive mineralization	OBAN	Orthopyroxene -bearing band
DIS	Disseminated mineralization	POD	Pod
BAN	Bands of oxide mineralization	OPOD	Orthopyroxene -bearing pod
ANO	Anorthosite hosted disseminated	VEIN	Vein
ORT	Orthopyroxene associated	COMP	composite ilmenite
CLI	Clinopyroxene associated	SAN	sandwich ilmenite

Appendix V (Continued)

Sample	CC054	CC054	CC072	CC072	CC072	CC072	CC072
Circle number	O	O	A	A	B	C	C
Analysis number	54-O-I1	54-O-I2	72-A-I1	72-A-I2	72-B-I2	72-C-I1	72-C-I2
Mineralization style	DIS	DIS	MAS	MAS	MAS	MAS	MAS
Descriptor	ORT	ORT	OPOD	OPOD	OPOD	OPOD	OPOD
Ilmenite texture	COMP	COMP	COMP	COMP	COMP	COMP	COMP
Exsolution?	y	y	n	n	n	n	n
Ti wt. % (EPMA)	28.9	28.8	30.1	30.2	30.4	29.6	29.7
^{24}Mg	7289	7135	20800	20600	20960	19730	19870
^{27}Al	404	358	1627	448	156	293	252
^{29}Si	415	280	245	293	558	137	158
^{31}P	<MDL	<MDL	<MDL	4	<MDL	<MDL	<MDL
^{44}Ca	<MDL	<MDL	<MDL	9	32	<MDL	<MDL
^{45}Sc	25	30	70	73	67	71	73
^{51}V	613	733	431	399	379	416	383
^{52}Cr	89	74	125	87	64	112	120
^{55}Mn	3826	3669	6870	6535	6035	6114	6317
^{57}Fe	390800	393900	357900	348000	341500	339900	339200
^{59}Co	111	113	121	120	118	117	116
^{60}Ni	73	66	58	55	52	54	52
^{63}Cu	3	3	3	3	1	2	2
^{65}Cu	5	6	6	6	4	5	5
^{69}Ga	2	1	2	1	0.3	1	1
^{74}Ge	<MDL	0.1	0.1	0.1	0.1	0.1	0.1
^{75}As	1	1	1	1	1	1	1
^{89}Y	0.1	0.1	0.1	0.2	0.2	0.2	0.2
^{90}Zr	99	128	124	129	120	129	130
^{93}Nb	39	40	4	5	5	5	4
^{95}Mo	0.4	0.3	0.4	0.4	0.4	0.4	0.3
^{118}Sn	2	3	2	2	2	1	2
^{121}Sb	0.03	0.04	0.1	0.1	0.04	0.1	0.03
^{178}Hf	4	4	4	4	4	4	4
^{181}Ta	2	2	0.1	0.1	0.1	0.1	0.1
^{182}W	0.1	0.1	0.02	0.01	0.01	0.01	0.01
^{208}Pb	1	1	1	1	1	1	1

MAS	Massive to semi-massive mineralization	OBAN	Orthopyroxene -bearing band
DIS	Disseminated mineralization	POD	Pod
BAN	Bands of oxide mineralization	OPOD	Orthopyroxene -bearing pod
ANO	Anorthosite hosted disseminated	VEIN	Vein
ORT	Orthopyroxene associated	COMP	composite ilmenite
CLI	Clinopyroxene associated	SAN	sandwich ilmenite

Appendix V (Continued)

Sample	CC072	CC072	CC072	CC072	CC072	CC072	CC072
Circle number	D	D	E	E	G	G	H
Analysis number	72-D-I1	72-D-I3	72-E-I1	72-E-I2	72-G-I1	72-G-I2	72-H-I2
Mineralization style	MAS	MAS	MAS	MAS	MAS	MAS	MAS
Descriptor	OPOD	OPOD	OPOD	OPOD	OPOD	OPOD	OPOD
Ilmenite texture	COMP	COMP	COMP	COMP	COMP	COMP	COMP
Exsolution?	n	n	n	n	n	n	n
Ti wt. % (EPMA)	31.1	31.0	31.0	31.0	31.0	31.3	31.0
^{24}Mg	22270	21430	28670	23680	22300	21490	20820
^{27}Al	175	187	15700	6950	451	264	245
^{29}Si	406	218	360	552	301	<MDL	445
^{31}P	<MDL	<MDL	<MDL	5	<MDL	<MDL	4
^{44}Ca	<MDL	<MDL	<MDL	<MDL	<MDL	<MDL	10
^{45}Sc	53	63	56	68	51	76	71
^{51}V	311	382	373	417	546	557	540
^{52}Cr	88	69	268	209	69	63	39
^{55}Mn	6274	6170	6710	6583	6463	5946	5667
^{57}Fe	335900	343800	368800	362700	375900	360900	353100
^{59}Co	121	119	165	146	130	123	123
^{60}Ni	54	53	105	79	71	58	55
^{63}Cu	2	2	3	6	2	1	1
^{65}Cu	6	6	7	10	5	5	4
^{69}Ga	0.4	0.4	13	7	2	1	1
^{74}Ge	0.1	0.1	<MDL	0.1	0.1	0.1	0.2
^{75}As	1	1	1	1	1	0.4	1
^{89}Y	0.2	0.2	0.1	0.2	0.2	0.1	0.2
^{90}Zr	91	112	91	114	120	139	155
^{93}Nb	4	5	5	5	5	5	9
^{95}Mo	0.4	0.4	1	0.5	0.4	0.5	0.4
^{118}Sn	1	1	1	1	2	2	2
^{121}Sb	0.03	0.1	0.1	0.1	0.04	0.02	0.04
^{178}Hf	3	4	3	3	5	4	4
^{181}Ta	0.1	0.1	0.1	0.1	0.2	0.2	0.4
^{182}W	0.01	0.01	0.01	0.01	0.00	0.01	0.01
^{208}Pb	1	1	2	1	2	1	1

MAS	Massive to semi-massive mineralization	OBAN	Orthopyroxene -bearing band
DIS	Disseminated mineralization	POD	Pod
BAN	Bands of oxide mineralization	OPOD	Orthopyroxene -bearing pod
ANO	Anorthosite hosted disseminated	VEIN	Vein
ORT	Orthopyroxene associated	COMP	composite ilmenite
CLI	Clinopyroxene associated	SAN	sandwich ilmenite

Appendix V (Continued)

Sample	CC074	CC074	CC074	CC074	CC074	CC074	CC074
Circle number	A	A	A	B	B	C	C
Analysis number	74-A-I1	74-A-I2	74-A-I4	74-B-I1	74-B-I2	74-C-I1	74-C-I2
Mineralization style	DIS	DIS	DIS	DIS	DIS	DIS	DIS
Descriptor	CLI	CLI	CLI	CLI	CLI	CLI	CLI
Ilmenite texture	COMP	COMP	COMP	COMP	COMP	COMP	COMP
Exsolution?	y	y	y	n	n	n	n
Ti wt. % (EPMA)	29.2	29.3	29.2	29.2	29.4	29.4	29.3
^{24}Mg	3079	3150	3205	2469	2664	3000	2715
^{27}Al	258	245	18070	143	155	812	385
^{29}Si	1450	<MDL	430	1490	990	1107	651
^{31}P	14	<MDL	<MDL	200	9	<MDL	<MDL
^{44}Ca	18	<MDL	24	500	15	32	15
^{45}Sc	32	32	27	32	31	29	27
^{51}V	925	944	811	903	900	850	900
^{52}Cr	406	402	1169	347	337	304	292
^{55}Mn	9853	9830	10160	10788	11170	9730	9120
^{57}Fe	434800	444100	405200	404500	411500	411300	419100
^{59}Co	92	97	205	83	88	73	90
^{60}Ni	49	54	102	45	48	32	36
^{63}Cu	2	2	2	2	2	2	10
^{65}Cu	6	6	6	10	6	6	13
^{69}Ga	2	2	32	1	1	1	1
^{74}Ge	0.1	0.2	0.2	0.2	0.2	0.1	0.2
^{75}As	2	2	2	2	1	2	2
^{89}Y	0.1	0.2	0.2	0.3	0.1	0.2	0.3
^{90}Zr	52	51	25	36	34	47	43
^{93}Nb	16	17	5	11	11	14	14
^{95}Mo	1	1	1	1	1	1	1
^{118}Sn	3	3	3	3	3	2	3
^{121}Sb	0.1	0.1	0.1	0.1	0.1	0.1	0.1
^{178}Hf	2	2	1	1	2	2	2
^{181}Ta	1	1	0.1	0.4	0.4	1	0.5
^{182}W	0.04	0.1	0.01	0.02	0.02	0.03	0.04
^{208}Pb	2	2	2	2	1	1	2

MAS	Massive to semi-massive mineralization	OBAN	Orthopyroxene -bearing band
DIS	Disseminated mineralization	POD	Pod
BAN	Bands of oxide mineralization	OPOD	Orthopyroxene -bearing pod
ANO	Anorthosite hosted disseminated	VEIN	Vein
ORT	Orthopyroxene associated	COMP	composite ilmenite
CLI	Clinopyroxene associated	SAN	sandwich ilmenite

Appendix V (Continued)

Sample	CC074	CC074	CC074	CC074	CC074	CC076	CC076
Circle number	D	D	E	E	F	B	C
Analysis number	74-D-I1	74-D-13	74-E-I1	74-E-I2	74-F-I1	76-B-I1	76-C-I1
Mineralization style	DIS	DIS	DIS	DIS	DIS	MAS	MAS
Descriptor	CLI	CLI	CLI	CLI	CLI	VEIN	VEIN
Ilmenite texture	COMP	COMP	COMP	COMP	COMP	COMP	SAN
Exsolution?	y	n	y	y	n	n	y
Ti wt. % (EPMA)	28.7	28.7	29.3	29.2	28.6	28.4	28.3
^{24}Mg	3076	3433	3915	3742	2578	5558	5521
^{27}Al	2570	160	402	260	324	237	3460
^{29}Si	3760	804	<MDL	<MDL	528	385	282
^{31}P	<MDL	5	<MDL	<MDL	<MDL	<MDL	<MDL
^{44}Ca	870	13	<MDL	<MDL	<MDL	<MDL	24
^{45}Sc	29	27	29	31	25	52	54
^{51}V	769	712	843	813	947	1393	1420
^{52}Cr	273	288	432	405	417	267	733
^{55}Mn	12530	7906	7310	7131	9651	9928	11023
^{57}Fe	412000	384400	409800	421300	418800	400400	370600
^{59}Co	120	94	105	103	100	68	79
^{60}Ni	56	39	45	46	42	18	19
^{63}Cu	7	1	1	2	5	1	6
^{65}Cu	11	5	5	5	8	4	9
^{69}Ga	5	1	2	2	2	1	7
^{74}Ge	0.2	0.1	0.1	0.1	0.1	0.2	0.1
^{75}As	2	2	1	1	2	0.5	1
^{89}Y	0.2	0.1	0.1	0.1	0.1	0.1	0.1
^{90}Zr	46	26	39	52	26	13	6
^{93}Nb	19	13	14	19	18	15	12
^{95}Mo	1	1	1	0.5	1	1	1
^{118}Sn	2	2	2	2	2	0.1	0.03
^{121}Sb	0.1	0.04	0.04	0.02	0.1	0.2	0.1
^{178}Hf	2	1	2	2	1	0.5	0.1
^{181}Ta	1	1	1	1	1	0.5	0.3
^{182}W	0.1	0.03	0.03	0.04	0.1	0.2	0.1
^{208}Pb	2	2	1	1	2	1	1

MAS	Massive to semi-massive mineralization	OBAN	Orthopyroxene -bearing band
DIS	Disseminated mineralization	POD	Pod
BAN	Bands of oxide mineralization	OPOD	Orthopyroxene -bearing pod
ANO	Anorthosite hosted disseminated	VEIN	Vein
ORT	Orthopyroxene associated	COMP	composite ilmenite
CLI	Clinopyroxene associated	SAN	sandwich ilmenite

Appendix V (Continued)

Sample	CC076	CC076	CC076	CC076	CC076	CC076
Circle number	D	D	D	F	G	K
Analysis number	76-D-I1	76-D-I2	76-D-I3	76-F-I1	76-G-I1	76-K-I1
Mineralization style	MAS	MAS	MAS	MAS	MAS	MAS
Descriptor	VEIN	VEIN	VEIN	VEIN	VEIN	VEIN
Ilmenite texture	COMP	COMP	COMP	COMP	COMP	COMP
Exsolution?	y	y	y	y	y	y
Ti wt. % (EPMA)	29.9	28.9	29.1	29.0	28.3	28.4
^{24}Mg	5787	5539	5535	5547	5286	5556
^{27}Al	351	310	311	279	249	1220
^{29}Si	1990	424	481	390	264	234
^{31}P	17	5	<MDL	<MDL	<MDL	<MDL
^{44}Ca	81	12	<MDL	<MDL	<MDL	<MDL
^{45}Sc	61	68	67	62	67	69
^{51}V	1896	1698	1633	2012	1633	1864
^{52}Cr	315	252	262	224	276	295
^{55}Mn	9050	8545	8576	8670	8229	8519
^{57}Fe	521800	472100	477800	498400	456000	468800
^{59}Co	76	68	68	70	65	71
^{60}Ni	19	17	16	14	15	19
^{63}Cu	3	1	1	2	1	1
^{65}Cu	5	3	4	4	4	4
^{69}Ga	3	2	2	2	2	3
^{74}Ge	0.2	0.2	0.2	<MDL	0.2	0.1
^{75}As	<MDL	1	1	1	0.3	0.4
^{89}Y	0.1	0.1	0.1	0.1	0.1	0.1
^{90}Zr	17	26	26	30	27	25
^{93}Nb	20	19	18	18	19	15
^{95}Mo	1	1	1	1	1	1
^{118}Sn	3	2	2	2	2	2
^{121}Sb	0.3	0.2	0.2	0.2	0.2	0.2
^{178}Hf	1	2	2	2	2	2
^{181}Ta	1	1	1	1	1	0.4
^{182}W	0.1	0.03	0.03	0.04	0.02	0.03
^{208}Pb	2	1	1	1	1	1

MAS	Massive to semi-massive mineralization	OBAN	Orthopyroxene -bearing band
DIS	Disseminated mineralization	POD	Pod
BAN	Bands of oxide mineralization	OPOD	Orthopyroxene -bearing pod
ANO	Anorthosite hosted disseminated	VEIN	Vein
ORT	Orthopyroxene associated	COMP	composite ilmenite
CLI	Clinopyroxene associated	SAN	sandwich ilmenite

Appendix V (Continued)

Sample	CC008	CC008	CC008	CC008	CC008	CC010
Circle	B	B	D	D	H	A
Source file	08-B-H1.D	08-B-H2.D	08-D-H1.D	08-D-H2.D	08-H-H2.D	10-A-H1.D
Mineralization type	MAS	MAS	MAS	MAS	MAS	MAS
Descriptor	BAN	BAN	BAN	BAN	BAN	OBAN
Mineral host	PLE	PLE	PLE	PLE	ILM	PLE
Mineral analyzed	PLE	PLE	PLE	PLE	PLE	PLE
Al wt. % (EPMA)*	31.0	31.0	30.7	30.7	30.8	31.3
^{24}Mg	138800	143400	140890	74400	73730	86900
^{29}Si	5020	4830	1240	<MDL	2300	900
^{31}P	39	70	<MDL	<MDL	<MDL	21
^{44}Ca	56	39	<MDL	<MDL	300	19
^{45}Sc	1	1	0.5	<MDL	2	<MDL
^{47}Ti	<MDL	<MDL	<MDL	780	22800	<MDL
^{51}V	1102	1375	1223	751	1780	793
^{52}Cr	3560	3622	4160	1923	3110	2275
^{55}Mn	3801	3799	3537	2056	2390	2500
^{57}Fe	517600	578400	534000	286000	464000	337000
^{59}Co	1473	1423	1500	940	1054	869
^{60}Ni	1660	1583	1506	909	963	1113
^{63}Cu	1	0.5	1	1	6	1
^{66}Zn	7480	8550	7990	5960	5710	8680
^{69}Ga	460	444	461	230	301	266
^{74}Ge	1	0.4	0.1	1	0.5	0.3
^{75}As	5	5	8	<MDL	1	2
^{89}Y	<MDL	<MDL	<MDL	<MDL	0.02	<MDL
^{90}Zr	0.05	0.03	0.1	0.1	2	0.03
^{93}Nb	<MDL	<MDL	<MDL	<MDL	0.4	<MDL
^{95}Mo	0.1	0.2	0.5	<MDL	0.1	0.1
^{118}Sn	0.01	0.2	<MDL	0.1	1	0.1
^{121}Sb	0.1	0.02	0.1	0.05	0.01	0.1
^{178}Hf	<MDL	<MDL	<MDL	<MDL	0.1	<MDL
^{181}Ta	<MDL	<MDL	<MDL	<MDL	0.03	<MDL
^{182}W	<MDL	<MDL	<MDL	0.00	<MDL	0.02
^{208}Pb	0.4	0.4	0.3	1	0.3	0.4

MAS	Massive to semi-massive mineralization	OBAN	Orthopyroxene -bearing band
DIS	Disseminated mineralization	POD	Pod
BAN	Bands of oxide mineralization	OPOD	Orthopyroxene -bearing pod
ANO	Anorthosite hosted disseminated	VEIN	Vein
ORT	Orthopyroxene associated	MAG	Magnetite
CLI	Clinopyroxene associated	ILM	Ilmenite PLE

* Internal calibrant was taken from EPMA analyses performed on the same grain as LA-ICPMS analyses; when LA-ICPMS analyses were performed on pleonaste without EPMA analyses, the internal calibrant used was the average of all texturally similar pleonaste in the sample

Appendix V (Continued)

Sample	CC010	CC010	CC010	CC010	CC010	CC010
Circle	A	B	B	E	H	I
Source file	10-A-H2.D	10-B-H1.D	10-B-H2.D	10-E-H1.D	10-H-H1.D	10-I-H1.D
Mineralization type	MAS	MAS	MAS	MAS	MAS	MAS
Descriptor	OBAN	OBAN	OBAN	OBAN	OBAN	OBAN
Mineral host	PLE	PLE	PLE	MAG	MAG	MAG
Mineral analyzed	PLE	PLE	PLE	PLE	PLE	PLE
Al wt. % (EPMA)*	31.3	31.2	31.2	32.2	31.8	31.8
^{24}Mg	78000	67240	95000	85670	84320	75200
^{29}Si	<MDL	<MDL	630	6030	2900	2030
^{31}P	6	<MDL	19	<MDL	<MDL	16
^{44}Ca	<MDL	<MDL	<MDL	22	79	<MDL
^{45}Sc	0.1	<MDL	<MDL	1	2	0.2
^{47}Ti	<MDL	<MDL	<MDL	4900	25300	1120
^{51}V	785	506	924	433	1380	1198
^{52}Cr	2120	2098	3150	2076	2642	2335
^{55}Mn	2122	1631	2600	2311	2964	1876
^{57}Fe	321000	227000	386000	262400	447000	361000
^{59}Co	827	719	1084	1410	1423	906
^{60}Ni	1071	832	1392	1121	1119	866
^{63}Cu	1	0.2	1	59	24	39
^{66}Zn	5970	3711	8600	4595	4860	3780
^{69}Ga	239	217	294	372	384	233
^{74}Ge	0.4	0.3	0.2	0.2	1	0.3
^{75}As	5	6	4	2	1	4
^{89}Y	<MDL	<MDL	<MDL	<MDL	<MDL	<MDL
^{90}Zr	0.03	0.01	0.02	2	3	0.1
^{93}Nb	<MDL	<MDL	<MDL	<MDL	<MDL	<MDL
^{95}Mo	0.1	0.1	0.1	0.1	0.2	0.2
^{118}Sn	0.1	0.1	0.02	0.3	1	0.4
^{121}Sb	0.1	0.04	0.02	0.00	-0.01	0.1
^{178}Hf	<MDL	<MDL	<MDL	0.03	0.1	0.01
^{181}Ta	<MDL	<MDL	<MDL	<MDL	<MDL	<MDL
^{182}W	0.01	<MDL	0.01	<MDL	<MDL	0.02
^{208}Pb	1	0.1	0.4	0.3	0.2	0.4

MAS	Massive to semi-massive mineralization	OBAN	Orthopyroxene -bearing band
DIS	Disseminated mineralization	POD	Pod
BAN	Bands of oxide mineralization	OPOD	Orthopyroxene -bearing pod
ANO	Anorthosite hosted disseminated	VEIN	Vein
ORT	Orthopyroxene associated	MAG	Magnetite
CLI	Clinopyroxene associated	ILM	Ilmenite
		PLE	Pleonaste

Appendix V (Continued)

Sample	CC010	CC013	CC013	CC013	CC025	CC025
Circle	M	A	I	L	A	D
Source file	10-M-H1.D	13-A-H1.D	13-I-H1.D	13-L-H1.D	25-A-H1.D	25-D-H2.D
Mineralization type	MAS	MAS	MAS	MAS	MAS	MAS
Descriptor	OBAN	BAN	BAN	BAN	POD	POD
Mineral host	MAG	MAG	PLE	PLE	MAG	PLE
Mineral analyzed	PLE	PLE	PLE	PLE	PLE	PLE
Al wt. % (EPMA)*	31.9	30.4	30.9	31.6	30.0	30.0
^{24}Mg	63800	65850	61270	63290	53760	47560
^{29}Si	6410	860	260	<MDL	2100	2590
^{31}P	8	<MDL	10	9	<MDL	<MDL
^{44}Ca	61	<MDL	22	<MDL	<MDL	24
^{45}Sc	1	0.4	<MDL	0.2	<MDL	1
^{47}Ti	2900	4450	<MDL	<MDL	720	<MDL
^{51}V	2560	546	577	545	598	484
^{52}Cr	3157	3560	2326	3120	6000	4067
^{55}Mn	1983	2125	2120	2020	1558	1607
^{57}Fe	577000	240600	227100	238900	369000	327000
^{59}Co	969	765	655	738	1405	1237
^{60}Ni	929	755	741	803	1207	1155
^{63}Cu	72	1	4	1	8	<MDL
^{66}Zn	3210	3164	3270	4100	5560	5580
^{69}Ga	331	206	221	217	413	363
^{74}Ge	1	0.3	0.4	0.3	<MDL	<MDL
^{75}As	3	3	4	3	<MDL	1
^{89}Y	0.03	<MDL	<MDL	<MDL	<MDL	<MDL
^{90}Zr	1	1	0.01	0.03	4	3
^{93}Nb	<MDL	<MDL	<MDL	<MDL	<MDL	<MDL
^{95}Mo	0.1	<MDL	0.2	0.2	0.3	0.3
^{118}Sn	1	0.1	0.1	0.1	0.03	0.3
^{121}Sb	0.2	0.02	0.1	0.1	0.4	0.2
^{178}Hf	0.01	0.00	<MDL	<MDL	0.03	0.1
^{181}Ta	1	0.01	<MDL	<MDL	<MDL	<MDL
^{182}W	0.3	<MDL	<MDL	0.00	<MDL	0.01
^{208}Pb	1	1	0.3	0.3	<MDL	<MDL

MAS	Massive to semi-massive mineralization	OBAN	Orthopyroxene -bearing band
DIS	Disseminated mineralization	POD	Pod
BAN	Bands of oxide mineralization	OPOD	Orthopyroxene -bearing pod
ANO	Anorthosite hosted disseminated	VEIN	Vein
ORT	Orthopyroxene associated	MAG	Magnetite
CLI	Clinopyroxene associated	ILM	Ilmenite
		PLE	Pleonaste

Appendix V (Continued)

Sample	CC025	CC025	CC054	CC054	CC054	CC054
Circle	H	I	A	A	D	F
Source file	25-H-H1.D	25-I-H1.D	54-A-H1.D	54-A-H2.D	54-D-H1.D	54-F-H1.D
Mineralization type	MAS	MAS	DIS	DIS	DIS	DIS
Descriptor	POD	POD	ORT	ORT	ORT	ORT
Mineral host	MAG	MAG	PLE	PLE	MAG	MAG
Mineral analyzed	PLE	PLE	PLE	PLE	PLE	PLE
Al wt. % (EPMA)*	30.0	30.0	32.0	32.0	31.1	29.8
^{24}Mg	49630	42650	39710	42000	42430	39910
^{29}Si	2070	2570	390	300	3020	9140
^{31}P	<MDL	25	21	21	14	189
^{44}Ca	55	34	19	54	73	352
^{45}Sc	0.4	<MDL	<MDL	0.2	0.3	2
^{47}Ti	2590	<MDL	<MDL	<MDL	4600	<MDL
^{51}V	1053	602	577	603	510	530
^{52}Cr	5020	4411	2037	2053	2793	2760
^{55}Mn	1564	1084	1747	1786	1426	1368
^{57}Fe	422000	281800	332000	326200	267200	291500
^{59}Co	1133	664	552	552	713	725
^{60}Ni	1016	630	755	782	755	765
^{63}Cu	2	2	1	1	4	235
^{66}Zn	5520	6871	5328	4808	4989	5160
^{69}Ga	283	210	184	182	188	167
^{74}Ge	0.4	0.1	1	1	0.2	0.4
^{75}As	<MDL	1	4	5	4	3
^{89}Y	<MDL	<MDL	<MDL	<MDL	<MDL	0.3
^{90}Zr	2	0.04	<MDL	<MDL	1	0.3
^{93}Nb	<MDL	<MDL	<MDL	<MDL	0.3	<MDL
^{95}Mo	0.1	0.1	0.1	0.1	0.1	0.3
^{118}Sn	0.2	0.01	0.2	0.1	0.1	0.3
^{121}Sb	0.3	0.1	0.05	0.04	<MDL	0.2
^{178}Hf	0.03	<MDL	<MDL	<MDL	0.02	0.01
^{181}Ta	<MDL	<MDL	<MDL	<MDL	0.01	<MDL
^{182}W	0.01	0.01	0.01	0.02	<MDL	0.2
^{208}Pb	0.04	0.1	0.5	0.5	0.2	1

MAS	Massive to semi-massive mineralization	OBAN	Orthopyroxene -bearing band
DIS	Disseminated mineralization	POD	Pod
BAN	Bands of oxide mineralization	OPOD	Orthopyroxene -bearing pod
ANO	Anorthosite hosted disseminated	VEIN	Vein
ORT	Orthopyroxene associated	MAG	Magnetite
CLI	Clinopyroxene associated	ILM	Ilmenite
		PLE	Pleonaste

Appendix V (Continued)

Sample	CC054	CC072	CC072	CC072	CC072	CC072
Circle	F	A	B	B	D	E
Source file	54-F-H2.D	72-A-H1.D	72-B-H1.D	72-B-H2.D	72-D-H1.D	72-E-H1.D
Mineralization type	DIS	MAS	MAS	MAS	MAS	MAS
Descriptor	ORT	OPOD	OPOD	OPOD	OPOD	OPOD
Mineral host	MAG	MAG	MAG	MAG	MAG	MAG
Mineral analyzed	PLE	PLE	PLE	PLE	PLE	PLE
Al wt. % (EPMA)*	29.8	31.1	31.1	31.1	31.1	31.1
^{24}Mg	44400	193100	95600	96300	80900	82400
^{29}Si	11600	<MDL	1630	1820	1590	1030
^{31}P	140	31	14	17	<MDL	10
^{44}Ca	219	30	38	38	<MDL	45
^{45}Sc	1	1	2	5	0.3	0.1
^{47}Ti	<MDL	1020	26600	55000	<MDL	<MDL
^{51}V	567	942	508	620	427	414
^{52}Cr	3118	5470	3260	3163	2326	2406
^{55}Mn	1531	3200	2860	3490	1482	1430
^{57}Fe	307000	458000	266000	334000	195100	191000
^{59}Co	876	1141	659	630	500	487
^{60}Ni	876	1240	622	627	523	477
^{63}Cu	182	21	53	436	14	1
^{66}Zn	5820	9500	6700	5920	4080	3830
^{69}Ga	192	414	207	209	183	187
^{74}Ge	0.3	0.4	0.4	0.4	0.3	0.2
^{75}As	3	8	3	3	4	3
^{89}Y	0.1	<MDL	0.02	0.1	<MDL	<MDL
^{90}Zr	0.1	0.1	2	6	0.04	0.04
^{93}Nb	<MDL	<MDL	1	1	<MDL	<MDL
^{95}Mo	0.2	0.1	0.2	0.2	0.1	0.1
^{118}Sn	0.2	0.3	1	1	0.1	0.1
^{121}Sb	0.03	0.1	0.1	0.1	0.04	0.1
^{178}Hf	0.01	<MDL	0.1	0.2	0.00	<MDL
^{181}Ta	<MDL	0.4	<MDL	0.1	<MDL	<MDL
^{182}W	0.2	9	0.1	0.1	0.01	0.01
^{208}Pb	1	1	0.5	1	0.1	0.2

MAS	Massive to semi-massive mineralization	OBAN	Orthopyroxene -bearing band
DIS	Disseminated mineralization	POD	Pod
BAN	Bands of oxide mineralization	OPOD	Orthopyroxene -bearing pod
ANO	Anorthosite hosted disseminated	VEIN	Vein
ORT	Orthopyroxene associated	MAG	Magnetite
CLI	Clinopyroxene associated	ILM	Ilmenite
		PLE	Pleonaste

Appendix V (Continued)

Sample	CC072	CC072	CC072	CC074	CC074	CC076
Circle	E	K	K	D	E	A
Source file	72-E-H2.D	72-K-H1.D	72-K-H2.D	74-D-H1.D	74-E-H1.D	76-A-H2.D
Mineralization type	MAS	MAS	MAS	DIS	DIS	MAS
Descriptor	OPOD	OPOD	OPOD	CLI	CLI	VEIN
Mineral host	MAG	PLE	PLE	MAG	MAG	ILM
Mineral analyzed	PLE	PLE	PLE	PLE	PLE	PLE
Al wt. % (EPMA)*	31.1	31.1	31.1	31.1	31.1	29.9
^{24}Mg	83300	75900	91400	46200	36040	39500
^{29}Si	990	580	500	6690	6000	830
^{31}P	17	<MDL	7	6	63	<MDL
^{44}Ca	<MDL	<MDL	29	680	149	29
^{45}Sc	0.2	0.4	0.4	2	<MDL	18
^{47}Ti	<MDL	<MDL	<MDL	46700	<MDL	27750
^{51}V	405	500	705	981	388	648
^{52}Cr	2350	2068	2750	7160	4733	3040
^{55}Mn	1440	1711	2058	5310	2674	2420
^{57}Fe	198000	228200	287000	492000	282100	209100
^{59}Co	513	472	586	1901	1333	324
^{60}Ni	493	557	686	936	661	219
^{63}Cu	10	0.2	1	4	3	1
^{66}Zn	3910	3680	5820	12610	9380	6320
^{69}Ga	177	177	212	326	251	305
^{74}Ge	0.2	0.3	0.3	0.4	0.2	<MDL
^{75}As	4	2	3	6	4	3
^{89}Y	<MDL	<MDL	<MDL	0.1	<MDL	<MDL
^{90}Zr	<MDL	0.03	<MDL	1	<MDL	59
^{93}Nb	<MDL	<MDL	<MDL	2	<MDL	1
^{95}Mo	0.1	<MDL	0.2	1	<MDL	0.1
^{118}Sn	0.1	0.1	0.1	1	<MDL	10
^{121}Sb	0.03	0.1	0.1	0.03	<MDL	0.1
^{178}Hf	<MDL	<MDL	<MDL	0.03	<MDL	3
^{181}Ta	<MDL	<MDL	<MDL	0.1	<MDL	0.1
^{182}W	0.01	<MDL	<MDL	0.02	<MDL	0.01
^{208}Pb	0.2	0.3	1	2	0.4	1

MAS	Massive to semi-massive mineralization	OBAN	Orthopyroxene -bearing band
DIS	Disseminated mineralization	POD	Pod
BAN	Bands of oxide mineralization	OPOD	Orthopyroxene -bearing pod
ANO	Anorthosite hosted disseminated	VEIN	Vein
ORT	Orthopyroxene associated	MAG	Magnetite
CLI	Clinopyroxene associated	ILM	Ilmenite
		PLE	Pleonaste

Appendix V (Continued)

Sample	CC076	CC076	CC076
Circle	A	B	G
Source file	76-A-H3.D	76-B-H1.D	76-G-H1.D
Mineralization type	MAS	MAS	MAS
Descriptor	VEIN	VEIN	VEIN
Mineral host	PLE	PLE	PLE
Mineral analyzed	PLE	PLE	PLE
Al wt. % (EPMA)*	29.9	29.9	29.9
^{24}Mg	48600	45170	44700
^{29}Si	<MDL	1360	390
^{31}P	<MDL	9	12
^{44}Ca	<MDL	21	<MDL
^{45}Sc	<MDL	0.2	<MDL
^{47}Ti	1090	<MDL	<MDL
^{51}V	549	507	576
^{52}Cr	2620	3158	4270
^{55}Mn	3383	3164	3537
^{57}Fe	237800	250600	295100
^{59}Co	527	410	453
^{60}Ni	225	234	260
^{63}Cu	1	0.2	2
^{66}Zn	12000	9810	11900
^{69}Ga	195	214	224
^{74}Ge	0.3	<MDL	0.2
^{75}As	<MDL	2	3
^{89}Y	<MDL	<MDL	<MDL
^{90}Zr	0.3	0.05	0.03
^{93}Nb	<MDL	<MDL	<MDL
^{95}Mo	0.1	0.1	0.2
^{118}Sn	0.3	0.1	0.04
^{121}Sb	0.01	0.1	0.1
^{178}Hf	0.01	0.00	<MDL
^{181}Ta	<MDL	<MDL	<MDL
^{182}W	<MDL	<MDL	0.01
^{208}Pb	0.3	0.2	0.4

MAS	Massive to semi-massive mineralization	OBAN	Orthopyroxene -bearing band
DIS	Disseminated mineralization	POD	Pod
BAN	Bands of oxide mineralization	OPOD	Orthopyroxene -bearing pod
ANO	Anorthosite hosted disseminated	VEIN	Vein
ORT	Orthopyroxene associated	MAG	Magnetite
CLI	Clinopyroxene associated	ILM	Ilmenite
		PLE	Pleonaste

Appendix VI. **LA-ICPMS and EPMA spot and line analysis locations on BSE images and photomicrographs, respectively.**
CC008 circle A LA-ICPMS

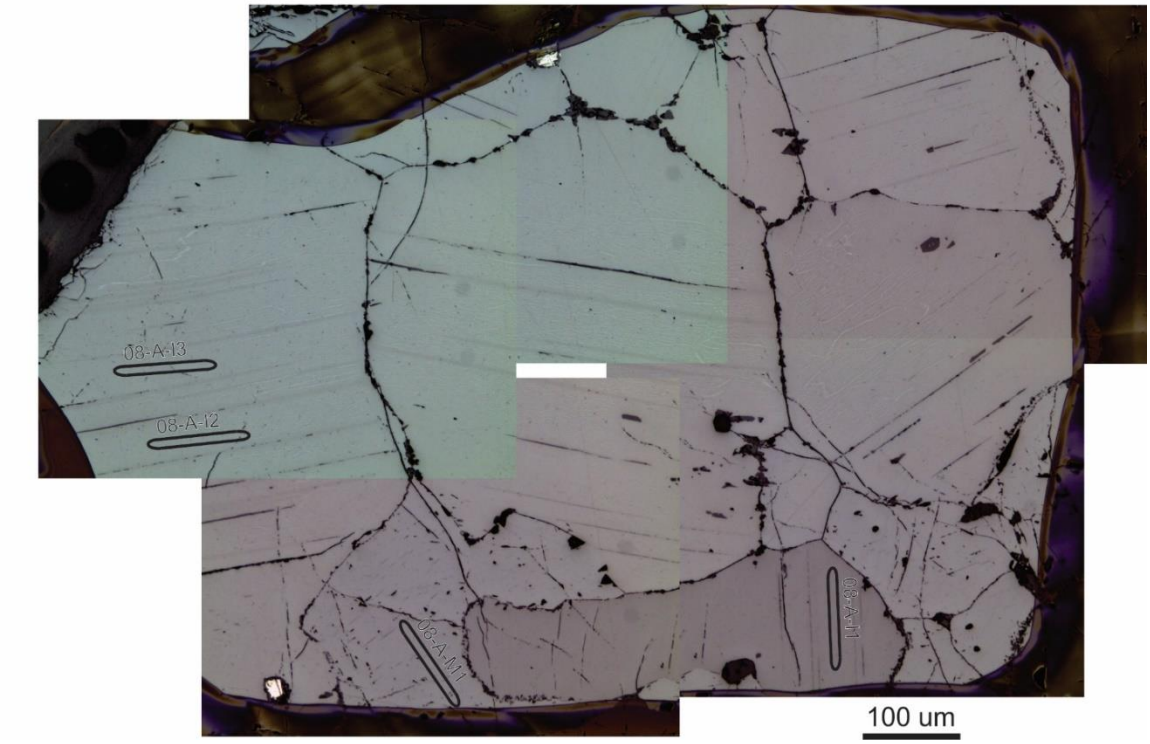

CC008 circle A EPMA

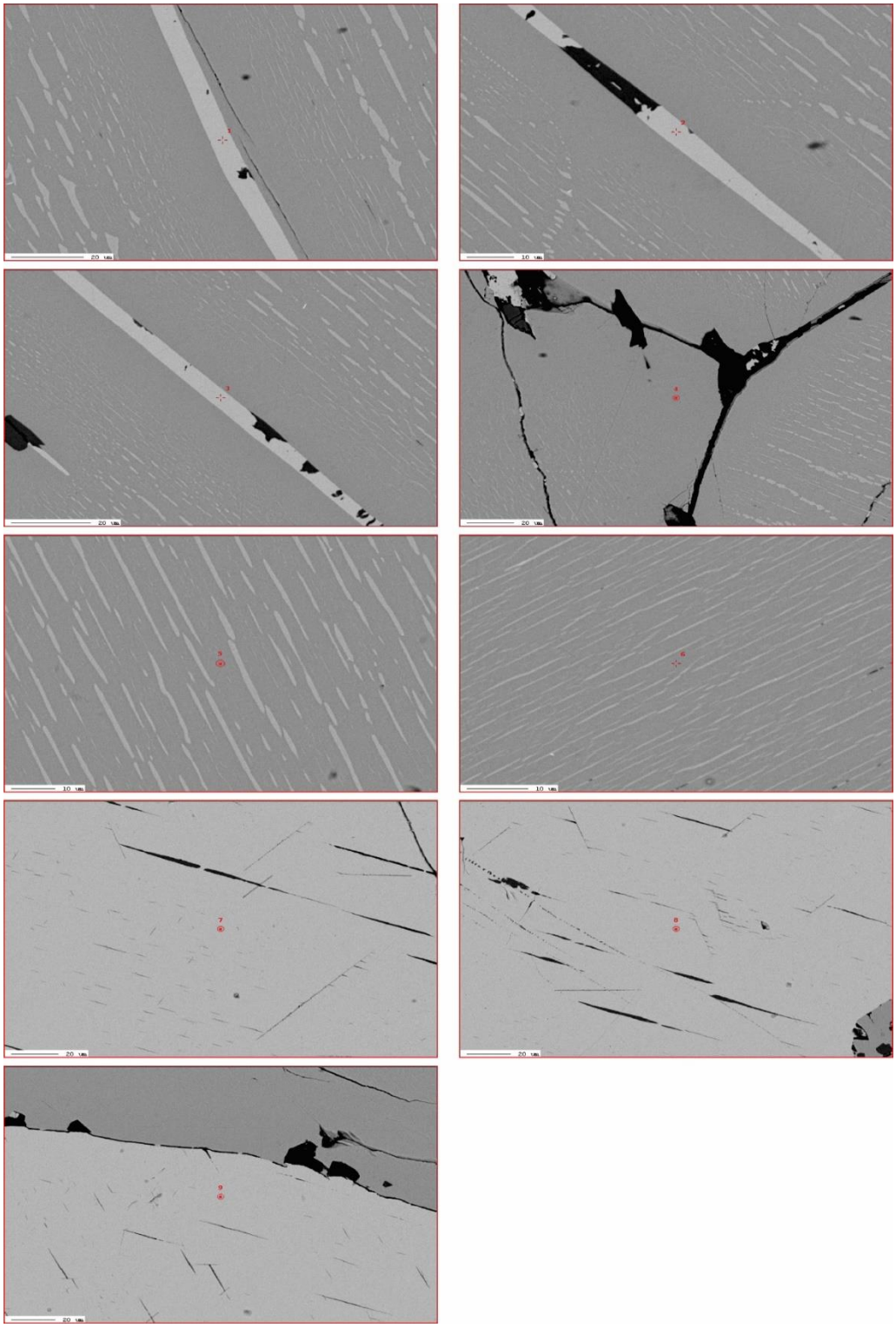

CC008 circle B LA-ICPMS

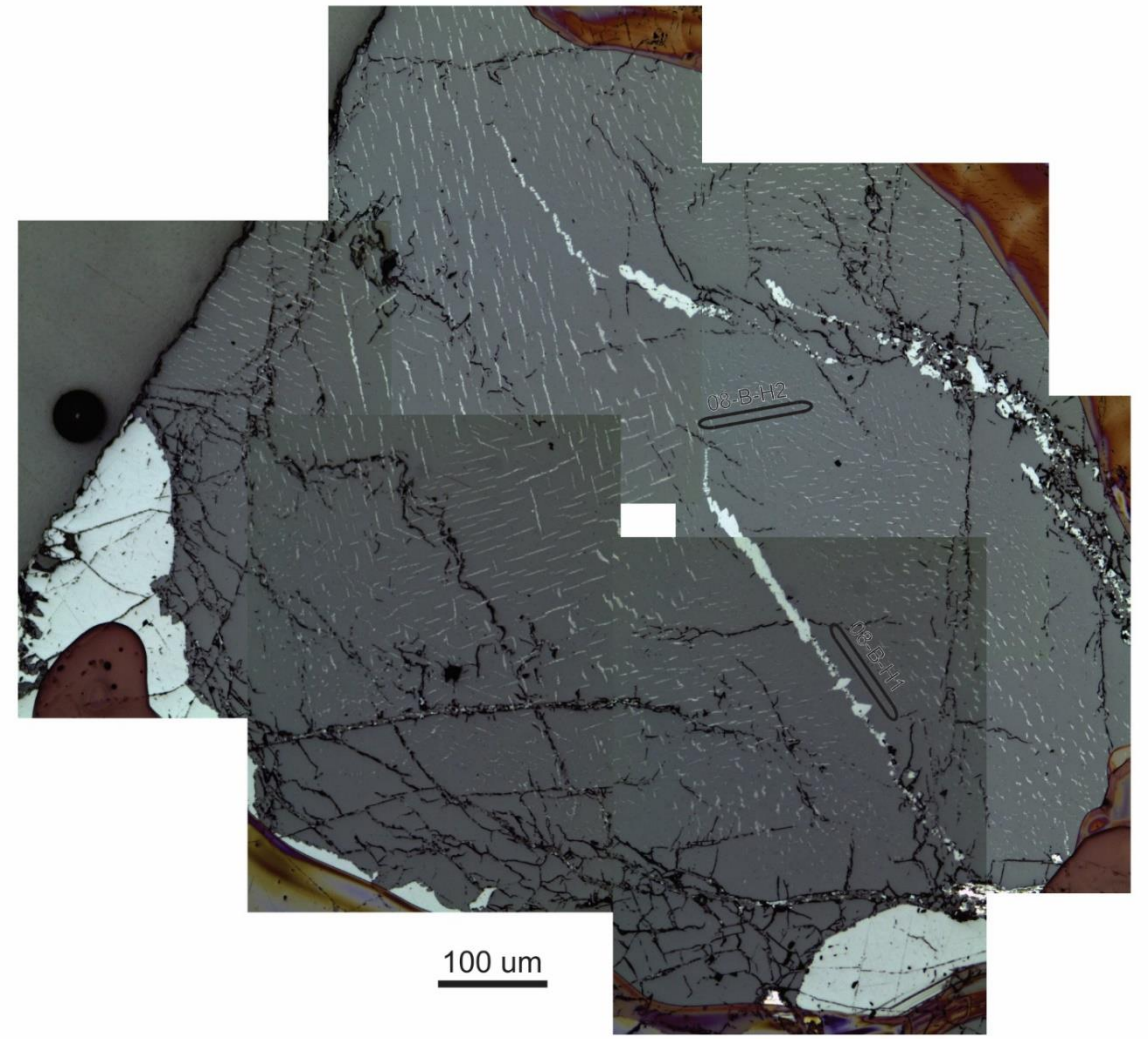
08-B-H2
08-B-H1
100 um

CC008 circle B EPMA

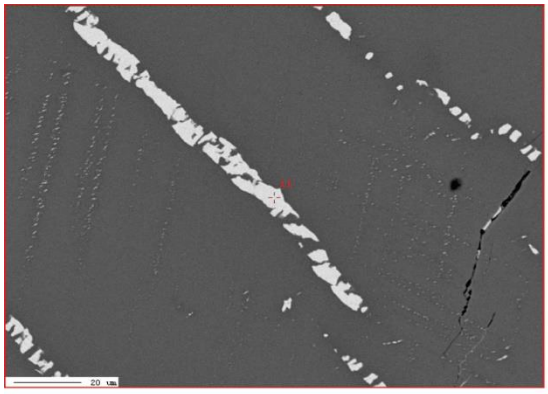

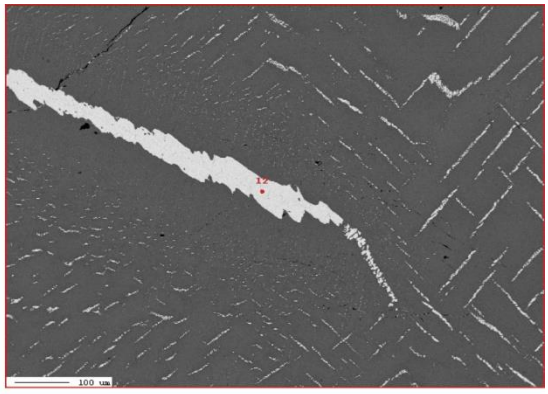

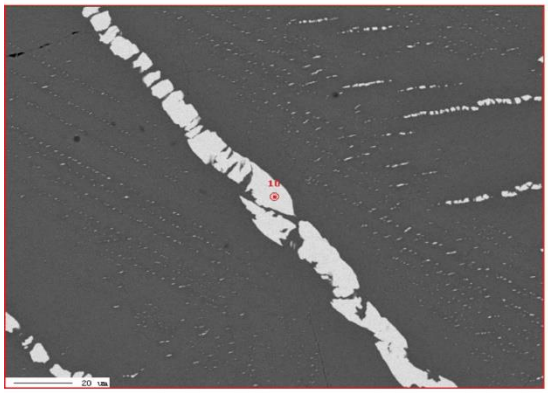

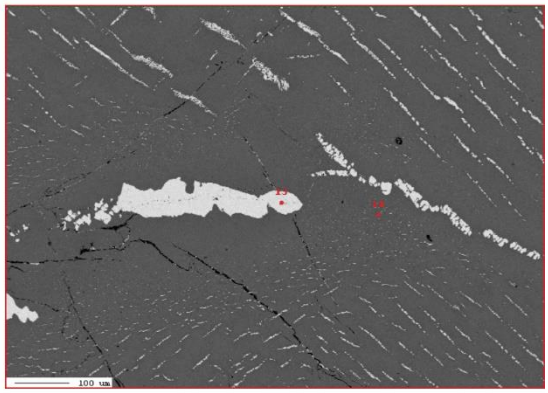

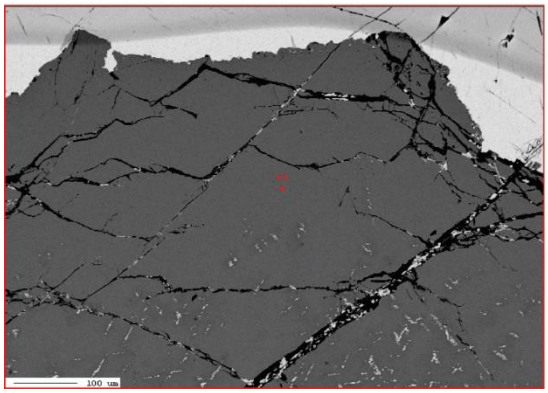

CC008 circle C EPMA

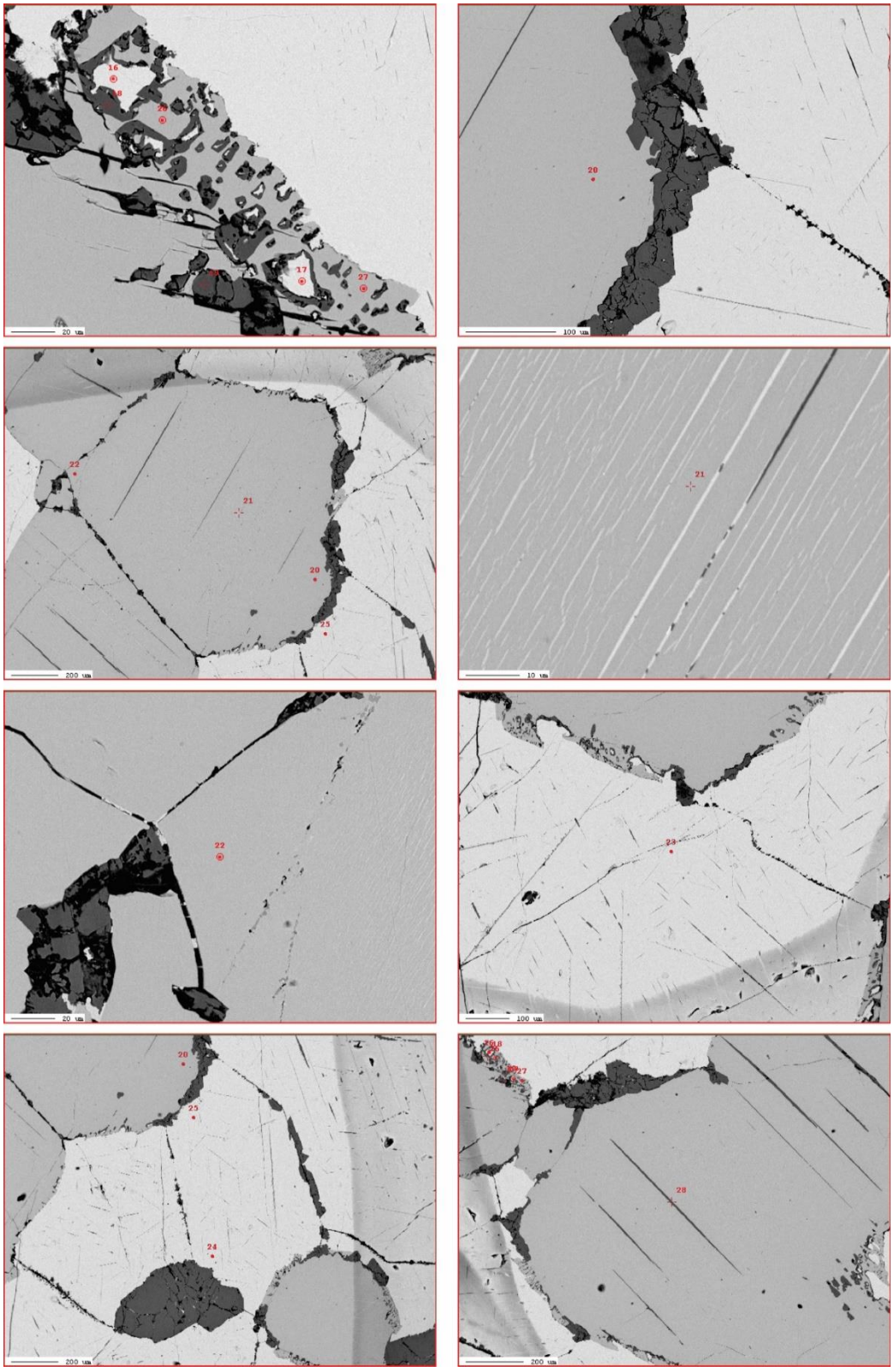

CC008 circle D LA-ICPMS

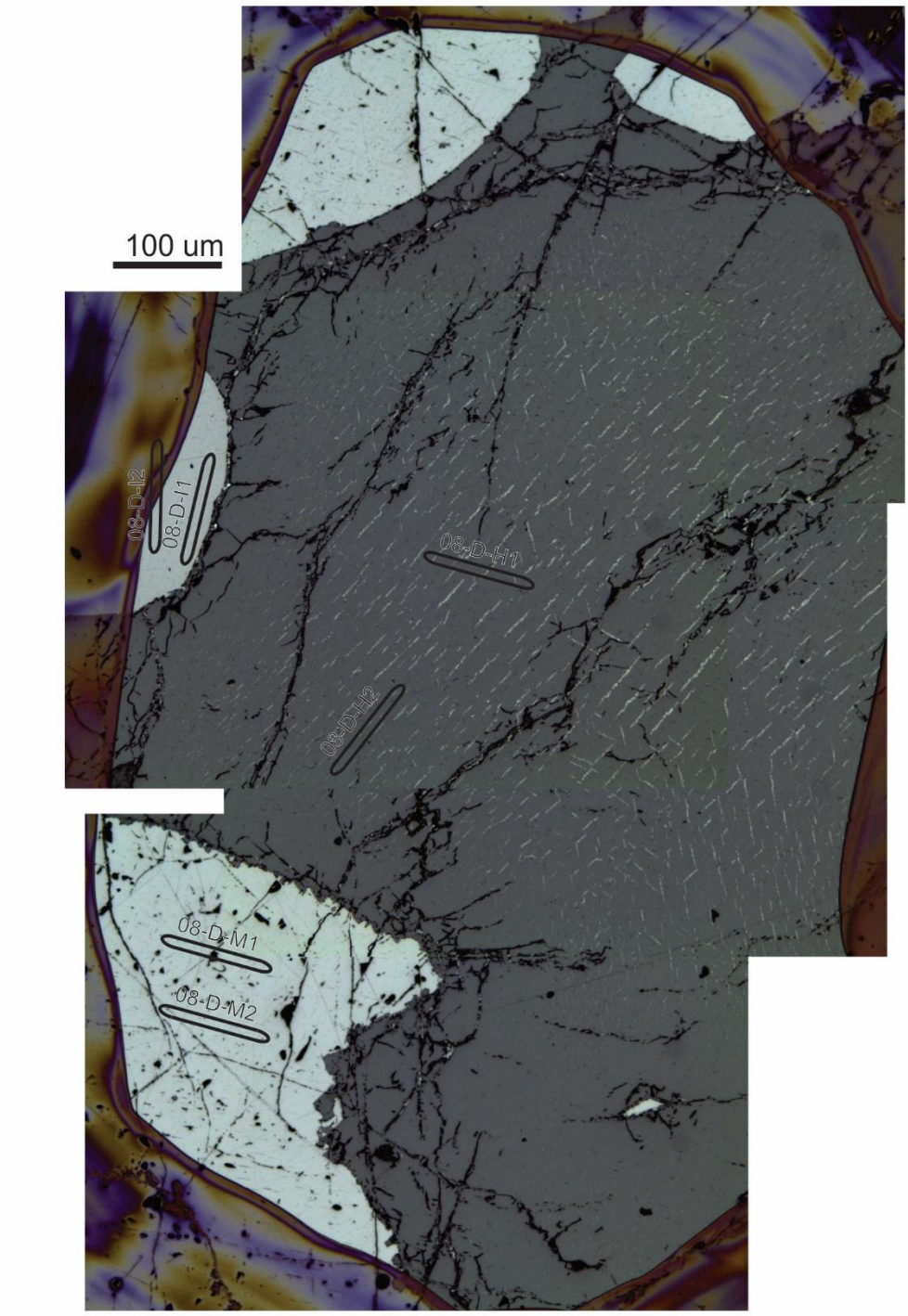
100 um
08-D-I2
08-D-I1
08-D-H1
08-D-H2
08-D-M1
08-D-M2

CC008 circle D EPMA

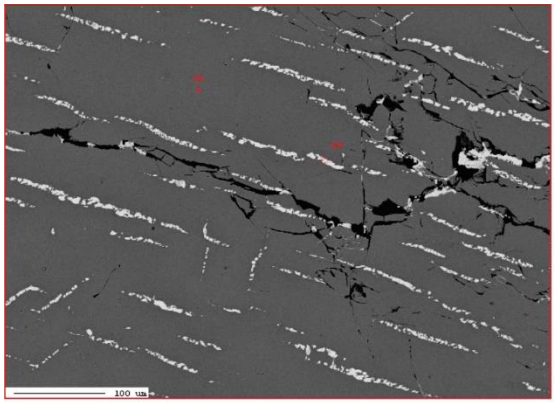

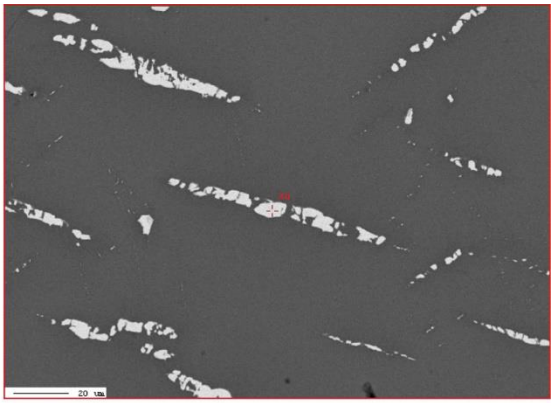

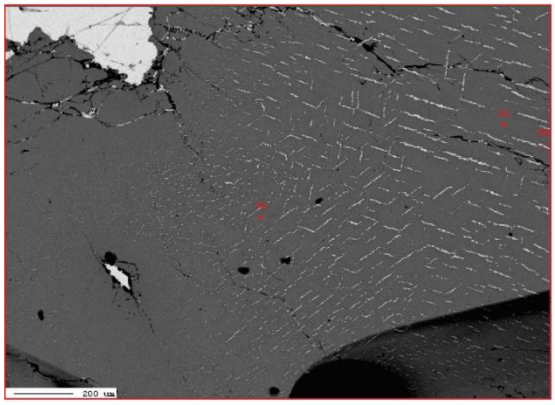

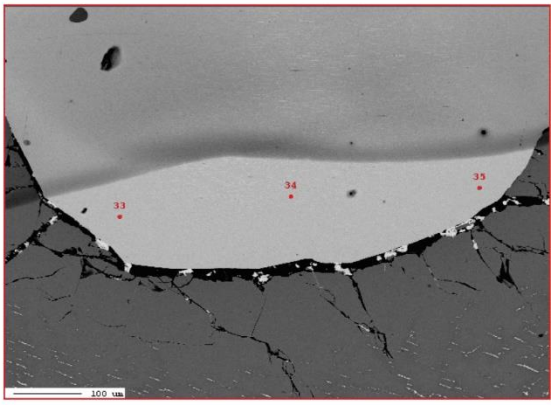

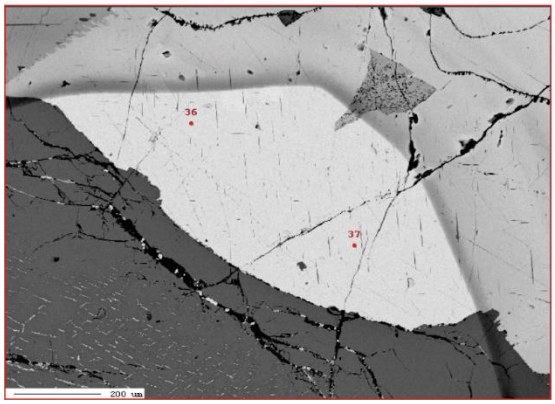

CC008 circle E EPMA

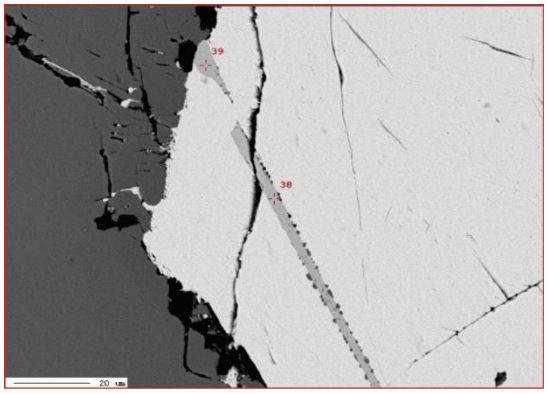

CC008 circle F LA-ICPMS

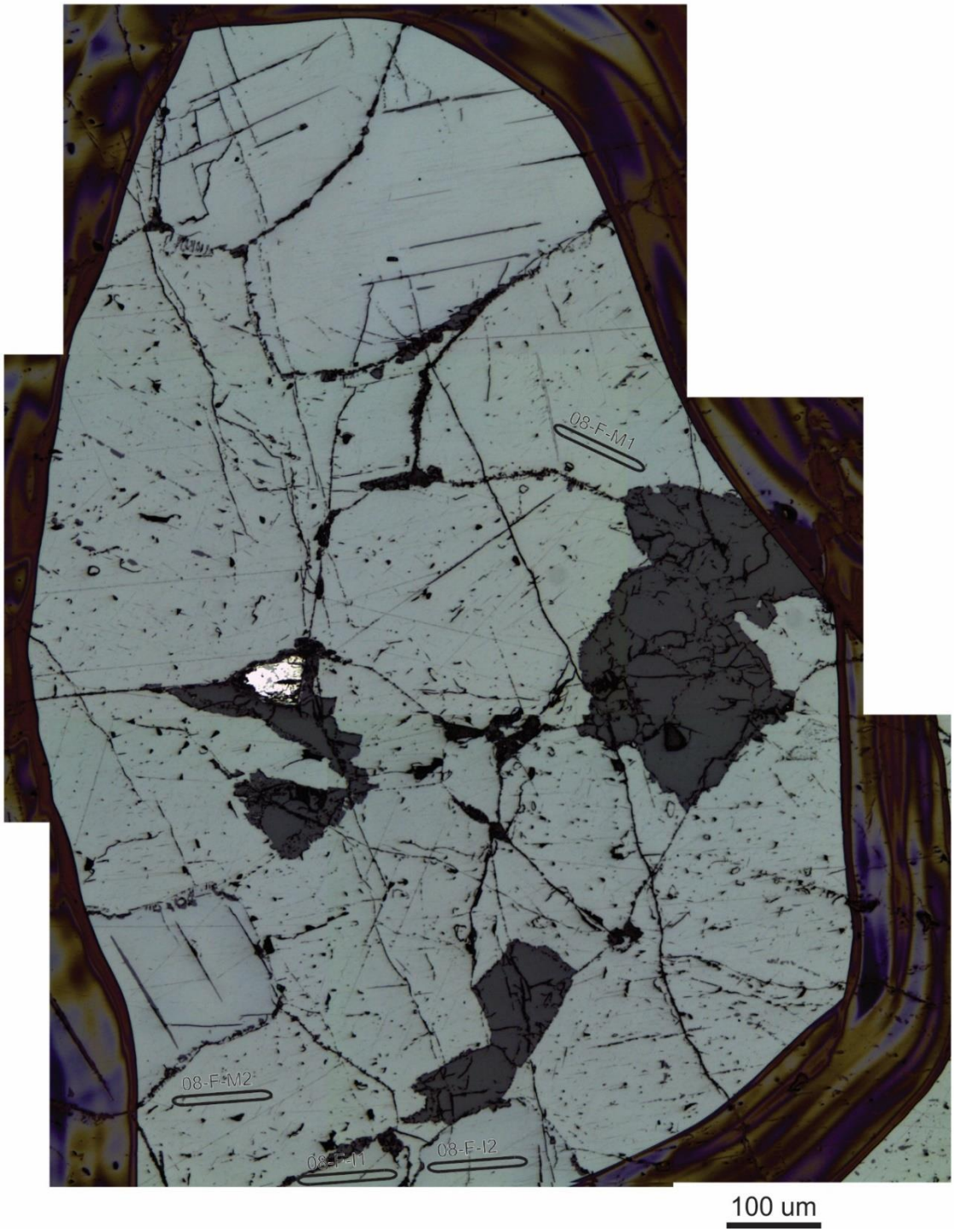

CC008 circle F EPMA

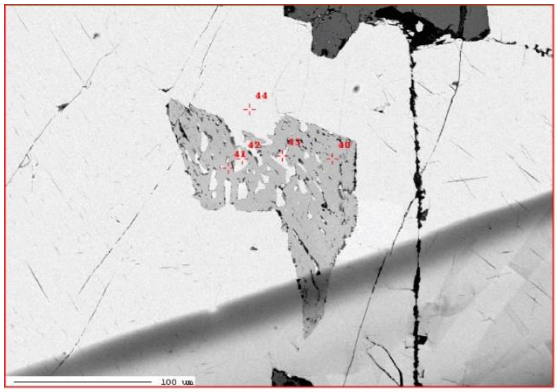

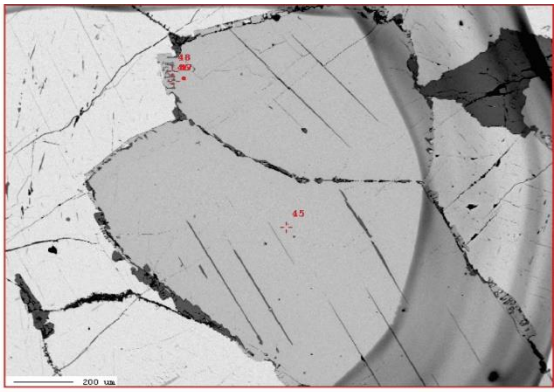

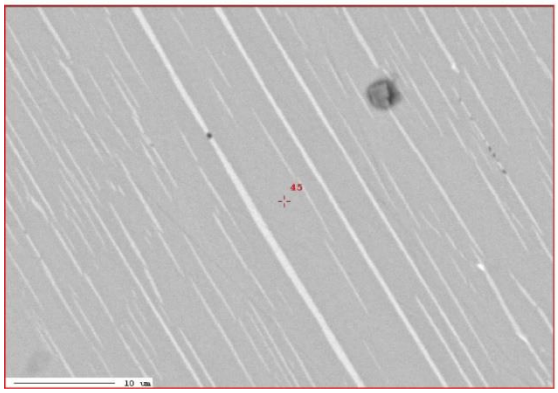

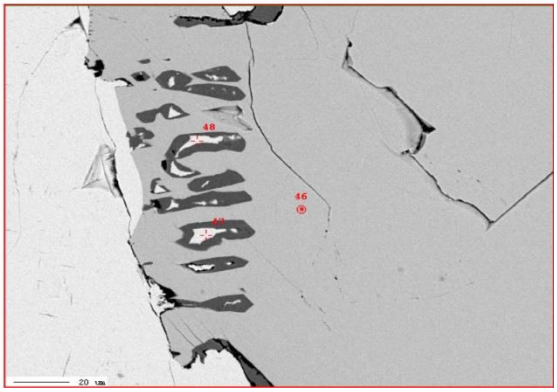

CC008 circle H LA-ICPMS

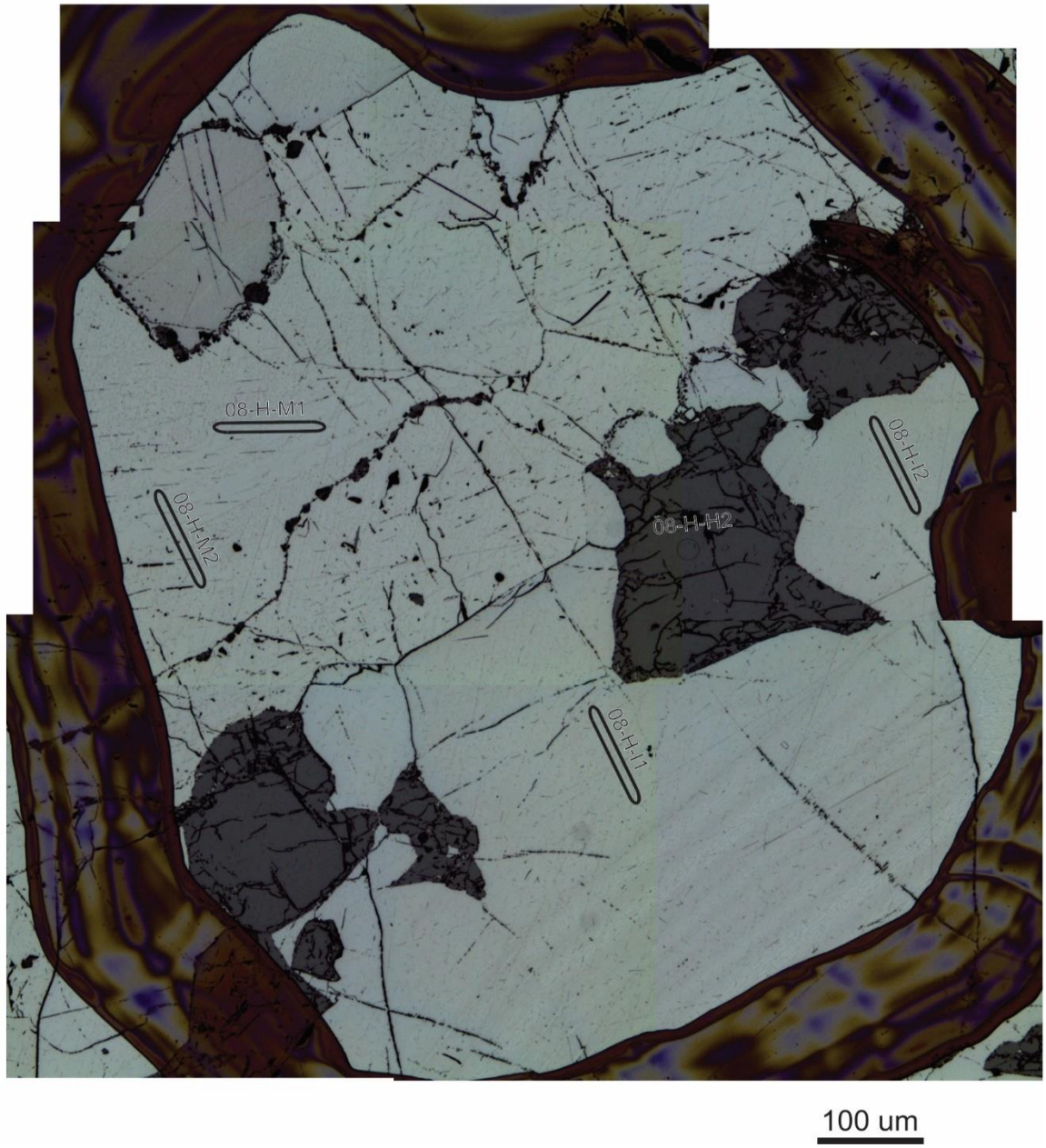

CC008 circle I EPMA

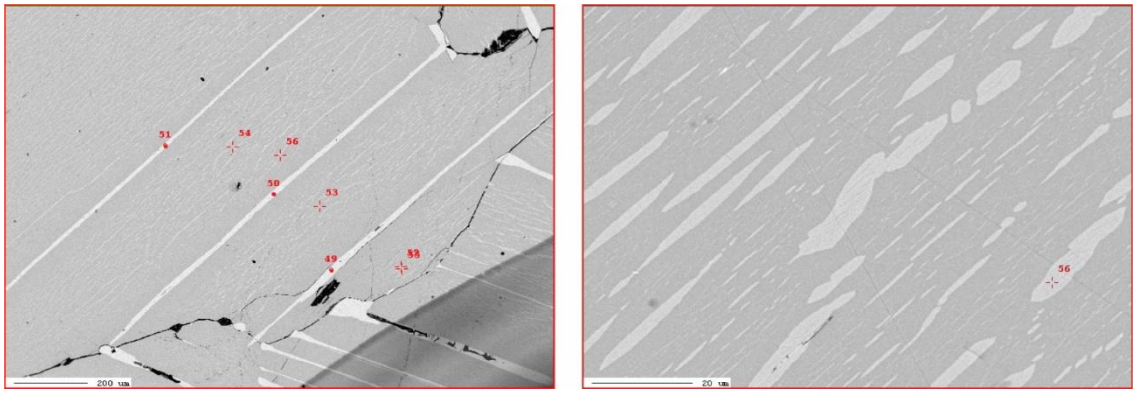

CC008 circle J LA-ICPMS

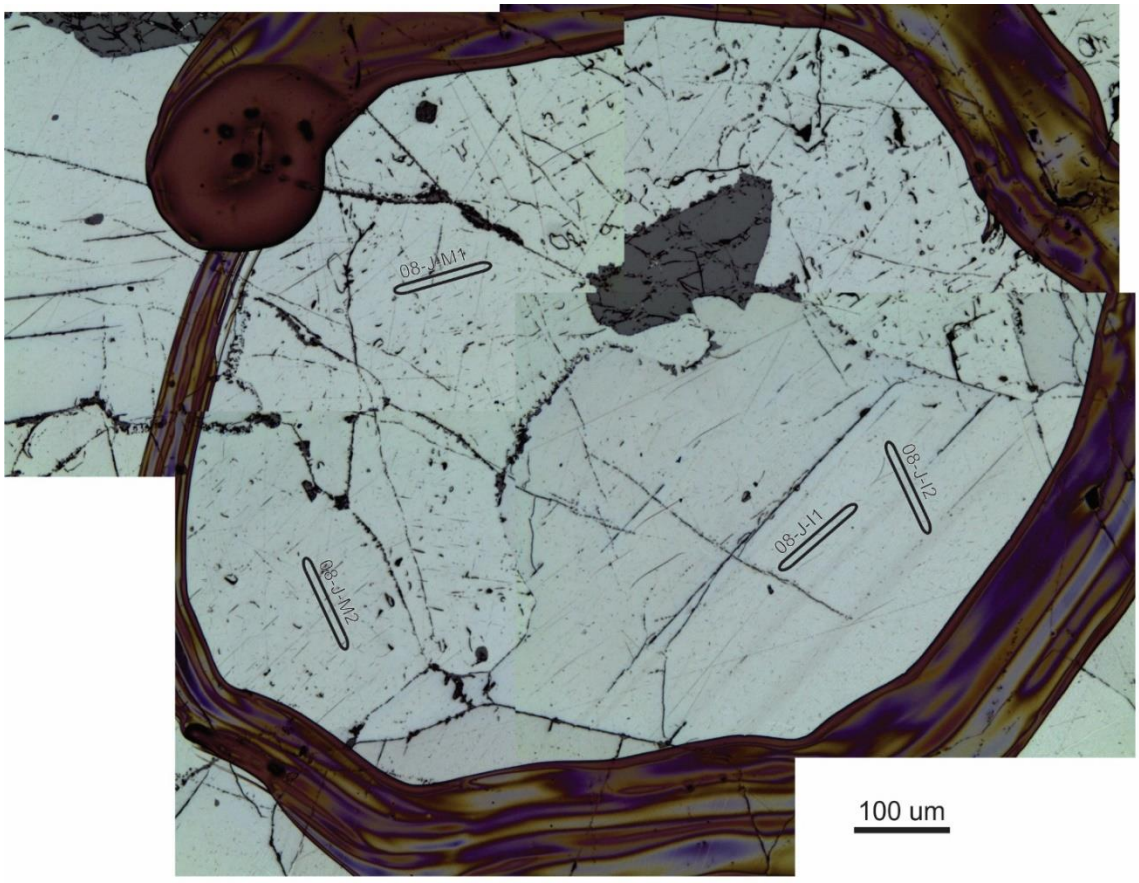

CC010 circle A LA-ICPMS

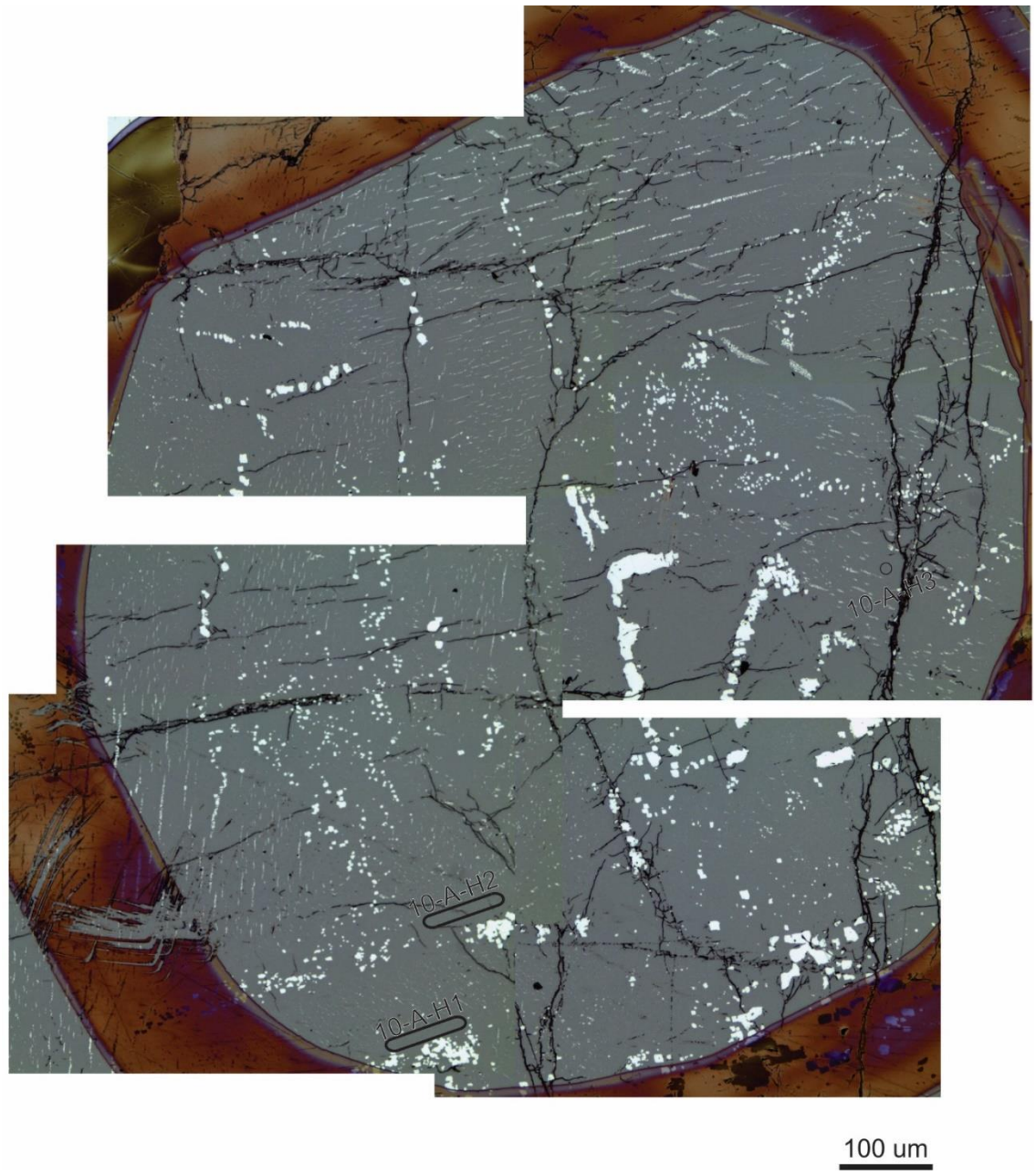

CC010 circle A EPMA

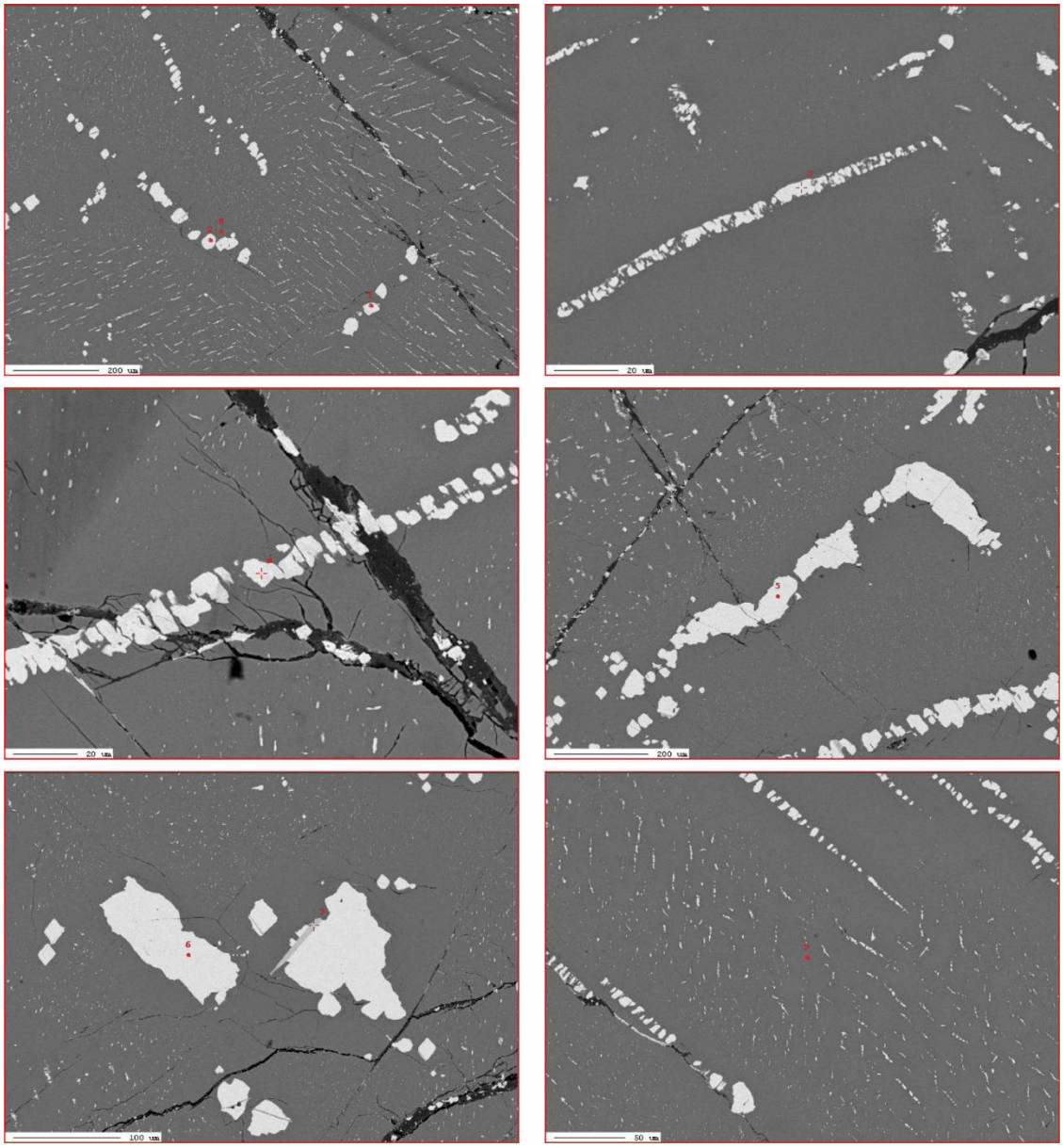

CC010 circle B LA-ICPMS

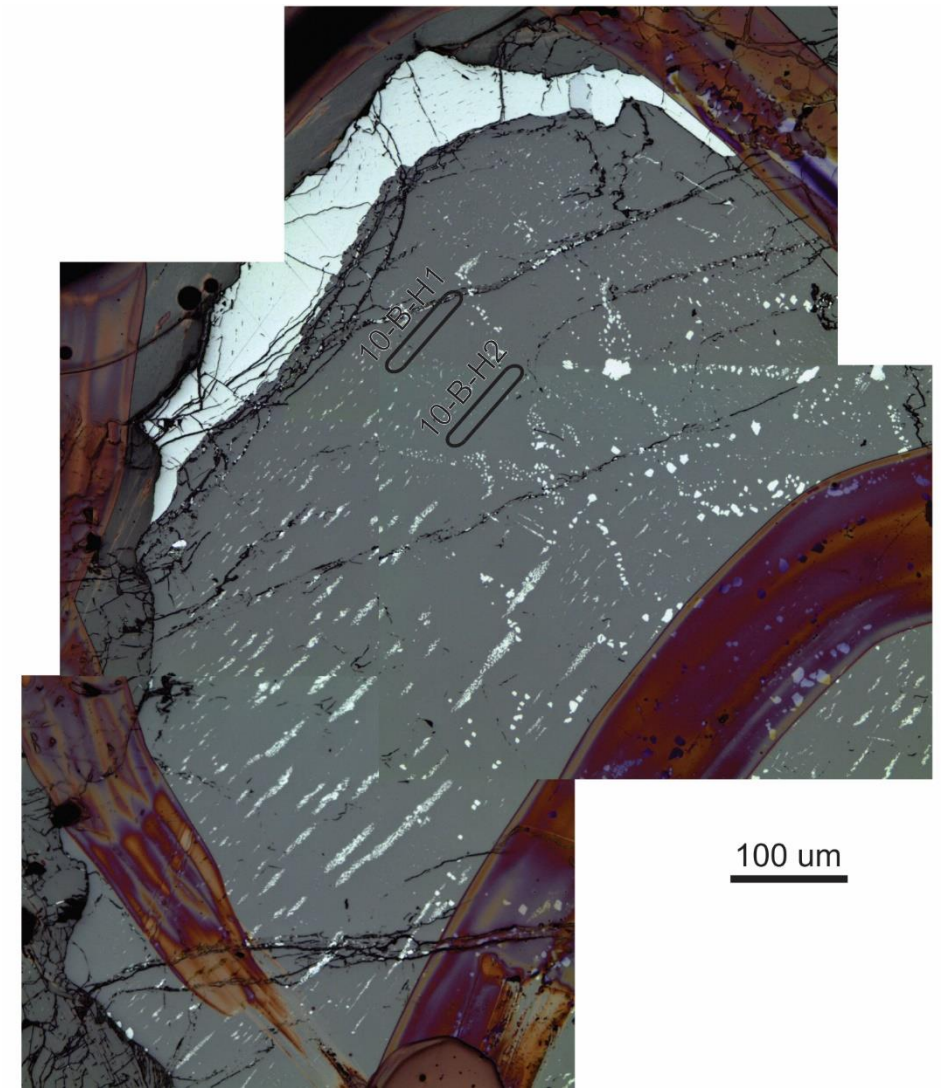

CC010 circle D LA-ICPMS

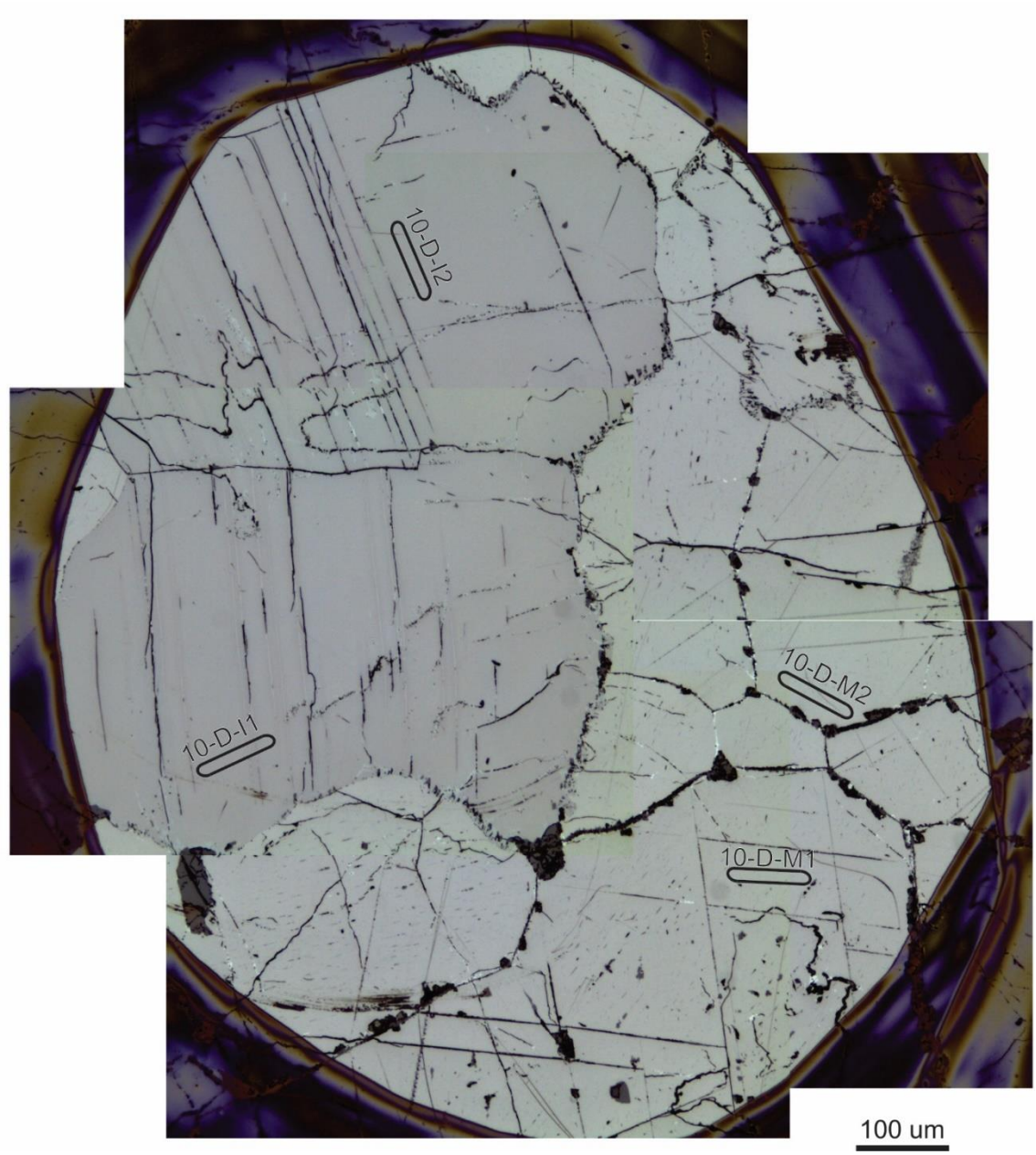

CC010 circle D EPMA

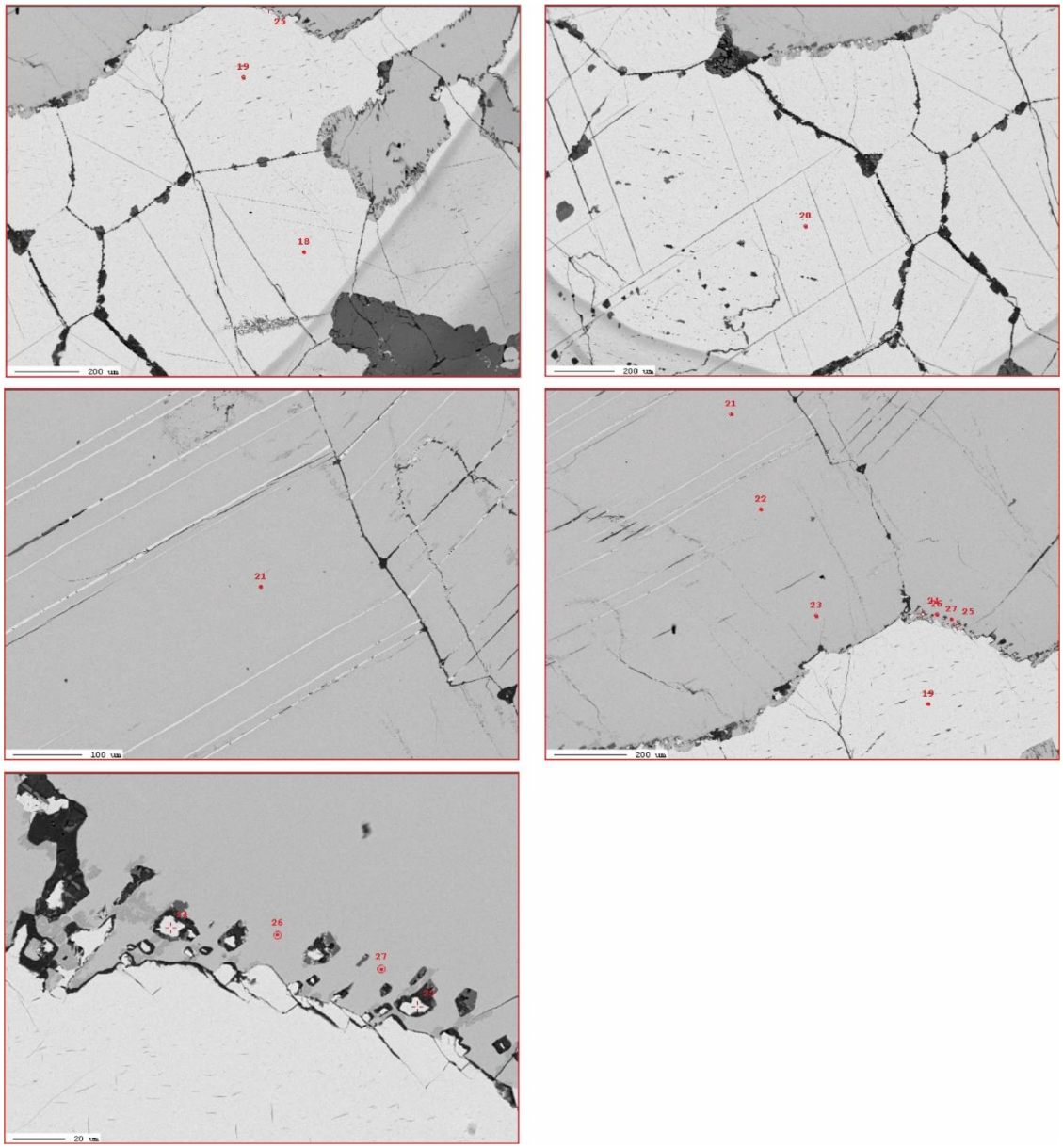

CC010 circle E LA-ICPMS

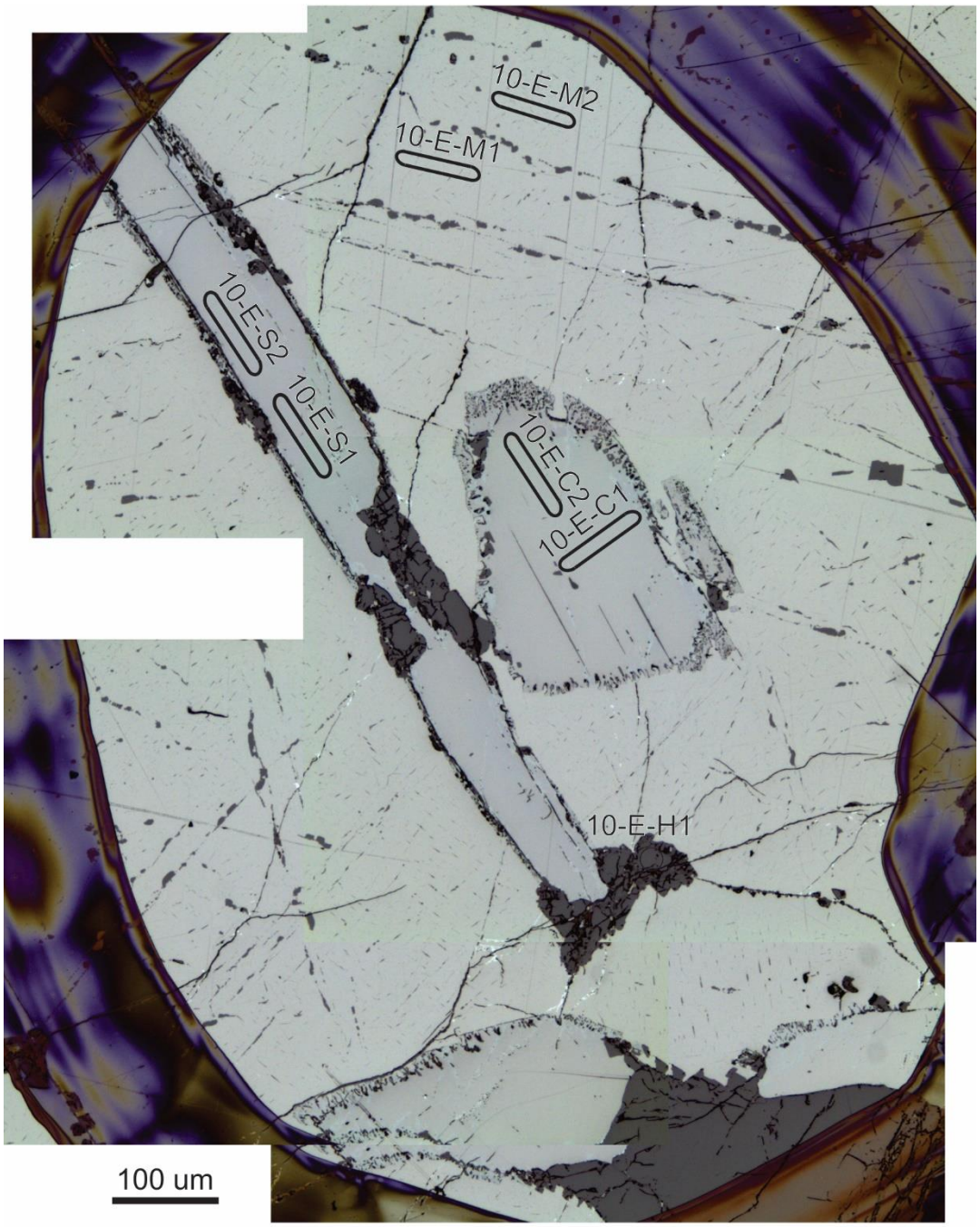

CC010 circle E EPMA

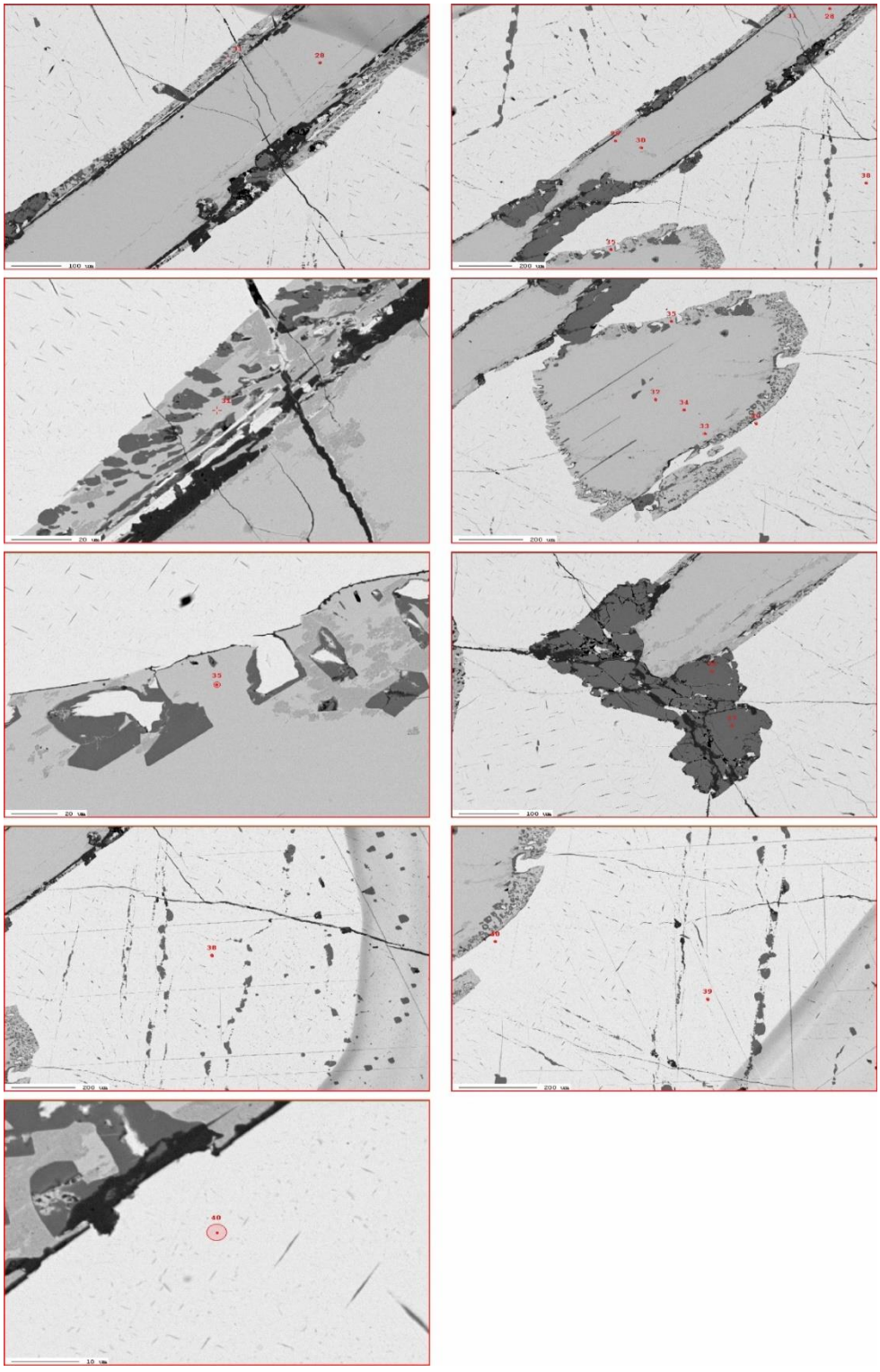

CC010 circle F LA-ICPMS

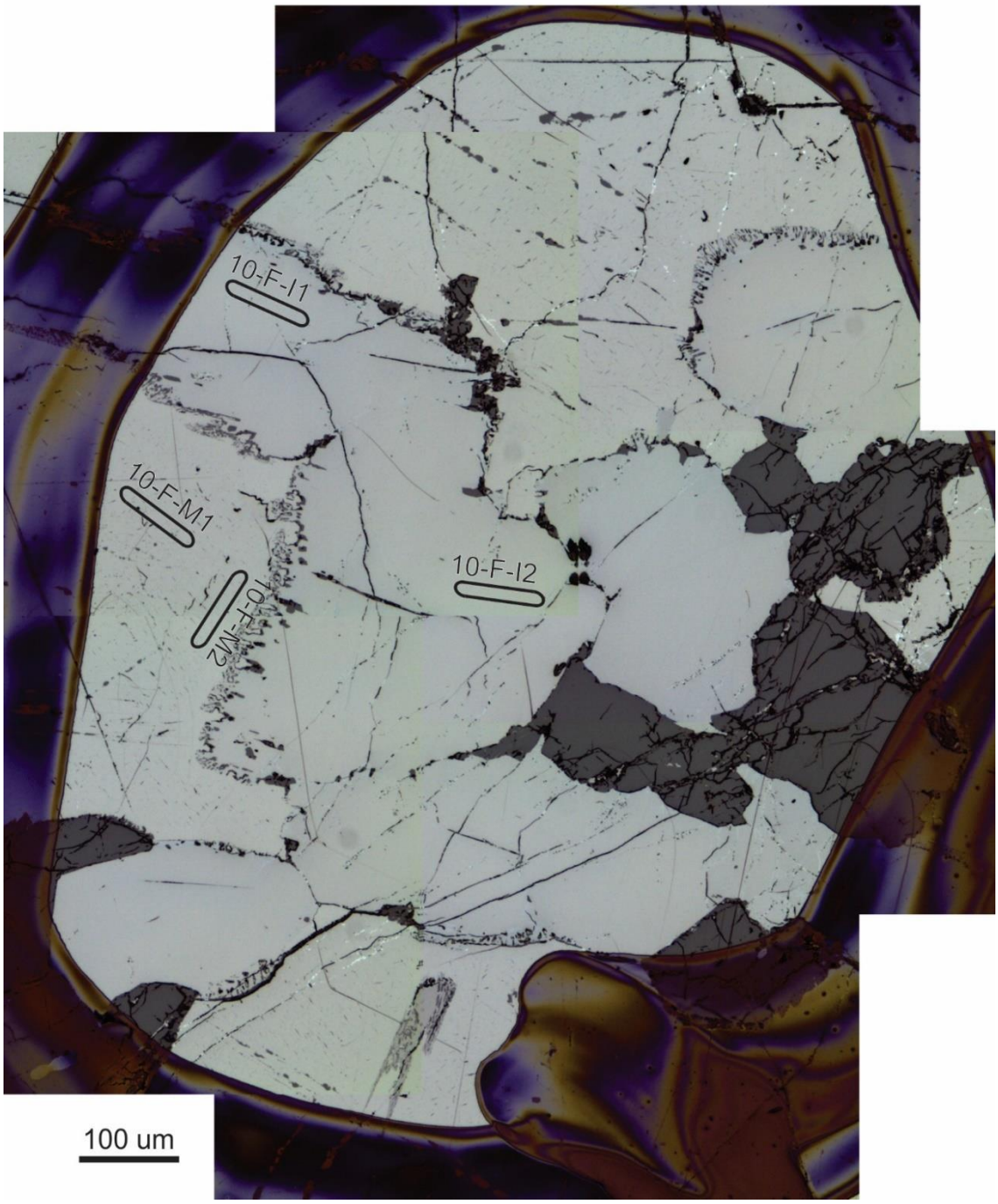

CC010 circle F EPMA

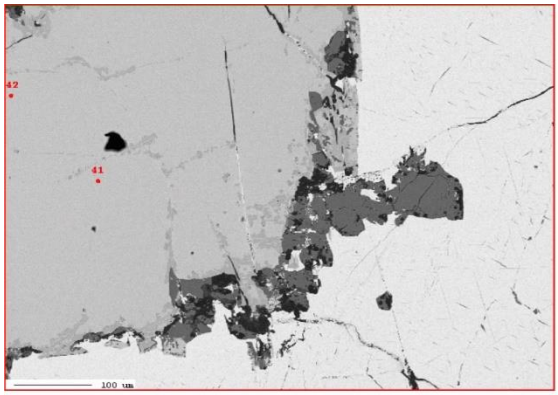

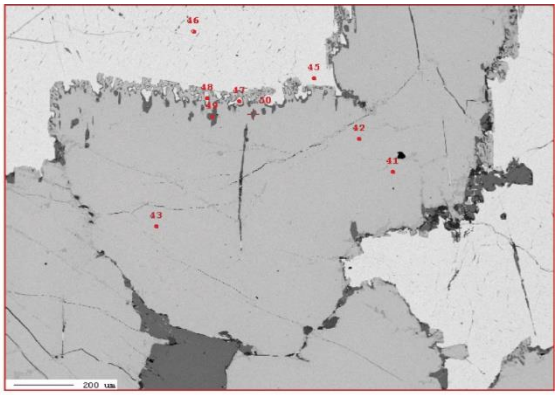

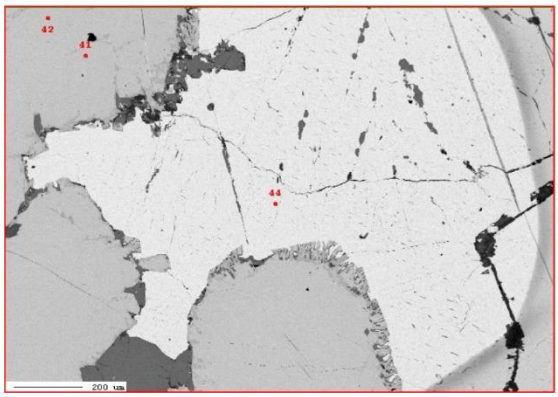

CC010 circle H LA-ICPMS

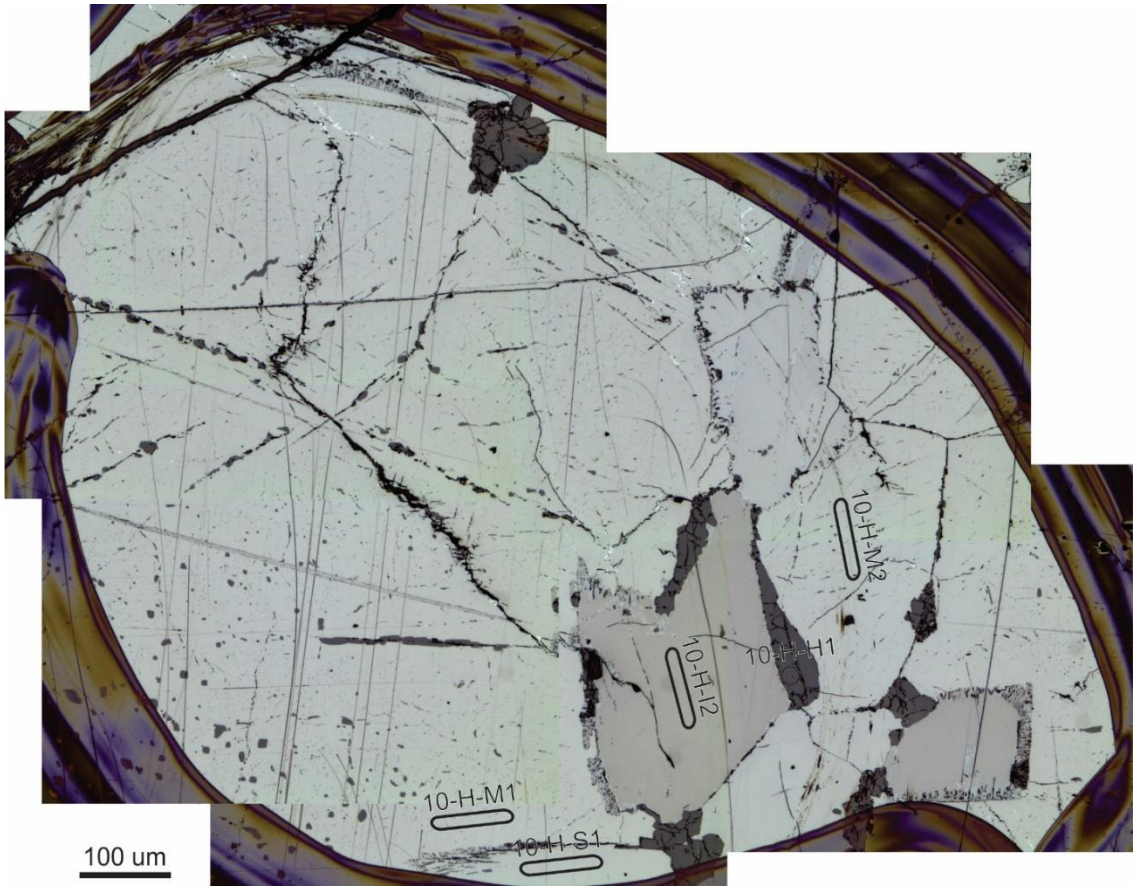

CC010 circle H EPMA

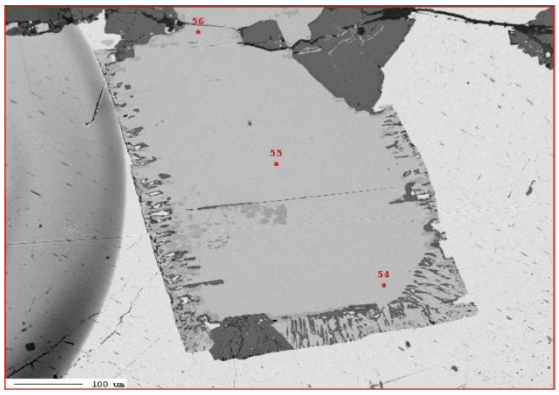

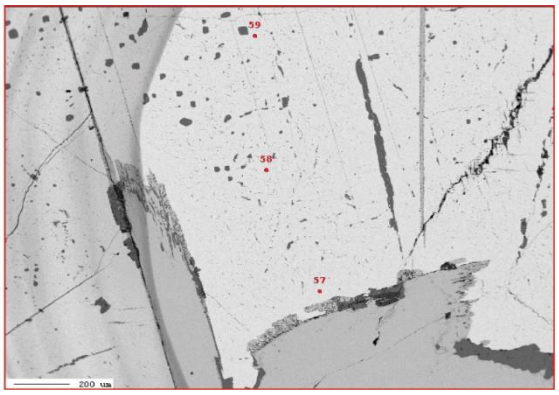

CC010 circle I LA-ICPMS

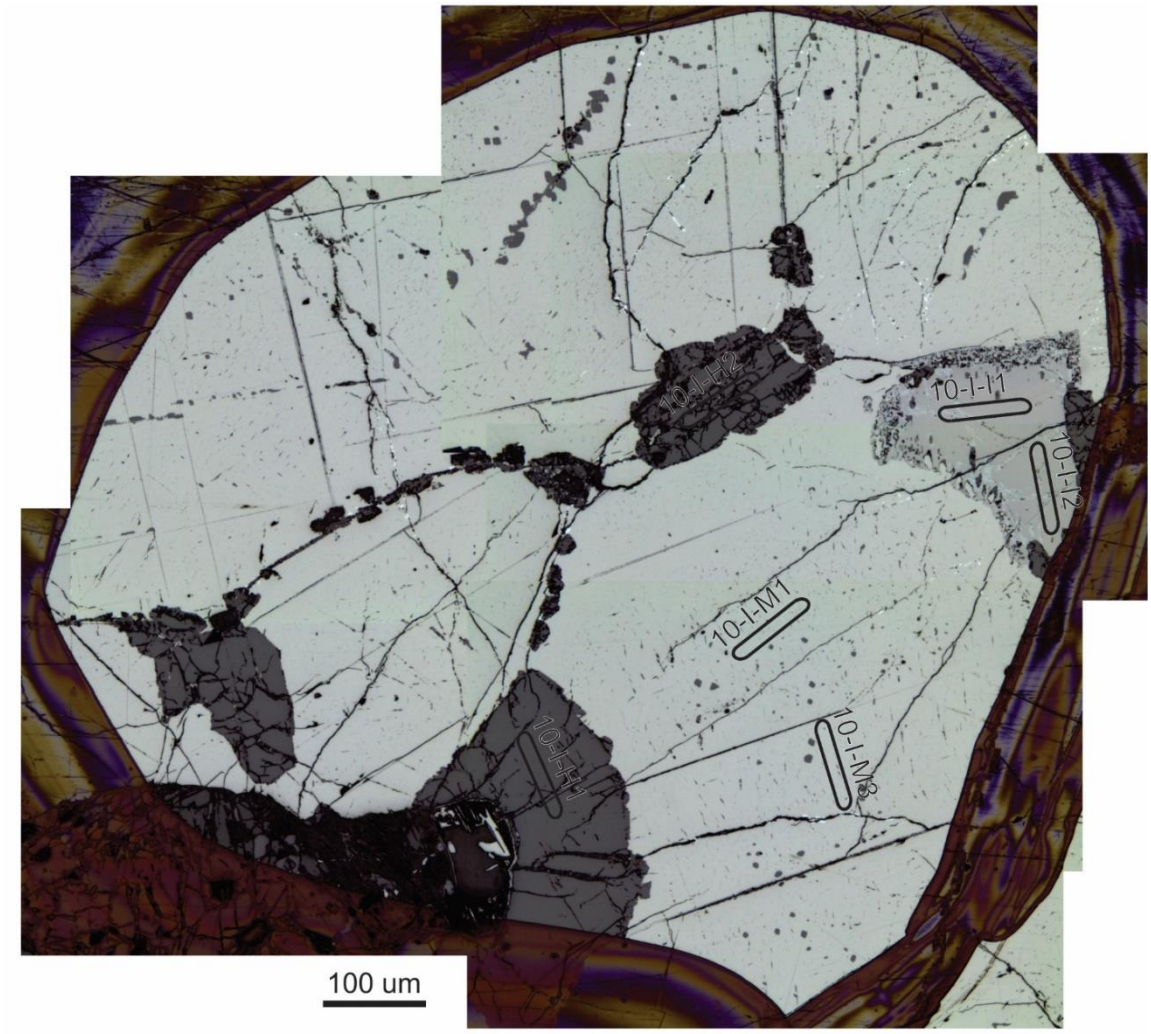

CC010 circle I EPMA

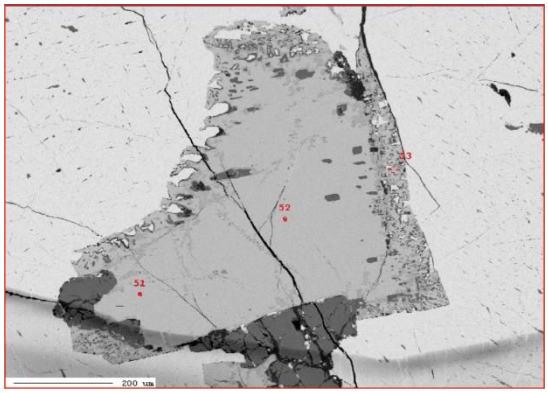

CC010 circle L LA-ICPMS

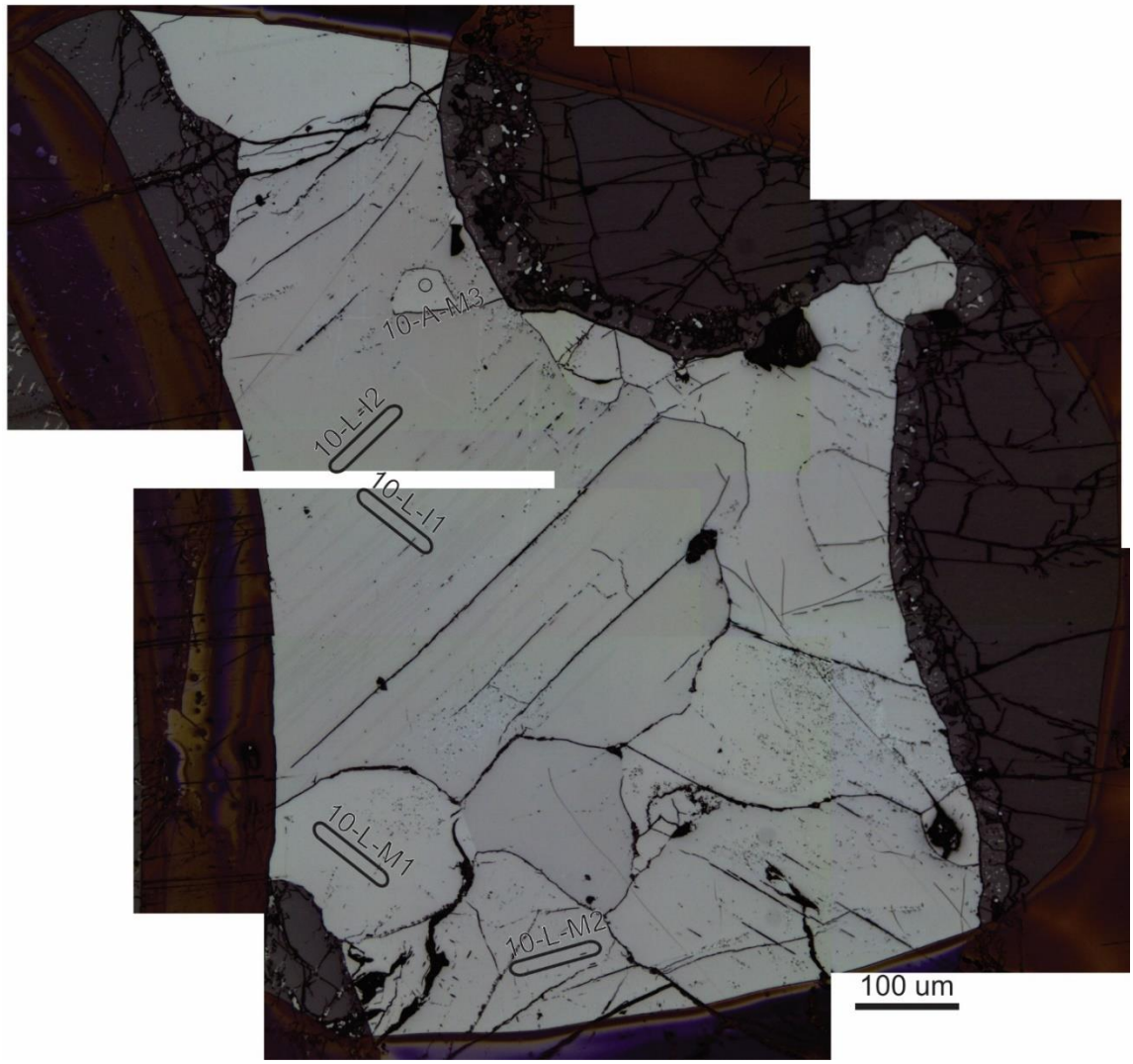

CC010 circle L EPMA

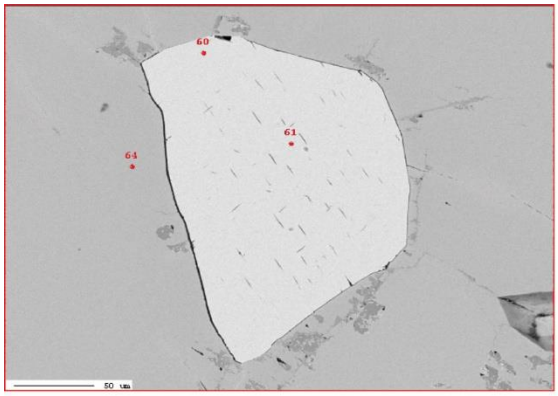

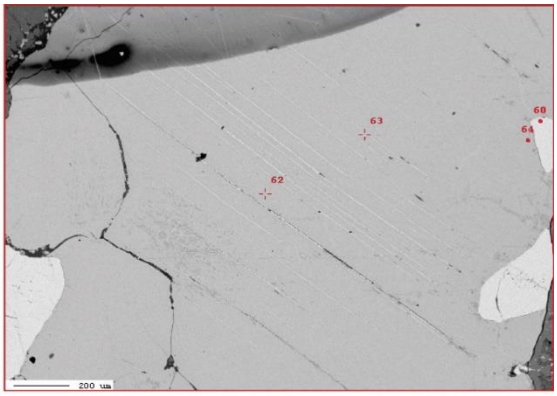

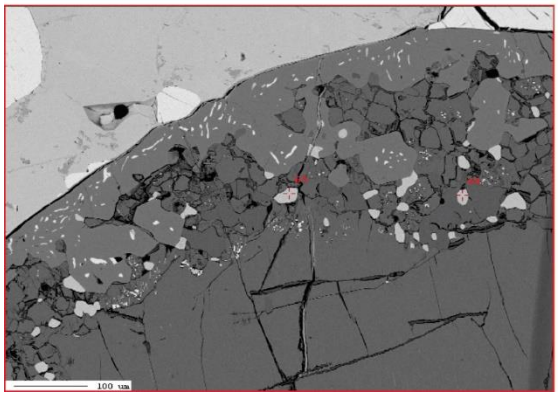

CC010 circle M LA-ICPMS

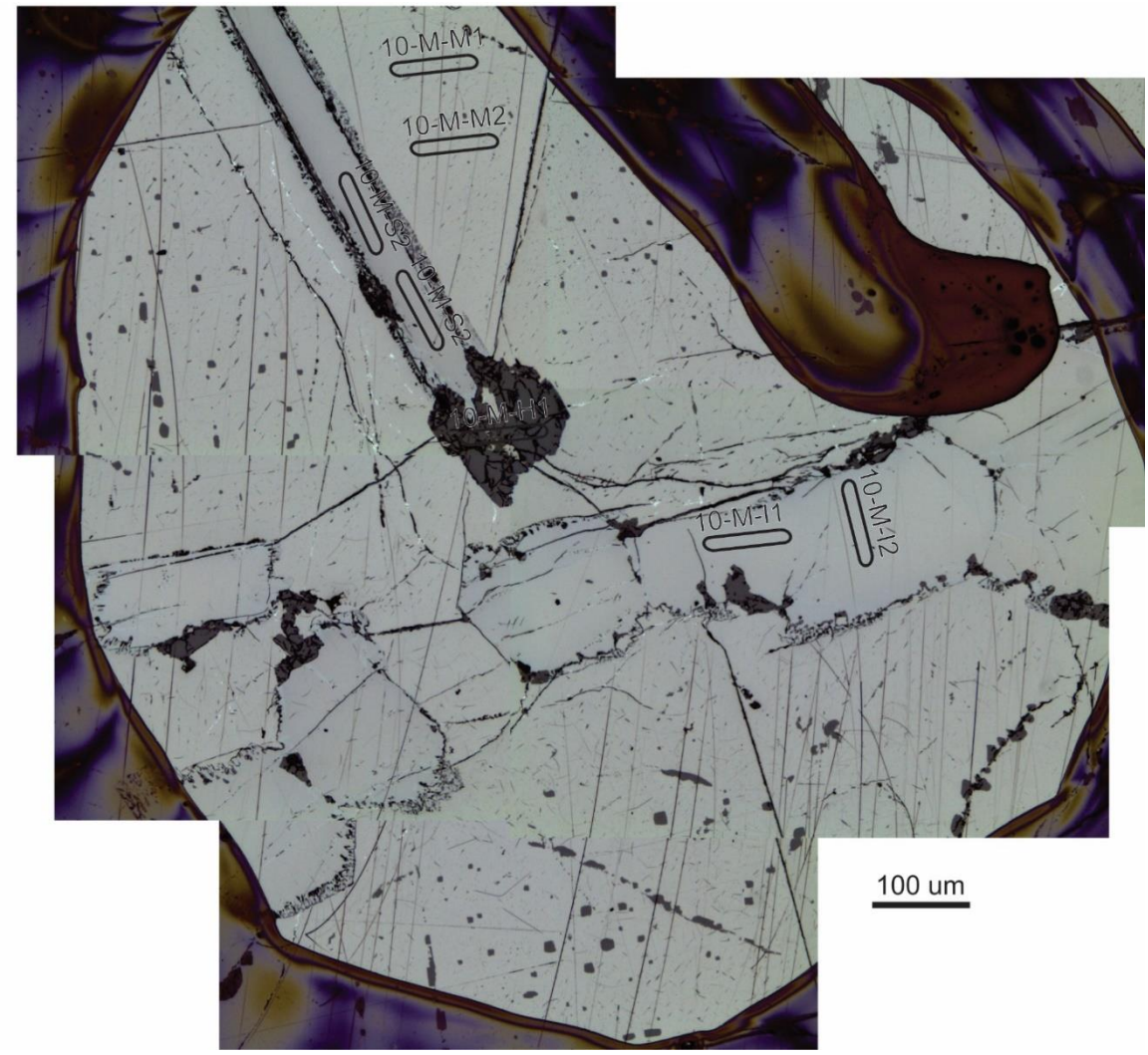

CC010 circle M EPMA

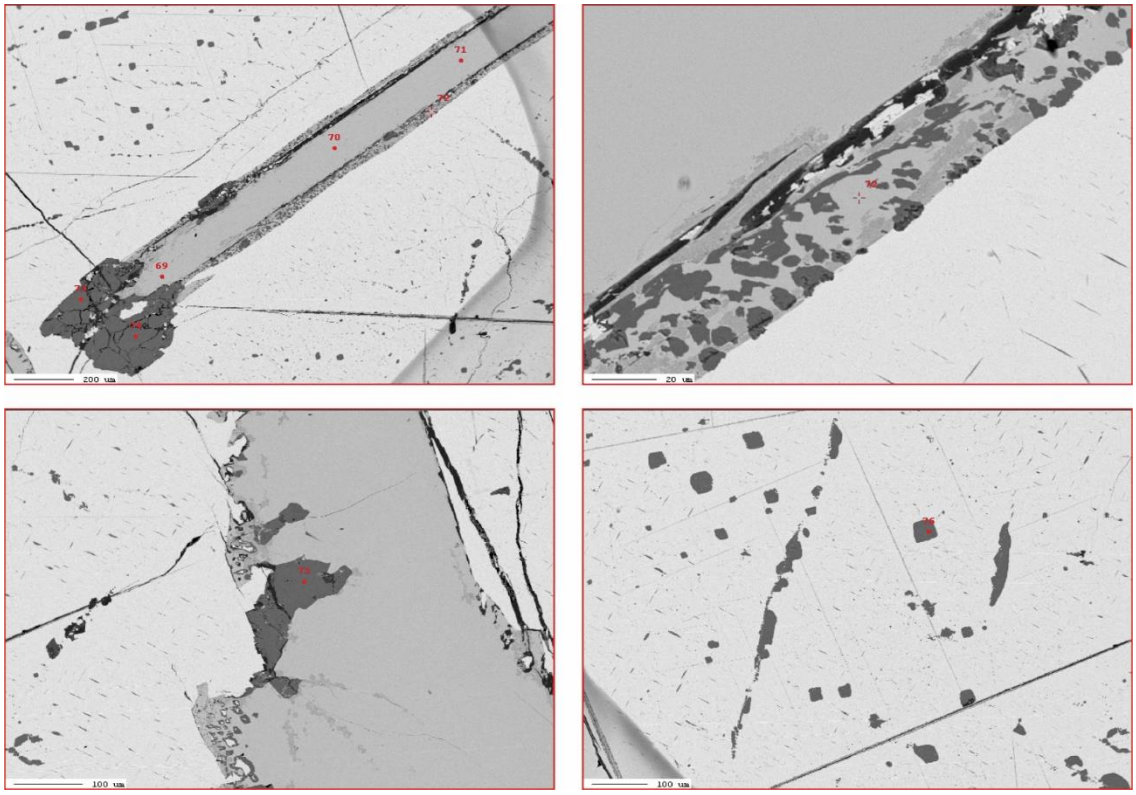

CC010 circle O LA-ICPMS

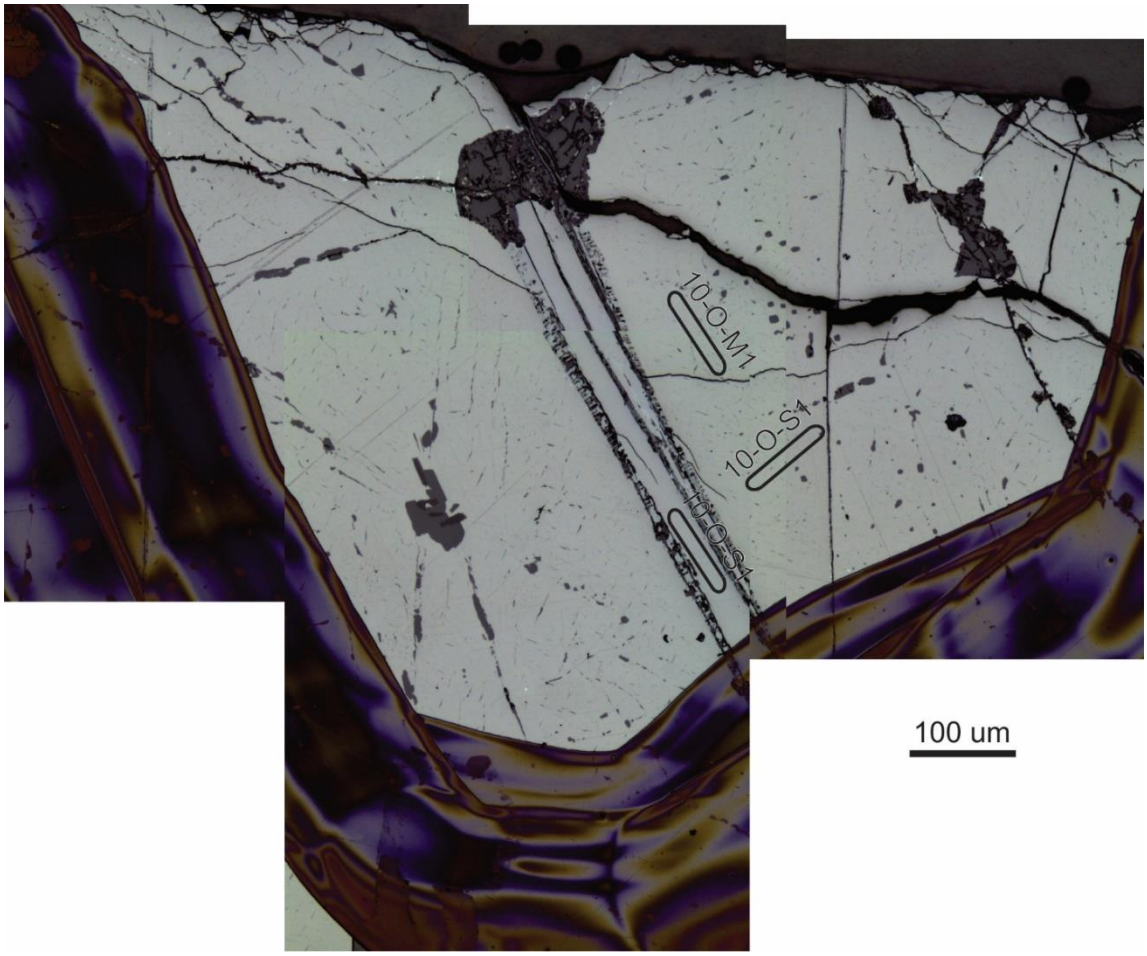

CC010 circle O EPMA

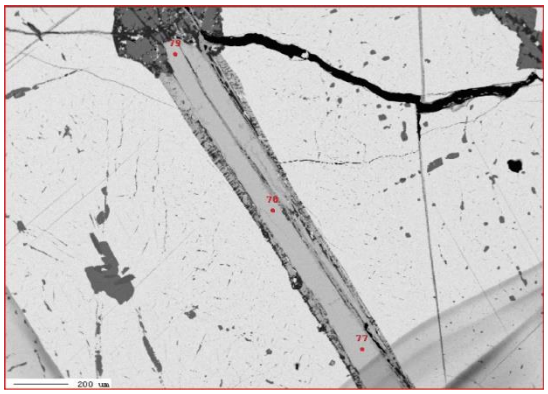

CC013 circle A LA-ICPMS

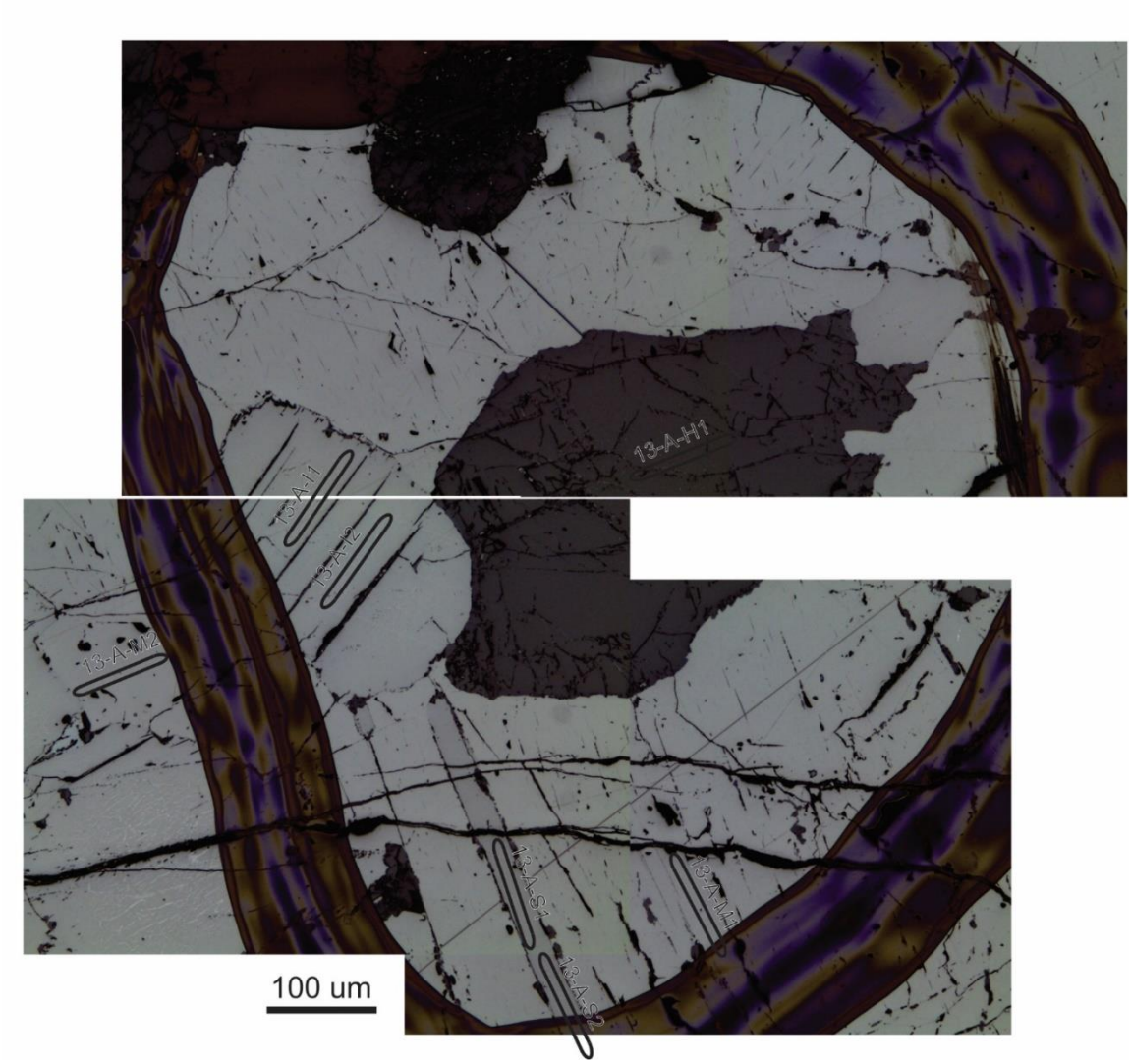

CC013 circle A EPMA

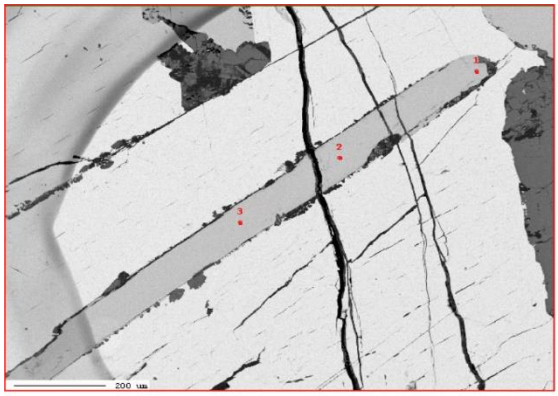

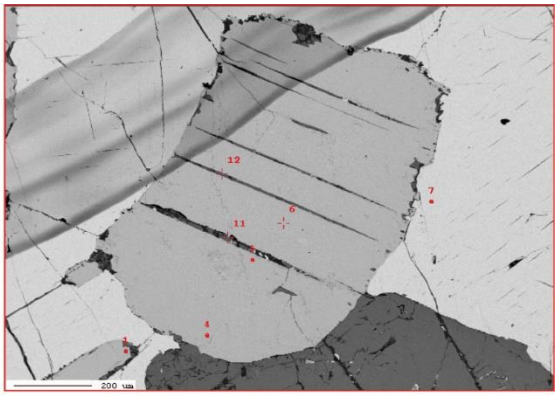

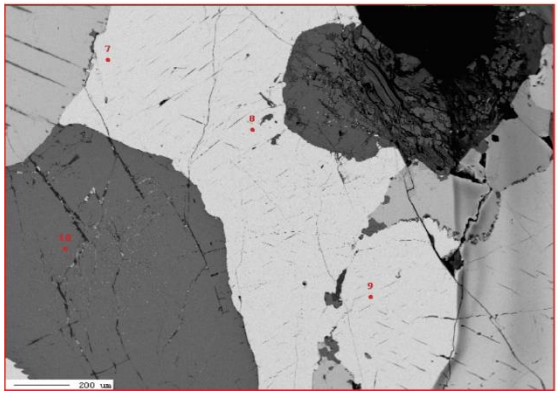

CC013 circle B LA-ICPMS

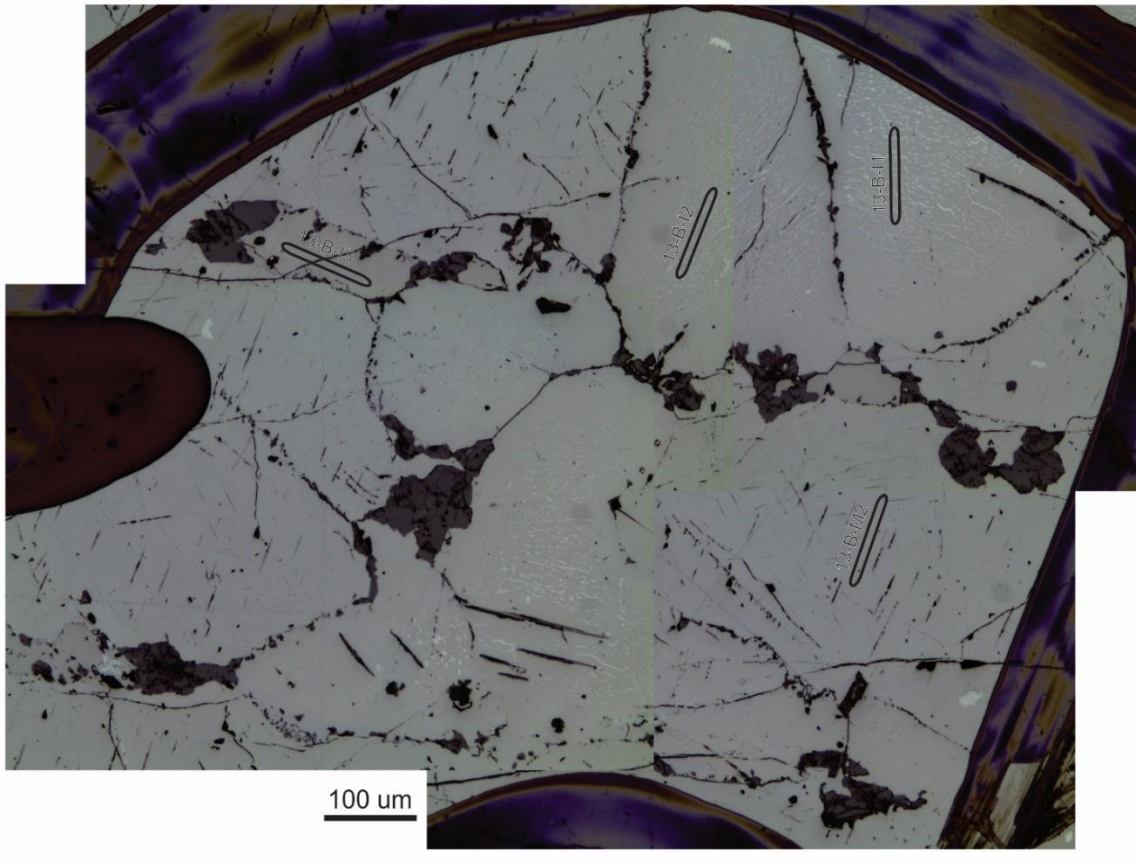

CC013 circle B EPMA

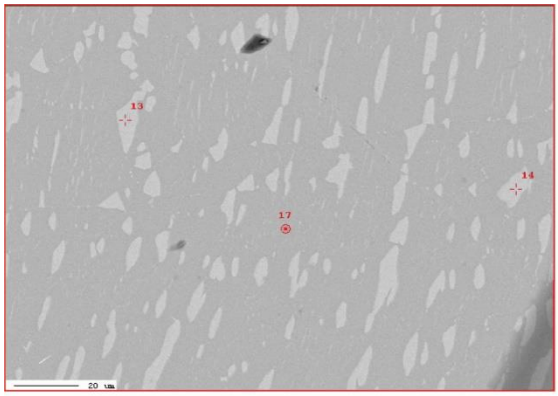

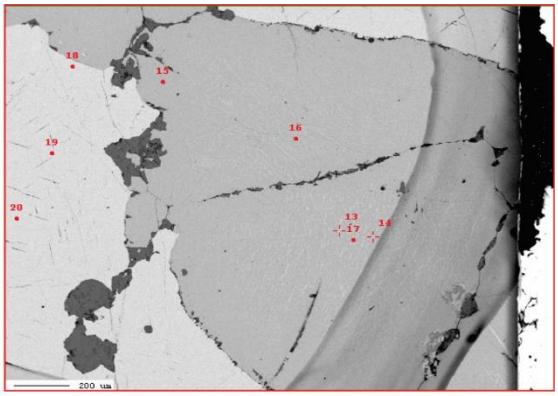

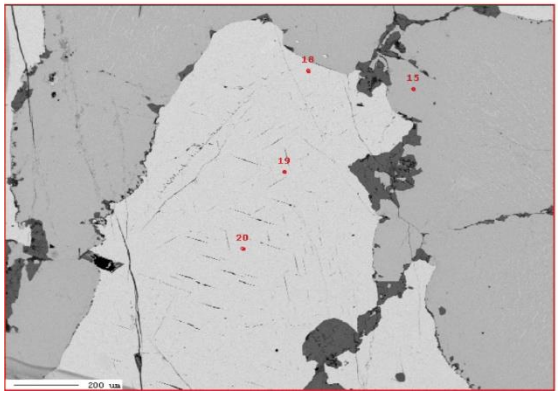

CC013 circle C LA-ICPMS

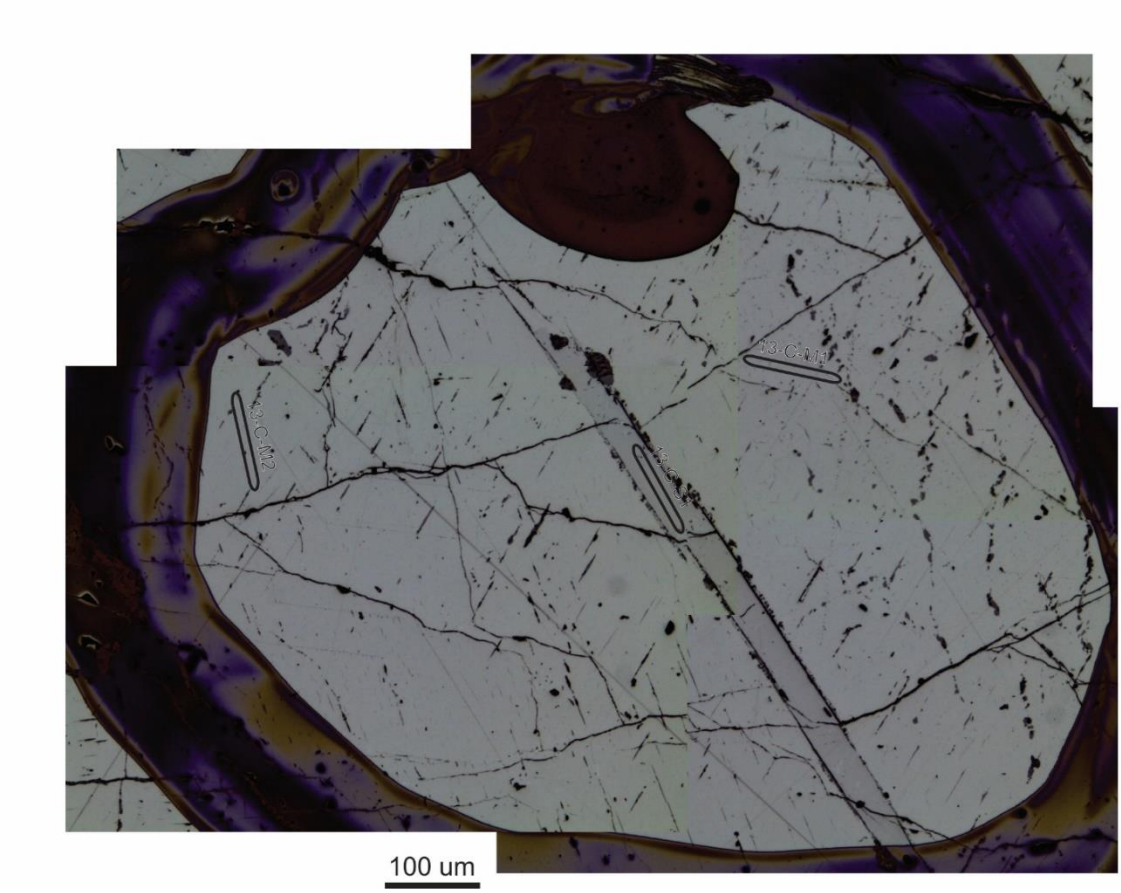

CC013 circle C EPMA

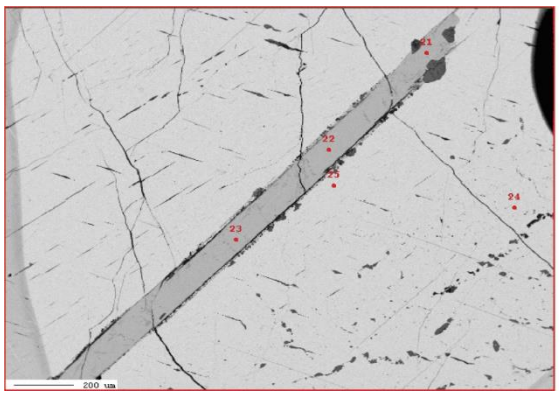

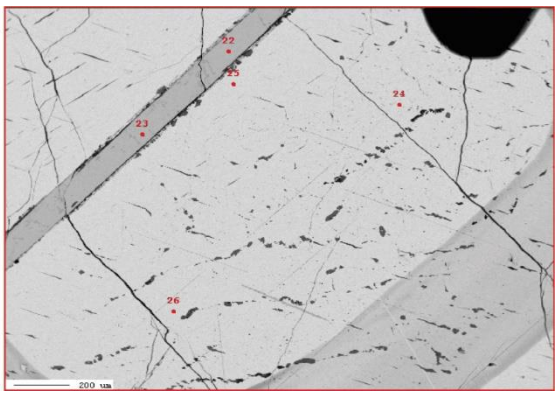

CC013 circle D LA-ICPMS

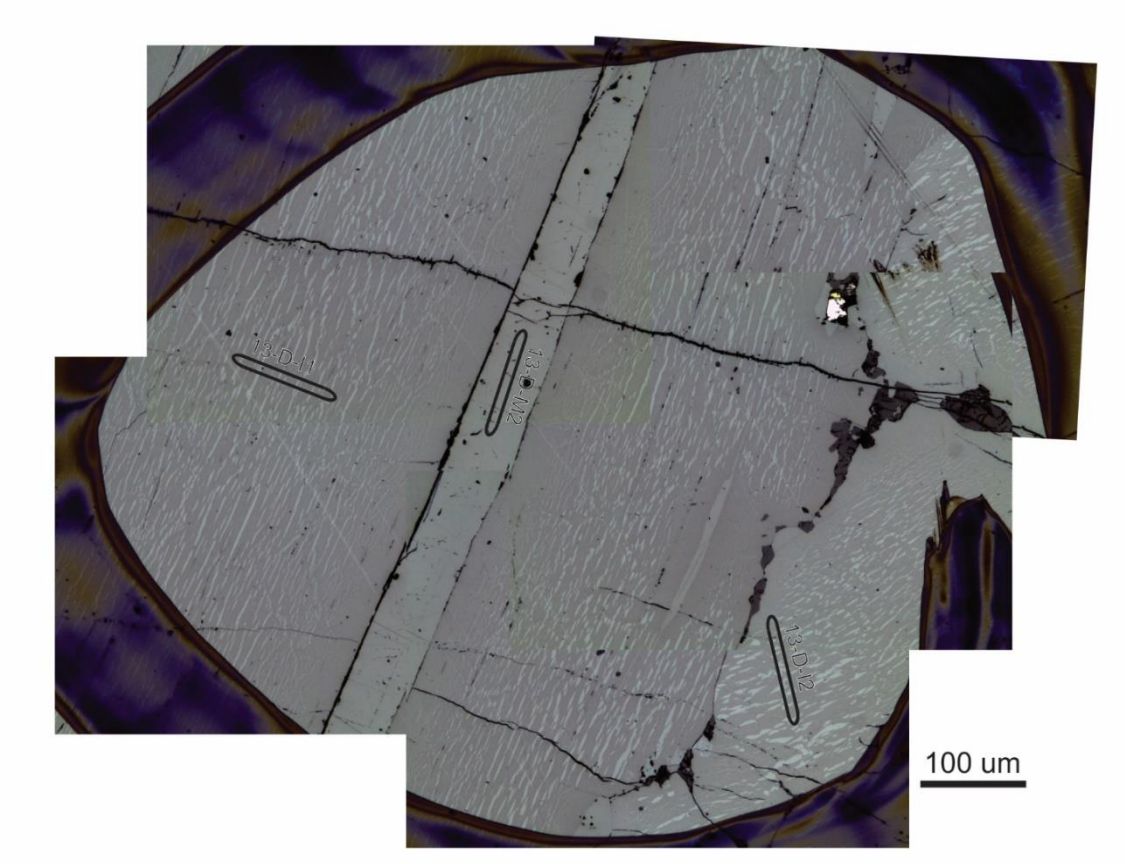

CC013 circle D EPMA

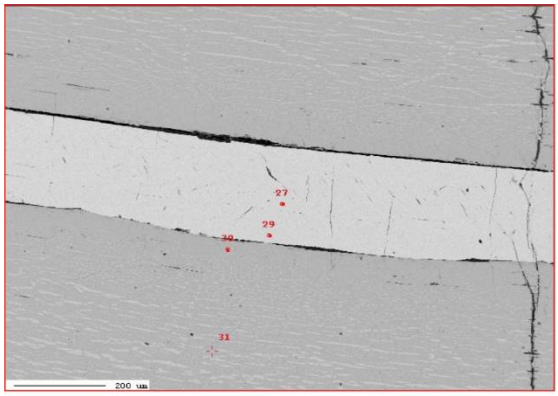

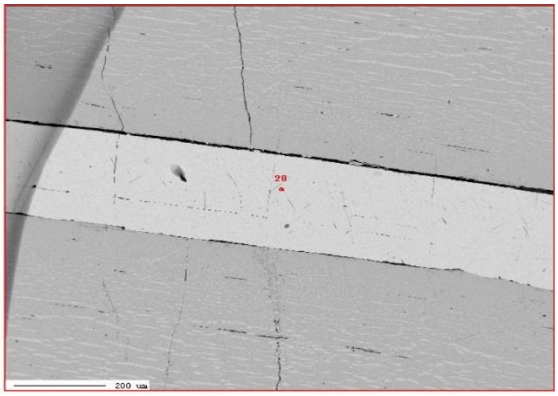

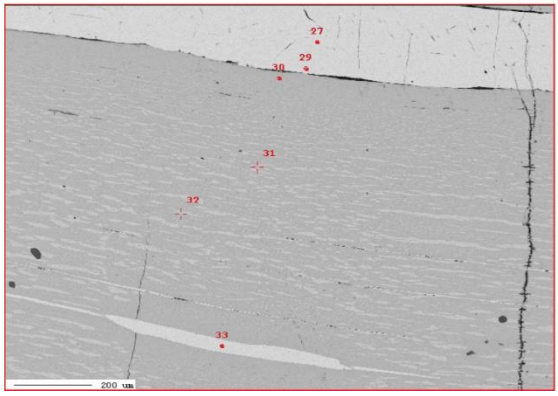

CC013 circle E LA-ICPMS

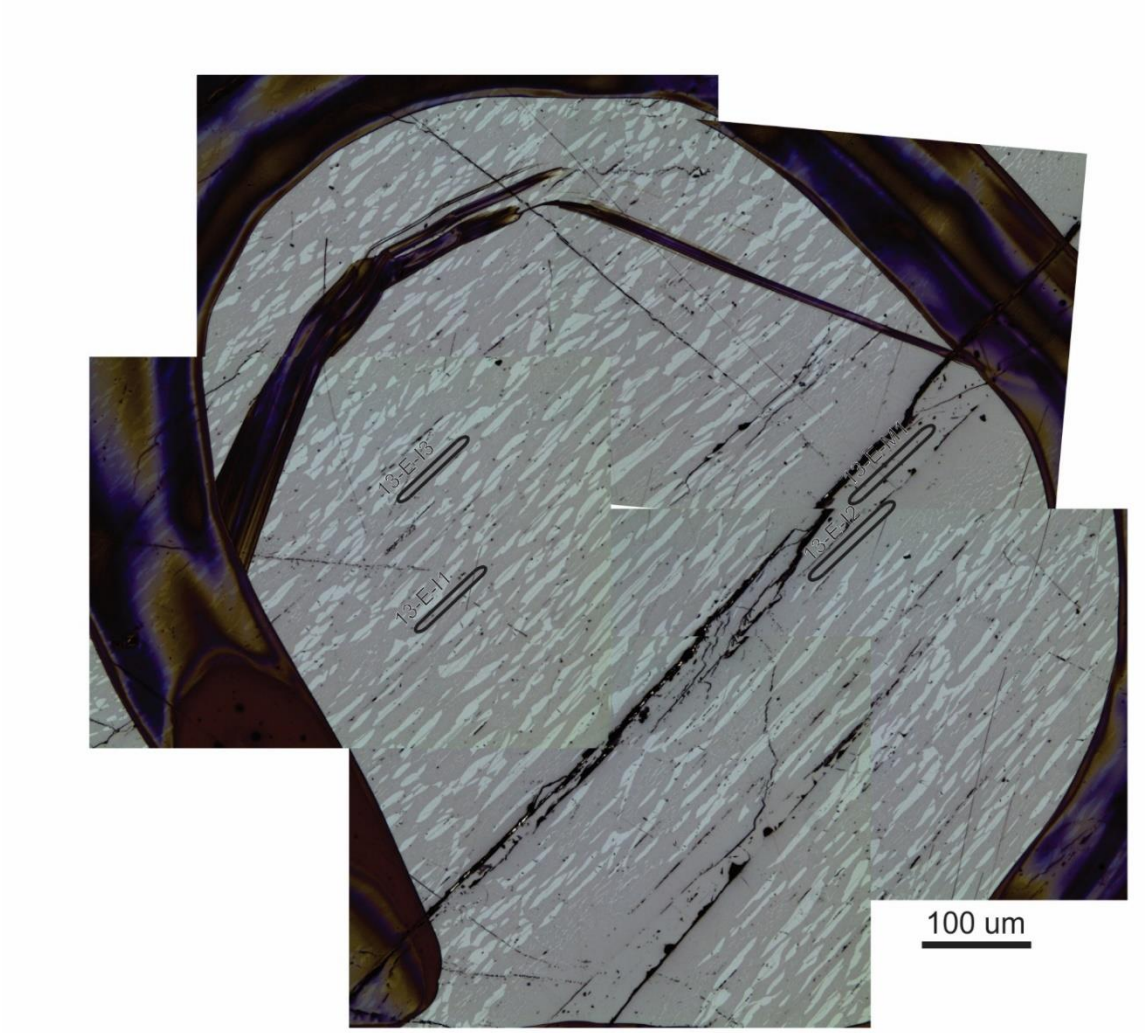

CC013 circle E EPMA

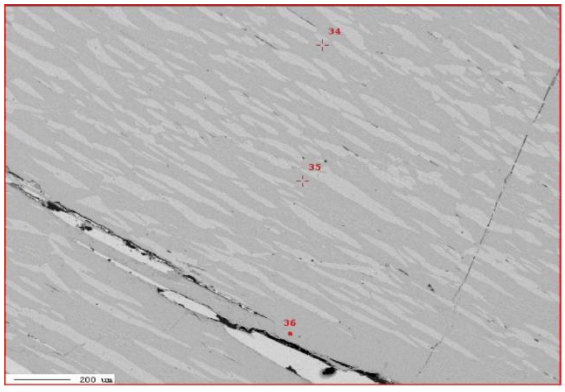

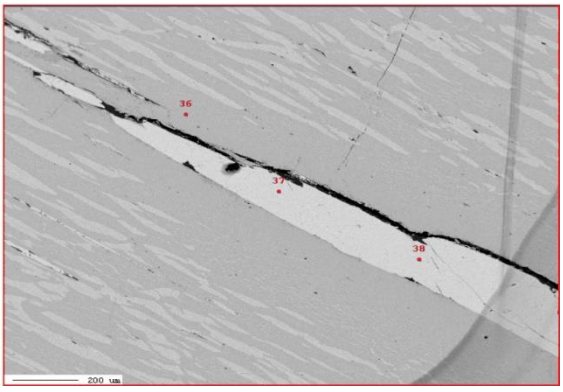

CC013 circle F LA-ICPMS

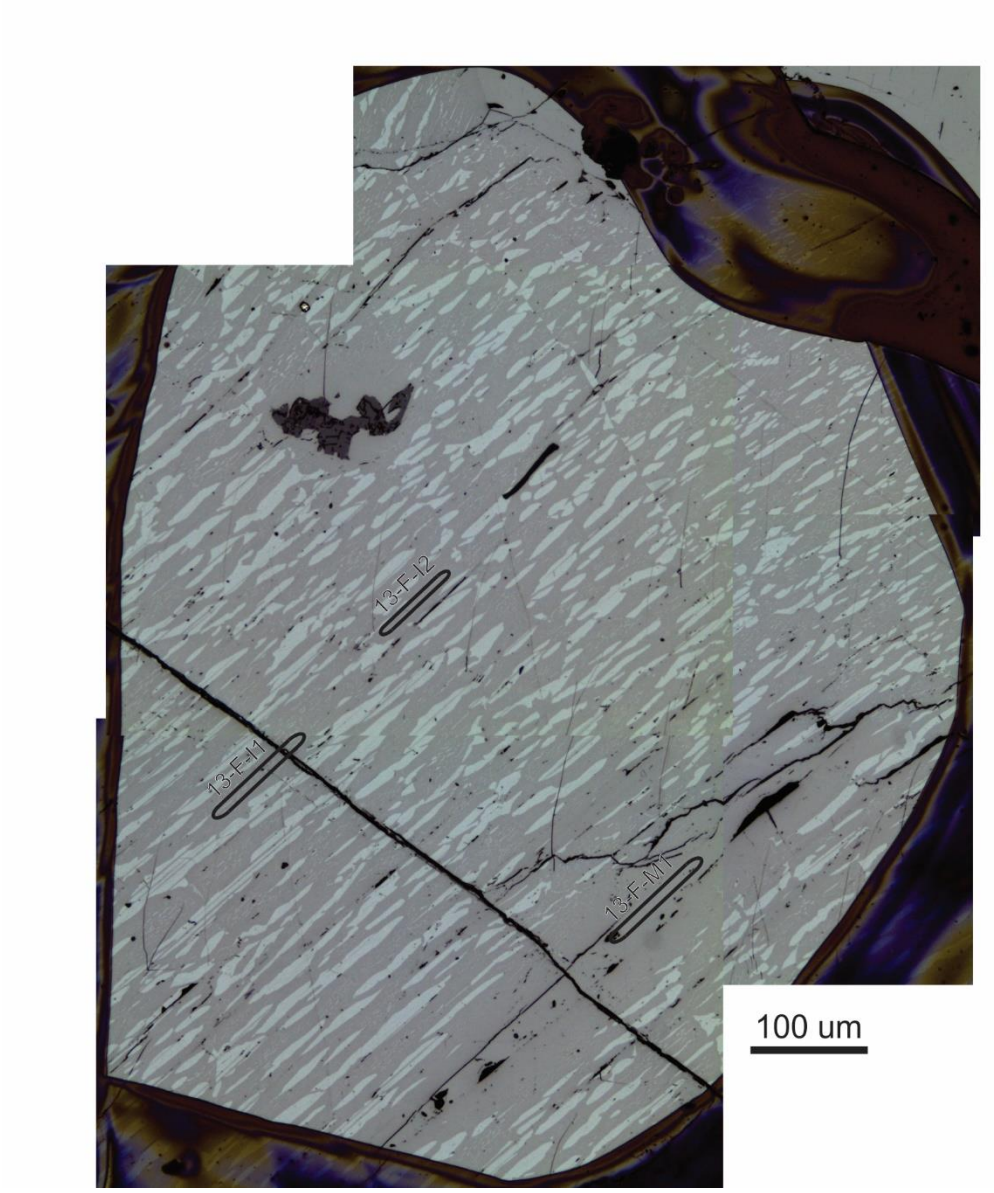

CC013 circle H LA-ICPMS

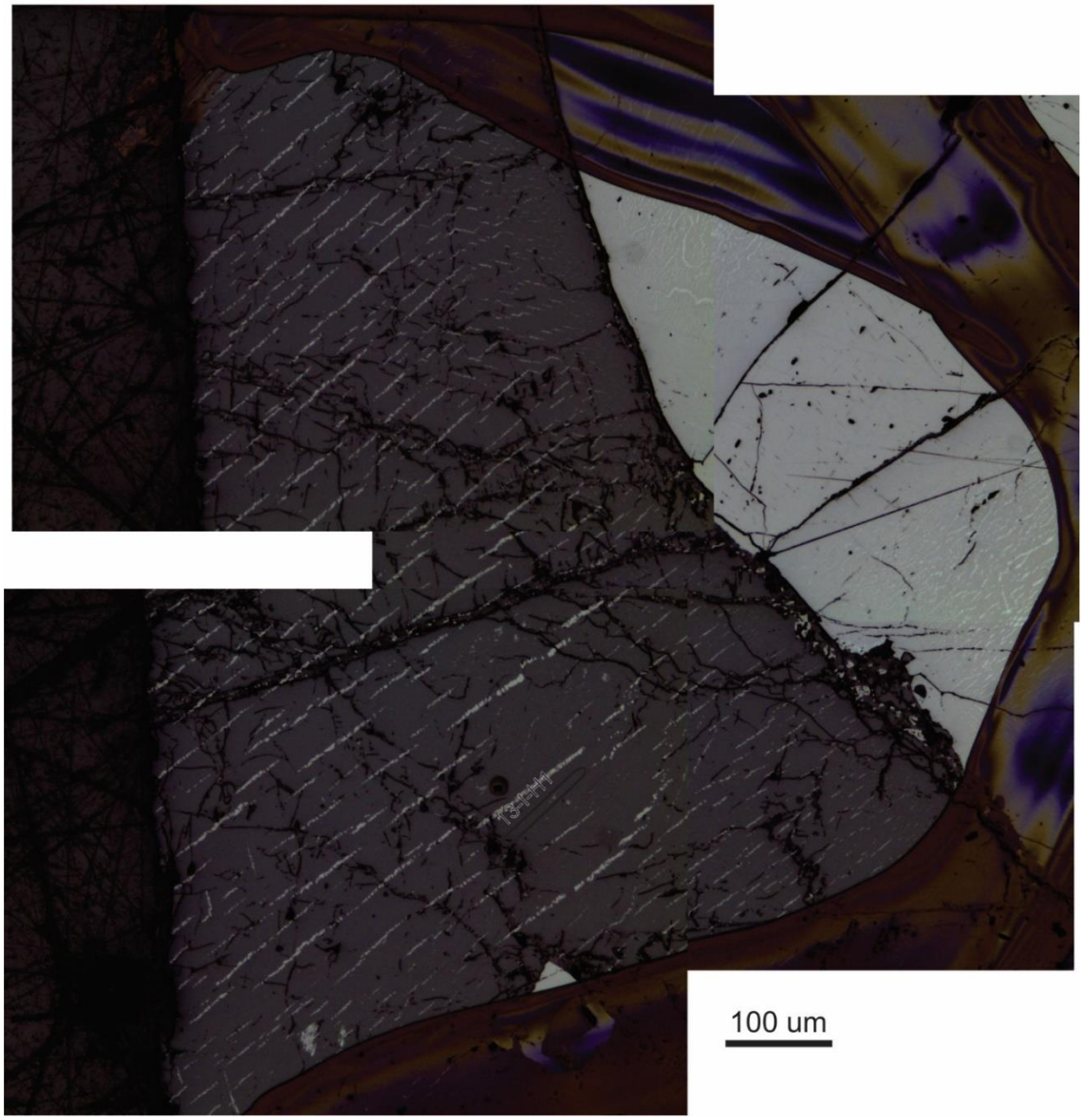

CC013 circle I EPMA

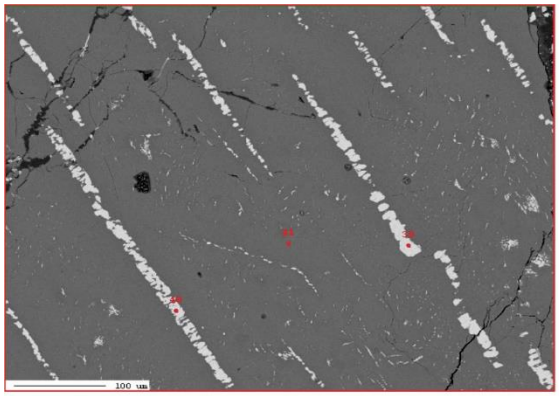

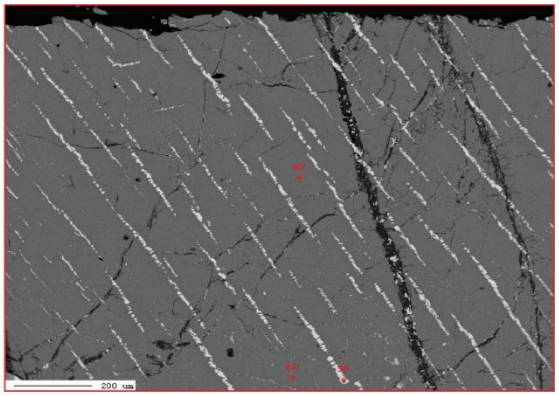

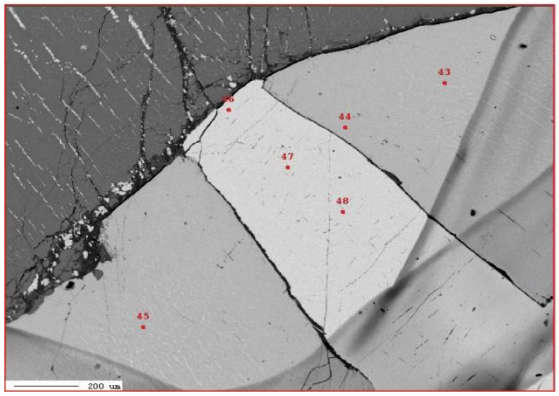

CC013 circle L LA-ICPMS

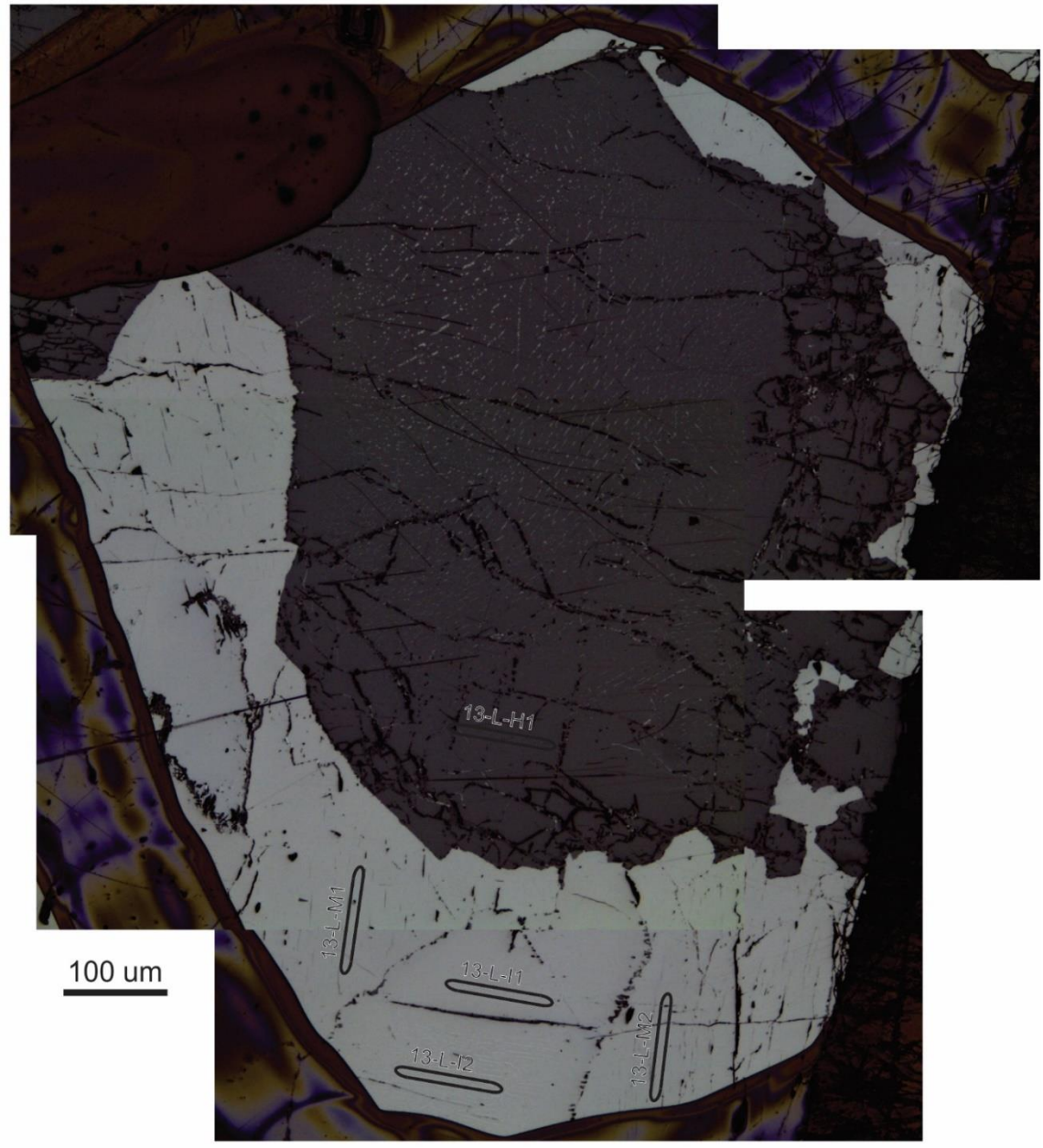

CC013 circle L EPMA

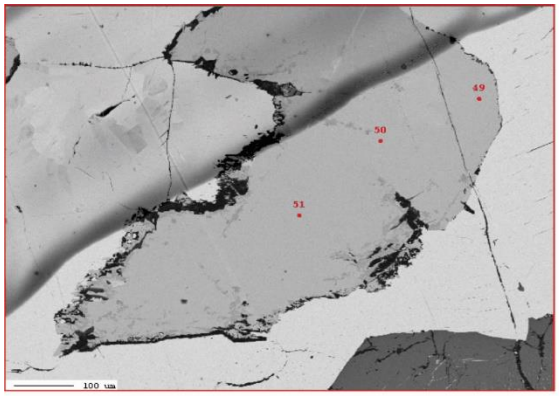

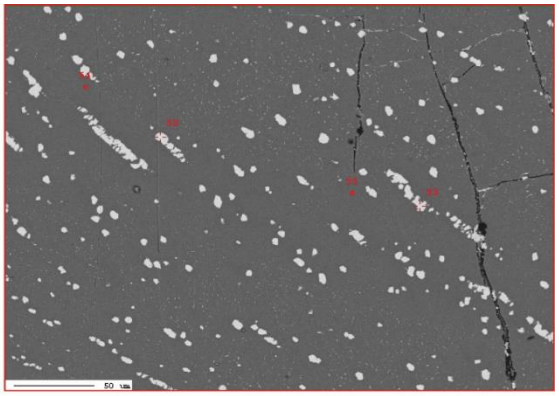

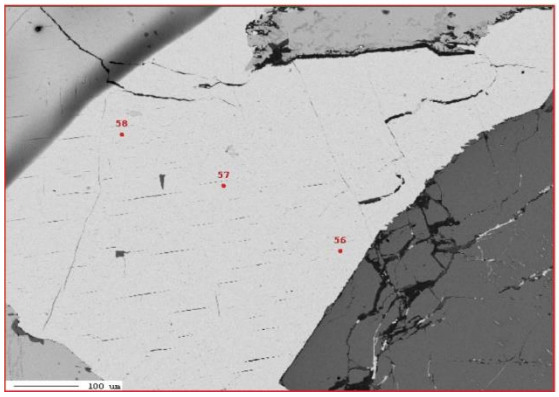

CC013 circle M EPMA

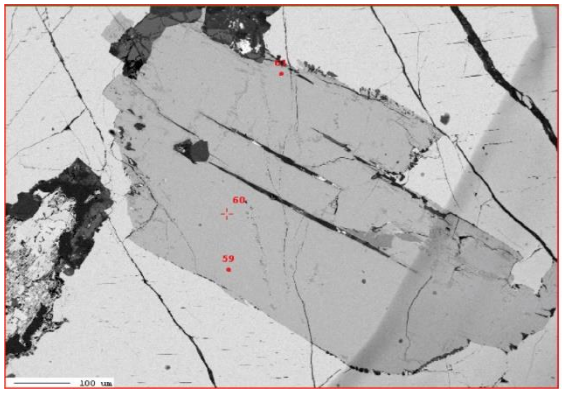

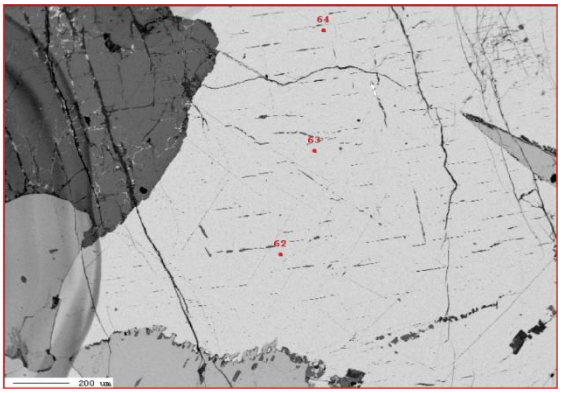

CC013 circle P LA-ICPMS

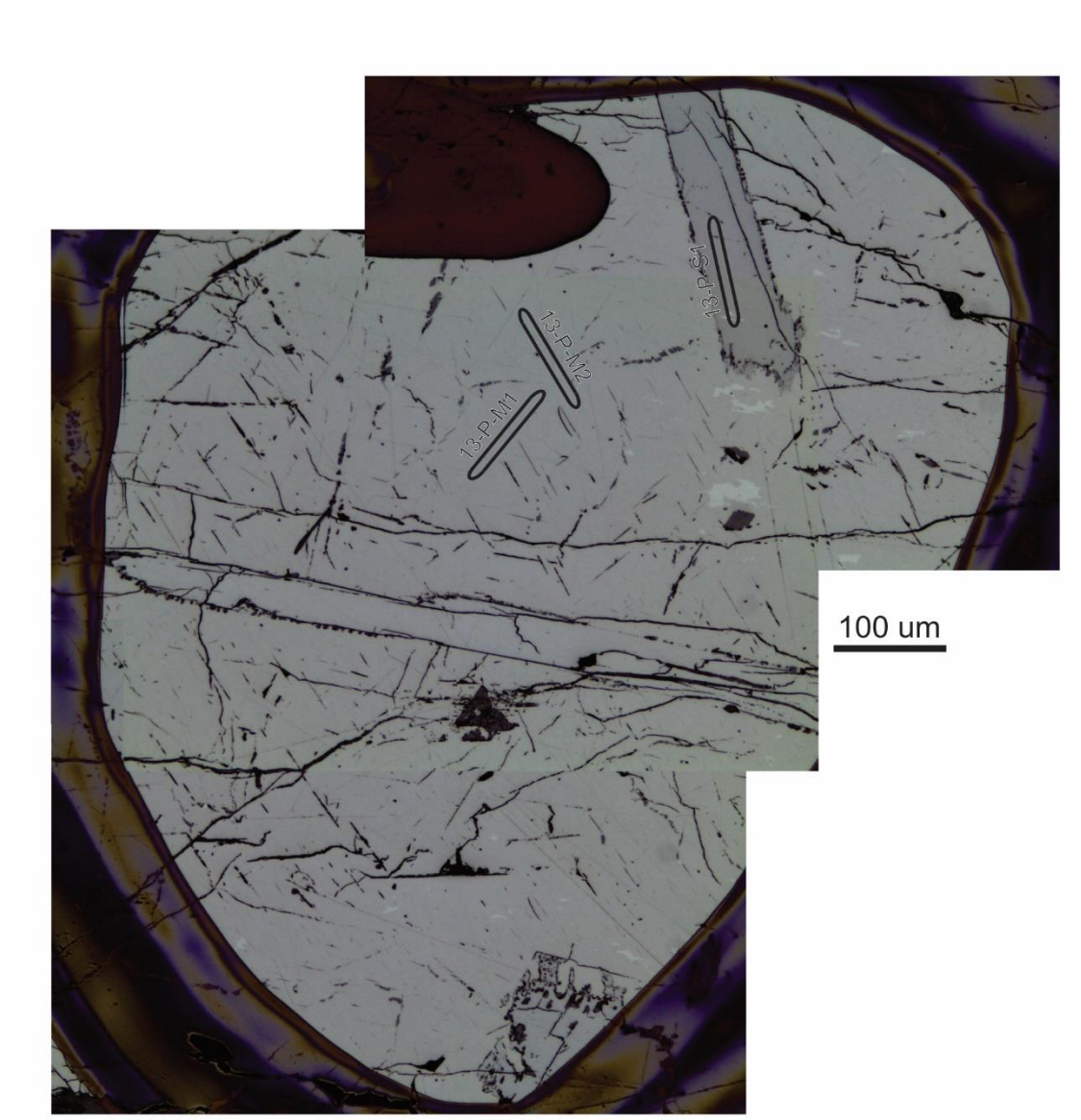

CC013 circle P EPMA

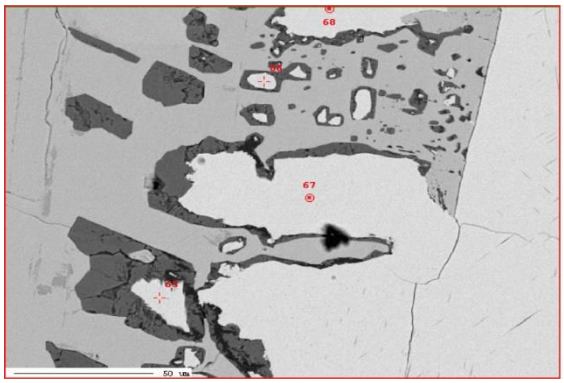

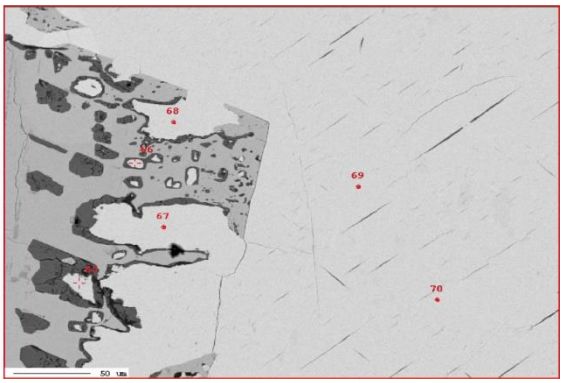

CC025 circle A EPMA

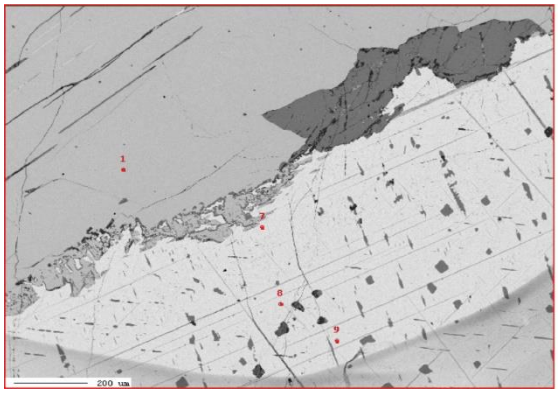

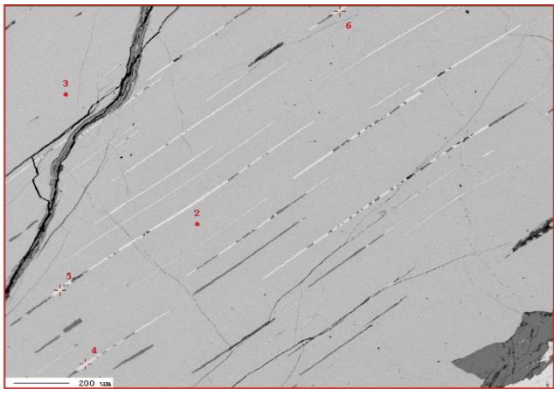

CC025 circle B EPMA

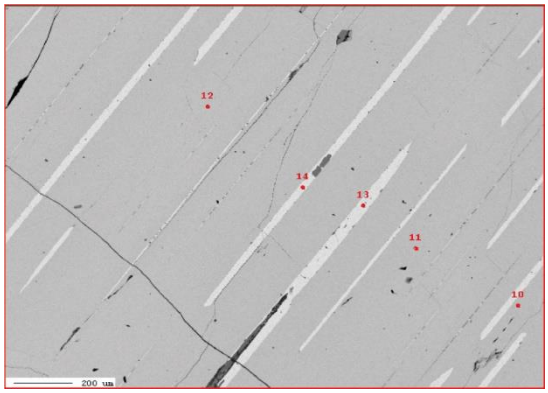

CC025 circle C LA-ICPMS

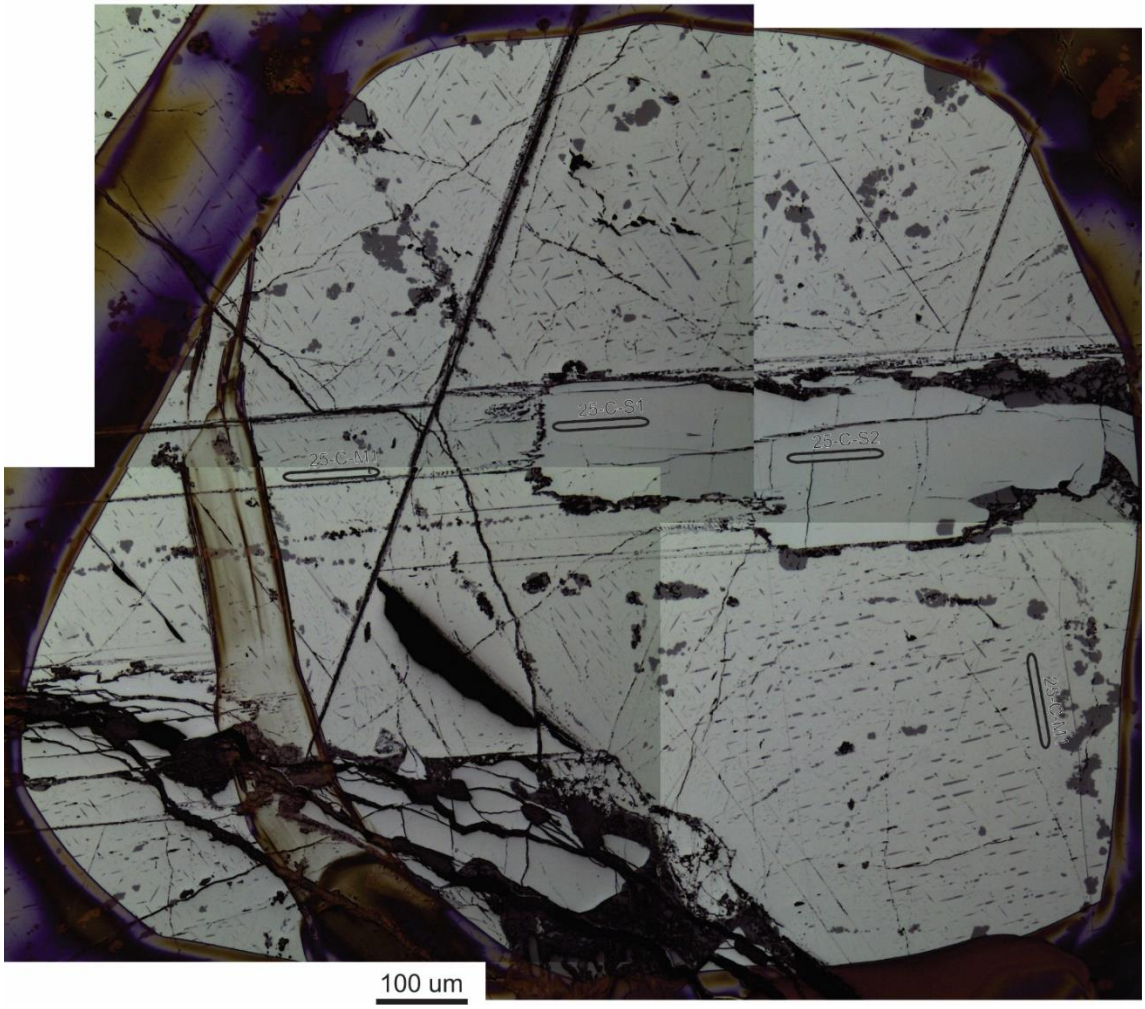

CC025 circle C EPMA

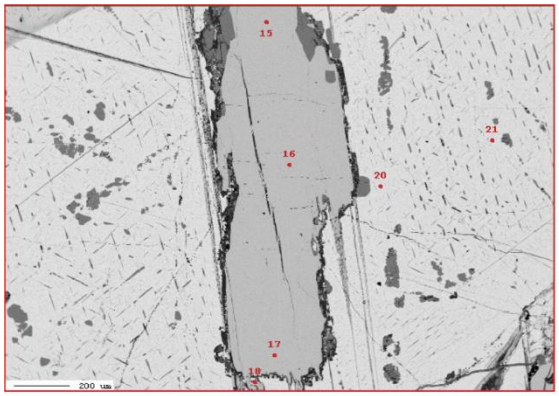

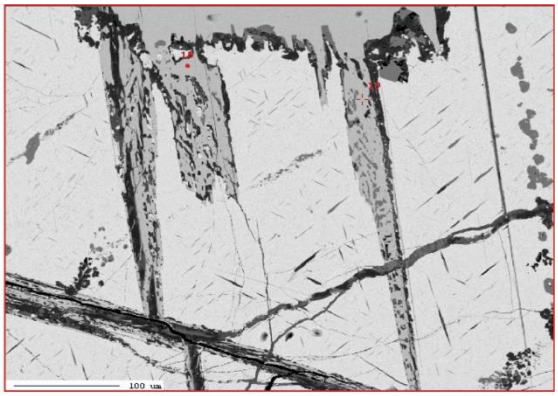

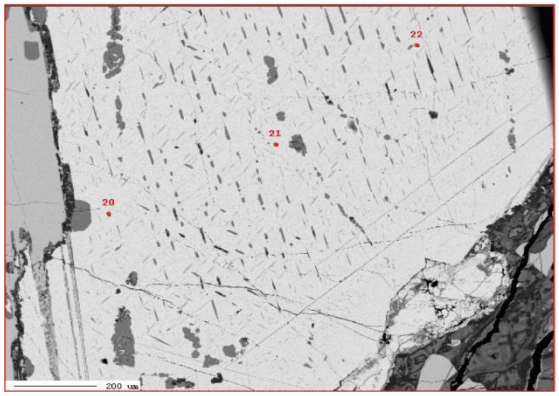

CC025 circle D LA-ICPMS

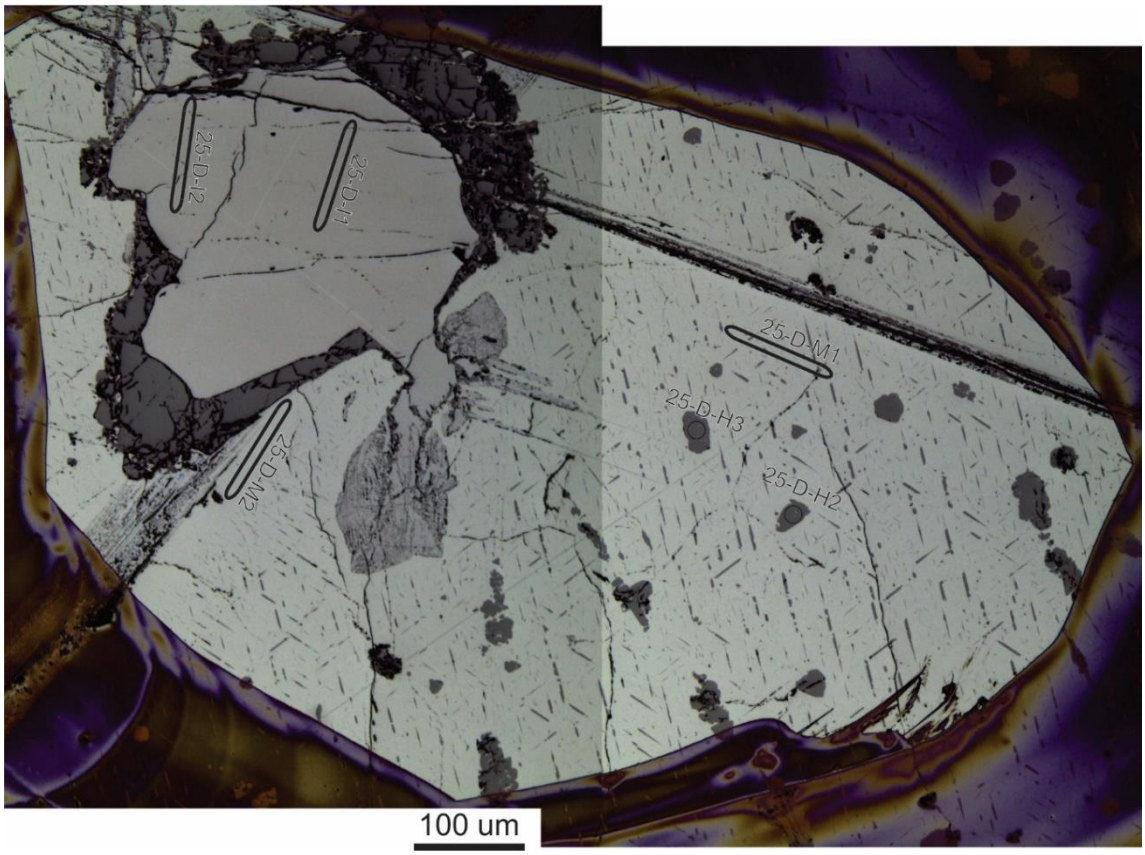

CC025 circle D EPMA

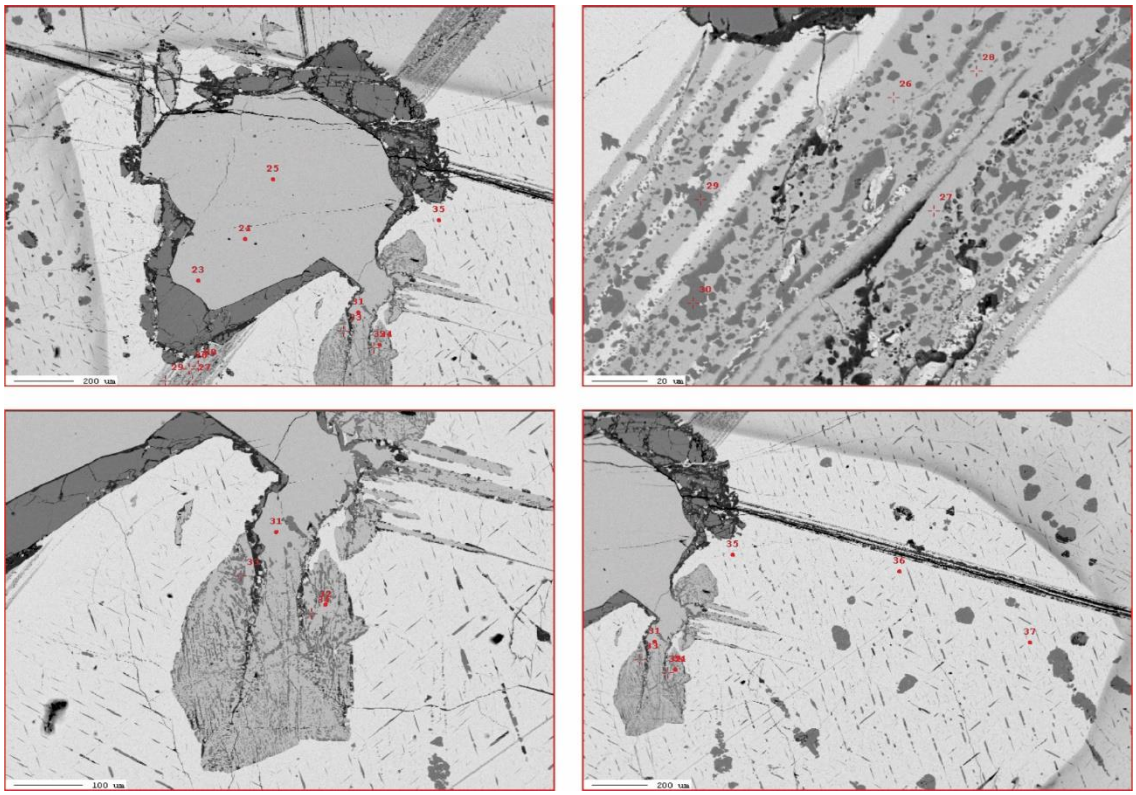

CC025 circle E LA-ICPMS

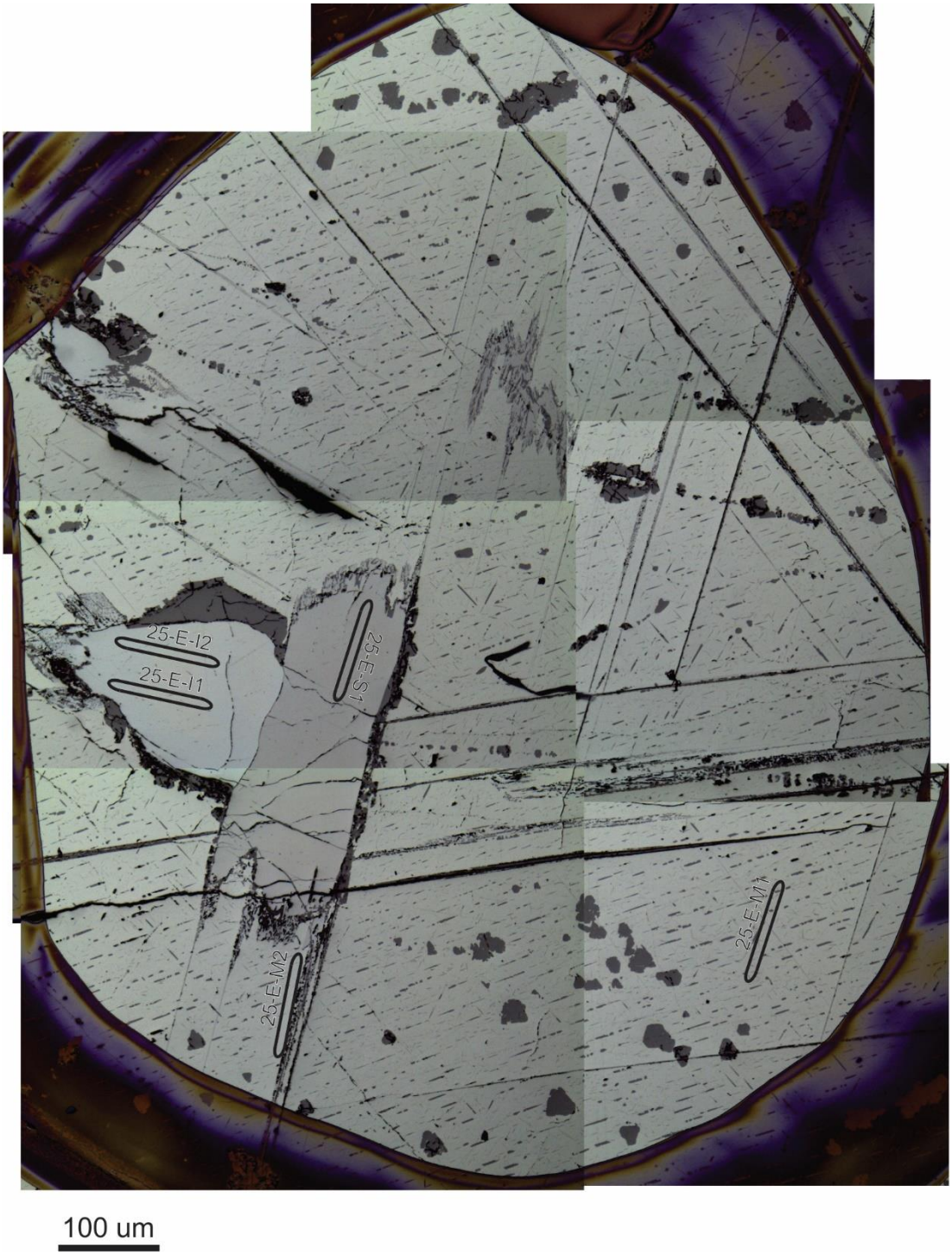

CC025 circle E EPMA

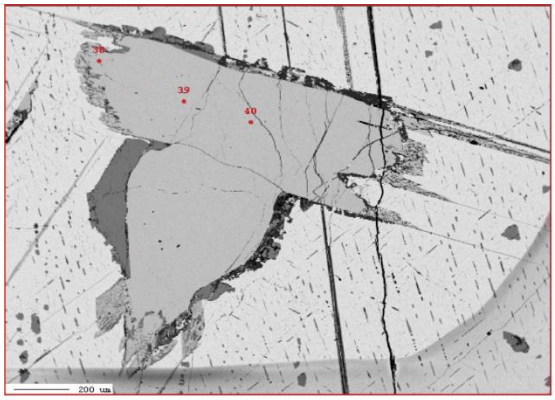

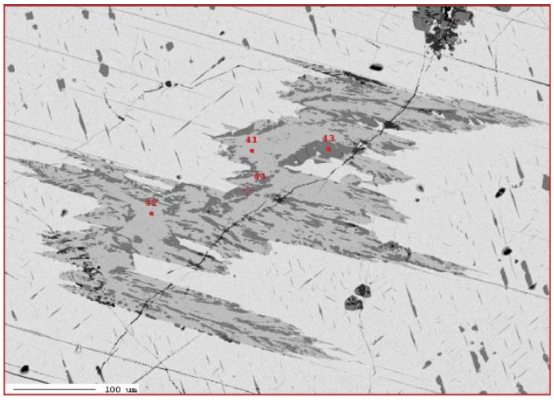

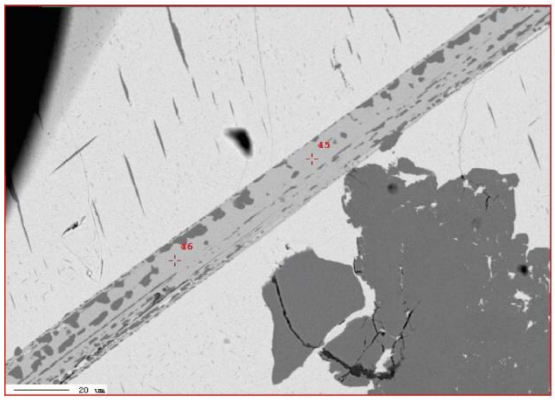

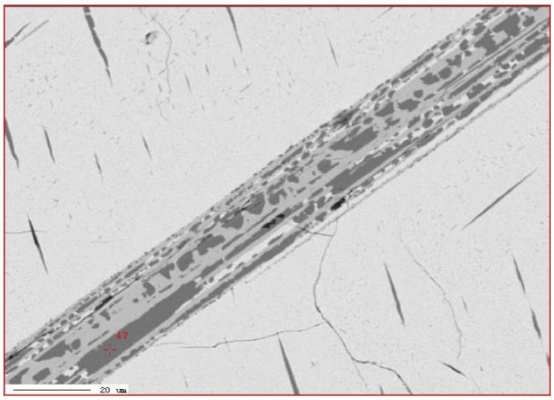

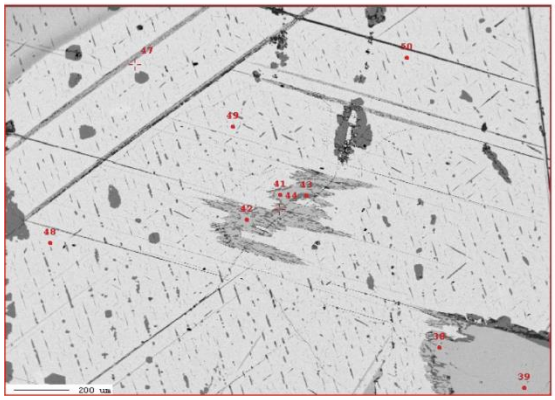

CC025 circle F LA-ICPMS

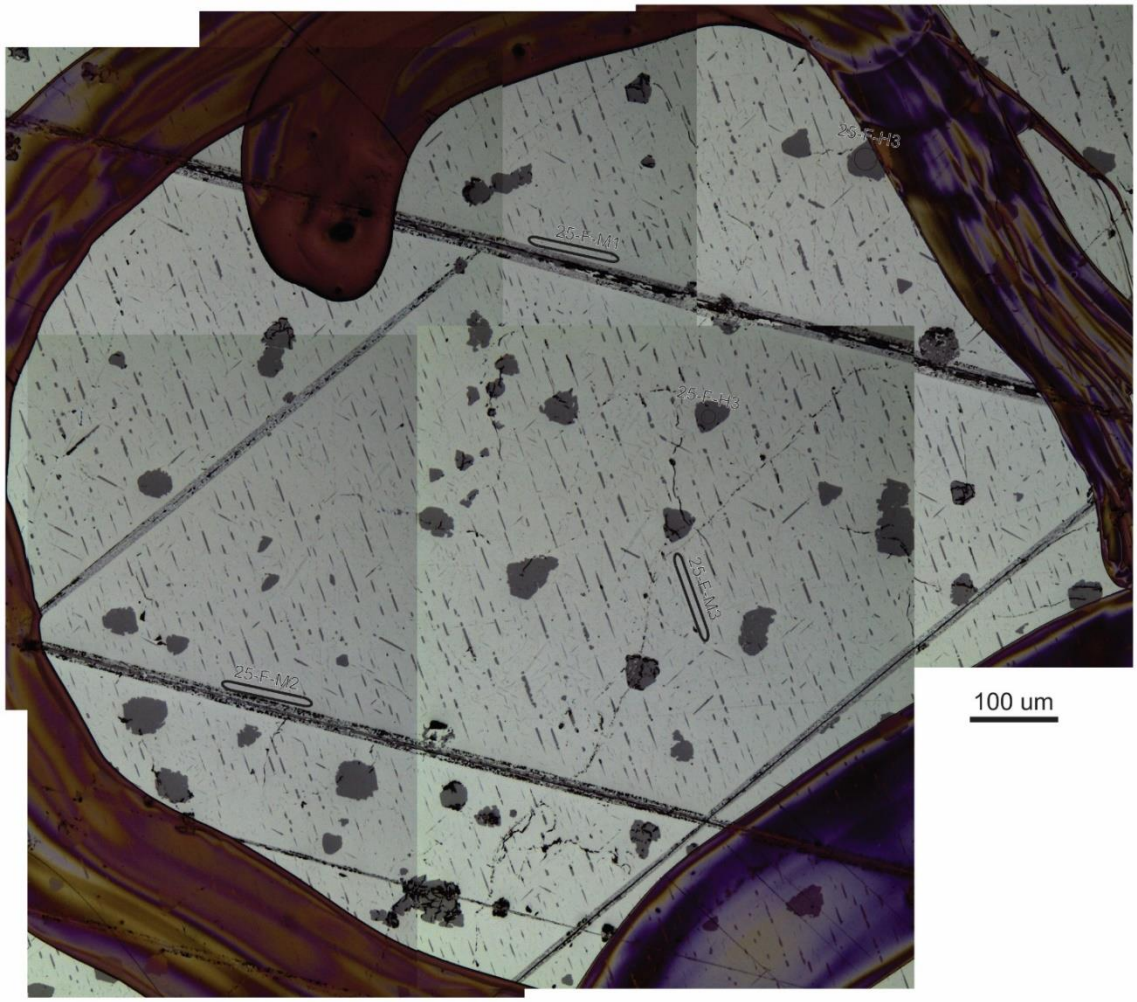

CC025 circle G LA-ICPMS

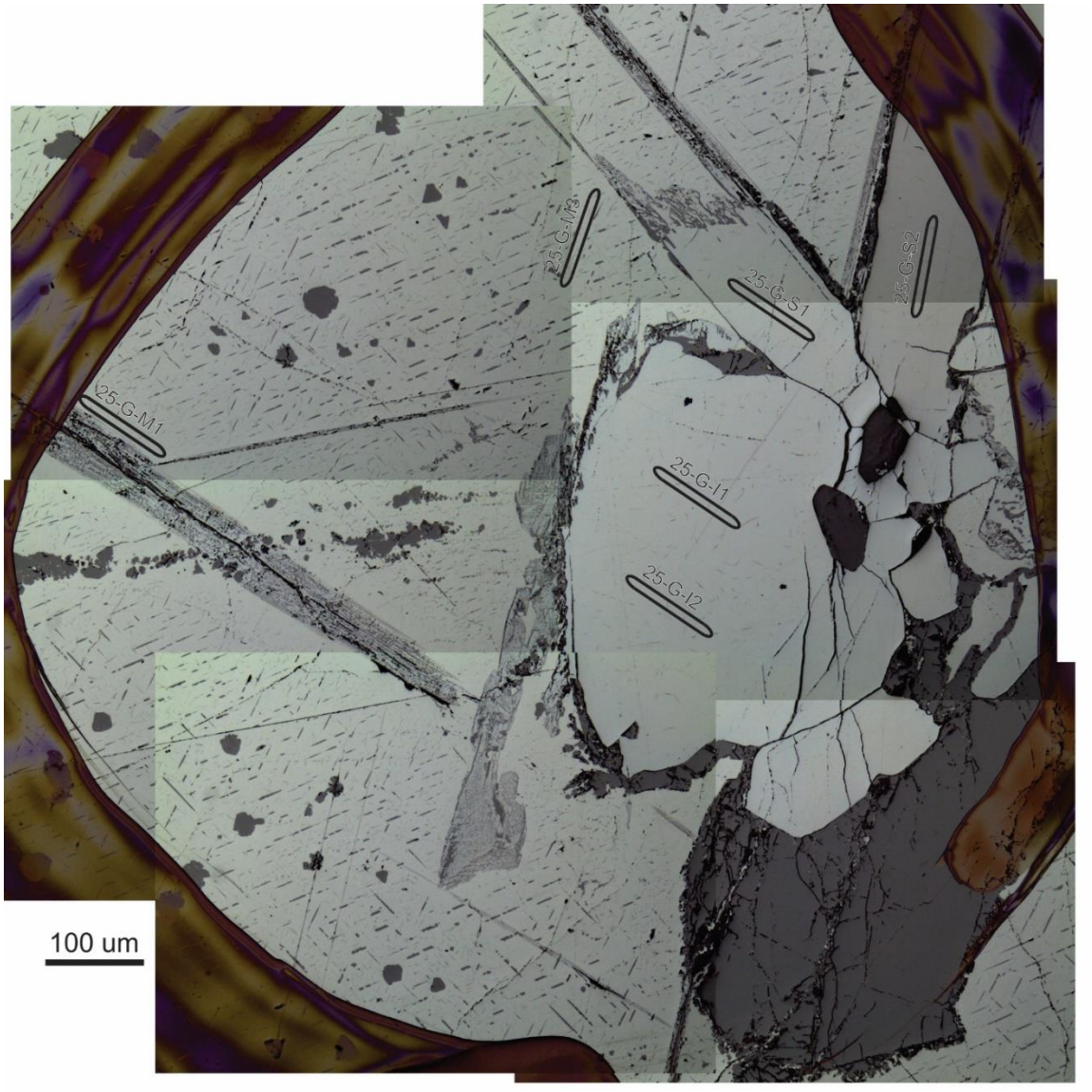

CC025 circle G EPMA

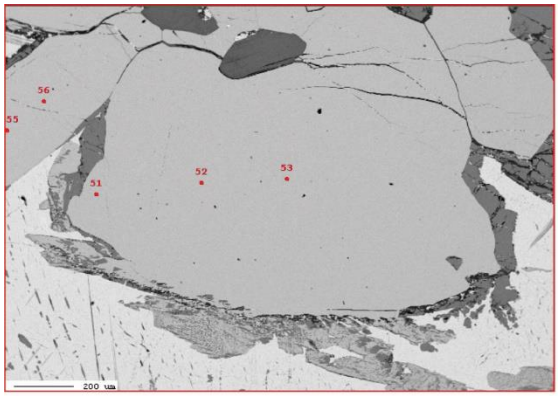

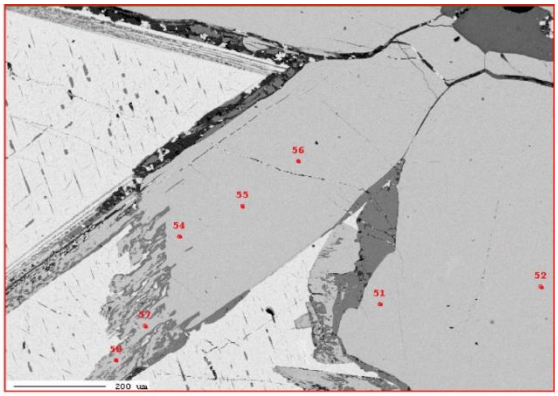

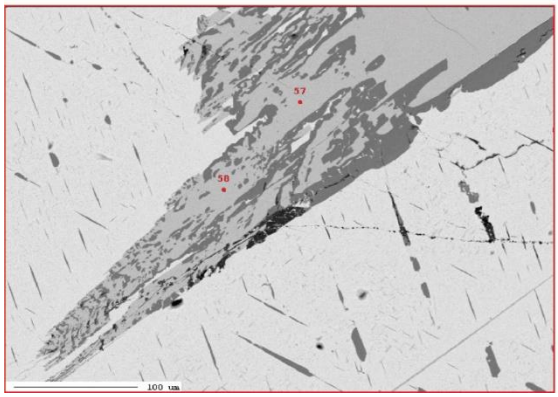

CC025 circle H LA-ICPMS

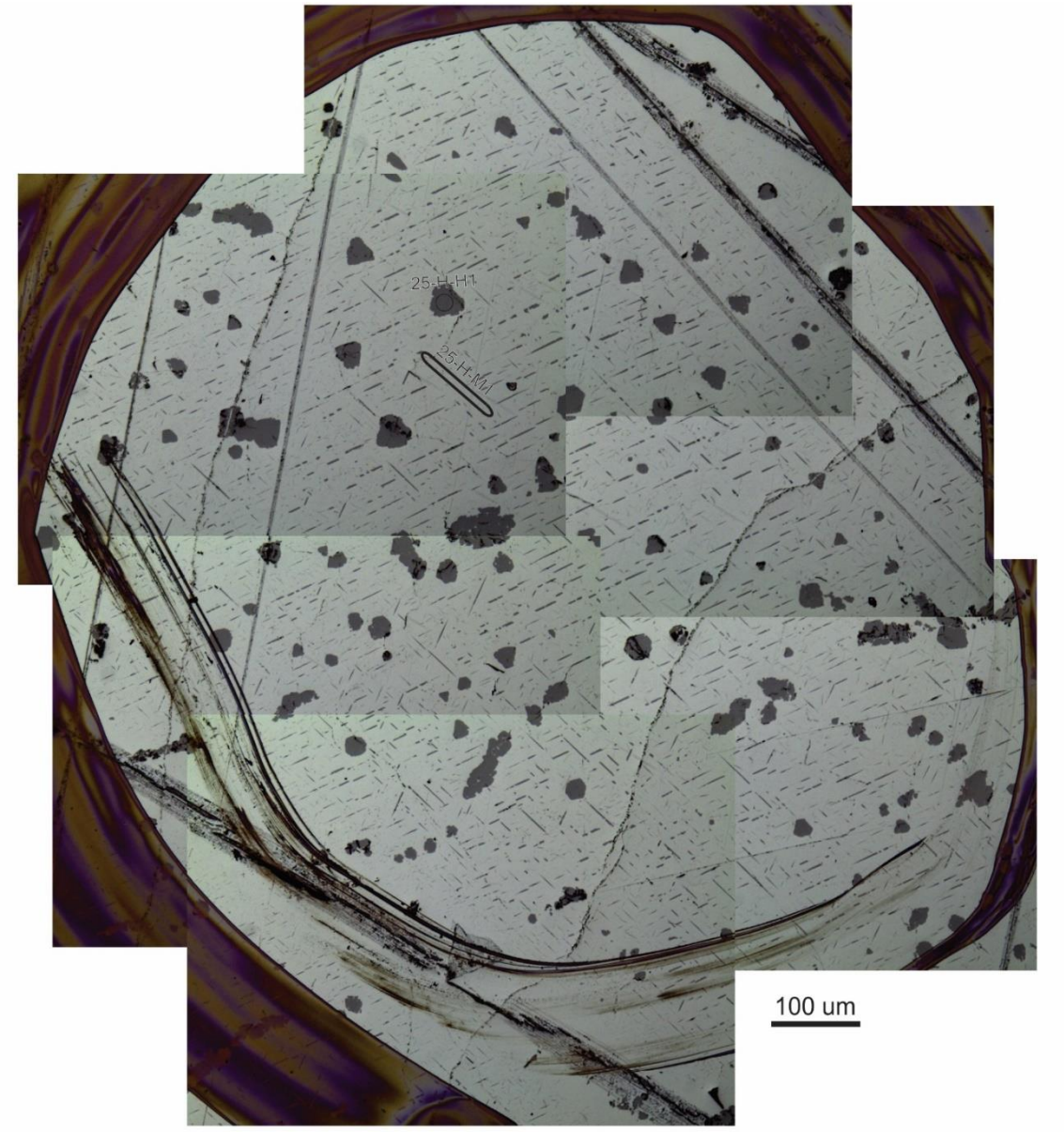

CC025 circle I LA-ICPMS

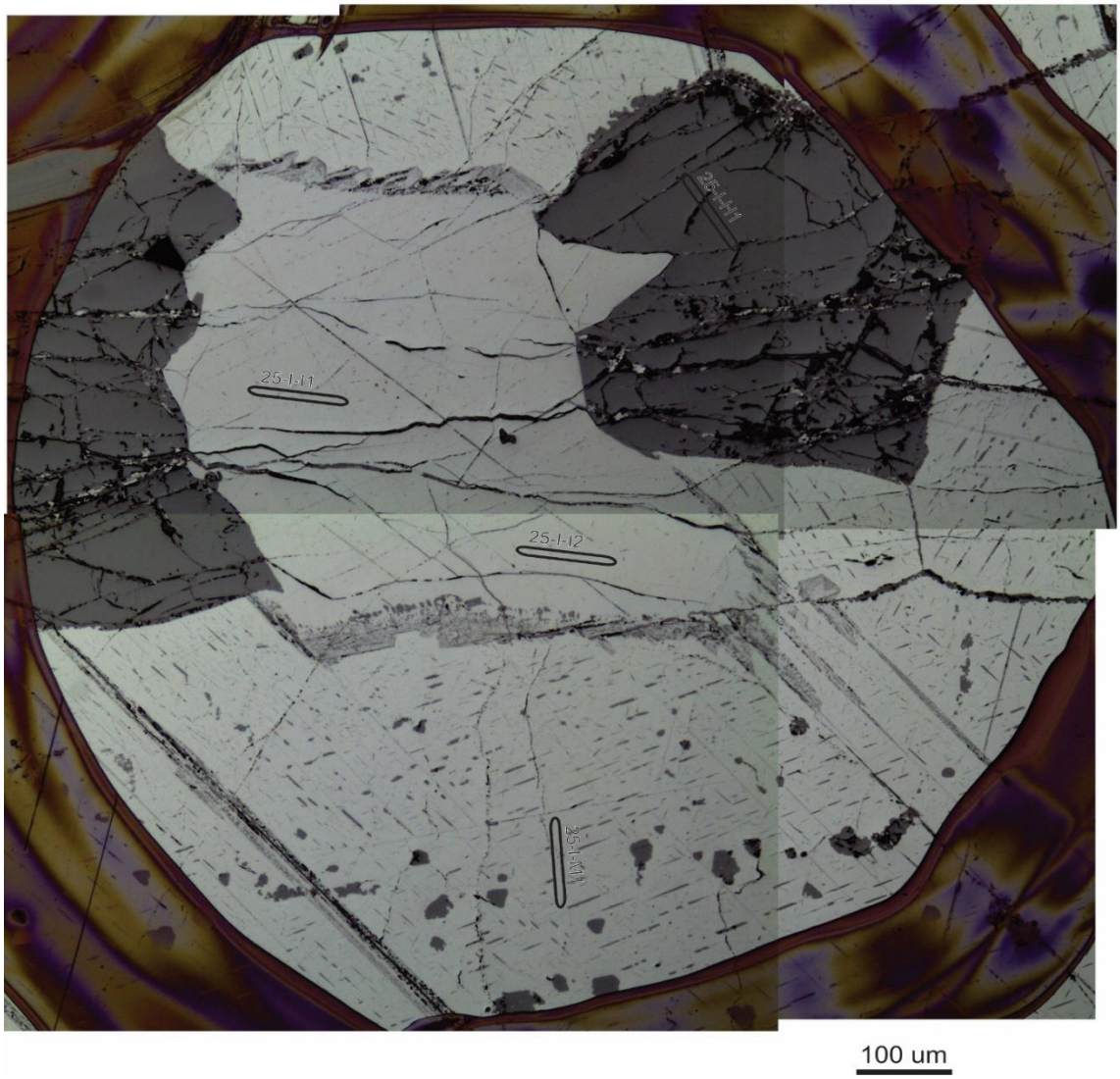

CC025 circle I EPMA

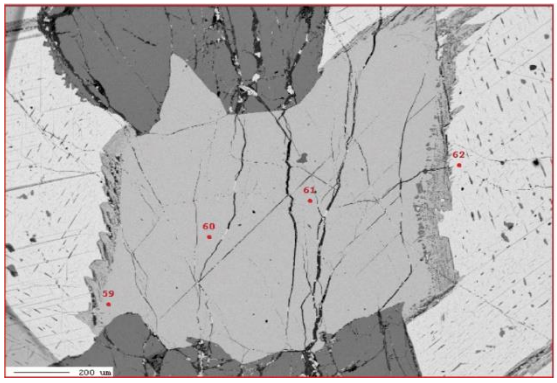

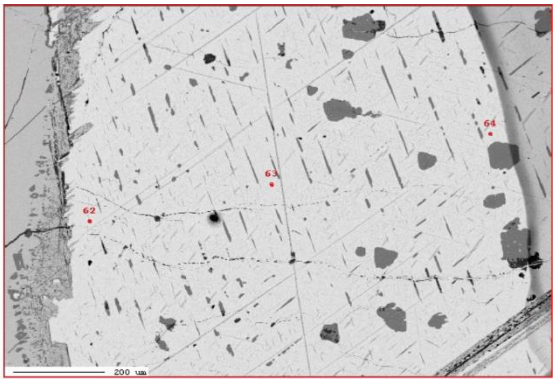

CC025 circle K LA-ICPMS

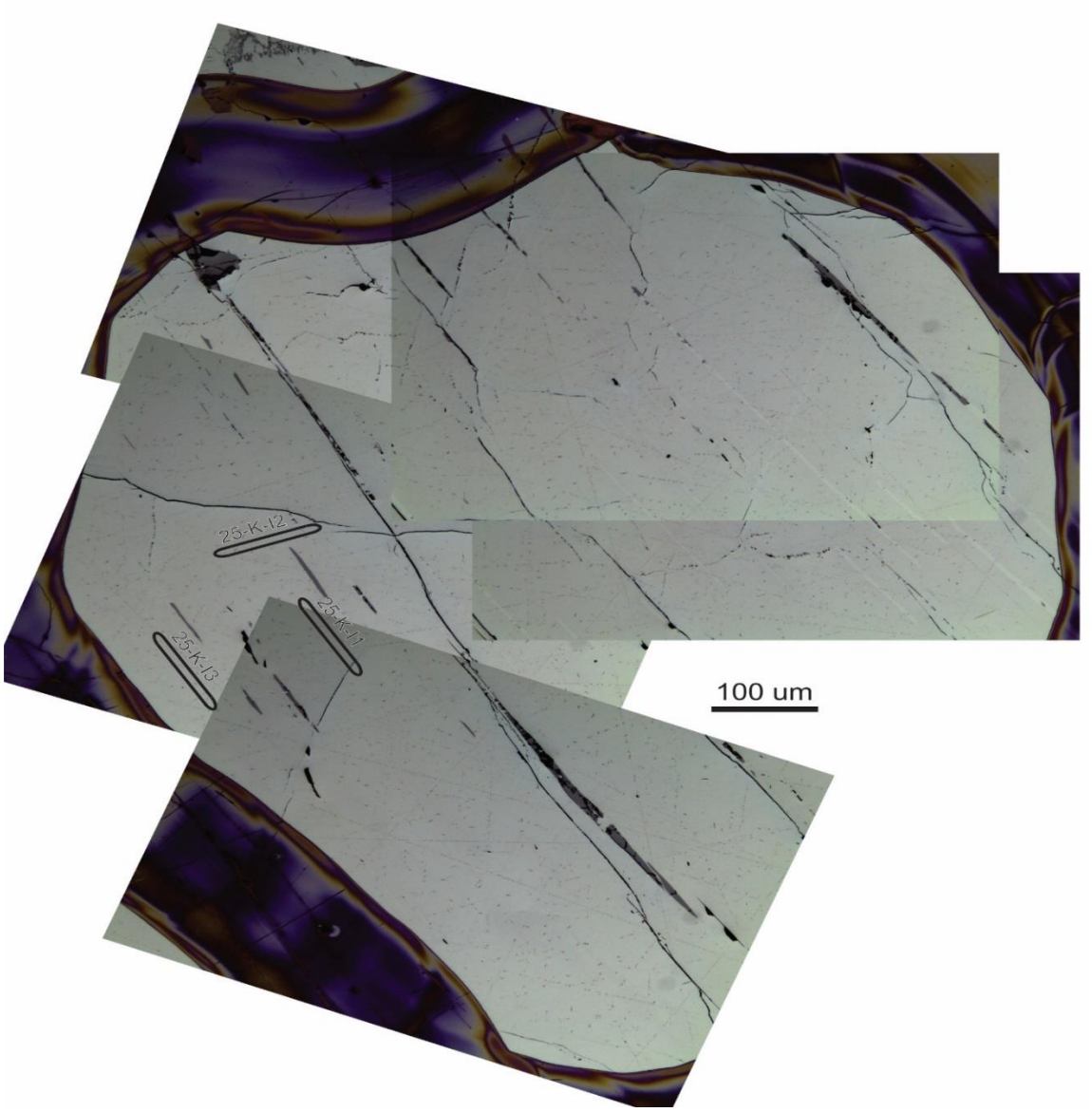

CC025 circle K EPMA

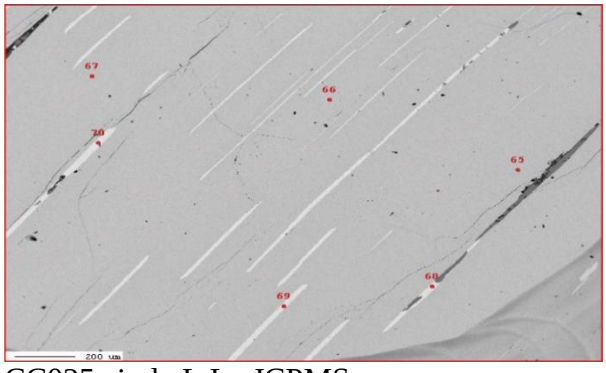

CC025 circle L La-ICPMS

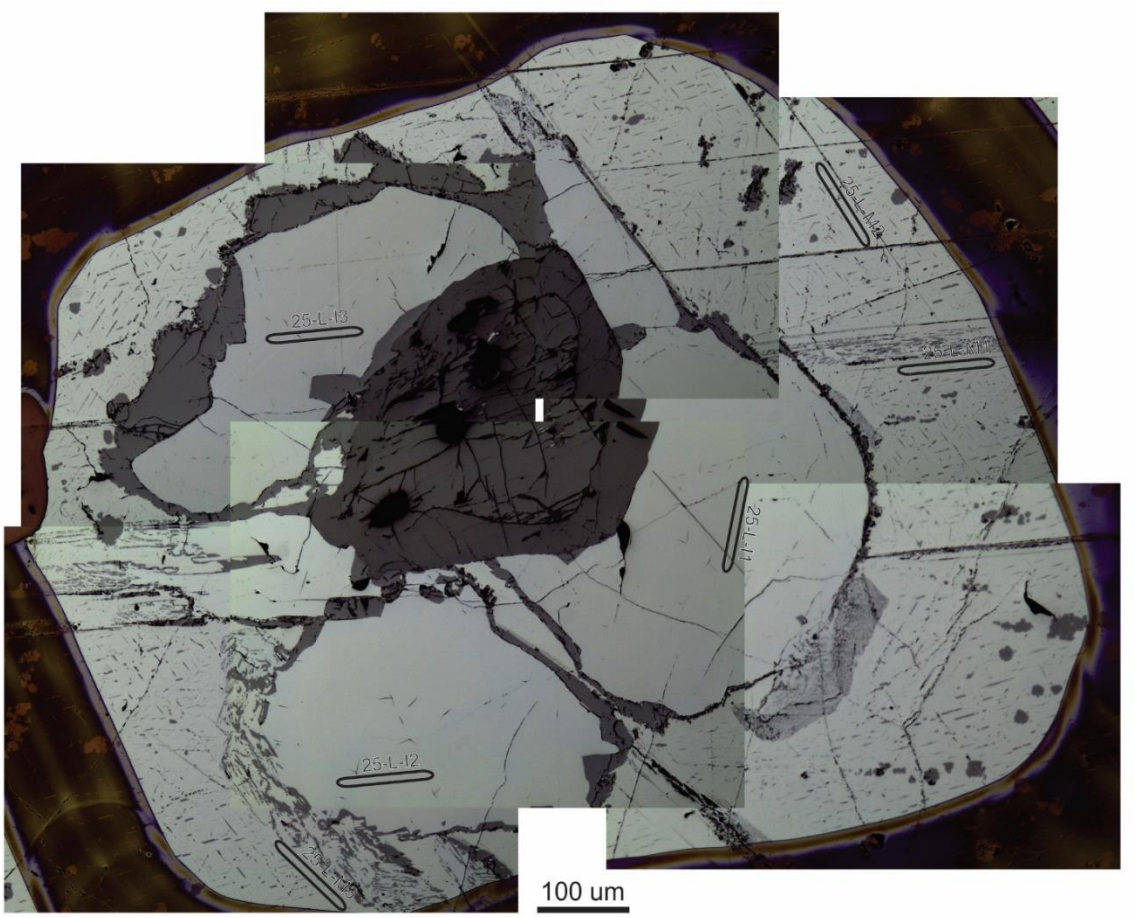
25-L-13
25-L-11
25-L-12
100 um

CC031 circle A LA-ICPMS

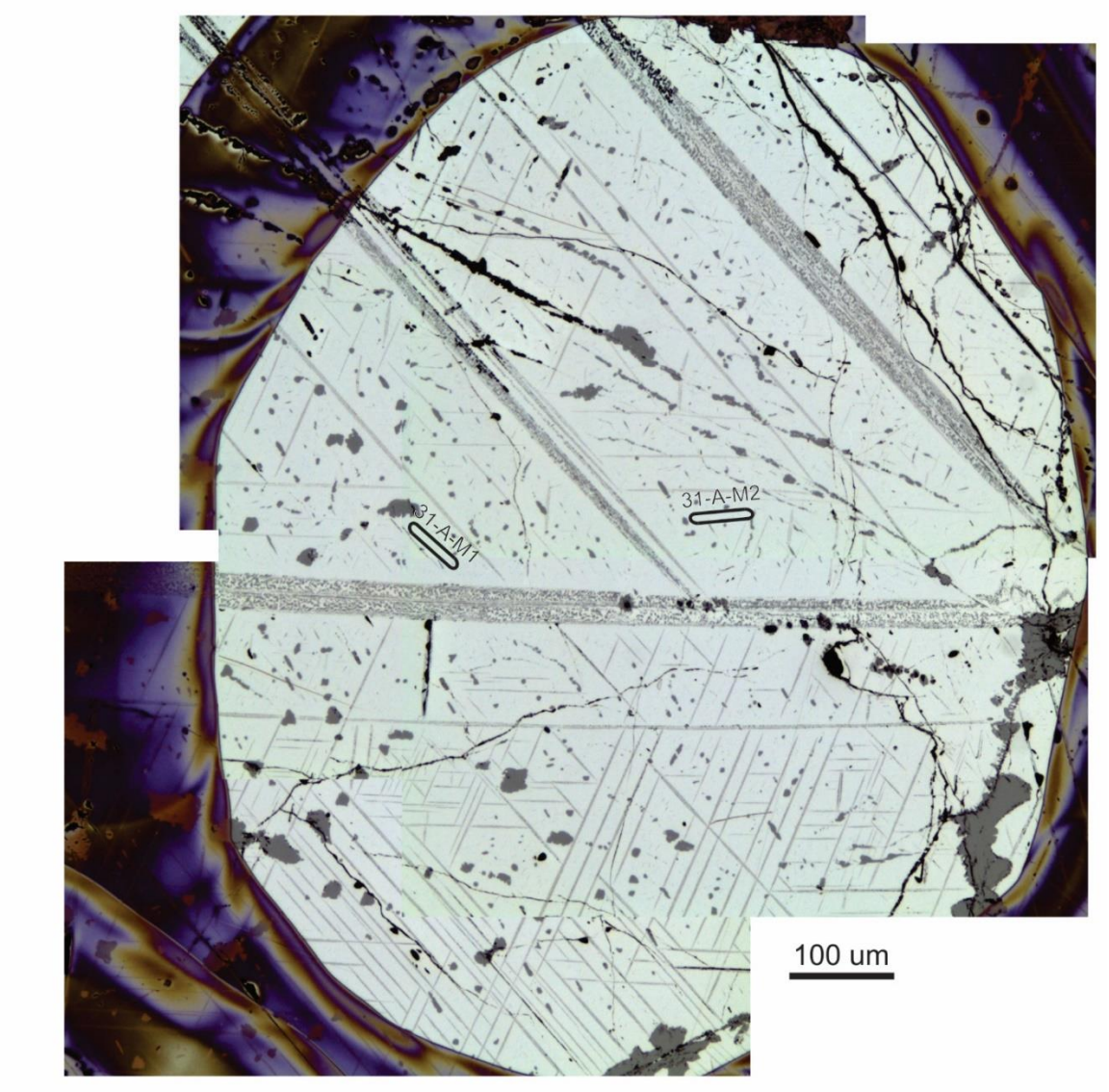

CC031 circle A EPMA

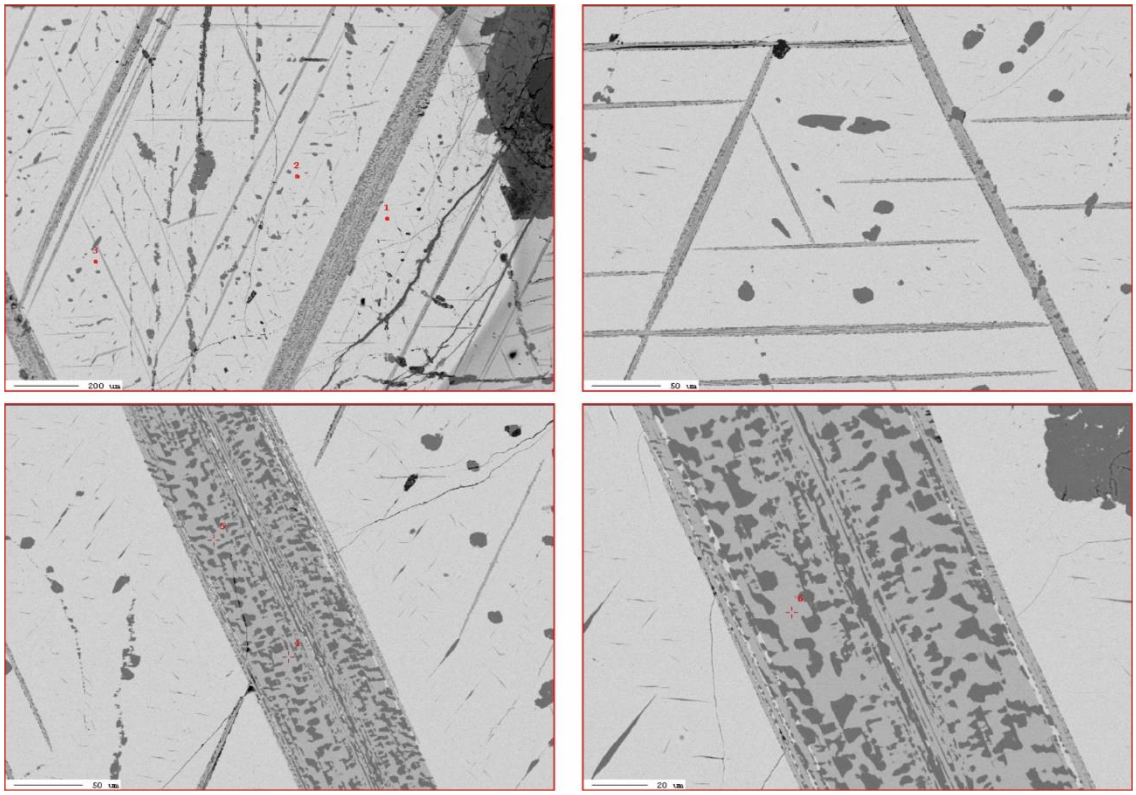

CC031 circle B LA-ICPMS

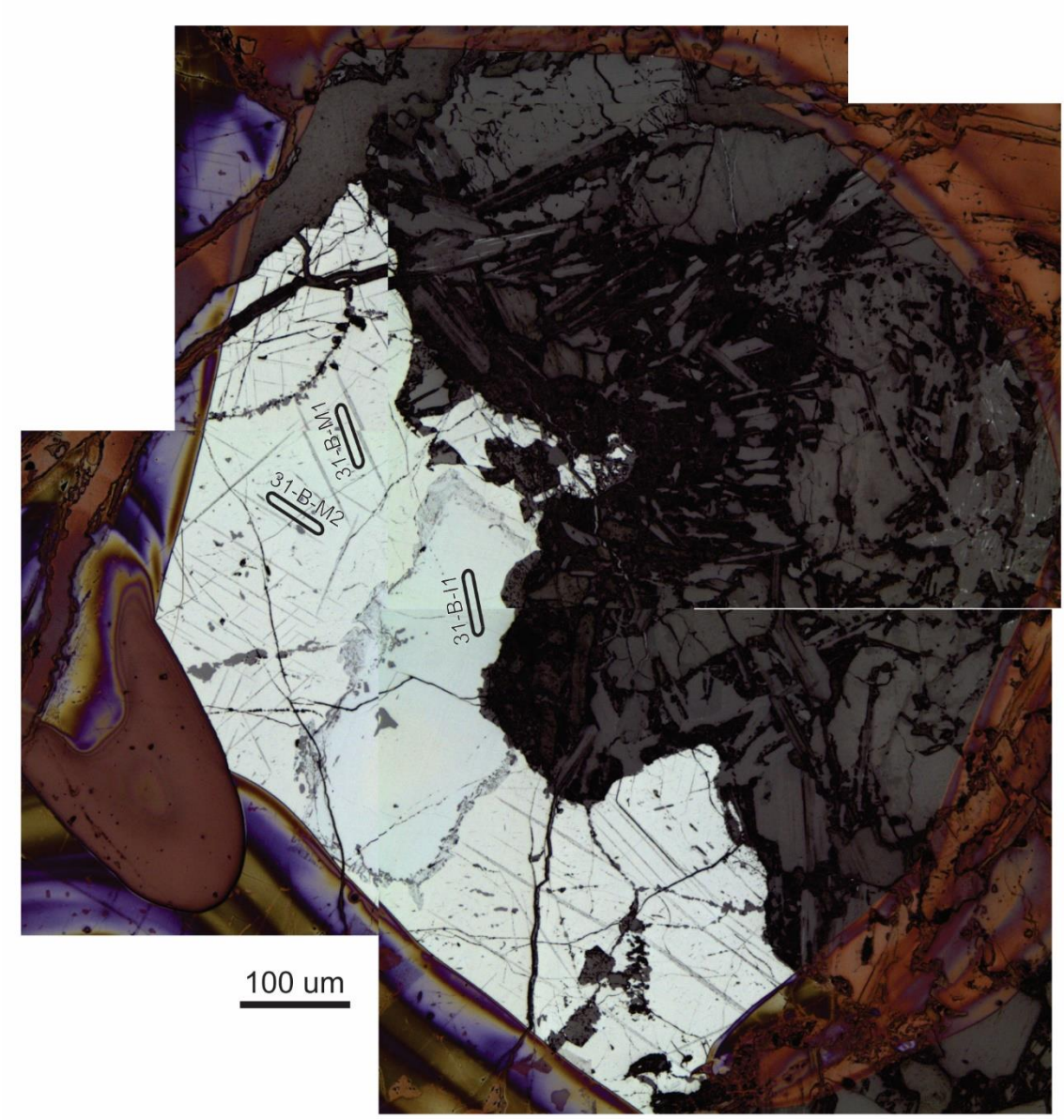

CC031 circle B EPMA

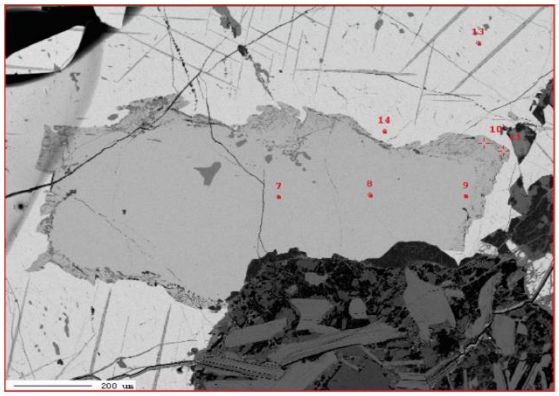

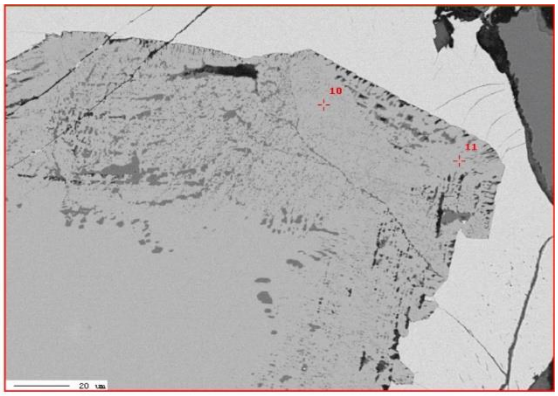

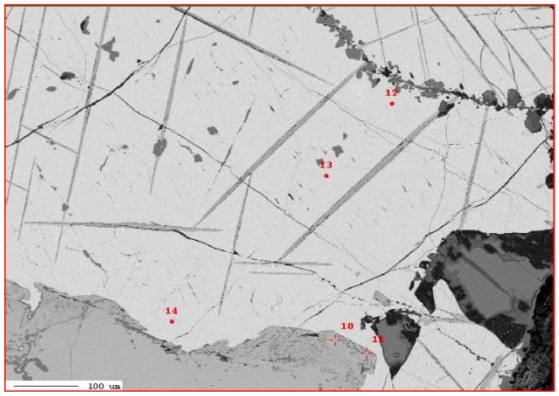

CC031 circle C LA-ICPMS

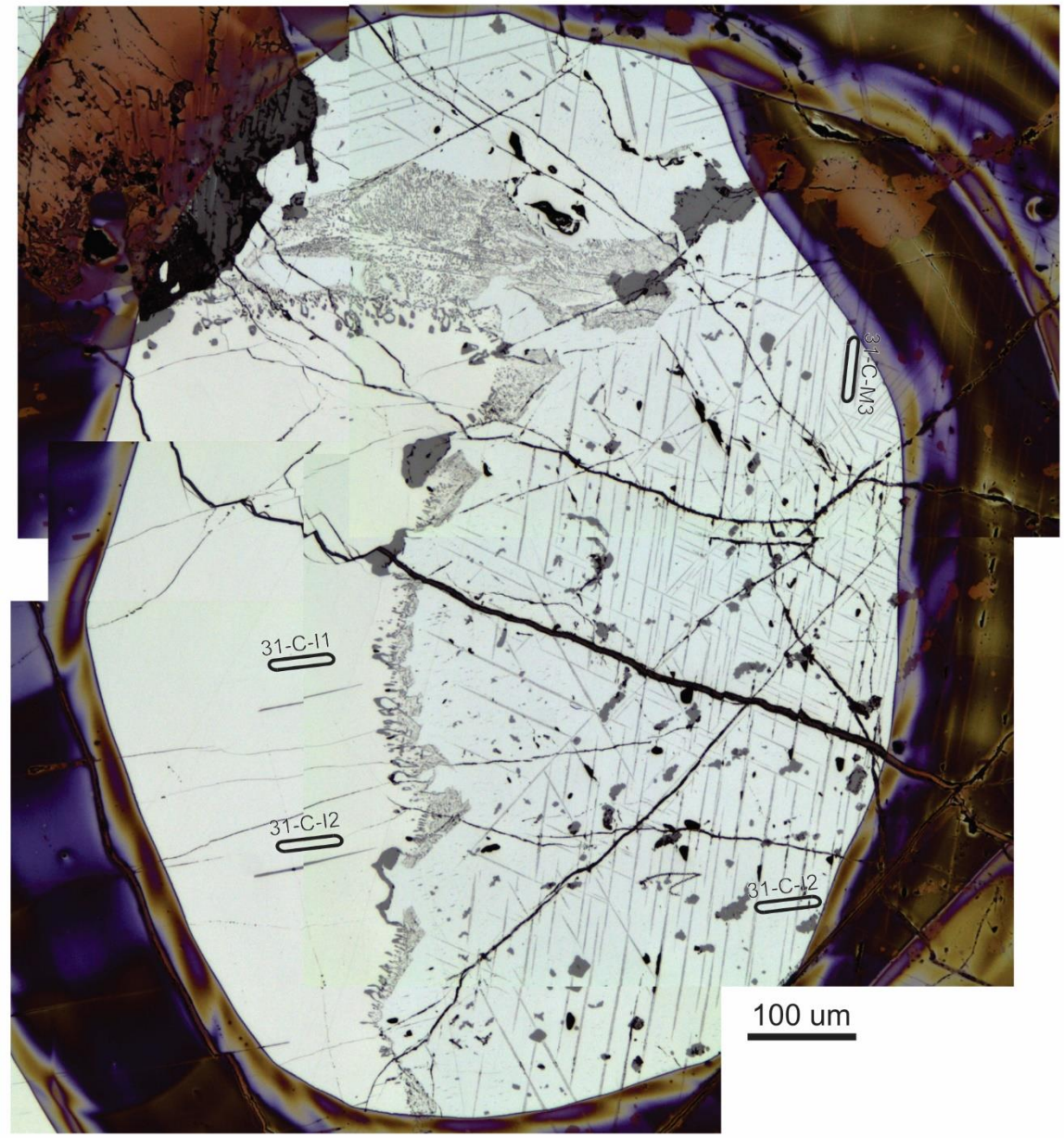

CC031 circle C EPMA

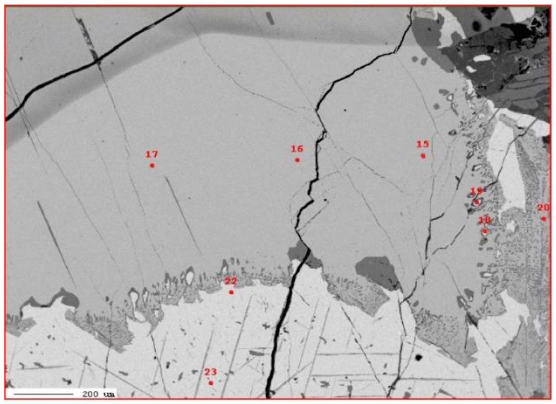

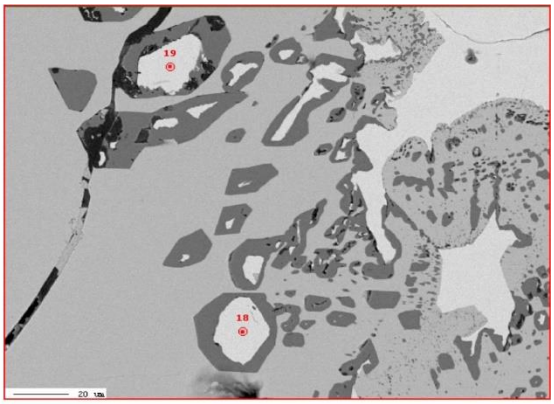

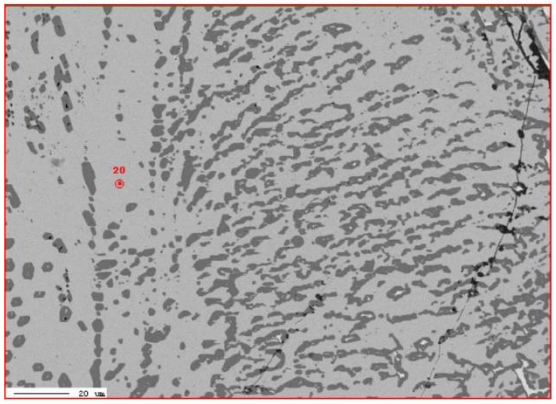

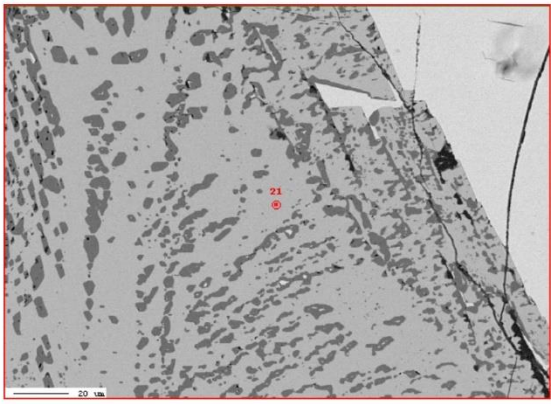

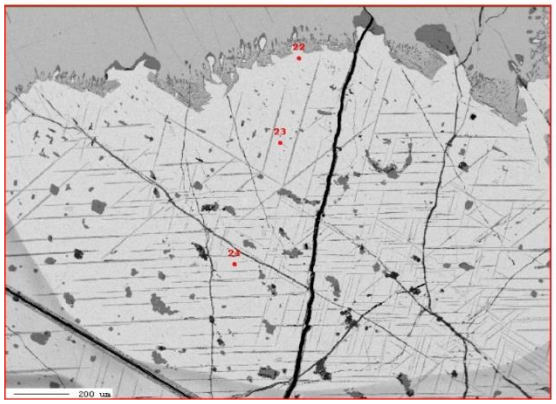

CC031 circle D LA-ICPMS

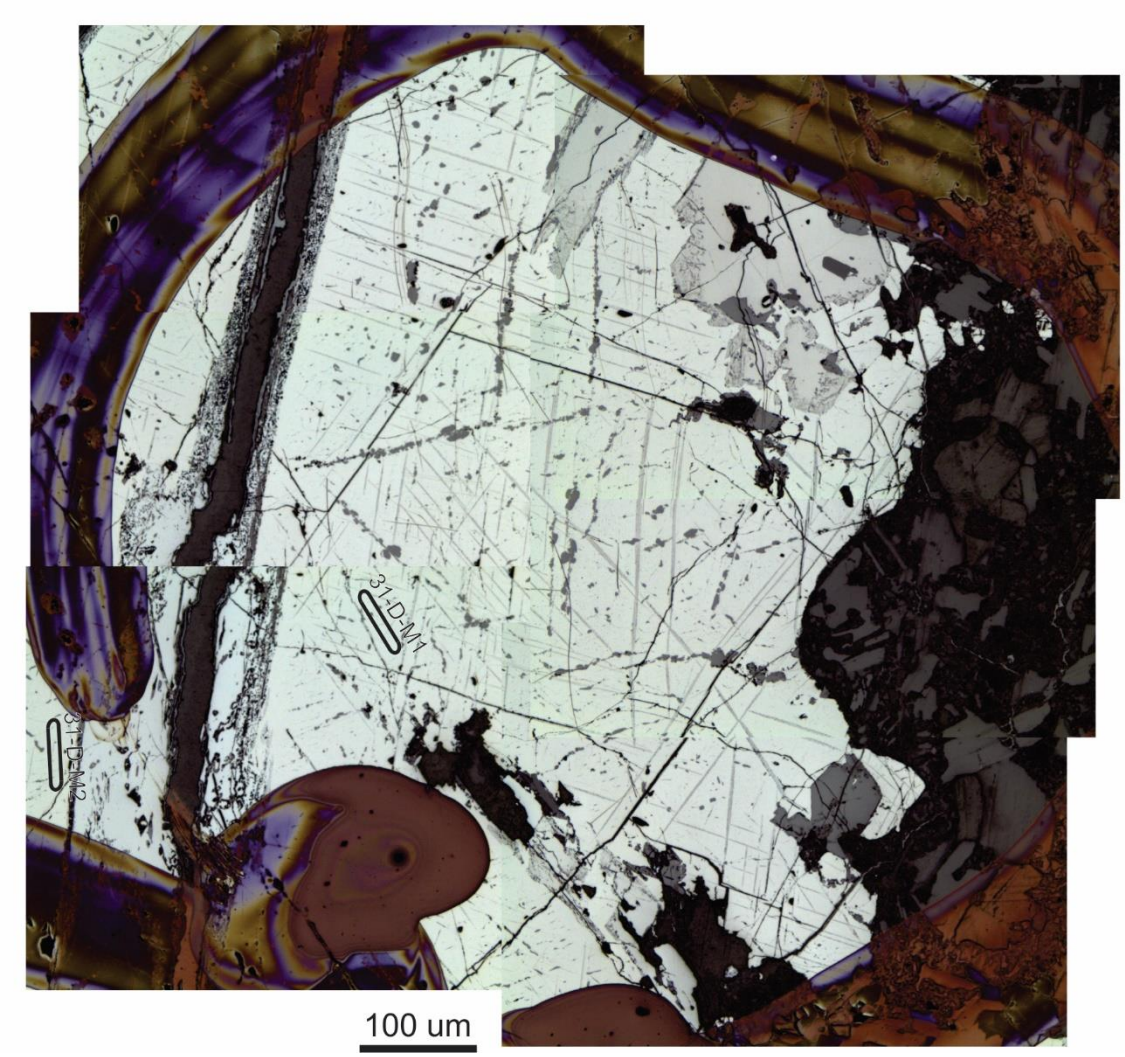

CC031 circle D EPMA

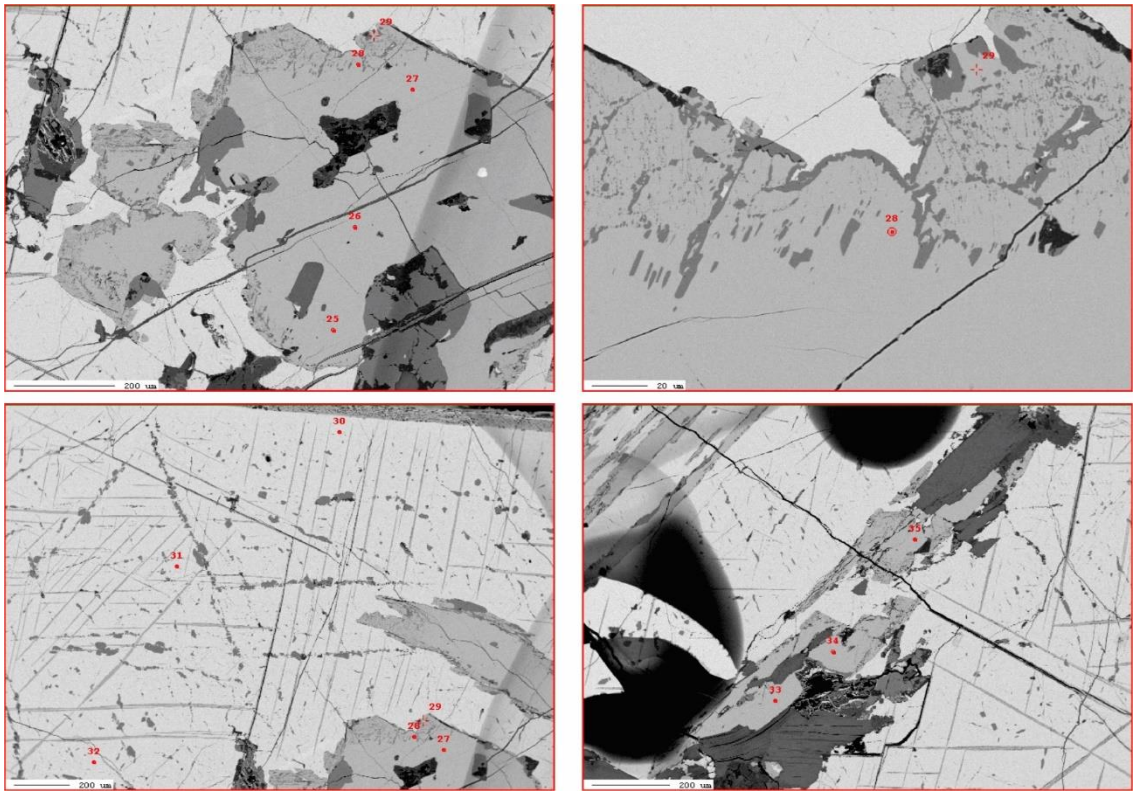

CC031 circle E LA-ICPMS

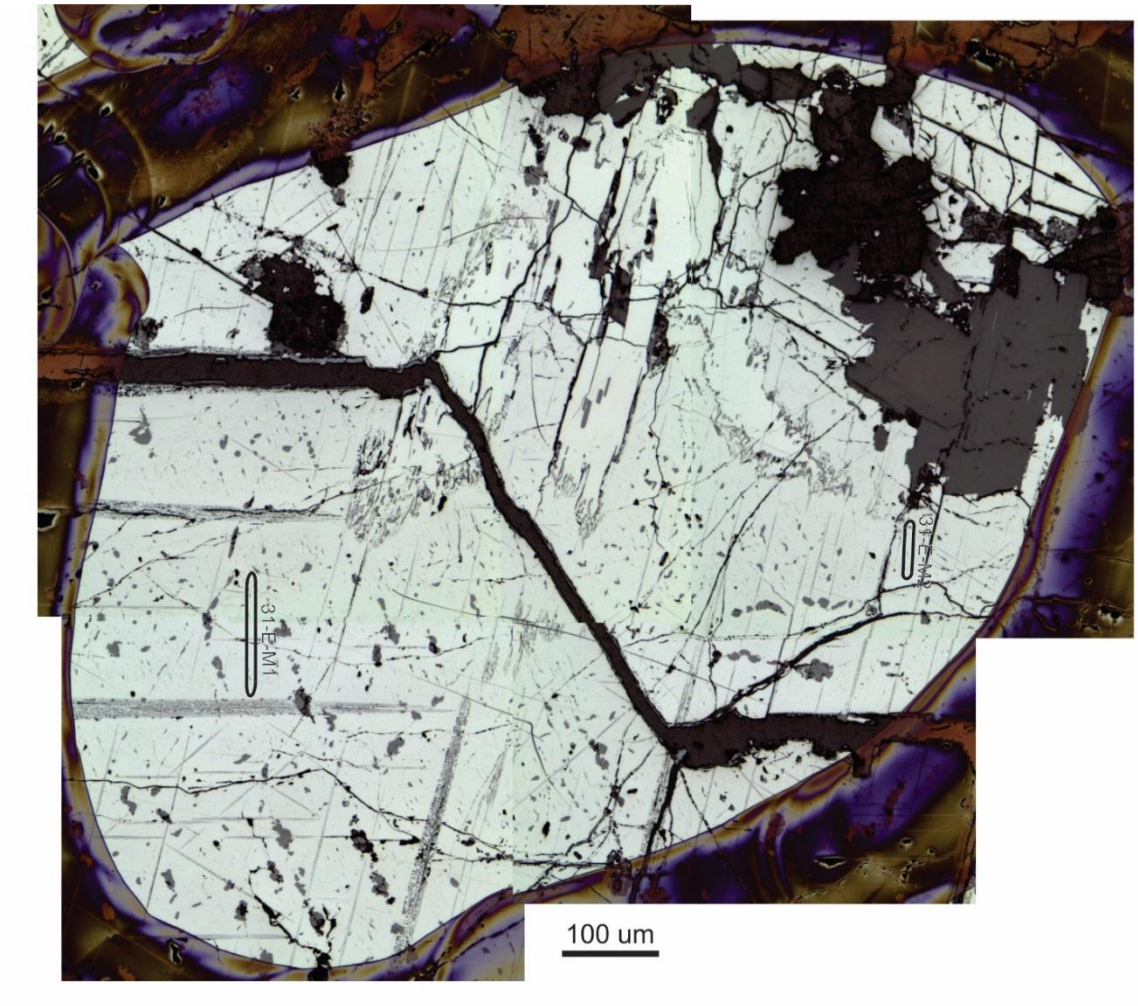

CC031 circle E EPMA

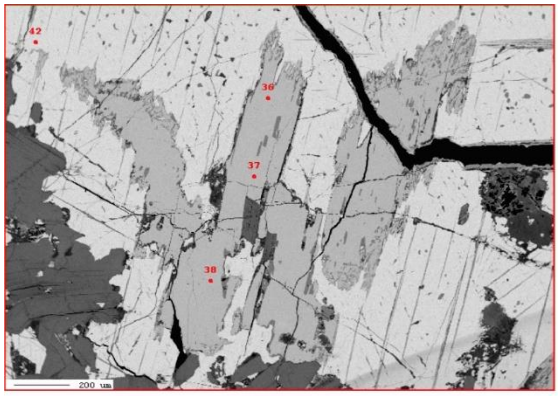

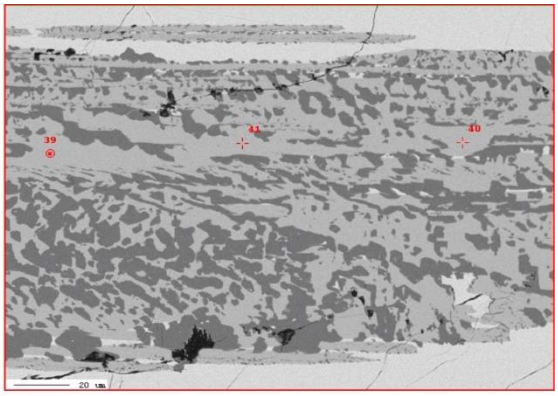

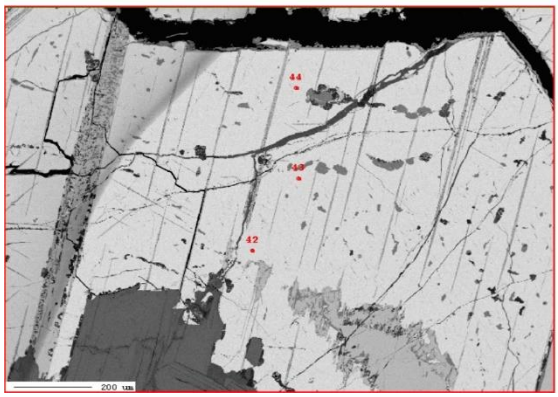

CC031 circle F LA-ICPMS

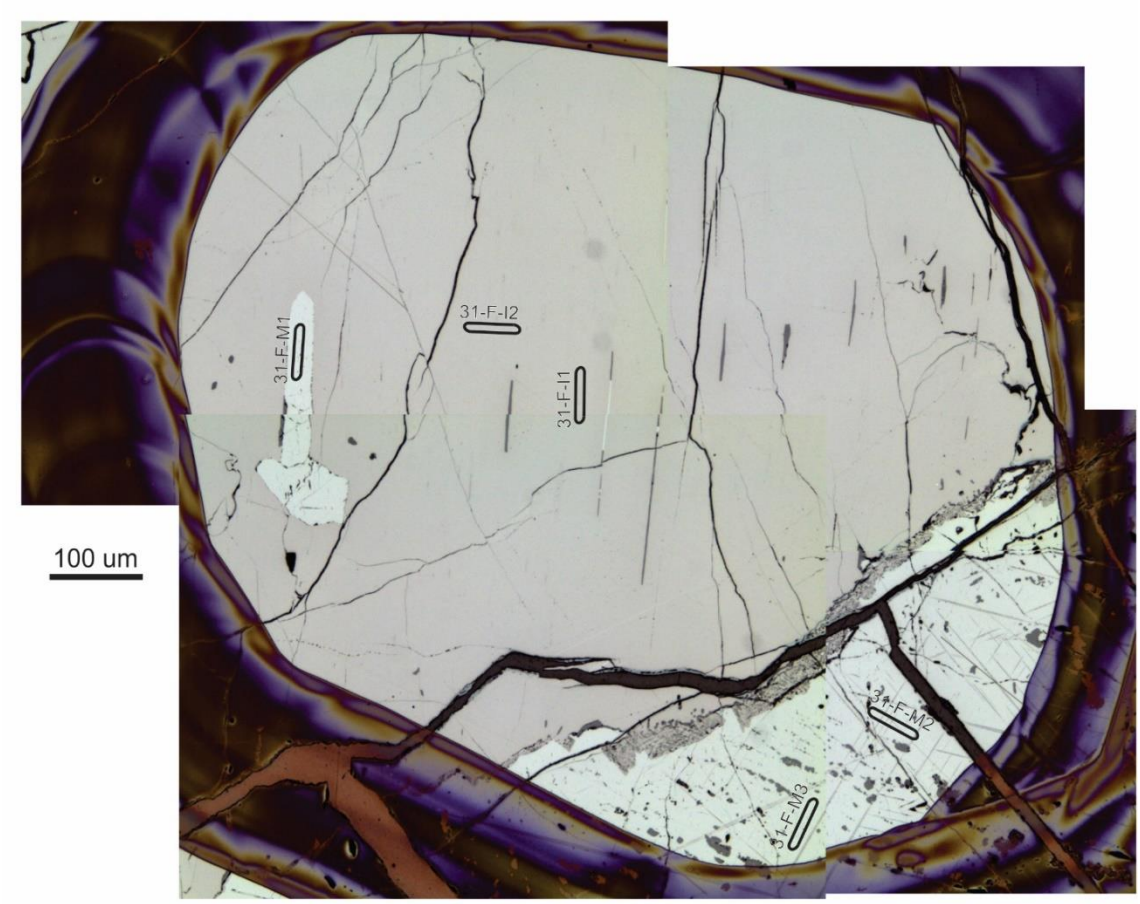

CC031 circle F EPMA

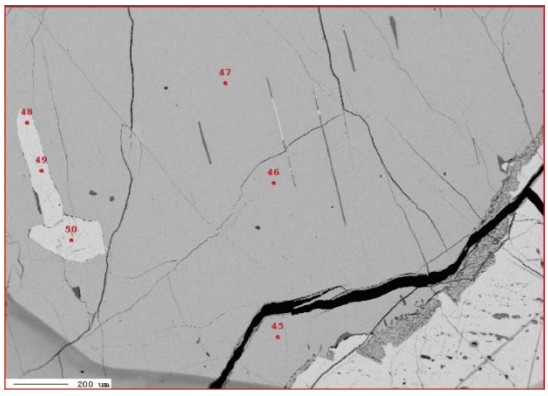

CC031 circle G EPMA

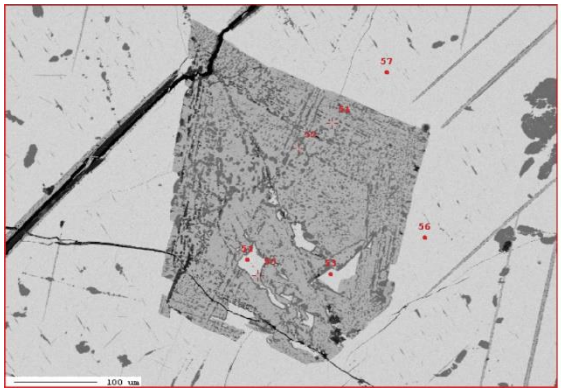

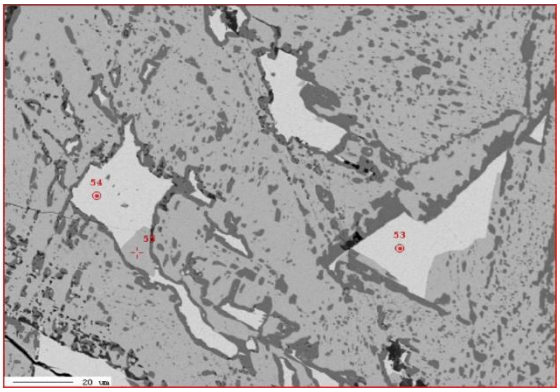

CC031 circle H LA-ICPMS

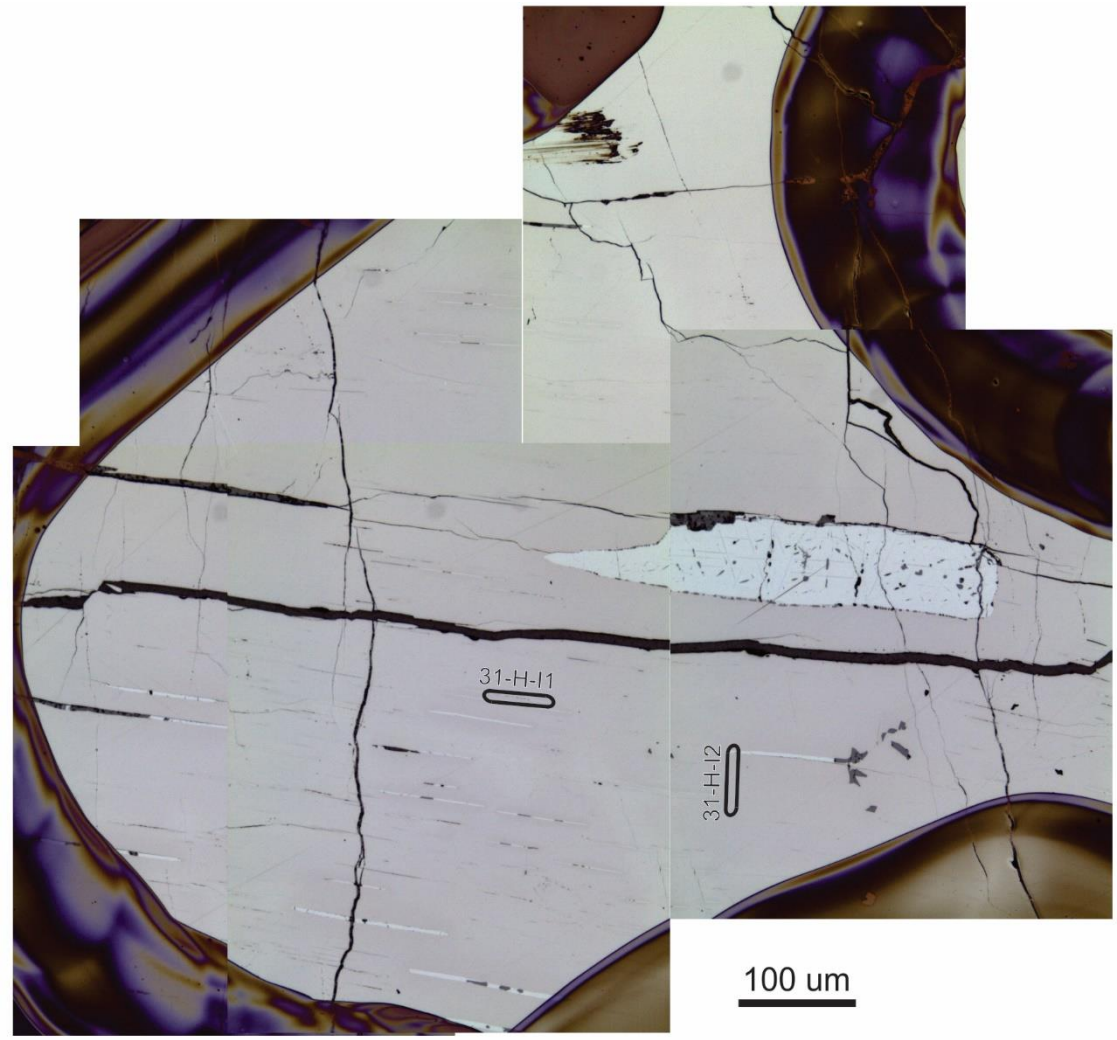

CC031 circle H EPMA

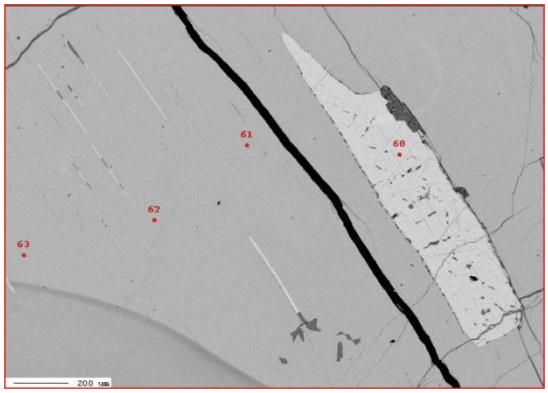

CC031 circle I LA-ICPMS

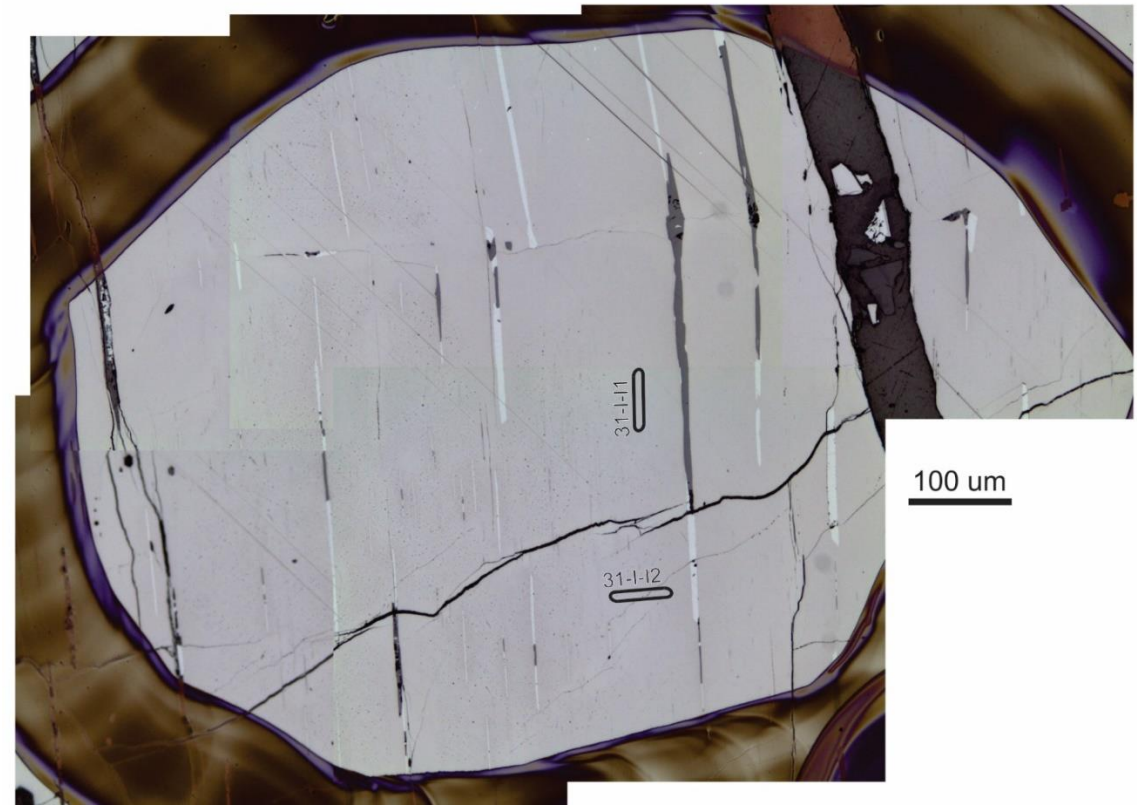

CC031 circle I EPMA

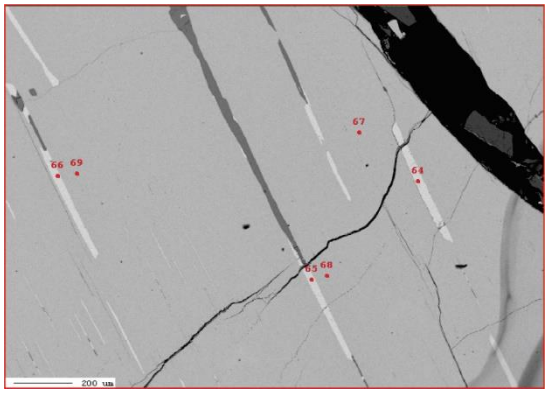

CC054 circle A LA-ICPMS

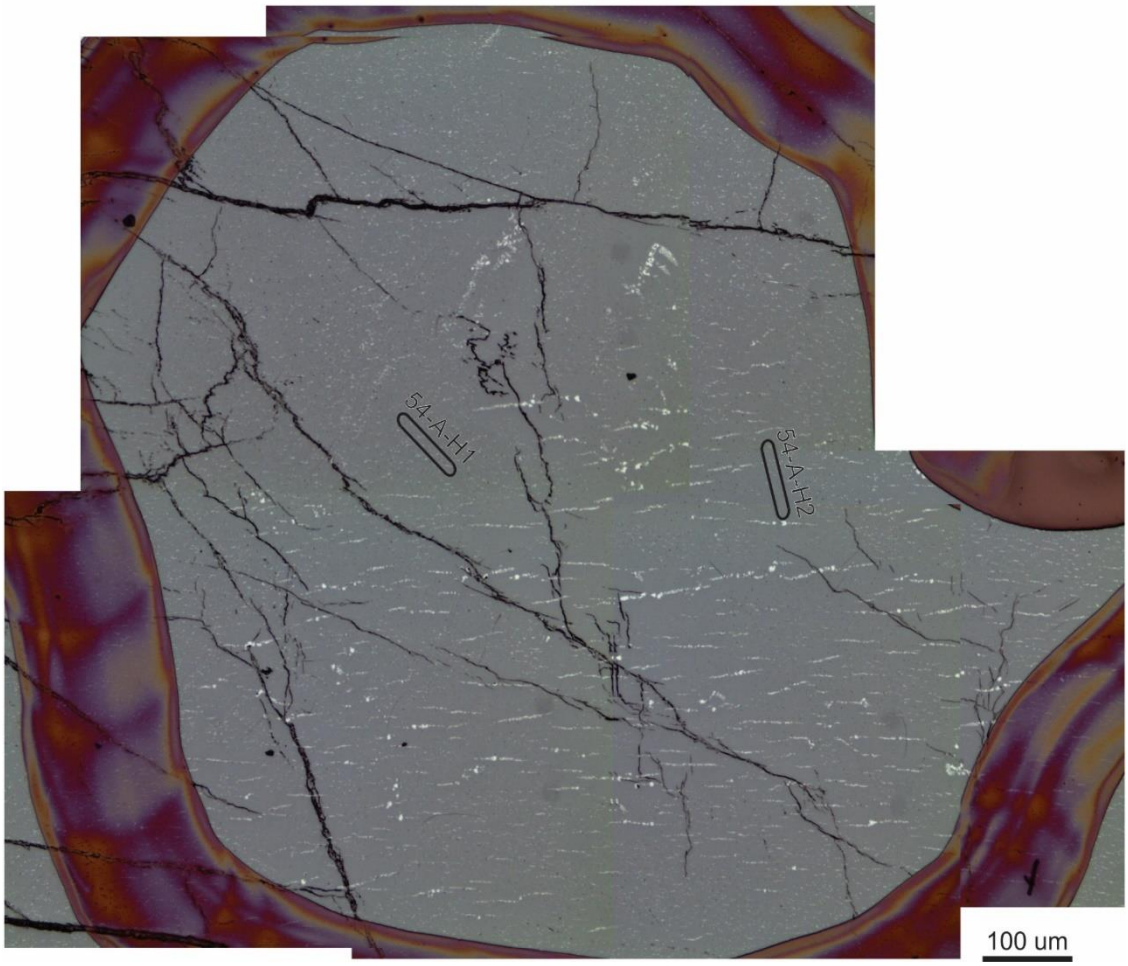

CC054 circle B LA-ICPMS

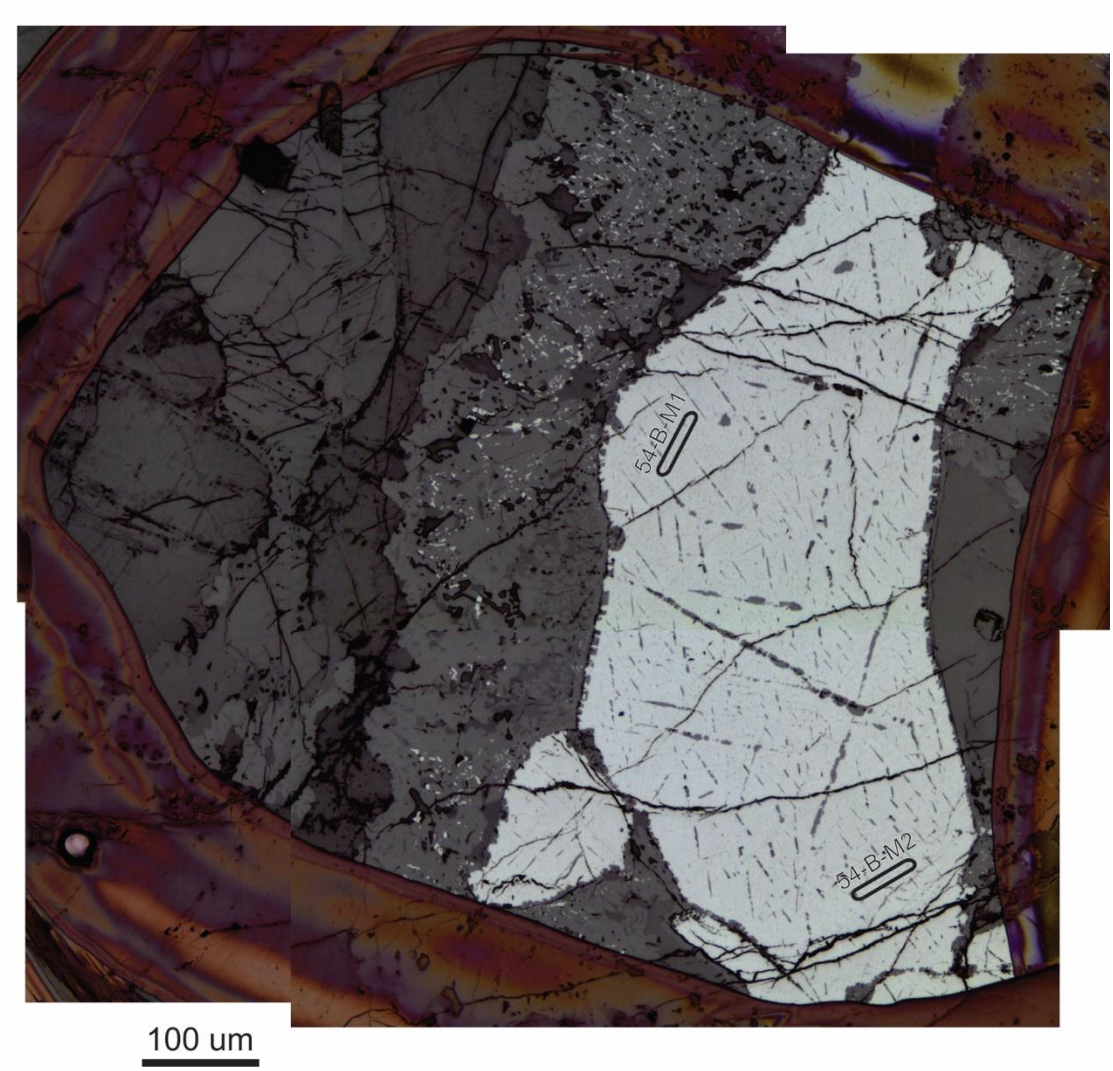

CC054 circle B EPMA

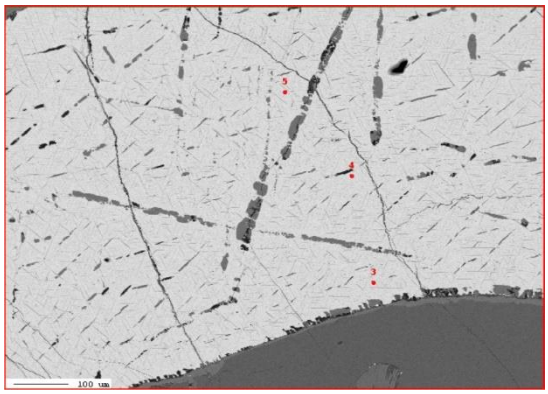

CC054 circle C LA-ICPMS

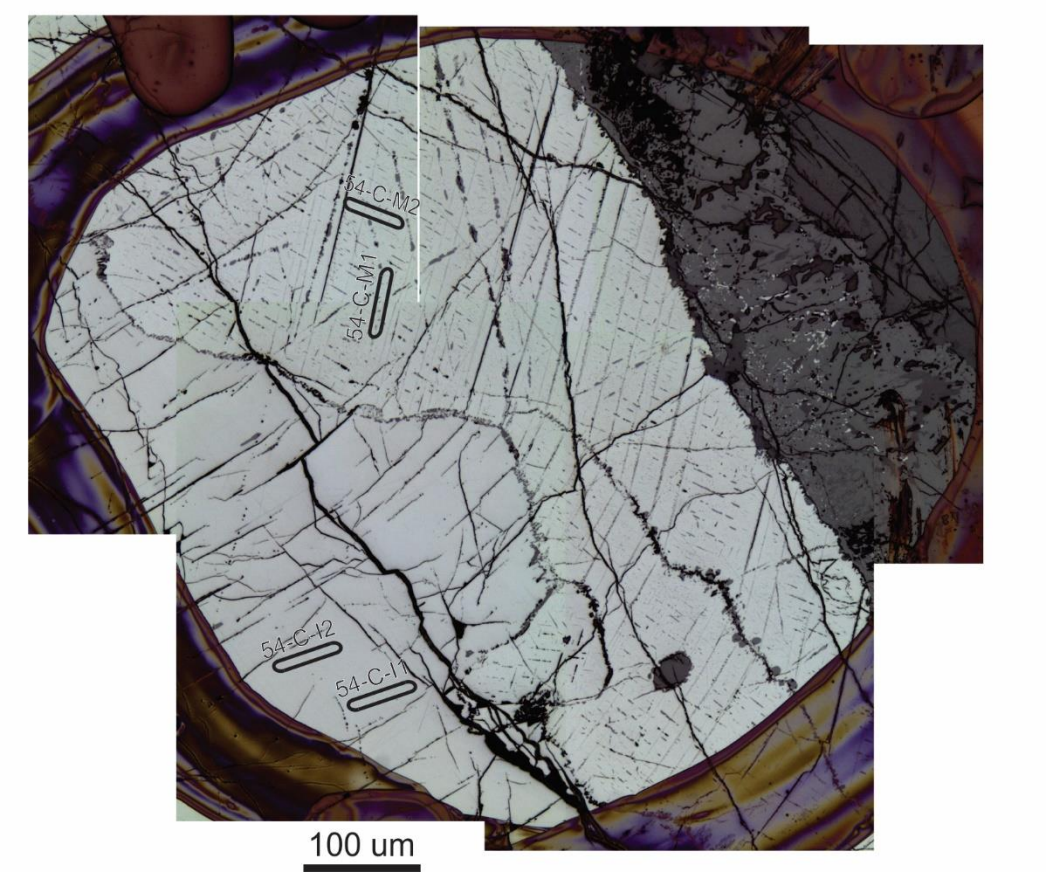

CC054 circle C EPMA

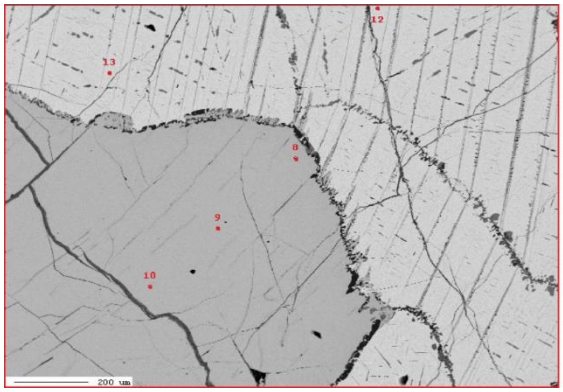

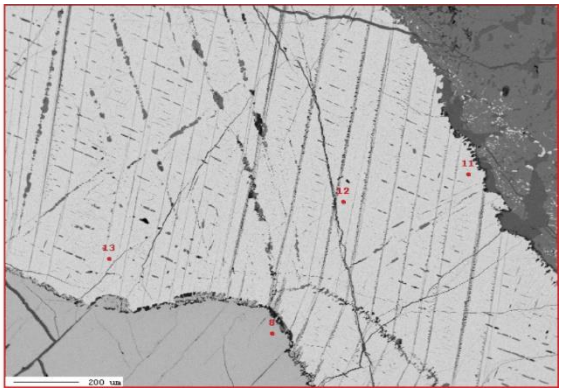

CC054 circle D LA-ICPMS

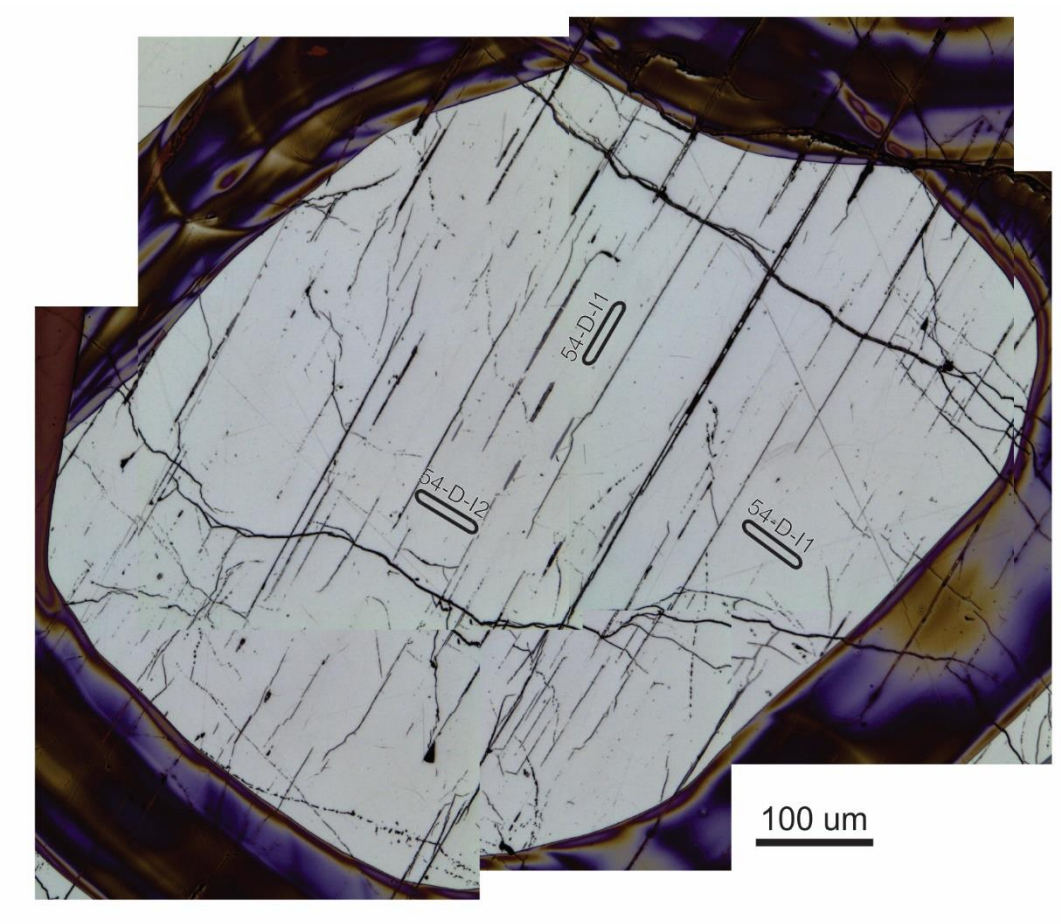

CC054 circle D EPMA

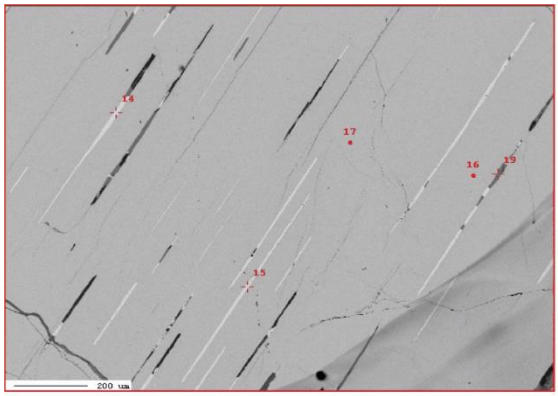

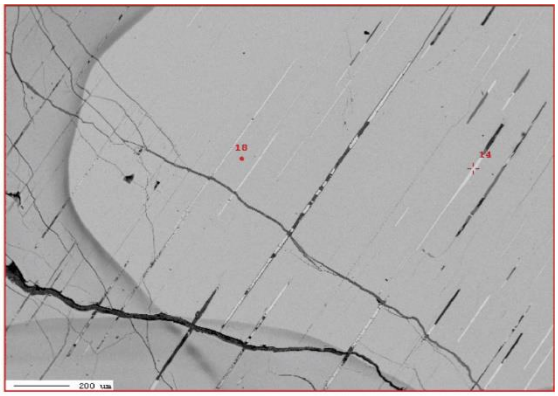

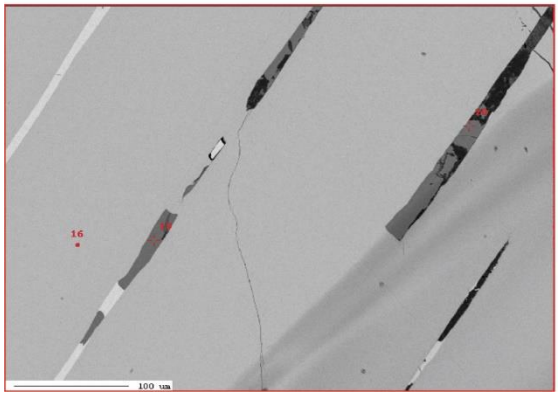

CC054 circle E EPMA

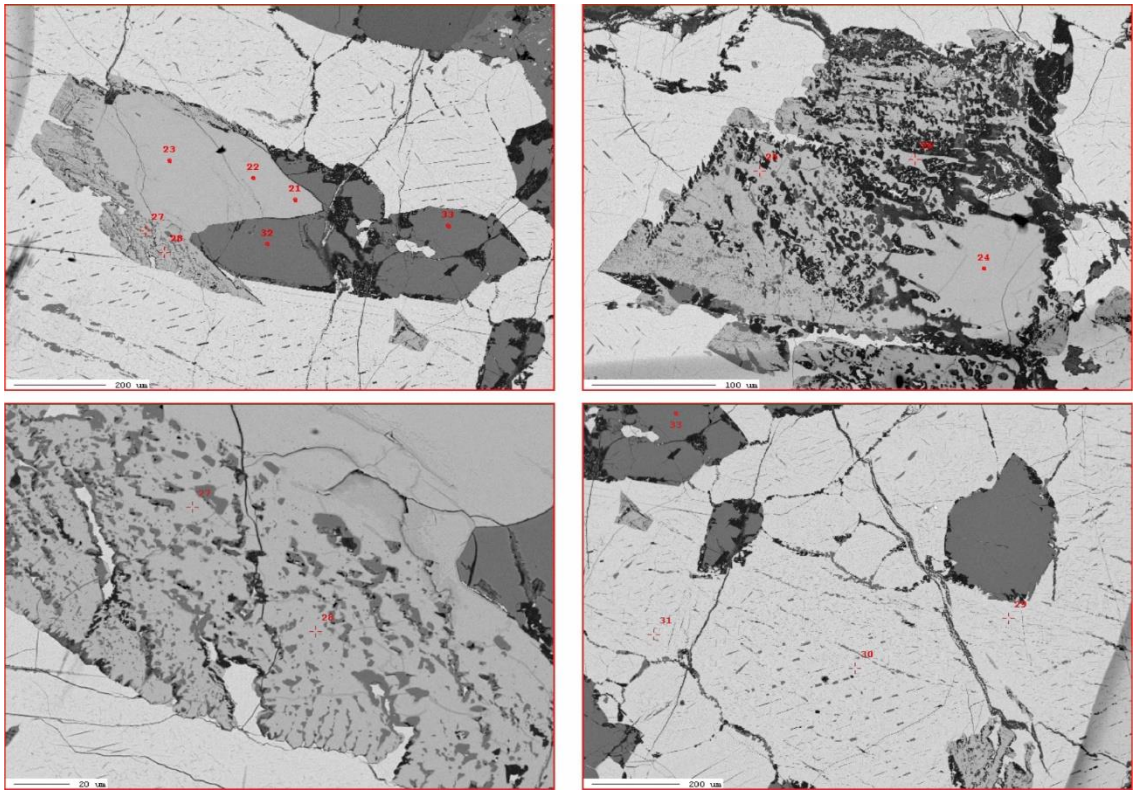

CC054 circle F LA-ICPMS

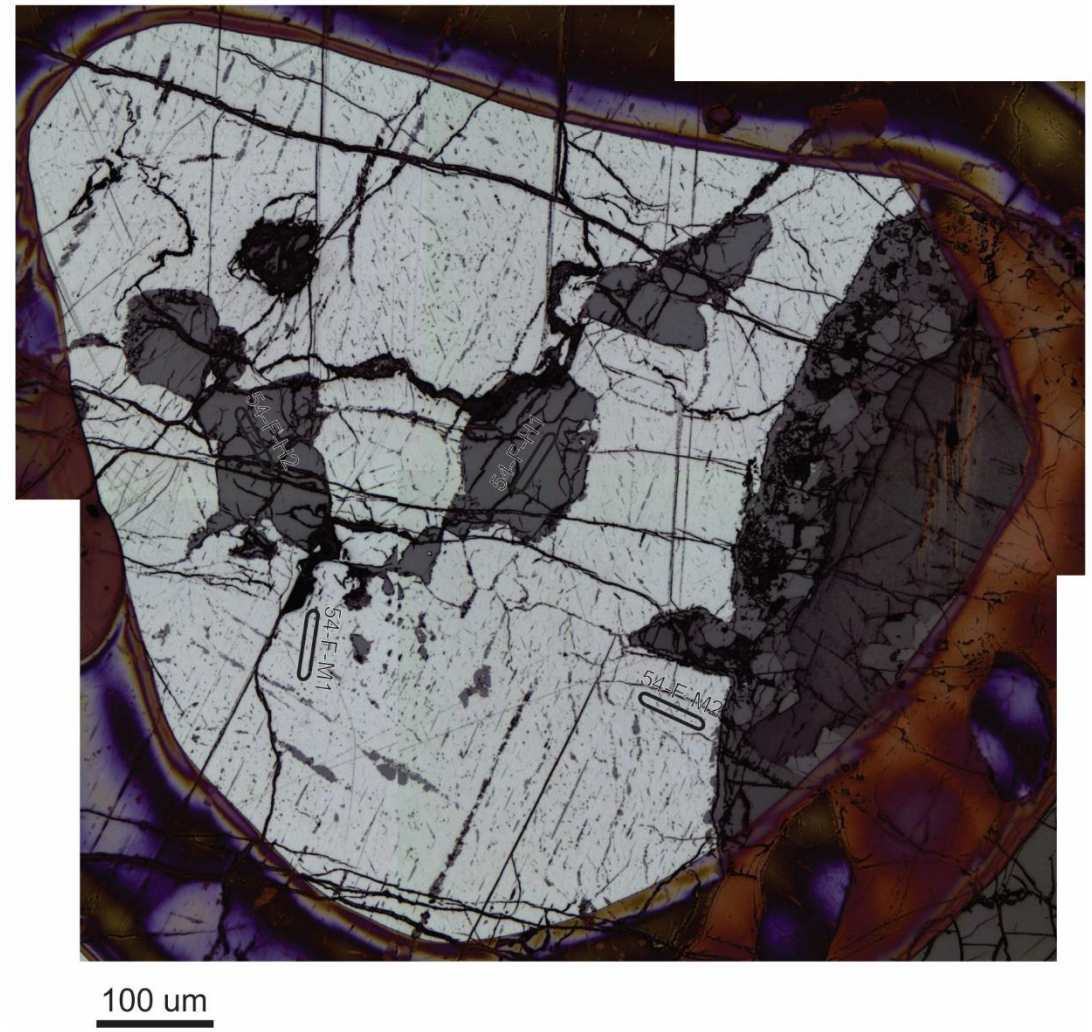

CC054 circle F EPMA

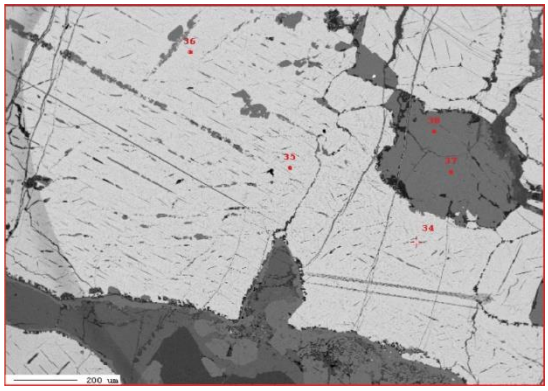

CC054 circle G LA-ICPMS

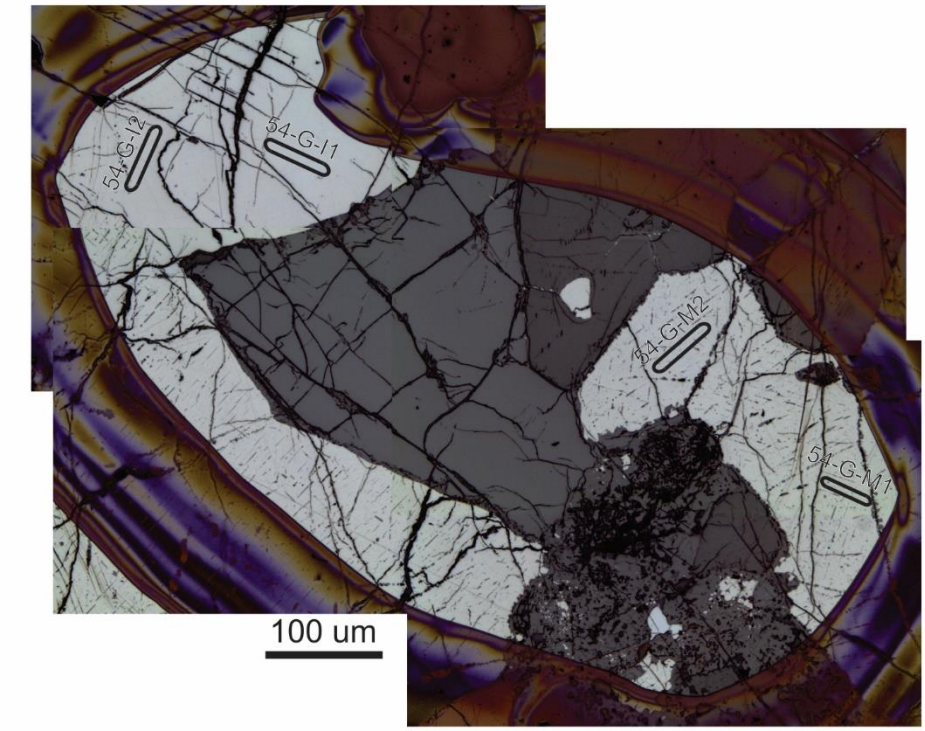

CC054 circle G EPMA

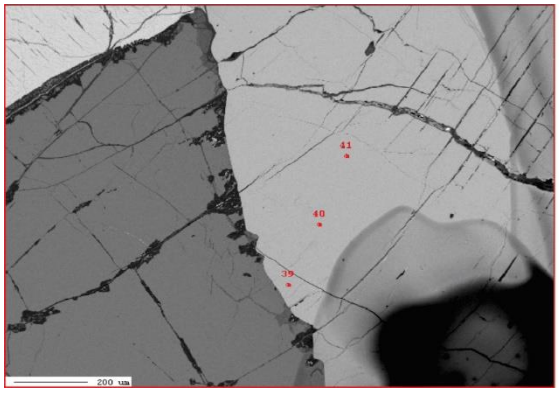

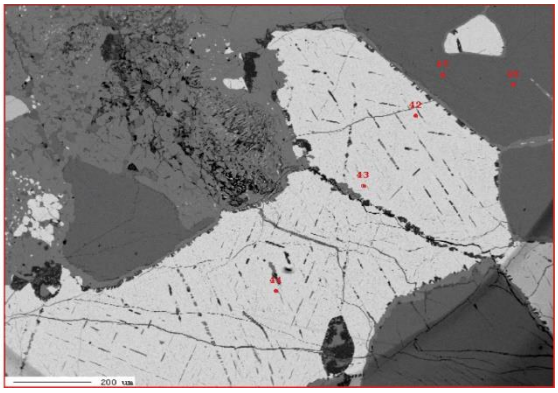

CC054 circle H EPMA

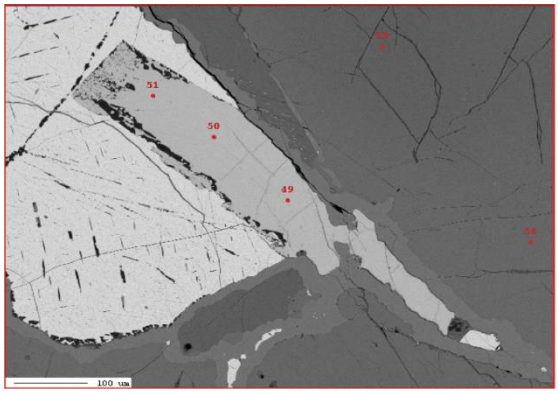

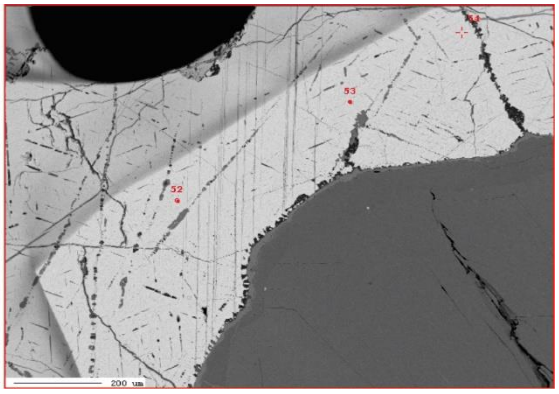

CC054 Circle I LA-ICPMS

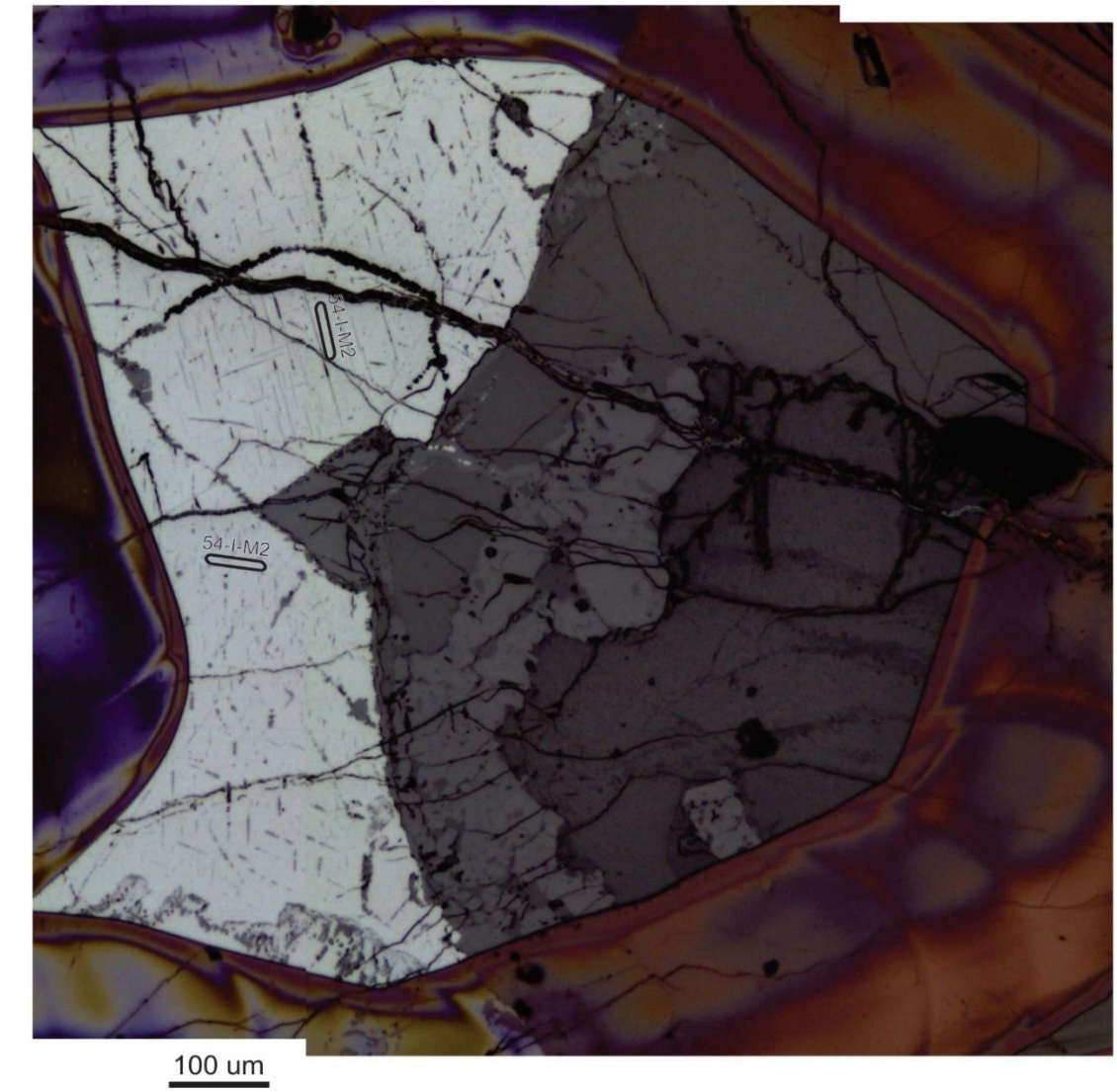

CC054 circle J EPMA

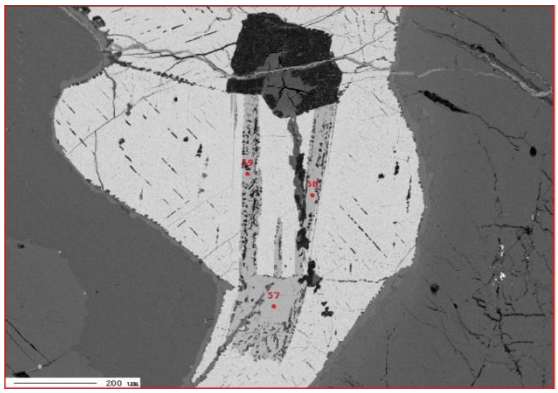

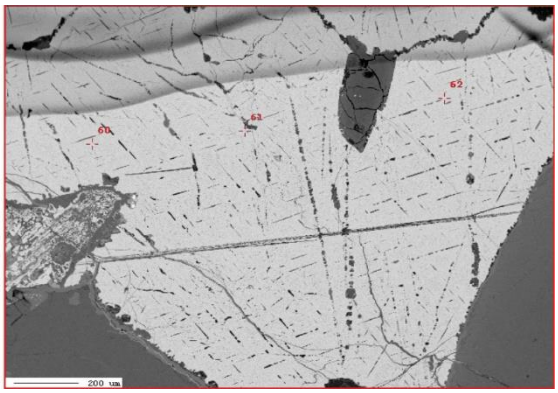

CC054 circle L LA-ICPMS

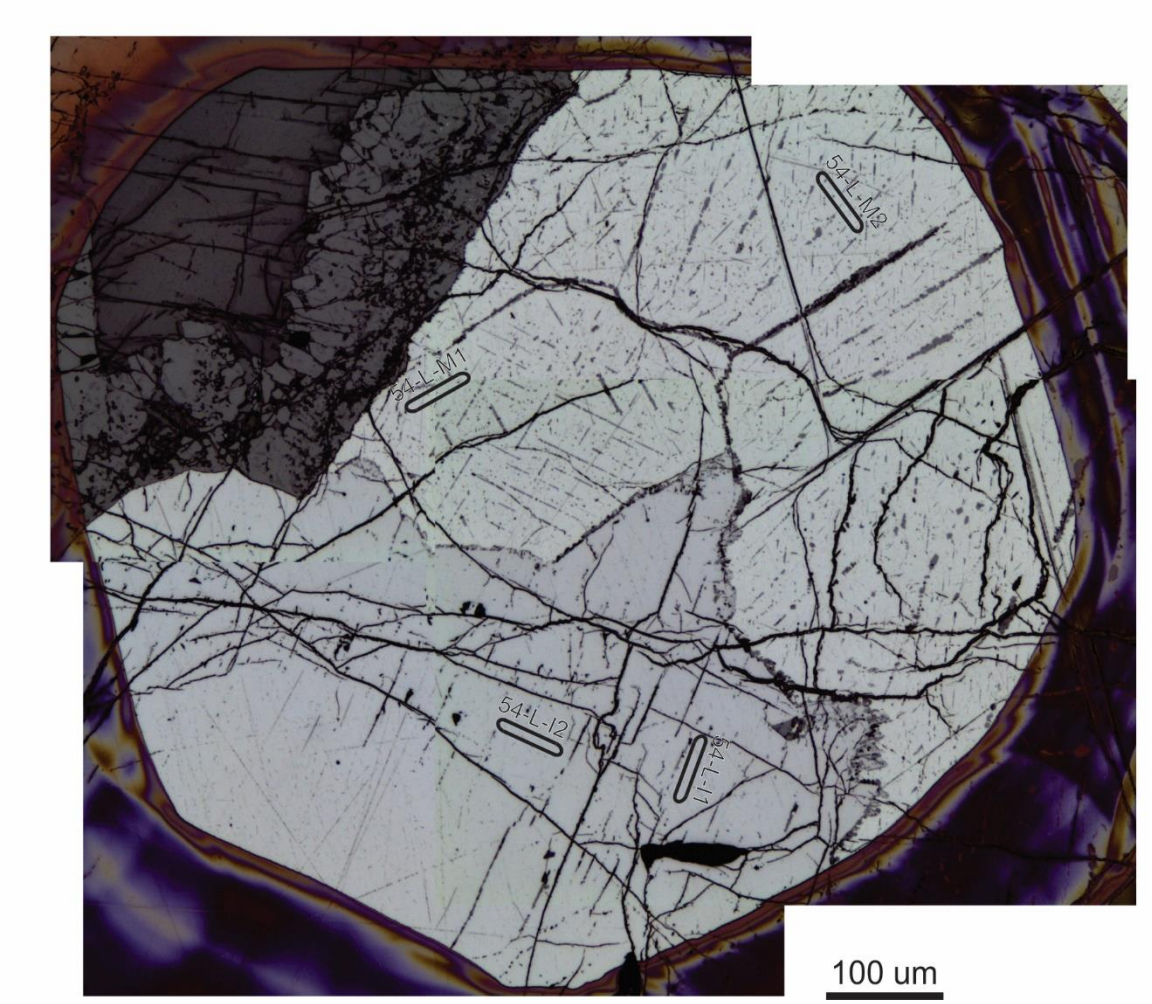

CC054 circle L EPMA

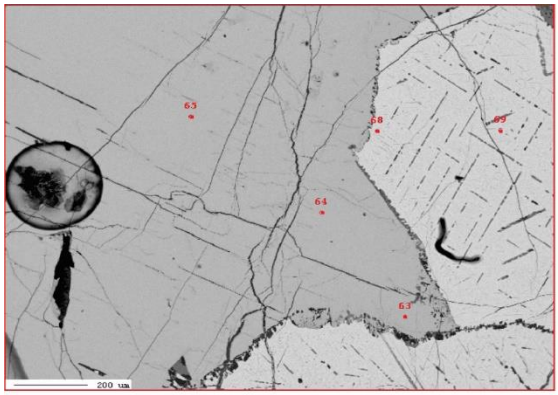

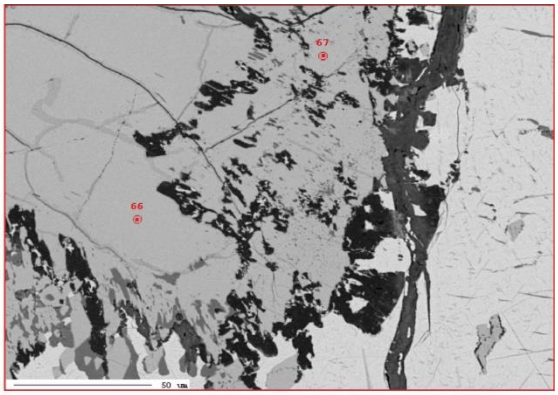

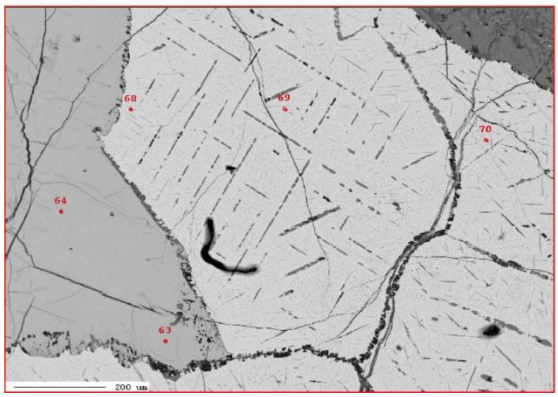

CC054 circle M LA-ICPMS

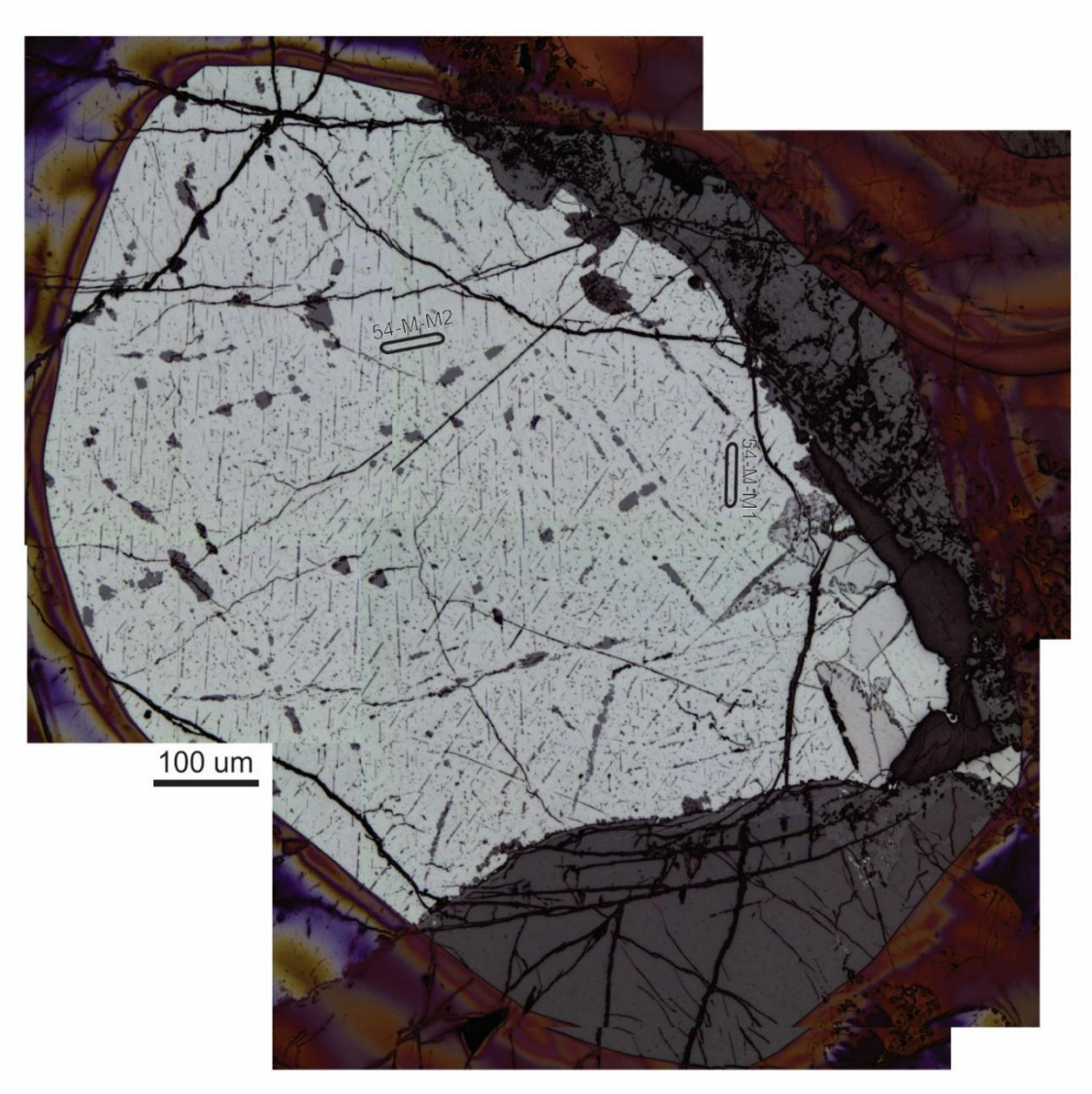

CC054 circle O LA-ICPMS

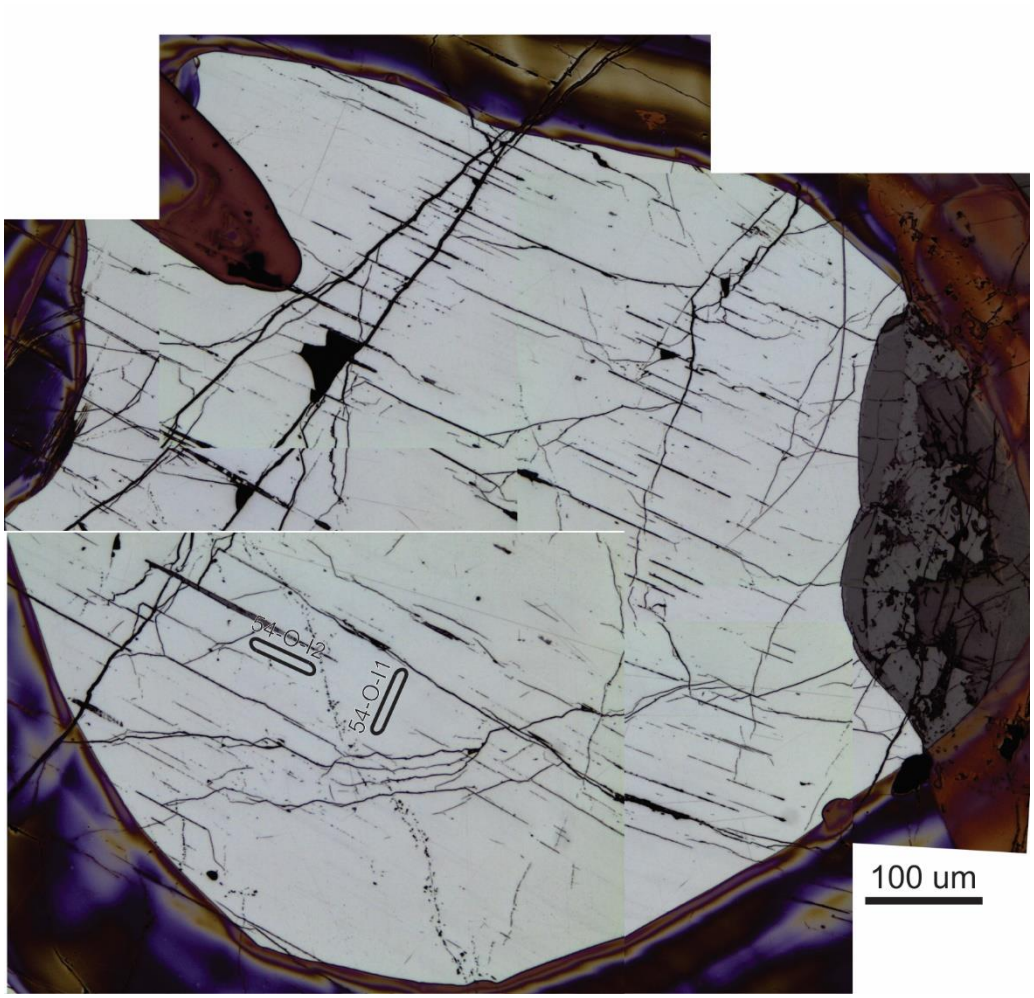

CC054 circle O EPMA

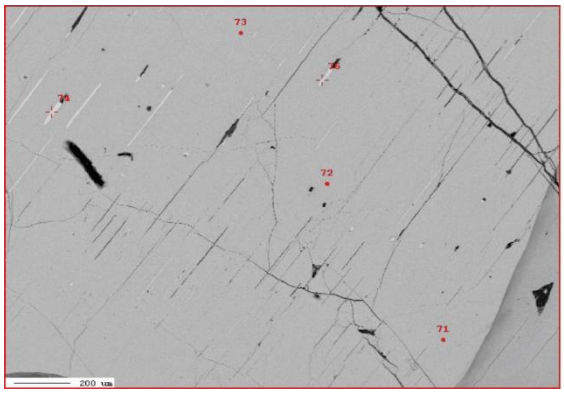

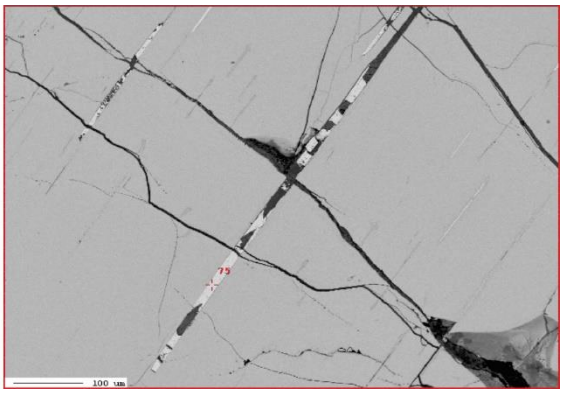

CC072 circle A LA-ICPMS

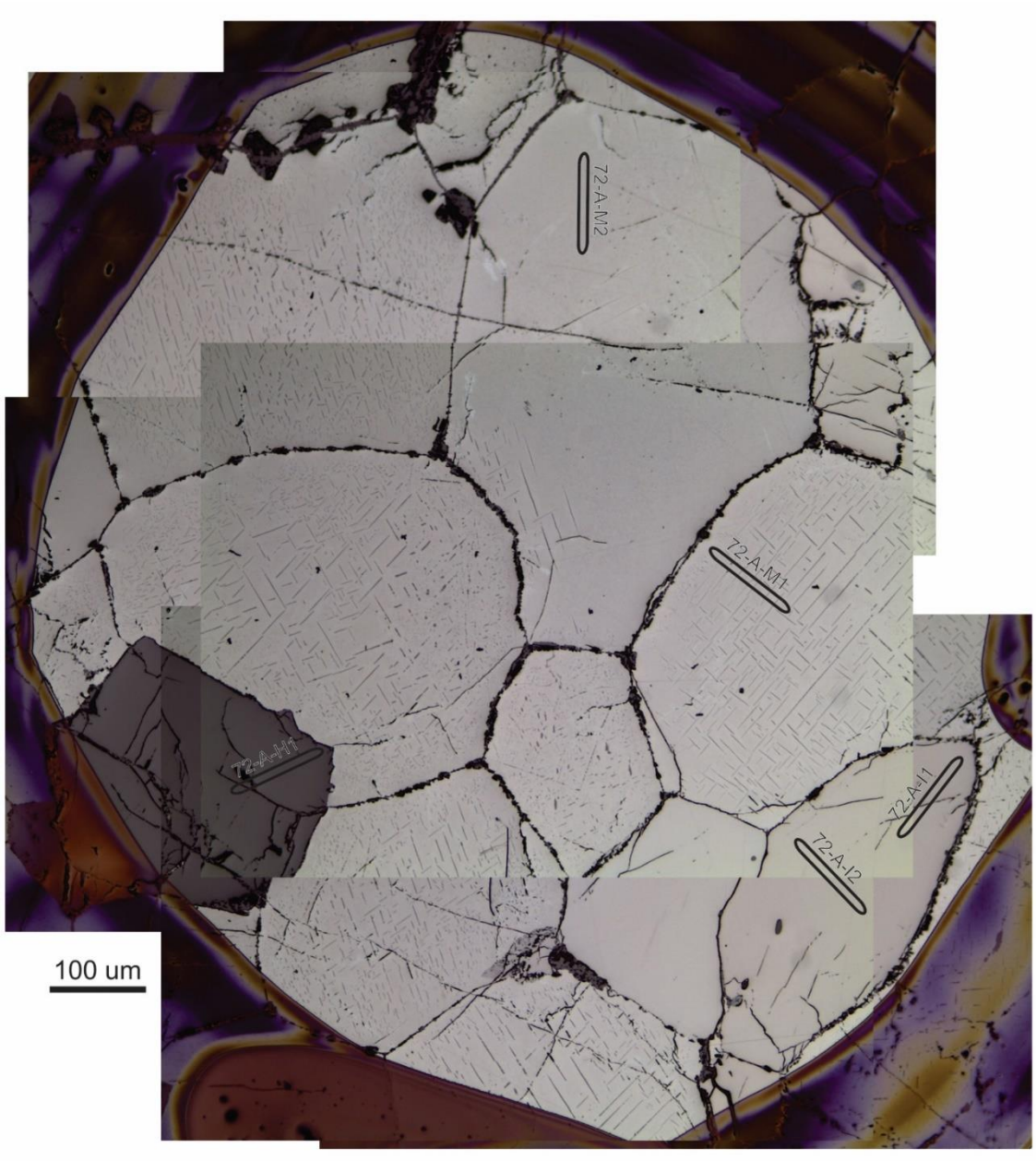

CC072 circle A EPMA

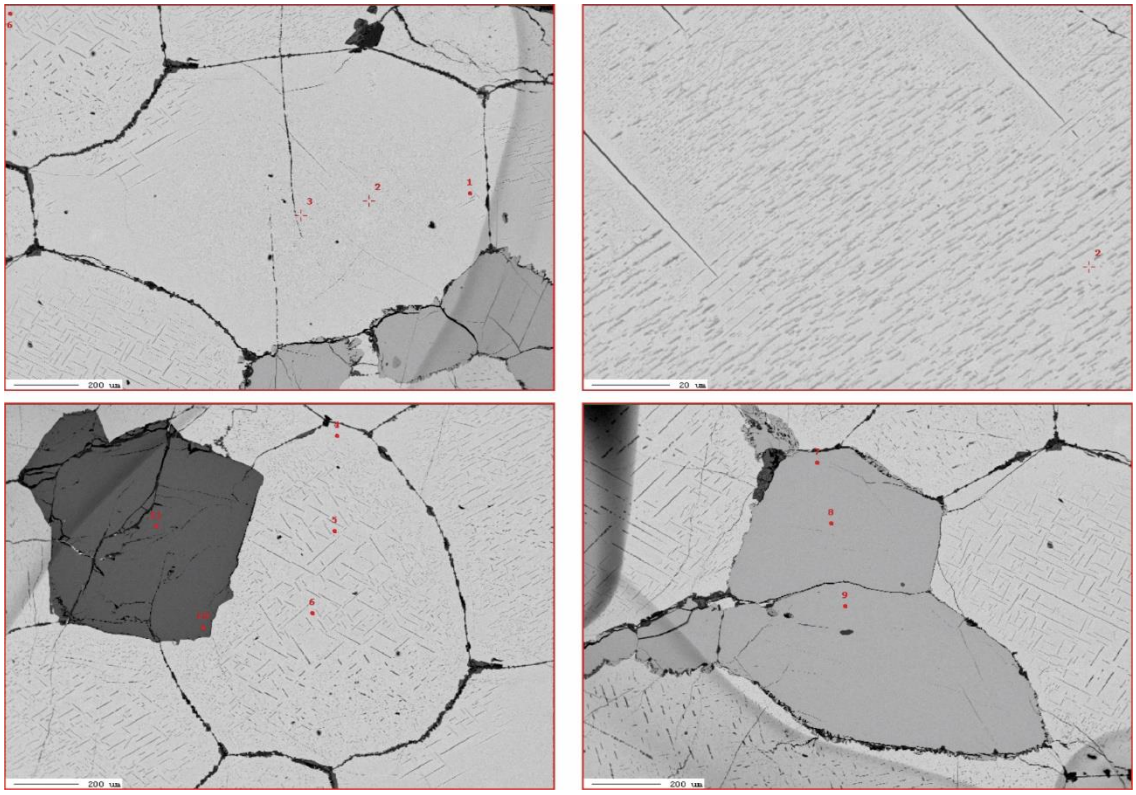

CC072 circle B LA-ICPMS

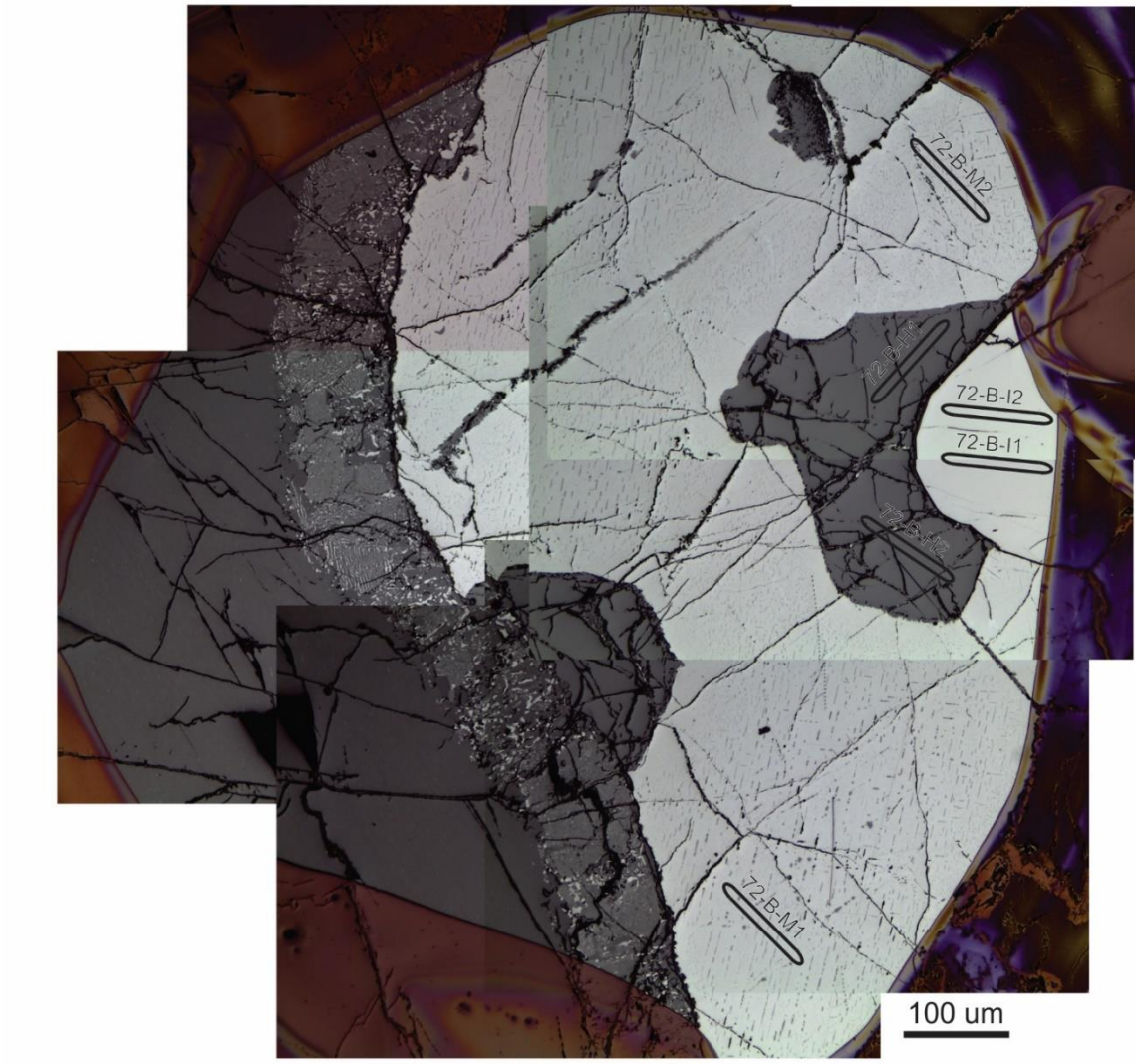

CC072 circle B EPMA

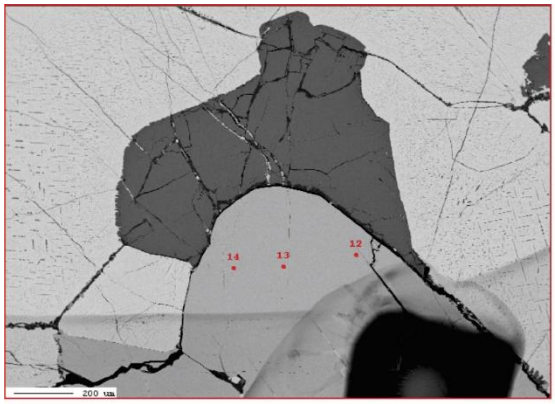

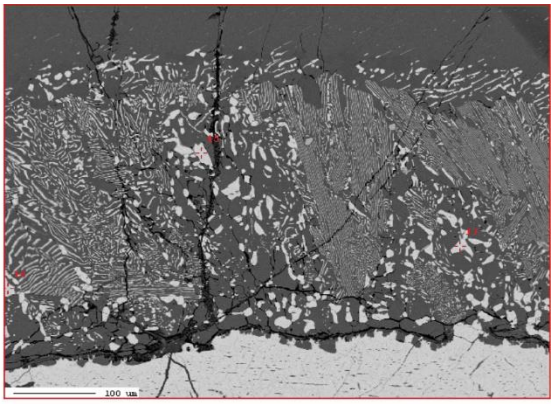

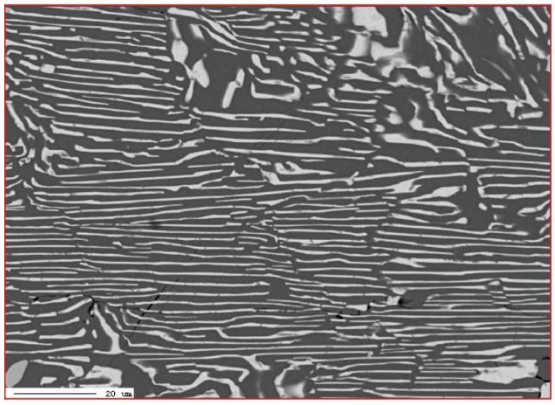

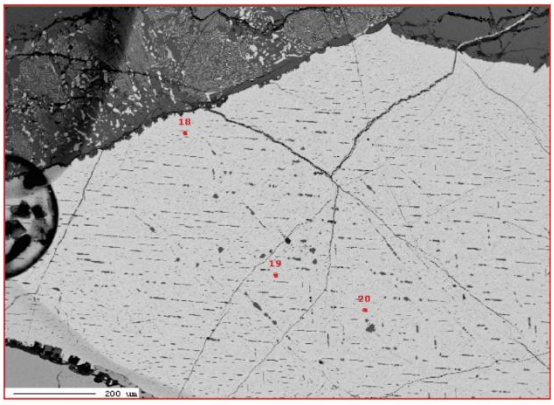

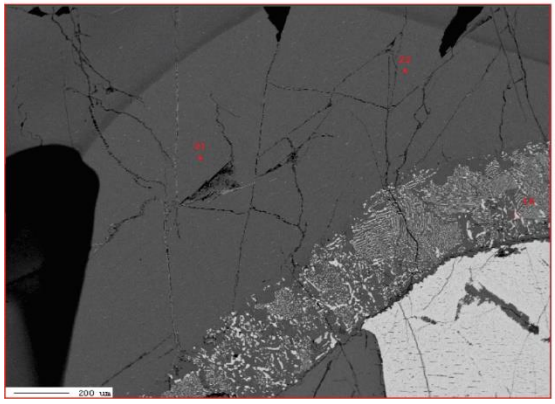

CC072 circle C LA-ICPMS

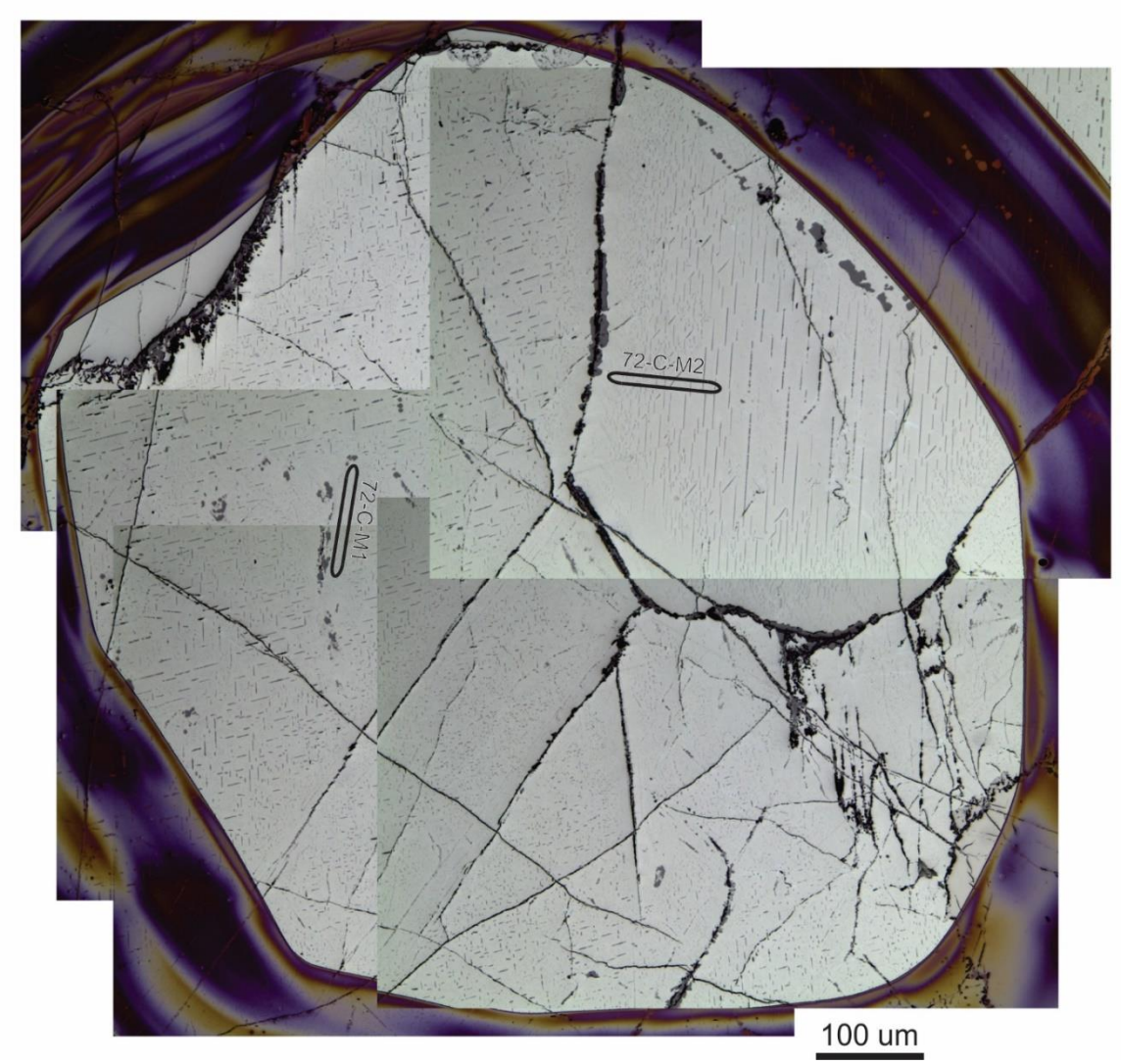

CC072 circle C EPMA

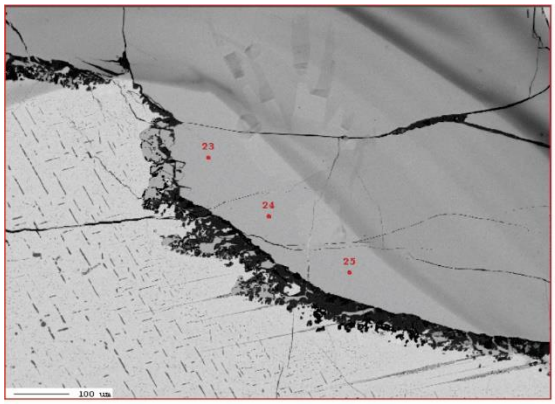

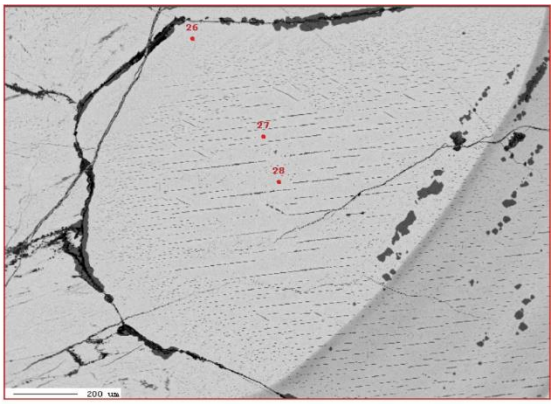

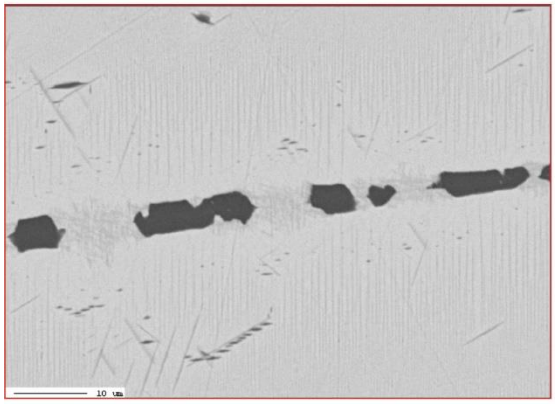

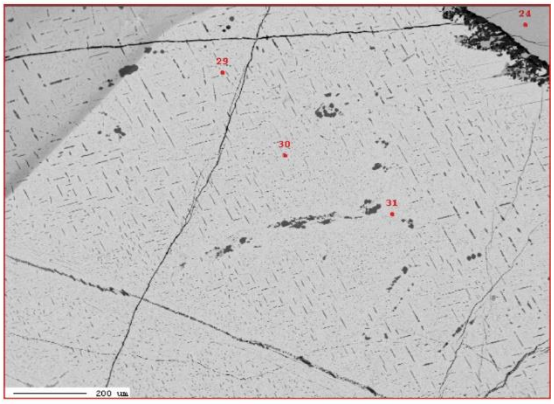

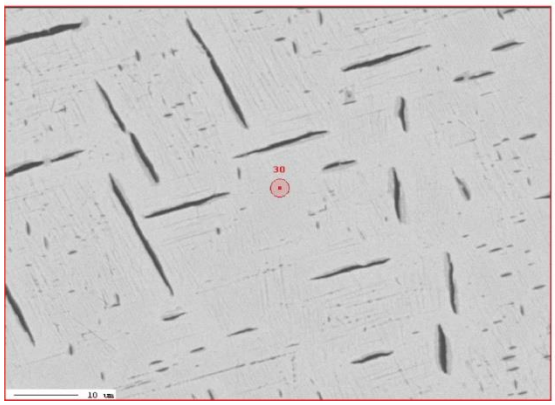

CC072 circle D LA-ICPMS

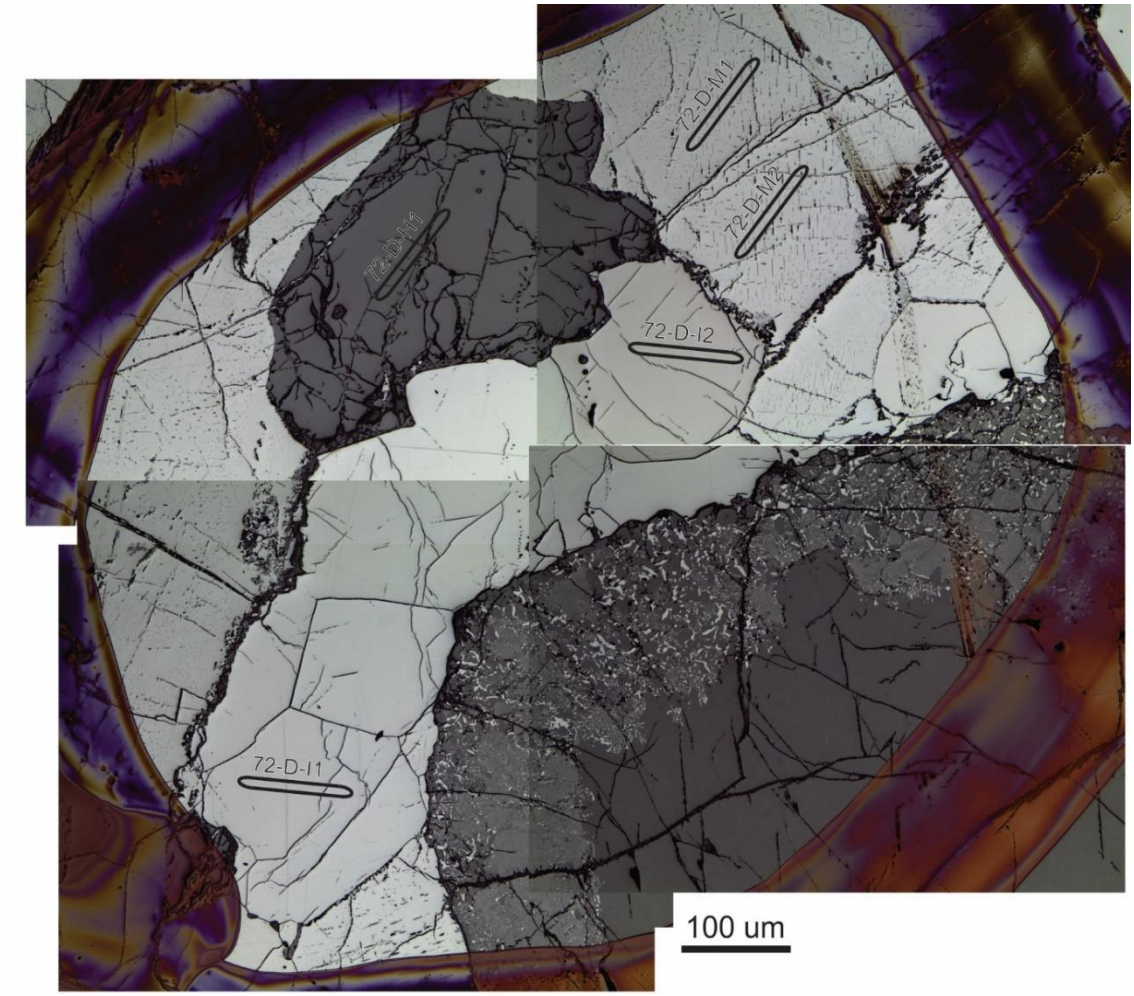

CC072 circle D EPMA

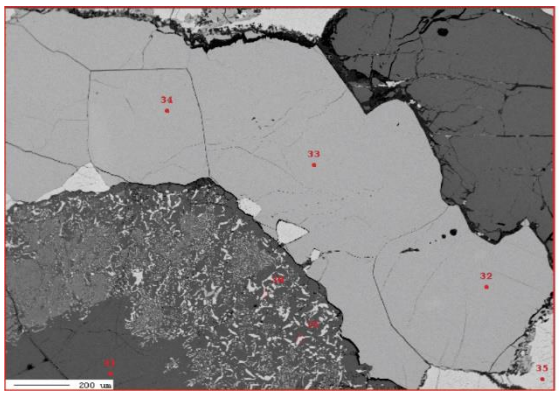

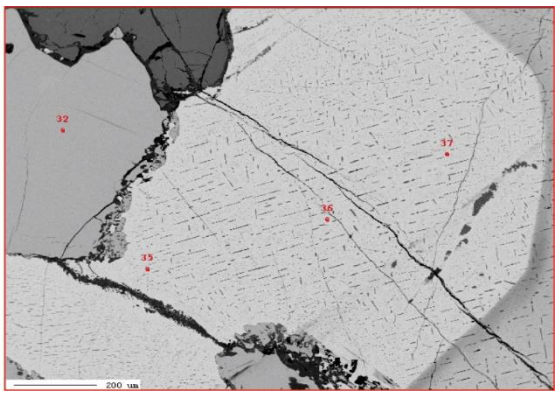

CC072 circle E LA-ICPMS

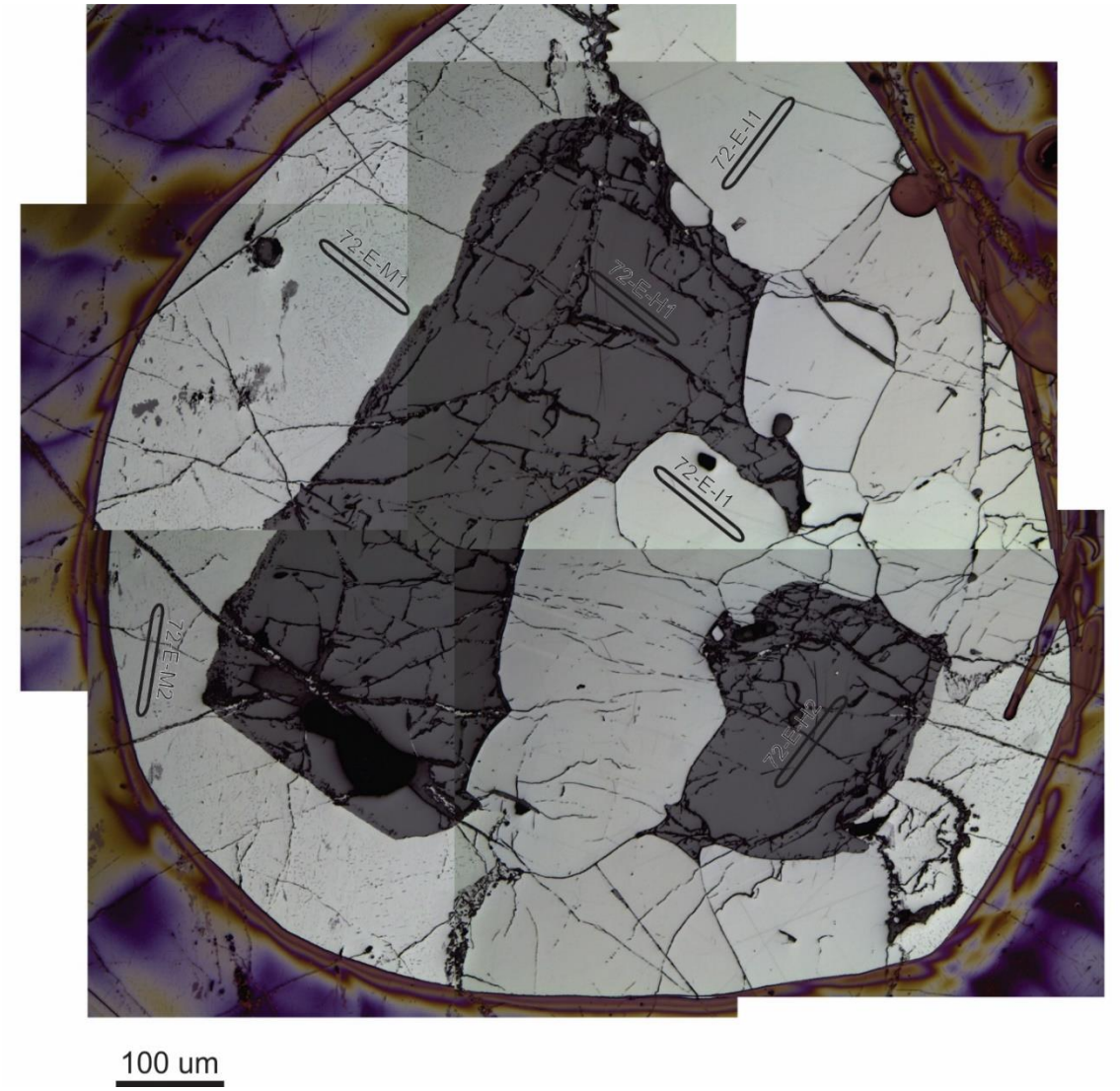

CC072 circle E EPMA

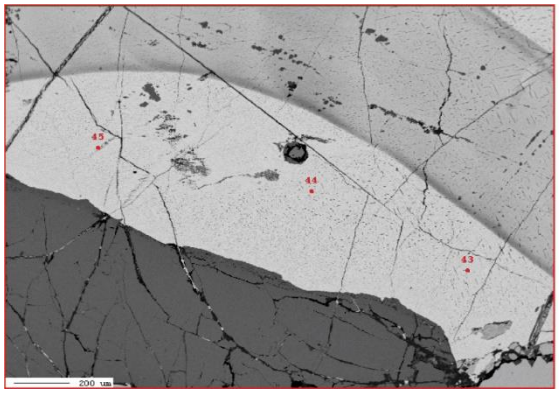

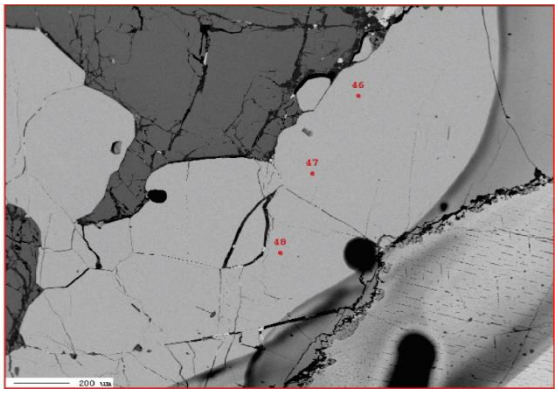

CC072 circle G LA-ICPMS

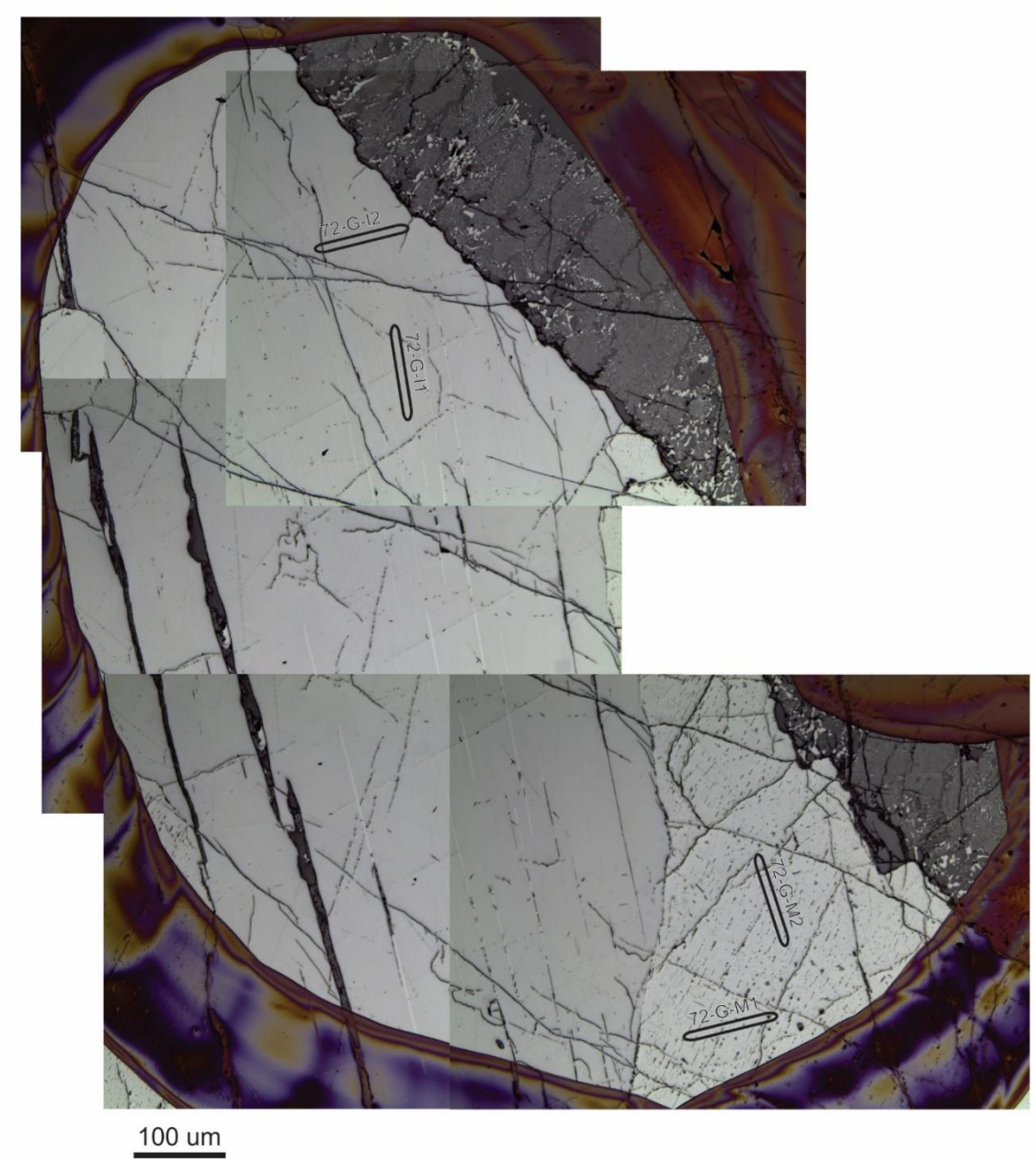
72-G-I2
72-G-I1
72-G-M2
72-G-M1
100 um

CC072 circle G EPMA

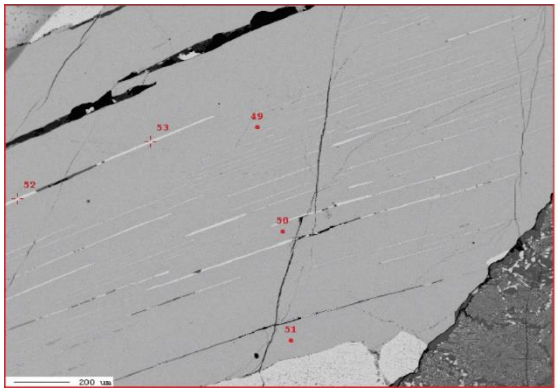

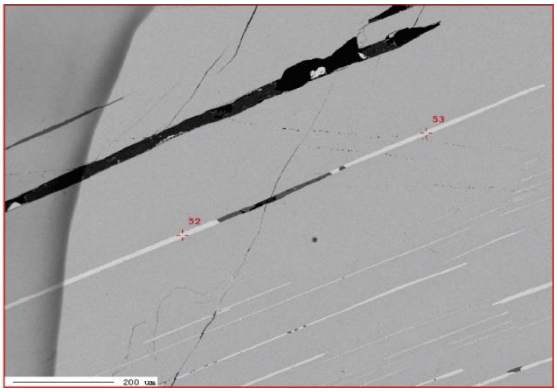

CC072 circle H LA-ICPMS

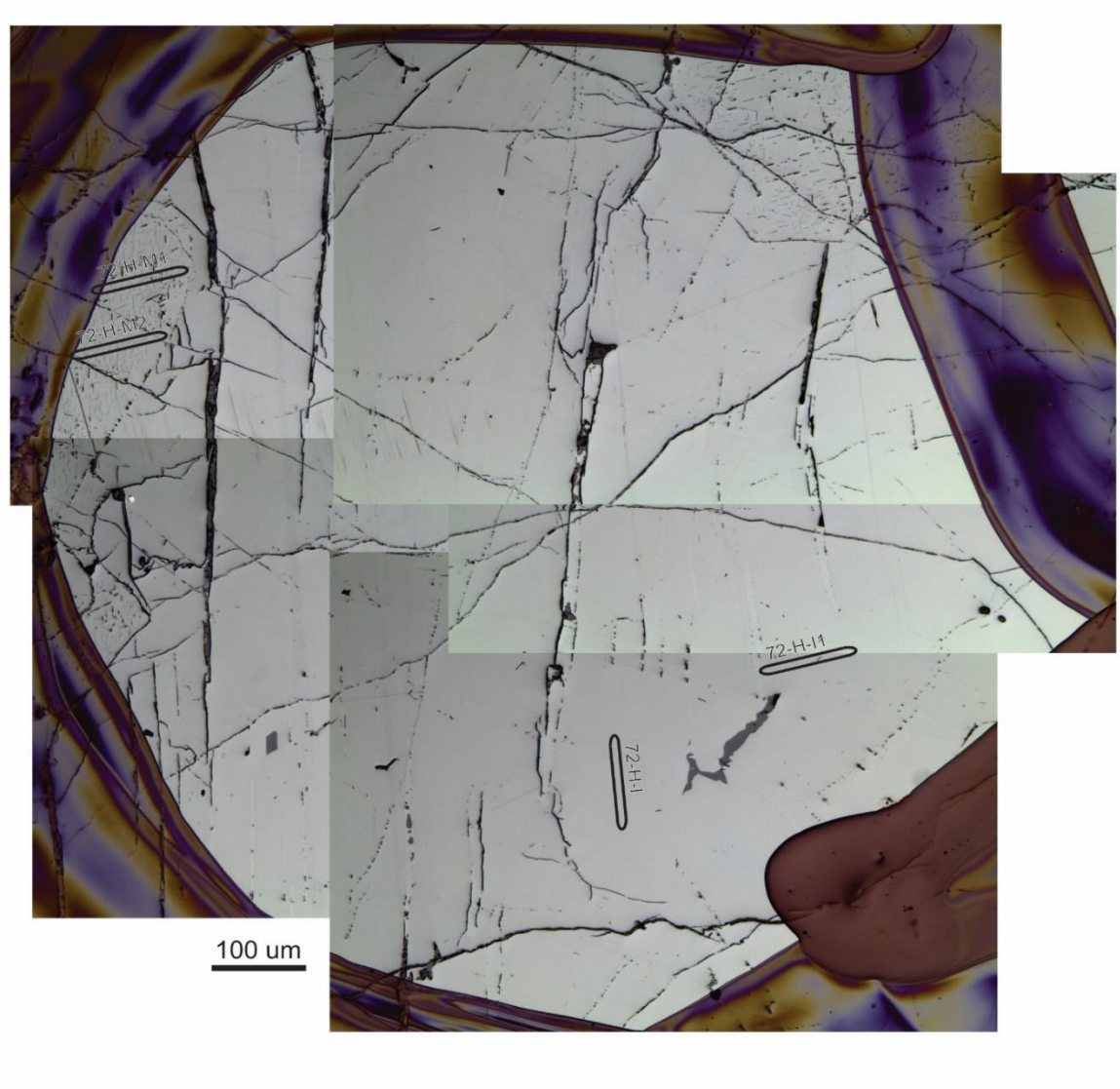

CC072 circle H EPMA

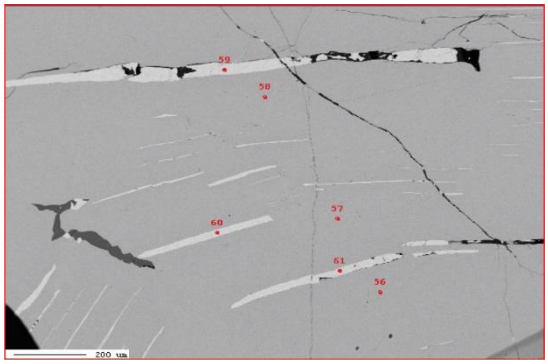

CC072 circle I LA-ICPMS

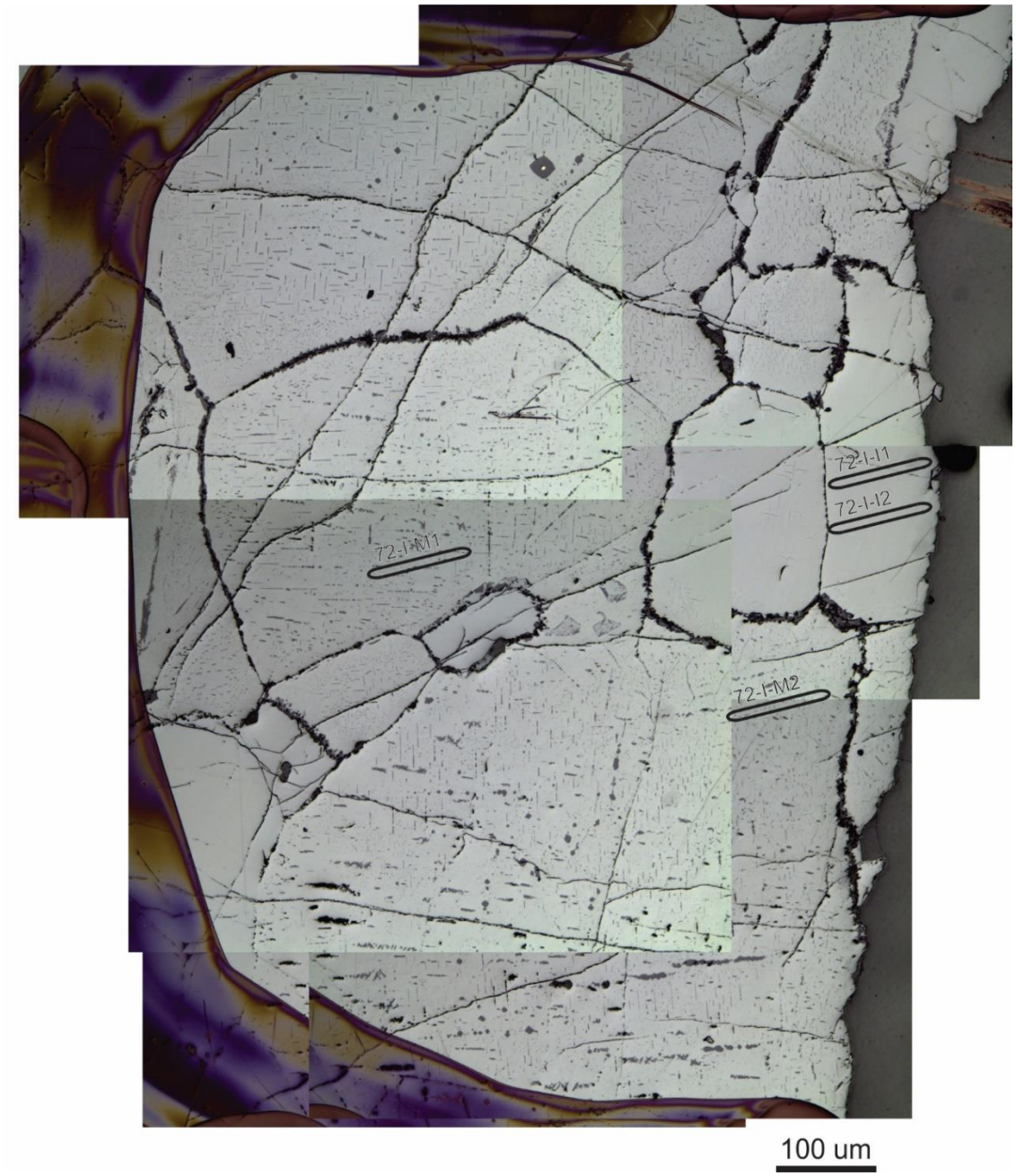
72-I-I1
72-I-I2
72-I-M1
72-I-M2
100 um

CC072 circle I EPMA

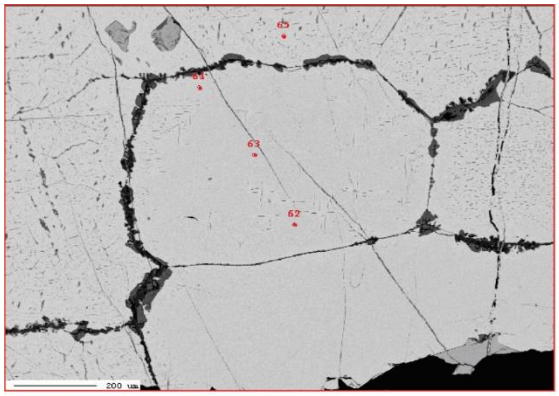

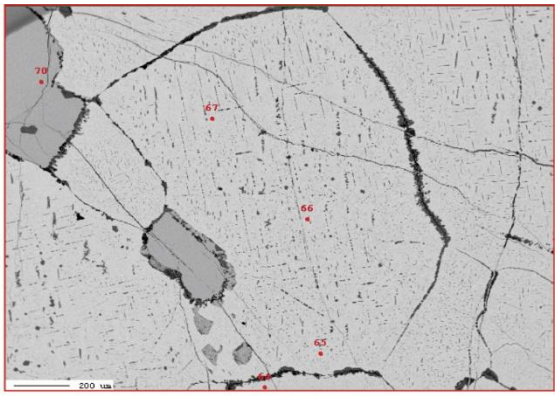

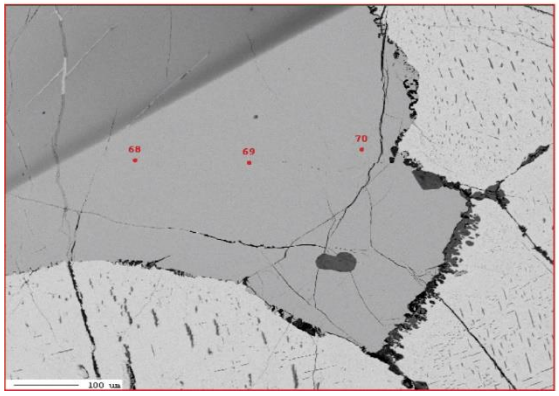

CC072 circle K LA-ICPMS

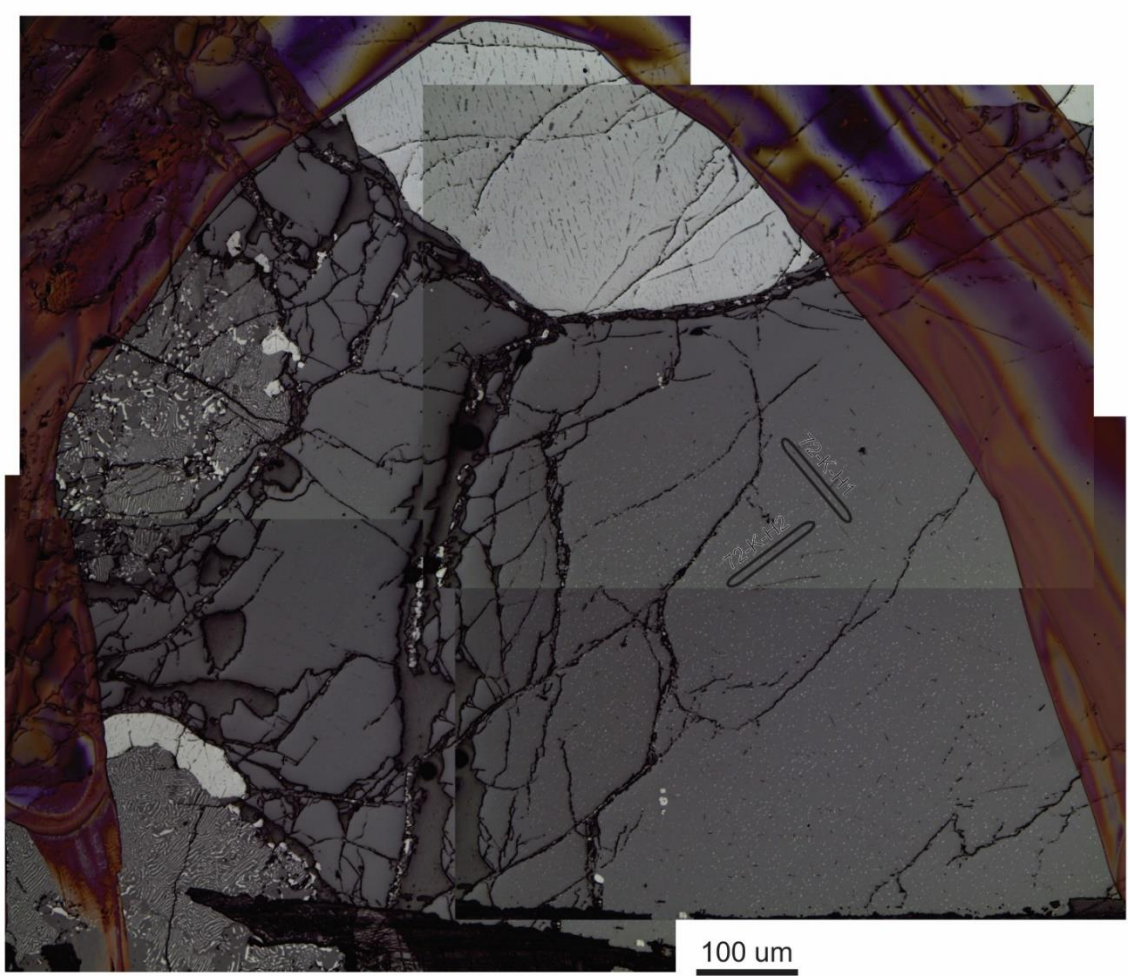

CC074 circle A LA-ICPMS

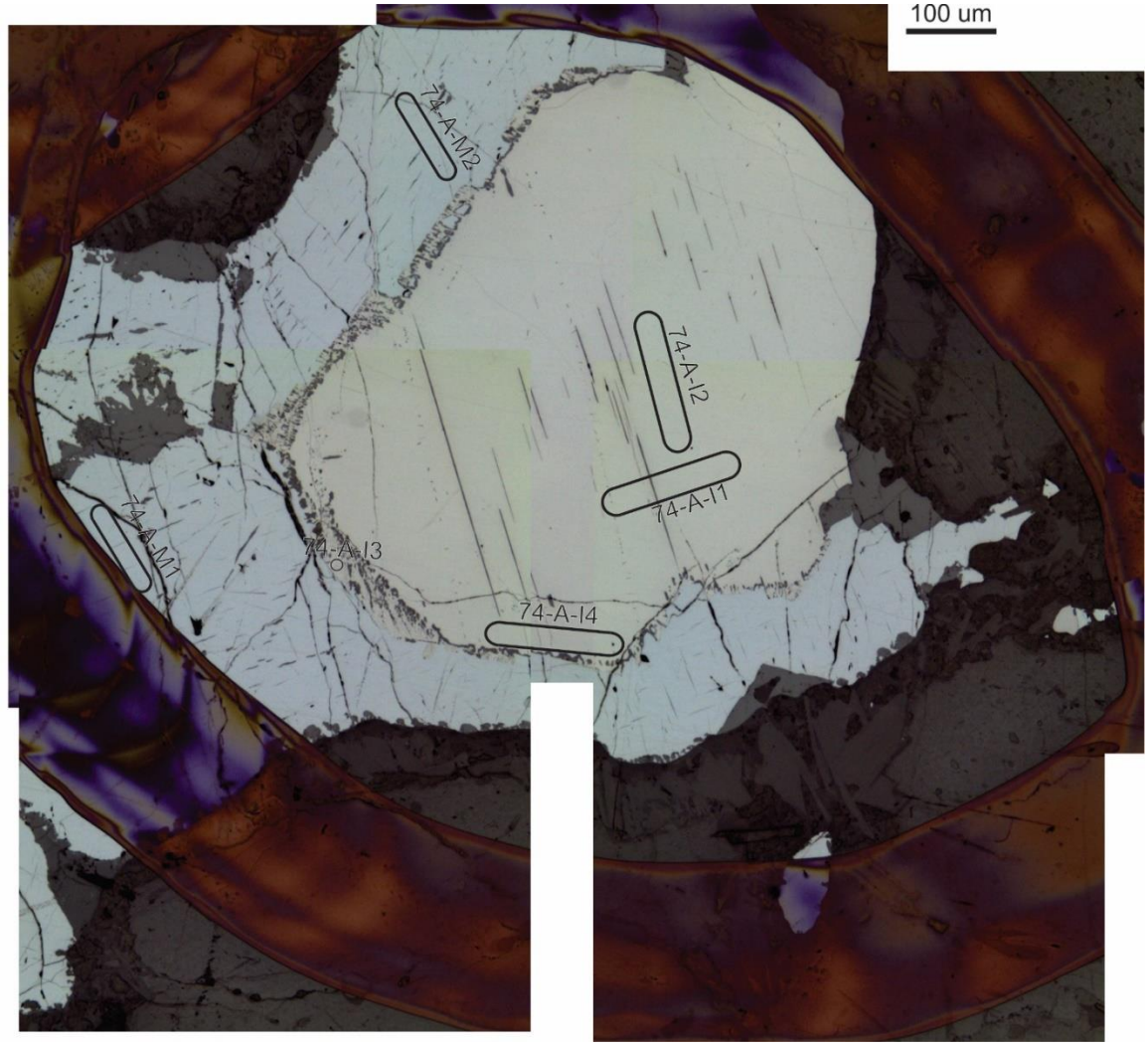

CC074 circle A EPMA

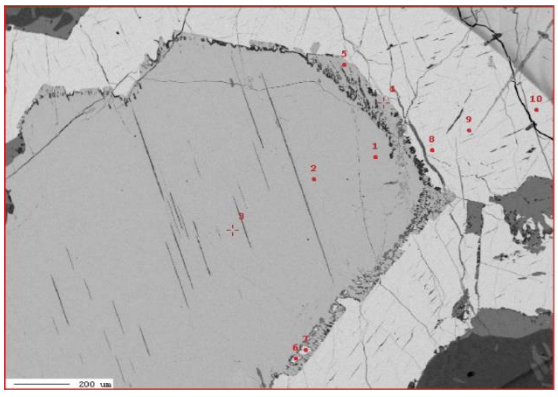

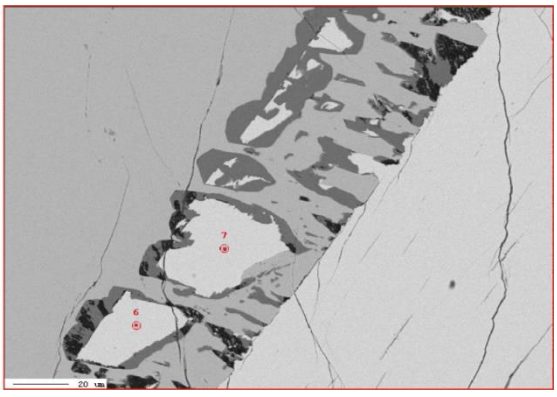

CC074 circle B LA-ICPMS

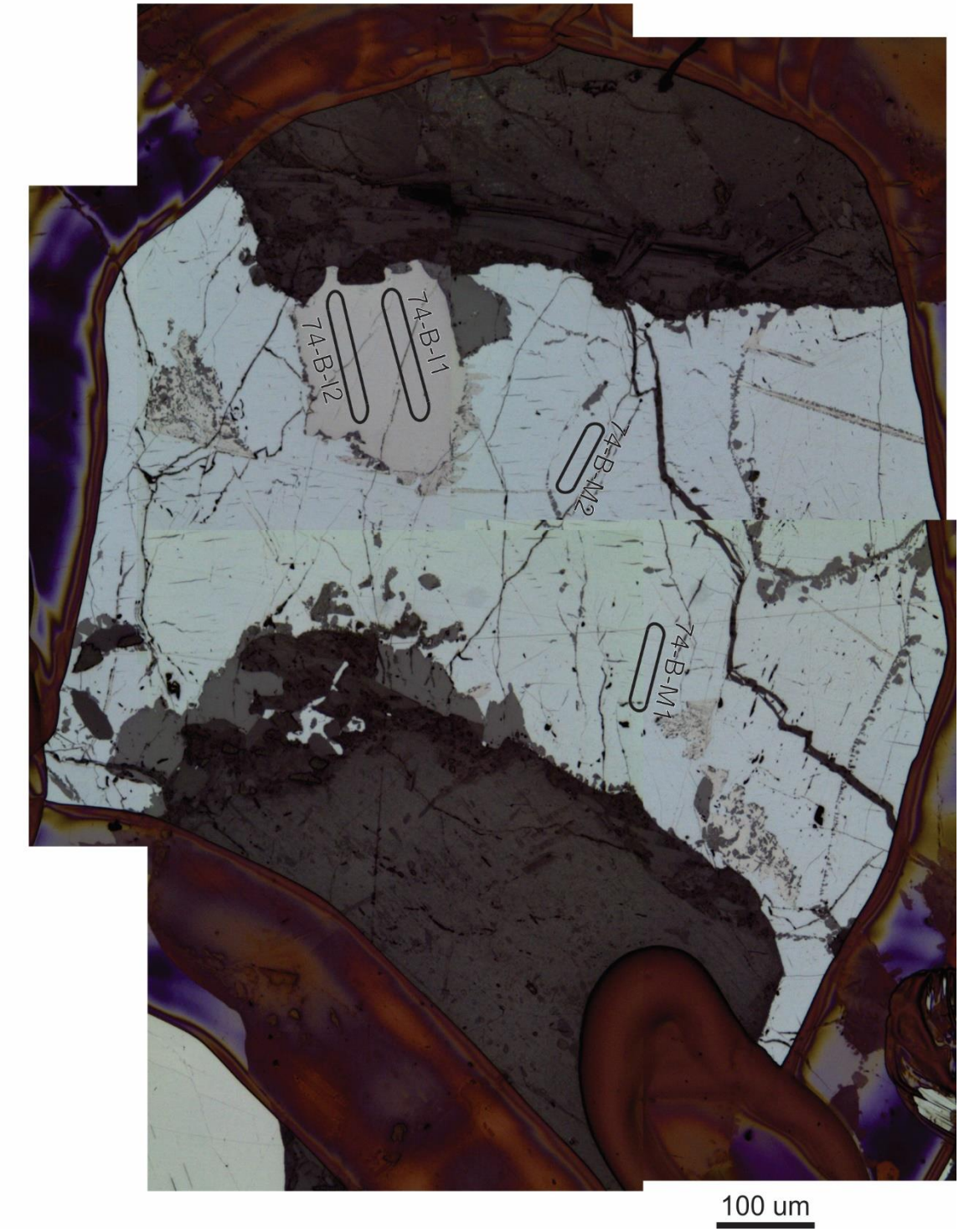

CC074 circle B EPMA

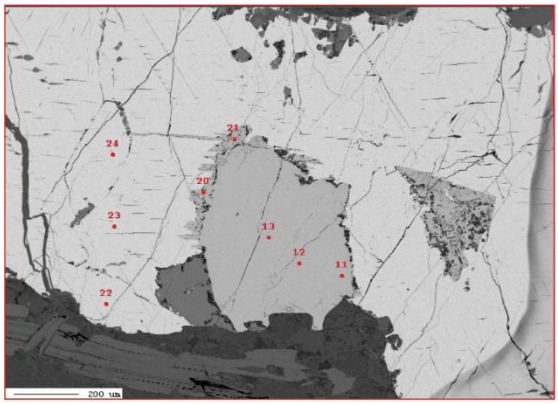

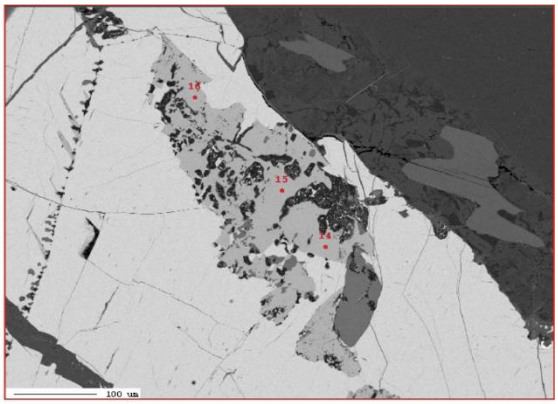

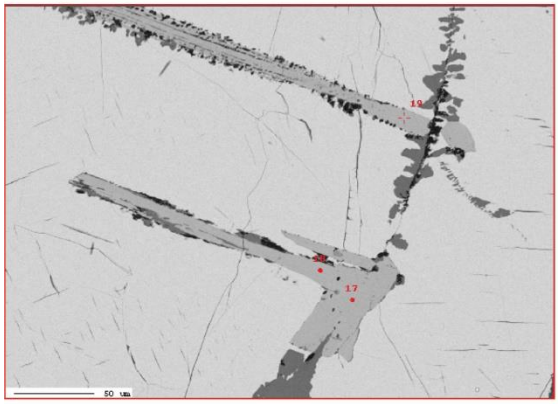

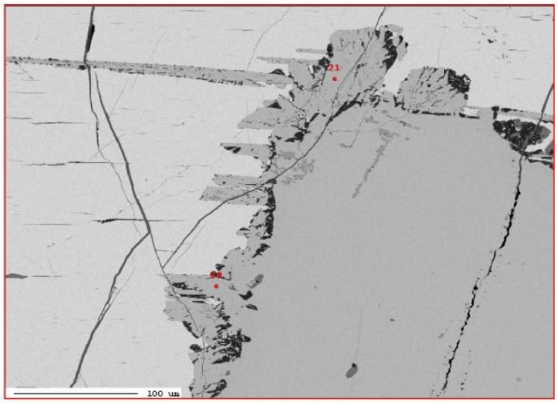

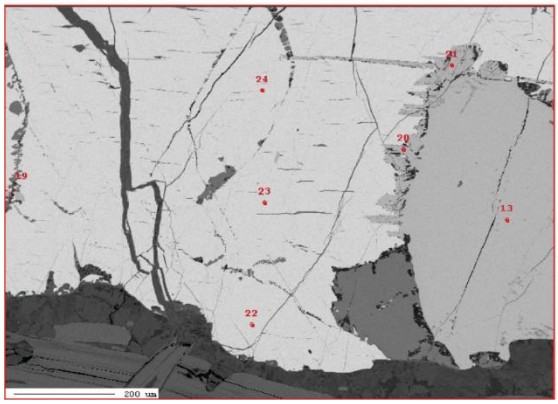

CC074 circle C LA-ICPMS

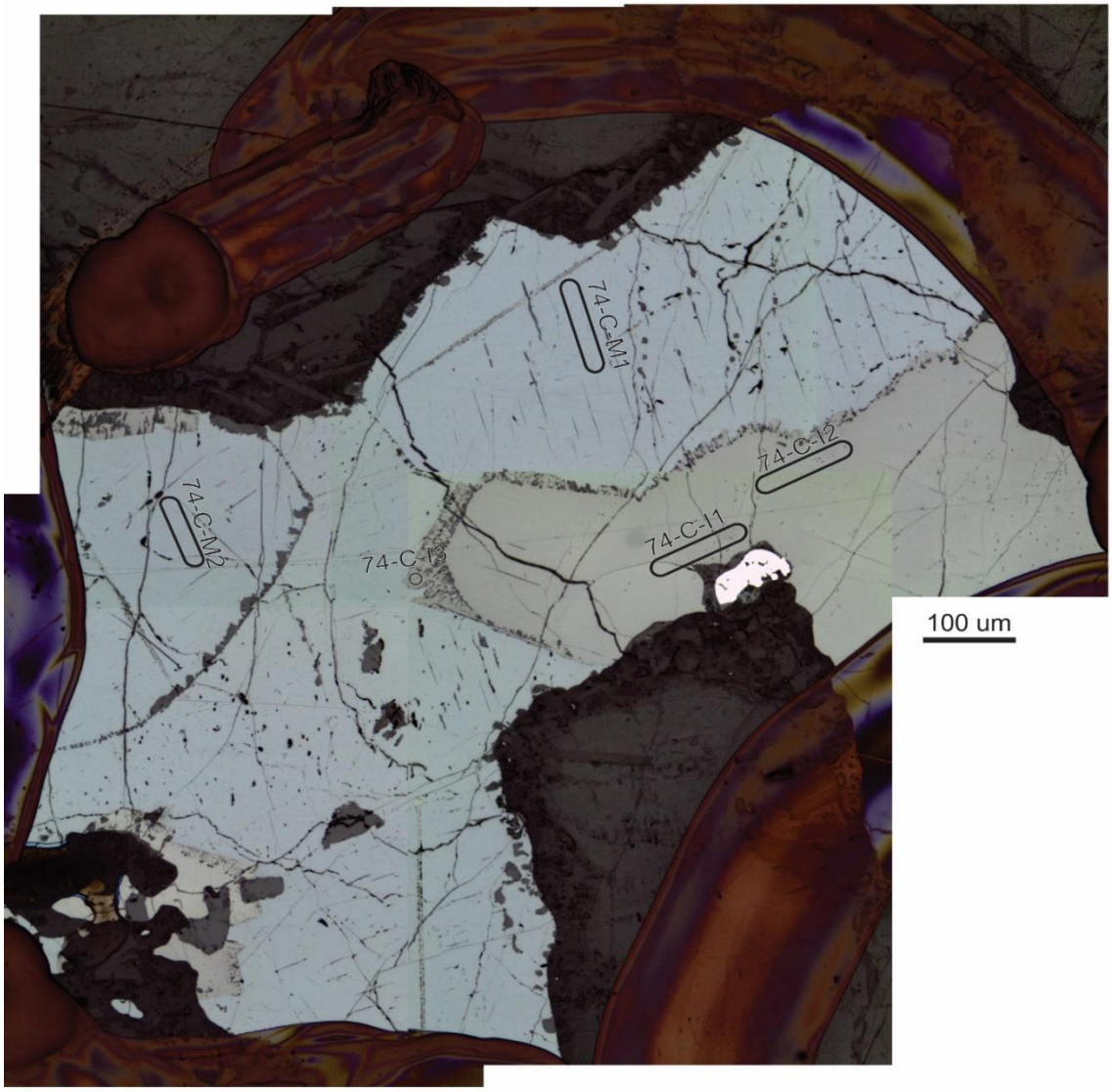

CC074 circle C EPMA

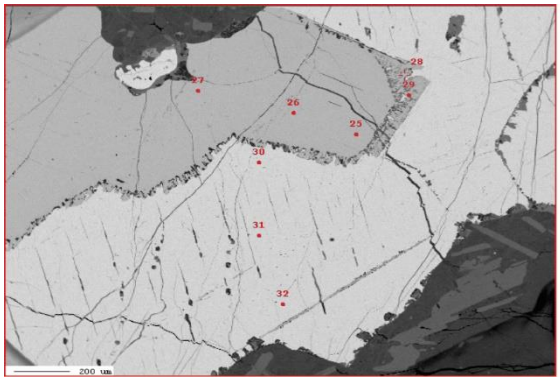

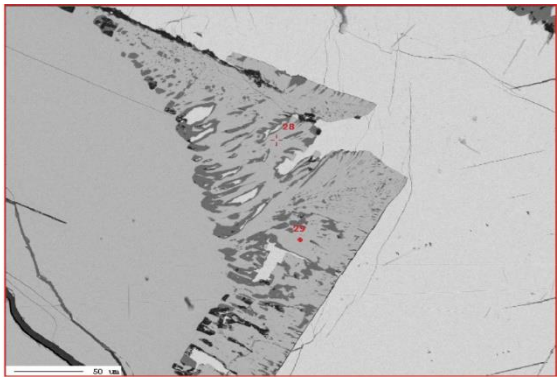

CC074 circle D LA-ICPMS

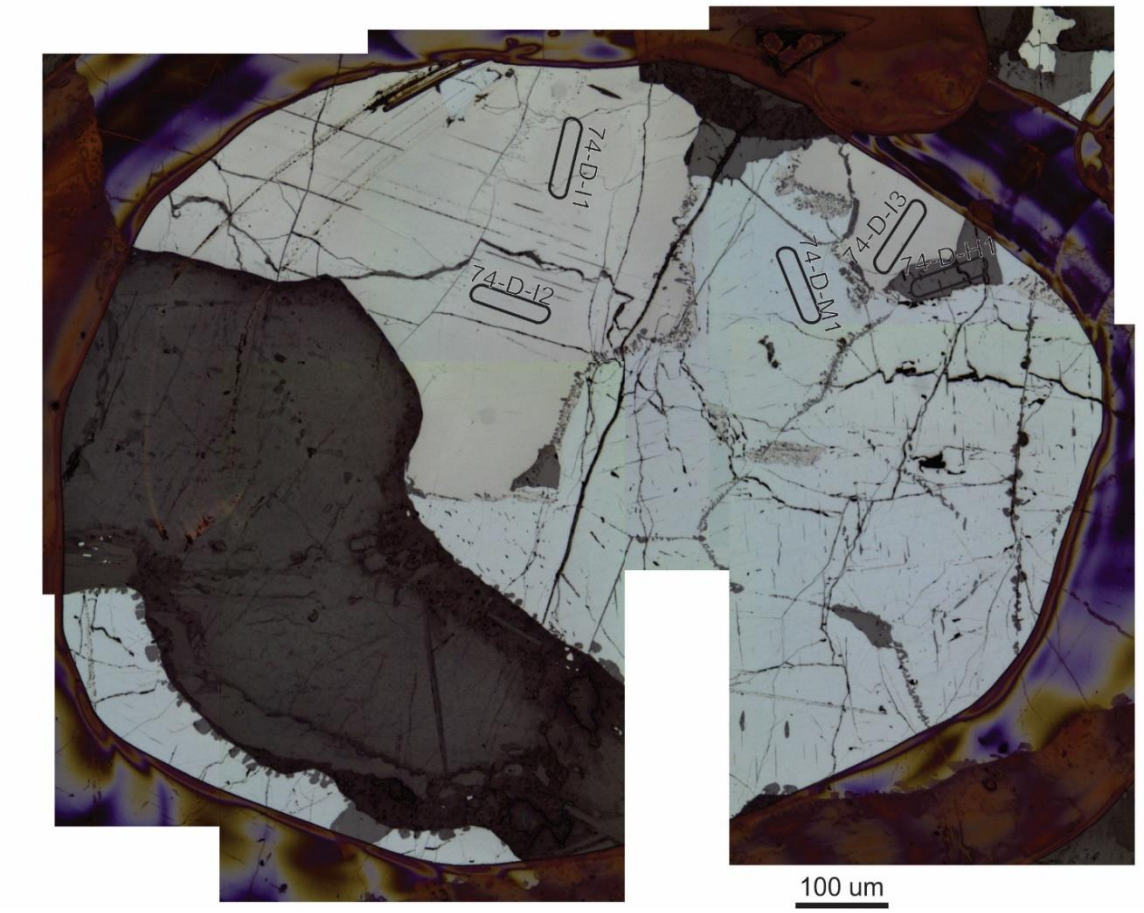
74-D-I1
74-D-I2
74-D-I3
74-D-H1
74-D-M1
100 um

CC074 circle D EPMA

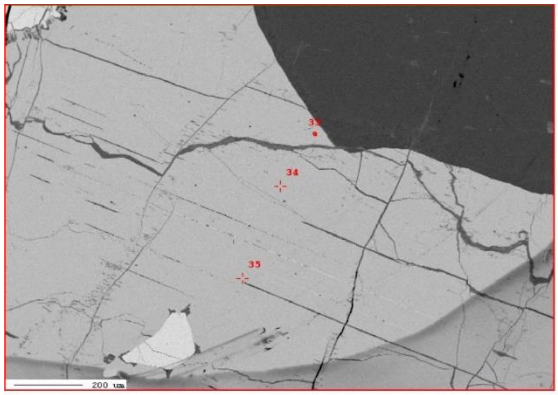

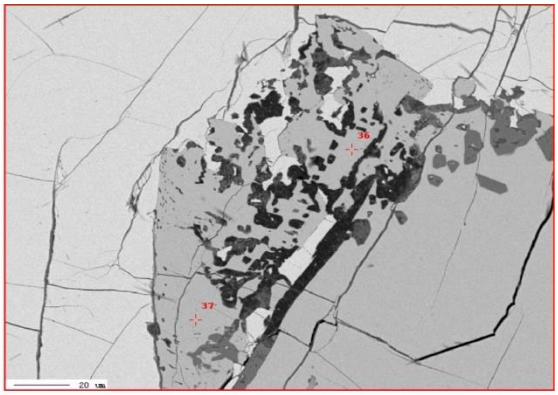

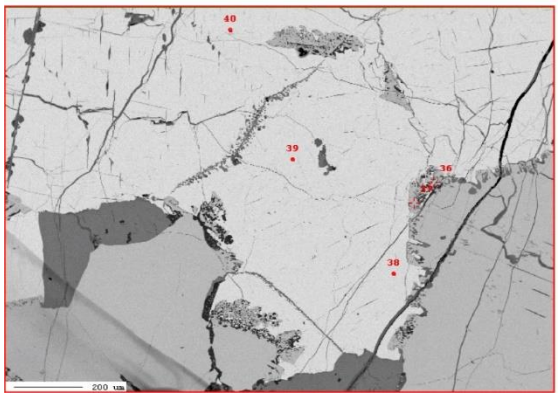

CC074 circle E LA-ICPMS

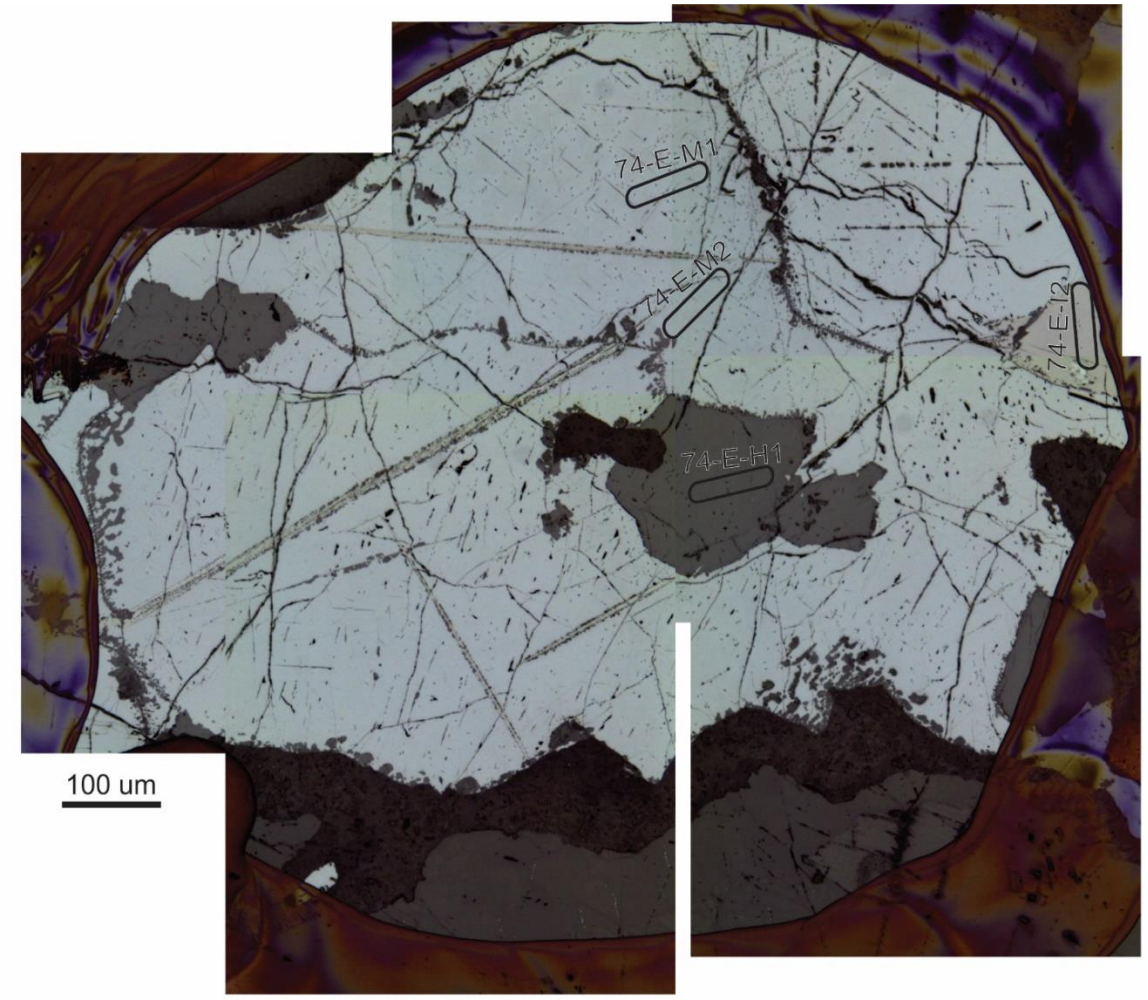

CC074 circle E EPMA

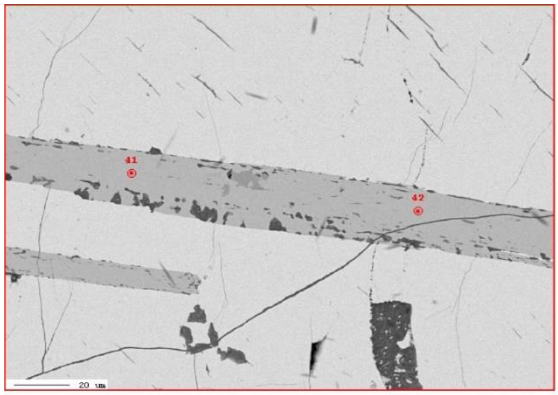

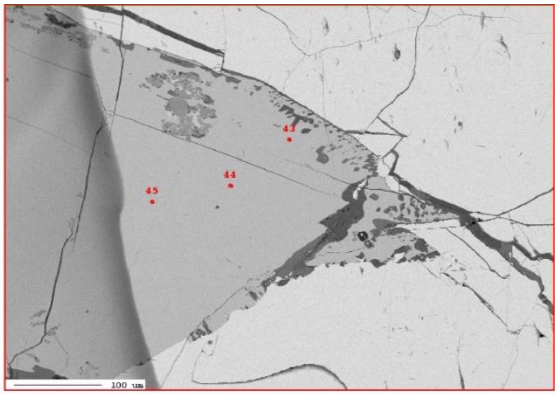

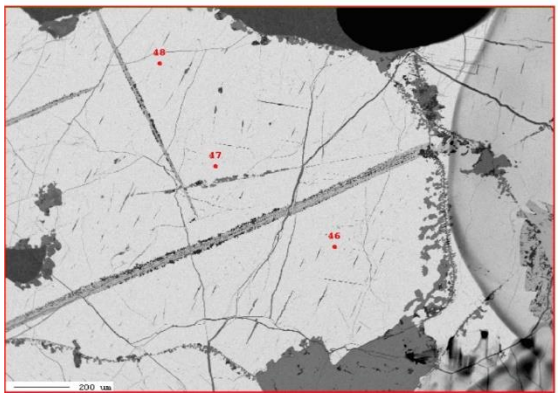

CC074 circle F LA-ICPMS

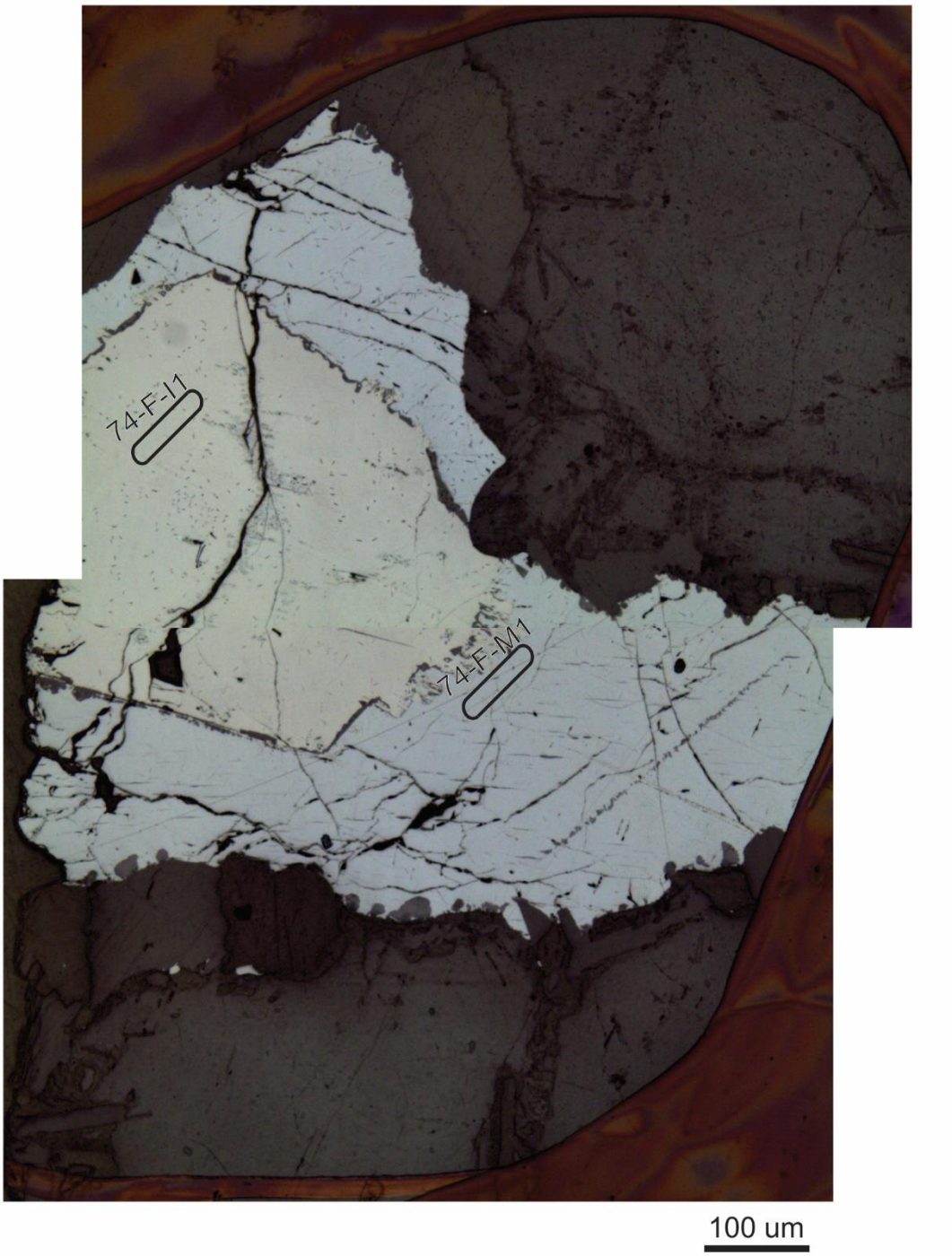

CC074 circle F EPMA

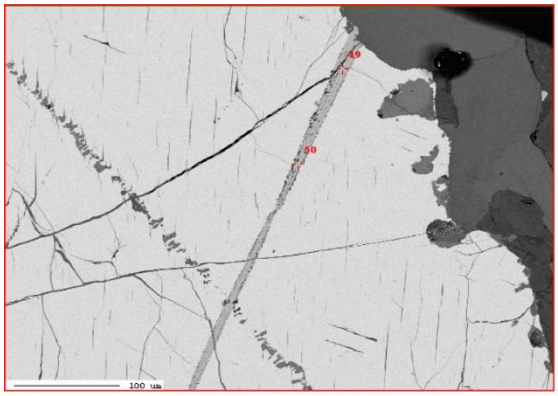

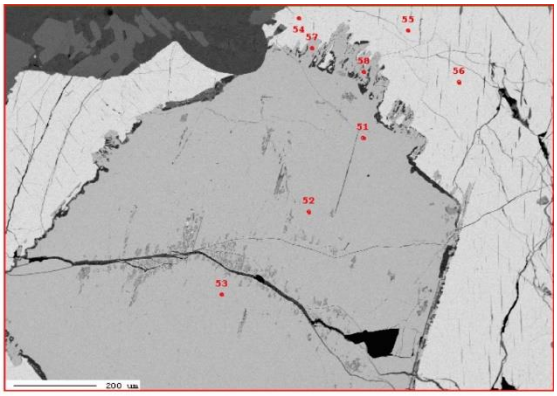

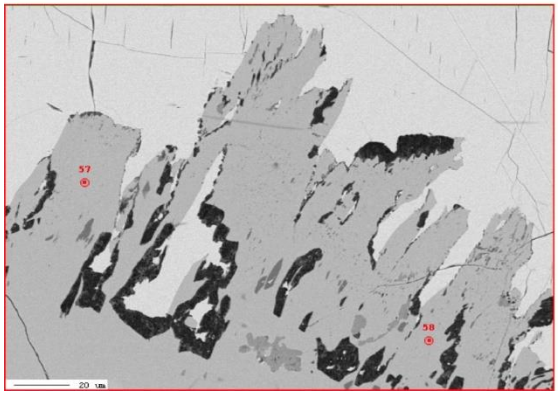

CC076 circle A LA-ICPMS

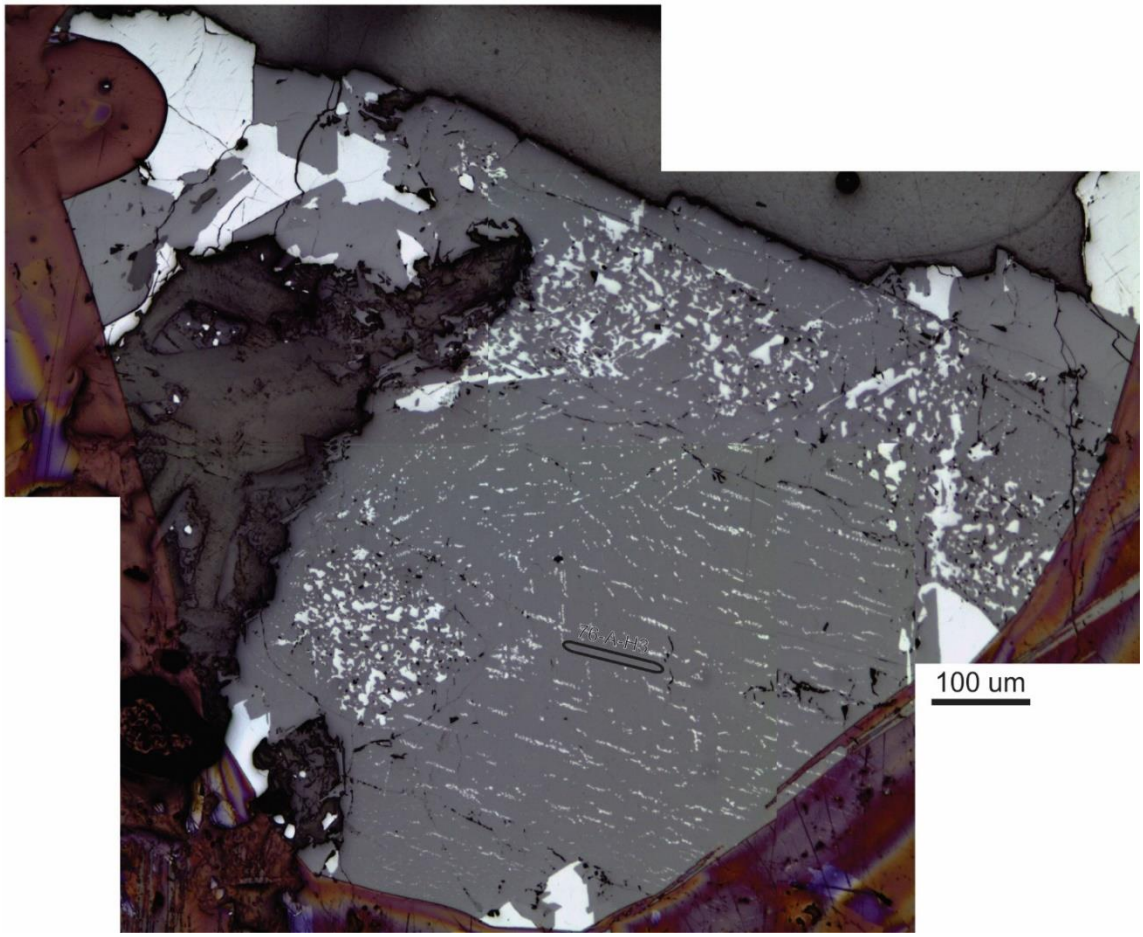

CC076 circle B LA-ICPMS

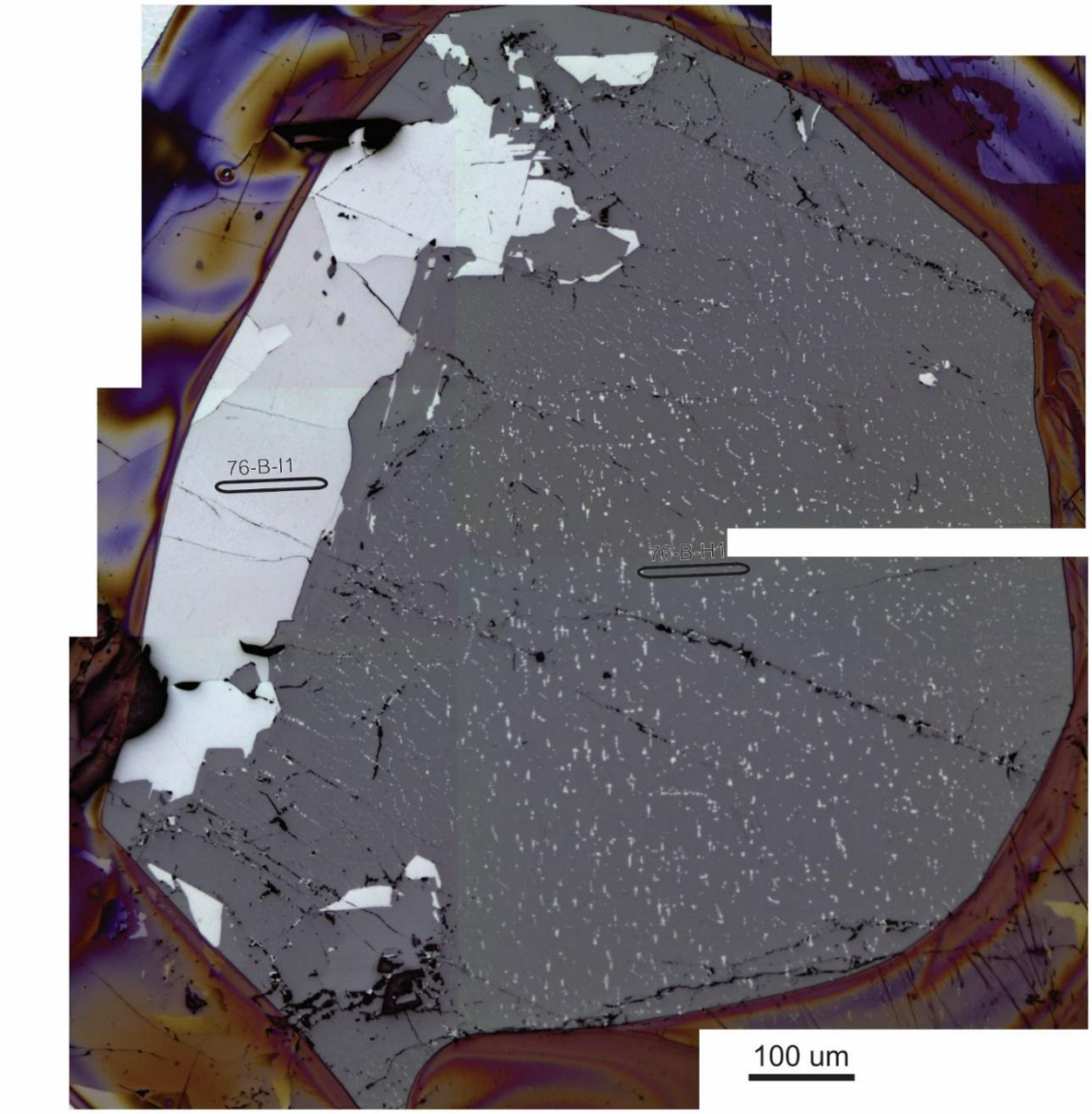

CC076 circle B EPMA

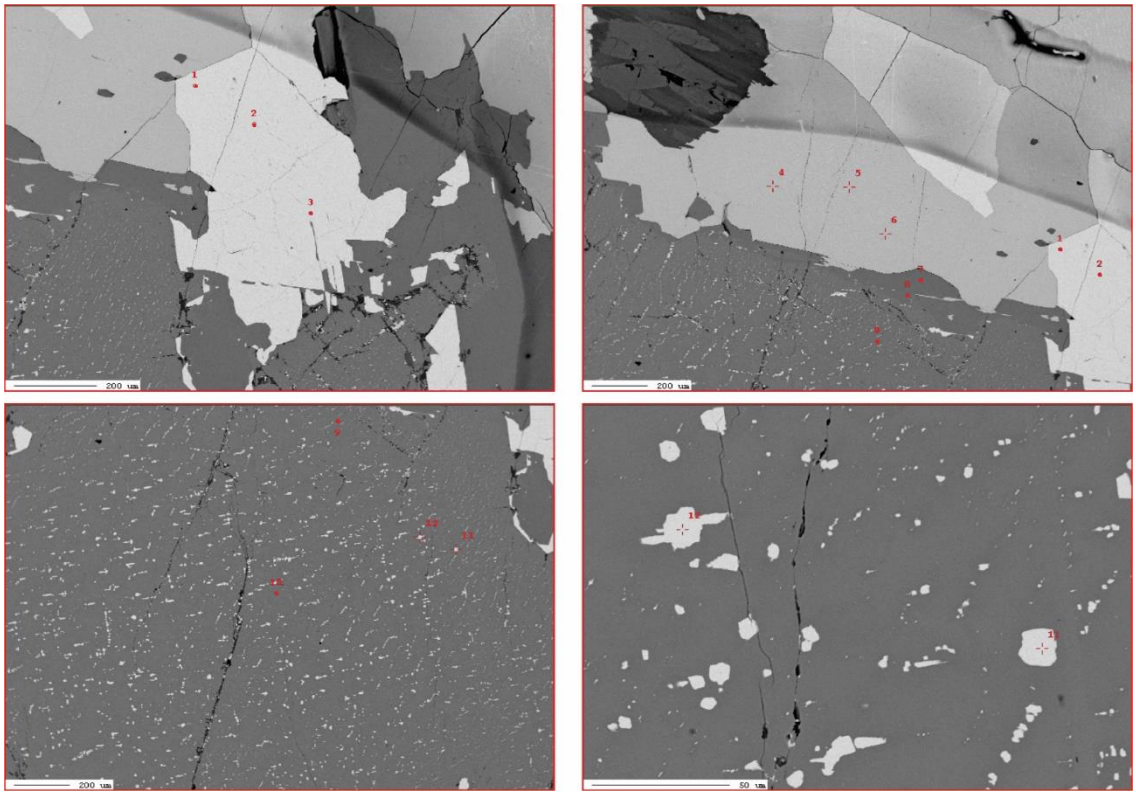

CC076 circle C LA-ICPMS

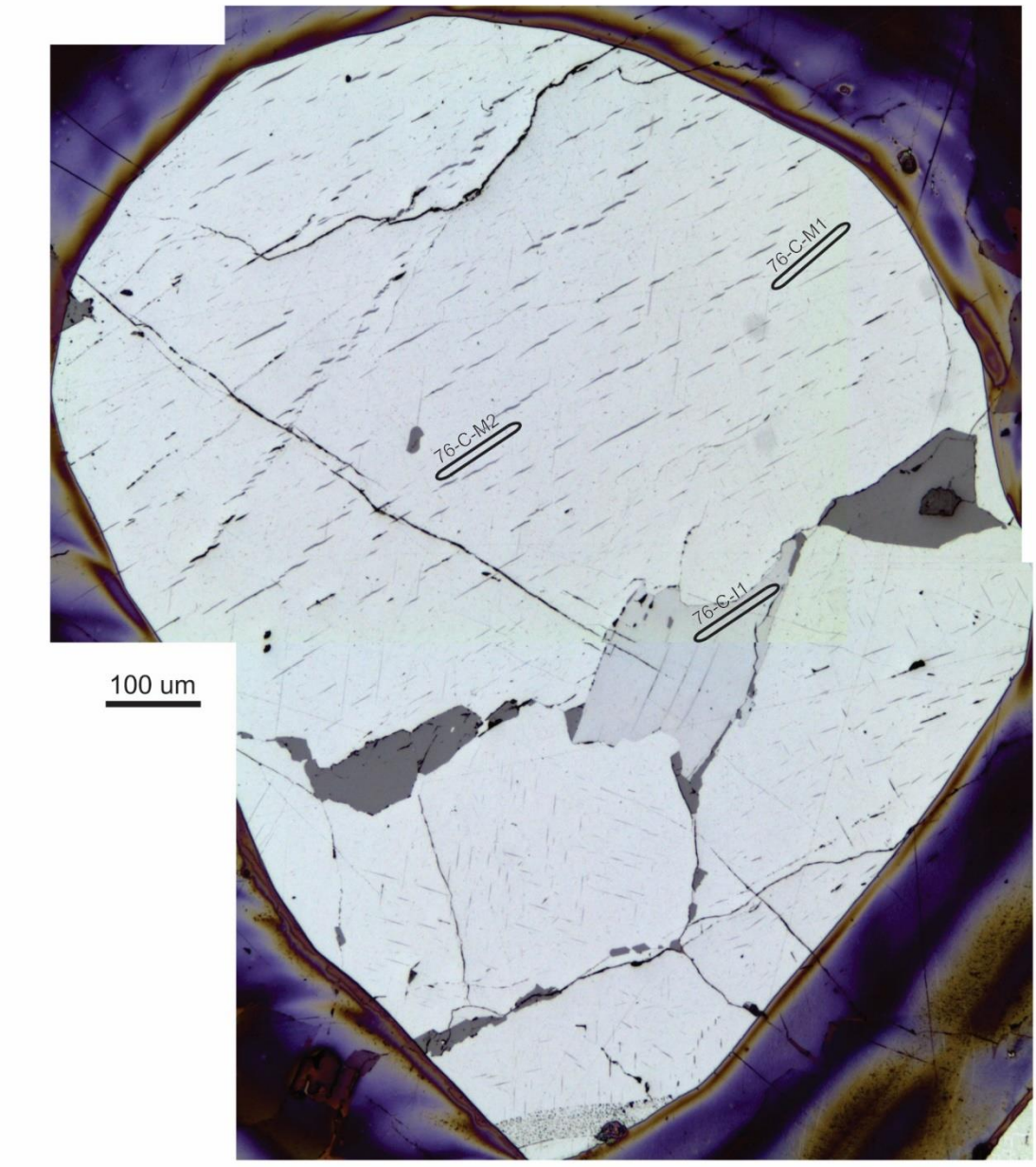

CC076 circle C EPMA

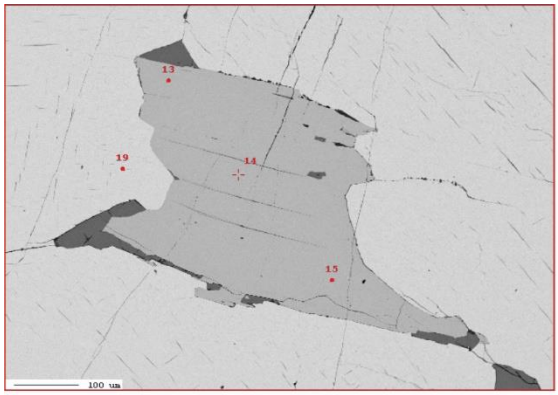

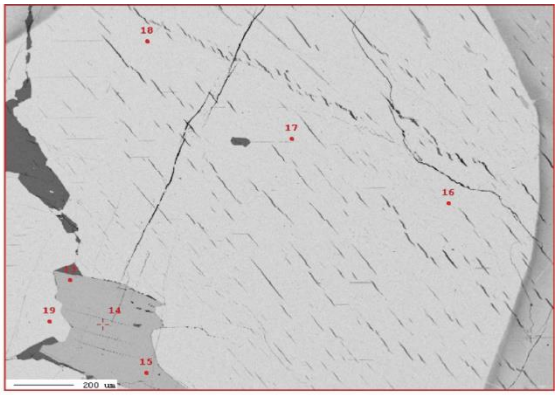

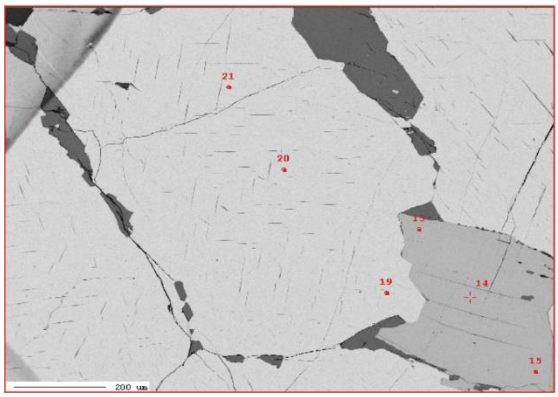

CC076 circle D LA-ICPMS

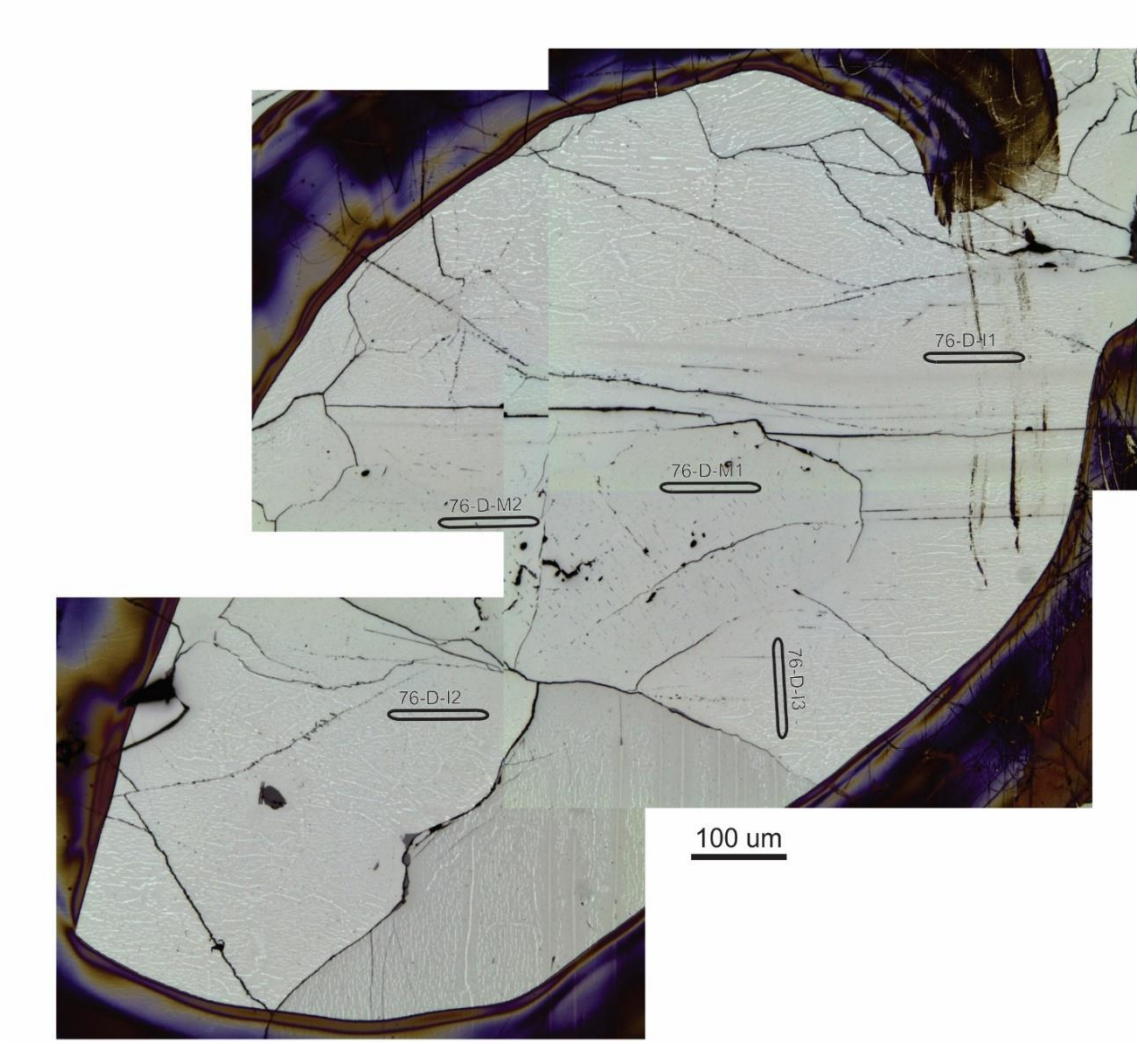

CC076 circle D EPMA

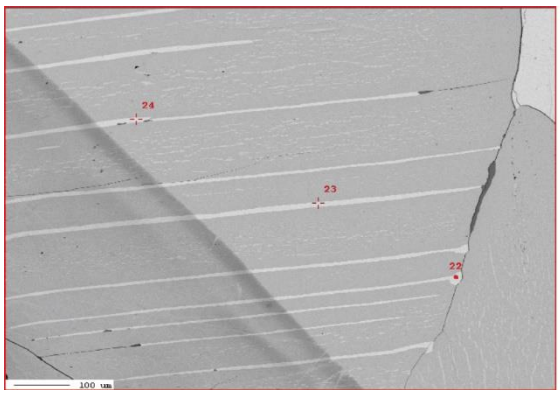

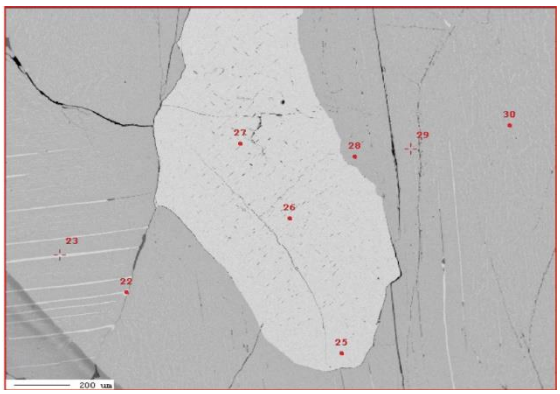

CC076 circle F LA-ICPMS

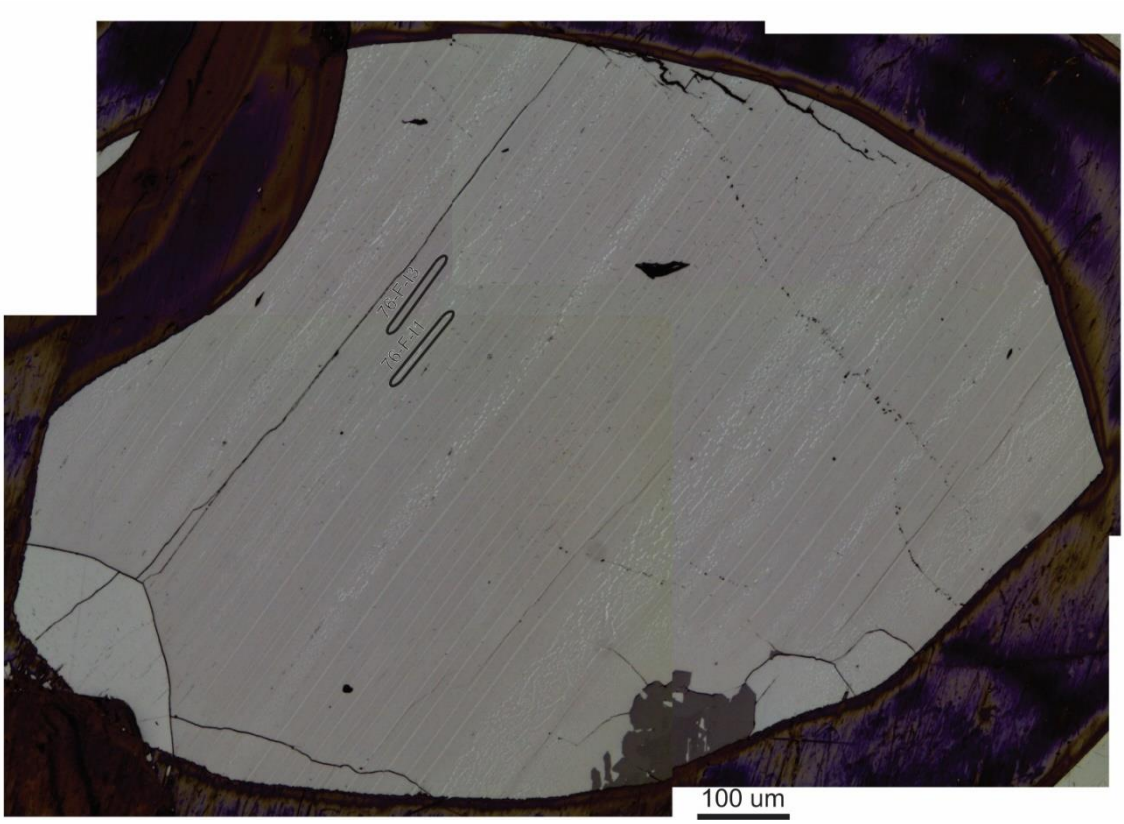

CC076 circle F EPMA

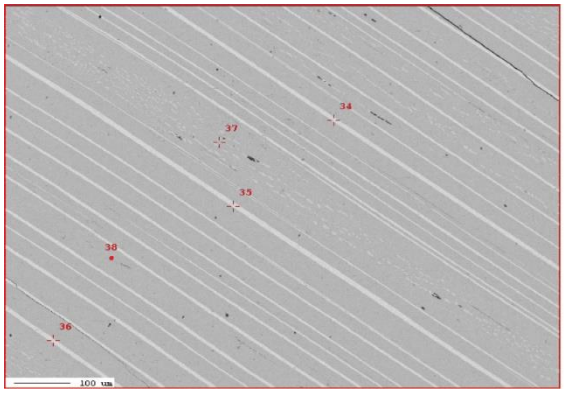

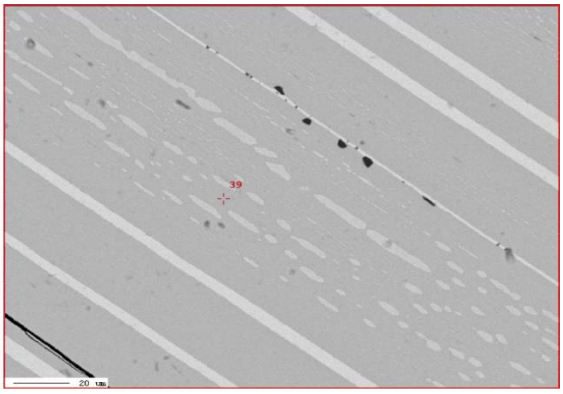

CC076 Circle G LAICPMS

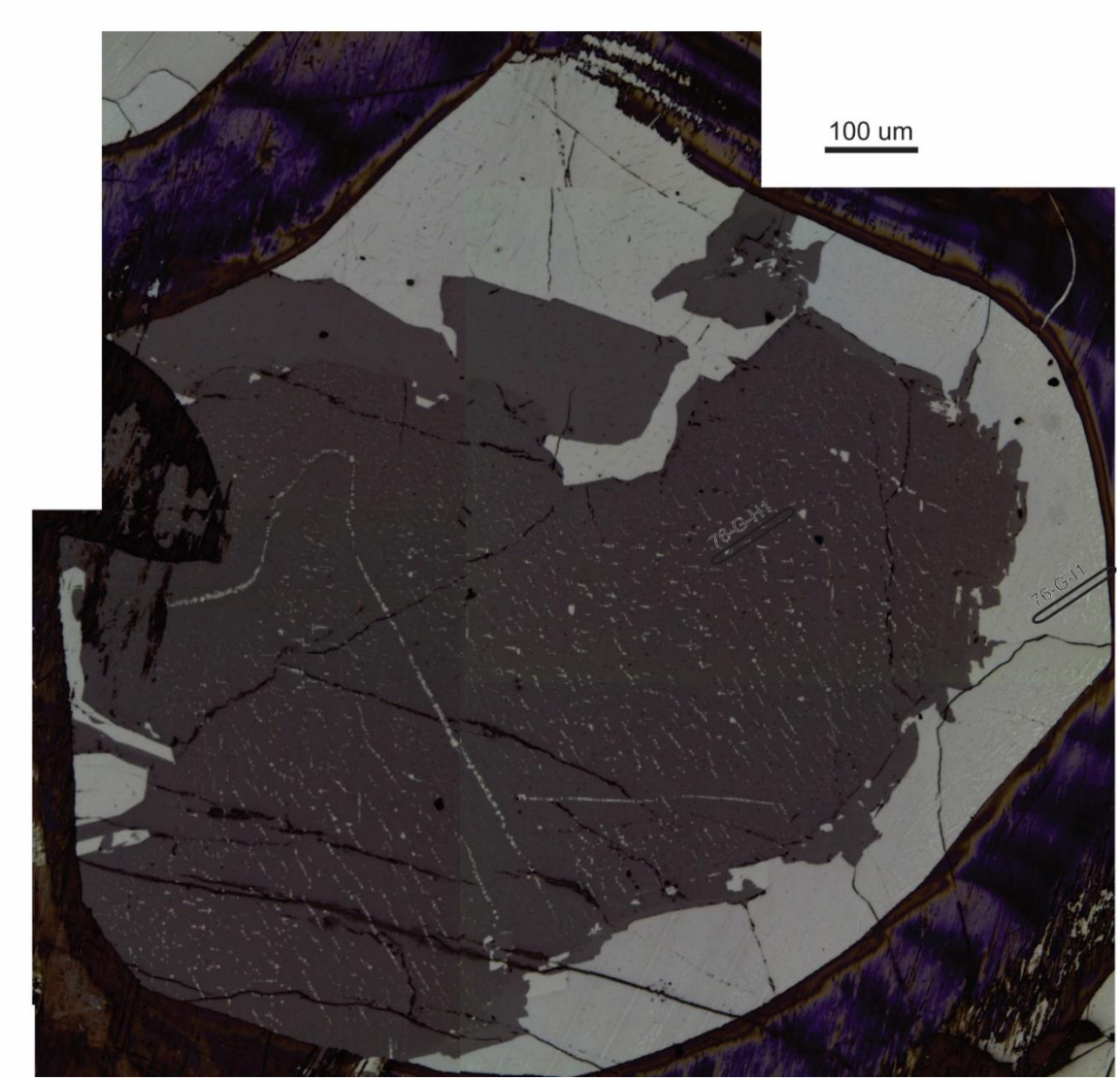

CC076 circle G EPMA

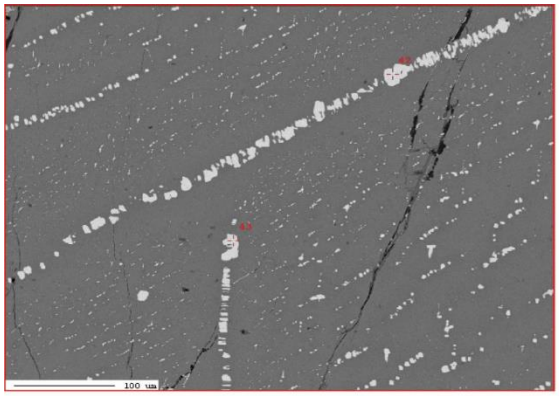

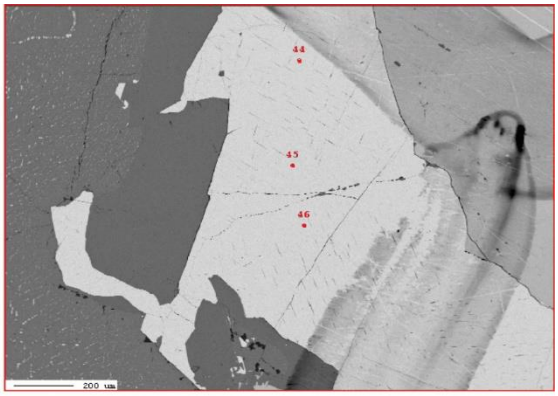

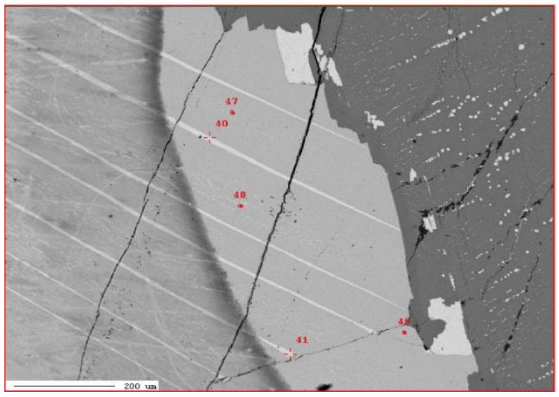

CC076 circle K LA-ICPMS

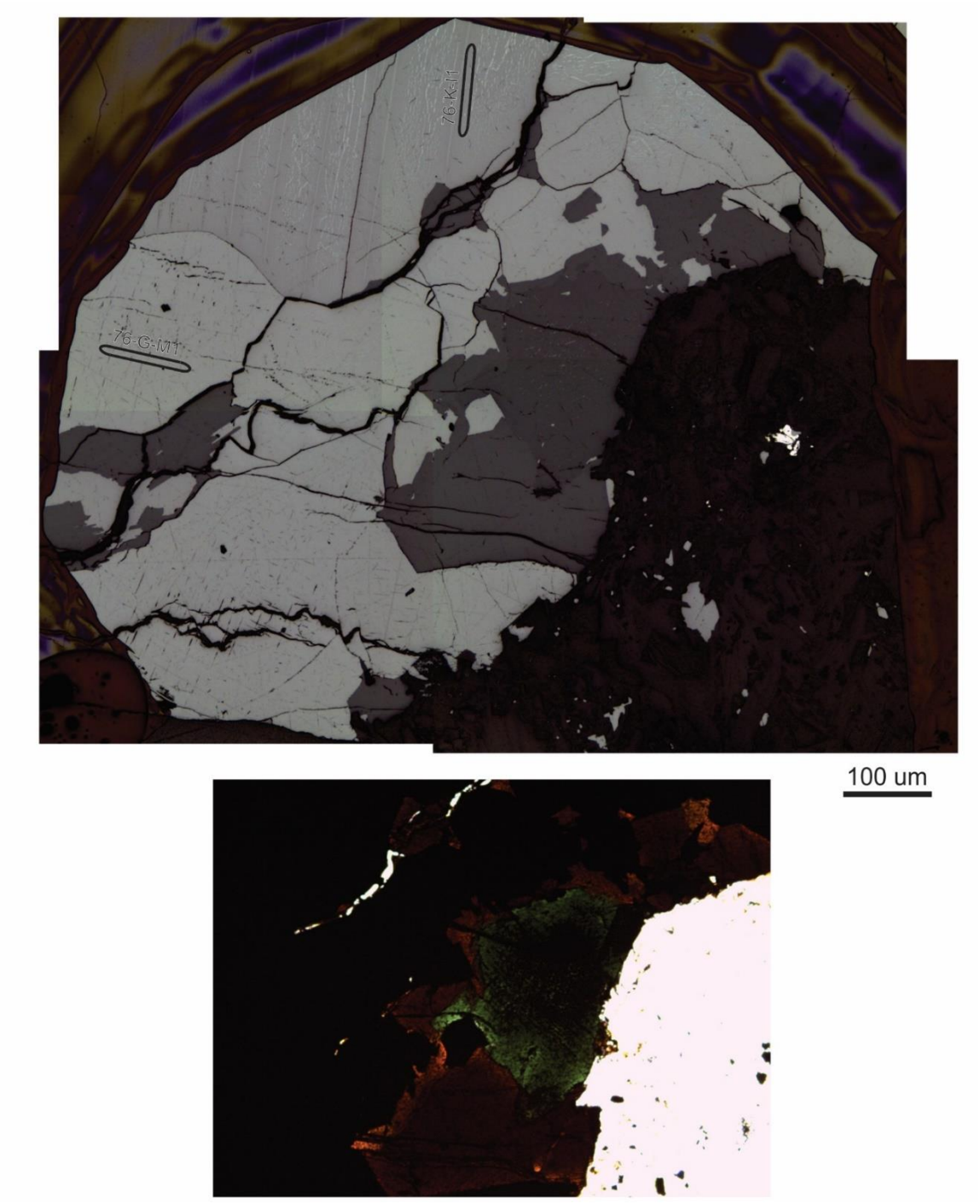

CC076 circle L LA-ICPMS

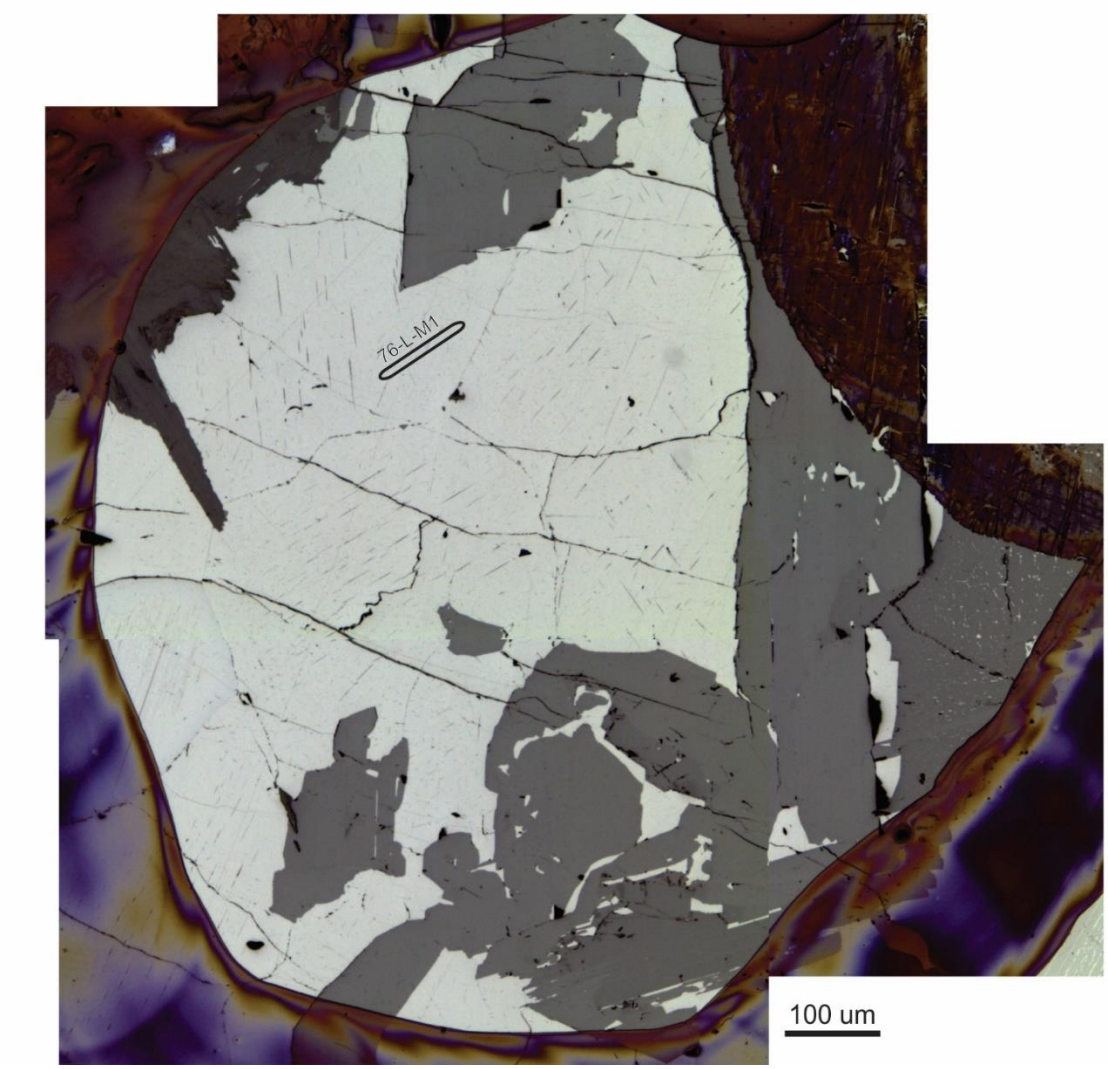

Appendix VII: LA-ICPMS secondary standards

Table aVII: LA-ICPMS secondary standards

Source	GSE Certificate Value GEOREM Average	GSE This study (n=15) Average	Gp6 Certificate value GEOREM Average	Gp6 This study (n=13) Average
^{24}Mg	21106	21077	51318	49616
^{27}Al	68804	68348	92145	85829
^{29}Si	250994	246793	224259	217000
^{31}P	70	28	611	514
^{44}Ca	52858	52247	86787	82534
^{45}Sc	530	532	36.75	35
^{47}Ti	450	413	7012	6351
^{49}Ti	450	419	7012	6336
^{51}V	440	440	238	256
^{52}Cr	400	368	300.2	313
^{53}Cr	400	370	300.2	318
^{55}Mn	590	589	1255	1286
^{59}Co	380	381	46.9	47
^{60}Ni	440	416	145.7	144
^{63}Cu	380	363	89.5	73
^{65}Cu	380	369	89.5	79
^{66}Zn	460	442	70.8	79
^{69}Ga	490	501	16.02	27
^{71}Ga	490	510	16.02	15
^{74}Ge	320	318	1.26	1
^{75}As	260	260	N.R.	N.R.
^{89}Y	410	433	19.33	17
^{90}Zr	410	404	55.1	48
^{92}Zr	410	408	55.1	27
^{93}Nb	420	429	4.16	4
^{95}Mo	390	382	N.R.	N.R.
^{118}Sn	280	277	1.33	3
^{121}Sb	450	432	0.13	0
^{178}Hf	395	409	1.52	1
^{181}Ta	390	416	0.28	0
^{182}W	430	441	N.R.	N.R.
^{208}Pb	378	406	3.28	4

N.R.- Not recorded

Appendix VII (Continued)